Halogen Bonding Interlocked Host Systems for Recognition and Sensing of Charged Guests

Hui Min Tay

Somerville College



A thesis submitted for the degree of Doctor of Philosophy

Trinity Term 2024

Abstract

Halogen Bonding Interlocked Host Systems for Recognition and Sensing of Charged Guests

***Hui Min Tay**, Somerville College, University of Oxford*

Abstract of Thesis Submitted for the Degree of Doctor of Philosophy, Trinity Term 2024

This thesis describes the development of cation and anion template-directed methodologies to prepare interlocked host molecules for the recognition of charged guests, principally anions and ion-pairs. The use of halogen bonding motifs as both anion templating and binding motifs is explored as a strategy to enhance the ion recognition properties of the interlocked hosts.

Chapter 1 introduces the field of supramolecular chemistry and outlines the key principles underlying host-guest chemistry. Advances in the design of receptors for anion and ion-pair recognition are reviewed, with a particular focus on receptors utilising halogen bonding (XB) interactions. The template-directed preparation of mechanically interlocked molecules and their applications in host-guest recognition and sensing is discussed.

Chapter 2 describes the ion-pair binding properties of neutral heteroditopic XB catenanes and rotaxanes prepared via an alkali metal cation template-directed approach. The binding of alkali metal cations, halide anions and their respective ion-pairs by the interlocked hosts is investigated by ^{1}H NMR titration studies, revealing significant positive cooperativity between cation and anion binding events. Crystallographic analysis is used to probe the binding modes and stoichiometries of the catenane receptors. The ion-pair binding capabilities of the receptors are also exploited for the selective solid-liquid extraction of alkali metal halide salts.

Chapter 3 describes the use of a novel chloride anion template-directed strategy to prepare neutral XB [2]catenane and [2]rotaxane interlocked host molecules. ^{1}H NMR binding studies of the host molecules in aqueous-acetone solvent mixtures demonstrate a mechanical bond induced anti-Hofmeister halide anion binding preference, which is exploited to develop selective interlocked systems for anion membrane transport and sensing.

Chapter 4 details the use of orthogonal cation and anion template-directed strategies to prepare a heteroditopic [3]catenane possessing interlocked binding cavities for both the cationic and anionic guests. Crystallographic studies suggest the catenane is capable of stabilising a sodium chloride ion-pair in a host-separated binding mode. Modifications to the [3]catenane design with the aim of improving its yield and ion recognition capabilities are presented.

Chapter 5 presents the main conclusions of this thesis.

Chapter 6 details the experimental procedures employed in this work, including synthetic protocols and characterisation of novel compounds.

Acknowledgements

I am immensely grateful to the many people who have supported me during this journey and helped make this thesis a reality.

Firstly, I would like to thank my supervisor, Professor Paul Beer, for his invaluable support and guidance during my DPhil. From a research perspective, his wealth of chemical knowledge, constant stream of 'crazy ideas' and willingness to let me explore projects of interest have created a conducive research environment in which I was able to thrive. As a mentor, Paul has been extremely kind and understanding, from the very beginning when he accommodated the many travel restrictions that I faced during the pandemic, all the way to extending financial support during my final term of thesis writing.

I am very fortunate to have been mentored by several outstanding senior members of the group: Dr Andrew Docker, who has been an indispensable source of project inspiration and chemistry advice; Dr Richard Tse, for his guidance on the work in Chapter 2 and entrusting me with many useful compounds; Dr Vihanga Munasinghe, who warmly welcomed me into the Beer group and showed me the ropes.

It has been a pleasure working alongside some brilliant chemists and lovely individuals over the last three years: Dr Robert Hein, Dr Krzysztof Bak, Dr Edward (TJ) Mitchell, Dr Heike Kuhn, Dr Zongyao Zhang, Dr Laura Bickerton, Dr Arya Arun, Dr Jamie Wilmore, Dr Toby Johnson, Dr Manzoor Ahmad and Andrew Taylor. Our conversations, pub nights and mini-battles for control over the lab speakers have added colour and vibrance to my time in the Beer group, which I will look back on fondly. A special shout-out goes to my late-night lab buddy Arya, who has become one of my closest friends in Oxford thanks to her fantastic music taste, solid life advice and shared appreciation of fast food.

I would like to acknowledge my colleagues in the Department for their contributions to this thesis, in particular Professor Matthew Langton and Dr Toby Johnson for conducting the anion transport studies in Chapter 3; Dr Amber Thompson and Dr Heike Kuhn for their help with X-ray crystallography; Dr Nick Rees and the members of the NMR facility for troubleshooting my titration experiments and obtaining NMR characterisation of many interlocked structures.

I would not have made it to Oxford if not for the groundwork laid by my previous supervisors. I would especially like to thank Dr Carol Hua and Professor Brendan Abrahams, my Honours supervisors at the University of Melbourne, for encouraging my passion for research and helping me with the application process, as well as Dr Nick White at the Australian National University, who introduced me to the field of supramolecular chemistry. I am also very grateful to Professors Craig Hutton and Ethan Goddard-Borger, who kindly opened their research groups to an untested second-year undergraduate student six years ago.

My DPhil has been made all the more enjoyable by the people I met along the way. I would like to acknowledge my friends and teammates from the Oxford University Badminton Club, in particular Yi, Yuying, Chuanqi and Rash for the countless good memories on and off the court. A big thanks to my 'mates' from Australia, especially Yifei, Adele, Yasmine and Lachlan, who have gone the extra mile (literally) to stay in touch. Finally, I would like to thank Tom for his steadfast support during the final year of my DPhil.

None of this would be possible without my family: 婆婆, who constantly asks after my health and well-being; Joo Kai, for sorting out my tech issues; and last but definitely not least, Mum and Dad, for your unconditional love and care at every step of this journey. I will never be able to express how much it means to me, and I hope that I can make you proud.

Publications

'Optical sensing of anions by macrocyclic and interlocked hosts.'

H. M. Tay and P. D. Beer, *Org. Biomol. Chem.* **2021**, *19*, 4652-4677.

'Anti-Hofmeister Anion Selectivity via a Mechanical Bond Effect in Neutral Halogen-Bonding [2]Rotaxanes.'

A. Docker, Y. C. Tse, H. M. Tay, A. J. Taylor, Z. Zhang and P. D. Beer*, Angew. Chem. Int. Ed.* **2022**, *61*, e202214523.

'Halogen-Bonding Heteroditopic [2]Catenanes for Recognition of Alkali Metal/Halide Ion Pairs.'

H. M. Tay, Y. C. Tse, A. Docker, C. Gateley, A. L. Thompson, H. Kuhn, Z. Zhang and P. D. Beer, *Angew. Chem. Int. Ed.* **2023**, *62*, e202214785.

'Alkali Metal Halide Ion-Pair Binding in Conformationally Dynamic Halogen Bonding Heteroditopic [2]Rotaxanes.'

H. M. Tay, A. Docker, Y. C. Tse and P. D. Beer, *Chem. Eur. J.* **2023**, *29*, e202301316.

'Exploiting the Catenane Mechanical Bond Effect for Selective Halide Anion Transmembrane Transport.'

H. M. Tay, T. G. Johnson, A. Docker, M. J. Langton and P. D. Beer, *Angew. Chem. Int. Ed.* **2023**, *62*, e202312745.

'Squaramide-Based Heteroditopic [2]Rotaxanes for Sodium Halide Ion-Pair Recognition.'

A. Arun, A. Docker, H. M. Tay and P. D. Beer, *Chem. Eur. J.* **2023**, *29*, e202301446.

'A Halogen-Bonding [2]Rotaxane Shuttle for Chloride-Selective Optical Sensing.'

H. M. Tay, A. Docker, A. Taylor and P. D. Beer, *Chem. Eur. J.* **2024**, e202400952.

'*Ammonium Halide Selective Ion Pair Recognition and Extraction with a Chalcogen Bonding Heteroditopic Receptor.'*

A. Docker, Y. C. Tse, H. M. Tay, Z. Zhang and P. D. Beer, *Dalton Trans.* **2024**, *53*, 11141-11146.

'Selective Sodium Halide over Potassium Halide Binding and Extraction by a Heteroditopic Halogen Bonding [2]Catenane.'

H. M. Tay, A. Docker, C. Hua and P. D. Beer, *Chem. Sci.* **2024**, *Advance Article.*

Abbreviations

δ	*chemical shift*
β_x	*binding constant*
λ	*wavelength*
μ	*micro*
Δ	*change in (a physical quantity)*
ν	*frequency*
°	*degree*
°C	*degrees Celsius*
Å	*Ångstrom*
A^-	*anion*
abs	*absorption*
a.u.	*arbitrary units*
aq.	*aqueous*
Ar	*aromatic*
AMT	*active metal template*
Br^-	*bromide ion*
BODIPY	*boron-dipyrromethene (4,4-difluoro-4-bora-3a,4a-diaza-s-indacene)*
BAr^{F-}	*tetrakis[3,5-bis(trifluoromethyl)phenyl]borate*
bipy	*2,2'-bipyridine*
Boc	*di-tert-butyl dicarbonate*
br	*broad*
Bu	*butyl*
cat.	*catalytic*
Ch	*chalcogen*
ChB	*chalcogen bonding*
Cl^-	*chloride ion*

conc.	*concentrated*
COSY	*homonuclear correlation spectroscopy*
CuAAC	*copper(I)-catalysed azide-alkyne cycloaddition*
D	*donor*
d	*doublet*
d	*deuterated*
DBU	*1,8-diazabicyclo[5.4.0]undec-7-ene*
DCM	*dichloromethane*
dd	*doublet of doublets*
DEG	*di(ethylene glycol)*
DFT	*density functional theory*
DIPEA	*N,N-di-iso-propylethylamine*
DMAP	*4-dimethylaminopyridine*
DMF	*N,N-dimethylformamide*
DMSO	*dimethyl sulfoxide*
DNA	*deoxyribonucleic acid*
e.g.	*exempli gratia*
e^-	*electron*
EDTA	*ethylenediaminetetraacetate*
eq., equiv.	*equivalents*
ESI	*electrospray ionisation (mass spectrometry)*
Et	*ethyl*
et al.	*et alia*
EtOAc	*ethyl acetate*
E.T.	*energy transfer*
EWG	*electron withdrawing groups*
g	*gram*
G	*Gibbs free energy*
Grubbs' I/ II	*Grubbs' first/ second generation catalyst*

H	*enthalpy*
HB	*hydrogen bonding*
HRMS	*high resolution mass spectrometry*
$H_2PO_4^-$	*dihydrogen phosphate ion*
HSO_4^-	*hydrogen sulfate ion*
Hz	*Hertz*
ICT	*Isothermal titration calorimetry*
i.e.	*id est*
I^-	*iodide ion*
ITC	*Isothermal titration calorimetry*
J	*coupling constant*
K	*Kelvin (Temperature SI Unit)*
K_a	*association constant*
K_{app}	*apparent association constant*
K_d	*dissociation constant*
L	*litre*
M	*molar (moles per litre)*
m/z	*mass to charge ratio*
Me	*methyl*
MIM	*mechanically-interlocked molecule*
MS	*mass spectrometry*
Ms	*mesyl*
NDI	*naphthalenediimide*
NMR	*nuclear magnetic resonance*
NO_3^-	*nitrate ion*
NO_2^-	*nitrite ion*
o	*ortho*
o/n	*overnight*
OAc^-	*acetate ion*

OBz^-	*benzoate ion*
PEG	*polyethylene glycol*
PET	*photo-induced electronic transfer*
ppm	*parts per million*
prep TLC	*preparative thin layer chromatography*
pH	$-log_{10}[H^+]$
Ph	*phenyl*
pKa	$-log_{10}K_a$
q	*quartet*
quant.	*quantitative*
quin.	*quintet*
R	*chemical substituent*
rt / RT	*room temperature*
RCM	*ring-closing metathesis*
Rf	*retention factor*
ROESY	*Rotating-frame Nuclear Overhauser Enhancement Spectroscopy*
S	*entropy*
s	*second, singlet*
sat.	*saturated*
SLE	*solid-liquid extraction*
T	*temperature*
t	*triplet*
TBA	*tetrabutylammonium*
TBTA	*tris[(1-benzyl-1,2,3-triazol-4-yl)methyl]amine*
TEG	*tri(ethylene glycol)*
t, tert	*tertiary*
TFA	*trifluoroacetic acid*
THF	*tetrahydrofuran*

TLC	*thin layer chromatography*
TMS	*trimethylsilyl (protecting group)*
Ts	*tosyl*
UV	*ultra-violet*
v/v	*volume/ volume percent*
vis.	*visible*
vs.	*versus*
VT	*variable temperature*
wt.	*weight*
XB	*halogen bond*
XRD	*X-ray diffraction*

Table of Contents

Abstract ..... **i**

Acknowledgements ..... **iii**

Publications ..... **v**

Abbreviations ..... **vi**

Table of Contents ..... **xi**

Chapter 1: Introduction **1**

1.1 Supramolecular Chemistry **1**

1.2 Anion Recognition **3**

1.2.1 Importance of Anions 3

1.2.2 Challenges in Anion Recognition 4

1.2.3 Supramolecular Anion Receptors 7

1.2.3.1 Electrostatic Interactions in Anion Recognition 7

1.2.3.2 Hydrogen Bonding Interactions in Anion Recognition 9

1.2.3.2.1 Cationic Hydrogen Bonding Anion Binding Motifs 10

1.2.3.2.2 Neutral Hydrogen Bonding Anion Binding Motifs 13

1.2.3.3 Sigma-hole Interactions in Anion Recognition 19

1.2.3.3.1 Halogen Bonding Anion Receptors 22

1.2.3.3.2 Chalcogen Bonding Anion Receptors 28

1.2.3.4 Anion-π Interactions in Anion Recognition 30

1.3 Ion-Pair Recognition **32**

1.3.1 Heteroditopic Ion-Pair Receptors 33

1.3.1.1 Separated Ion-pair Receptors 33

1.3.1.2 Contact Ion-pair Receptors 36

1.3.2 Applications of Ion-Pair Receptors 38

1.3.2.1 Ion-pair Sensing 38

1.3.2.2 Extraction and Solubilisation of Salts 39

1.3.2.3 Membrane Transport 40

1.4 Mechanically Interlocked Molecules 42

1.4.1 Template-directed Syntheses of MIMs 44

1.4.1.1 Cation Template-Directed Approaches 44

1.4.1.1.1 Passive Metal Templates 45

1.4.1.1.2 Active Metal Templates 45

1.4.1.2 Anion Template-Directed Approaches 46

1.4.2 MIM-based Hosts for Charged Guest Recognition 48

1.4.2.1 MIMs for Cation Recognition and Sensing 49

1.4.2.2 MIMs for Anion Recognition 51

1.4.2.3 MIMs for Ion-pair Recognition and Sensing 54

1.5 Thesis Aims 58

1.6 References for Chapter 1 59

Chapter 2: Alkali Metal Cation Template-Directed Synthesis of Interlocked Architectures for Ion-Pair Recognition 67

2.1 Introduction 67

2.1.1 Cooperativity in Ion-Pair Receptors 68

2.1.2 Catenane-based Heteroditopic Ion-Pair Receptors 72

2.1.3 Alkali Metal Template-Directed Synthesis of MIMs 73

2.1.4 Project Aims 74

2.2 Homo[2]catenanes for Ion-Pair Recognition 75

2.2.1 Synthesis and Characterisation 76

2.2.1.1 Synthesis of XB Macrocycles 76

2.2.1.2 Pseudo[2]rotaxane Studies 77

2.2.1.3 Synthesis and Characterisation of Homo[2]Catenanes 78

2.2.2 ^{1}H NMR Ion Binding Studies 83

2.2.2.1 Alkali Metal Cation Binding Studies....83
2.2.2.2 Anion Binding Studies....86
2.2.2.3 Alkali Metal Halide Ion-Pair Binding Studies....90
2.2.2.4 Ion Binding Properties of Hetero[2]catenane 2.2·HBXB^{DEG}....96
2.2.3 Solid-Liquid Extraction Studies....100
2.3 A Hetero[2]catenane for Enhanced Ion-Pair Binding....102
2.3.1 Synthesis and Characterisation....102
2.3.2 ^{1}H NMR Ion Binding Studies....104
2.3.2.1 Cation Binding Studies....105
2.3.2.2 Anion Binding Studies....107
2.3.2.3 Ion-Pair Binding Studies....110
2.3.3 X-ray Crystallographic Analysis of Ion-Pair Binding....112
2.3.4 Preferential Solid-Liquid Extraction of NaX over KX Salts....114
2.4 Conformationally Dynamic [2]Rotaxane Systems for Ion-Pair Binding....116
2.4.1 Synthesis and Characterisation....117
2.4.2 ^{1}H NMR Co-conformational Analysis of [2]Rotaxanes....120
2.4.3 ^{1}H NMR Ion Binding Studies....125
2.4.3.1 Cation Binding Studies....125
2.4.3.2 Anion Binding Studies....129
2.4.3.3 Ion-Pair Binding....132
2.5 Conclusions and Future Work....139
2.5.1 Future Work....140
2.6 References for Chapter 2....141
Chapter 3: Anion Template-Directed Synthesis of Interlocked Host Structures for Anion Sensing and Transport....145
3.1 Introduction....145
3.1.1 Anion Template Directed Synthesis....145

3.1.2 Anion Transport by Mechanically Interlocked Molecules 149
3.1.3 Anion Sensing by Dynamic Multi-station Rotaxane Shuttles 151
3.1.4 Chapter Aims 154
3.2 A Potent Dinitro-Functionalised Halogen Bonding Donor Motif..... 156
3.2.1 Synthesis of Dinitro-Functionalised Acyclic Receptor..... 156
3.2.2 ^{1}H NMR Anion Binding Studies..... 157
3.3 Catenanes for Anion Binding..... 160
3.3.1 Anion Template-Directed Synthesis of Neutral Hetero[2]Catenanes..... 160
3.3.2 ^{1}H NMR Anion Binding Studies..... 165
3.3.3 Cation Binding Studies 172
3.3.4 Effects of Methylation on the Anion Binding Properties of the [2]Catenanes 172
3.3.5 Anion Transport Studies 180
3.4 A Multi-station Rotaxane Shuttle for Selective Chloride Sensing..... 186
3.4.1 Synthesis and Characterisation 187
3.4.2 ^{1}H NMR Anion Binding Studies..... 191
3.4.3 UV-Vis Studies 197
3.5 Conclusions and Future Work..... 199
3.5.1 Future Work 200
3.6 References for Chapter 3..... 202
Chapter 4: Preparation of Higher-Order Catenanes via Orthogonal Template-Directed Strategies 205
4.1 Introduction..... 205
4.1.1 Strategies for the Preparation of Higher Order [n]Catenanes (n > 2) 206
4.1.1.1 Linear [3]Catenanes..... 206
4.1.1.2 Higher Order [n]Catenanes (n > 3)..... 209
4.1.2 Applications of Higher Order Catenanes 214
4.1.3 Chapter Aims 216

4.2 A Heteroditopic [3]Catenane for Ion-Pair Recognition 217

4.2.1 Synthesis 217

4.2.1.1 Sodium Cation Template-Directed Formation of a [2]Catenane 218

4.2.1.2 Chloride Anion Template-Directed Formation of a [3]Catenane 223

4.2.2 Characterisation 223

4.2.2.1 ^{1}H NMR and Mass Spectrometric Studies 223

4.2.2.2 Single Crystal X-ray Diffraction Studies 227

4.3 Modifications to [3]Catenane Design 229

4.3.1 Expanded Central Macrocycles 229

4.3.2 Perfluorophenyl (PFP)-functionalised Central Macrocycles 232

4.3.3 A Coumarin-containing Central Macrocycle 235

4.4 Conclusions and Future Work 238

4.4.1 Future Work 239

4.5 References for Chapter 4 240

Chapter 5: Conclusions 243

Chapter 6: Experimental 250

6.1 General Considerations 250

6.1.1 Chemicals and Solvents 250

6.1.2 Instrumentation 250

6.1.3 ^{1}H NMR Titration Protocol 251

6.1.4 Solid-liquid Extraction Protocol 252

6.1.5 Optical Studies 252

6.2 Synthesis and Characterisation of Novel Compounds 253

6.2.1 Compounds from Chapter 2 253

6.2.2 Compounds from Chapter 3 277

6.2.3 Compounds from Chapter 4 293

6.3 References for Chapter 6 317

Appendix **319**

CHAPTER 1

Introduction

Chapter 1: Introduction

1.1 Supramolecular Chemistry

Supramolecular chemistry, or the reversible association of chemical entities via intermolecular non-covalent interactions, represents the current 'cutting edge' in the chemist's quest to build assemblies of ever-increasing complexity using a bottom-up approach. Despite being a relatively young field, supramolecular chemistry has advanced swiftly; in comparison to the centuries of effort required to develop the tools necessary to construct molecules from atoms, the corresponding leap from molecules to supramolecular assemblies has occurred over just a few decades.[1] Underpinning this rapid growth is an understanding of non-covalent interactions, which play a pivotal role in everyday processes, from the cleaning action of soaps and detergents, to the encoding of genetic information in the double helical structure of DNA, and even the unusually high boiling point of water. Attempts to rationalise these phenomena have driven intense, if somewhat unsystematic, investigations into the nature of the underlying intermolecular interactions, laying the groundwork for modern supramolecular chemistry.

The birth of supramolecular chemistry as a distinct field can be traced back to the serendipitous discovery of crown ethers by Pedersen in 1967, when dibenzo[18]crown-6 was isolated as a reaction side product. In his seminal paper, Pedersen described a series of macrocyclic polyethers capable of complexing alkali and alkaline earth metal ions via convergent ion-dipole interactions between the cation and the oxygen atoms of the polyether ring (**Figure 1.1a**).[2] This is widely regarded as the first example of 'host-guest chemistry', in which a small guest molecule or ion is bound within the cavity of a larger host. Subsequent work by Lehn and Cram on the preparation and host-guest chemistry of cryptands[3-4] (**Figure 1.1b**) and spherands[5-6] (**Figure 1.1c**) respectively, established that the encapsulation of alkali

metal cationic guests in pre-organised, three-dimensional cavities can serve as a powerful strategy to improve both the affinity and selectivity of binding. For these pioneering studies, Pedersen, Lehn and Cram were jointly awarded the 1987 Nobel Prize in Chemistry.[7-9] Over the subsequent decades, a plethora of macrocyclic host molecules were introduced,[10] including calixarenes,[11] cyclodextrins,[12] cucurbiturils,[13] cyclophanes[14] and pillararenes.[15]

The next milestone in the field was independently achieved by Sauvage and Stoddart, who developed template-directed methods based on Cu(I)-phenanthroline coordination[16] and π-π donor-acceptor interactions[17] respectively to prepare mechanically interlocked molecules (MIMs) such as rotaxanes (**Figure 1.1d**) and catenanes (**Figure 1.1e**). Not only did the interlocked cavities of MIMs present new opportunities for designing binding sites tailored to target guests, the inherent dynamic nature of interlocked host molecules propelled host-guest chemistry beyond simple guest binding and into the realm of nanotechnology. Indeed, many exciting developments in the field arise from the use of interlocked host molecules as increasingly sophisticated sensors,[18] switches[19-20] and molecular machines.[21-22]

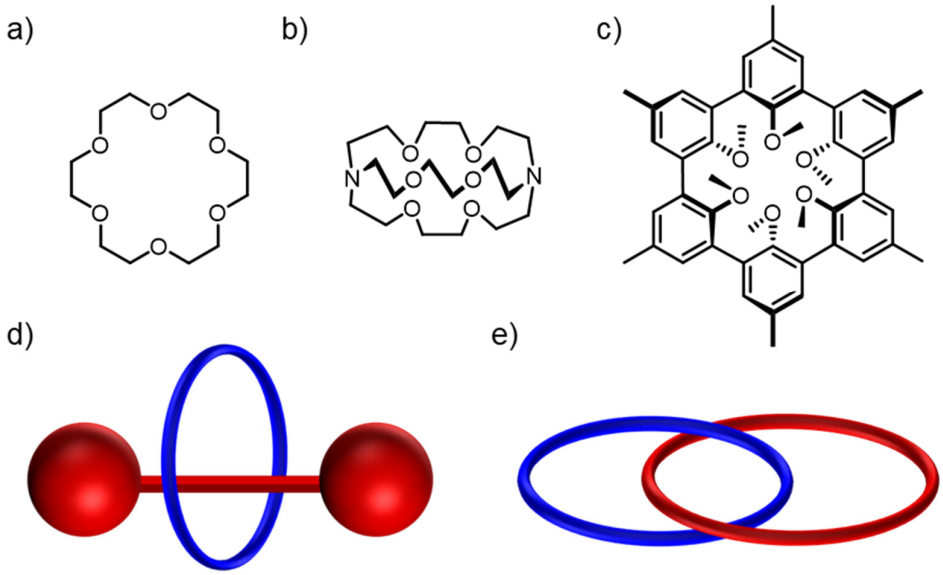


Figure 1.1. *Representative chemical structures of early supramolecular host molecules, including: (a) Crown ethers; (b) Cryptands; (c) Spherands. Carton representations of mechanically interlocked molecules, including: (d) [2]Rotaxanes; (e) [2]Catenanes.*

This thesis describes the development of novel template-directed methods for the preparation of catenanes and rotaxanes, and the subsequent application of these interlocked host molecules for the recognition of charged guest species, particularly anions and ion-pairs. With this in mind, this introductory chapter provides a survey of the challenges and strategies associated with the design of host molecules for anion and ion-pair binding, followed by an overview of mechanically interlocked molecules used in charged guest recognition. Finally, the aims of the novel work of this thesis will be outlined.

1.2 Anion Recognition

1.2.1 Importance of Anions

Within the broader area of supramolecular host-guest chemistry, the sub-field of anion recognition has expanded rapidly over the last two decades or so, driven by a growing awareness of the vital role anions play in a myriad of biological,[23-25] environmental[26-28] and industrial[29-30] processes. Phosphate-containing nucleotides are the building blocks of important biomolecules such as DNA, RNA and ATP, which are key components of many essential cellular processes, including replication, transcription and metabolism.[31] Even simple halide anions have dedicated biological systems for their regulation and transport, the failure of which can have severe and wide-ranging effects on human health. Abnormalities in chloride transport is implicated in a variety of diseases, including cystic fibrosis, myotonia congenita, osteopetrosis, epilepsy and even some cardiac diseases.[32-33] Likewise, mis-regulation of iodide transport into the thyroid gland is known to disrupt the production of essential hormones required for normal metabolism.[34]

The anthropogenic injection of anions into the biosphere as a result of various industrial processes also poses a significant threat to human health and the environment. Nitrate and phosphate fertilisers are used in large scale in arable farming to increase crop yields. The

leaching of these anions into nearby rivers and lakes can severely impact aquatic ecosystems through a combination of eutrophication, water acidification and toxicity towards aquatic animals.[35-36] The radioactive pertechnetate ($^{99}TcO_4^-$) anion, a by-product of the nuclear fission industry, is a particularly hazardous component of nuclear waste streams due to its long half-life ($t_{1/2} = 2.13 \times 10^5$ years) and environmental mobility.[29] Gold mining operations produce highly toxic arsenate salts which leads to elevated levels of arsenic-associated health problems in nearby communities.[37] Developing methods to detect and remove these toxic anion contaminants from waste streams therefore constitutes a potential strategy to mitigate the detrimental impact of industrial activity on human health and the environment. In this context, supramolecular host molecules capable of selective anion recognition represent a promising starting point for the design of systems for anion sensing, extraction and transport.

1.2.2 Challenges in Anion Recognition

Despite the considerable demand for anion receptors and sensors, progress in the area of supramolecular anion binding has lagged behind its sister field of cation recognition. This relatively slower pace of development is attributed to the greater challenges associated with anion binding, which stem from several intrinsic properties of anions, namely their large ionic radii, variable geometries, pH dependence and high energies of solvation.[38]

Anions typically possess larger ionic radii than isoelectronic cations, as seen from a comparison of the spherical halide anions and alkali metal cations (**Table 1.1**).[39] This results in anions having lower charge densities and hence experiencing relatively weaker electrostatic interactions with positively-charged groups or dipoles. In addition, anions typically display higher solvation enthalpies relative to cations (**Table 1.1**).[40] This presents a particular challenge in aqueous-containing solvent media due to the extensive hydration of anions by surrounding

water molecules. The need to de-solvate target anionic guests prior to receptor complexation therefore imposes a steep enthalpic penalty to anion binding.

***Table 1.1**. Ionic radii and free energies of hydration of halide anions and alkali metal cations*[39, 41]

Anion	Ionic Radius (Å)	ΔG_{hyd} (kJ mol^{-1})	Cation	Ionic Radius (Å)	ΔG_{hyd} (kJ mol^{-1})
F^-	1.33	−465	Na^+	1.02	−365
Cl^-	1.81	−340	K^+	1.38	−295
Br^-	1.96	−315	Rb^+	1.57	−275
I^-	2.20	−275	Cs^+	1.67	−250

The extent of anion hydration is correlated with the 'Hofmeister series' (**Figure 1.2**), initially proposed by Franz Hofmeister in 1888 based on his empirical observations regarding the tendency of different ions to either increase or decrease the solubility of proteins in water.[42] While the precise position of a salt on the series proved to be a combination of multiple factors, including its degree of hydration and interaction with the dipoles on the protein backbone,[43-45] generally speaking, the Hofmeister series provides a classification of anions according to their hydration enthalpies, with latter members of the series being more extensively hydrated. These hydrophilic anions such as fluoride and sulfate typically exhibit lower host-guest binding affinities in aqueous-containing solvent mixtures compared to hydrophobic anions like iodide and perchlorate, an effect termed the 'Hofmeister bias'. The need for supramolecular receptors and sensors capable of functioning in aqueous solvent systems for various environmental and biological applications has intensified efforts to counteract the Hofmeister bias, but examples of synthetic receptors demonstrating anti-Hofmeister selectivity are still relatively scarce.[46-50]

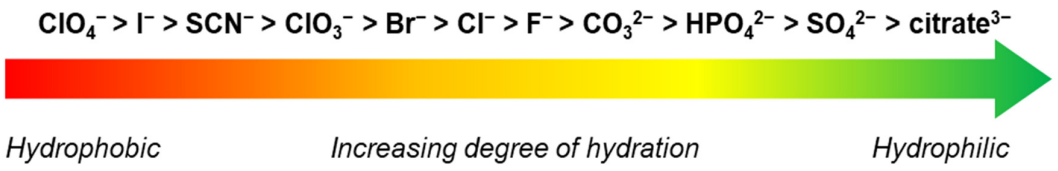


***Figure 1.2.** The Hofmeister series of anion hydration.*

Many anions of interest, even simple inorganic ones, exist in a variety of geometries ranging from linear to octahedral (**Figure 1.3**). This complicates the synthesis of anion receptors by imposing additional restrictions on binding site geometries, often requiring careful arrangement of binding motifs within the receptor scaffold, to achieve host-guest complementarity, which is essential for the strong and selective binding of target anions.[51]

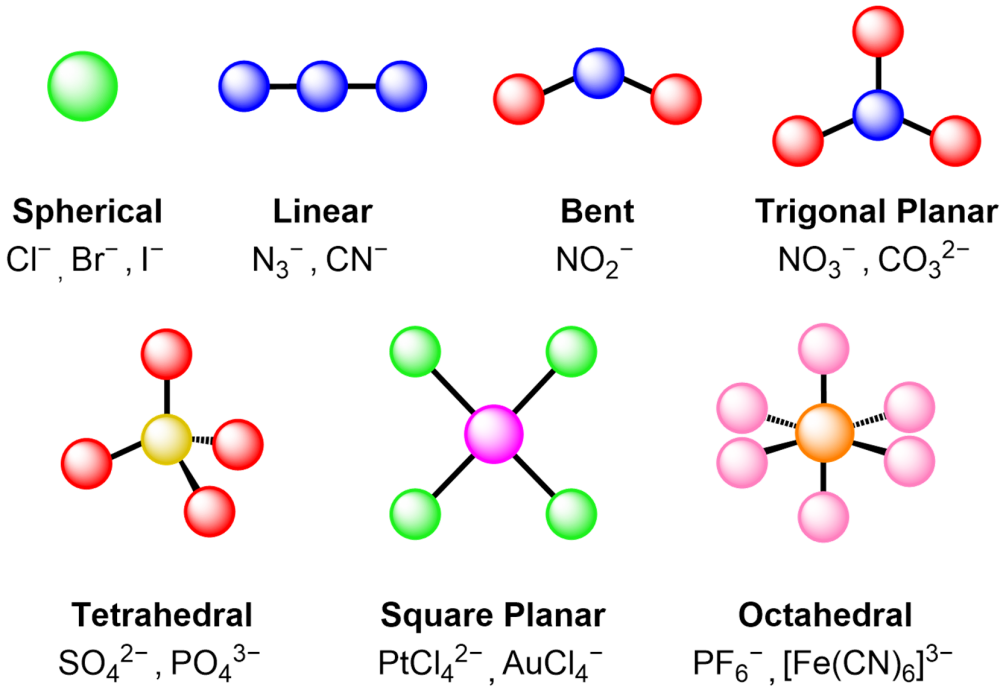


Figure 1.3. *Examples of common anion geometries.*

A further consideration in anion binding is the sensitivity of both the anionic guest and the receptor to varying pH conditions. Most anions are conjugate bases that undergo protonation under acidic conditions, lowering or negating their binding affinity to a positively-charged host molecule. This is of particular concern for highly charged oxoanions which undergo multiple acid-base equilibria, such as PO_4^{3-}, SO_4^{2-} and CO_3^{2-}, as the predominant species present in solution can vary considerably with changes in pH.[52] In addition, early anion receptors relied on acidic polyammonium groups that are susceptible to deprotonation under

basic conditions, further limiting the pH window within which anion binding and sensing can occur.[53]

1.2.3 Supramolecular Anion Receptors

Although Park and Simmons reported the first supramolecular anion receptor in 1968,[54] featuring a lipophilic diprotonated macrobicyclic bis-ammonium cryptand capable of encapsulating halide anions in acidic aqueous media, the field of anion receptor chemistry was slow to advance until the latter half of the 20th century. A diverse range of receptors now exist which display differing anion selectivities and the ability to function in a variety of solvent media. Behind this progress is the expanding repertoire of non-covalent interactions used in anion binding, from traditional electrostatic interactions and hydrogen bonding to more exotic interactions like halogen bonding, chalcogen bonding and anion-π interactions. The following section outlines some of these non-covalent interactions and prominent examples of their incorporation into anion receptor design.

1.2.3.1 Electrostatic Interactions in Anion Recognition

Exploiting the Coulombic attraction between oppositely charged ions or dipoles is arguably the first strategy that comes to mind when tasked with designing an anion receptor. Electrostatic interactions can be classified based on the type of the charged species involved: ion-ion, ion-dipole and dipole-dipole. Ion-ion interactions typically possess the highest stabilisation energies (100-300 kJ/mol), which are comparable in strength to covalent bonding, while the stabilisation energies of ion-dipole and dipole-dipole interactions are considerably weaker at 50-200 kJ/mol and 5-50 kJ/mol respectively. Ion-ion interactions are also capable of operating over the longest distances due to their low distance (r) dependence ($E \propto 1/r$), followed by ion-dipole ($E \propto 1/r^2$) and dipole-dipole ($E \propto 1/r^3$) interactions. However, the non-directionality of ion-ion interactions presents a major limitation in the context of anion receptor

design. Consequently, reports of selective anion receptors that utilise electrostatic ion-ion interactions as the primary binding motif are rare.

One example is a series of tetracationic quaternary ammonium cages reported by Schmidtchen (**Figure 1.4a**),[55] which are capable of binding halide anions in pure water. The cages exhibit a Hofmeister binding preference, wherein the most strongly solvated chloride anion shows the lowest binding affinity to the cage receptors (K_a = 10-20 M^{-1}), whereas bromide and iodide were bound more strongly (K_a = 150-250 M^{-1}). No significant selectivity for bromide or iodide was achieved despite varying the cavity size of the cages, which the authors attribute to the flexibility of the alkyl linkers.

Charge matching was found to be crucial in determining anion selectivity of a flexible tripodal receptor reported by Garratt and co-workers (**Figure 1.4b**).[56] The tricationic receptor, which contains three 1,4-diazobicyclo (DABCO) substituents appended to the 1,3,5-positions of a central benzene scaffold, was capable of binding tricarboxylate anions in aqueous solution with moderate affinities (K_a = 60-200 M^{-1}). In addition, co-crystals of the receptor with ferricyanide showed a 1:1 complex in which the receptor adopts a *cis* conformation that enables all three charged DABCO groups to interact with the anion.

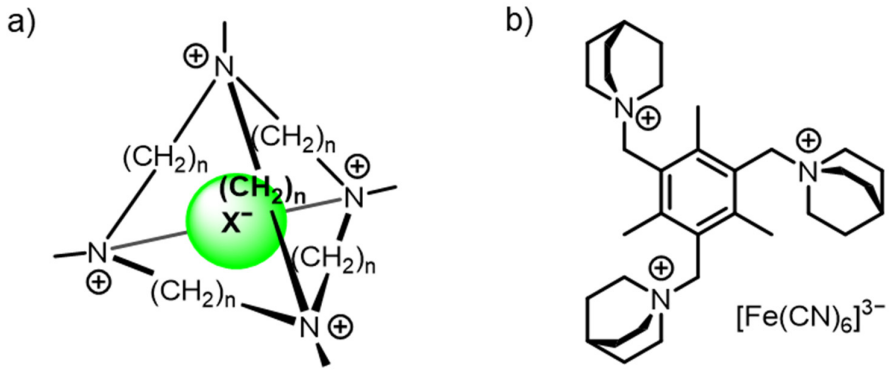


Figure 1.4. *Chemical structures of cationic anion receptors, including: (a) Schmidtchen's tetracationic quaternary ammonium cage; (b) Garratt's tricationic tripodal receptor.*

Despite the scarcity of receptors utilising predominantly ion-ion interactions for anion binding, electrostatic interactions remain an important part of the supramolecular toolkit. The incorporation of positive charged groups into the structures of anion receptors is a common strategy to enhance the potency of other non-covalent binding motifs as well as achieve solubility of receptors in aqueous-containing solvent media.

1.2.3.2 Hydrogen Bonding Interactions in Anion Recognition

Hydrogen bonding (HB) is defined as the attractive interaction between a hydrogen atom that is covalently bonded to an electronegative atom (donor) and another electronegative atom bearing a lone pair of electrons (acceptor). This is typically denoted D-H···A, where the donor D is often a nitrogen, oxygen or fluorine atom, but can also be a carbon atom if the latter is bonded to a sufficiently electron-withdrawing group, while the acceptor A is a Lewis base or anion.

The strength of hydrogen bonds varies considerably, with interaction energies spanning 4-60 kJ/mol, depending on factors such as: the basicity of the acceptor, the electron-withdrawing ability of the donor, the geometry of the system, the presence of charged groups in the system, and the solvent polarity, with HB strength being significantly diminished in protic solvent media. In the solid-state, the strength of a hydrogen bond can be approximated via the crystallographically-determined distance between the donor and acceptor, with typical O···O distances falling in the range 2.50-2.80 Å, while longer bonds indicate a weaker interaction. Hydrogen bonds generally exhibit a linear directionality, but this preference is not stringent and the crystal structures of many hydrogen bonded systems contain D-H···A angles that deviate from 180°.

Hydrogen bonding is heavily utilised in biotic anion receptors such as sulfate- and phosphate-binding proteins, which contain arrays of complementary HB donors designed to

achieve strong and specific binding of target anions. Drawing inspiration from nature, supramolecular chemists have integrated a variety of charged and neutral HB donor groups into synthetic anion receptors (**Figure 1.5**).

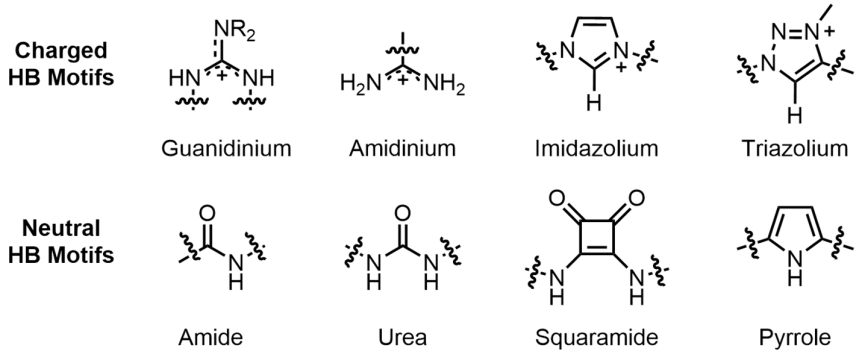


Figure 1.5. *Common hydrogen bonding motifs used in anion recognition*

1.2.3.2.1 Cationic Hydrogen Bonding Anion Binding Motifs

Inspired by the pioneering work of Park and Simmons (**Figure 1.6a**),[54] early efforts towards the synthesis of anion receptors focused on the incorporation of polyammonium hydrogen bonding motifs into macrocyclic or cage-like host architectures. A prominent figure in this area was Lehn, who built an extensive family of polyammonium-based anion receptors of varying sizes and geometries,[3] including an ellipsoidal cage which exhibits a preference for linear anions such as N_3^- (**Figure 1.6b**)[4] and a series of hexacationic macrocycles capable of size-based discrimination between dicarboxylate anions in aqueous solution buffered at pH 5 (**Figure 1.6c**).[57]



Figure 1.6. *Polyammonium-based HB receptors: (a) Park and Simmons' initial bicyclic cage; (b)-(c) Lehn's cage and macrocycles*

Despite the potential of polyammonium cages for anion recognition in competitive solvent media, a significant limitation of these systems is their pH sensitivity, with great care often required to ensure that the solution is sufficiently acidic to protonate the ammonium groups yet basic enough to prevent protonation of any potential anionic guests. For this reason, guanidinium has gained popularity as a hydrogen bond donor motif due to its ability to remain protonated over a wide pH range, a property which stems from the high pK_a (13.6) of the guanidinium cation. In addition, guanidinium is capable of acting as a bidentate hydrogen bond donor, making it particularly useful for binding Y-shaped anions like oxoanions and carboxylates. The degree of pre-organisation can be further enhanced by incorporating the guanidinium group into a rigid bicyclic ring, thereby directing the two hydrogen bond donors parallel to each other.[58]

Schmidtchen reported an acyclic bis(guanidinium)-functionalised receptor capable of selectively binding tetrahedral anions via convergent HB interactions with the two guanidinium moieties on the arms of the receptor (**Figure 1.7a**). ^{1}H NMR titration experiments conducted in unbuffered water determined a 1:1 host-guest binding stoichiometry, with a particular preference for the biologically relevant mononucleotide thymidine-5'-phosphate ($K_a \approx 10^6$ M^{-1}).[59] Mendoza and co-workers reported a chiral acyclic guanidinium receptor which exhibited a stronger binding affinity for the *L*- enantiomer of *N*-acetyl tryptophan (K_a = 1051 and 534 M^{-1} for the *L*- and *D*-enantiomers respectively in $CDCl_3$) (**Figure 1.7b**). Impressively, the receptor was capable of preferentially extracting *N*-acetyl-*L*-tryptophan into chloroform from a racemic mixture in water, representing the first reported instance of enantioselective anion recognition.[60]

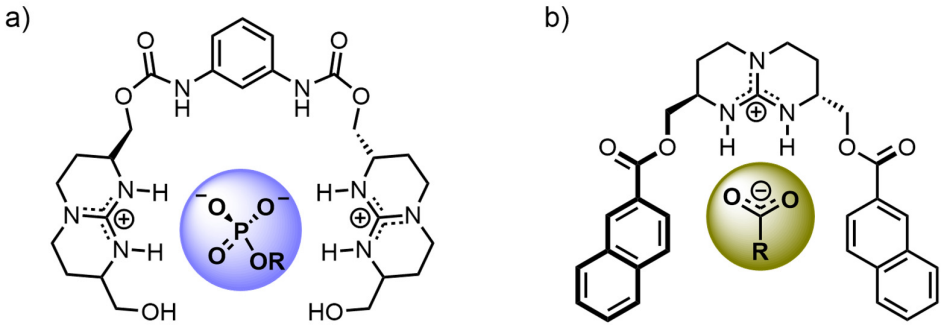


Figure 1.7. *Guanidinium-based HB receptors: (a) Schmidtchen's bis(guanidinium) receptor; (b) Mendoza's chiral receptor.*

Driven by a growing awareness of charge-assisted C-H hydrogen bonding interactions, imidazolium and triazolium groups have emerged as promising pH-independent anion binding motifs. Kim and co-workers synthesised a macrocyclic tetra(imidazolium)-functionalised receptor which displayed a marked preference for fluoride over other anions, with a 1:1 host-guest binding constant of 28900 M^{-1} in DMSO-d_6, whereas all other anions formed less stable 1:2 host-guest complexes (**Figure 1.8a**). The difference in binding properties was attributed to the convergent formation of four C-H···F^- hydrogen bonds which anchor the small fluoride guest in the macrocyclic cavity, as shown by X-ray crystallographic analysis of the receptor-fluoride complex.[61]

In recent years, the synthesis of anion receptors based on triazolium donor motifs has become an increasingly attractive prospect owing to the facile synthesis of triazoles via click chemistry procedures. An early example of a triazolium-functionalised anion receptor was reported by Pandey and co-workers, who appended triazolium groups to a deoxycholic acid scaffold (**Figure 1.8b**). The resulting receptor showed selective binding to the tetrahedral $H_2PO_4^-$ anion over halides and acetate in $CDCl_3$, which the authors attribute to size and shape complementarity between the $H_2PO_4^-$ anion and the binding pocket formed by the two triazolium functionalised arms of the receptor.[62]

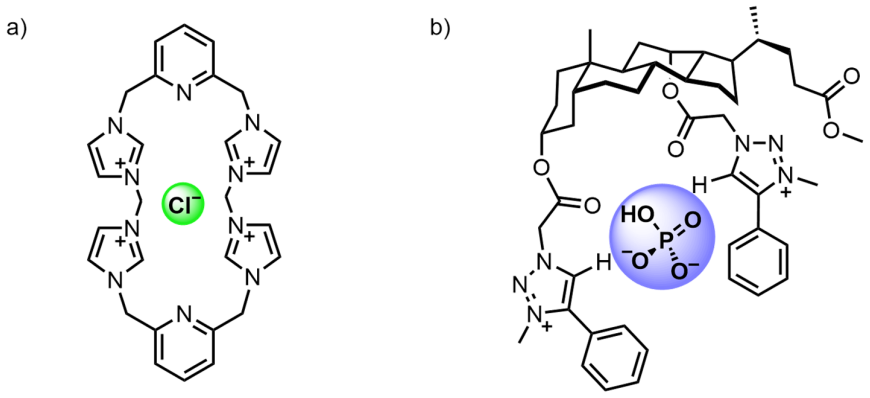


Figure 1.8. *Receptors containing C-H HB donor motifs, including (a) imidazolium; (b) triazolium.*

1.2.3.2.2 Neutral Hydrogen Bonding Anion Binding Motifs

Although the incorporation of positively charged motifs into anion receptors can provide an advantage in terms of enhanced binding strength and increased aqueous solubility, this often comes at the cost of selectivity or functionality. For instance, cationic receptors are more likely to be toxic, which limits their use in biological applications.[63] In addition, even weakly coordinating counter-anions may compete with the target guest for binding to the receptor in aqueous solvent systems. The development of neutral anion binding motifs and their integration into pre-organised macrocyclic or cage host architectures has therefore garnered increasing attention as a strategy to achieve potent and selective anion recognition in both organic and aqueous solvent media.

As a versatile and synthetically accessible N-H hydrogen bond donor, the amide motif has been widely exploited in a range of anion receptors. In a seminal study, Crabtree reported an acyclic isophthalamide-based receptor which, despite its deceptively simple structure, displayed notable halide binding (K_a = 6.1 × 10^4 M^{-1} (Cl^-), 7.1 × 10^3 M^{-1} (Br^-), and 4.6 × 10^2 M^{-1} (I^-)) in CD_2Cl_2 solution.[64] X-ray crystallographic studies indicates that the receptor adopts a *syn-syn* conformation upon halide binding, allowing it to act as a bidentate chelating HB donor motif (**Figure 1.9a**).

The binding affinities and selectivities of amide-based anion receptors can be further augmented by incorporation of amide functionalities into macrocyclic host architectures. This is exemplified in a series of cyclopeptide-derived anion receptors reported by Kubik and co-workers.[65] The group synthesised a cyclic hexapeptide comprising alternating L-proline and 6-aminopicolinic acid subunits (**Figure 1.9b**), which formed 2:1 stoichiometric host-guest sandwich complexes with various anions in the competitive 80% D_2O/CD_3OD (v/v) solvent mixture.[66] The receptor displayed a binding preference for iodide and sulfate (overall stability constants, log K_a = 5.21 (I^-) and 5.09 (SO_4^{2-})), presumably due to size complementarity between the large anions and the macrocyclic cavity.[67] Covalently linking two such cyclopeptides to form a "molecular oyster" enabled anion binding in pure water (**Figure 1.9c**), with iodide and sulfate again exhibiting strongest binding to the receptor (log K_a = 3.62 (I^-) and 3.31 (SO_4^{2-})).[68]

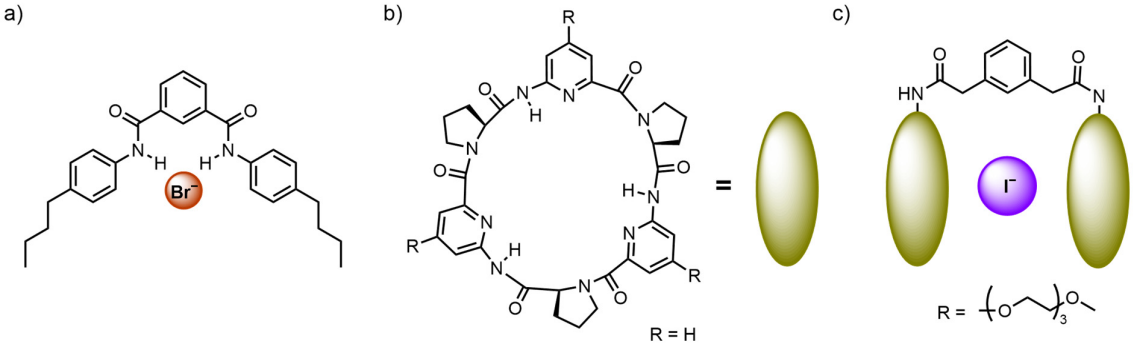


Figure 1.9. *Amide-based HB receptors: (a) Crabtree's isophthalamide receptor; (b)-(c) Kubik's cyclic hexapeptide and "molecular oyster".*

Urea and thiourea moieties are useful bidentate HB motifs capable of forming stable complexes with oxoanions and carboxylate anions, reflecting the complementary Y-shaped geometry of the HB donor and acceptor motifs.[69] Hossain and co-workers have, over the years, synthesised an extensive library of di-, tri- and hexa-functionalised urea- and thiourea-based receptors and systematically investigated the effects of geometry, linker type and substituent

groups on the anion binding properties of the receptors.[70] As anticipated, the tripodal receptors showed greater anion affinity than the dipodal analogues, attributed to a combination of having more HB donors available as well as a better defined binding cavity. In particular, the thiourea-based tripodal receptor functionalised with electron-withdrawing *o*-nitrobenzene chromophores (**Figure 1.10a**) displayed impressive binding affinities for sulfate (log K_a = 6.4) and fluoride (log K_a = 5.1) in DMSO solution. This was exploited for selective naked-eye colorimetric sensing of sulfate via a displacement assay, in which displacement of the bound fluoride from the receptor by sulfate resulted in a colour change from deep red to pale yellow.[71]

The strategy of integrating HB donor motifs into macrocyclic hosts was once again used to great effect by Gale and co-workers, who synthesised a fluorinated tetraurea macrocycle capable of binding chloride in competitive aqueous-containing solvent mixtures (**Figure 1.10b**). Although initially designed to bind the anionic guest within the macrocyclic cavity, the macrocycles were instead found to aggregate in aqueous-containing solvents, forming sandwich-like complexes containing a solvent-excluded binding site suitable for chloride binding between the faces of the stacked macrocycles. This gave rise to unprecedented chloride association constants of 10^5-10^6 M^{-1} in 60% water/acetonitrile (v/v).[72]

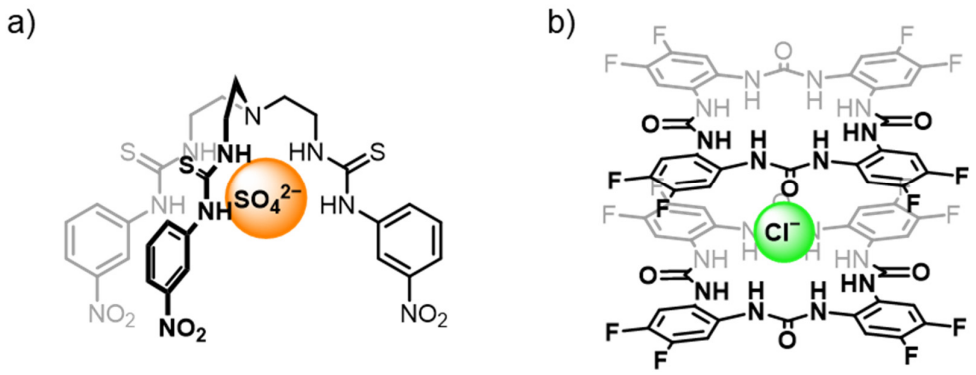


Figure 1.10. *Urea and thiourea-based HB receptors: (a) Hossain's tripod; (b) Gale's macrocycle.*

Squaramides are a family of conformationally rigid cyclobutene ring derivatives which, like ureas and thioureas, possess the capability to function as a bidentate HB donor motif.[73-74] The use of squaramides in anion recognition was first demonstrated by Costa and co-workers, who prepared a tripodal tris(squaramide)-functionalised receptor based on a 1,3,5-substituted benzene scaffold (**Figure 1.11a**). The receptor was found to bind tricarboxylate anions possessing complementary pseudo-C_3 symmetry in 10% D_2O/DMSO-d_6 (v/v), with ^{1}H NMR titration studies determining anion association constants of $K_a = 3.9 \times 10^3$ M^{-1} for trimesic acid and 7.7×10^3 M^{-1} for *cis*-cyclohexenetricarboxylate.[75]

The incorporation of squaramide motifs into macrocyclic receptors was undertaken by Jolliffe and co-workers (**Figure 1.11b**). In particular, a water-soluble tris(squaramide)-functionalised macrocycle displayed remarkable binding affinity for sulfate, as well as impressive selectivity over other tetrahedral divalent anions such as selenate, dihydrogen phosphate and chromate, in aqueous solvent mixtures of up to 50% D_2O/DMSO-d_6 (v/v).[76]

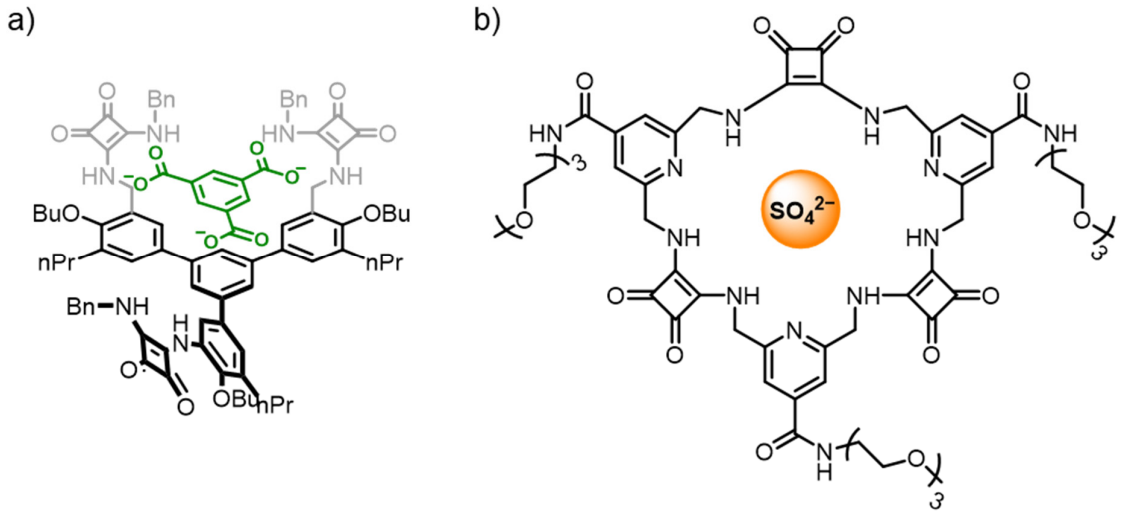


Figure 1.11. *Squaramide-based HB receptors: (a) Costa's initial tripodal receptor; (b) Jolliffe's water-soluble macrocycle.*

Pyrrole hydrogen bond donor groups have also found utility in anion recognition, in particular the macrocyclic calix[4]pyrrole moiety which was first employed as an anion

receptor by Sessler in 1996 (**Figure 1.12a**). In this seminal study, the authors demonstrated via X-ray crystallography the tendency of calix[4]pyrroles to adopt a cone-like conformation in the presence of a halide anion, facilitating convergent binding of the halide via four N-H···X^- interactions.[77]

A drawback of the calix[4]pyrrole motif is its small cavity size, which renders it unable to encapsulate even the small fluoride anion, as evidenced by X-ray crystallographic studies that show the fluoride guest perching on the rim of the cone-like calix[4]pyrrole. As such, considerable research effort has been directed towards modifying the parent calix[4]pyrrole to tune its anion binding properties.[78] One promising approach is the introduction of straps on one face of the calix[4]pyrrole, enabling the incorporation of additional binding motifs as well as anion encapsulation in the binding pocket formed between the calix[4]pyrrole and the strap. Lee and co-workers synthesised a series of strapped calix[4]pyrroles which displayed enhanced chloride binding relative to the parent calix[4]pyrrole (**Figure 1.12b**). In particular, the receptor bearing a pyrrole moiety in the strap showed remarkable affinity for chloride (K_a = 1.8 × 10^7 M^{-1} in acetonitrile), attributed to the formation of multiple N-H···Cl^- and C-H···Cl^- interactions from the donor groups in the calix[4]pyrrole and the strap.[79] Further enhancements in anion binding affinity were achieved by introducing a bipyrrole-containing strap, resulting in receptors that displayed a particularly high affinity for sulfate over other anions (**Figure 1.12c**). This prompted their use in the extraction and solubilisation of sulfate in organic solvents, as demonstrated in a series of solid-liquid and liquid-liquid extraction studies which indicated selective sulfate over chloride extraction by the strapped calix[4]pyrroles.[80]

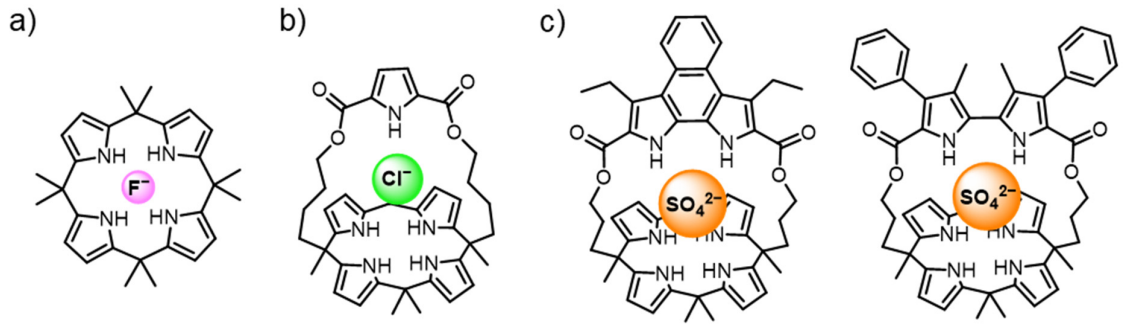


Figure 1.12. *Calix[4]pyrrole-based HB receptors: (a) Parent calix[4]pyrrole. (b)-(d) Sessler's bicyclic strapped calix[4]pyrroles.*

Neutral anion receptors utilising C-H hydrogen bond donors as the primary binding motif are relatively rare, largely due to the perceived weaker strength of C-H hydrogen bonds relegating them to secondary contacts. However, recent work has begun to challenge this conventional wisdom by demonstrating the remarkable anion binding potential of rigid macrocyclic or cage hosts containing pre-organised cavities decorated with multiple C-H donor groups.

The utility of C-H hydrogen bonding interactions in anion binding was elegantly demonstrated by Flood and co-workers, who reported a cryptand-like cage functionalised with six triazole motifs which have their polarised C-H hydrogen bond donors directed towards the interior of the cage (**Figure 1.13a**). An X-ray crystal structure of the receptor bound to Cl^- showed the halide guest residing in the cavity of the cage, stabilised by six C-H hydrogen bonds originating from the triazole moieties. This resulted in unprecedented chloride affinity ($K_a \approx 10^{17}$ M^{-1} in CD_2Cl_2 and 10^8 M^{-1} in DMSO-d_6), alongside impressive selectivity over larger halide anions, attributed to small size and rigidity of the cage precluding the larger halides from accessing the binding cavity. The high chloride affinity of the receptor was exploited to extract alkali metal salts from water into dichloromethane solution – an impressive feat considering the high solvation enthalpies of these salts.[81]

In another exemplary demonstration of using CH hydrogen bonds for potent anion recognition, Flood and co-workers synthesised a C_5-symmetric cyanostilbene macrocycle, dubbed "cyanostar", on a gram scale via a one-pot macrocyclization procedure, which yielded the target macrocycle in 81% yield (**Figure 1.13b**). The presence of electron-withdrawing cyano groups activates the CH hydrogen bond donors, which, alongside its bowl-like conformation, facilitated the strong binding of large and traditionally weakly-coordinating anions such as BF_4^-, ClO_4^- and PF_6^- in 40% CD_3OD/CD_2Cl_2 (v/v) through the formation of 2:1 stoichiometric host-guest sandwich complexes.[82]

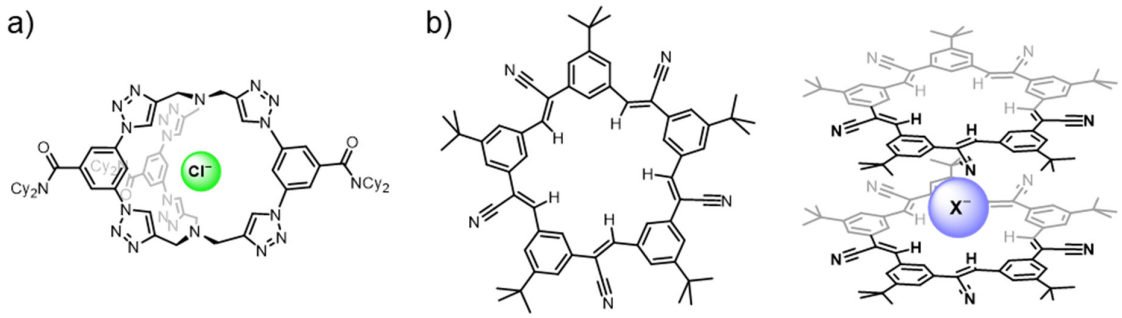


Figure 1.13. *Neutral C-H donor HB receptors: (a) Flood's cage; (b) Cyanostar macrocycle.*

1.2.3.3 Sigma-hole Interactions in Anion Recognition

When an atom of group 14-17 is covalently bonded to an electron-withdrawing group, polarisation of the covalent bond results in an anisotropic distribution of electron density on the surface of the atom, creating one or more electron-deficient regions known as sigma-holes (**Figure 1.14**). These sigma-holes are able to participate in attractive non-covalent interactions with Lewis basic acceptors (A), giving rise to a series of sigma-hole interactions named after the group the donor atom belongs to, with elements from groups 17, 16, 15 and 14 forming halogen bonding (XB), chalcogen bonding (ChB), pnictogen bonding (PnB) and tetrel bonding (TrB) interactions respectively.[83-84]

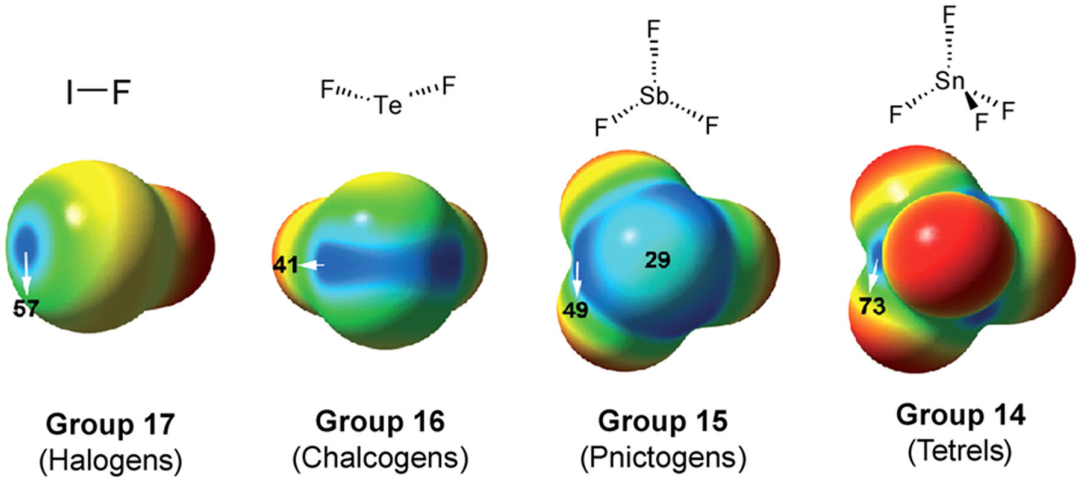


Figure 1.14. *Computed molecular electrostatic potential (MEP) surfaces of group 14-17 elements bonded to fluoride. MEP values of the σ-holes (blue) are indicated in kJ mol^{-1}. Adapted with permission from Bauzá and Frontera.*[84]

There has been considerable debate in early literature reports surrounding the nature of sigma-hole interactions. The electrostatic attraction between the partially positive sigma-hole of the donor atom and the lone electron pair of the acceptor is readily accepted as a major contributor to the formation of sigma-hole interactions. However, the role played by dispersion and charge transfer interactions has been increasingly highlighted in a number of recently published studies. Using K-edge X-ray absorption spectroscopy, Beer and co-workers showed that the halogen bonding interactions with halide anions contains a substantial charge-transfer component, revealing a degree of covalency that is on par with transition metal coordination complexes.[85] A theoretical study into halogen bonding by Arunan and co-workers suggested that the observed lengthening of the covalent bond containing the halogen donor atom upon the formation of XB interactions is consistent with donation of electron density from the Lewis basic acceptor into the σ* orbital of the halogen donor.[86] These and other studies have led to the general consensus that sigma-hole interactions can be described by a combination of electrostatic and covalent contributions.

The number of sigma holes that can be formed on a donor atom is related to the atom's valency. In general, a monovalent halogen atom can only possess one sigma hole, which is formed directly opposite the covalent bond. In contrast, chalcogens, pnictogens and tetrels can contain up to two, three and four sigma holes respectively (**Figure 1.14**). This leads to different geometries available to the different classes of sigma hole interactions; for instance, crystal structures of XB complexes typically contain highly linear halogen bonds, with R-X···A bond angles of >170°, whereas the analogous bond angles in ChB interactions are centred around 80° and 170°.[87] Regardless of the geometry adopted, a key feature shared by sigma-hole interactions is their stringent directionality, evidenced in the more restricted distribution of bond angles relative to hydrogen bonded complexes.[88] The increasing multivalency of the donor atoms going from the halogens to tetrels also leads to decreasing steric accessibility of the sigma-holes, as seen from the calculated molecular electrostatic potential surface of tetrel bonding SnF_4, in which the sigma-holes are obstructed by the four covalently-bonded fluorine atoms (**Figure 1.14**).

The strength of sigma-hole interactions depends on a number of factors, including the polarisability of the donor atom and the electron-withdrawing ability of the covalently bonded group (R). Heavier donor atoms tend to be more polarisable and less electronegative, giving rise to sigma-holes with greater positive potential. Therefore, the majority of XB-based anion receptors utilise iodine donor atoms, which affords anion binding energies comparable to traditional HB donor motifs. On the other hand, the heavier tetrel and pnictogen atoms exhibit increasing metallic character and tendency to participate in traditional coordination chemistry, making them less desirable as donor atoms in anion recognition motifs.[89]

Increasing the electron-withdrawing ability of the group bonded to the donor atom has proven to be an effective method of increasing the potency of the sigma-hole interaction. For

this reason, many sigma-hole anion receptors contain cationic moieties, such as triazolium and pyridinium, covalently attached to the donor group. The use of neutral electron-withdrawing perfluoroarene and nitro-substituted groups has also been shown to strengthen sigma-hole interactions.[90]

Of the sigma-hole interactions, halogen bonding is by far the most widely used in anion recognition, owing to its considerable interaction energy, steric accessibility of the sigma hole and the ease of incorporating XB motifs such as halo-triazoles into receptor scaffolds.[91-93] Other advantages of XB interactions include its stringent linear directionality, pH-independence, and the intrinsic hydrophobicity of XB donor atoms, which assists in desolvation of anions. As such, XB interactions have become a valuable addition to the toolkit of non-covalent interactions used to construct supramolecular anion receptors. Recently, several prominent studies have also begun to explore the potential of chalcogen bonding anion binding motifs, which will be discussed in the following sections.

1.2.3.3.1 Halogen Bonding Anion Receptors

A range of polarised XB donor motifs have been incorporated into anion receptors, of which haloperfluoroaerenes, halotriazoles, halotriazoliums and haloimidazoliums are the most common (**Figure 1.15**).[94]

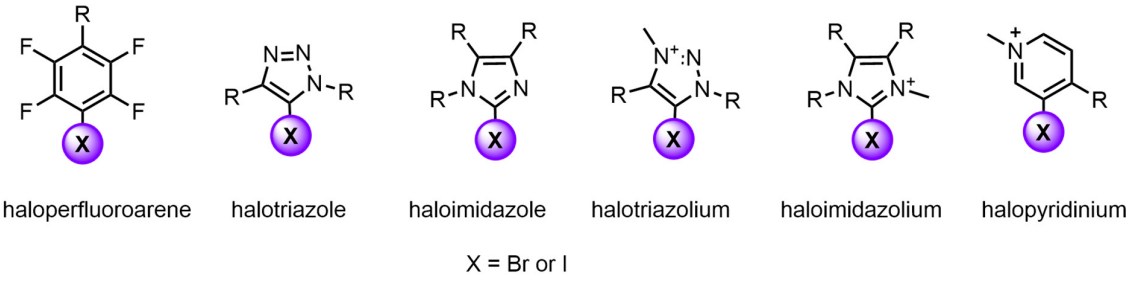


Figure 1.15. *Common halogen bonding donor motifs used in anion recognition.*

Due to the electron-withdrawing ability of fluorine atoms, iodoperfluoroarenes are capable of forming strong XB interactions with anions and feature heavily in early reports of XB anion receptors. The first example of integrating halogen bond donor motifs into an anion receptor was reported in 2005 by Resnati and co-workers, who synthesised a tripodal heteroditopic receptor comprising a tris(polyoxyethylene)amine cation recognition site and 4-iodotetetrafluorophenyl anion recognition sites (**Figure 1.16a**). ^{1}H NMR competition studies conducted in 60:35:5 $CDCl_3/CD_3OD/D_2O$ (v/v/v) showed the XB receptor was able to bind an NaI ion-pair with significantly higher affinity than the non-XB pentafluorophenyl analogue ($K_a^{XB} = 2.6 \times 10^5\ M^{-1}$; $K_a^{HB} = 1.3 \times 10^4\ M^{-1}$). However, single crystal X-ray analysis suggested that only one iodine donor in the receptor participates in XB interactions with the iodide guest due to the divergent arrangement of the donor motifs.[95] Therefore, there is scope to further enhance the anion binding affinity of the receptor by judicious arrangement of the XB donor motifs to enable convergent XB interactions with the target anion.

This was accomplished by Taylor and co-workers, who synthesised a tripodal XB anion receptor capable of multidentate halogen bonding through the cooperative action of ortho-substituted iodoperfluoroarene donor groups (**Figure 1.16b**). As anticipated, the tris(2-iodotetrafluorophenyl)-functionalised receptor showed a marked enhancement in halide binding affinity over monodentate and bidentate analogues. ^{19}F NMR binding studies conducted in acetone-d_6 indicated a preference for halides over oxoanions. The strongest binding was observed in the case of chloride ($K_a = 1.9 \times 10^4\ M^{-1}$), whereas the receptor exhibited no measurable affinities towards TsO^-, HSO_4^- and NO_3^-. The apparent preference of the XB receptor for the softer halide anions was attributed to significant charge-transfer and dispersion contributions to the XB···anion interaction.[96]

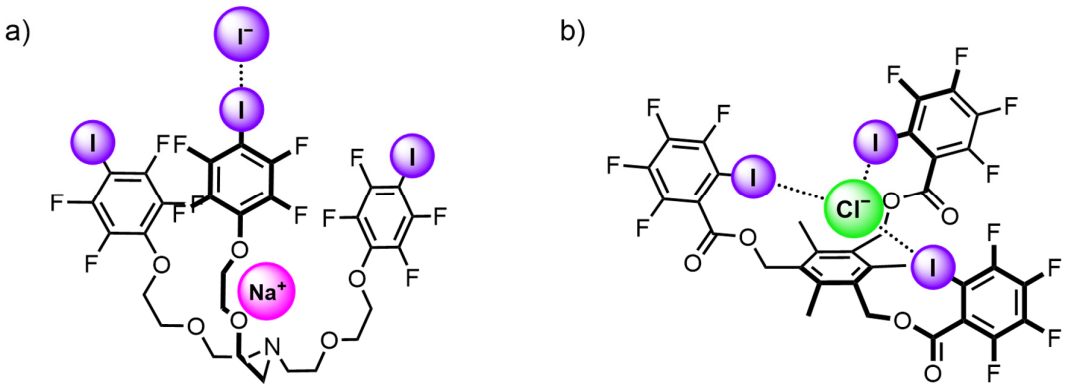


Figure 1.16. *Early XB anion receptors reported by (a) Resnati; (b) Taylor.*

In recent years, the 5-iodo-1,2,3-triazole moiety has risen in popularity as a polarised XB donor group due to the ease with which it can be integrated into receptor frameworks via copper(I)-catalysed azide-alkyne cycloaddition (CuAAC) "click" reactions. An extensive family of acyclic and macrocyclic anion receptors featuring the iodotriazole group or its cationic iodotriazolium derivative have been reported, with prominent examples discussed below showcasing the diverse range of receptor architectures into which this XB donor group has been incorporated.

Schubert and co-workers designed a cleft-like bis(iodotriazole)-functionalised anion receptor that exploits the dual ability of the iodotriazole motif to act as an XB donor through the iodine atom and a HB acceptor through the nitrogen atoms (**Figure 1.17**). The introduction of hydroxy groups at the 2,7-positions of the carbazole spacer, which form intramolecular HB interactions with the triazole nitrogen atoms, served to restrict the rotational freedom of the iodotriazole donor groups, forcing the receptor to adopt a syn/syn conformation optimal for bidentate anion binding. Single crystal X-ray analysis and NMR studies indicated that the pre-organised receptor formed 2:1 stoichiometric host-guest complexes with halide anions, with the two receptors oriented in an orthogonal conformation. Isothermal calorimetry (ITC) titrations conducted in THF further indicated a favourable entropic contribution to binding for

the pre-organised receptor relative to the more conformationally flexible receptor, which is reflected in the higher 1:1 anion binding constants exhibited by the former (K_1^{unorg} = 2.34 × 10^3 M^{-1} and K_1^{preorg} = 7.09 × 10^4 M^{-1}).[97]

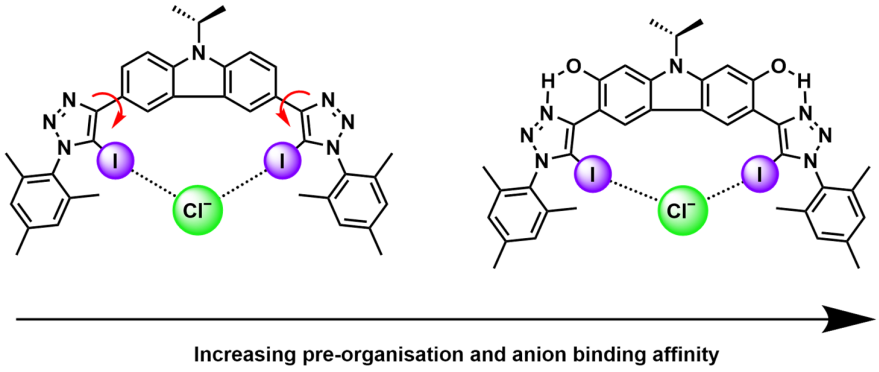


Figure 1.17. *Schubert's cleft-like XB receptors, demonstrating the use of hydroxy substituents to increase receptor pre-organisation.*

Iodotriazole donor motifs were integrated into foldamer structural frameworks by the Beer group to afford a series of XB foldamers for anion recognition (**Figure 1.18**). Notably, the XB foldamers show improved anion binding affinities and an increased preference for halide guests relative to HB analogues in $CDCl_3$. Crystallographic studies confirm that the XB foldamer encapsulates an iodide guest via four convergent halogen bonding interactions, with an Na^+ counterion coordinated to a peripheral tri(ethylene glycol) (TEG) chain (**Figure 1.18a**). Chiral BINOL groups were also incorporated into the foldamer structure to enable chiral discrimination capabilities (**Figure 1.18b**).[98] A neutral tetradentate XB foldamer functionalised with multiple hydrophilic TEG chains was subsequently synthesised (**Figure 1.18c-d**), which exhibits exceptionally strong and selective binding of iodide anions in pure water. This was accomplished by exploiting the intrinsic hydrophobicity of the iodine donor atoms to engender a hydrophobic collapse of the receptor in water, forming a dehydrated binding cavity for anion binding. The combination of multidentate XB···I^- interactions and the shielded microenvironment resulted in record-breaking iodide binding affinities, with 2:1 stoichiometric

host-guest cumulative association constants (β_2) of up to 1.68×10^{11} M^{-2}, the highest out of all known neutral and cationic sigma-hole anion receptors reported to date.[99]

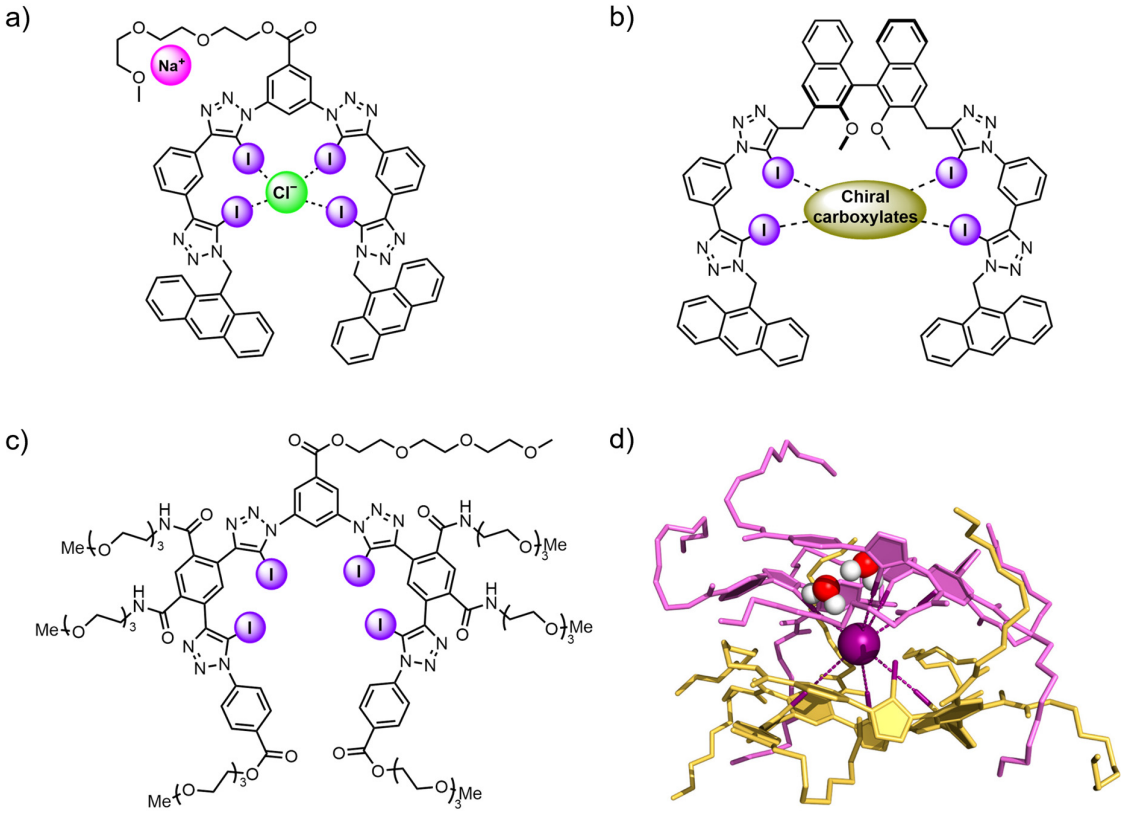


Figure 1.18. *Beer's XB foldamers for: a) Fluorescence sensing of halides; b) Chiral discrimination of carboxylates; c) Anion binding in water. d) MD snapshot of a self-assembled 2:1 sandwich complex between the water-soluble XB foldamer and an iodide guest. Reproduced from Borissov et. al.*[99]

Macrocyclic XB receptors based on iodotriazole donor motifs have also been explored. Building on their extensive investigations into the use of cyclic peptides for anion recognition, Kubik and co-workers synthesised a macrocyclic pseudopeptide containing three iodotriazole moieties (**Figure 1.19a**), which preferentially bound chloride over bromide and iodide in 2.5% D_2O/DMSO-d_6 (v/v).[100] Sessler and co-workers prepared a box-like macrocycle comprising four iodotriazole donors (**Figure 1.19b**), which formed 1:2 host-guest complexes with halides in $CDCl_3$. Interestingly, Sessler's macrocycle exhibited the reverse selectivity trend to Kubik's cyclopeptide, with a modest preference for iodide binding over the lighter halides. This was

attributed to a reduction in the electrostatic repulsion between the two guest anions in the case of the larger, charge-diffuse iodide.[101]

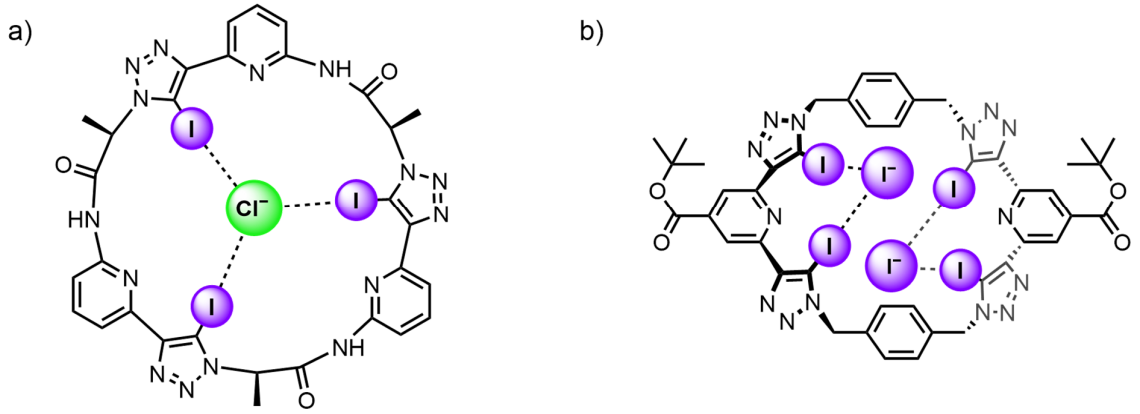


Figure 1.19. *Macrocyclic iodotriazole-based XB receptors: (a) Kubik's pseudo-cyclopeptide; (b) Sessler's cyclophane-like box.*

As is the case with HB receptors, incorporating positive charges into the framework of XB receptors is a common strategy to augment the anion binding affinities of the receptors in polar solvents. One method to achieve this is through methylation of the triazole group to form an iodotriazolium group. This approach was used by Zapata and co-workers, who synthesised a dicationic XB receptor wherein a naphthalene spacer group is functionalised with bis(iodotriazolium) binding motifs alongside terminal pyrene groups for fluorescent anion sensing (**Figure 1.20a**). The receptor showed relatively strong binding to $HP_2O_7^{3-}$ (K_a = 9.84 × 10^3 M^{-1} in 90% CD_3CN/CD_3OD (v/v)), which notably represents a 5.5-fold enhancement in affinity over the non-halogenated triazolium analogue.[102]

Cationic groups can also be incorporated adjacent to the iodotriazole motif, most commonly via the use of a pyridinium spacer group. The pyridinium-3,5-bis(iodotriazole) donor motif was introduced by Robinson[85] and subsequently utilised to great effect by Mitchell and co-workers to prepare a series of XB receptors for hydrosulfide sensing (**Figure 1.20b**). The incorporation of coumarin fluorophores as well as hydrophilic TEG chains enabled the

receptor to function as a fluorescent sensor in pure water. Fluorescence titration experiments in pH 7.4 aqueous HEPES buffer solution demonstrated significant quenching of the receptor's fluorescence in the presence of HS^- but not halide anions, enabling for the first time reversible chemosensing of HS^- in pure water.[103]

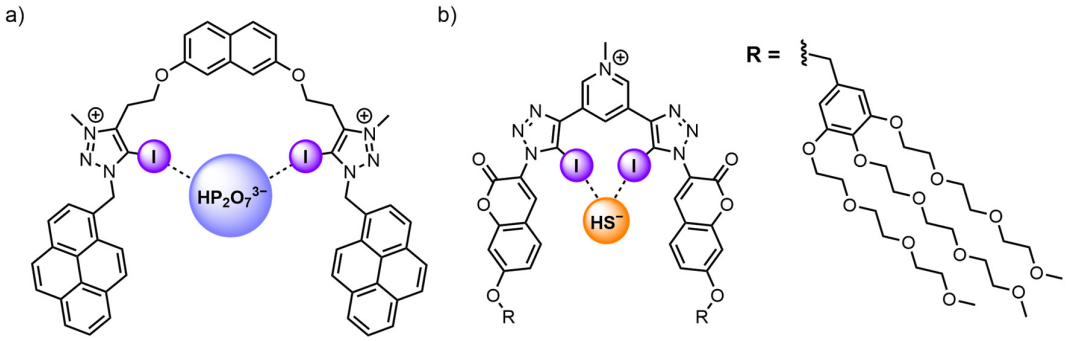


Figure 1.20. *Cationic XB receptors: (a) Zapata's bis(iodotriazolium)-based receptor; (b) Beer's bis(iodotriazole)pyridinium-based receptor.*

1.2.3.3.2 Chalcogen Bonding Anion Receptors

Compared to halogen bonding, the field of anion recognition by chalcogen bonding (ChB) receptors is still in its infancy. The development of ChB receptors has been hampered by the inherent instability of the C-Te bond, which makes them sensitive to moisture and vulnerable to nucleophilic attack and metal-insertion reactions. Nonetheless, several promising ChB donor motifs have recently been reported, which bodes well for the future development of the field.

Taylor and co-workers synthesised a series of benzo-fused chalcogenodiazoles, which are five-membered aromatic heterocycles containing highly deficient chalcogen atoms (**Figure 1.21a**). By varying the substituent group attached to the benzene ring, the anion binding affinities of the resulting receptors could be tuned by several orders of magnitude. In particular, the tetrafluorophenyl variant displayed an impressive chloride binding constant of 1.3×10^5 M^{-1} in dry THF, as determined by UV-vis titrations. However, the receptors were unstable to

aqueous-containing solvent media and basic anions, with decomposition occurring in the presence of F^-, $CH_3CO_2^-$, $H_2PO_4^-$, and HSO_4^-.[104]

Subsequently, the same group reported the use of chalcogenophenes as ChB anion receptors with improved stability. Although chalcogenophenes are intrinsically electron-rich heterocycles, by attaching electron-withdrawing perfluoroaryl substituents, the tellurium donor atom can be made sufficiently electrophilic to interact with anions, albeit with modest binding affinities (K_a (Cl^-) = 310 M^{-1} in THF). Improved anion affinities were obtained through the use of a bidentate ChB receptor, in which the two tellurophene donor motifs are connected by an ethynylene spacer to allow sufficient space for the tellurium donors to cooperatively bind a halide anion (**Figure 1.21b**). This resulted in a dramatic enhancement in anion affinity, giving rise to a chloride association constant of 2290 M^{-1} under the same solvent conditions.[105]

Building on the success of iodotriazole-based XB donors, Beer and co-workers turned to the preparation of analogous 5-telluromethyl-1,2,3-triazoles, which proved to be highly tuneable and surprisingly stable ChB donor motifs. In a seminal study, a series of bidentate 3,5-bis(telluromethyltriazole)pyridine receptors were synthesised and the electron-withdrawing nature of the aryl substituents was systematically varied to modulate the ChB donor potency (**Figure 1.21c**). The attachment of perfluorophenyl (PFP) substituents to the 1-position of the triazole led to marked enhancements in the halide affinities of the ChB receptors, which appear more sensitive to the local electronic environment than analogous XB and HB receptors. Further enhancements in ChB donor potency were afforded by the introduction of electron-withdrawing substituents directly to the Te(II) donor atom, with the most potent analogues displaying $K_a(Cl^-)$ values in excess of 10^5 M^{-1} in acetone-d_6.[106] The stability of telluromethyltriazole groups was further demonstrated by their incorporation into a foldamer

capable of binding iodide anions as a 2:1 stoichiometric host-guest complex with a remarkable β_2 of 2.64×10^7 M^{-2} in pure water.[99]

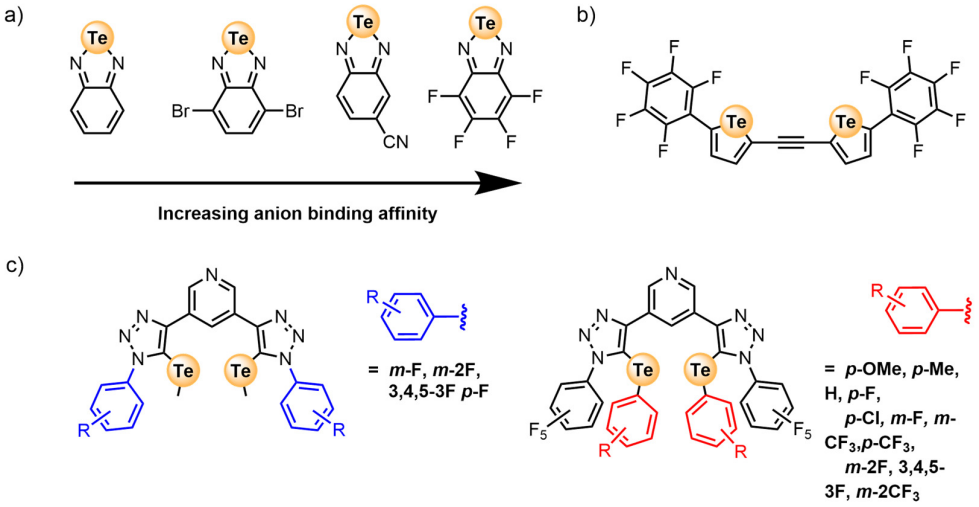


Figure 1.21. *Chalcogen bonding anion receptors based on: (a) Chalcogenodiazoles; (b) Chalcogenophens; (c) Telluromethyl- or telluroaryl triazoles*

1.2.3.4 Anion-π Interactions in Anion Recognition

Anion-π interactions are defined as attractive non-covalent contacts between an electron-deficient aromatic system and an anion.[107] Relative to other non-covalent interactions, anion-π interactions remain an underexplored area, largely because the attractive interaction between an anion and a negatively charged π electron cloud appears counterintuitive at first glance. In fact, the electrostatic contribution to anion-π interactions is correlated with the quadrupole moment (Q_{zz}) of the aromatic ring, which can be positive in highly electron-deficient aromatic systems *e.g.* Q_{zz}(hexafluorobenzene) = +9.50 B, where 1 B = 3.336×10^{-40} C m^2.[108] Anion-induced polarisation also contributes significantly to the formation of anion-π interactions, with highly polarisable aromatic systems such as *s*-tetrazine forming stronger interactions with anions. Although traditionally considered a 'weak' interaction, several theoretical studies suggested that anion-π interactions can exhibit considerable binding energies of up to 20-50 kJ mol^{-1}, comparable to hydrogen bonding.[109-111]

Nonetheless, the use of anion-π interactions as the primary binding motif in anion receptors remains relatively uncommon due to the weak nature of these interactions in solution-phase anion binding. This was demonstrated in a study by Wang and co-workers, who synthesised four tetra-homocorona[4]arenes containing electron-deficient tetrazine units (**Figure 1.22a**). Despite possessing rectangular box-like cavities complementary in size and shape to linear anions such as azide and thiocyanate, the receptors exhibited relatively low binding affinities for these anions, with association constants in the range 23-166 M^{-1} for azide and 3-22 M^{-1} for thiocyanate in acetonitrile. A detectable fluorescence response to azide and thiocyanate binding was observed, with gradual quenching of the tetrazine emission observed when the anions were introduced into acetonitrile solutions of the receptors.[112]

Improved anion recognition properties and sensing capabilities were achieved by increasing the pre-organisation of the host. The same group subsequently designed a C_3-symmetric cage receptor based on benzene triimide (BTI) anion-π donor groups (**Figure 1.22b**). The receptor was found to bind N_3^-, SCN^- and I^-, with a remarkable affinity for N_3^- in particular (K_a = 15372 M^{-1} in acetone). The formation of charge-transfer interactions between the electron-deficient BTI moieties and azide led to a naked-eye colour change of the solution from colourless to bright orange. A co-crystal of the cage with azide showed that the anion is sandwiched between the two BTI planes with intermolecular distances of 2.830-2.873 Å, indicating the presence of strong anion-π interactions.[113]

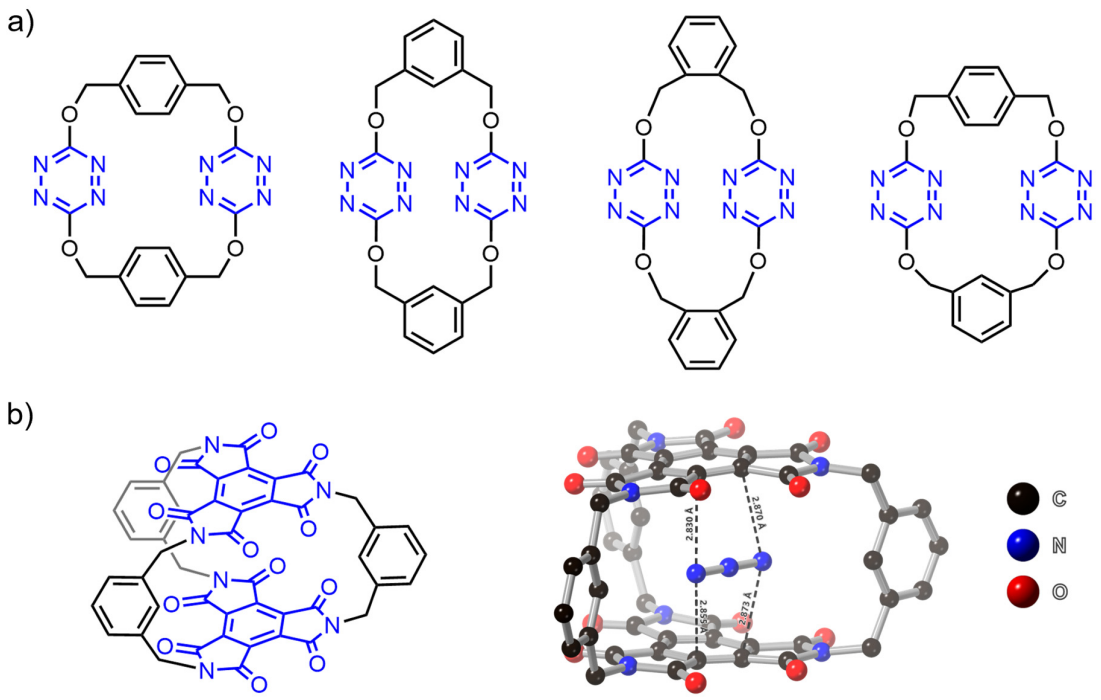


Figure 1.22. *Receptors based on anion-π interactions: (a) Wang's tetrazine-containing macrocycles; (b) BTI-functionalised cage.*

1.3 Ion-Pair Recognition

An inherent disadvantage of monotopic anion receptors is the need to overcome the energetic cost of separating the target anionic guest from its counterion, which may inhibit anion binding to the receptor. Heteroditopic ion-pair receptors containing binding sites for both a cationic and anionic guest offer a potential solution to this issue, and indeed have shown improved binding affinities for ion-pairs or constituent ions relative to monotopic receptor analogues.[114] This is often a result of proximal electrostatic attraction between the oppositely charged guests, though several examples also exist of elegant receptor designs that exploit cooperative allosteric effects, whereby the binding of one charged guest, typically the cation, pre-organises the receptor to bind the counter-ion pair guest species.[115]

1.3.1 Heteroditopic Ion-Pair Receptors

Ion-pair receptors can be broadly classified based on their binding modes into contact ion-pair or separated ion-pair receptors (**Figure 1.23**). Contact ion-pairs are formed when the two bound ions are held in close proximity to each other within the receptor, as determined by X-ray crystallographic studies. In other cases, when the cation and anion binding sites are distal to each other, the co-bound ion-pair may be separated by solvent molecules or the receptor framework.[116] Representative examples of the various types of ion-pair receptors are discussed in the following sections.

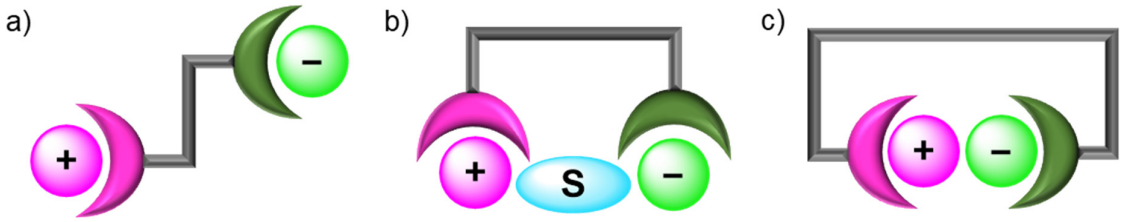


Figure 1.23. *Ion-pair binding modes in heteroditopic receptors: (a) Host-separated; (b) Solvent-separated; (c) Direct contact.*

1.3.1.1 Separated Ion-pair Receptors

Solvent-separated or host-separated ion-pairs typically result when the cation and anion binding sites are spatially separated from each other on the receptor framework. Such receptor design may be prompted by the convenience of a modular synthetic strategy, in which heteroditopicity is achieved by coupling established cation and anion binding motifs. This approach was employed by Sessler and co-workers, who prepared an ion-pair receptor by linking the well-known calix[4]pyrrole anion binding site to a crown-6-calix[4]arene for cation binding (**Figure 1.24a**). The receptor was found to bind a caesium fluoride ion-pair in a solvent-separated binding mode, as shown by X-ray crystallographic analysis. ^{1}H NMR studies suggested that that Cs^{+} binding 'switches on' the F^{-} affinity of the receptor in 10% $CD_3OD/CDCl_3$ (v/v), with no spectral changes elicited by addition of TBAF alone. The

receptor also appears to be highly selective for CsF over other alkali metal halide salts, presumably due to size complementarity of the cation and anion binding cavities for the respective guest ions.[117]

A major appeal of separated ion-pair receptors is the scope to exploit allosteric cooperativity through informed receptor design. One such example, reported by Reinhoudt and co-workers, involves a calix[4]arene-based receptor functionalised with urea groups on the upper rim for anion binding and ethyl ester groups on the lower rim for cation binding (**Figure 1.24b**). The free receptor exists in a pinched cone conformation stabilised by intramolecular hydrogen bonding between the urea moieties, which are not available to bind to a halide guest. However, the authors showed through qualitative ^{1}H NMR studies in $CDCl_3$ that the pre-complexation of a sodium cation by the ester groups converts the receptor into a symmetrical cone conformation in which intramolecular HB interactions are disrupted, thereby switching on the anion binding capabilities of the receptor. The strength of ion-pair binding was evidenced by the receptor's ability to extract sodium halide salts into $CDCl_3$ solution.[118]

Kubo and co-workers reported a heteroditopic receptor based on bis(thiourea)-substituted dibenzo-diaza-30-crown-10 (**Figure 1.24c**), which exploits the highly flexible nature of the dibenzo-30-crown-10 ether macrocycle to elicit positive allosteric cooperativity towards potassium diphenylphosphate ion-pairs. ^{1}H NMR binding studies in CD_3CN suggested that the K^+ cation was bound in a concave cavity formed by the crown ether. Pre-complexation of K^+ to the receptor resulted in a 19-fold enhancement in the apparent diphenylphosphate association constant, which was attributed to the increased Lewis acidity of the thiourea protons as well as the K^+-assisted stabilisation of a folded receptor conformation that pre-organises the thiourea donors for convergent anion complexation.[119]

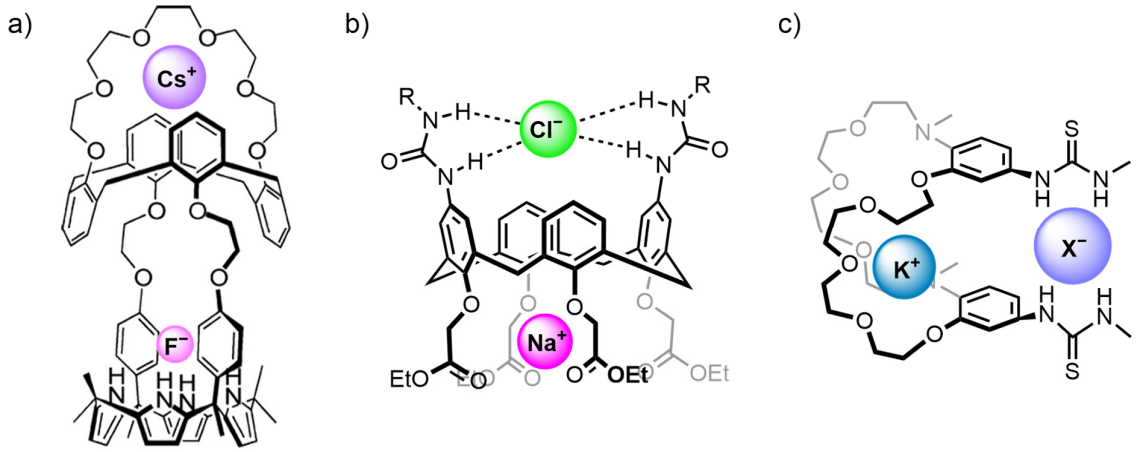


Figure 1.24. *Examples of host- or solvent-separated ion-pair binding: (a) Sessler's solvent-separated strapped calix[4]pyrrole receptor; (b) Reinhoudt's urea-functionalised calix[4]arene receptor; Kubo's thiourea-functionalised DBC10 receptor.*

In another elegant demonstration of utilising allosteric cooperativity in receptor design, Beer and co-workers have reported a series of KX-selective ion-pair receptors that exploit the tendency of benzo-15-crown-5 ether (B15C5) to form 2:1 sandwich complexes with potassium ions.[120] One example features a subsequent 1,3-bis(iodotriazole)benzene-based XB ion-pair receptor functionalised with B15C5 groups (**Figure 1.25a**). Pre-complexation of the receptor to K^+ or Rb^+ facilitated the formation of an intramolecular sandwich complex which led to significant enhancements of up to 700-fold in the apparent anion association constants of the receptor, whereas Na^+-complexation resulted in only a 15-fold enhancement arising from electrostatic effects.[121] Recently, the group reported a ChB heteroditopic receptor based on a 3,5-bis-tellurotriazole nitro-benzene scaffold, with B15C5 units directly appended to the tellurium-incorporated triazoles (**Figure 1.25b**). The receptor showed marked selectivity for potassium chloride over other alkali metal chloride salts, with crystallographic studies confirming the formation of an intramolecular co-facial bis-B15C5 K^+ sandwich complex. The receptor was shown to solubilise KCl in $CDCl_3$ through a series of solid-liquid and liquid-liquid

extraction studies, and preliminary U-tube membrane transport experiments further indicated its capability to selectively transport KCl across a membrane.[122]

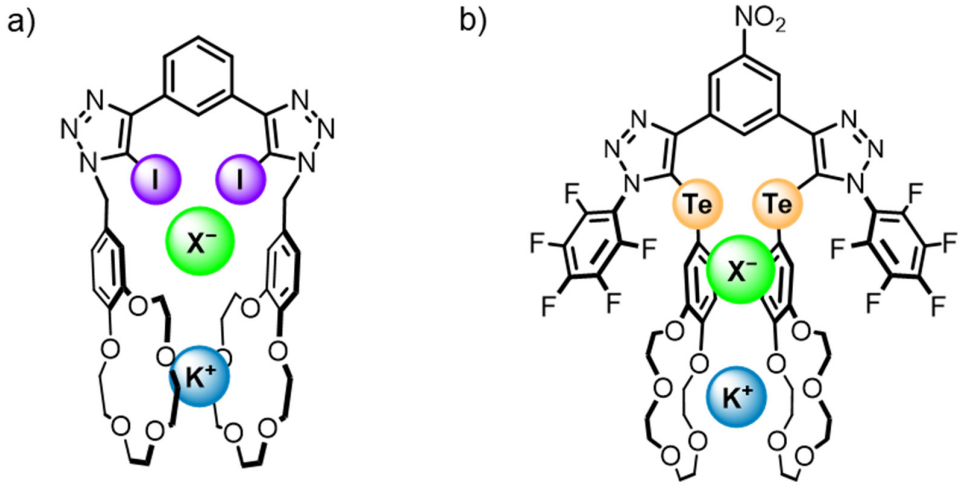


Figure 1.25. *Beer's host-separated ion-pair receptors showing allosteric cooperativity, utilising (a) XB and (b) ChB interactions.*

1.3.1.2 Contact Ion-pair Receptors

Contact ion-pair receptors reduce the Coulombic penalty associated with separating the two ions by allowing them to remain in contact within the receptor framework. This can, in some cases, lead to dramatically enhanced ion-pair binding affinities.[123]

A popular receptor scaffold used in ion-pair binding is a macrobicyclic crown ether strapped by a 1,3-phenyldicarboxamide anion binding motif, first introduced by Smith and co-workers in 2000 (**Figure 1.26a**). The receptor proved to be capable of binding a range of salts, with a particular preference for sodium and potassium halide ion pairs. Importantly, a crystal structure of the receptor bound to NaCl revealed a solvent-separated ion-pair binding mode wherein a chloroform molecule bridges the two guests.[124] This prompted the authors to synthesise a second-generation receptor with a smaller distance between the anion and cation binding sites to promote direct contact between the bound ion-pairs (**Figure 1.26a**), which was confirmed by crystallographic studies of the NaCl- and KCl-bound receptors. Unfortunately,

as the ion-pair binding properties of the two receptors were studied in different solvent systems (3:1 DMSO-d_6/CD_3CN vs. pure DMSO-d_6 for the first- and second-generation receptors respectively), a direct comparison of their binding affinities was not possible. However, it is interesting to note that, relative to the solvent-separated ion-pair receptor, the contact ion-pair receptor showed a markedly greater selectivity for KCl over NaCl in DMSO-d_6, which was attributed to a better fit between the receptor cavity and the larger KCl ion-pair.[125]

Extending the approach of enforcing contact ion-pair binding by confining the guests within a bicyclic macrocycle cavity, Beer and co-workers designed a heteroditopic calix[4]diquinone receptor with an isophthalamide strap (**Figure 1.26c**). The resulting receptor exhibited no discernible binding affinity for either alkali metal cations or halide anions alone in CD_3CN, but showed dramatically enhanced halide binding affinities (apparent $K_a > 10^4\ M^{-1}$) in the presence of 1 equivalent of the metal cation. Likewise, the binding affinities of the receptor for Na^+ and NH_4^+ were only switched on in the presence of 1 equivalent of TBACl. The authors likened this behaviour to that of a Boolean AND gate, hinting at the potential of heteroditopic receptors to function as molecular logic gates.[126]

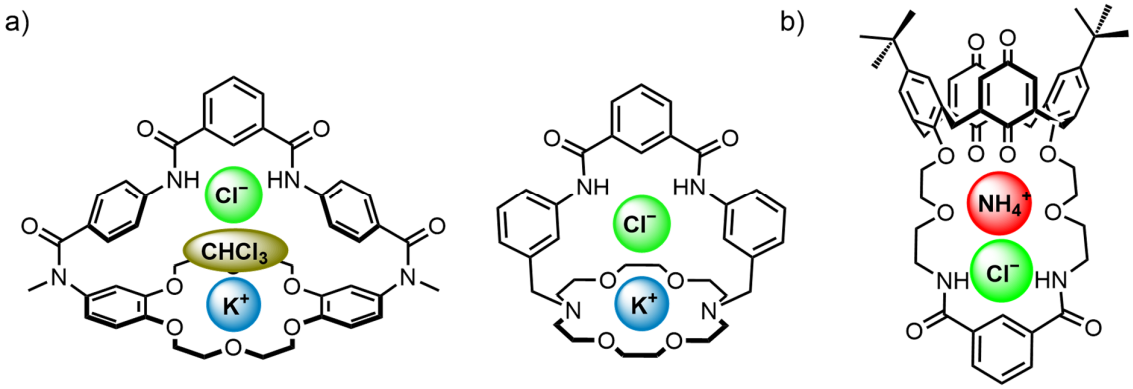


Figure 1.26. *Examples of direct contact ion-pair binding: (a) Smith's bicyclic isophthalamide macrocycles; (b) Beer's strapped calix[4]diquinone receptor.*

1.3.2 Applications of Ion-Pair Receptors

The high binding affinities and modulated selectivity profiles demonstrated by ion-pair receptors have encouraged their use in a range of applications, including ion sensing, salt extraction/solubilisation and transmembrane transport.[127]

1.3.2.1 Ion-pair Sensing

Sensing of ion-pairs rather than isolated ions can provide more accurate qualitative and quantitative data on the concentration of salts in the analysis sample, particularly in biological systems where the nature of the counterion may lead to different physiological effects. Recent years have seen a growing number of supramolecular ion-pair chemosensors, which are typically prepared by appending various chromophores, fluorophores or electroactive signalling groups into receptor frameworks.

Sessler and co-workers functionalised a heteroditopic calix[4]arene-calix[4]pyrrole ion-pair receptor at the β-pyrrolic position with a chromophoric indane substituent (**Figure 1.27a**). The resulting ion-pair sensor mirrored the binding properties of the parent receptor, displaying a strong affinity for caesium ion-pairs such as CsF, CsCl and $CsNO_3$, but not to the constituent ions separately. Extraction of various caesium ion-pairs into a solution of the receptor in nitrobenzene was accompanied by a subtle darkening of the solution from orange to red or brown depending on the anion. Notably, the use of other alkali metal halides led to minimal changes in the UV-vis spectrum of the receptor, highlighting its potential to function as a selective caesium ion-pair colourimetric sensor.[128]

Fluorescent chemosensors for ammonium sulfate ion-pairs was developed by Jabin and co-workers by appending terminal pyrene units to calix[6]arene tris(urea)-based receptors (**Figure 1.27b**). The authors showed that the receptor was capable of cooperative ammonium sulfate recognition in the protic solvent mixture 1:11 $CD_3OD/CDCl_3$ (v/v). Ion-pair binding

resulted in an increase in the fluorescence corresponding to the pyrene monomer emission and a decrease in the excimer emission, which was attributed to the bulky sulfate anion forcing the pendant pyrene-functionalised arms apart and inhibiting excimer formation.[129]

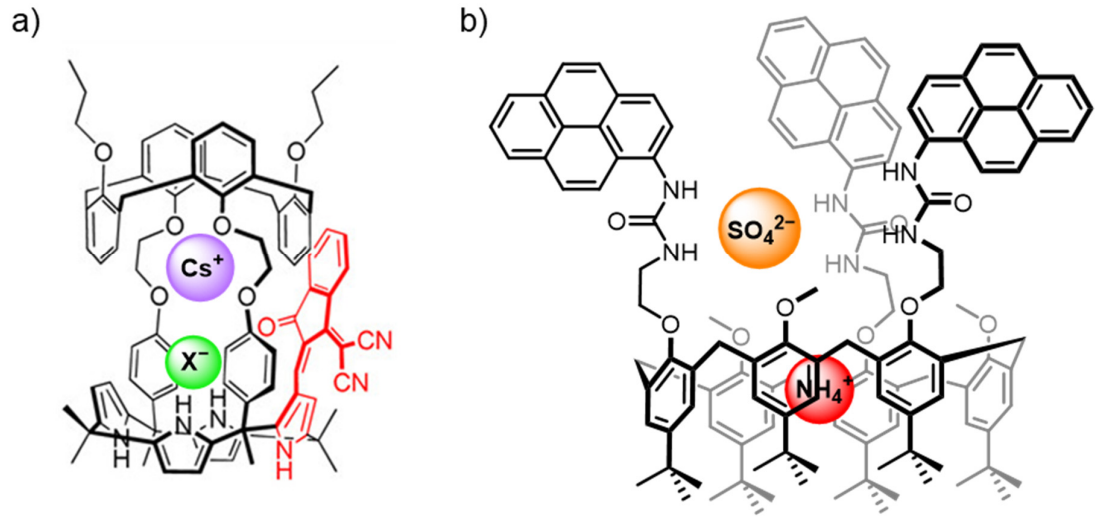


Figure 1.27. *Heteroditopic receptors for ion-pair sensing: (a) Sessler's indane-substituted calix[4]arene-calix[4]pyrrole; (b) Jabin's pyrene-functionalised calix[6]arene tris(urea) receptor.*

1.3.2.2 Extraction and Solubilisation of Salts

Extraction methodologies are widely used in a range of industrial processes for separating mixtures and waste remediation. The development of extractants to control the selectivity and efficiency of these processes is therefore of great commercial relevance. In order to achieve solid-liquid and liquid-liquid extraction of ion-pairs, the binding affinity of the receptor needs to be sufficiently strong to overcome respectively the lattice enthalpy and solvation enthalpy of the target salt. This means that salts comprising smaller and more charge-dense ions are generally more challenging to extract.

A considerable number of ion-pair receptors have been reported to function as salt extracting agents with varying degrees of efficiency and selectivity. Ghosh and co-workers reported a simple crown ether-based pentafluorophenyl urea-functionalised ditopic receptor

which showed selective extraction of solid KBr in the presence of KCl and KNO_3 (**Figure 1.28a**).[130] A similar receptor design was employed by Romanski and co-workers, who prepared an acyclic ion-pair receptor bearing a squaramide anion binding unit and a crown ether cation binding motif (**Figure 1.28b**). The receptor was capable of extracting sodium chloride from aqueous media into nitrobenzene-d_5, an impressive feat considering the high solvation enthalpy of the alkali metal halide salt.[131] A range of receptors based on functionalised calix[n]arenes, calix[4]pyrroles and strapped crown ethers have also demonstrated alkali metal halide salt extractant capabilities.[132-137]

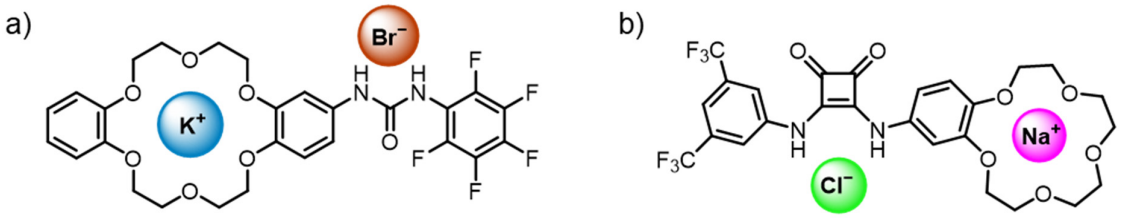


Figure 1.28. *Heteroditopic receptors for salt extraction: (a) Ghosh's urea-functionalised DB18C6 receptor; (b) Romanski's squaramide-functionalised B15C5 receptor.*

1.3.2.3 Membrane Transport

Ion transport through cellular membranes is crucial in maintaining the normal functioning of biological systems, with defective ion transport implicated in a number of diseases. Synthetic ion transporters are therefore of therapeutic relevance, spurring the development of many cation and anion transporters.[138-141] The potential advantages of ion-pair transporters in terms of improving activity and selectivity of ion transport are increasingly being recognised. However, due to the inherent difficulty of designing assays that reliably determine co-transport of ion-pairs across a membrane, only a limited number of ion-pair transporters have been reported to date.

Smith and co-workers described a macrobicyclic ion-pair host capable of transporting both NaCl and KCl across unilamellar 1-palmitoyl-2-oleoylphosphatidylcholine (POPC)

vesicles (**Figure 1.29a**). The authors used a Cl^- selective electrode to show that the receptor was capable of facilitating rapid Cl^- efflux from POPC vesicles. ^{35}Cl and ^{23}Na NMR studies provided further evidence for the co-transport of NaCl across the membrane. Importantly, a 1:1 mixture of the analogous monotopic azacrown ether cation and amide anion receptors failed to induce Cl^- efflux under identical conditions, highlighting the importance of the neutral heteroditopic receptor contact ion-pair complex design in facilitating transmembrane transport.[142] Using a similar experimental set-up, caesium chloride transport across POPC vesicles was subsequently demonstrated by Sessler and co-workers using calix[4]pyrrole-based receptors as ion carriers (**Figure 1.29b**).[143]

More recently, Jeong and co-workers synthesised an acyclic receptor containing a urea anion binding site and an azacrown ether for cation binding (**Figure 1.29c**), which was shown to be capable of transporting Cl^- from the inside of POPC vesicles into an external Na_2SO_4 solution. The authors deduced that this is only possible via a Na^+/Cl^- symport mechanism, meaning that the receptor facilitates co-transport of an NaCl ion-pair, because the high hydrophilicity and low membrane permeability of SO_4^{2-} precludes the more commonly-observed antiport mechanism. Analogous studies using a series of POPC vesicles containing different alkali metal chloride salts suggested that NaCl transport occurs with highest efficiency, presumably due to the size complementarity between the azacrown-5 ether binding site and the sodium ion guest.[144]

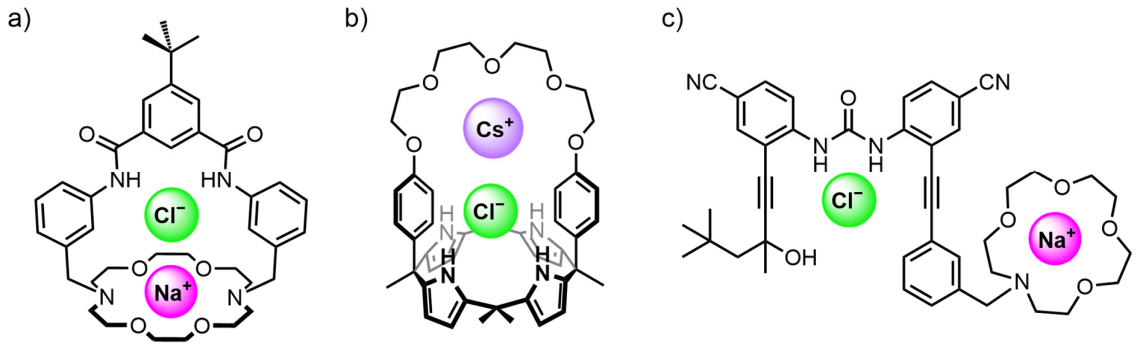


Figure 1.29. *Heteroditopic receptors for ion-pair transport: (a) Smith's bicyclic receptor; (b) Sessler's strapped calix[4]pyrrole; (c) Jeong's urea-functionalised azacrown ether rececptor.*

1.4 Mechanically Interlocked Molecules

Mechanical bonding is a phenomenon in which two or more objects are held together by physical entanglement in space. Mechanically interlocked systems are ubiquitous in our daily lives; we create a mechanical bond each time we do up a button, put on a necklace, or chain a bicycle to a rack. On a molecular level, entanglement gives rise to the class of mechanically interlocked molecules (MIMs), which consists of components that are connected as a result of their entanglement in space rather than via traditional covalent bonds.[145] The fascinating topologies of MIMs, as well as the unusual chemical and physical properties arising from their dynamic interlocked nature, has drawn tremendous research attention over the past two decades, culminating in the 2016 Nobel Prize in Chemistry being awarded to Jean-Pierre Sauvage and Fraser Stoddart for their work on MIM-based molecular machines, together with Ben Feringa's pioneering contributions on non-interlocked rotor molecular machine designed analogues. [146-148]

The two major subsets of MIMs are based on [*n*]catenane and [*n*]rotaxane topologies, where *n* denotes the number of interlocked components. [*n*]Catenanes consists of two or more interlocked macrocycles in which each macrocycle is threaded through the cavity of at least one other in a manner resembling links in a chain. Catenanes are topologically complex

molecules which can be described mathematically by the number of rings and crossing points in a two-dimensional projection of the catenane. The simplest catenane is known as a 'Hopf link' and consists of two rings and two crossing points, but molecules based on more complex [*n*]catenane topologies have also been reported, including Borromean Rings (3 rings and 6 crossings) a Solomon Link (2 rings and 4 crossings) and a "Star of David" (2 rings and 6 crossings) (**Figure 1.30**).[149]

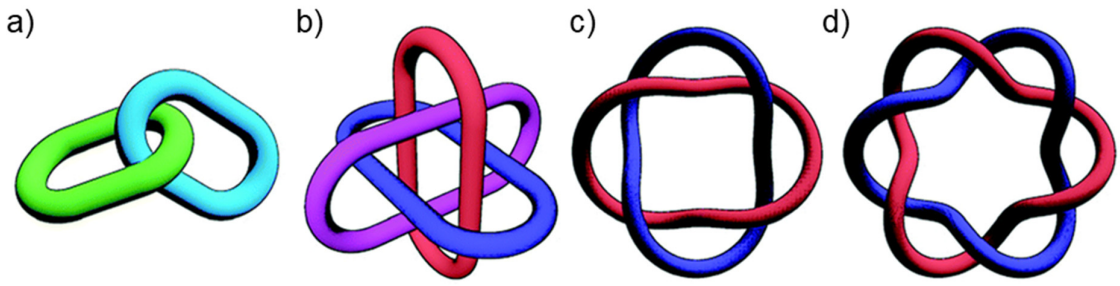


Figure 1.30. *Examples of named catenane topologies: (a) Hopf link; (b) Borromean Rings; (c) Solomon Link; (d) "Star of David". Adapted with permission from Pérez and Lewis.*[150]

In an [*n*]rotaxane, one or more macrocyclic components is threaded by a linear axle component. Unlike catenanes, rotaxanes are considered trivial species from a mathematical perspective because they can in principle be separated by continuous deformation. However, in practice this is prevented by appending bulky stopper groups to the terminals of the axle that sterically prevent de-threading of the macrocycle (**Figure 1.31**).

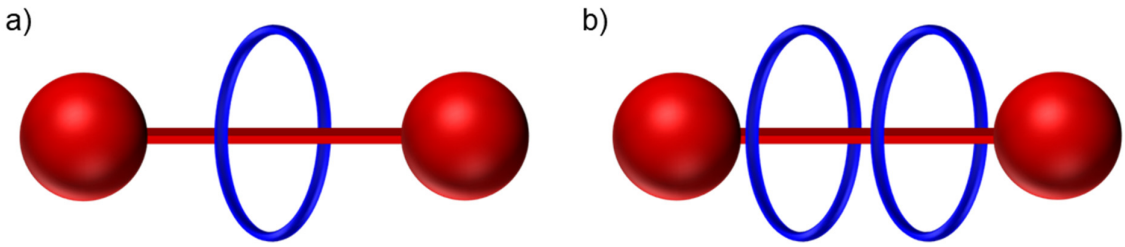


Figure 1.31. *Commonly encountered rotaxane topologies: a) A [2]rotaxane; (b) A [3]rotaxane.*

1.4.1 Template-directed Syntheses of MIMs

A statistical approach for the preparation of [2]catenanes was first proposed by Wasserman in 1960, who used an acyloin condensation reaction to cyclise a diester around a deuterated cyclohexane macrocycle.[151] Although indirect evidence for successful [2]catenane formation was obtained via IR spectroscopic detection of deuterium-labelled components, the prohibitively low yields (0.0001%) of the interlocked product stymied progress in the field of MIMs for many years.

The 1980s saw a revolution in the field of interlocked molecules with the pioneering work of Jean-Pierre Sauvage and Fraser Stoddart on template-directed synthetic approaches to dramatically improve the efficiency of MIM synthesis. Sauvage's seminal study in 1983, which described a Cu(I) template-directed synthesis of a metallo[2]catenane in 27% yield,[16] was followed closely by Stoddart's use of the aromatic donor-acceptor interactions between paraquat (methyl viologen) and hydroquinone moieties to prepare a catenane in 70% yield.[17]

These trailblazing studies paved the way for the development of a variety of template-directed strategies for MIM synthesis, which utilise a range of non-covalent interactions to facilitate the assembly of precursors into a complex that is pre-organised for mechanical bond formation. The following sections briefly highlight prominent examples of cation and anion templates used to direct mechanical bond formation.

1.4.1.1 Cation Template-Directed Approaches

The predictable chelation numbers and binding geometries of transition metal ions, as well as their ability to form a variety of strong and well-defined stereochemical ligand complexes, has resulted in metal-ligand coordination interactions forming the basis of the majority of template-directed syntheses of MIMs.

1.4.1.1.1 Passive Metal Templates

Classical template-directed synthetic approaches utilise passive metal templates, in which coordination interactions between the metal ion and appropriately functionalised ligand precursors serves to pre-organise the latter in a geometry suitable for mechanical bond formation via a chemical reaction. The efficacy of this approach was first demonstrated by Sauvage and co-workers, who exploited the tetrahedral coordination geometry of Cu(I) to arrange two phenanthroline ligands in an orthogonal orientation suitable for [2]catenane formation by intra-ligand cyclisation. The yield of the [2]catenane forming step could be improved to 42% by using a pre-formed macrocycle to facilitate pseudo[2]rotaxane assembly (**Figure 1.32**). By modification of the phenanthroline ligands, a plethora of topologically complex molecules could be accessed, highlighting the versatility of this passive metal strategy.[152-158] Sauvage's approach inspired the development of many alternative transition metal templates displaying a range of ligand preferences and binding modes, including systems based on octahedral, trigonal bipyramidal, square planar and linear coordination geometries.[159]

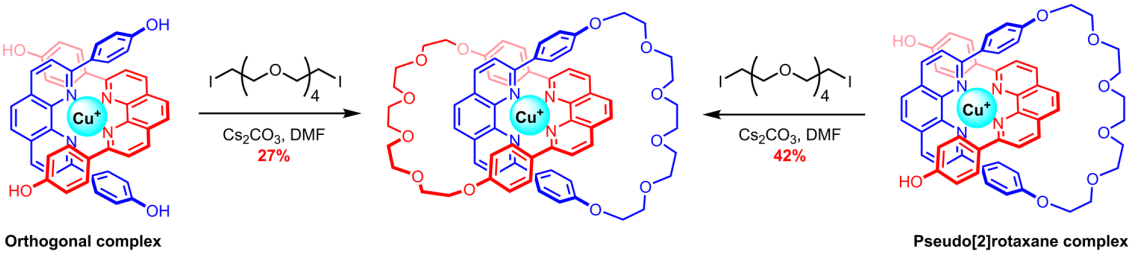


Figure 1.32. *Sauvage's Cu(I) template-directed synthesis of homo[2]catenane via formation of an orthogonal complex (left) or pseudorotaxane assembly (right).*

1.4.1.1.2 Active Metal Templates

Exploiting the ability of transition metal ions to catalyse azide-alkyne cycloaddition reactions, in 2006 Leigh and co-workers introduced a novel active metal template (AMT) strategy for MIM synthesis, in which the metal serves the dual roles of pre-organising the

components and, crucially, catalysing the chemical reaction used to form the mechanical bond. The most common application is the use of a Cu(I) ion that binds in the cavity of a pre-formed pyridine-containing macrocycle and catalyses a CuAAC reaction between azide and alkyne precursors inside the macrocyclic cavity to form a permanently threaded species (**Figure 1.33**). Using this approach, the authors achieved rotaxane yields as high as 94% using sub-stoichiometric quantities of the Cu(I) template.[160] Encouraged by the efficacy of this approach, the active metal template strategy has been extended to exploit a range of metal-mediated bond forming reactions including Pd(II)-mediated oxidative Heck reactions,[161] Ni(II)-mediated sp^3-sp^3 couplings[162] and other Cu(I)-mediated reactions.[163-164]

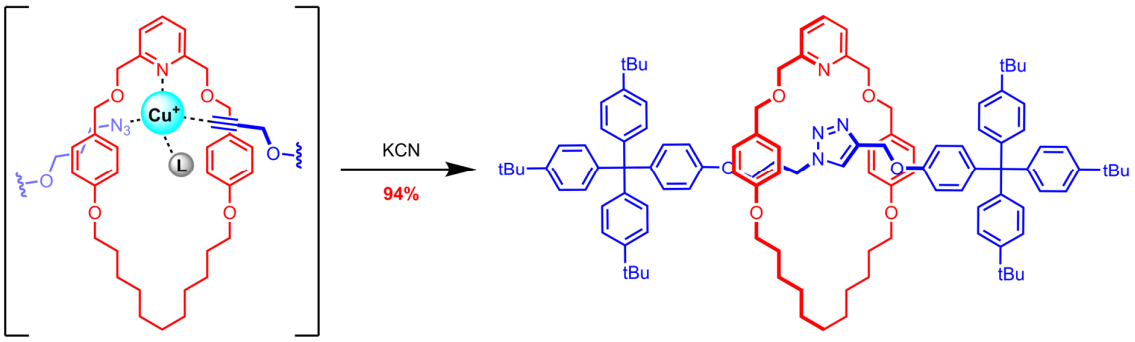


Figure 1.33. *Leigh's Cu(I) catalysed active metal template synthesis of [2]rotaxanes.*

1.4.1.2 Anion Template-Directed Approaches

Mirroring the slower development of anion host-guest chemistry relative to its sister field of cation recognition, the use of anion templates in MIM synthesis is less common, with only a handful of anion-templated MIMs reported to date.

An early example of anion template-directed [2]rotaxane formation was reported by Vögtle and co-workers in 1999 (**Figure 1.34**). This strategy utilises the hydrogen bonding interactions between a tetralactam macrocycle and a bulky phenolate-containing axle precursor

to induce the formation of a threaded complex, which was subsequently reacted with an aryl bromide axle precursor to afford a [2]rotaxane in an impressive 95% yield.[165]

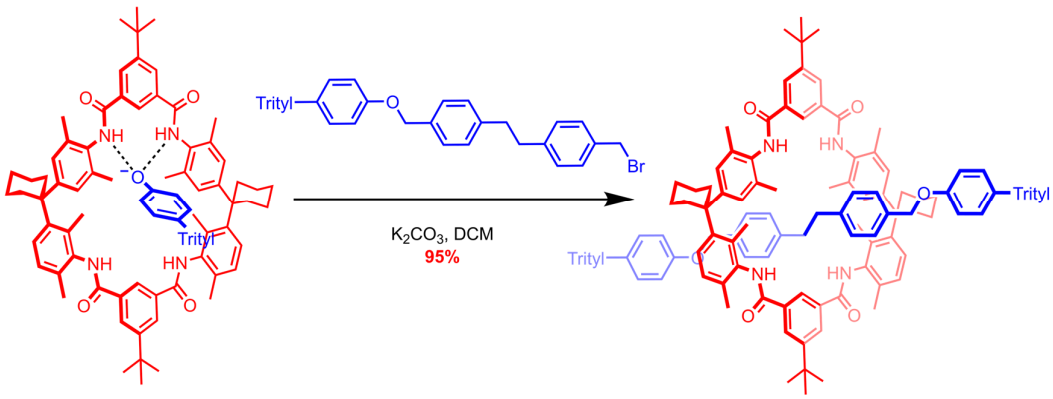


Figure 1.34. *Vögtle's phenolate-directed synthesis of a [2]rotaxane.*

The propensity of Flood's cyanostar macrocycle to sandwich large anions was exploited to assemble a pseudorotaxane complex in which dipropargylphosphate is threaded through the cavities of two cyanostar macrocycles. Stoppering of this complex via a CuAAC reaction with bulky organic azides gave the target [3]rotaxane in 24% yield.[82]

The use of a discrete anion as an external template that can be removed post-MIM synthesis was pioneered by Beer in 2002 (**Figure 1.35**).[166] The authors exploited the orthogonal complexation of a chloride anion by a cationic 3,5-bis-amido-N-methylpyridinium axle and an isophthalamide containing macrocycle precursor to assemble a complex that was pre-organised to undergo macrocycle clipping around the axle via a Grubbs' catalysed ring closing metathesis reaction. A distinct advantage of this approach is the retainment of an interlocked anion binding cavity following the removal of the template, which endows the resulting MIMs with potent anion recognition capabilities. As such, this approach has been employed extensively for the preparation of various catenane[167-170] and rotaxane[171-173] hosts for anion recognition and sensing. The use of alternative inorganic anion templates, including bromide,[174] nitrate,[175-176] sulfate[177-179] and nitrite,[180] has also been explored. In recent years, the development of anion

template-directed strategies based on halogen bonding donor motifs has proven to be a powerful strategy to prepare XB interlocked host molecules capable of strong and selective anion binding in competitive solvent media.[50, 90, 93, 181-182]

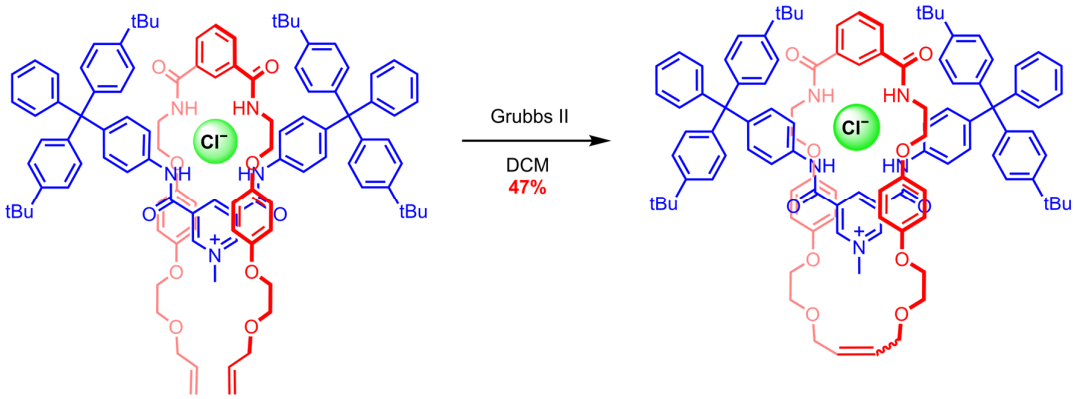


Figure 1.35. *Beer's chloride template-directed synthesis of a [2]rotaxane.*

1.4.2 MIM-based Hosts for Charged Guest Recognition

The unusual topologies and dynamic nature of MIMs have made them promising candidates for a diverse range of applications, including as molecular machines, switches and catalysts.[22, 183] In the field of host-guest recognition and sensing, the use of MIMs offers distinct advantages over acyclic or macrocyclic receptors. MIMs present a unique opportunity to generate pre-organised 3D binding sites which can be tailored to the specific geometric requirements of a target guest by functionalisation with appropriate recognition motifs. In addition, the binding cavities of MIMs provide a solvent-shielded hydrophobic environment to reduce the thermodynamic cost of binding charged guests, which typically results in MIM-based cation and anion receptors displaying superior binding affinities over acyclic and/or macrocyclic analogues.[184] The notable enhancements in guest binding selectivity and potency observed in MIM-based hosts has been generalised in terms of a "mechanical bond effect" (MBE), analogous to the well-established chelate and macrocyclic effects in coordination chemistry.[185]

1.4.2.1 MIMs for Cation Recognition and Sensing

The use of metal template-directed approaches for MIM synthesis often results in interlocked products that possess recognition motifs suitable for metal cation binding and recognition. Despite the existence of many non-interlocked ligand systems capable of effective metal ion binding, the unique properties of MIMs can give rise to unusual behaviour upon cation binding. For instance, Goldup and co-workers employed a CuAAC-AMT methodology to prepare a series of [2]rotaxanes containing different numbers of nitrogen donor groups (**Figure 1.36**). The confinement of various transition metal ions within the binding cavities of the rotaxanes in CH_3CN was found to enforce unusual metal coordination geometries, including five-coordinate Co^{2+} and Ni^{2+} complexes observed by X-ray crystallography. The redox properties of metal ions could also be modulated by encapsulation within the [2]rotaxane binding cavities, with Cu^{+} in particular showing a significant enhancement in electrochemical stability.[186]

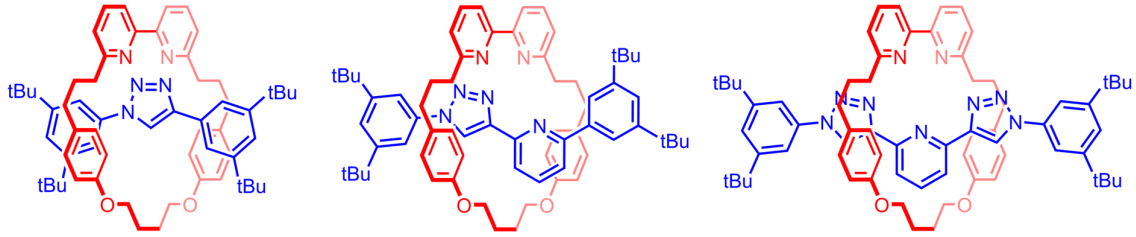


Figure 1.36. *Goldup's series of [2]rotaxanes for transition metal recognition.*

Conversely, the coordination preferences of metal ions can be used to exert co-conformational control over dynamic MIM systems, which was poignantly demonstrated in a [2]rotaxane synthesised by Loeb and co-workers (**Figure 1.37**). The [2]rotaxane was capable of binding metal cations via convergent coordination interactions in 1:1 $CD_3CN/CDCl_3$ (v/v), utilising nitrogen donors from the axle and oxygen or olefinic donors from the macrocycle. Importantly, crystallographic and 2D NMR studies showed that the addition of cations with

different coordination preferences induced a rotation of the macrocycle to enable access to the most favourable binding environment. The hard Li^+ cation binds to the rotaxane via the macrocycle polyether oxygen atoms, whereas Cu^+ binding is accompanied by a macrocycle circum-rotation to enable participation of the olefinic π-donor.[187]

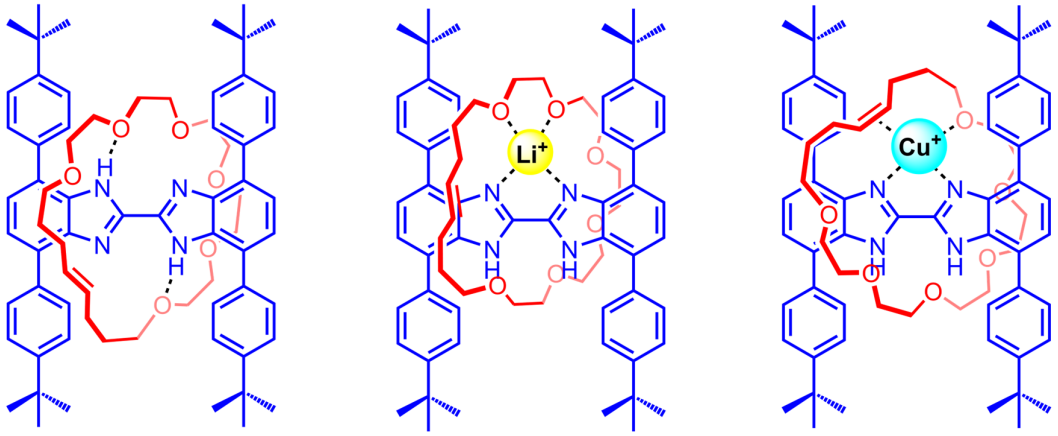


Figure 1.37. *Loeb's dynamic [2]rotaxane capable of adopting different co-conformations upon binding Li^+ (middle) and Cu^+ (right).*

The incorporation of reporter groups to the structural framework of MIM cation hosts is an effective means of endowing MIMs with sensing capabilities.[188-190] In one example, Leung and co-workers synthesised fluorescent [2]rotaxanes stoppered with anthracene or BODIPY units (**Figure 1.38**). Binding of Au^{3+} to the rotaxanes in the competitive 1:1 H_2O/MeCN (v/v) solvent mixture led to a significant fluorescence turn-on, which was exploited for Au^{3+} imaging in HeLa cells.[191]

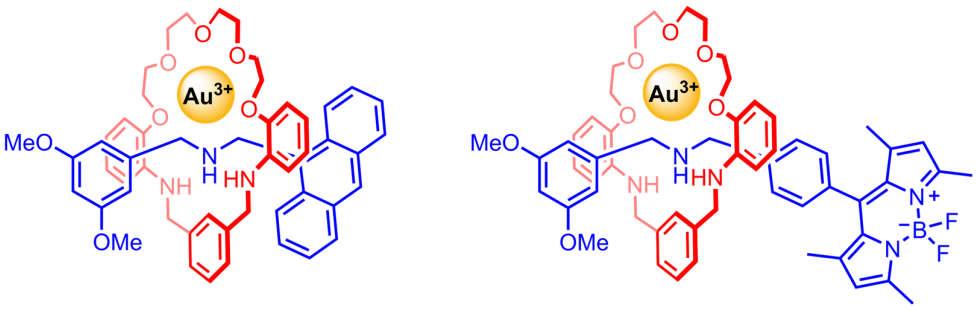


Figure 1.38. *Leung's fluorophore-stoppered rotaxanes for sensing of Au^{3+}.*

1.4.2.2 MIMs for Anion Recognition

Facilitated by the development of anion template-directed methodologies for MIM preparation, the design and synthesis of MIM-based anion hosts and sensors has advanced significantly over the past two decades.

Early examples of anion binding MIMs primarily utilised cationic hydrogen bonding donor groups as both the templating and binding motifs. Utilising their previously-developed chloride anion template-directed approach, Beer and co-workers synthesised a [2]catenane which displays a marked preference for binding chloride over oxoanions in 1:1 $CD_3OD/CDCl_3$ (v/v) (**Figure 1.39a**). This selectivity trend is the reverse of that observed in the acyclic pyridinium precursor, demonstrating the importance of the interlocked host topology in dictating anion binding selectivity.[167]

The integration of halogen bonding motifs into interlocked host architectures has given rise to MIMs with enhanced anion binding and sensing properties. A particularly impressive example features a bis(iodotriazole)pyridinium-containing rotaxane stoppered with permethylated β-cyclodextrins which demonstrates XB-mediated anion recognition in pure water for the first time (**Figure 1.39b**). The rotaxane displayed strong binding of iodide anions in water (K_a = 2200 M^{-1}), which was two orders of magnitude higher than the analogous HB rotaxanes containing bis-triazole or bis-amide donor groups in their axles. Thermodynamic binding data suggested that the enhanced iodide binding in the XB rotaxane arises from the favourable enthalpy of XB···I^- interactions, whereas the weaker anion association of the HB rotaxanes is entropically driven.[93] Recently, it was shown that appending electron-deficient perfluoroaryl substituents to the bis(iodotriazole) XB donor motif can further increase the anion binding potency of XB MIMs, as suggested by an impressive rotaxane yield of 91% achieved via a chloride anion template-directed synthesis (**Figure 1.39c**).[90]

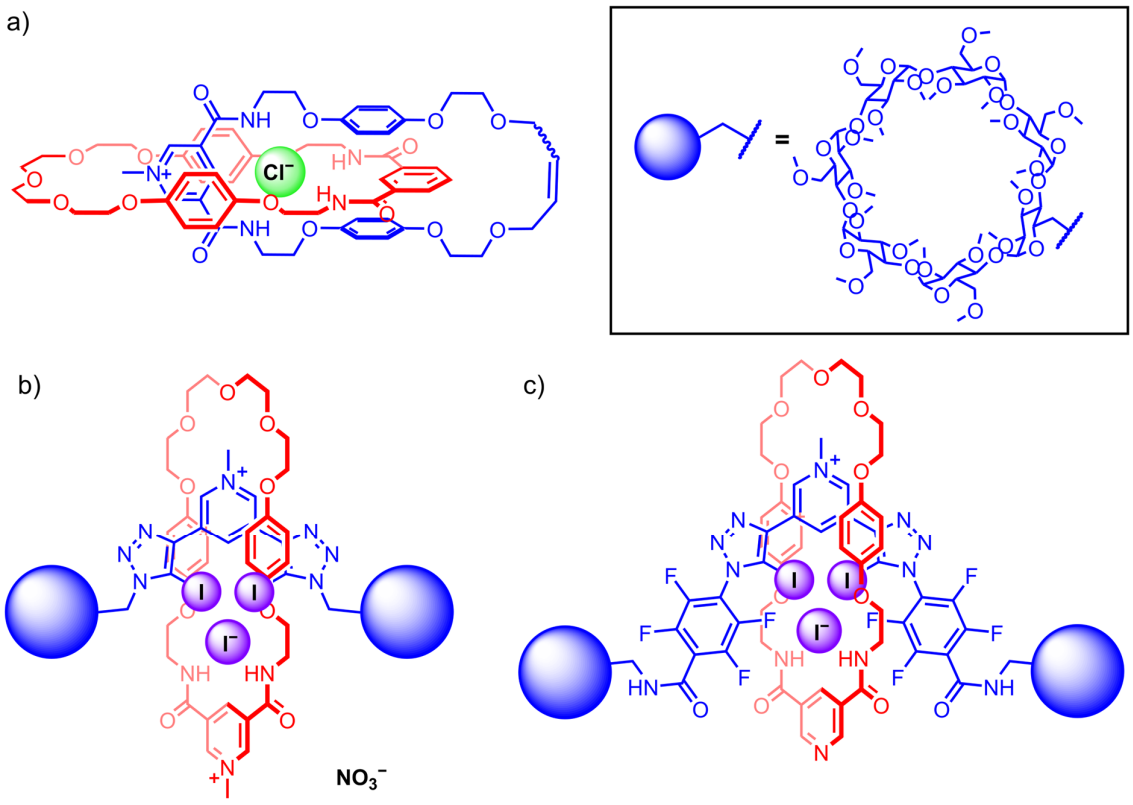


Figure 1.39. *Anion binding MIMs: (a) A [2]catenane; (b) A water-soluble [2]rotaxane; (c) A pentafluorophenyl-substituted [2]rotaxane. Inset: Structure of permethylated β-cyclodextrin rotaxane stoppers.*

A range of anion sensing rotaxanes[180, 192-198] and catenanes[199-200] have been developed by appending reporter groups to the host framework. A notable example is a chiral [3]rotaxane which possesses a central (*S*)-BINOL fluorophore flanked by two halogen bonding 3,5-bis(iodotriazole)pyridinium motifs in the axle, which displayed significant fluorescence quenching upon addition of dicarboxylate anions (**Figure 1.40a**). Importantly, the [3]rotaxane was capable of discriminating both enantiomers (K_S/K_R for glutamate = 5.7 ± 0.3) and geometric isomers ($K_{fumarate}/K_{malonate}$ = 4.4 ± 0.3) in 60:39:1 $CHCl_3/CH_3OH/H_2O$ (v/v/v).[201] In another example, a zinc metalloporphyrin signalling group was incorporated into a hetero-[2]catenane (**Figure 1.40b**). Pyridyl coordination to the apical site of Zn(II) centre served to pre-organise the interlocked cavity for chloride recognition, which was bound via six convergent CH···Cl^- and NH···Cl^- hydrogen bonds. The encapsulation of chloride by the

catenane induced a gradual blueshift of the Soret band absorbance as well as slight increases in emission intensity.[202]

Surprisingly, despite the useful luminescent properties of lanthanide ions in sensing and imaging,[203] the only report of optical anion sensing by a lanthanide-containing MIM featured a europium-containing [2]rotaxane, which was synthesised via a nitrite anion template-directed route (**Figure 1.39c**).[180] After removal of the nitrite template, it was found that fluoride addition caused substantial quenching of the Eu(III) emission in acetone/H_2O (99:1 v/v). The increase in fluorescence lifetime and changes in the intensity of the hypersensitive $\Delta J = 2$ bands in the fluoride-bound rotaxane suggested that the guest ion was coordinated directly to the Eu(III) centre, although charge-assisted hydrogen bonds from the axle also played a role in enhancing the affinity of the rotaxane for fluoride, as suggested by the reduced binding strength of the non-interlocked macrocyclic component. Nitrite and acetate led to weaker fluorescence quenching, which was attributed to a different mode of binding wherein these anions were associated with organic groups in the binding cavity rather than directly coordinated to the emissive Eu(III) centre.

Exploiting the inherent co-conformational dynamism of interlocked architectures, MIMs that undergo anion-induced co-conformational movements have been developed as novel anion sensors. These systems are mostly based on multi-station rotaxanes, wherein a photophysical response is produced upon translocation of the macrocycles between photoactive and anion binding stations to facilitate convergent anion binding by the donor groups of both interlocked components, which will be discussed further in Chapter 3.[91, 170, 173, 204-206]

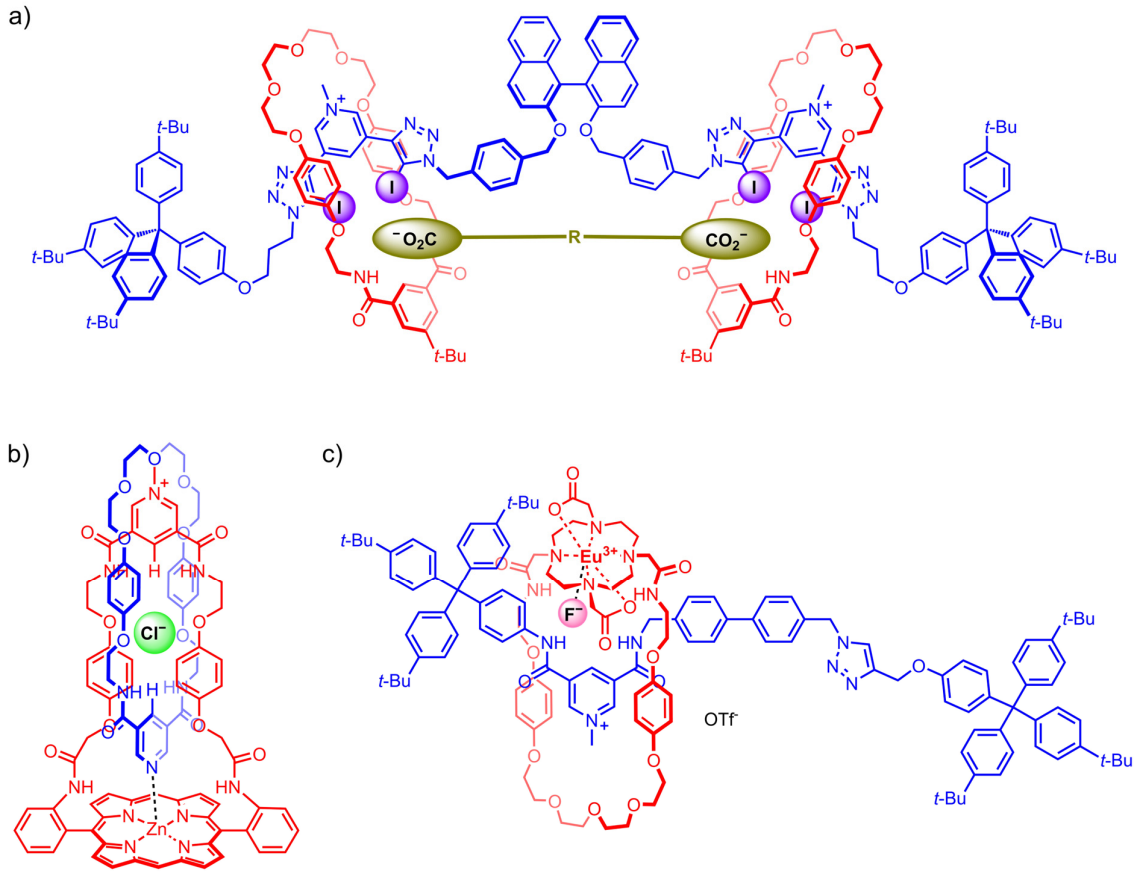


Figure 1.40. *MIMs for anion sensing: (a) A BINOL-functionalised [3]rotaxane; (b) A Zn-porphyrin-functionalised hetero[2]catenane; (c) A Eu(III)-containing [2]rotaxane.*

1.4.2.3 MIMs for Ion-pair Recognition and Sensing

The multi-component nature of MIMs makes them promising scaffolds upon which multiple cation and anion binding sites can be incorporated, facilitating a modular approach to constructing complex heteroditopic and multitopic receptors for ion-pair recognition. Surprisingly, however the design of mechanically interlocked heteroditopic receptors remains an underexplored area, with the handful of reported examples typically limited to rotaxane architectures utilising hydrogen bonding (HB) as the primary means by which anion binding is achieved.[207-213]

The first example of ion-pair binding by heteroditopic MIM was reported by Smith and co-workers in 2002,[209] who prepared [2]rotaxanes containing various diester-functionalised axles threaded through a macrobicyclic wheel, which was previously been demonstrated to bind NaCl and KCl ion-pairs with significant positive cooperativity (**Figure 1.41a**).[124] Although the rotaxanes remained capable of binding KCl in 3:1 DMSO-d_6/CD_3CN (v/v) as an axle-separated ion-pair complex, closer inspection of the ^1H NMR binding data revealed no positive cooperativity, which the authors attributed to the axle insulating through-space electrostatic attraction between the co-bound ions. Cooperative ion-pair binding by a heteroditopic MIM was only demonstrated for the first time in 2014 by Beer and co-workers, who prepared a [2]rotaxane containing a calix[4]diquinone-and isophthalamide-functionalised macrocycle encircling a bis-amide pyridine-*N*-oxide axle (**Figure 1.41b**). Convergent sodium cation binding by the calix[4]diquinone and the pyridine-*N*-oxide served to disrupt intramolecular HB interactions and generate an anion binding cavity containing four amide NH donors. The combination of electrostatic and allosteric effects elicited significant positive cooperativity in the cation and anion binding events, with the strength of chloride binding enhanced by 15-fold in the presence of a co-bound sodium ion in 4:1 $CDCl_3$/CD_3OD (v/v).[207]

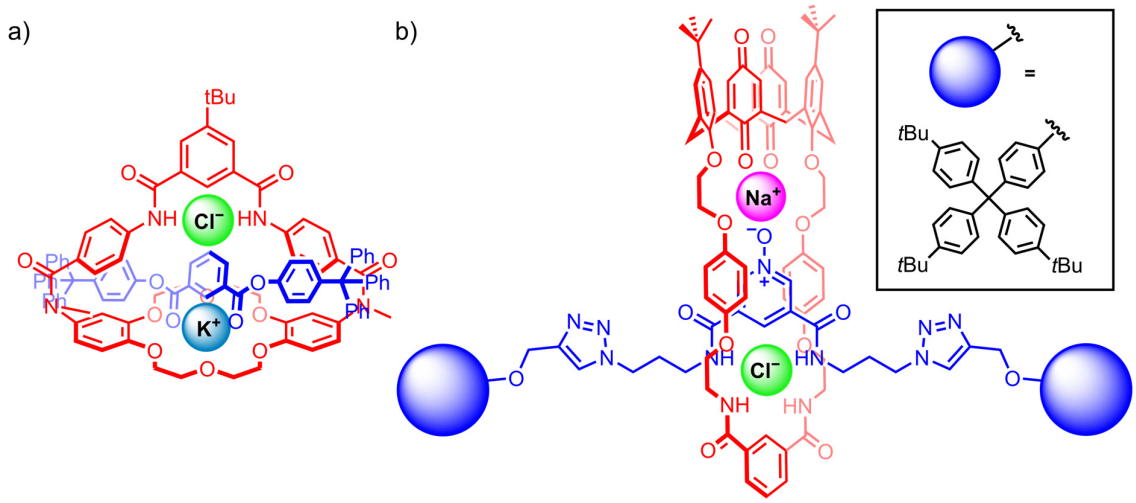


Figure 1.41. *Early ion-pair binding rotaxanes: (a) Smith's bicyclic wheel [2]rotaxane; (b) Beer's calix[4]diquinone- and pyridyl-N-oxide-functionalised [2]rotaxane.*

A similar approach was utilised by Goldup and co-workers in a simple [2]rotaxane capable of selective HCl recognition (**Figure 1.42**). The free rotaxane exhibits strong intramolecular hydrogen bonds between the urea station of the axle and the bipyridine group of the macrocycle that precludes the binding of anions. Protonation of the bipyridine forces the macrocycle to move away from the urea station and onto the adjacent triazole station, allowing the 'freed' urea group to bind anions via HB interactions. A marked preference for chloride ($K_a > 10^4$ in 1:1 $CDCl_3/CD_3CN$) was observed, which is accompanied by a fluorescence enhancement that the authors attribute to a combination of receptor rigidification as well as the formation of π-π interactions with the axle naphthalimide group.[211]

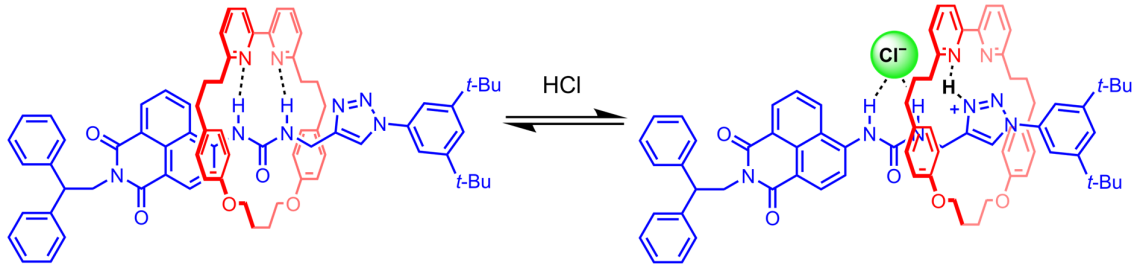


Figure 1.42. *Goldup's dynamic [2]rotaxane shuttle capable for cooperative HCl ion-pair binding.*

Recently, Beer and co-workers incorporated XB donor groups into a heteroditopic rotaxane for selective binding of lithium halide salts,[214] which are growing in industrial importance with the development of lithium-based battery technologies.[215] The rotaxane was synthesised via a CuAAC reaction and contains a bis(iodotriazole)-functionalised macrocycle as well as an iodotriazole-functionalised axle component (**Figure 1.43**). Cooperative binding of lithium bromide and iodide ion-pairs by the rotaxanes was observed in $CDCl_3/CD_3CN$ mixtures, which is impressive considering the high lattice enthalpy of lithium halide salts. Importantly, the non-interlocked axle and macrocycle components were unable to bind lithium halide ion-pairs. Crystallographic and DFT studies suggested that the favourable binding cooperativity observed in the interlocked hosts arises from a positive allosteric effect, in which Li^+ complexation by the macrocycle pyridyl and axle triazole donors pre-organises the iodotriazole XB motifs on the macrocycle and axle to participate in convergent anion binding.

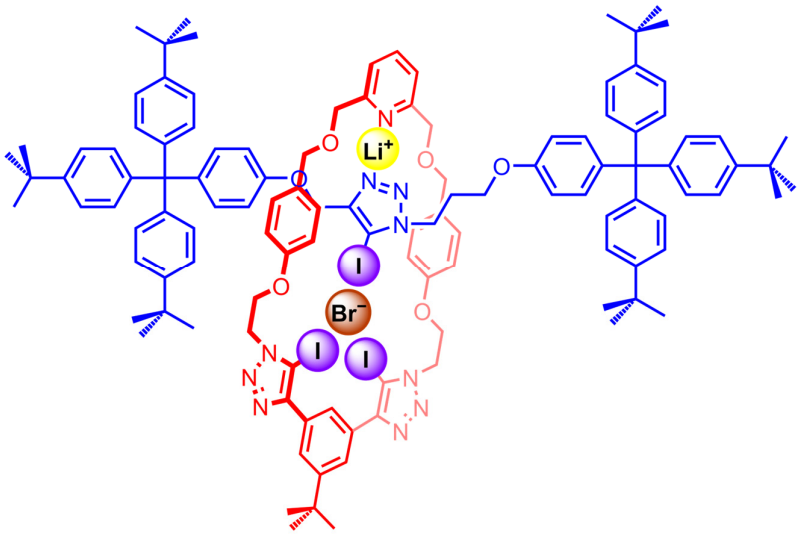


Figure 1.43. *Beer's XB [2]rotaxane for lithium halide binding.*

1.5 Thesis Aims

The rapid growth of supramolecular host-guest chemistry over the past few decades has intensified the search for novel strategies to improve the binding and recognition properties of anion and ion-pair receptors. In particular, the integration of halogen bonding donor motifs into anion and ion-pair host designs has emerged as a promising alternative to traditional hydrogen bonding interactions. Receptors based on interlocked host topologies have also been shown to exhibit considerable advantages over non-interlocked analogues. Despite the perceived advantages of integrating these two strategies, efforts to prepare interlocked receptors containing XB donor groups have thus far been limited. In particular, the development of heteroditopic MIM-based XB receptors for ion-pair recognition remains an underexplored area.

This thesis describes the development of novel cation- and anion-templated methodologies for the preparation of XB containing catenanes and rotaxanes for the selective recognition of anions and ion-pairs, highlighting in particular the utility of halogen bonding donor groups as both templating and binding motifs. The application of the interlocked systems in the extraction, sensing and transport of charged guest species is also explored.

Chapter Two describes the synthesis and ion-pair binding properties of a family of neutral heteroditopic XB catenanes and rotaxanes prepared by an alkali metal cation template-directed approach. Extensive quantitative ^{1}H NMR titration studies with alkali metal cations, halide anions and their respective ion-pairs reveal significant positive cooperativity between cation and anion binding events. Crystallographic analysis is used to probe the binding modes and stoichiometries of the catenane receptors, corrobating the solution-state NMR binding data. The ion-pair binding capabilities of the MIM receptors are also exploited for the development of alkali metal halide salt selective solid-liquid extraction agents.

Chapter Three describes the development of a novel chloride anion template-directed methodology for the preparation of neutral interlocked molecules which utilises the exceptionally strong anion binding properties of an activated 4,6-dinitro-1,3-bis-iodotriazole XB donor motif. ^{1}H NMR anion binding studies in aqueous-acetone solvent mixtures demonstrate an mechanical bond induced anti-Hofmeister halide anion binding preference, which is exploited to develop selective interlocked systems for anion membrane transport and sensing.

Chapter Four describes synthetic efforts to prepare higher order heteroditopic catenanes possessing interlocked binding cavities for both the cationic and anionic guests by integrating the cation- and anion-templated methodologies introduced in the previous chapters. A variety of [3]catenane designs are outlined, alongside the synthetic challenges associated with each route. Preliminary evidence for the formation of the target [3]catenanes is also presented.

1.6 References for Chapter 1

1. J. F. Stoddart, *Nature Chem.* **2009**, *1*, 14-15.
2. C. J. Pedersen, *J. Am. Chem. Soc.* **1967**, *89*, 7017-7036.
3. E. Graf, J. M. Lehn, *J. Am. Chem. Soc.* **1976**, *98*, 6403-6405.
4. J. M. Lehn, E. Sonveaux, A. K. Willard, *J. Am. Chem. Soc.* **1978**, *100*, 4914-4916.
5. D. J. Cram, *Science* **1983**, *219*, 1177-1183.
6. D. J. Cram, *Science* **1988**, *240*, 760-767.
7. J.-M. Lehn, *Angew. Chem. Int. Ed.* **1988**, *27*, 89-112.
8. C. J. Pedersen, *Angew. Chem. Int. Ed. Engl.* **1988**, *27*, 1021-1027.
9. D. J. Cram, *Angew. Chem. Int. Ed. Engl.* **1988**, *27*, 1009-1020.
10. Q. Shi, X. Wang, B. Liu, P. Qiao, J. Li, L. Wang, *Chem. Commun.* **2021**, *57*, 12379-12405.
11. A. Ikeda, S. Shinkai, *Chem. Rev.* **1997**, *97*, 1713-1734.
12. G. Crini, *Chem. Rev.* **2014**, *114*, 10940-10975.
13. S. J. Barrow, S. Kasera, M. J. Rowland, J. del Barrio, O. A. Scherman, *Chem. Rev.* **2015**, *115*, 12320-12406.
14. P. G. Ghasemabadi, T. Yao, G. J. Bodwell, *Chem. Soc. Rev.* **2015**, *44*, 6494-6518.
15. K. Yang, Y. Pei, J. Wen, Z. Pei, *Chem. Commun.* **2016**, *52*, 9316-9326.
16. C. O. Dietrich-Buchecker, J. P. Sauvage, J. M. Kern, *J. Am. Chem. Soc.* **1984**, *106*, 3043-3045.
17. P. R. Ashton, T. T. Goodnow, A. E. Kaifer, M. V. Reddington, A. M. Z. Slawin, N. Spencer, J. F. Stoddart, C. Vicent, D. J. Williams, *Angew. Chem. Int. Ed. Engl.* **1989**, *28*, 1396-1399.
18. M. J. Langton, P. D. Beer, *Acc. Chem. Res.* **2014**, *47*, 1935-1949.
19. H.-Y. Zhou, Y. Han, C.-F. Chen, *Mater. Chem. Front.* **2020**, *4*, 12-28.
20. A. Saura-Sanmartin, *Beilstein J. Org. Chem.* **2023**, *19*, 873-880.

21. F. M. Raymo, J. F. Stoddart, in *Magnetism: A Supramolecular Function* (Ed.: O. Kahn), Springer Netherlands, Dordrecht, **1996**, pp. 33-51.
22. A. W. Heard, S. M. Goldup, *ACS Cent. Sci.* **2020**, *6*, 117-128.
23. M. P. Anderson, R. J. Gregory, S. Thompson, D. W. Souza, S. Paul, R. C. Mulligan, A. E. Smith, M. J. Welsh, *Science* **1991**, *253*, 202.
24. F. Delange, *Thyroid* **1994**, *4*, 107-128.
25. J. L. Way, *Annu. Rev. Pharmacol. Toxicol.* **1984**, *24*, 451-481.
26. V. H. Smith, D. W. Schindler, *Trends. Ecol. Evol.* **2009**, *24*, 201-207.
27. J. H. P. Watson, D. C. Ellwood, *Nucl. Eng. Des.* **2003**, *226*, 375-385.
28. P. K. Dasgupta, J. V. Dyke, A. B. Kirk, W. A. Jackson, *Environ. Sci. Technol.* **2006**, *40*, 6608-6614.
29. D. Banerjee, D. Kim, M. J. Schweiger, A. A. Kruger, P. K. Thallapally, *Chem. Soc. Rev.* **2016**, *45*, 2724-2739.
30. M. D. Rao, K. K. Singh, C. A. Morrison, J. B. Love, *RSC Adv.* **2020**, *10*, 4300-4309.
31. T. Hunter, *Philosophical Transactions of the Royal Society B: Biological Sciences* **2012**, *367*, 2513-2516.
32. D.-y. Duan, L. L. H. Liu, N. Bozeat, Z. M. Huang, S. Y. Xiang, G.-l. Wang, L. Ye, J. R. Hume, *Acta Pharmacol. Sin.* **2005**, *26*, 265-278.
33. L. Puljak, G. Kilic, *Biochimica et Biophysica Acta (BBA) - Molecular Basis of Disease* **2006**, *1762*, 404-413.
34. N. Carrasco, *Biochimica et Biophysica Acta (BBA) - Reviews on Biomembranes* **1993**, *1154*, 65-82.
35. J. A. Camargo, Á. Alonso, *Environment International* **2006**, *32*, 831-849.
36. V. H. Smith, G. D. Tilman, J. C. Nekola, *Environ. Pollut.* **1999**, *100*, 179-196.
37. R. Eisler, in *Reviews of Environmental Contamination and Toxicology*, Springer New York, New York, NY, **2004**, pp. 133-165.
38. N. H. Evans, P. D. Beer, *Angew. Chem. Int. Ed.* **2014**, *53*, 11716-11754.
39. R. Shannon, *Acta Crystallographica Section A* **1976**, *32*, 751-767.
40. Y. Marcus, *J. Chem. Soc., Faraday Trans.* **1991**, *87*, 2995-2999.
41. E. J. W. Whittaker, R. Muntus, *Geochim. Cosmochim. Acta* **1970**, *34*, 945-956.
42. F. Hofmeister, *Archiv für experimentelle Pathologie und Pharmakologie* **1888**, *24*, 247-260.
43. B. Kang, H. Tang, Z. Zhao, S. Song, *ACS Omega* **2020**, *5*, 6229-6239.
44. R. S. Carnegie, C. L. D. Gibb, B. C. Gibb, *Angew. Chem. Int. Ed.* **2014**, *53*, 11498-11500.
45. C. L. D. Gibb, B. C. Gibb, *J. Am. Chem. Soc.* **2011**, *133*, 7344-7347.
46. A. J. Grooms, J. F. Neal, K. C. Ng, W. Zhao, A. H. Flood, H. C. Allen, *J. Phys. Chem. A* **2020**, *124*, 5621-5630.
47. K. Kavallieratos, B. A. Moyer, *Chem. Commun.* **2001**, 1620-1621.
48. A. L. Sisson, J. P. Clare, A. P. Davis, *Chem. Commun.* **2005**, 5263-5265.
49. M. K. Chae, J.-m. Suk, K.-S. Jeong, *Tetrahedron Lett.* **2010**, *51*, 4240-4242.
50. A. Docker, Y. C. Tse, H. M. Tay, A. J. Taylor, Z. Zhang, P. D. Beer, *Angew. Chem. Int. Ed.* **2022**, *61*, e202214523.
51. D. Lichosyt, S. Wasiłek, P. Dydio, J. Jurczak, *Chem. Eur. J.* **2018**, *24*, 11683-11692.
52. P. D. Beer, P. A. Gale, *Angew. Chem. Int. Ed.* **2001**, *40*, 486-516.
53. M. Teresa Albelda, M. Alexandra Bernardo, E. Garcia-España, M. Luz Godino-Salido, S. V. Luis, M. João Melo, F. Pina, C. Soriano, *J. Chem. Soc., Perkin Transactions 2* **1999**, 2545-2549.
54. C. H. Park, H. E. Simmons, *J. Am. Chem. Soc.* **1968**, *90*, 2431-2432.
55. F. P. Schmidtchen, *Angew. Chem. Int. Ed. Engl.* **1977**, *16*, 720-721.
56. P. J. Garratt, A. J. Ibbett, J. E. Ladbury, R. O'Brien, M. B. Hursthouse, K. M. Abdul Malik, *Tetrahedron* **1998**, *54*, 949-968.
57. M. W. Hosseini, J. M. Lehn, *J. Am. Chem. Soc.* **1982**, *104*, 3525-3527.
58. G. Müller, J. Riede, F. P. Schmidtchen, *Angew. Chem. Int. Ed. Engl.* **1988**, *27*, 1516-1518.
59. F. P. Schmidtchen, *Tetrahedron Lett.* **1989**, *30*, 4493-4496.

60. A. Echavarren, A. Galan, J. M. Lehn, J. De Mendoza, *J. Am. Chem. Soc.* **1989**, *111*, 4994-4995.
61. K. Chellappan, N. J. Singh, I.-C. Hwang, J. W. Lee, K. S. Kim, *Angew. Chem. Int. Ed.* **2005**, *44*, 2899-2903.
62. A. Kumar, P. S. Pandey, *Org. Lett.* **2008**, *10*, 165-168.
63. M. A. Mintzer, M. W. Grinstaff, *Chem. Soc. Rev.* **2011**, *40*, 173-190.
64. K. Kavallieratos, S. R. de Gala, D. J. Austin, R. H. Crabtree, *J. Am. Chem. Soc.* **1997**, *119*, 2325-2326.
65. S. Kubik, *Acc. Chem. Res.* **2017**, *50*, 2870-2878.
66. S. Kubik, R. Goddard, R. Kirchner, D. Nolting, J. Seidel, *Angew. Chem. Int. Ed.* **2001**, *40*, 2648-2651.
67. S. Kubik, R. Goddard, *Proceedings of the National Academy of Sciences* **2002**, *99*, 5127-5132.
68. F. Sommer, Y. Marcus, S. Kubik, *ACS Omega* **2017**, *2*, 3669-3680.
69. D. E. Gómez, L. Fabbrizzi, M. Licchelli, E. Monzani, *Org. Biomol. Chem.* **2005**, *3*, 1495-1500.
70. S. Kundu, T. K. Egboluche, M. A. Hossain, *Acc. Chem. Res.* **2023**, *56*, 1320-1329.
71. M. Emami Khansari, M. H. Hasan, C. R. Johnson, N. A. Williams, B. M. Wong, D. R. Powell, R. Tandon, M. A. Hossain, *ACS Omega* **2017**, *2*, 9057-9066.
72. X. Wu, P. Wang, P. Turner, W. Lewis, O. Catal, D. S. Thomas, P. A. Gale, *Chem* **2019**, *5*, 1210-1222.
73. L. A. Marchetti, L. K. Kumawat, N. Mao, J. C. Stephens, R. B. P. Elmes, *Chem* **2019**, *5*, 1398-1485.
74. V. Amendola, G. Bergamaschi, M. Boiocchi, L. Fabbrizzi, M. Milani, *Chem. Eur. J.* **2010**, *16*, 4368-4380.
75. R. Prohens, S. Tomàs, J. Morey, P. M. Deyà, P. Ballester, A. Costa, *Tetrahedron Lett.* **1998**, *39*, 1063-1066.
76. L. Qin, A. Hartley, P. Turner, R. B. P. Elmes, K. A. Jolliffe, *Chem. Sci.* **2016**, *7*, 4563-4572.
77. P. A. Gale, J. L. Sessler, V. Král, V. Lynch, *J. Am. Chem. Soc.* **1996**, *118*, 5140-5141.
78. I. Saha, J. T. Lee, C.-H. Lee, *Eur. J. Org. Chem.* **2015**, *2015*, 3859-3885.
79. D.-W. Yoon, D. E. Gross, V. M. Lynch, J. L. Sessler, B. P. Hay, C.-H. Lee, *Angew. Chem. Int. Ed.* **2008**, *47*, 5038-5042.
80. S. K. Kim, J. Lee, N. J. Williams, V. M. Lynch, B. P. Hay, B. A. Moyer, J. L. Sessler, *J. Am. Chem. Soc.* **2014**, *136*, 15079-15085.
81. Y. Liu, W. Zhao, C.-H. Chen, A. H. Flood, *Science* **2019**, *365*, 159-161.
82. S. Lee, C.-H. Chen, A. H. Flood, *Nature Chem.* **2013**, *5*, 704-710.
83. J. Y. C. Lim, P. D. Beer, *Chem* **2018**, *4*, 731-783.
84. A. Bauzá, A. Frontera, *Angew. Chem. Int. Ed.* **2015**, *54*, 7340-7343.
85. S. W. Robinson, C. L. Mustoe, N. G. White, A. Brown, A. L. Thompson, P. Kennepohl, P. D. Beer, *J Am Chem Soc* **2015**, *137*, 499-507.
86. A. Shahi, E. Arunan, *Phys. Chem. Chem. Phys.* **2014**, *16*, 22935-22952.
87. A. Bauzá, D. Quiñonero, P. M. Deyà, A. Frontera, *CrystEngComm* **2013**, *15*, 3137-3144.
88. A. Bauzá, T. J. Mooibroek, A. Frontera, *ChemPhysChem* **2015**, *16*, 2496-2517.
89. M. H. Kolář, P. Hobza, *Chem. Rev.* **2016**, *116*, 5155-5187.
90. T. Bunchuay, A. Docker, A. J. Martinez-Martinez, P. D. Beer, *Angew. Chem. Int. Ed.* **2019**, *58*, 13823-13827.
91. T. A. Barendt, S. W. Robinson, P. D. Beer, *Chem. Sci.* **2016**, *7*, 5171-5180.
92. B. Chowdhury, S. Sinha, P. Ghosh, *Chem. Eur. J.* **2016**, *22*, 18051-18059.
93. M. J. Langton, S. W. Robinson, I. Marques, V. Félix, P. D. Beer, *Nature Chem.* **2014**, *6*, 1039-1043.
94. A. Brown, P. D. Beer, *Chem. Commun.* **2016**, *52*, 8645-8658.
95. A. Mele, P. Metrangolo, H. Neukirch, T. Pilati, G. Resnati, *J. Am. Chem. Soc.* **2005**, *127*, 14972-14973.

96. M. G. Sarwar, B. Dragisic, S. Sagoo, M. S. Taylor, *Angew. Chem. Int. Ed.* **2010**, *49*, 1674-1677.
97. R. Tepper, B. Schulze, H. Görls, P. Bellstedt, M. Jäger, U. S. Schubert, *Org. Lett.* **2015**, *17*, 5740-5743.
98. A. Borissov, J. Y. C. Lim, A. Brown, K. E. Christensen, A. L. Thompson, M. D. Smith, P. D. Beer, *Chem. Commun.* **2017**, *53*, 2483-2486.
99. A. Borissov, I. Marques, J. Y. C. Lim, V. Félix, M. D. Smith, P. D. Beer, *J. Am. Chem. Soc.* **2019**, *141*, 4119-4129.
100. D. Mungalpara, S. Stegmüller, S. Kubik, *Chem. Commun.* **2017**, *53*, 5095-5098.
101. T. Zhao, V. M. Lynch, J. L. Sessler, *Org. Biomol. Chem.* **2022**, *20*, 980-983.
102. F. Zapata, A. Caballero, P. Molina, I. Alkorta, J. Elguero, *J. Org. Chem.* **2014**, *79*, 6959-6969.
103. E. J. Mitchell, A. J. Beecroft, J. Martin, S. Thompson, I. Marques, V. Félix, P. D. Beer, *Angew. Chem. Int. Ed.* **2021**, *60*, 24048-24053.
104. G. E. Garrett, G. L. Gibson, R. N. Straus, D. S. Seferos, M. S. Taylor, *J. Am. Chem. Soc.* **2015**, *137*, 4126-4133.
105. G. E. Garrett, E. I. Carrera, D. S. Seferos, M. S. Taylor, *Chem. Commun.* **2016**, *52*, 9881-9884.
106. A. Docker, C. H. Guthrie, H. Kuhn, P. D. Beer, *Angew. Chem. Int. Ed.* **2021**, *60*, 21973-21978.
107. B. L. Schottel, H. T. Chifotides, K. R. Dunbar, *Chem. Soc. Rev.* **2008**, *37*, 68-83.
108. C. Garau, A. Frontera, D. Quiñonero, P. Ballester, A. Costa, P. M. Deyà, *ChemPhysChem* **2003**, *4*, 1344-1348.
109. I. Alkorta, I. Rozas, J. Elguero, *J. Am. Chem. Soc.* **2002**, *124*, 8593-8598.
110. D. Quiñonero, C. Garau, C. Rotger, A. Frontera, P. Ballester, A. Costa, P. M. Deyà, *Angew. Chem. Int. Ed.* **2002**, *41*, 3389-3392.
111. M. Mascal, A. Armstrong, M. D. Bartberger, *J. Am. Chem. Soc.* **2002**, *124*, 6274-6276.
112. H.-B. Liu, Q. Zhang, M.-X. Wang, *Angew. Chem. Int. Ed.* **2018**, *57*, 6536-6540.
113. D.-H. Tuo, Y.-F. Ao, Q.-Q. Wang, D.-X. Wang, *Org. Lett.* **2019**, *21*, 7158-7162.
114. A. J. McConnell, A. Docker, P. D. Beer, *ChemPlusChem* **2020**, *85*, 1824-1841.
115. S. K. Kim, J. L. Sessler, *Chem. Soc. Rev.* **2010**, *39*, 3784-3809.
116. A. J. McConnell, P. D. Beer, *Angew. Chem. Int. Ed.* **2012**, *51*, 5052-5061.
117. J. L. Sessler, S. K. Kim, D. E. Gross, C.-H. Lee, J. S. Kim, V. M. Lynch, *J. Am. Chem. Soc.* **2008**, *130*, 13162-13166.
118. J. Scheerder, J. P. M. van Duynhoven, J. F. J. Engbersen, D. N. Reinhoudt, *Angew. Chem. Int. Ed. Engl.* **1996**, *35*, 1090-1093.
119. T. Tozawa, Y. Misawa, S. Tokita, Y. Kubo, *Tetrahedron Lett.* **2000**, *41*, 5219-5223.
120. A. J. Evans, P. D. Beer, *Dalton Trans.* **2003**, 4451-4456.
121. A. J. Taylor, A. Docker, P. D. Beer, *Chemistry – An Asian Journal* **2023**, *18*, e202201170.
122. A. Docker, I. Marques, H. Kuhn, Z. Zhang, V. Félix, P. D. Beer, *J. Am. Chem. Soc.* **2022**, *144*, 14778-14789.
123. A. Frontera, M. Orell, C. Garau, D. Quiñonero, E. Molins, I. Mata, J. Morey, *Org. Lett.* **2005**, *7*, 1437-1440.
124. M. J. Deetz, M. Shang, B. D. Smith, *J. Am. Chem. Soc.* **2000**, *122*, 6201-6207.
125. J. M. Mahoney, A. M. Beatty, B. D. Smith, *J. Am. Chem. Soc.* **2001**, *123*, 5847-5848.
126. M. D. Lankshear, A. R. Cowley, P. D. Beer, *Chem. Commun.* **2006**, 612-614.
127. Q. He, G. I. Vargas-Zúñiga, S. H. Kim, S. K. Kim, J. L. Sessler, *Chem. Rev.* **2019**, *119*, 9753-9835.
128. Y. Yeon, S. Leem, C. Wagen, V. M. Lynch, S. K. Kim, J. L. Sessler, *Org. Lett.* **2016**, *18*, 4396-4399.
129. E. Brunetti, J.-F. Picron, K. Flidrova, G. Bruylants, K. Bartik, I. Jabin, *J. Org. Chem.* **2014**, *79*, 6179-6188.
130. B. Akhuli, P. Ghosh, *Chem. Commun.* **2015**, *51*, 16514-16517.

131. D. Jagleniec, S. Siennicka, Ł. Dobrzycki, M. Karbarz, J. Romański, *Inorg. Chem.* **2018**, *57*, 12941-12952.
132. P. R. A. Webber, P. D. Beer, *Dalton Trans.* **2003**, 2249-2252.
133. J. M. Mahoney, G. U. Nawaratna, A. M. Beatty, P. J. Duggan, B. D. Smith, *Inorg. Chem.* **2004**, *43*, 5902-5907.
134. Q. He, N. J. Williams, J. H. Oh, V. M. Lynch, S. K. Kim, B. A. Moyer, J. L. Sessler, *Angew. Chem. Int. Ed.* **2018**, *57*, 11924-11928.
135. Z.-H. Sun, F.-F. Pan, Triyanti, M. Albrecht, G. Raabe, *Eur. J. Org. Chem.* **2013**, *2013*, 7922-7932.
136. P. D. Beer, P. K. Hopkins, J. D. McKinney, *Chem. Commun.* **1999**, 1253-1254.
137. J. Romański, P. Piątek, *J. Org. Chem.* **2013**, *78*, 4341-4347.
138. J. T. Davis, P. A. Gale, R. Quesada, *Chem. Soc. Rev.* **2020**, *49*, 6056-6086.
139. X. Wu, E. N. W. Howe, P. A. Gale, *Acc. Chem. Res.* **2018**, *51*, 1870-1879.
140. L. E. Bickerton, A. Docker, A. J. Sterling, H. Kuhn, F. Duarte, P. D. Beer, M. J. Langton, *Chem. Eur. J.* **2021**, *27*, 11738-11745.
141. A. Barba-Bon, M. Nilam, A. Hennig, *ChemBioChem* **2020**, *21*, 886-910.
142. A. V. Koulov, J. M. Mahoney, B. D. Smith, *Org. Biomol. Chem.* **2003**, *1*, 27-29.
143. I.-W. Park, J. Yoo, B. Kim, S. Adhikari, S. K. Kim, Y. Yeon, C. J. E. Haynes, J. L. Sutton, C. C. Tong, V. M. Lynch, J. L. Sessler, P. A. Gale, C.-H. Lee, *Chem. Eur. J.* **2012**, *18*, 2514-2523.
144. J. H. Lee, J. H. Lee, Y. R. Choi, P. Kang, M.-G. Choi, K.-S. Jeong, *J. Org. Chem.* **2014**, *79*, 6403-6409.
145. C. J. Bruns, J. F. Stoddart, **2016**.
146. J. F. Stoddart, *Angew. Chem. Int. Ed.* **2017**, *56*, 11094-11125.
147. J.-P. Sauvage, *Angew. Chem. Int. Ed.* **2017**, *56*, 11080-11093.
148. B. L. Feringa, *Angew. Chem. Int. Ed.* **2017**, *56*, 11060-11078.
149. H. Y. Au-Yeung, Y. Deng, *Chem. Sci.* **2022**, *13*, 3315-3334.
150. N. Hoyas Pérez, J. E. M. Lewis, *Org. Biomol. Chem.* **2020**, *18*, 6757-6780.
151. E. Wasserman, *J. Am. Chem. Soc.* **1960**, *82*, 4433-4434.
152. J. Guilhem, C. Pascard, J. P. Sauvage, J. Weiss, *J. Am. Chem. Soc.* **1988**, *110*, 8711-8713.
153. C. O. Dietrich-Buchecker, C. Hemmert, A. K. Khemiss, J. P. Sauvage, *J. Am. Chem. Soc.* **1990**, *112*, 8002-8008.
154. F. Bitsch, C. O. Dietrich-Buchecker, A. K. Khemiss, J. P. Sauvage, A. Van Dorsselaer, *J. Am. Chem. Soc.* **1991**, *113*, 4023-4025.
155. C. Wu, P. R. Lecavalier, Y. X. Shen, H. W. Gibson, *Chem. Mater.* **1991**, *3*, 569-572.
156. J. Frey, T. Kraus, V. Heitz, J.-P. Sauvage, *Chem. Commun.* **2005**, 5310-5312.
157. Z. Xue, M. F. Mayer, *J. Am. Chem. Soc.* **2010**, *132*, 3274-3276.
158. J.-P. Collin, F. Durola, J. Frey, V. Heitz, F. Reviriego, J.-P. Sauvage, Y. Trolez, K. Rissanen, *J. Am. Chem. Soc.* **2010**, *132*, 6840-6850.
159. J. E. Beves, B. A. Blight, C. J. Campbell, D. A. Leigh, R. T. McBurney, *Angew. Chem. Int. Ed.* **2011**, *50*, 9260-9327.
160. V. Aucagne, K. D. Hänni, D. A. Leigh, P. J. Lusby, D. B. Walker, *J. Am. Chem. Soc.* **2006**, *128*, 2186-2187.
161. J. D. Crowley, K. D. Hänni, A.-L. Lee, D. A. Leigh, *J. Am. Chem. Soc.* **2007**, *129*, 12092-12093.
162. S. M. Goldup, D. A. Leigh, R. T. McBurney, P. R. McGonigal, A. Plant, *Chem. Sci.* **2010**, *1*, 383-386.
163. S. Hoekman, M. O. Kitching, D. A. Leigh, M. Papmeyer, D. Roke, *J. Am. Chem. Soc.* **2015**, *137*, 7656-7659.
164. S. Saito, E. Takahashi, K. Nakazono, *Org. Lett.* **2006**, *8*, 5133-5136.
165. G. M. Hübner, J. Gläser, C. Seel, F. Vögtle, *Angew. Chem. Int. Ed.* **1999**, *38*, 383-386.
166. J. A. Wisner, P. D. Beer, M. G. B. Drew, M. R. Sambrook, *J. Am. Chem. Soc.* **2002**, *124*, 12469-12476.

167. M. R. Sambrook, P. D. Beer, J. A. Wisner, R. L. Paul, A. R. Cowley, *J. Am. Chem. Soc.* **2004**, *126*, 15364-15365.
168. M. D. Lankshear, N. H. Evans, S. R. Bayly, P. D. Beer, *Chem. Eur. J.* **2007**, *13*, 3861-3870.
169. K.-Y. Ng, V. Felix, S. M. Santos, N. H. Rees, P. D. Beer, *Chem. Commun.* **2008**, 1281-1283.
170. T. A. Barendt, L. Ferreira, I. Marques, V. Félix, P. D. Beer, *J. Am. Chem. Soc.* **2017**, *139*, 9026-9037.
171. S. R. Bayly, T. M. Gray, M. J. Chmielewski, J. J. Davis, P. D. Beer, *Chem. Commun.* **2007**, 2234-2236.
172. M. R. Sambrook, P. D. Beer, M. D. Lankshear, R. F. Ludlow, J. A. Wisner, *Org. Biomol. Chem.* **2006**, *4*, 1529-1538.
173. T. A. Barendt, I. Rašović, M. A. Lebedeva, G. A. Farrow, A. Auty, D. Chekulaev, I. V. Sazanovich, J. A. Weinstein, K. Porfyrakis, P. D. Beer, *J. Am. Chem. Soc.* **2018**, *140*, 1924-1936.
174. N. L. Kilah, M. D. Wise, C. J. Serpell, A. L. Thompson, N. G. White, K. E. Christensen, P. D. Beer, *J. Am. Chem. Soc.* **2010**, *132*, 11893-11895.
175. M. J. Langton, L. C. Duckworth, P. D. Beer, *Chem. Commun.* **2013**, *49*, 8608-8610.
176. M. J. Langton, P. D. Beer, *Chem. Commun.* **2014**, *50*, 8124-8127.
177. K. M. Bąk, B. Trzaskowski, M. J. Chmielewski, *Chem. Sci.* **2024**, *15*, 1796-1809.
178. B. Huang, S. M. Santos, V. Felix, P. D. Beer, *Chem. Commun.* **2008**, 4610-4612.
179. Y. Li, K. M. Mullen, T. D. W. Claridge, P. J. Costa, V. Felix, P. D. Beer, *Chem. Commun.* **2009**, 7134-7136.
180. M. J. Langton, O. A. Blackburn, T. Lang, S. Faulkner, P. D. Beer, *Angew. Chem. Int. Ed.* **2014**, *53*, 11463-11466.
181. G. Turner, A. Docker, P. D. Beer, *Dalton Trans.* **2021**, *50*, 12800-12805.
182. J. Y. C. Lim, I. Marques, V. Félix, P. D. Beer, *Angew. Chem. Int. Ed.* **2018**, *57*, 584-588.
183. J. E. M. Lewis, M. Galli, S. M. Goldup, *Chem. Commun.* **2017**, *53*, 298-312.
184. K. M. Bąk, K. Porfyrakis, J. J. Davis, P. D. Beer, *Mater. Chem. Front.* **2020**, *4*, 1052-1073.
185. J. T. Wilmore, P. D. Beer, *Adv. Mater.* **2024**, *36*, 2309098.
186. M. Cirulli, A. Kaur, J. E. M. Lewis, Z. Zhang, J. A. Kitchen, S. M. Goldup, M. M. Roessler, *J. Am. Chem. Soc.* **2019**, *141*, 879-889.
187. G. Baggi, S. J. Loeb, *Angew. Chem. Int. Ed.* **2016**, *55*, 12533-12537.
188. M. Denis, J. Pancholi, K. Jobe, M. Watkinson, S. M. Goldup, *Angew. Chem. Int. Ed.* **2018**, *57*, 5310-5314.
189. T. Shukla, A. K. Dwivedi, R. Arumugaperumal, C.-M. Lin, S.-Y. Chen, H.-C. Lin, *Dyes Pigm.* **2016**, *131*, 49-59.
190. K. Hiratani, M. Kaneyama, Y. Nagawa, E. Koyama, M. Kanesato, *J. Am. Chem. Soc.* **2004**, *126*, 13568-13569.
191. S.-M. Chan, F.-K. Tang, C.-S. Kwan, C.-Y. Lam, S. C. K. Hau, K. C.-F. Leung, *Mater. Chem. Front.* **2019**, *3*, 2388-2396.
192. A. Brown, T. Lang, K. M. Mullen, P. D. Beer, *Org. Biomol. Chem.* **2017**, *15*, 4587-4594.
193. M. J. Langton, P. D. Beer, *Chem. Eur. J.* **2012**, *18*, 14406-14412.
194. L. M. Hancock, E. Marchi, P. Ceroni, P. D. Beer, *Chem. Eur. J.* **2012**, *18*, 11277-11283.
195. M. J. Langton, I. Marques, S. W. Robinson, V. Félix, P. D. Beer, *Chem. Eur. J.* **2016**, *22*, 185-192.
196. R. C. Knighton, S. Dapin, P. D. Beer, *Chem. Eur. J.* **2020**, *26*, 5288-5296.
197. B. R. Mullaney, A. L. Thompson, P. D. Beer, *Angew. Chem. Int. Ed.* **2014**, *53*, 11458-11462.
198. M. J. Langton, Y. Xiong, P. D. Beer, *Chem. Eur. J.* **2015**, *21*, 18910-18914.
199. A. Caballero, F. Zapata, N. G. White, P. J. Costa, V. Félix, P. D. Beer, *Angew. Chem. Int. Ed.* **2012**, *51*, 1876-1880.
200. J. M. Mercurio, A. Caballero, J. Cookson, P. D. Beer, *RSC Adv.* **2015**, *20*, 9298-9306.
201. J. Y. C. Lim, I. Marques, V. Félix, P. D. Beer, *Chem. Commun.* **2018**, *54*, 10851-10854.
202. A. Brown, M. J. Langton, N. L. Kilah, A. L. Thompson, P. D. Beer, *Chem. Eur. J.* **2015**, *21*, 17664-17675.

203. C. Allain, S. Faulkner, *Future Med. Chem.* **2010**, *2*, 339-350.
204. T. A. Barendt, A. Docker, I. Marques, V. Félix, P. D. Beer, *Angew. Chem. Int. Ed.* **2016**, *55*, 11069-11076.
205. R. Arumugaperumal, V. Srinivasadesikan, M. V. Ramakrishnam Raju, M.-C. Lin, T. Shukla, R. Singh, H.-C. Lin, *ACS Appl. Mater. Interfaces* **2015**, *7*, 26491-26503.
206. R. Arumugaperumal, V. Parthiban, T. Shukla, R. Putikam, R. Singh, S.-P. Wu, M.-C. Lin, H.-C. Lin, *Sens. Actuators, B* **2018**, *270*, 382-395.
207. R. C. Knighton, P. D. Beer, *Chem. Commun.* **2014**, *50*, 1540-1542.
208. A. Brown, K. M. Mennie, O. Mason, N. G. White, P. D. Beer, *Dalton Trans.* **2017**, *46*, 13376-13385.
209. M. J. Deetz, R. Shukla, B. D. Smith, *Tetrahedron* **2002**, *58*, 799-805.
210. J. R. Romero, G. Aragay, P. Ballester, *Chem. Sci.* **2017**, *8*, 491-498.
211. M. Denis, L. Qin, P. Turner, K. A. Jolliffe, S. M. Goldup, *Angew. Chem. Int. Ed.* **2018**, *57*, 5315-5319.
212. D.-H. Li, B. D. Smith, *J. Org. Chem.* **2019**, *84*, 2808-2816.
213. A. Arun, A. Docker, H. Min Tay, P. D. Beer, *Chem. Eur. J.* **2023**, *29*, e202301446.
214. V. K. Munasinghe, J. Pancholi, D. Manawadu, Z. Zhang, P. D. Beer, *Chem. Eur. J.* **2022**, *28*, e202201209.
215. G. Martin, L. Rentsch, M. Höck, M. Bertau, *Energy Storage Mater.* **2017**, *6*, 171-179.

CHAPTER 2

Alkali Metal Cation Template-Directed Synthesis of Interlocked Architectures for Ion-Pair Recognition

Chapter 2: Alkali Metal Cation Template-Directed Synthesis of Interlocked Architectures for Ion-Pair Recognition

2.1 Introduction

The design of heteroditopic host systems capable of strong and selective recognition of ion-pairs has emerged as an important research focus within the field of supramolecular chemistry. By exploiting the positive cooperativity associated with binding oppositely charged species, ion-pair receptors typically exhibit superior binding properties over monotopic cation/anion receptors.[1-5] The favourable affinity and selectivity profiles displayed by heteroditopic ion-pair receptors have enabled their use in a myriad of applications, including salt extraction/solubilisation,[6-16] membrane transport[17-18] and the recognition of biologically-relevant zwitterions, as discussed in **Section 1.3**.[19-20]

The pre-organised and solvent-shielded cavities of MIMs present unique opportunities to design three dimensional binding sites, which through non-covalent donor/acceptor group decoration can be tuned to achieve size and shape complementarity towards a target guest.[21-28] The resulting improvements in binding affinity and selectivity over non-interlocked receptor analogues has motivated the construction of numerous MIM-based cation[29-33] and anion[34-39] receptors over the years.

In contrast, the design of mechanically interlocked heteroditopic receptors remains an under-explored area, with the handful of reported examples typically limited to [2]rotaxane topologies discussed in **Section 1.4.2.3**.[40-45] The scarcity of MIM-based heteroditopic receptors is attributed to the inherent synthetic difficulties associated with the preparation of complex interlocked scaffolds possessing multiple binding sites in appreciable yields. Catenane-based

architectures are a particular challenge due to their topologically complex nature, which necessitates at least two macrocycle-forming steps to obtain even the simplest [2]catenane topology. Despite these difficulties, the highly pre-organised binding cavities and unique modes of co-conformational dynamism available to catenanes make them highly desirable scaffolds for the development of novel ion-pair receptors and sensors.

In the following sections, the concept of cooperative guest binding will be introduced in the context of ion-pair recognition, highlighting commonly used methods to analyse and quantitatively determine the degree of cooperativity in the overall ion-pair binding event. The use of catenanes in ion-pair recognition is discussed, followed by a potential cation template-directed strategy for the preparation of catenane heteroditopic receptors.

2.1.1 Cooperativity in Ion-Pair Receptors

Cooperativity plays a significant role in ion-pair binding systems due to the presence of multiple binding sites. In general, cooperativity results from the coupling of two or more interactions such that the overall observed result is different from what would be expected if the interactions occurred in isolation. Positive or negative cooperativity can occur, depending on whether the interactions favour or disfavour each other.[46] In the case of ion-pair receptors, it is generally accepted that the coupling of cation and anion binding to the receptor typically results in positive cooperativity due to favourable electrostatic, and sometimes conformational, effects. However, the quantification of cooperativity, and in some cases even an accurate determination of ion-pair binding affinities, is challenging due to the multitude of contributing binding equilibria that have to be considered (**Figure 2.1a**). The receptor may bind to the cation or anion alone, represented by K_1 and K_2 respectively, or to both ions simultaneously as an ion-pair (K_3). Formation of the cation-bound receptor complex may cooperatively enhance the receptor's affinity for the anion (K_4) and vice versa (K_5). In addition, external ion-pairing in

solution (K_{IP}) may compete with ion-pair binding to the receptor, resulting in precipitation of the salt. This is of particular concern in non-polar solvents where ion-pairing effects are stronger due to reduced solvation of the individual ions.

One of the most comprehensive studies of cooperativity in ion-pair binding was undertaken by Flood and co-workers (**Figure 2.1b**). Using a series of semi-flexible aryl-triazole-ether macrocycles as model ion-pair receptors, the authors conducted extensive experimental and theoretical investigations to determine the overall cooperativity factor of ion-pair binding (α, where $\alpha = \beta_{overall}/K_{cation}K_{anion}$) and to delineate the respective contributions of electrostatic and allosteric effects for various alkali metal salts. Their findings indicated that electrostatic effects are the major contributor to positive cooperativity in these systems, accounting for 70-80% of the overall cooperativity, but allosteric effects are less sensitive to increases in solvent polarity. Electrostatic cooperativity was more pronounced for smaller ions if the ions were allowed to make direct contact with each other. On the basis of this analysis, the authors suggest that semi-flexible receptors are ideal for maximising electrostatic cooperativity.[4]

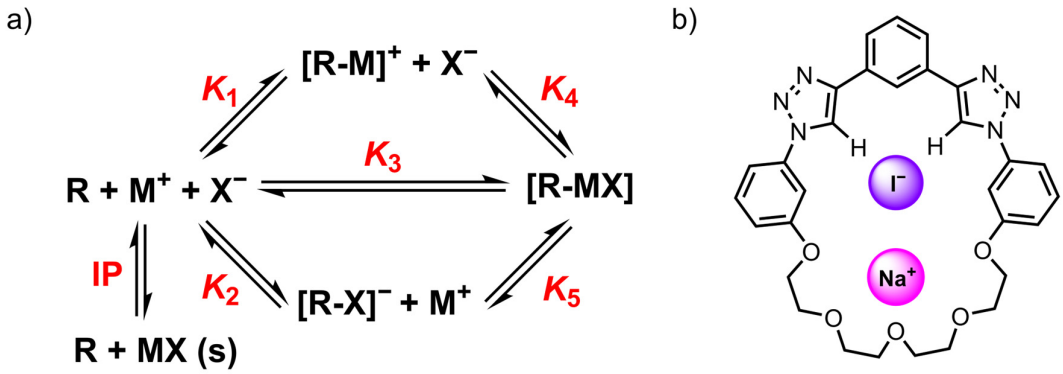


Figure 2.1. *(a) Schematic showing possible equilibria associated with ion-pair binding; (b) Flood's heteroditopic macrocycle used to study cooperativity in ion-pair binding.*

Although the ability to quantitatively analyse ion-pair binding equilibria in such detail is impressive, the experimental and computational effort required was substantial and

potentially unfeasible for complex or synthetically demanding ion-pair receptors. A less rigorous but nonetheless useful measure of cooperativity can be obtained by determining the *apparent* cation or anion association constants ($K_{app\text{-}cation}$ or $K_{app\text{-}anion}$) of the receptor-counterion complex, which is typically generated *in situ* by pre-complexing the receptor with a stoichiometric amount of the desired counterion (**Figure 2.2a**). Comparing the determined value of K_{app} to the corresponding ion association constant of the free receptor (K_{cation} or K_{anion}) would therefore serve as an indication of the extent to which the receptor's binding affinity for a given ion is enhanced in the presence of the co-bound counterion.[11, 47] A key assumption of this approach is that the formation of the receptor-counterion complex is quantitative, as the presence of uncomplexed receptor can promote competing equilibria that will substantially complicate measurement of K_{app}. Therefore, the guest ion that binds more strongly to the free receptor, usually the cation, is typically chosen for pre-complexation to facilitate the determination of $K_{app\text{-}anion}$.

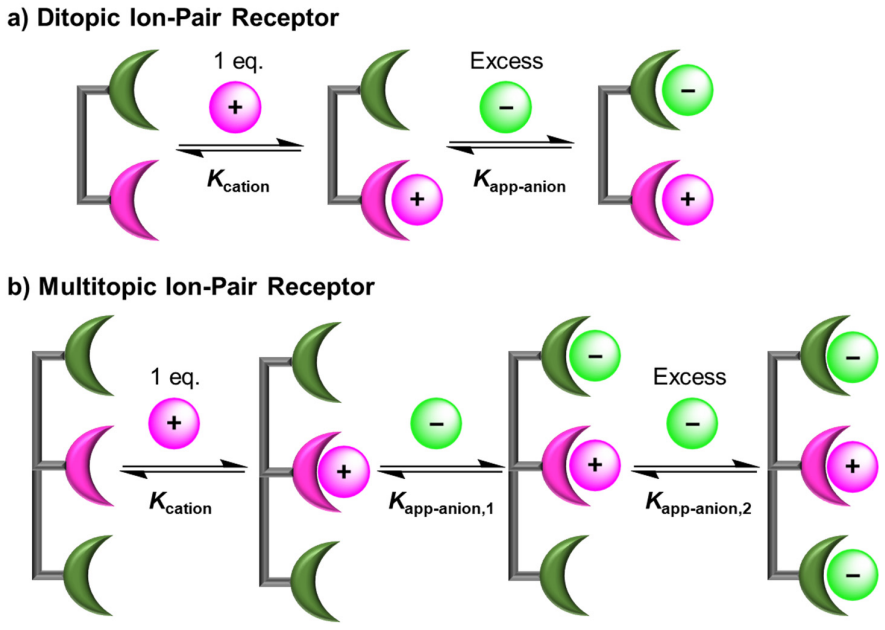


Figure 2.2. *Schematic showing the determination of apparent anion association constants in ion-pair receptors. a) A ditopic receptor with one associated K_{app} value; b) A multitopic receptor with stepwise K_{app} values associated with consecutive binding processes.*

In the case of multitopic receptors possessing more than one cation or anion binding site, the determination of $K_{app\text{-}anion}$ may be further complicated by multiple binding events that lead to the formation of higher-order complexes upon addition of the excess guest ion (**Figure 2.2b**). While multiple ion binding events can occur in any receptor that contains more than one binding site for the ion in question, this possibility is markedly increased in ion-pair receptors due to the electrostatic cooperativity between the cation and anion binding processes. In such situations, 1:2 host-guest binding models have to be considered during the determination of K_{app}. As noted in a study by Thordarson and co-workers, there are four 1:2 host-guest binding models typically used to analyse ^{1}H NMR titration data.[48] These models differ in their assumptions regarding: the relationship between the first and second binding constants (K_1 and K_2 respectively), and the chemical shifts induced by the formation of a 1:1 and 1:2 complex ($\Delta\delta_1$ and $\Delta\delta_2$ respectively), as summarised in **Table 2.1**.

Table 2.1. *Properties of the different 1:1 and 1:2 host-guest binding models*[a]

Binding model	**Relationship between K_1 and K_2**	**Relationship between $\Delta\delta_1$ and $\Delta\delta_2$**	**No. of fitted parameters**
1:1	N/A[b]	N/A[b]	2
1:2 Statistical	$K_1 = 4K_2$	$\Delta\delta_1 = \Delta\delta_2$	2
1:2 Non-cooperative	$K_1 = 4K_2$	$\Delta\delta_1 \neq \Delta\delta_2$	3
1:2 Additive	$K_1 \neq 4K_2$	$\Delta\delta_1 = \Delta\delta_2$	3
1:2 Full	$K_1 \neq 4K_2$	$\Delta\delta_1 \neq \Delta\delta_2$	4

[a] K_1 and K_2 denote the stepwise binding constants; $\Delta\delta_1$ and $\Delta\delta_2$ denote the movement of the NMR signal of interest upon the formation of a 1:1 and 1:2 complex respectively. [b] Only K_1 and $\Delta\delta_1$ are relevant in the 1:1 binding model.

To determine which model best describes the data, the authors compared the co-variance values (cov_{fit}) obtained from fitting the binding isotherms to each of the four 1:2 models to that of the classical 1:1 host-guest binding model, with a lower cov_{fit} value indicating a better fit to the data. However, as noted by the authors, models with a higher number of fitted parameters can give rise to an artificially better quality of fit. Therefore, both the quality of fit

and the number of fitted parameters have to be considered in determining the most appropriate binding model. The authors proposed that the cov_{fit} value of a model with a higher number of fitted parameters should be at least 3 times lower than that of a simpler model for it to be considered a genuinely better fit to the titration data.

2.1.2 Catenane-based Heteroditopic Ion-Pair Receptors

To the best of our knowledge, the sole example of a heteroditopic [2]catenane capable of ion-pair recognition was reported by Beer and co-workers in 2021.[49] The hetero[2]catenane was synthesised via a sodium cation template-directed strategy which exploits the convergent complexation of a sodium ion by a calix[4]diquinone-functionalised macrocycle and an acyclic pyridyl-*N*-oxide bis(pentafluorophenyl ester) to direct pseudo-[2]rotaxane formation (**Figure 2.3a**). An amide condensation reaction with a bis(amine) afforded the target catenane in 7% yield, which was isolated as the NaCl ion-pair adduct. Evidence for the ion-pair binding capabilities of the catenane was obtained via solid-state crystallographic studies which reveals

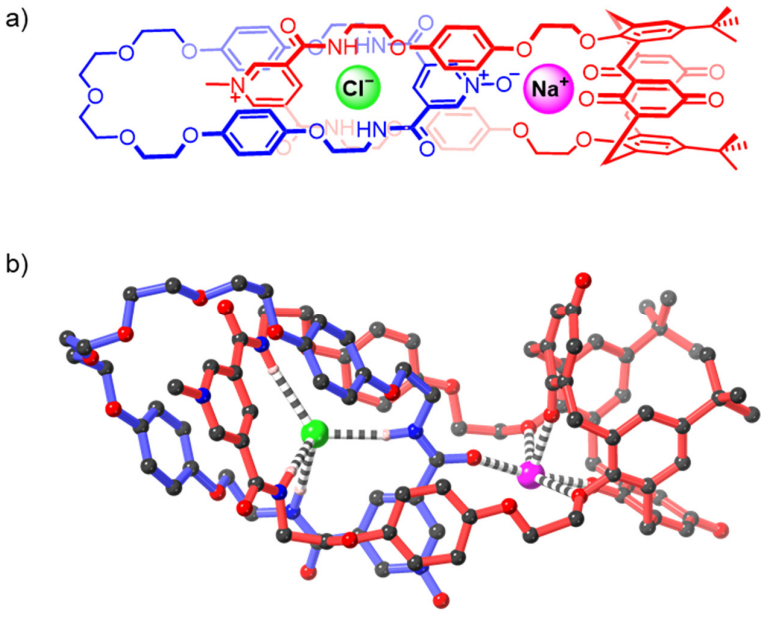


Figure 2.3. *a) Chemical structure of a heteroditopic [2]catenane for ion-pair recognition; b) SCXRD structure of the [2]catenane bound to NaCl*

the [2]catenane bound to NaCl as a host-separated ion-pair (**Figure 2.3b**). Unfortunately, the low yield of the compound precluded detailed solution-state binding studies to elucidate the ion-pair binding properties of the catenane.

2.1.3 Alkali Metal Template-Directed Synthesis of MIMs

Despite the low toxicity and relatively inexpensive nature of alkali metal cations, their use in metal template-directed synthesis of MIMs has remained relatively underexplored, presumably due to the lower stability and less predictable geometries of alkali metal complexes. While the above heteroditopic [2]catenane synthesis demonstrates the potential efficacy of using alkali metal cations to direct the formation of MIMs, this strategy requires the multistep preparation of synthetically complex precursors, in particular the strapped calix[4]diquinone macrocycle.

A notable example of using alkali metal ions as a passive template in MIM synthesis was reported by Chiu and co-workers in 2013, who showed that a sodium cation can direct the orthogonal arrangement of two di(ethylene glycol) chains to facilitate the formation of a [2]catenane following cyclisation via an imine condensation (**Figure 2.4**).[50] The same group subsequently demonstrated that [2]catenanes of varying macrocycle size could be prepared using different alkali metal cation templates, highlighting the importance of ensuring size complementarity between the metal template and the target interlocked structure.[51]

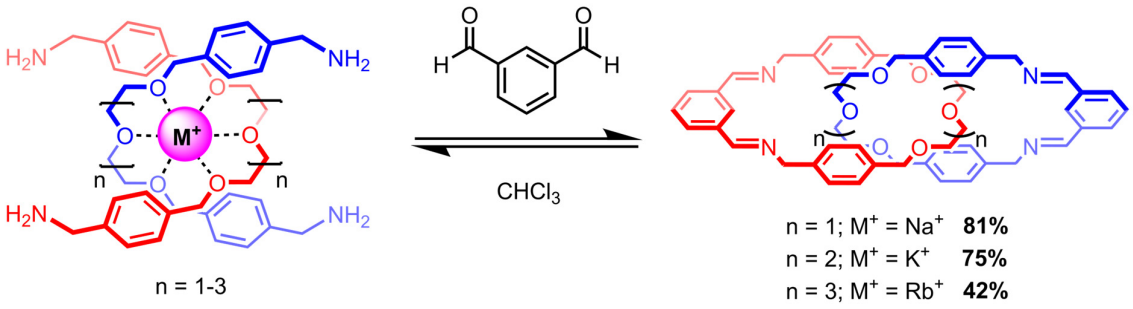


Figure 2.4. *Chiu's alkali metal template-directed synthesis of homo[2]catenanes.*

2.1.4 Project Aims

This chapter aims to develop an alkali metal template-directed synthetic strategy for the preparation of neutral heteroditopic catenanes and rotaxanes for ion-pair recognition (**Figure 2.5**). The target host designs consist of oligo(ethylene glycol) cation recognition units and bis(iodotriazole)-based halogen bonding donors for anion binding.

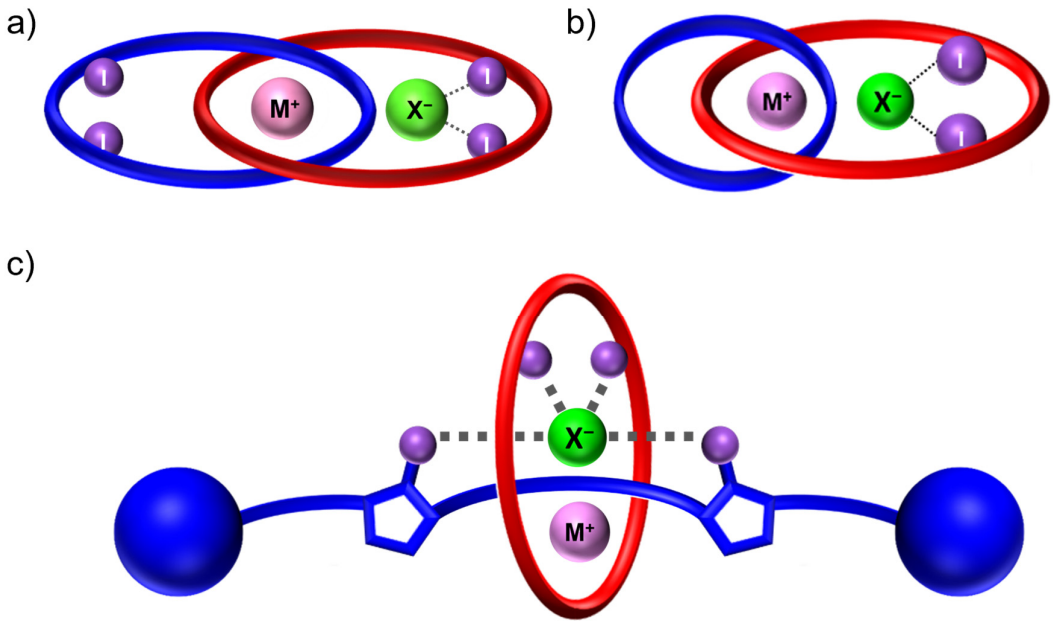


Figure 2.5. *Cartoon representations of the heteroditopic MIM-based receptors studied in this chapter: a) Homo[2]catenanes; b) Hetero[2]catenanes; c) [2]Rotaxanes. Pink spheres, green and purple spheres represent cationic guests, anionic guests and iodine XB donors respectively.*

The cation, anion and ion-pair binding properties of the initially-prepared homo[2]catenane hosts (**Figure 2.5a**) were investigated via detailed ^{1}H NMR spectroscopic studies, which revealed positive cooperative ion-pair recognition behaviour in which XB-mediated halide recognition is enhanced by alkali metal cation pre-complexation. The postulated ion-pair binding modes were corroborated by single crystal X-ray diffraction studies. By modification of the cation binding site, a second-generation hetero[2]catenane was synthesised which displayed dramatically improved ion-pair binding affinities as well as

notable sodium over potassium halide selectivity (**Figure 2.5b**). Solid-liquid extraction studies demonstrated the potential of the catenanes to function as salt extracting agents. The profound effects of topology on the ion-pair recognition behaviour of the interlocked hosts was elucidated through comparative binding studies conducted on a series of 'mechanical bond isomeric' [2]rotaxanes (**Figure 2.5c**).

2.2 Homo[2]catenanes for Ion-Pair Recognition

Inspired by Chiu's elegant use of alkali metal cation templates to direct the synthesis of functional interlocked topologies,[50-56] we exploited this approach to construct XB heteroditopic homo[2]catenane host systems for ion-pair binding. Conceivably, the target [2]catenanes could be prepared via the sodium cation-templated self-assembly of a pseudo-[2]rotaxane complex between an oligo(ethylene glycol)-functionalised XB macrocycle and a bis-azide, followed by a CuAAC-mediated cyclisation of the threaded bis-azide with a bis(iodoalkyne) to generate the second interlocked XB macrocycle (**Figure 2.6a**). The mechanical bond formation step would thereby simultaneously generate both cation and anion recognition sites. We envisaged that the homo[2]catenane products would be capable of cooperative alkali metal halide recognition, with the alkali metal cation bound via the interlocked cavity formed by the ethylene glycol groups of the macrocycles, while the halide anion would interact with the bis-iodotriazole XB donor groups (**Figure 2.6b**).

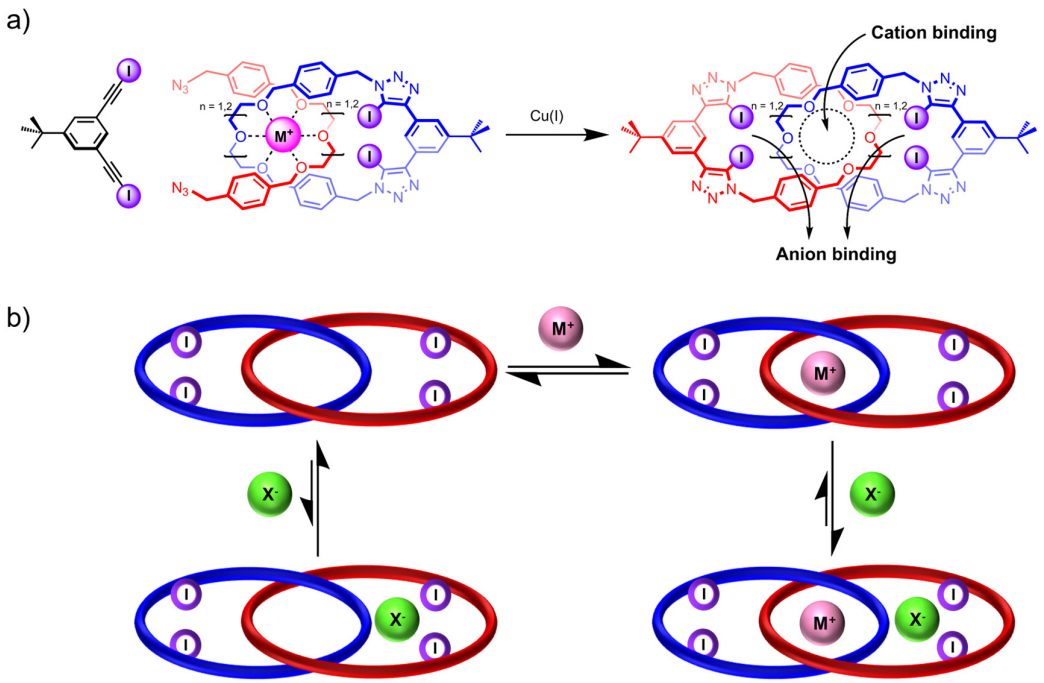
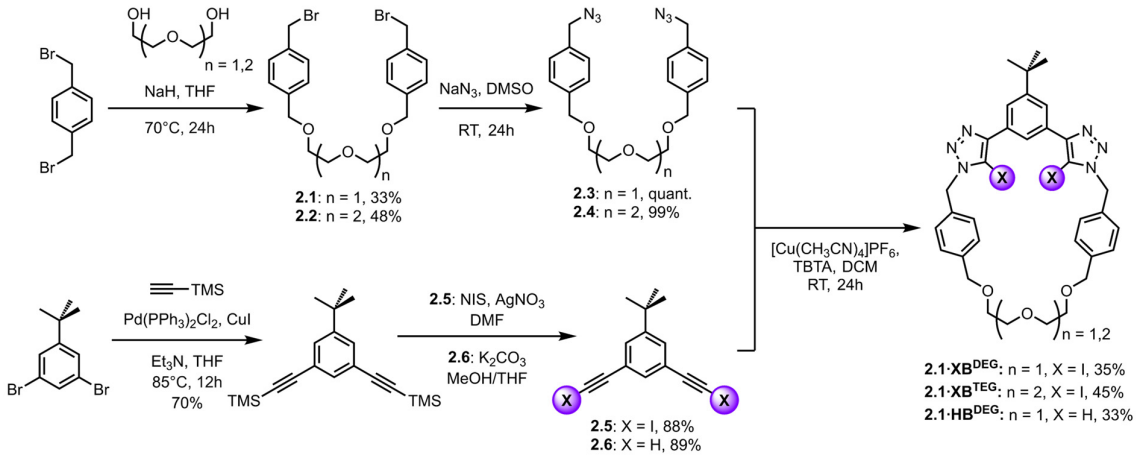


Figure 2.6. *a) Proposed alkali metal template-directed synthesis of heteroditopic [2]catenanes; b) Cartoon representation of cooperative alkali metal halide binding by catenane receptors.*

2.2.1 Synthesis and Characterisation

2.2.1.1 Synthesis of XB Macrocycles

To prepare the requisite oligo(ethylene glycol)-functionalised macrocycles **2.1·XB^{DEG}** and **2.1·XB^{TEG}**, di- and tri(ethylene glycol) were first alkylated with α,α'-dibromo-p-xylene in the presence of NaH in THF, affording dibromides **2.1** and **2.2** in 33% and 48% respective yields after purification by column chromatography. Quantitative azidation was achieved by stirring the dibromides with excess NaN_3 in DMSO, followed by aqueous work-up to give bis-azides **2.3** and **2.4**. A high-dilution CuAAC-mediated cyclisation between **2.3** or **2.4** and bis(iodo-alkyne) **2.5** in the presence of $[Cu(CH_3CN)_4]PF_6$ and TBTA in CH_2Cl_2 afforded XB macrocycles **2.1·XB^{DEG}** and **2.1·XB^{TEG}** in 35% and 45% yields respectively. An analogous HB macrocycle **2.1·HB^{DEG}** containing a bis(triazole) motif was synthesised in 33% yield via the reaction of **2.3** with bis(protoalkyne) **2.6** (**Scheme 2.1**).



Scheme 2.1. *Synthesis of XB macrocycles* ***2.1·XB^{DEG}*** *and* ***2.1·XB^{TEG}*** *and HB macrocycle* ***2.1·HB^{DEG}***.

2.2.1.2 Pseudo[2]rotaxane Studies

To confirm a sodium cation template could be used to assemble a pseudo[2]rotaxane topology, ^{1}H NMR spectra of XB macrocycle **2.1·XB^{DEG}** in the absence and presence of sodium tetrakis[3,5-bis(trifluoromethyl)phenyl]borate ($NaBAr^{F}$) and bis-azide **2.3** were recorded (**Figure 2.7**). Addition of 1 eq. $NaBAr^{F}$ to a solution of macrocycle **2.1·XB^{DEG}** in $CDCl_3$ led to notable perturbations in the proton resonances corresponding to H_g, H_h, H_i, which are proximal to the di(ethylene glycol) region of **2.1·XB^{DEG}**, indicating cation binding to the macrocycle. The subsequent addition of 1 eq. bis(azide) **3** to the mixture of **2.1·XB^{DEG}** and $NaBAr^{F}$ resulted in general upfield shifts of the proton resonances of **2.3**, with the largest changes ($\Delta\delta > 0.6$ ppm) occurring at the di(ethylene glycol) protons. This is consistent with the formation of an interpenetrated complex of **2.1·XB^{DEG}** and **2.3**, wherein the di(ethylene glycol) region of the bis-azide thread experiences increased shielding from the ring current of the macrocycle xylene spacers,[50] providing compelling evidence for the formation of the desired pseudo[2]rotaxane assembly. Similar indicative chemical shift perturbations were observed in the tri(ethylene glycol) proton resonances of TEG-based bis(azide) **2.4** in the presence of TEG-based XB macrocycle **2.1·XB^{TEG}** and $KBAr^{F}$.

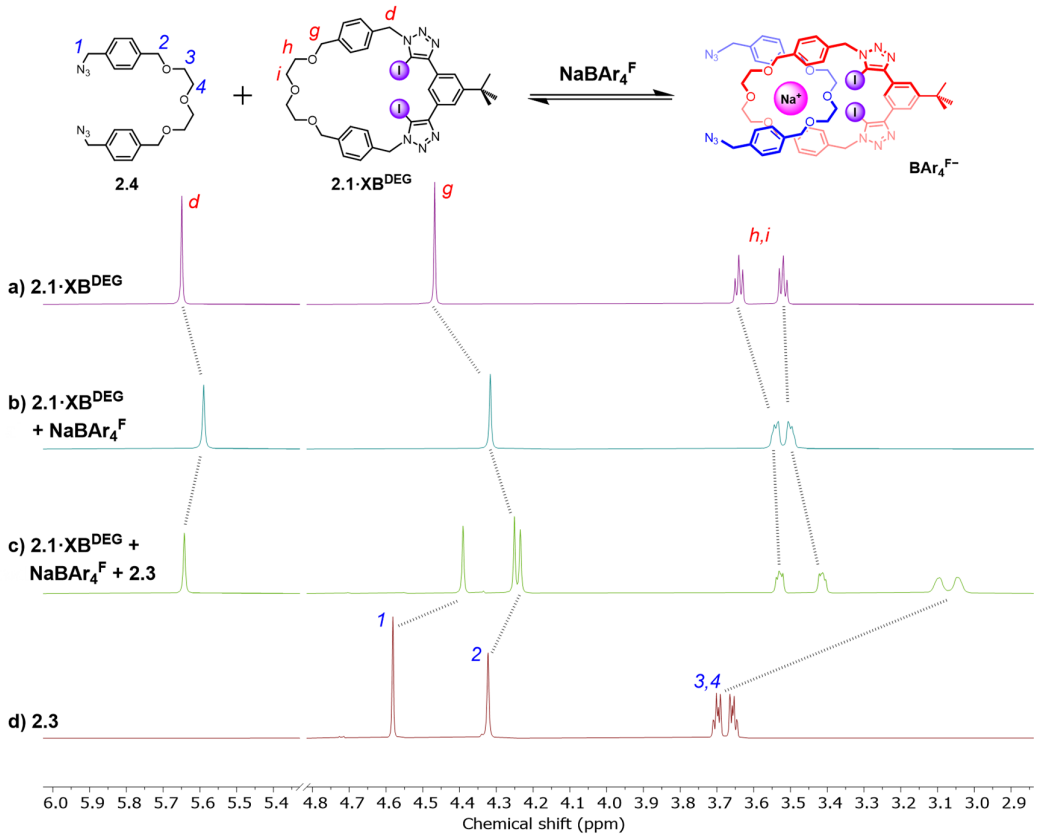
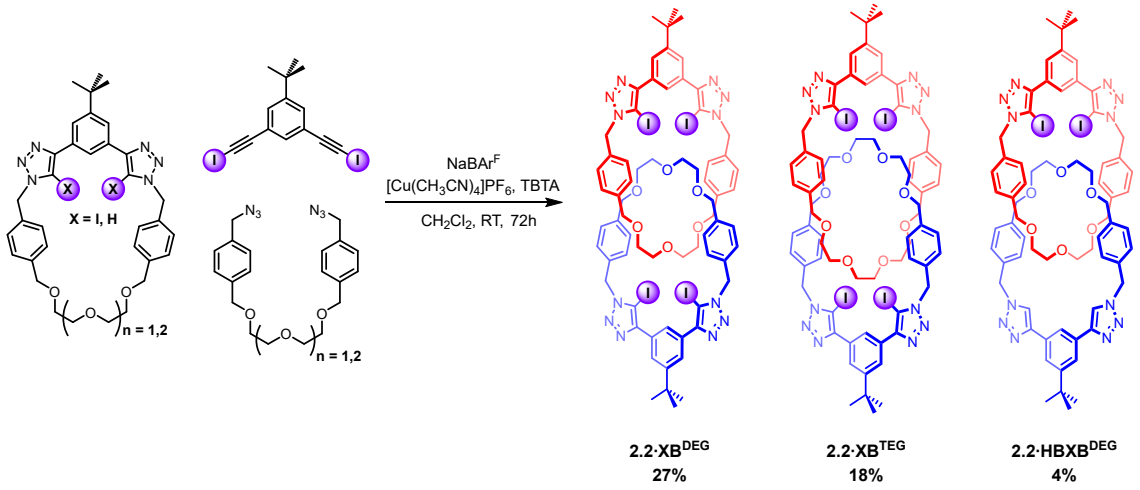


Figure 2.7. *Stacked ^{1}H NMR spectra of a)* ***2.1·XB^{DEG}****; b)* ***2.1·XB^{DEG}*** *+ 1 eq. NaBAr^F; c)* ***2.1·XB^{DEG}*** *+ 1 eq. NaBAr^F + 1 eq.* ***2.3****; d)* ***2.3***

2.2.1.3 Synthesis and Characterisation of Homo[2]Catenanes

Encouraged by the evidence of pseudo-[2]rotaxane formation, attention turned to the sodium cation template-directed synthesis of the target [2]catenanes (**Scheme 2.2**). In a typical reaction, an XB macrocycle and the corresponding bis-azide were stirred in CH_2Cl_2 in the presence of one equivalent of NaBAr^F for 30 minutes at room temperature to facilitate assembly of the interpenetrated pseudo-rotaxane complex, to which bis(iodo-alkyne) **2.5**, $[Cu(CH_3CN)_4]PF_6$ and TBTA were added. The reaction mixture was allowed to stir at room temperature overnight. After aqueous work-up with basic EDTA/NH_4OH and purification by preparative TLC, [2]catenanes **2.2·XB^{DEG}**, **2.2·XB^{TEG}** and **2.2·HBXB^{DEG}** were isolated in 27%, 18% and 4% yields respectively. Notably, the higher yield obtained for **2.2·XB^{DEG}** relative to

2.2·XB^{TEG} is in line with previous observations that Na^+ is a more suitable template for di(ethylene glycol) chains.[51] The lower yield of the hetero[2]catenane **2.2·HBXB^{DEG}** was likely due to the poor solubility of the Na^+-complexed HB macrocycle **2.1·HB^{DEG}** in CH_2Cl_2.



Scheme 2.2. *Synthesis of [2]catenanes via a sodium template-directed methodology.*

Comparing the ^{1}H NMR spectra of the [2]catenanes to that of their respective parent macrocycles reveals changes consistent with the formation of the mechanical bond, namely a splitting of the aryl spacer signals and upfield perturbations of the alkyl signals (**Figure 2.8**). In particular, the relatively large upfield perturbations of the poly(ethylene glycol) signals were attributed to the proximity of these methylene protons to the shielding ring current generated by the xylene spacers of the interlocked macrocycles.

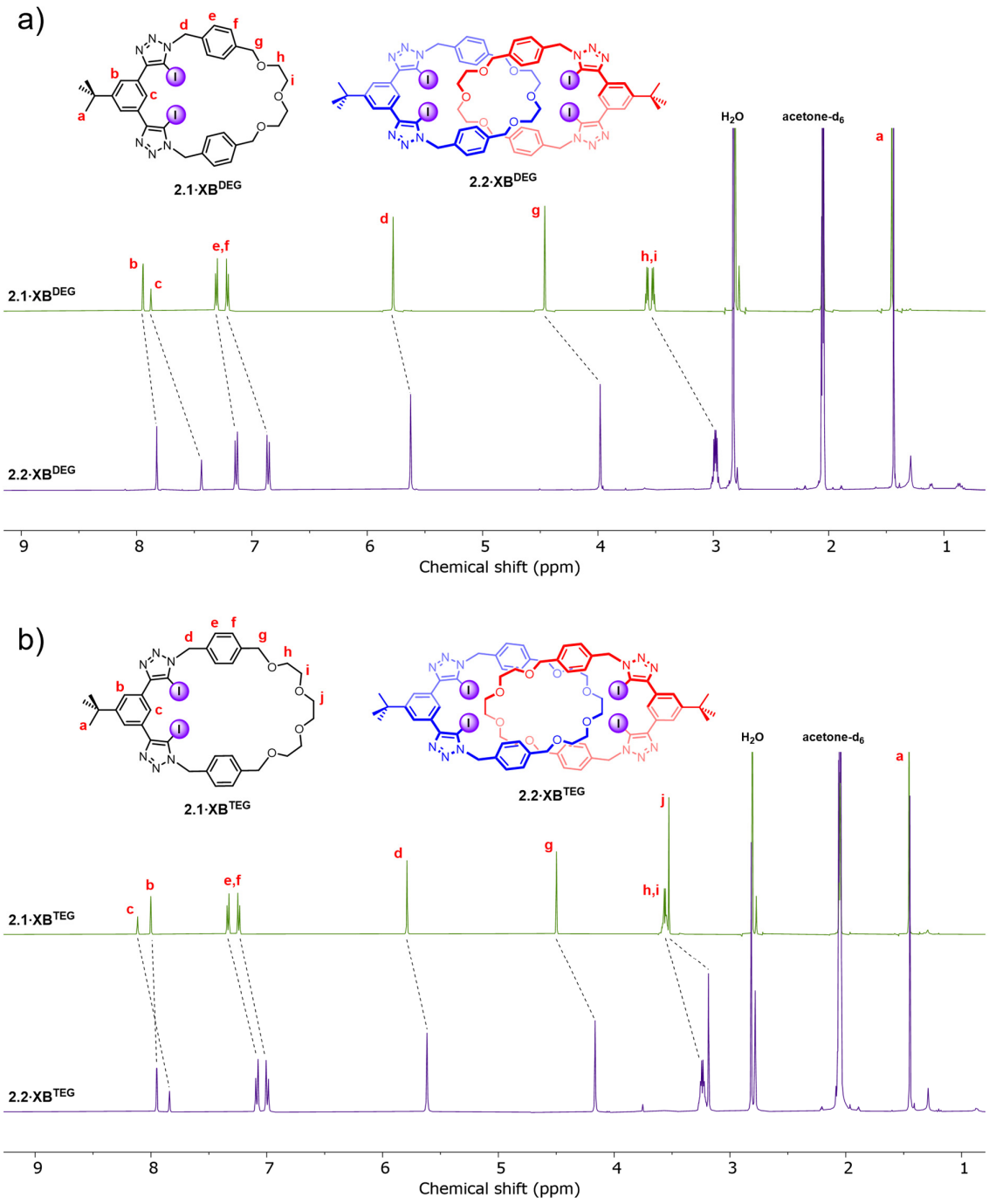


Figure 2.8. *Stacked ^{1}H NMR spectra of XB macrocycle (green) and [2]catenane (purple). a)* ***2.1·XB^{DEG}*** *and* ***2.2·XB^{DEG}****; b)* ***2.1·XB^{TEG}*** *and* ***2.2·XB^{TEG}****. (500 MHz, acetone-d$_6$, 298 K).*

To ascertain that the compounds isolated from the reactions were indeed the desired homo[2]catenanes instead of the topologically isomeric [2+2]macrocycles, which are expected to have similar ^{1}H NMR spectra and identical molecular ion peaks in ESI-MS, tandem mass spectrometry experiments were conducted on the two putative [2]catenanes (**Figure 2.9**). The [2]catenane would be expected to contain no or few peaks with *m/z* values between that of the parent macrocycle and the molecular ion peak of the [2]catenane as any bond cleavage resulting in ring-opening would cause the two interlocked rings to dissociate. When **2.2·XB^{DEG}** was subjected to a collision energy of 40 V, the only significant fragments detected in the range of interest (831 < *m/z* < 1662) had *m/z* 1506.20 and 1351.42, presumably due to the loss of I+N_2 moieties from one and two iodotriazole groups respectively. Notably, the bond breaking reactions that generate these fragments do not cause ring-opening of the macrocycle and is therefore consistent with the hypothesised [2]catenane topology. Peaks with *m/*z 1594.31 and 1439.36 were observed in the MS/MS spectrum of **2.2·XB^{TEG}**, likewise corresponding to sequential loss of I+N_2. For both compounds, an intense peak corresponding to a single parent macrocycle was observed, which likely arises from disassembly of the interlocked structure.

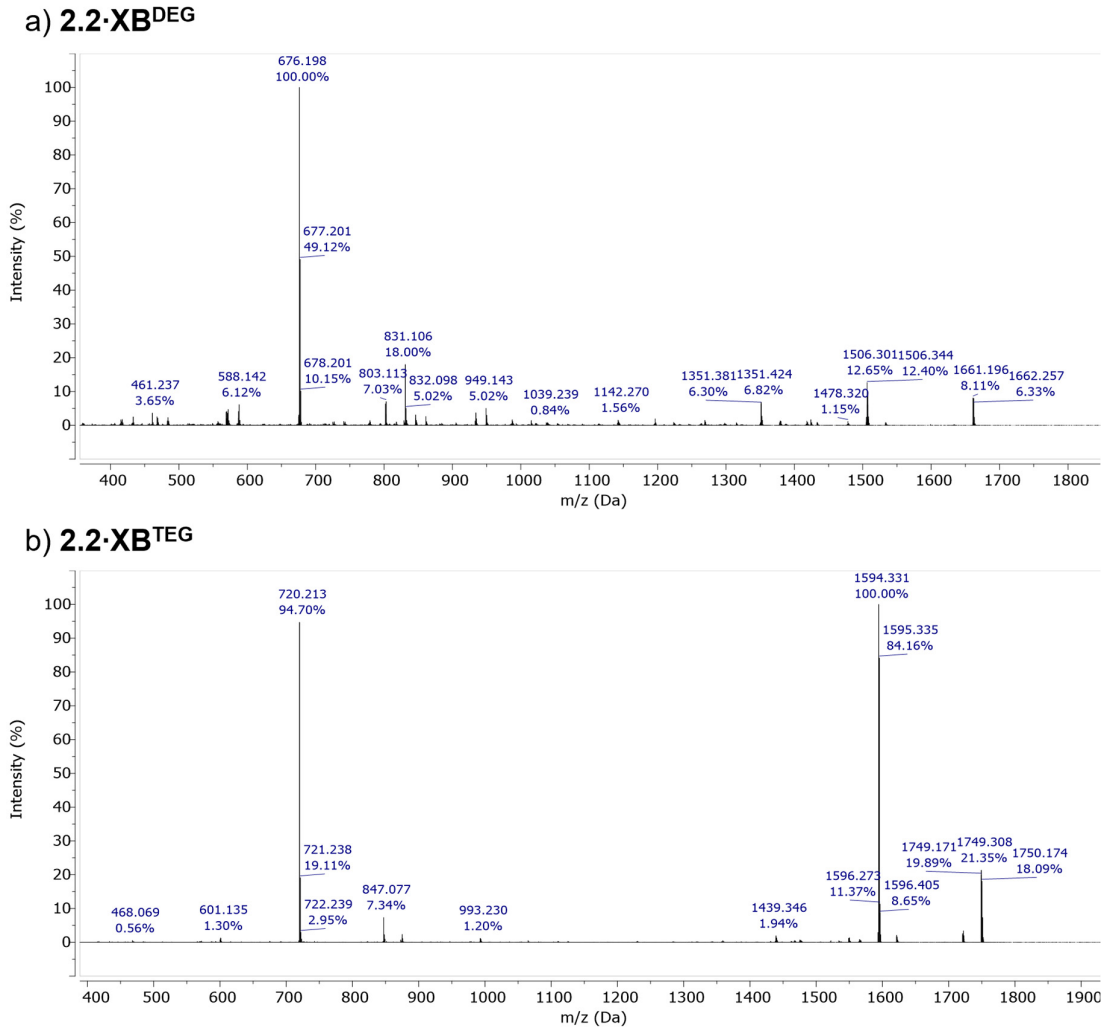


Figure 2.9. *High resolution tandem mass spectra of: a)* ***2.2·XB^{DEG}****; b)* ***2.2·X^{TEG}*** *(Xevo G2-S, collision energy: 40 V)*

Unequivocal evidence for the formation of an interlocked topology in **2.2·XB^{TEG}** was obtained by single crystal X-ray diffraction analysis (SCXRD). Crystals of **2.2·XB^{TEG}** suitable for analysis by SCXRD were obtained by slow evaporation of a solution of **2.2·XB^{TEG}** in 1:1 $CDCl_3/CD_3CN$. A structural solution obtained in the monoclinic space group *P*c and revealed the presence of [2]catenane units, confirming the interlocked topology of the compound (**Figure 2.10a**). An examination of the crystal packing revealed the presence of intermolecular halogen bonding interactions between the iodine donor atoms and triazole nitrogen atoms of

neighbouring [2]catenanes, giving rise to polymeric XB-stabilised chains running parallel to crystallographic *c* axis (**Figure 2.10b**).

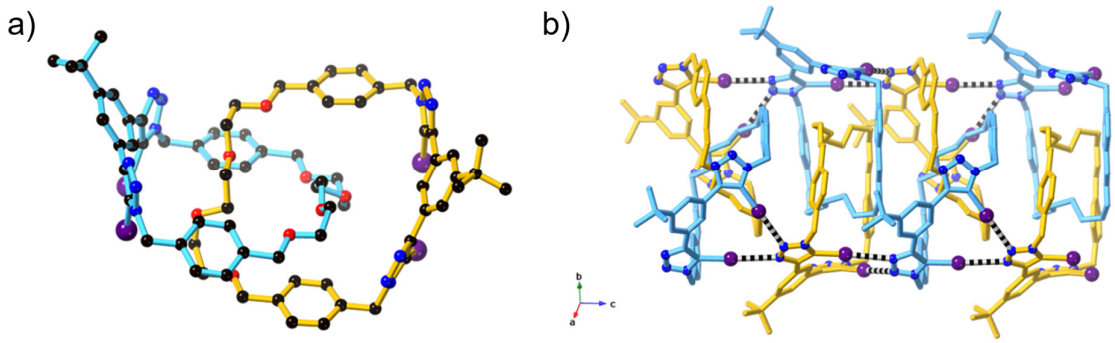


Figure 2.10. *Crystal structure of* ***2.2·XB^{TEG}****, showing: (a) a single [2]catenane unit, with atom colours are as follows: carbon (black), nitrogen (dark blue), oxygen (red), iodine (purple). (b) A stick model of the crystal packing, showing the network of intermolecular halogen bonding interactions between neighbouring [2]catenanes. Iodine and nitrogen atoms are highlighted in using purple and blue spheres respectively. Hydrogen atoms have been omitted for clarity.*

2.2.2 ^{1}H NMR Ion Binding Studies

2.2.2.1 Alkali Metal Cation Binding Studies

To establish the cation binding properties of the homo[2]catenanes **2.2·XB^{DEG}** and **2.2·XB^{TEG}**, ^{1}H NMR titration experiments were conducted by adding aliquots of NaBAr^{F} or KBAr^{F} to a 1 mM solution of the respective catenane in 1:1 $CDCl_3/CD_3CN$. The progressive addition of the cation led to perturbations in the resonances corresponding to the ethylene glycol protons, indicating that, as anticipated, alkali metal cation complexation occurs primarily via the polyether oxygen atoms (**Figure 2.11b).** Additional movements in proton resonances remote from the polyether signals, in particular upfield shifts of the internal benzene proton H_c, were ascribed to co-conformational changes occurring upon cation binding. Conceivably, cation binding might induce a rearrangement and structural rigidification of the polyether regions to form a suitable binding cavity (**Figure 2.11a**).

The movements of multiple proton signals proximal to the cation binding site were monitored and the resulting binding isotherms (**Figure 2.11c-d**) fitted to a global 1:1 host-guest stoichiometric binding model using Bindfit analysis[57] to determine the cation association constants (**Table 2.2**). The binding affinity of **2.2·XB^{TEG}** for both Na^+ and K^+ was found to be higher than that of **2.2·XB^{DEG}**, attributed to the larger number of oxygen donor atoms available for cation coordination in the tri(ethylene glycol) linkers of **2.2·XB^{TEG}**. The two [2]catenanes exhibit reversed preferences for metal cations, with **2.2·XB^{DEG}** having a >3-fold preference for Na^+ over K^+, while **2.2·XB^{TEG}** shows a >2-fold preference for K^+ over Na^+, the origin of which is presumably size complementarity between the shorter di(ethylene glycol) linker and the smaller Na^+ cation, as well as between the longer tri(ethylene glycol) linker and the larger K^+ cation.

Importantly, the parent macrocycles **2.1·XB^{DEG}** and **2.1·XB^{TEG}** showed negligible binding under identical solvent conditions, highlighting the pivotal role of the interlocked [2]catenane topology in enhancing cation affinity, presumably via a combination of providing a three-dimensional binding pocket for encapsulation of the cation as well as assisting in its desolvation.

Table 2.2. *Cation association constants (K_a/M^{-1}) for XB macrocycles and [2]catenanes determined by ^{1}H NMR titrations.*[a]

Cation	2.1·XB^{DEG}	2.1·XB^{TEG}	2.2·XB^{DEG}	2.2·XB^{TEG}
Na^+	N.B.[b]	N.B.	756	753
K^+	N.B.	N.B.	284	1734

[a]K_a values calculated using Bindfit with a 1:1 host-guest binding model. Errors are all <2%. All cations added as $BArF^-$ salts. Solvent = 1:1 $CDCl_3$/CD_3CN. T = 298 K. [Receptor] = 1.0 mM. [b]N.B. = No binding.

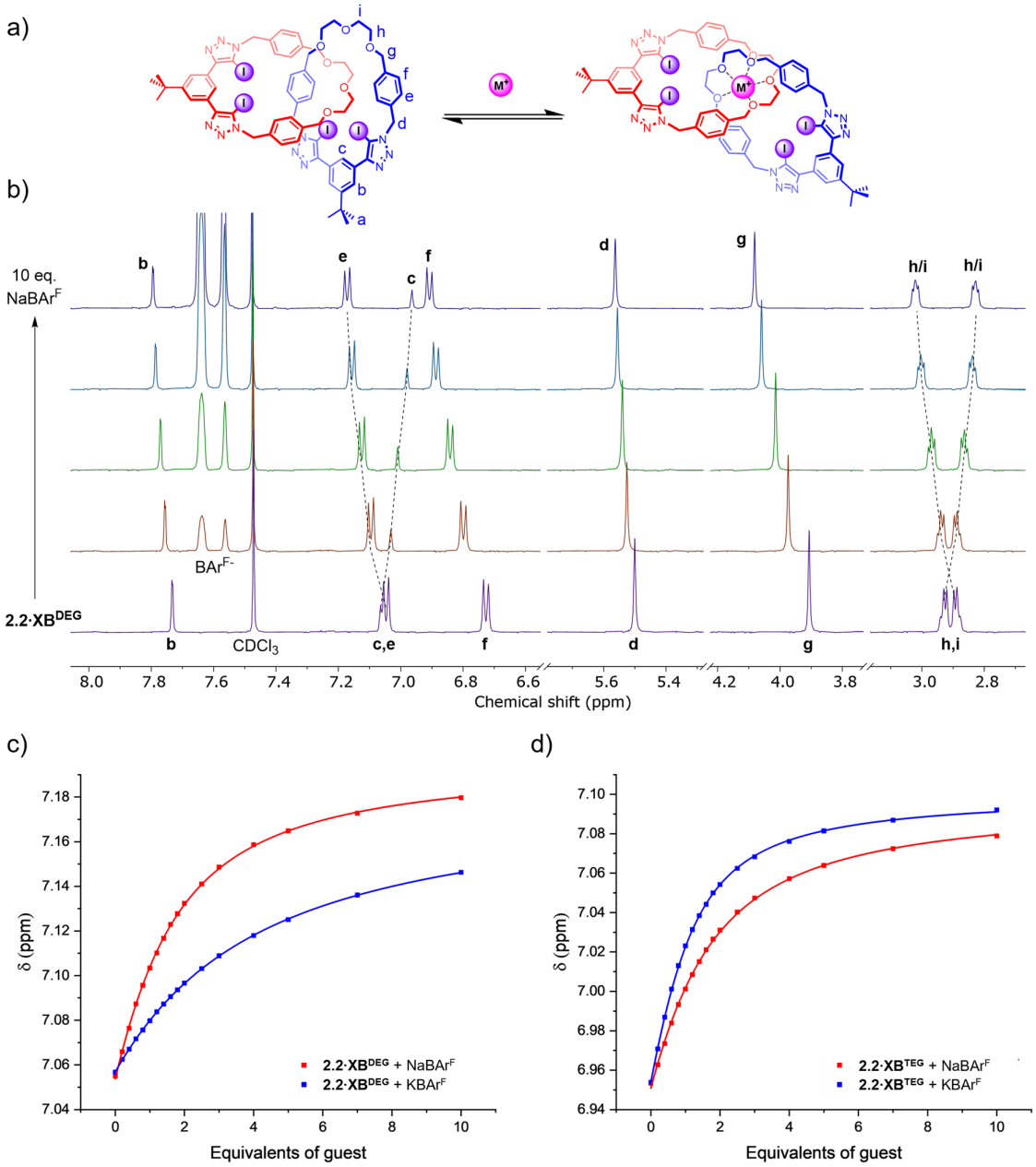


Figure 2.11. *[1]H NMR alkali metal cation binding studies of homo[2]catenanes* ***2.2·XB^{DEG}*** *and* ***2.2·XB^{TEG}***. *(a) Proposed cation binding mode; (b) Representative stacked [1]H NMR titration spectra of* ***2.2·XB^{DEG}*** *upon progressive addition of 10 eq. NaBAr^F (500 MHz, 1:1 $CD_3CN/CDCl_3$, 298 K); c)-d) Binding isotherms of* ***2.2·XB^{DEG}*** *and* ***2.2·XB^{TEG}*** *respectively with NaBAr^F (red) and KBAr^F (blue) generated by monitoring the chemical shifts of the aromatic xylene proton H_e, fitted to a 1:1 host-guest binding model.*

2.2.2.2 Anion Binding Studies

The anion binding properties of the XB catenane and macrocycle receptors were also investigated by ^{1}H NMR titration experiments conducted with halides as their tetrabutylammonium (TBA^+) salts, also in 1:1 $CDCl_3/CD_3CN$ solvent mixtures. As the concentration of the anionic guest was increased, the most significant perturbations were observed in the internal benzene proton H_c, which shifted progressively downfield, indicating an anion binding event occurring via XB interactions in the bis(iodotriazole)benzene cleft (**Figure 2.12a-b**).

The resulting binding isotherms were fitted to a 1:1 host-guest binding model using Bindfit analysis to determine the respective halide anion association constants (**Figure 2.12c-d, Table 2.3**). Interestingly, attempts to fit the anion binding isotherms of **2.2·XB^{DEG}** and **2.2·XB^{TEG}** to 1:2 host-guest binding models were unsuccessful, which is perhaps surprising given the [2]catenanes possess two bidentate XB binding motifs. However, the poor quality of fit obtained to all the 1:2 host-guest binding models suggests that the second anion binding association constant is too small to be measureable ($K_a < 10$ M^{-1}), presumably due to the modest XB···halide interactions being unable to overcome the electrostatic repulsion associated with binding two anionic guests. To account for the presence of two degenerate anion binding sites in the [2]catenanes, the observed association constants of **2.2·XB^{DEG}** and **2.2·XB^{TEG}** were treated with a statistical factor of 2.[46]

In general, the neutral XB macrocycles and [2]catenanes displayed relatively weak halide anion affinities in 1:1 $CDCl_3/CD_3CN$ ($K_a < 200$ M^{-1}). It is interesting to note that the statistically-adjusted anion K_a values of **2.2·XB^{DEG}** were significantly lower than the parent di(ethylene glycol)-based macrocycle **2.1·XB^{DEG}** for all three halides. This suggests that the mechanical bond reduces the anion binding strength of the individual bis(iodotriazole)benzene

XB donor motifs, possibly due to steric effects reducing access to the XB binding site. This is supported by the anion affinities determined for the larger catenane **2.2·XB^{TEG}** being comparable to that of the parent macrocycle **2.1·XB^{TEG}**.

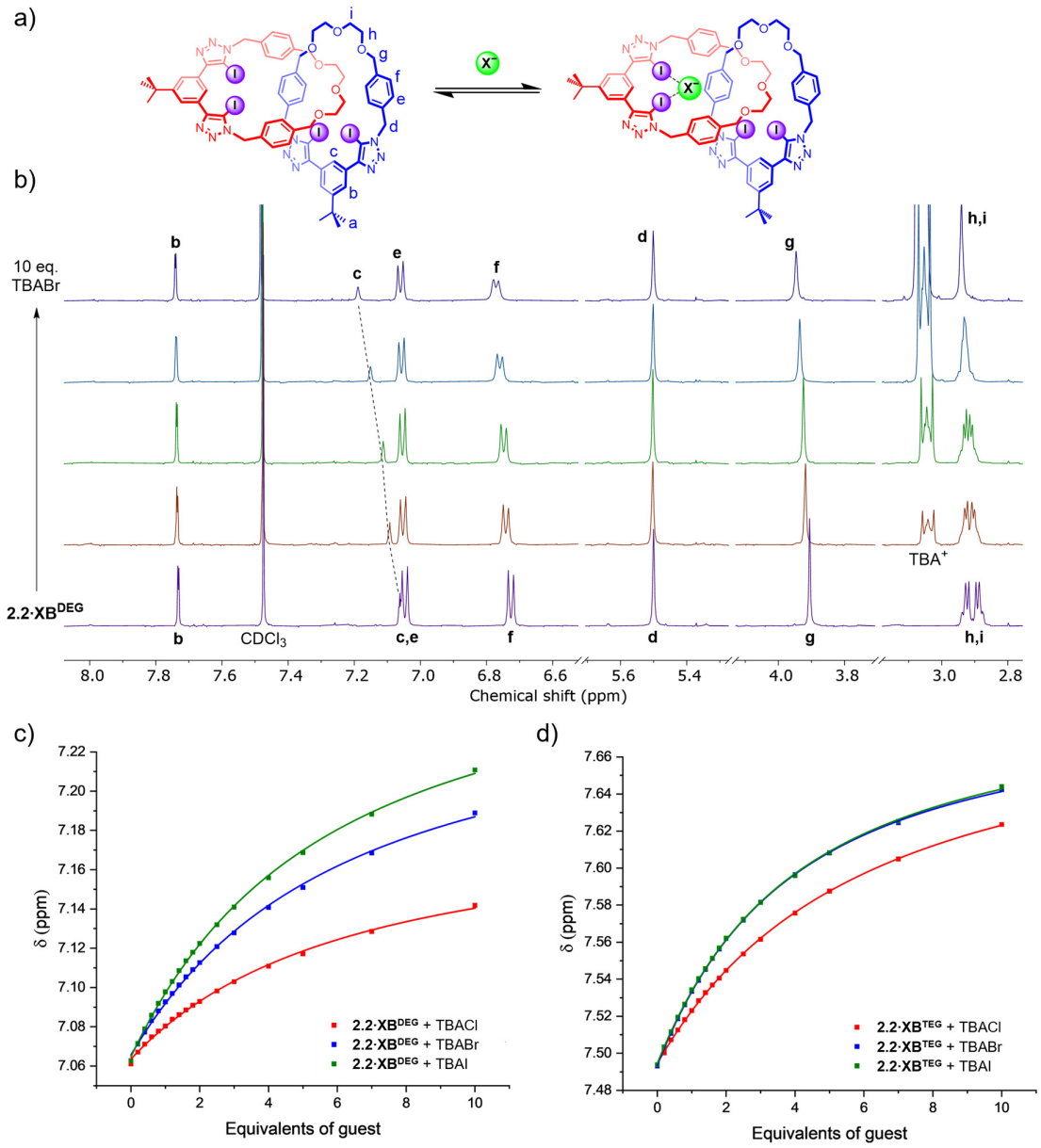


Figure 2.12. *^{1}H NMR halide anion binding studies of homo[2]catenanes **2.2·XB^{DEG}** and **2.2·XB^{TEG}**. (a) Proposed anion binding mode; (b) Representative stacked ^{1}H NMR titration spectra of **2.2·XB^{DEG}** upon progressive addition of 10 eq. TBABr (500 MHz, 1:1 CD$_3$CN/CDCl$_3$, 298 K); c)-d) Binding isotherms of **2.2·XB^{DEG}** and **2.2·XB^{TEG}** respectively with TBACl (red), TBABr (blue) and TBAI (green) generated by monitoring the chemical shifts of the internal benzene proton H$_c$, fitted to a 1:1 host-guest binding model.*

***Table 2.3**. Anion association constants (K_a/M^{-1}) for XB macrocycles and [2]catenanes determined by ^{1}H NMR titrations.[a]*

Anion	**2.1·XB^{DEG}**	**2.1·XB^{TEG}**	**2.2·XB^{DEG}**	**2.2·XB^{TEG}**
Cl^-	125	65	66[b]	84[b]
Br^-	154	97	78[b]	142[b]
I^-	186	146	87[b]	135[b]

[a]K_a values calculated using Bindfit with a 1:1 host-guest binding model. Errors (±) are all <5%. All anions added as TBA^+ salts. Solvent = 1:1 $CDCl_3/CD_3CN$. T = 298 K. [Receptor] = 1.0 mM. [b]The reported K_a values have been statistically corrected to determine the anion affinity of one bidentate XB donor motif, where $K_{a,reported} = K_{a,observed}/2$.

Evidence for the proposed chloride binding mode of **2.2·XB^{DEG}** was provided by solid state structural analysis. Crystals suitable for analysis by single crystal X-ray diffraction were obtained via diffusion of diethyl ether into a 1:1 $CDCl_3/CD_3CN$ solution of **2.2·XB^{DEG}** and excess TBACl. A structural solution in the tetragonal space group *P*4/n revealed a 1:1 complex of [2]catenane **2.2·XB^{DEG}** and TBACl stabilised by a network of intercomponent XB interactions. Each [2]catenane binds two chloride ions via XB interactions between the anion and the two independent bis(iodotriazole)benzene motifs on the interlocked macrocycles, as shown by the geometry as well as the I···Cl^- distances (3.156(4)-3.344(4) Å, which is 85-90% of the sum of the van der Waal radii of the two atoms) (**Figure 2.13a**). Each Cl^- is also bound by two pairs of XB interactions, with the second pair arising from the bis(iodotriazole)benzene motif of a [2]catenane in a neighbouring asymmetric unit, giving rise to an overall 1:1 binding stoichiometry.

In line with the weak anion association constants of **2.2·XB^{DEG}** determined via ^{1}H NMR binding studies, the chloride anions bind to the periphery of each macrocycle. It appears that an endotopic anion binding mode wherein the two bis-iodotriazole motifs cooperatively bind a single anion in the interlocked cavity is not sterically feasible. Instead, the [2]catenanes and chloride anions each act as two-connecting linkers and self-assemble to form a supramolecular tetramer stabilised by intercomponent halogen bonding (**Figure 2.13b**). Also notable is the

significant positional disorder in the di(ethylene glycol) regions of the macrocycles, which, in the absence of an alkali metal guest, exhibit considerable conformational flexibility.

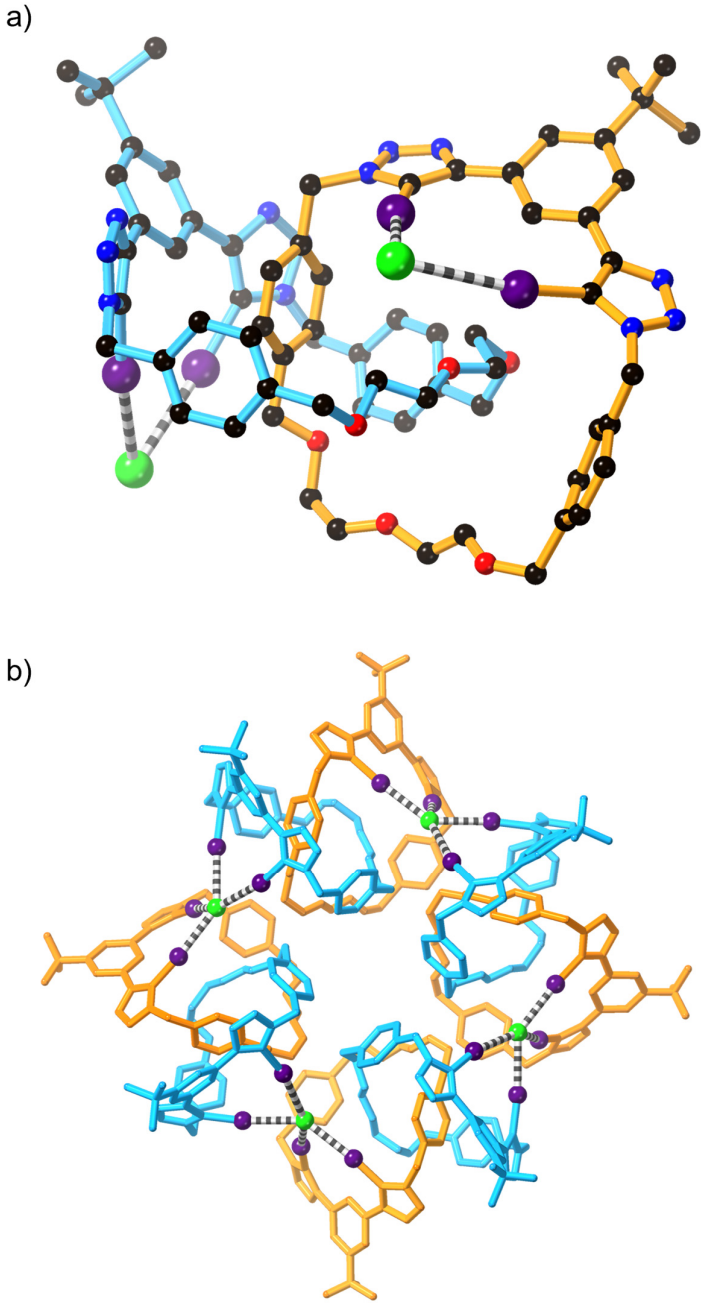


Figure 2.13. *Solid-state structure of* ***2.2·XB^{DEG}****·TBACl, showing: a) the XB interactions between a [2]catenane and two Cl¯ anions; b)the supramolecular tetramer comprising four [2]catenanes and chloride anions arranged around a crystallographic four-fold axis (right). Hydrogen atoms and TBA$^+$ counterions have been omitted for clarity. Where a ball-and-stick representation has been used, atom colours are as follows: black (C), blue (N), red (O), purple (I), green (Cl).*

2.2.2.3 Alkali Metal Halide Ion-Pair Binding Studies

Having determined both the cation and anion binding behaviour of the neutral XB [2]catenanes, their ability to recognise alkali metal halides as ion pairs was investigated. This was undertaken by adding aliquots of TBA halide salts to a 1 mM solution of the [2]catenane in the presence of 1 equivalent $MBAr^F$ (M = Na or K) (**Figure 2.14a**). It is important to note that under these conditions, only a fraction of the [2]catenane molecules in solution are initially complexed to the cationic guest, hence there remains at equilibrium a significant proportion of both free [2]catenane and cation. While it is possible to saturate the cation binding sites of the receptors by adding an excess of the metal salts, this would give rise to a high concentration of free cations which have a high propensity to undergo salt recombination and precipitation upon addition of the anion. The proportion of metal-complexed [2]catenane present in each ion-pair titration can be calculated from the respective cation association constants and are shown in **Table 2.4**.

Upon addition of Br^- and I^-, downfield shifts in the internal benzene proton H_c were seen in both [2]catenanes alongside perturbations of the signals at the ethylene glycol region, suggesting that binding of the anion simultaneously enhances cation binding to the [2]catenane. In contrast, addition of Cl^- led to salt recombination and precipitation of NaCl or KCl, reflecting the high lattice energy of the alkali metal chloride salts (**Figure 2.14b**).

Since metal complexation to the [2]catenane produces a monocationic species, there is a possibility of 1:2 host-guest binding that utilises both the anion binding sites. As such, all binding isotherms were fitted to both the 1:1 host-guest binding model, as well as four variants of the 1:2 host-guest binding model (**Figure 2.15c-d**, full details in **Appendix**). Following the approach developed by Thordarson and co-workers,[48] the co-variance values obtained from fitting the binding isotherms to each model were compared to determine the most appropriate

binding model. The binding models and corresponding K_1 and K_2 values obtained from this analysis are shown in **Table 2.4**.

Table 2.4. *Apparent anion association constants (K_a/M^{-1}) for XB homo[2]catenanes in the presence of 1 equiv. M^IBAr^F (M^I = Na, K) determined by ^1H NMR titrations.*[a]

Host	Cation	% bound	Anion	Binding model	K_1	K_2
2.2·XB^{DEG}	Na^+	34	Br^-	1:2 (Full)	1900	435
			I^-	1:2 (Full)	3080	787
	K^+	18	Br^-	1:1	216[b]	-
			I^-	1:1	244[b]	-
2.2·XB^{TEG}	Na^+	33	Br^-	1:1	373[b]	-
			I^-	1:1	409[b]	-
	K^+	47	Br^-	1:1	492[b]	-
			I^-	1:1	525[b]	-

[a]K_a values calculated using Bindfit with a 1:1 host-guest binding model. Errors (±) are all < 5%. All cations added as BAr^{F-} salts. Solvent = 1:1 $CDCl_3/CD_3CN$. T = 298 K. [Receptor] = 1.0 mM. [b]The reported K_a values have been statistically corrected to determine the anion affinity of one bidentate XB donor motif, where $K_{a,reported} = K_{a,observed}/2$.

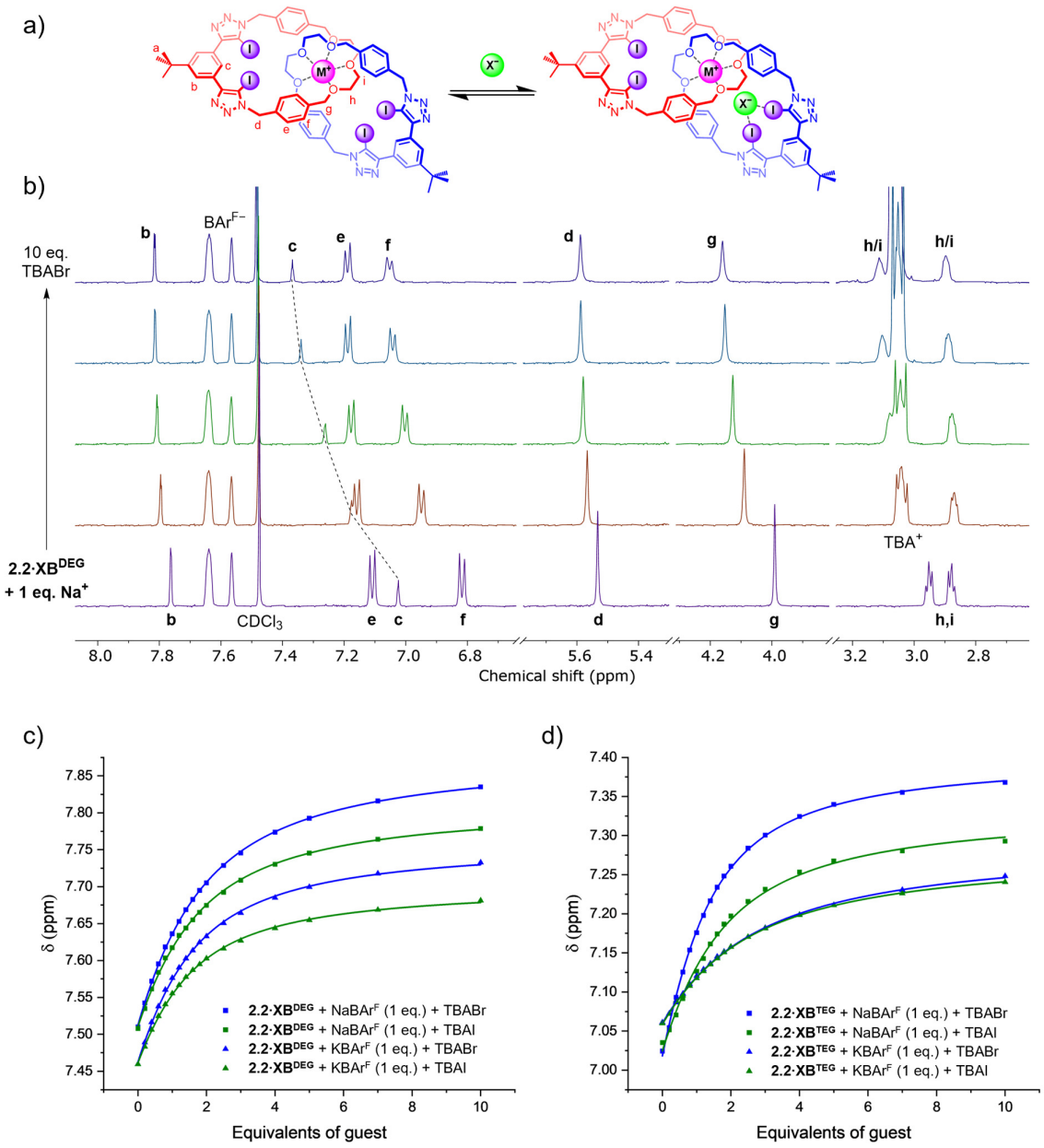


Figure 2.14. *^{1}H NMR ion-pair binding studies of homo[2]catenanes **2.2·XB^{DEG}** and **2.2·XB^{TEG}**. (a) Proposed ion-pair binding equilibrium; (b) Representative stacked ^{1}H NMR titration spectra of **2.2·XB^{DEG}** upon progressive addition of 10 eq. TBABr in the presence of 1 eq. NaBAr^F (500 MHz, 1:1 $CD_3CN/CDCl_3$, 298 K); c)-d) Binding isotherms of **2.2·XB^{DEG}** and **2.2·XB^{TEG}** respectively, pre-complexed with Na^+ (squares) or K^+ (diamonds) upon addition of TBABr (blue) and TBAI (green) generated by monitoring the chemical shifts of internal benzene proton H_c, fitted to either a 1:2 Full or 1:1 host-guest binding model (full details in text).*

Despite the introduction of a positive charge to the receptors, the apparent binding stoichiometry of **2.2·XB^{DEG}·K$^+$**, **2.2·XB^{TEG}·Na$^+$** and **2.2·XB^{TEG}·K$^+$** to both halide anions

remains at 1:1. Notable enhancements in the apparent K_1 values were observed for both halides **(Table 2.4**), which were attributed to cooperative electrostatic effects commonly observed in ion-pair receptors. All three [2]catenane-metal complexes exhibited moderately stronger binding to iodide over bromide. **2.2·XB^{TEG}·K$^+$** exhibited the strongest anion binding to both bromide and iodide, followed by **2.2·XB^{TEG}·Na$^+$**, while **2.2·XB^{DEG}·K$^+$** showed the weakest binding. This trend was rationalised by a combination of the intrinsically higher anion binding strength of **2.2·XB^{TEG}** compared to **2.2·XB^{DEG}** in the metal-free neutral state **(Table 2.3**), as well as the differing proportions of metal-bound complex initially present in solution (47% for **2.2·XB^{TEG}·K$^+$**, 33% for **2.2·XB^{TEG}·Na$^+$** and 17% for **2.2·XB^{DEG}·K$^+$**).

In contrast, **2.2·XB^{DEG}·Na$^+$** exhibited a 1:2 host-guest binding stoichiometry with Br^- and I^-. The binding isotherms of the two anions showed the best fit to the 1:2 (Full) model, which assumes there are two distinct anion binding sites in the receptor and changes in chemical shift (Δδ) corresponding to the 1:1 and 1:2 complexes are unrelated. Initially, the differences in binding stoichiometry between **2.2·XB^{DEG}·Na$^+$** and the other three metal-[2]catenane complexes were difficult to understand as all the receptors contain a bound alkali metal cation and two XB anion binding sites.

Crystallographic analysis of the ion-pair binding modes of the [2]catenanes in the solid state allowed us to rationalise this behaviour. Vapour diffusion of pentane into a 1:1 $CHCl_3$/CH_3CN solution of **2.2·XB^{DEG}** in the presence of 1 eq. $NaBAr^F$ and excess TBAI resulted in the formation of colourless needle-shaped single crystals suitable for X-ray diffraction studies. The asymmetric unit contains one **2.2·XB^{DEG}** catenane, a sodium cation, an iodide anion as well as a sodium-bound water molecule, giving an overall chemical composition of **2.2·XB^{DEG}·NaI·H$_2$O**. In sharp contrast to the structure of **2.2·XB^{DEG}·TBACl**, the di(ethylene glycol) chains of the two macrocycles are arranged orthogonally to form a

binding pocket in which a sodium cation resides (**Figure 2.15a**). This observed inter-ring circumrotation of the [2]catenane in the presence of a sodium cation is consistent with the postulated cation-induced conformational change in solution, as suggested by the chemical shift perturbations of proton signals distal to the cation binding site in ^{1}H NMR. Importantly, the cation forms coordination interactions with five di(ethylene glycol) oxygen atoms from the interlocked macrocycles and a sixth with a Na^{+}-ligated water molecule.

The anion binding mode in **2.2·XB^{DEG}·NaI·H$_2$O** is similar to **2.2·XB^{DEG}·TBACl**, where each [2]catenane binds two iodide ions via the bidentate XB donor motifs of the two interlocked macrocycles (I···I^{-}: 3.4592(19)- 3.6524(19)Å, 87-92% Σ_{vdW}), while each iodide ion bridges two adjacent [2]catenanes **(Figure 2.15a)**. Unlike **2.2·XB^{DEG}·TBACl**, however, this network of intercomponent XB interactions is propagated throughout the crystal, linking the [2]catenane units into 1D polymeric chains.

When **2.2·XB^{TEG}** was crystallised under similar conditions, needle-like crystals of chemical composition **2.2·XB^{TEG}·NaI** formed. Similar to **2.2·XB^{DEG}·NaI·H$_2$O**, sodium ions are encapsulated within the binding cavity formed by the tri(ethylene glycol) regions of the interlocked macrocycles and each [2]catenane unit binds two iodide anions via XB interactions (I···I^{-}: 3.4914(9)- 3.709(6) Å, 88-94% Σ_{vdW}) **(Figure 2.15b)** to form XB-stabilised polymeric chains. However, a key difference in the two structures lies in the coordination environment of the sodium ion; in **2.2·XB^{TEG}·NaI**, all six sodium coordination sites are occupied by polyether oxygens, presumably due to the presence of additional oxygen atoms in the longer tri(ethylene glycol) linkers. Consequently, this leaves no vacant coordination site to accommodate an external ligand such as water or an additional halide.

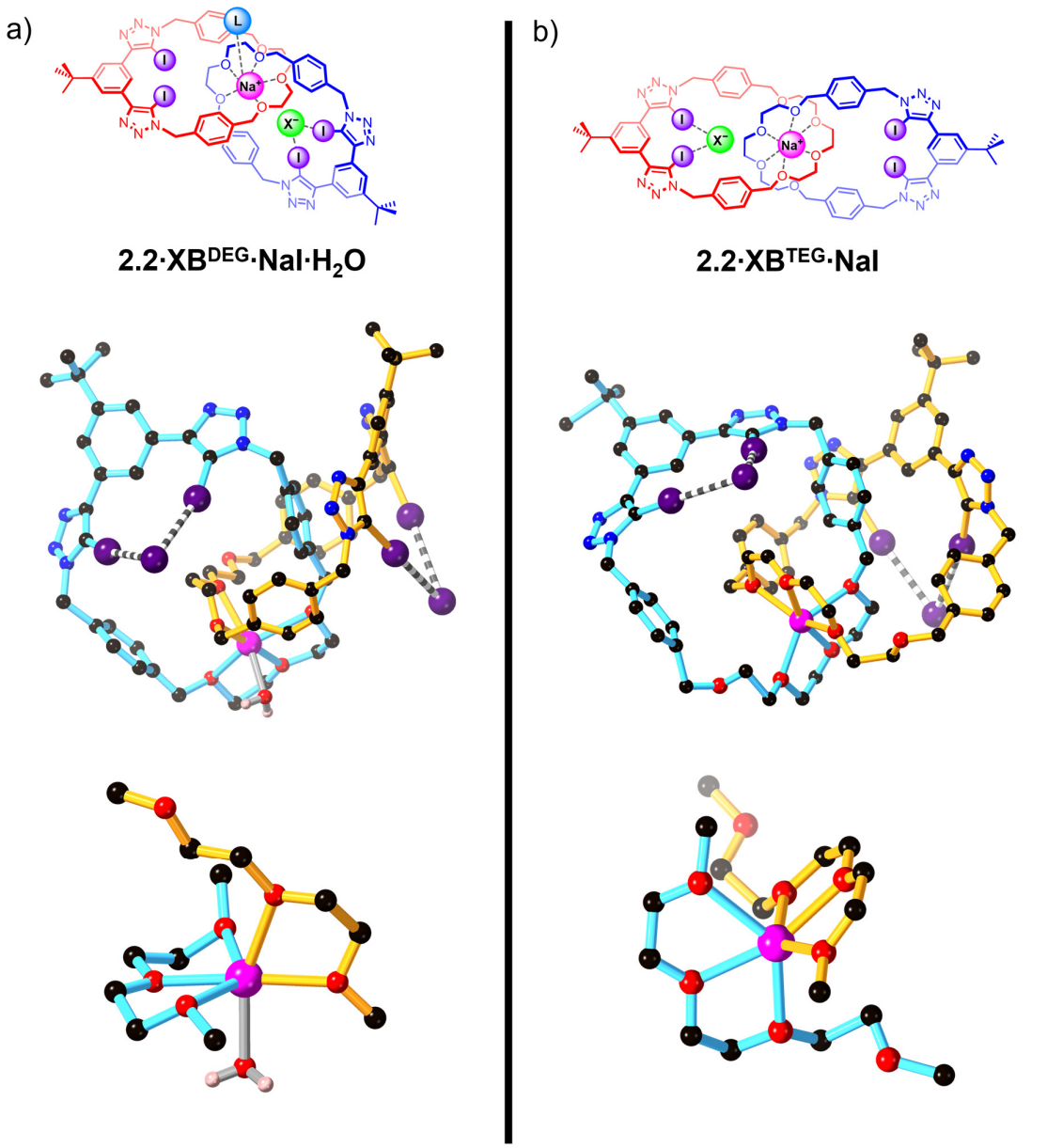


Figure 2.15. *Solid-state structures of (a)* ***2.2·XB^{DEG}·NaI·H$_2$O*** *and (b)* ***2.2·XB^{TEG}·NaI****, showing a single [2]catenane unit bound to a sodium cation and two iodide anions (middle) and a truncated representation of the ethylene glycol region (right,) highlighting the coordination environment around the sodium ion. Atom colours are as follows: black (carbon), blue (nitrogen), red (oxygen), purple (iodine), light pink (hydrogen), bright pink (sodium). The chemical structures of* ***2.2·XB^{DEG}*** *and* ***2.2·XB^{TEG}*** *are shown on the left for reference.*

Comparing the sodium cation coordination modes in the two structures suggests that the 1:2 stoichiometry of anion binding in **2.2·XB^{DEG}·Na$^+$** observed by solution-state ^{1}H-NMR arises from a contact ion-pair between coordinatively unsaturated Na^+ and the halide in addition

to XB-mediated anion binding (**Figure 2.16**). Importantly, this rationalises the higher apparent K_1 values of **2.2·XB^{DEG}·Na$^+$** for the two anions (K_1(Br$^-$) = 1900 M^{-1}, K_1(I$^-$) = 3080 M^{-1}) compared to the other three metal-[2]catenane complexes. As before, the stronger iodide binding is likely due to the lower lattice enthalpy of NaI making the competing salt recombination equilibrium less favourable.

Although it may be somewhat counterintuitive that **2.2·XB^{DEG}·K$^+$** did not exhibit the same 1:2 binding stoichiometry as **2.2·XB^{DEG}·Na$^+$**, given the larger ionic radius of potassium, this might be due to the low proportion of potassium-bound [2]catenane complex present in a 1 mM solution of **2.2·XB^{DEG}** and KBAr^F, meaning that the binding isotherm derived from the titration is in reality a superposition of anion binding to neutral **2.2·XB^{DEG}** (major, 83%) and **2.2·XB^{DEG}·K$^+$** (minor, 17%).

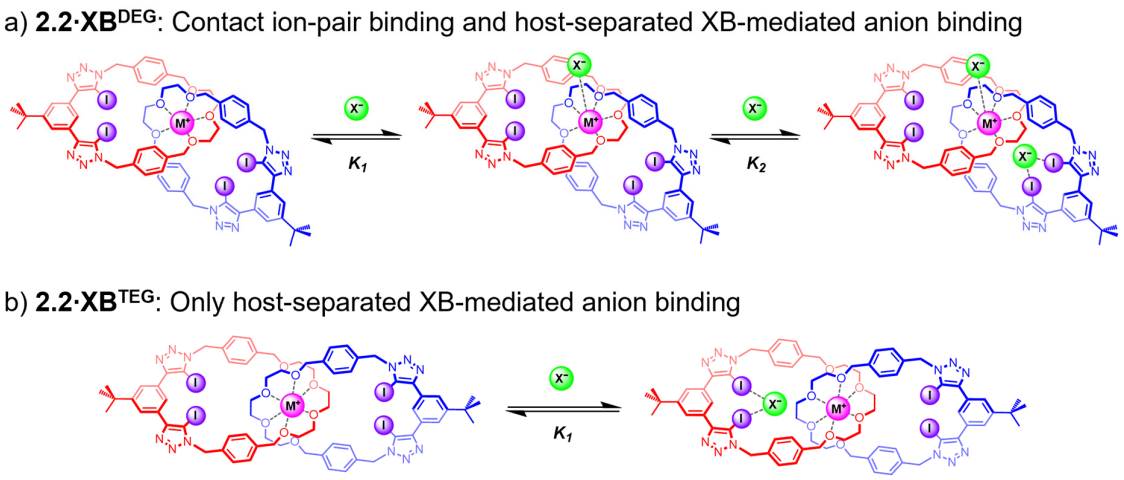


Figure 2.16. *Proposed ion-pair binding modes for a) **2.2·XB^{DEG}**; **2.2·XB^{TEG}**.*

2.2.2.4 Ion Binding Properties of Hetero[2]catenane 2.2·HBXB^{DEG}

To evaluate the contribution of XB interactions to the ion-pair recognition properties of the [2]catenane receptors, the hetero[2]catenane **2.2·HBXB^{DEG}** was subsequently prepared (**Scheme 2.2**), wherein one macrocycle features a bis(iodotriazole) XB donor motif and the

other a bis(prototriazole) HB donor motif. A comparison of the ^{1}H NMR spectrum of **2.2·HBXB^{DEG}** with that of the parent macrocycles revealed chemical shift perturbations indicative of mechanical bond formation (**Figure 2.17**). Analysis of **2.2·HBXB^{DEG}** by 2D ^{1}H-^{1}H ROESY NMR enabled a complete assignment of the proton resonances.

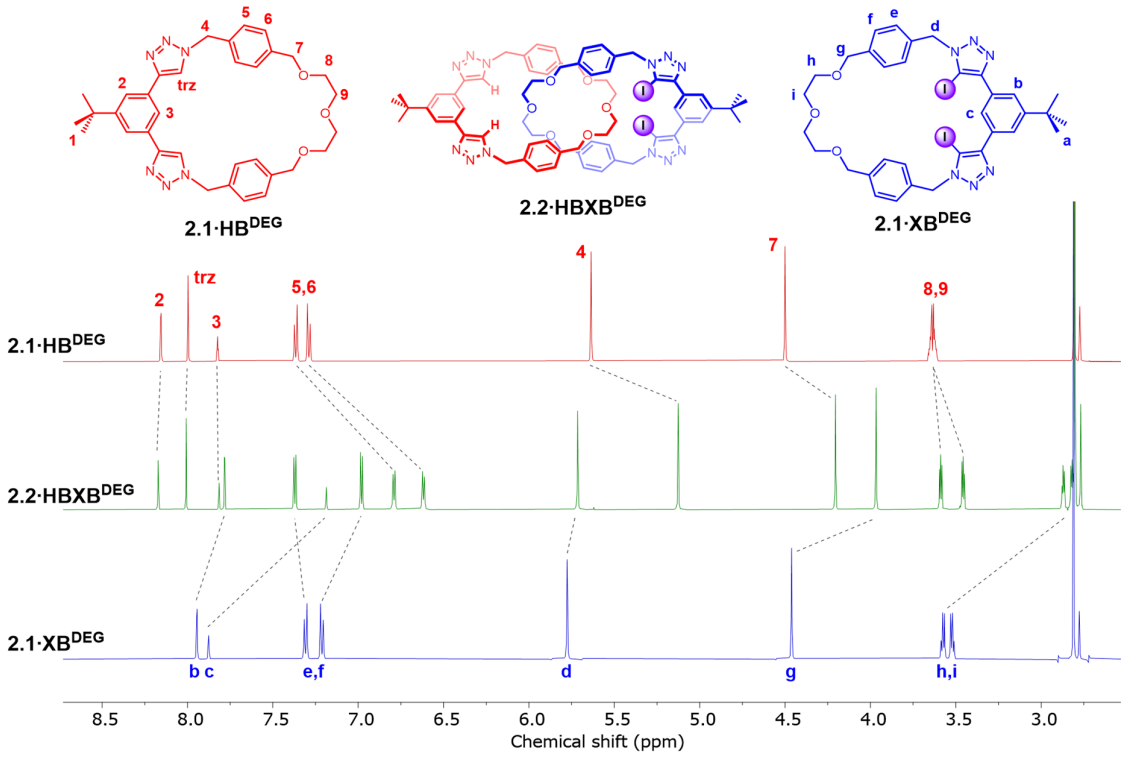


Figure 2.17. *Stacked ^{1}H NMR spectra of **2.1·HB^{DEG}** (top), **2.2·HBXB^{DEG}** (middle) and **2.1·XB^{DEG}** (bottom) (acetone-d_6, 500 MHz, 298 K);*

Crystals suitable for X-ray diffraction studies were obtained by slow evaporation of a cooled acetone solution of **2.2·HBXB^{DEG}**. The structure confirmed the interlocked [2]catenane topology of **2.2·HBXB^{DEG}** (**Figure 2.18**). Notably, the crystal structure features intercomponent CH···O hydrogen bonding interactions between the triazole donor atoms H_j and a polyether oxygen on the opposite ring (C···O distances: 3.333(8)-3.398(8) Å). As a result, the di(ethylene glycol) chains are not oriented in the optimal conformation to facilitate sodium cation complexation.

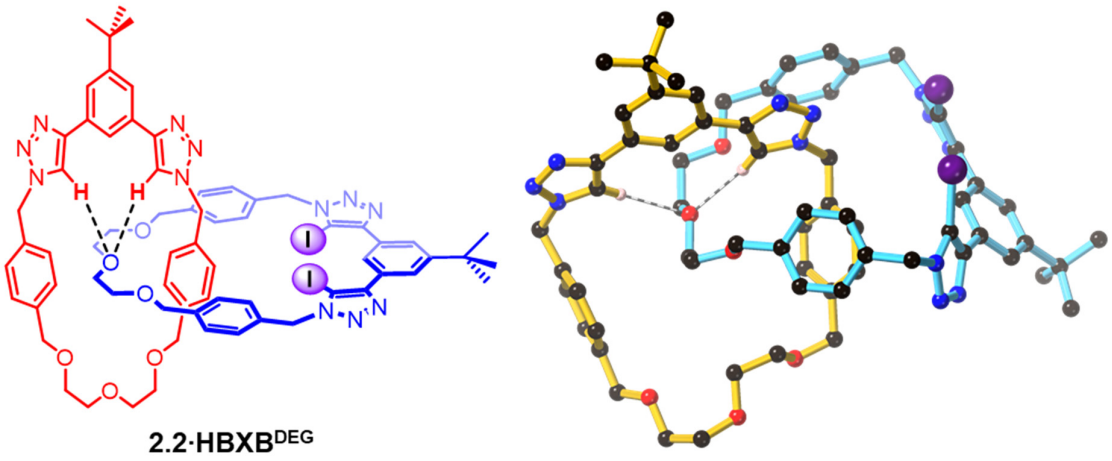


Figure 2.18. *Solid-state XRD structure of mixed HB/XB hetero[2]catenane* ***2.2·HBXB^{DEG}****, showing the HB interactions between H_j and a polyether oxygen atom. All other hydrogen atoms have been omitted for clarity. Atom colours are as follows: black (carbon), blue (nitrogen), red (oxygen), purple (iodine), pink (hydrogen). A chemical structure of the [2]catenane is shown on the left for reference.*

The binding affinities of **2.2·HBXB^{DEG}** for NaBAr^F and TBAI were determined in 1:1 $CDCl_3/CD_3CN$ (**Figure 2.19a-b**). Fitting the resulting isotherms to a 1:1 host-guest stoichiometric binding model in Bindfit gave K_a values of 36 M^{-1} for Na^+ and 31 M^{-1} for I^- (**Figure 2.19c**). The drastically reduced sodium cation affinity of **2.2·HBXB^{DEG}** relative to **2.2·XB^{DEG}** (K_a = 756 M^{-1}) was attributed to the reduced basicity of the polyether oxygens involved in intercomponent HB interactions, consistent with the conformation observed in the crystal structure of **2.2·HBXB^{DEG}**. The low iodide affinity of **2.2·HBXB^{DEG}** likely results from hindered access to the single bis(iodotriazole) anion binding cleft upon mechanical bond formation. Notably, the HB macrocycle **2.1·HB^{DEG}** exhibits no binding to I^- in this solvent system. The weak sodium binding of **2.2·HBXB^{DEG}** precluded a determination of an apparent iodide binding constant of **2.2·HBXB^{DEG}·Na$^+$** due to the low proportion (3%) of sodium-complexed receptor present in an equimolar mixture of **2.2·HBXB^{DEG}** and NaBAr^F.

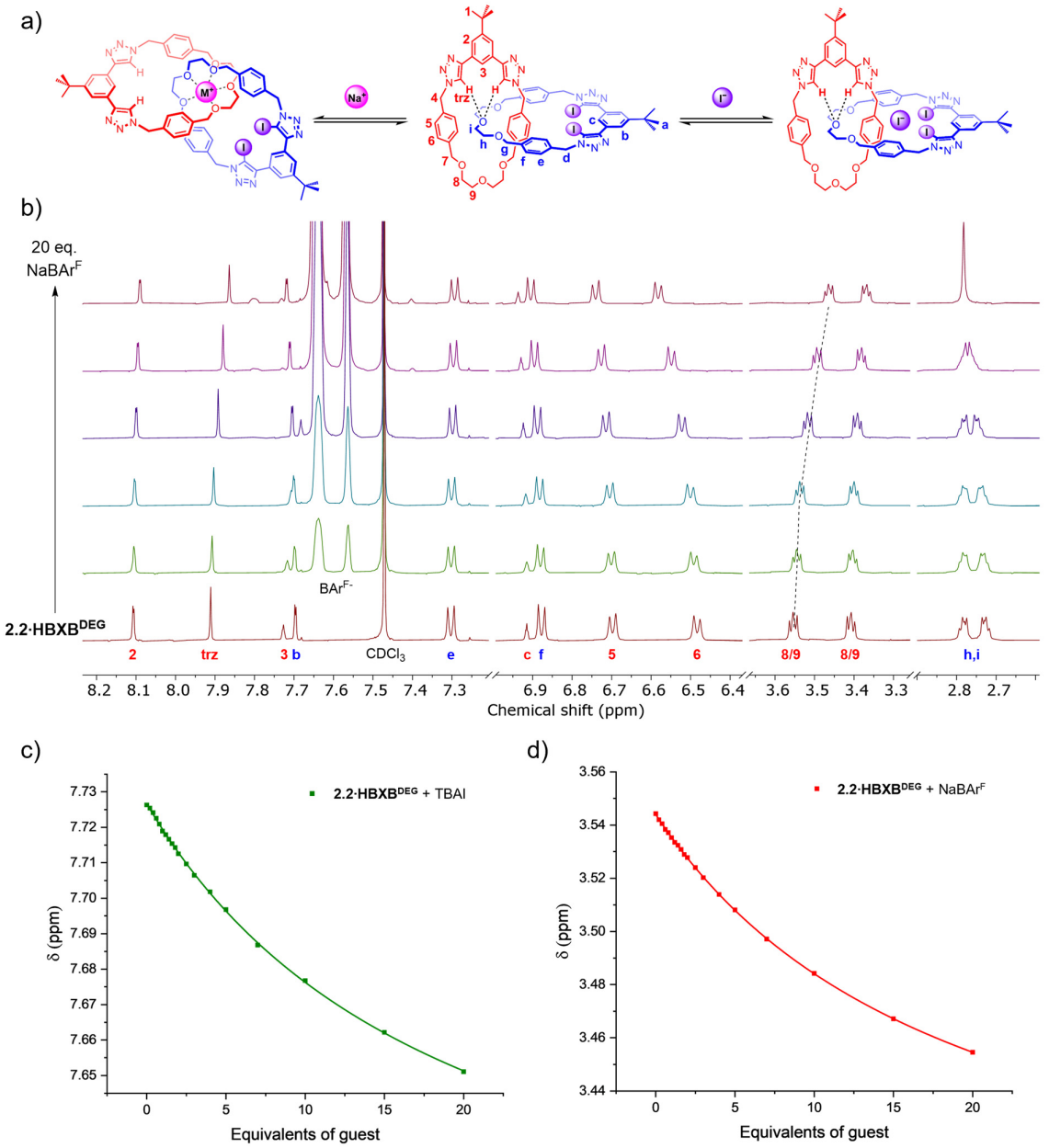


Figure 2.19. *[1]H NMR titration studies of* ***2.2·HBXB^{DEG}****. a) Proposed binding modes of cations (left) and anion (right); b)-c) Stacked [1]H NMR spectra of* ***2.2·HBXB^{DEG}*** *upon addition of NaBAr^F and TBAI respectively. (500 MHz, 1:1 $CD_3CN/CDCl_3$); e)-f) Binding isotherms of* ***2.2·HBXB^{DEG}*** *with NaBAr^F (monitoring ethylene glycol proton $H_{h/i}$) and TBAI (monitoring internal benzene proton H_3) respectively.*

2.2.3 Solid-Liquid Extraction Studies

Encouraged by the ion-pair recognition abilities of homo[2]catenanes **2.2·XB^{DEG}** and **2.2·XB^{TEG}**, the ability of these XB [2]catenanes to act as alkali metal halide salt extracting agents was investigated. Solid-liquid extraction (SLE) studies were conducted by sonicating a 1 mM $CDCl_3$ solution of the [2]catenane in the presence of excess solid NaX for **2.2·XB^{DEG}** or KX for **2.2·XB^{TEG}** ($X = Cl^-$, Br^-, I^-). After 30 minutes, the solution was filtered and a ^{1}H NMR spectrum recorded.

With solid NaI, the pre- and post-extraction ^{1}H NMR spectra of **2.2·XB^{DEG}** showed changes consistent with ion-pair binding, namely a splitting of the ethylene glycol protons H_h and H_i, alongside a downfield shift of internal benzene proton H_c (**Figure 2.20**), indicative of successful extraction. Notably, the subsequent addition of free [2]catenane **2.2·XB^{DEG}** to the solution gave rise to a second set of peaks corresponding to free **2.2·XB^{DEG}**, suggesting that the system is in slow exchange between the fully NaI-complexed and free receptors. An analogous study using NaBr gave rise to two sets of broad peaks, one corresponding to unbound **2.2·XB^{DEG}** while the other displays similar chemical shifts to that of NaI-bound **2.2·XB^{DEG}**, indicating partial extraction of NaBr by the [2]catenane. Integration of these respective signals estimated that 50% of the [2]catenane in solution was present as the NaBr-bound complex. In contrast, no extraction of NaCl occurred, which was attributed to the higher lattice enthalpy of NaCl.

Treating **2.2·XB^{TEG}** with potassium halide salts in analogous SLE experiments gave rise to a single set of peaks in all cases, indicative of systems in fast exchange. The extraction efficiencies were estimated from the magnitude of the observed chemical shift perturbations and found to be in the order: KCl << KBr < KI. Importantly, when the parent macrocycles **2.1·XB^{DEG}** and **2.1·XB^{TEG}** were subjected to the same SLE conditions with NaX and KX but

no evidence of salt extraction was observed, further testimony to the critical role of mechanical bond formation in enhancing the ion-pair recognition capabilities of the receptors.

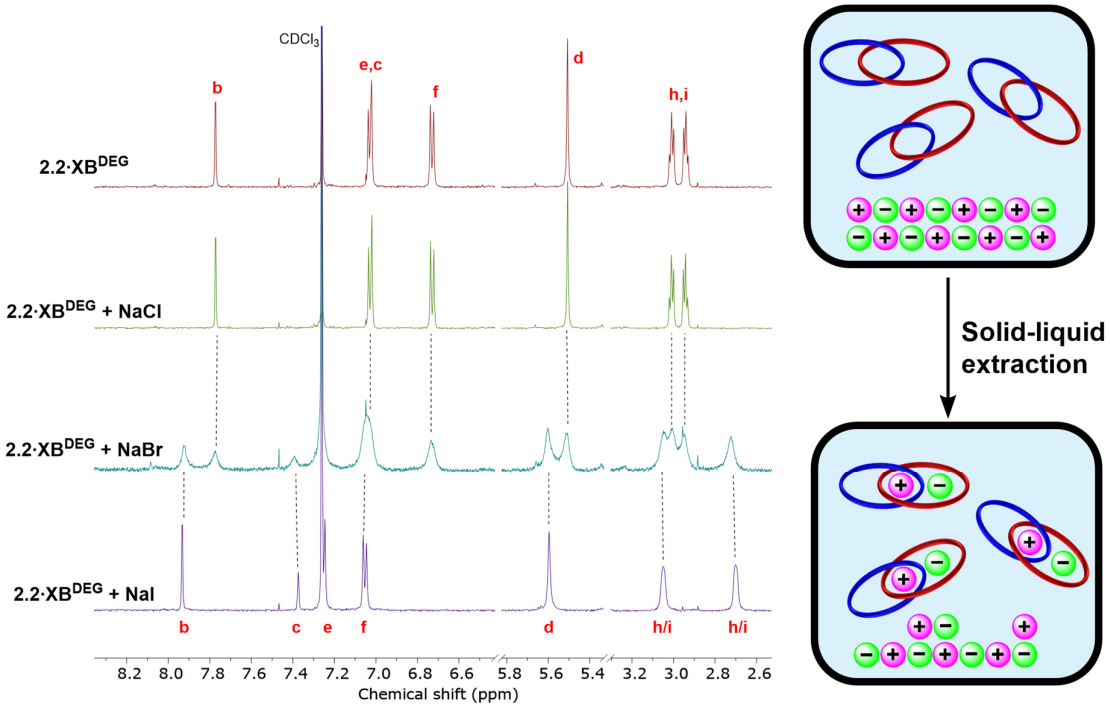


Figure 2.20. *Pre- and post-extraction spectra of* ***2.2·XB^{DEG}*** *with excess solid NaCl, NaBr and NaI ($CDCl_3$, 500 MHz, 298 K).*

2.3 A Hetero[2]catenane for Enhanced Ion-Pair Binding

A particularly notable feature of the homo[2]catenanes **2.2·XB^{DEG}** and **2.2·XB^{TEG}** is their ability to discriminate between sodium and potassium ions, which are the primary cationic biological electrolytes and underpin many of the functions requisite for life.[58-60] The shared monocationic nature and spherical geometry of sodium and potassium cations makes distinguishing these ions a significant challenge,[61] which likely accounts for the scarcity of heteroditopic ion-pair receptors capable of selectively binding sodium or potassium salts.[14, 62-63] While the above-described homo[2]catenane systems demonstrated the potential of exploiting the highly pre-organised binding cavities of catenanes to elicit sodium/potassium selectivity, the relatively moderate individual cation and anion affinities of these receptors precluded strong ion-pair binding as a whole. We therefore designed a second-generation heteroditopic [2]catenane ion-pair host system possessing a bis-di(ethylene glycol)-based cation binding site which significantly enhances its alkali metal binding affinity (**Figure 2.21**). ^{1}H NMR studies revealed a dramatic improvement in its ion-pair binding affinity relative to the homo[2]catenanes, with a marked preference for sodium over potassium halide salts.

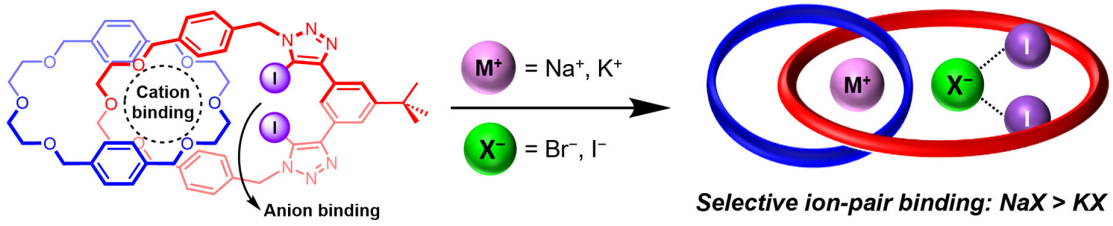


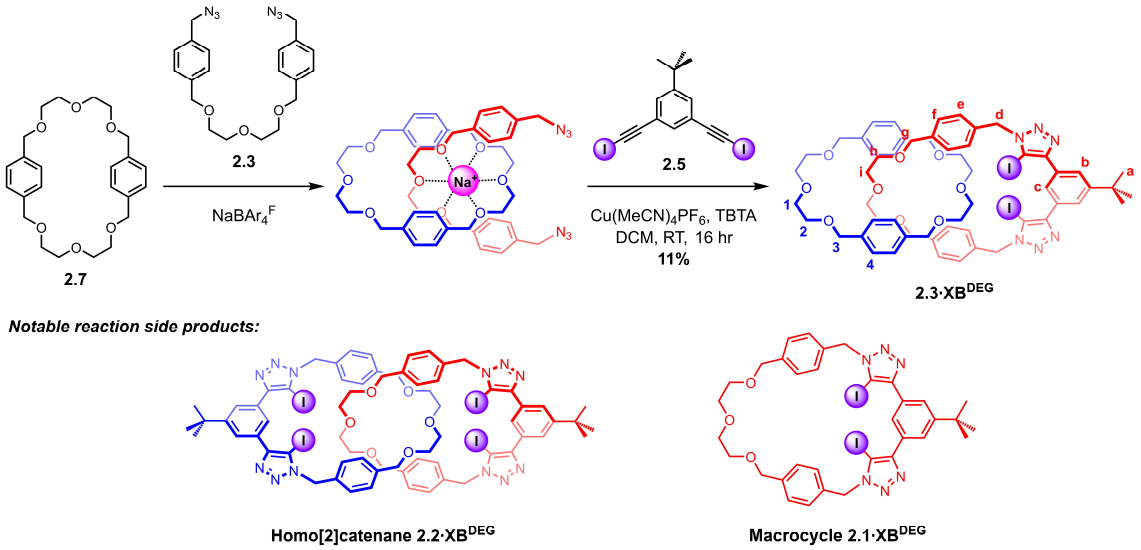
Figure 2.21. *Schematic showing the chemical structure (left) and cartoon representation (right) of a hetero[2]catenane which functions as a heteroditopic ion-pair receptor capable of potent and selective binding of sodium halides.*

2.3.1 Synthesis and Characterisation

We sought to prepare the target hetero[2]catenane via an alkali metal cation template-directed strategy, in which a sodium ion facilitates the formation of a pseudo[2]rotaxane

complex between di(ethylene)glycol-functionalised macrocycle **2.7** and bis(azide) **2.3**. Cyclisation of the latter by CuAAC reaction with bis(iodoalkyne) **2.7** would generate the second interlocked macrocycle and the bis(iodotriazole)benzene XB donor motif in a single step.

To this end, a solution of **2.7**, $NaBAr^F$ and bis(azide) **2.3** was allowed to stir in CH_2Cl_2 for 30 minutes, following which bis(iodoalkyne) **2.5** was added, followed by dropwise addition of $Cu(MeCN)_4PF_6$ and TBTA. After stirring the reaction overnight at room temperature, an aqueous work-up with basic EDTA solution and water, followed by iterative preparative thin-layer chromatographic purification, the target hetero[2]catenane **2.3·XB^{DEG}** was isolated in 11% yield (**Scheme 2.3**). The low yield relative to the homo[2]catenane systems was attributed to competing reactions that produced non-interlocked macrocycle **2.1·XB^{DEG}** as well as homo[2]catenane **2.2·XB^{DEG}**, both of which were isolated as by-products in low yields (<10%).



Scheme 2.3. *Synthesis of hetero[2]catenane **2.3·XB^{DEG}** using a sodium cation template-directed strategy. The chemical structures of notable reaction side products are shown*

Compared to the non-interlocked macrocycles **2.7** and **2.1·XB^{DEG}**, the ^{1}H NMR spectrum of [2]catenane **2.3·XB^{DEG}** in $CDCl_3$ solution (**Figure 2.22**) exhibited peak shifts that

are consistent with the formation of an interlocked topology. The proton signals arising from macrocycle **2.7** underwent significant upfield shifts in the spectrum of **2.3·XB^{DEG}**, attributed to their enforced proximity of these proton environments to the shielding ring currents of the xylene spacers in **2.1·XB^{DEG}**. Notably, the proton signals of the macrocycle **2.7** did not undergo desymmetrisation, suggesting that under ambient conditions in $CDCl_3$ the relative co-conformational circumrotation of the constituent macrocycles is fast relative to the NMR timescale. Significant shifts were also observed in the signals arising from macrocycle **2.1·XB^{DEG}**. In particular, the upfield shifts and coalescence of protons H_h and H_i indicate that the ethylene glycol region of **2.1·XB^{DEG}** is threaded through the cavity of **2.7**.

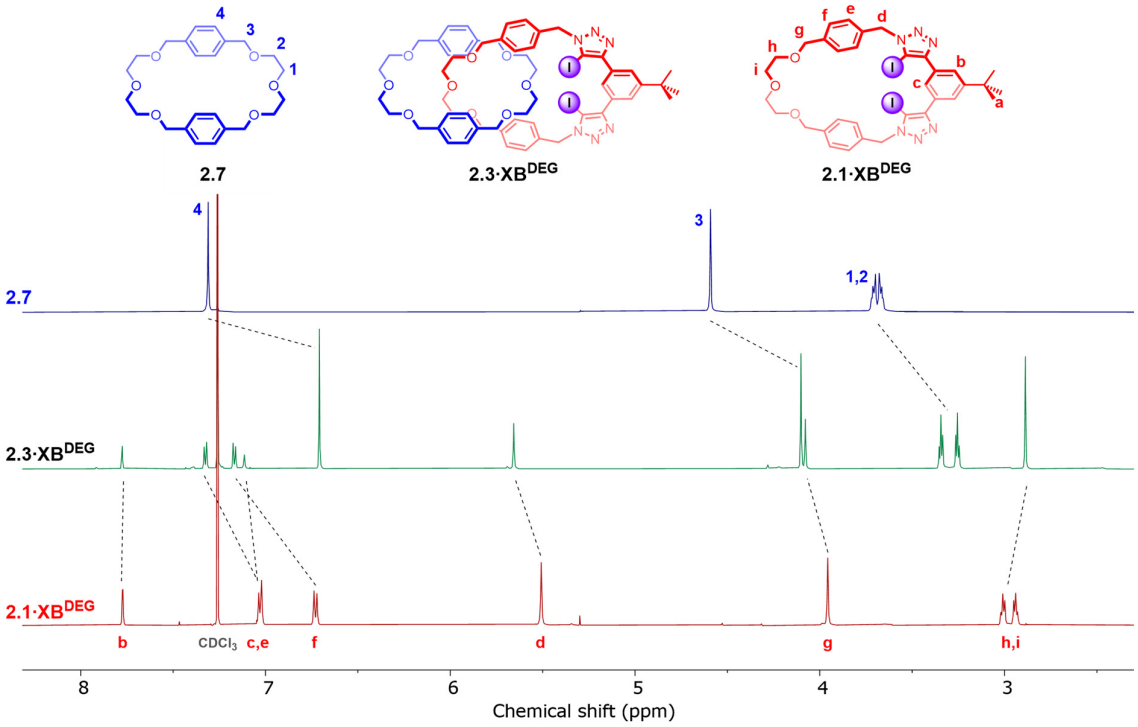


Figure 2.22. *Stacked ^{1}H NMR spectra of macrocycle **2.7** (top), [2]catenane **2.3·XB^{DEG}** (middle) and XB macrocycle **2.1·XB^{DEG}** (bottom) (500 MHz, $CDCl_3$, 298 K).*

2.3.2 ^{1}H NMR Ion Binding Studies

Attention was subsequently directed to investigating the potential of **2.3·XB^{DEG}** to function as an ion-pair receptor for alkali metal halide salts. To this end, the cation and anion

binding properties of the hetero[2]catenane receptor were first investigated separately, following which ion-pair binding studies were conducted to determine the overall binding of the receptor to alkali metal halide salts.

2.3.2.1 Cation Binding Studies

The cation binding affinities of **2.3·XB^{DEG}** were investigated via ^{1}H NMR binding studies with $M^{I}BAr^{F}$ salts (where M^{I} = Na^{+}, K^{+}) in 1:1 $CD_3CN/CDCl_3$, under identical conditions to those used in the binding studies of the homo[2]catenane systems.

Upon addition of $NaBAr^{F}$ and $KBAr^{F}$ to **2.3·XB^{DEG}**, large movements were observed in the ethylene glycol proton resonances of the two constituent macrocycles, as well as the proximal benzylic singlets H_g and H_3, indicating convergent coordination of the alkali metal cation by the polyether oxygen atoms of both macrocycles **(Figure 2.23a-b**). A substantial downfield shift of the xylene protons H_4 from macrocycle **2.7** was also observed, possibly due to a co-conformational rearrangement that rotates these aromatic groups away from the macrocyclic cavity of **2.1·XB^{DEG}** to accommodate the cation in the binding site.

The binding isotherms generated by monitoring the upfield movement of ethylene glycol proton H_i rapidly approached saturation after 1 equivalent of the cation was added (**Figure 2.23c**). Fitting the isotherms to a 1:1 host-guest stoichiometric binding model gave cation association constants with values in excess of 10^4 M^{-1}, indicating that alkali metal cation binding is too strong to be accurately quantified by ^{1}H NMR in this solvent system (**Table 2.5**). This represents a significant enhancement (>10-fold) in cation binding affinity relative to the homo[2]catenane **2.1·XB^{DEG}**, which was attributed to the presence of two ethylene glycol linkers in macrocycle **2.7**. The symmetric nature of macrocycle **2.7** would conceivably allow [2]catenane **2.3·XB^{DEG}** to adopt a larger number of co-conformations in which convergent cation coordination by the polyether regions of the two interlocked macrocycles is possible.

Importantly, analogous cation binding studies conducted on the non-interlocked macrocycles revealed no significant cation affinity, highlighting the salient role of the interlocked binding cavity in 'switching on' cation binding.

To enable a quantitative comparison of the binding affinities of **2.3·XB^{DEG}** for sodium and potassium ions, the cation binding studies were repeated in the more competitive solvent mixture 3:1 $CD_3CN/CDCl_3$. The sodium cation association constant remained too high to be quantified by ^{1}H NMR, but potassium cation binding was significantly attenuated (**Figure 2.23d**, **Table 2.5**). This verifies the expected binding preference of **2.3·XB^{DEG}** for sodium over potassium ions, presumably due to better size match between the di(ethylene glycol)-derived binding site and the smaller sodium cation.

Table 2.5. *Cation association constants (K_a/M^{-1}) for homo- and hetero[2]catenanes determined by ^{1}H NMR titrations.*[a]

Solvent	1:1 $CD_3CN/CDCl_3$		3:1 $CD_3CN/CDCl_3$
Receptor	**2.2·XB^{DEG}**	**2.3·XB^{DEG}**	
Na^+	756(11)	$> 10^4$	$> 10^4$
K^+	284(2)	$> 10^4$	3737(91)

[a] K_a values calculated using Bindfit with a 1:1 host-guest binding model. Errors are shown in parantheses. All cations added as BAr^{F-} salts. T = 298 K. [Receptor] = 1.0 mM.

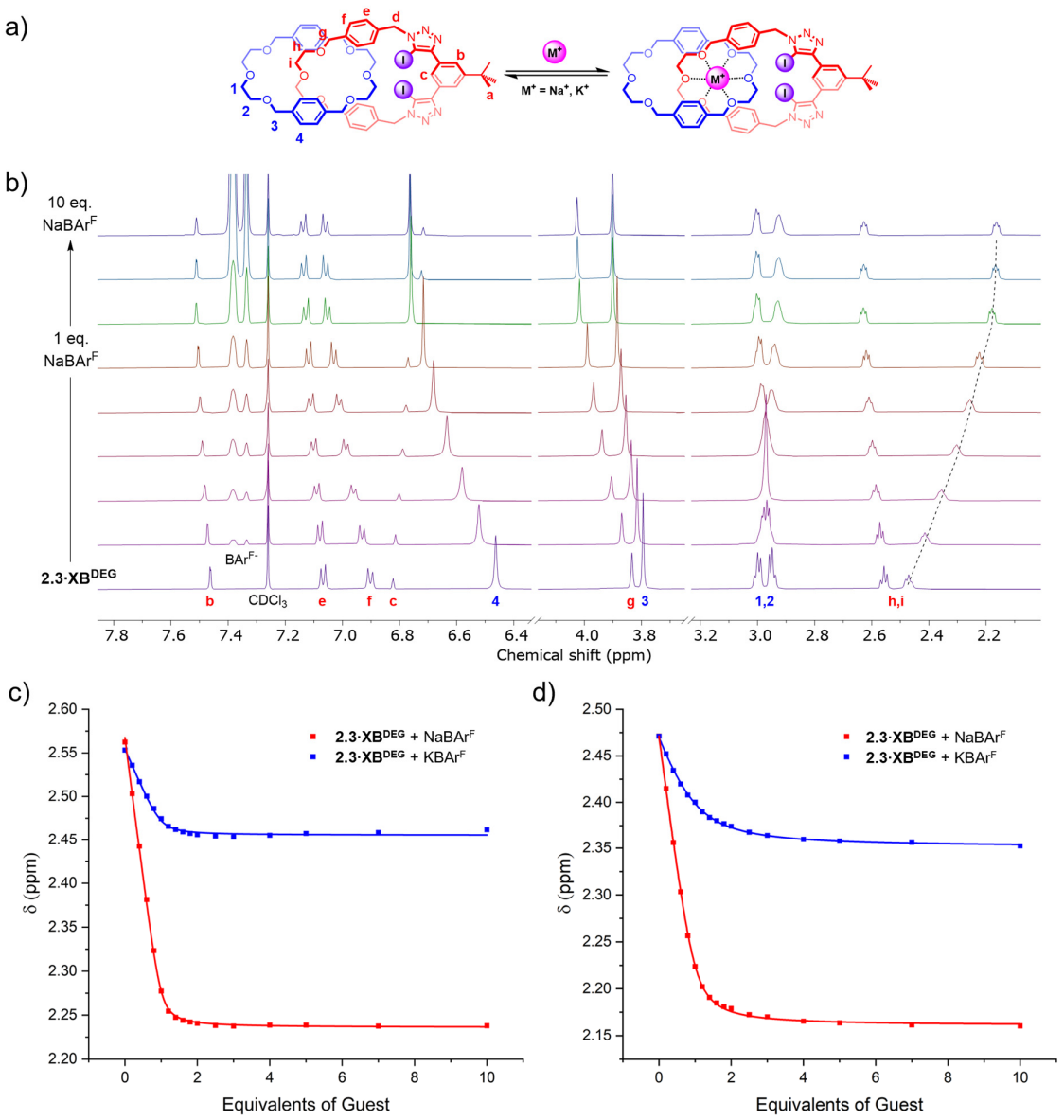


Figure 2.23. *^{1}H NMR alkali metal cation binding studies of hetero[2]catenane **2.3·XB^{DEG}**. (a) Proposed cation binding mode; (b) Representative stacked ^{1}H NMR titration spectra of **2.3·XB^{DEG}** upon progressive addition of 10 eq. NaBAr^F (500 MHz, 3:1 $CD_3CN/CDCl_3$, 298 K); c)-d) Binding isotherms of **2.3·XB^{DEG}** in 1:1 or 3:1 $CD_3CN/CDCl_3$ respectively with NaBAr^F (red) and KBAr^F (blue) generated by monitoring the chemical shifts of $H_{h/i}$, fitted to a 1:1 host-guest binding model.*

2.3.2.2 Anion Binding Studies

The anion binding affinity of [2]catenane **2.3·XB^{DEG}** was subsequently investigated via analogous ^{1}H NMR titrations with tetrabutylammonium halide salts (TBAX, where X = Cl, Br, I). In 1:1 $CD_3CN/CDCl_3$ solvent media, the addition of aliquots of TBAX resulted in significant

peak broadening and merging. Consequentially, the halide association constants of **2.3·XB^{DEG}** could not be determined in this solvent system. In contrast, the ^{1}H NMR signals of the [2]catenane host remained sharp in 3:1 $CD_3CN/CDCl_3$, which possibly reflects more facile co-conformational circum-rotation of the [2]catenane-anion complex in this solvent system. A significant downfield perturbation of the internal benzene signal H_c was observed, indicating that anion binding occurs via XB interactions with the bis(iodotriazole)benzene donor motif (**Figure 2.24a-b**).

Bindfit analysis of the resulting binding isotherms unexpectedly revealed that **2.3·XB^{DEG}** exhibits an approximately 2-fold higher halide association constants than its constituent XB macrocycle **2.1·XB^{DEG}** (**Figure 2.24c**, **Table 2.6**). This enhancement in anion binding affinity upon hetero[2]catenane formation was surprising since the mechanical bond between macrocycles **2.7** and **2.1·XB^{DEG}** ostensibly introduces no additional anion binding groups. We tentatively attribute this enhanced halide affinity to the formation of ancillary CH···X^- interactions involving the aromatic spacers of macrocycle **2.7**, which underwent downfield movements upon addition of TBA halide salts.

Another unexpected result obtained from comparing the anion binding constants of XB macrocycle **2.1·XB^{DEG}** determined in 1:1 and 3:1 $CD_3CN/CDCl_3$ is the increase in anion binding affinity in the more polar solvent mixture. A possible explanation for this observed enhancement is the disruption of intramolecular halogen bonding interactions between the iodotriazole XB donors and the poly(ether) oxygen acceptors in the more competitive solvent mixture, which may enable the catenane to participate in XB···anion interactions with the halide guest. These results represent a case in which altering the polarity of a solvent mixture can have unexpected effects on anion recognition, thereby highlighting the general need for a thorough consideration of solvation effects in the design of supramolecular host-guest systems.

Table 2.6. *Anion association constants (K_a/M^{-1}) for XB macrocycle* ***2.1·XB^{DEG}*** *and hetero[2]catenane* ***2.3·XB^{DEG}*** *determined by ^{1}H NMR titrations.*[a]

Solvent	1:1 $CD_3CN/CDCl_3$		3:1 $CD_3CN/CDCl_3$	
Receptor	**2.1·XB^{DEG}**	**2.3·XB^{DEG}**	**2.1·XB^{DEG}**	**2.3·XB^{DEG}**
Br^-	154(2)	N.D.[b]	261(2)	506(44)
I^-	186(2)	N.D.[b]	277(2)	437(29)

[a] K_a values calculated using Bindfit with a 1:1 host-guest binding model. Errors are shown in parantheses. All anions added as TBA^+ salts. Solvent = 3:1 $CD_3CN/CDCl_3$. T = 298 K. [Receptor] = 1.0 mM. [b]Not determined due to poor resolution of ^{1}H NMR signals.

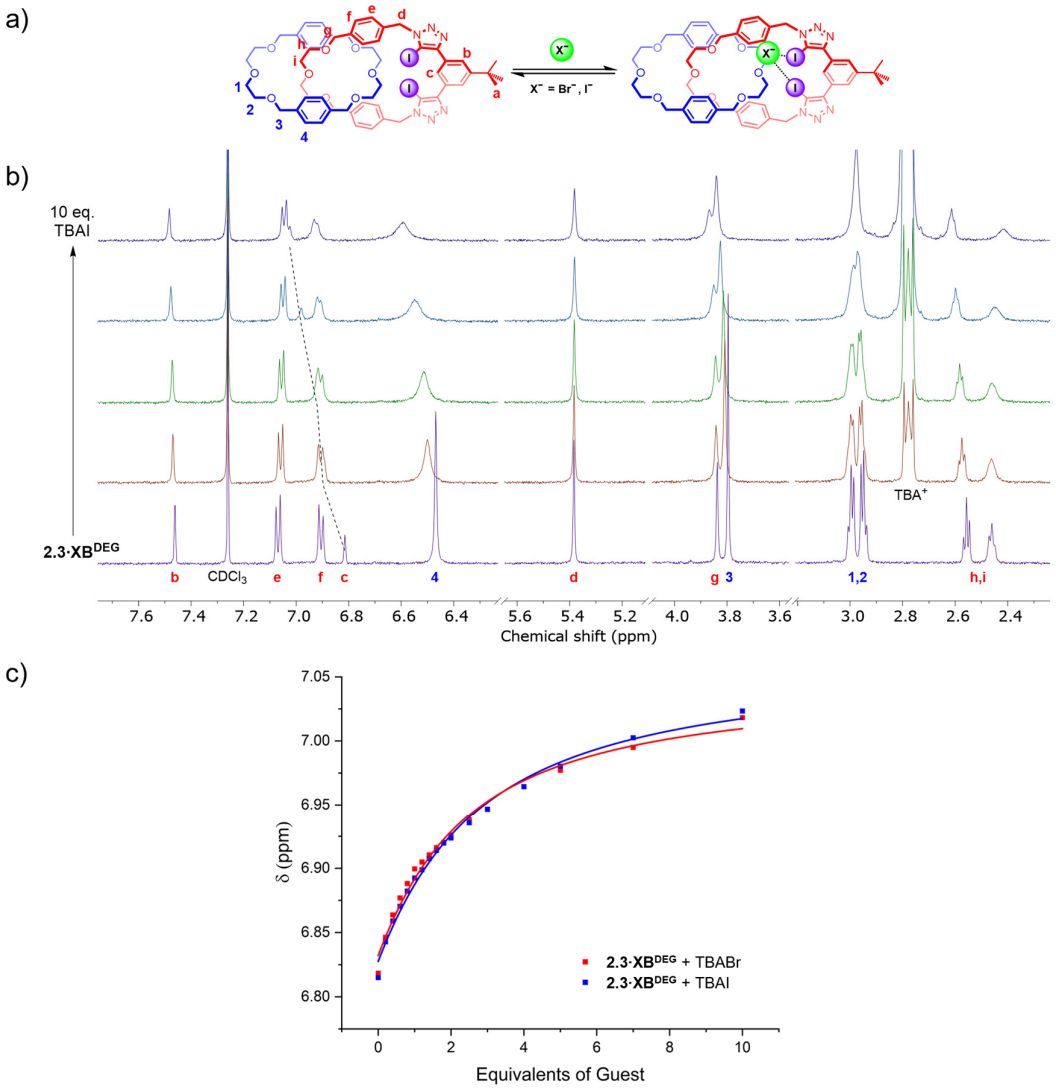


Figure 2.24. *^{1}H NMR halide anion binding studies of hetero[2]catenane* ***2.3·XB^{DEG}****. (a) Proposed cation binding mode; (b) Representative stacked ^{1}H NMR titration spectra of* ***2.3·XB^{DEG}*** *upon progressive addition of 10 eq. TBAI (500 MHz, 3:1 $CD_3CN/CDCl_3$, 298 K); c) Binding isotherms of* ***2.3·XB^{DEG}*** *in 3:1 $CD_3CN/CDCl_3$ with TBABr (red) and TBAI (blue) generated by monitoring the chemical shifts of H_c, fitted to a 1:1 host-guest binding model.*

2.3.2.3 Ion-Pair Binding Studies

Having established that the binding affinity of **2.3·XB^{DEG}** for alkali metal cations is sufficient to ensure near-quantitative complexation to 1 equivalent of sodium or potassium in 1:1 $CD_3CN/CDCl_3$, ^1H NMR ion-pair binding studies were conducted by adding aliquots of TBAX salts (X = Cl, Br, I) to a 1 mM solution of **2.3·XB^{DEG}** pre-complexed to an equimolar amount of MBAr^F (M = Na, K).

Addition of Br^- and I^- resulted in prominent downfield shifts of the internal benzene proton H_c, confirming that anion binding remains primarily mediated by XB interactions (**Figure 2.25a-b**). Importantly, adding up to 10 equivalents of Br^- or I^- causes little to no perturbation of the ethylene glycol proton signals, indicating that the cation binding sites of the catenane remains saturated throughout the titration. In contrast, addition of chloride induces chemical shift changes that are consistent with external ion-pairing and salt recombination, in particular a gradual movement of the di(ethylene glycol) proton resonances to a state resembling the free receptor. This suggests that the ion-pair binding ability of **2.3·XB^{DEG}** remains insufficient to overcome the high lattice enthalpies of NaCl and KCl despite its improved cation affinities.

Binding isotherms for Br^- and I^- were generated by monitoring the downfield shift of H_c and fitted to a 1:1 host-guest binding model to determine apparent anion association constants (K_{app}) of the monocationic catenane-Na^+ complexes (**Figure 2.25c-d**). The apparent bromide and iodide binding constants were found to be in excess of 10^4 M^{-1}, thereby demonstrating a dramatic enhancement in the anion binding affinity of [2]catenane **2.3·XB^{DEG}** in the presence of a co-bound sodium cation. The corresponding K_{app} values of the catenane-K^+ complex were found to be significantly lower **(Table 2.7**), suggesting a binding preference for sodium halide over potassium halide salts by the [2]catenane receptor. Importantly, the

similar chemical shift perturbation profiles observed in the NaX and KX titrations, namely a downfield shift of H_c upon addition of Br^- and I^- and no significant changes in the ethylene glycol proton signals, indicates that ion-pair binding of KBr and KI by the receptor nonetheless remains the dominant process, outcompeting the salt recombination equilibrium. These studies demonstrate strong positive cooperativity between the cation and anion binding events which enables the heteroditopic [2]catenane to act as a potent ion-pair receptor.

In order to quantitatively determine the apparent anion binding constants of the catenane-sodium complexes, the ion-pair binding studies were repeated in the more competitive solvent system 3:1 $CD_3CN/CDCl_3$. The K_{app} values of the sodium halide salts were indeed found to be 2 to 5-fold higher than the analogous potassium salts (**Table 2.7**), indicating that the size-driven selectivity of the [2]catenane **2.3·XB^{DEG}** for sodium over potassium ions translates to its ion-pair recognition properties.

Table 2.7. *Apparent anion association constants (K_{app}/M^{-1}) for catenane-cation complexes of 2.3·XB^{DEG} determined by ^1H NMR titrations.*

Solvent	**Cation**	**Anion**	**K_{app} (M^{-1})**
1:1 $CD_3CN/CDCl_3$	Na^+	Cl^-	Salt recombination
		Br^-	$> 10^4$
		I^-	$> 10^4$
	K^+	Cl^-	Salt recombination
		Br^-	3178(269)
		I^-	2357(268)
3:1 $CD_3CN/CDCl_3$	Na^+	Br^-	4179(204)
		I^-	5392(522)
	K^+	Br^-	1480(69)
		I^-	1243(96)

[a] K_{app} values calculated using Bindfit with a 1:1 host-guest binding model. Errors are shown in parantheses. All cations added as BAr^{F-} salts and anions as TBA^+ salts. T = 298 K. [Receptor] = [$MBAr^F$] = 1.0 mM.

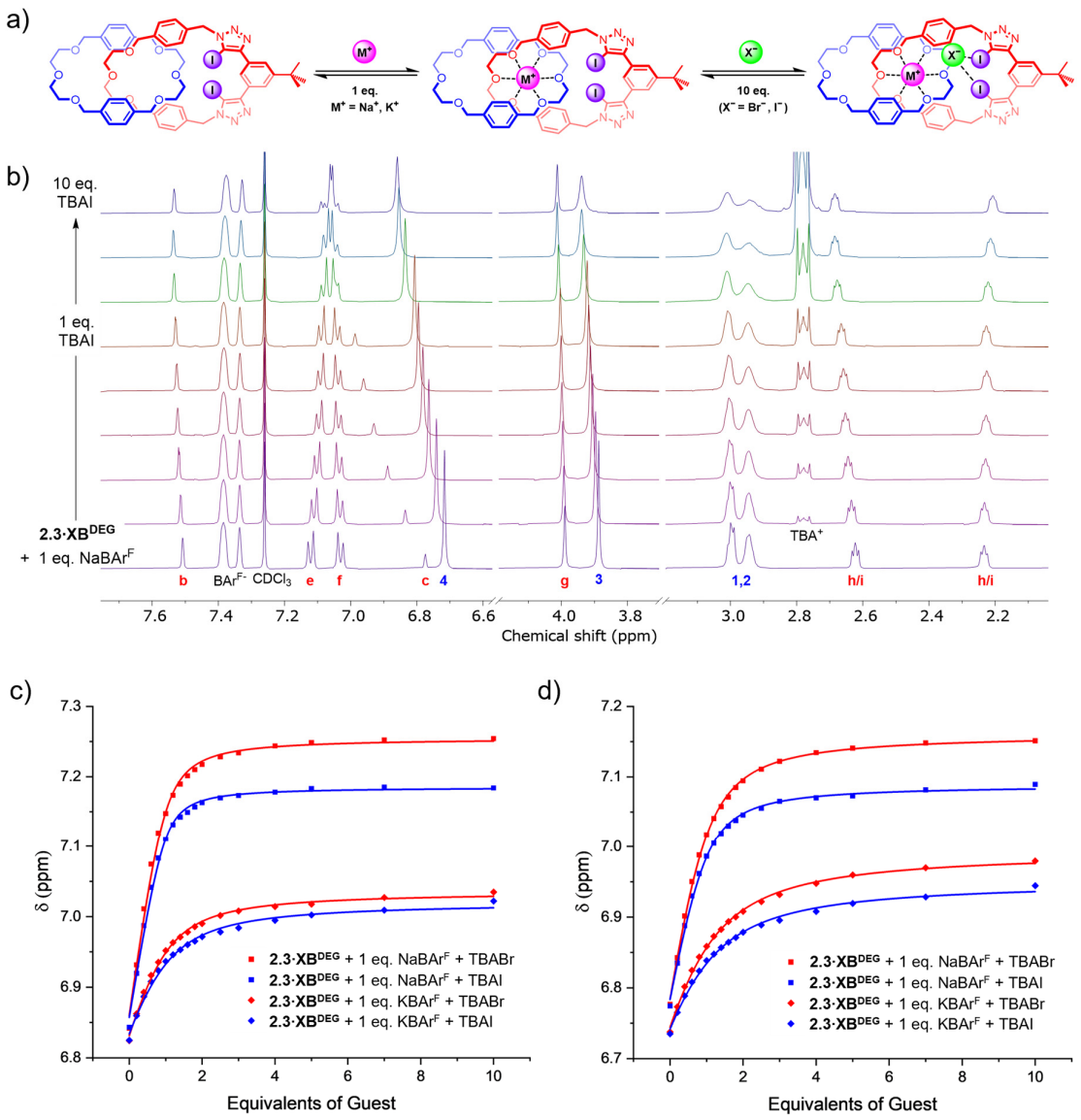


Figure 2.25. *^{1}H NMR ion-pair binding studies of hetero[2]catenane **2.3·XB^{DEG}**. (a) Proposed ion-pair binding equilibrium; (b) Representative stacked ^{1}H NMR titration spectra of **2.3·XB^{DEG}** upon progressive addition of 10 eq. TBAI in the presence of 1 eq. NaBAr^F (500 MHz, 3:1 $CD_3CN/CDCl_3$, 298 K); Binding isotherms of **2.3·XB^{DEG}** in: c) 1:1 $CD_3CN/CDCl_3$; d) 3:1 $CD_3CN/CDCl_3$, pre-complexed with Na^+ (squares) or K^+ (diamonds) upon addition of TBABr (blue) and TBAI (green), generated by monitoring the chemical shifts of internal benzene proton H_c, fitted to a 1:1 host-guest binding model.*

2.3.3 X-ray Crystallographic Analysis of Ion-Pair Binding

Solid-state x-ray crystallographic analysis confirmed the proposed host-separated ion-pair binding mode of **2.3·XB^{DEG}**. Single crystals suited for analysis by SCXRD were obtained

by slow evaporation of a 1:1 $CD_3CN/CDCl_3$ solution containing **2.3·XB^{DEG}** in the presence of 1 eq. $NaBAr^F$ and excess TBAI. The solid-state crystal structure revealed a 1:1 complex of catenane **2.3·XB^{DEG}** bound to an NaI ion-pair, in which the guest ions are bound in a separated ion-pair binding mode consistent with solution-phase NMR studies (**Figure 2.26**). The polyether regions of the two macrocyclic components **2.7** and **2.1·XB^{DEG}** are arranged in an orthogonal geometry to form a three-dimensional interlocked cation binding pocket. The sodium cation resides within this binding pocket where it is convergently bound by three oxygen atoms each from **2.7** and **2.1·XB^{DEG}** in a distorted six-coordinate distorted octahedral coordination geometry. In contrast, the iodide anion is perched on the periphery of the XB macrocycle **2.1·XB^{DEG}** where it is bound via XB interactions with the bis(iodotriazole)benzene motif, as evidenced in the short I···I− distances (3.460(4)-3.482(4) Å, which is 87-98% of the sum of the van der Waal radii of the two atoms).

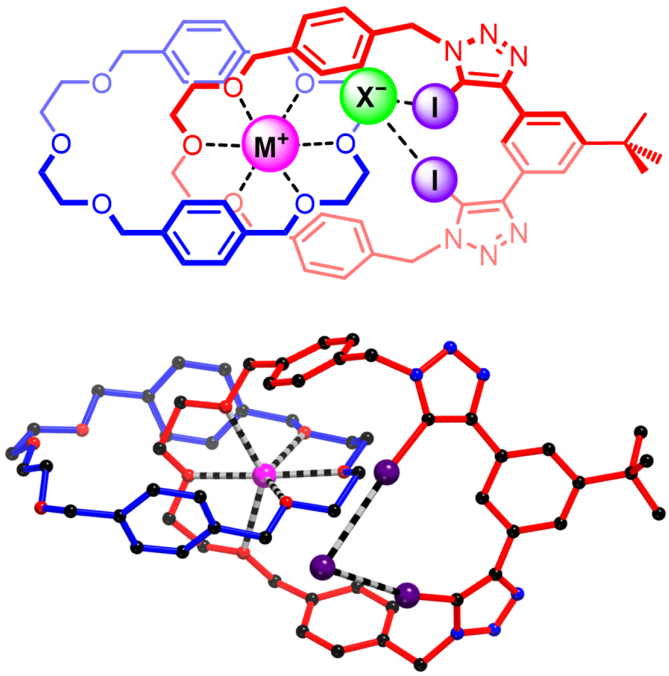


Figure 2.26. *Solid-state XRD structure of **2.3·XB^{DEG}** bound to an NaI ion-pair in a host-separated binding mode. Hydrogen atoms have been omitted for clarity. Atom colours are as follows: black (carbon), blue (nitrogen), red (oxygen), purple (iodine), pink (sodium). The chemical structure of the catenane is shown on the left for reference.*

2.3.4 Preferential Solid-Liquid Extraction of NaX over KX Salts

The ability of hetero[2]catenane **2.3·XB^{DEG}** to extract and solubilise alkali metal halide salts in organic solvents was investigated via a series of solid-liquid extraction studies. In a typical experiment, a 1 mM $CDCl_3$ solution of **2.3·XB^{DEG}** was sonicated in the presence of a fixed excess mass quantity of solid MX salt (M = Na, K; X = Br^-, I^-).

The pre- and post-extraction ^{1}H NMR spectra of **2.3·XB^{DEG}** revealed large perturbations following treatment with NaBr and NaI (**Figure 2.27**) which are consistent with the changes observed upon ion-pair binding in the solution-state ^{1}H NMR titration studies. Notably, a significant upfield shift of internal benzene proton H_c was observed, as well as de-symmetrisation of the ethylene glycol protons $H_{h/i}$, which are respectively diagnostic of anion and cation binding by the [2]catenane. The subsequent addition of 0.25 equivalents of free hetero[2]catenane **2.3·XB^{DEG}** to this solution resulted in the appearance of a minor set of peaks corresponding to the unbound receptor, confirming that the ion-pair bound [2]catenane complex exists in slow exchange with the free catenane on the NMR timescale. These results suggest complete stoichiometric extraction of both NaX salts, with the post-extraction solution containing only the ion-pair bound [2]catenane complex.

In contrast, the post-extraction spectrum of **2.3·XB^{DEG}** following treatment with KBr and KI featured two distinct set of catenane-derived peaks. In the case of KBr, shown in **Figure 2.27**, the major set corresponds to the free catenane, while the minor set exhibits chemical shifts similar to that of the **2.3·XB^{DEG}·NaBr** ion-pair bound complex. Addition of 0.25 equivalents of free hetero[2]catenane **2.3·XB^{DEG}** to this sample resulted in an increase in the intensity of the major set of peaks relative to the minor set, confirming that these peaks arise from the free receptor. This indicates that the catenane is only capable of partially extracting KBr into solution phase, with the free and bound receptors undergoing slow exchange on the NMR

timescale. Integration of the peaks estimates that 43% of the receptor present in solution exists as the ion-pair bound complex.

The higher observed efficiency of sodium halide extraction by **2.3·XB^{DEG}** prompted a further investigation into the extraction preferences of the catenane receptor via a competitive NaX/KX solid-liquid extraction experiment. To this end, in an analogous procedure to the above-described experiments, a 1 mM $CDCl_3$ solution of **2.3·XB^{DEG}** was exposed to a mixture of NaBr/KBr or NaI/KI present in excess. This resulted in post-extraction spectra identical to those obtained from treatment of the receptor solely with the corresponding sodium halide salt (**Figure 2.27**), providing promising evidence that **2.3·XB^{DEG}** is capable of preferential sodium halide extraction over the corresponding potassium halide salts. Importantly, this shows that despite the higher lattice enthalpies of sodium over potassium halide salts, the mechanical bond effect enables size-based discrimination to achieve sodium halide selective ion-pair recognition and extraction.

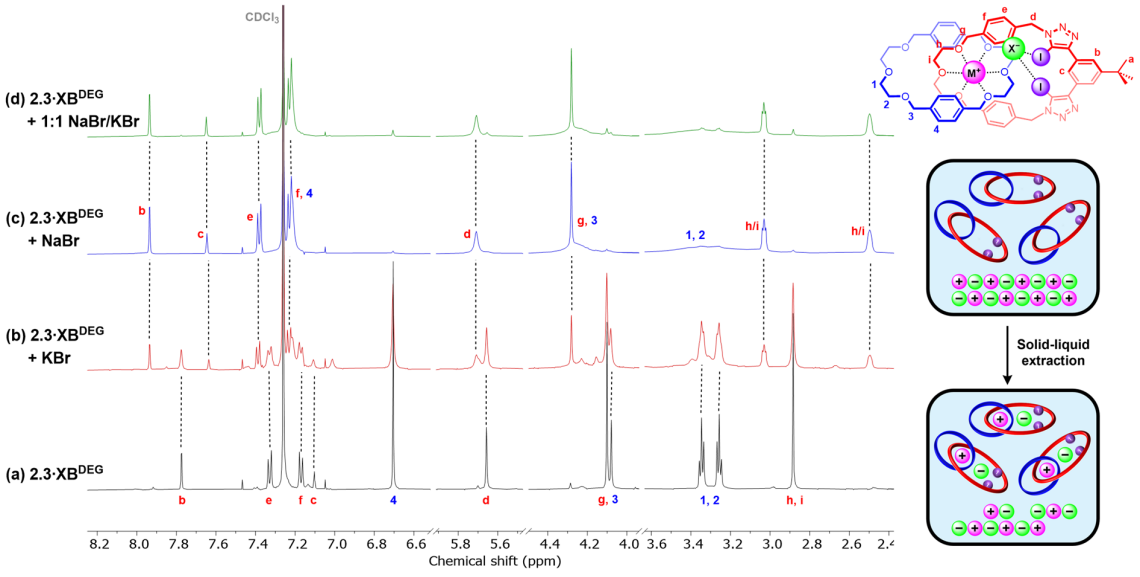


Figure 2.27. *Solid-liquid extraction studies of alkali metal bromide salts, showing truncated ^{1}H NMR spectra of: (a) free catenane receptor **2.3·XB^{DEG}**, and post-extraction spectra of **2.3·XB^{DEG}** following treatment with (b) 10 mg KBr; (c) 10 mg NaBr; (d) 5 mg NaBr and 5 mg KBr ($CDCl_3$, 298 K, 500 MHz). The inset on the right shows the structure of **2.3·XB^{DEG}** bound to an MX ion-pair (top) and a schematic illustrating the SLE experiment (bottom).*

2.4 Conformationally Dynamic [2]Rotaxane Systems for Ion-Pair Binding

The intriguing ion-pair binding properties of homo- and hetero[2]catenanes prompted us to investigate their XB heteroditopic [2]rotaxane analogues as ion-pair receptors for alkali metal halide salts (**Figure 2.28**). The target [2]rotaxanes could conceivably be prepared by performing a stoppering-type reaction of the intermediate pseudo[2]rotaxane assembly with bulky terphenyl-substituted iodoalkynes as stoppering groups. To the best of our knowledge, comparative studies of "mechanical bond isomers" is unprecedented in the context of ion-pair recognition by interlocked structures, which is surprising considering the markedly different conformational behaviours of rotaxanes and catenanes. A systematic comparison of the cation, anion and ion-pair recognition properties of heteroditopic [2]rotaxanes and [2]catenanes containing chemically analogous binding sites may therefore serve to inform and guide the design of future MIM-based ion-pair receptors.

In this section, we describe the synthesis of four heteroditopic [2]rotaxanes containing poly(ethylene)-glycol based cation binding sites and XB iodotriazole or mixed XB/HB iodotriazole/prototriazole anion binding sites. ^{1}H NMR binding studies showed that despite the [2]rotaxanes possessing weaker individual cation and anion binding affinities, their ion-pair binding properties were enhanced relative to the analogous [2]catenanes. The notably higher level of positive cooperativity between the cation and anion binding events highlights the potential advantages of greater co-conformational adaptive behaviour in mechanically interlocked ion-pair hosts.

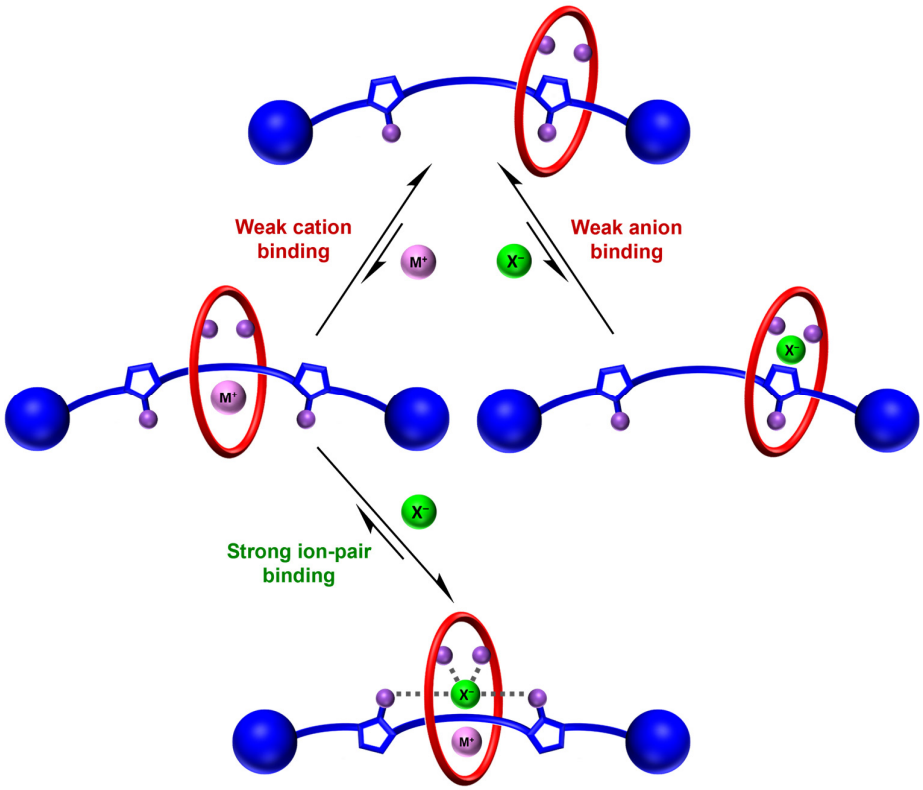


Figure 2.28. *Cartoon representation of the target conformationally dynamic heteroditopic [2]rotaxanes, highlighting the strong positive cooperativity in ion-pair binding.*

2.4.1 Synthesis and Characterisation

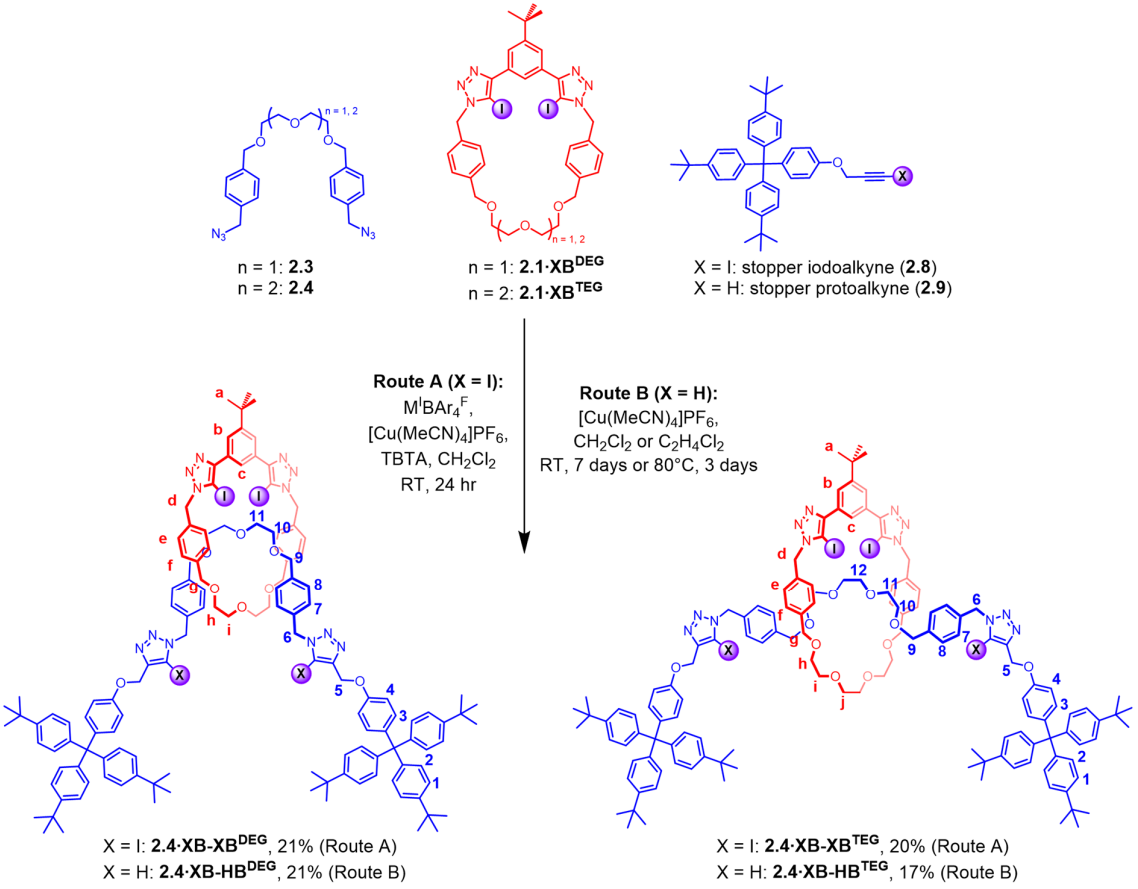
The all-halogen bonding [2]rotaxanes **2.4·XB-XB^{DEG}** and **2.4·XB-XB^{TEG}**, which are based on di- and tri(ethylene glycol) cation binding motifs respectively, were readily synthesised via an alkali metal template-directed pseudo[2]rotaxane formation followed by a double stoppering CuAAC reaction between the threaded bis(azide) and iodoalkyne stopper **2.8**. In a typical reaction, the macrocycles **2.1·XB^{DEG}** or **2.1·XB^{TEG}** were pre-complexed with 1 eq. MBAr^{F} (M = Na^+ or K^+) and the corresponding bis(azide) **2.3** or **2.4** in CH_2Cl_2, to which was added 2.5 eq. stopper iodoalkyne **2.8**, followed by dropwise addition of $Cu(CH_3CN)_4PF_6$ and TBTA to facilitate rotaxane formation via a CuAAC reaction. After stirring at room temperature for 24 hours, mass spectrometric analysis of the reaction mixtures revealed peaks with m/z = 2565 and 2652, corresponding to the $[M+H]^+$ adducts of the desired rotaxanes.

Aqueous work-up with EDTA/NH_4OH and purification by preparative thin-layer chromatography afforded the target rotaxanes **2.4·XB-XB^{DEG}** and **2.4·XB-XB^{TEG}** in 21% and 20% yields respectively (**Scheme 2.4**, Route A).

In contrast, we were unable to prepare the mixed HB/XB rotaxanes **2.4·XB-HB^{DEG}** and **2.4·XB-HB^{TEG}**, which contain iodotriazole groups in the macrocycle and prototriazole groups in the axle, by employing a similar alkali metal template strategy with an alkyne stopper **2.9**. When the stopper proto-alkyne was added to the reaction mixture, immediate precipitation occurred, which persisted despite prolonged sonication. After two days, TLC analysis of the reaction mixture showed nearly complete consumption of the bis(azide), but the target [2]rotaxane was not observed on ESI mass spectrometry and purification of the crude yielded only non-interlocked axle product. This may suggest the formation of a highly insoluble Cu(I) acetylide complex which is presumably active towards CuAAC reaction, but incapable of effectively participating in a CuAAC reaction with the Na^+ templated pseudo[2]rotaxane complex.

We therefore turned to an alternative active metal template strategy to prepare the target [2]rotaxanes. Motivated by our previous demonstration that iodotriazoles are bifunctional motifs capable of acting as ligands for Cu(I) coordination in an active metal template reaction,[64] we pre-complexed the macrocycles **2.1·XB^{DEG}** or **2.1·XB^{TEG}** with $[Cu(MeCN)_4]PF_6$ by stirring at room temperature for 30 min. Subsequently, 4 eq. of the relevant bis(azide) **2.3** or **2.4** as well as 8 eq. of stopper alkyne **2.9** were added. After several days, aqueous work-up and purification by preparative TLC afforded **2.4·XB-HB^{DEG}** and **2.4·XB-HB^{TEG}** in 21% and 17% yields respectively (**Scheme 2.4**, Route B). Notably, although the rotaxane yields obtained were comparable to the alkali metal cation template-directed strategy, the CuAAC-AMT methodology required a considerable excess of both the bis(azide) and stopper alkyne

components as well as longer reaction times and/or elevated temperatures to achieve commensurate yields (3 days for **3·XB-HB^{DEG}** at 80 °C or 7 days for **3·XB-HB^{TEG}** at room temperature).



Scheme 2.4. *Synthesis of [2]rotaxanes via metal cation template-directed pseudo-[2]rotaxane formation to prepare all-XB rotaxanes (Route A) or Cu^{I}-mediated active metal templation to prepare mixed XB-HB rotaxanes (Route B).*

The four [2]rotaxanes were fully characterised by ^{1}H NMR, ^{13}C NMR and HR-MS. The ^{1}H NMR resonances of several macrocycle and axle protons, in particular the signals corresponding to H_6-$H_{11(12)}$ (axle) and H_d-$H_{i(j)}$ (macrocycle), were difficult to distinguish solely on the basis of chemical shift as both interlocked components were derived from the same bis(azide) core. ^{1}H-^{1}H COSY and ROESY 2D NMR techniques were therefore employed to obtain an unambiguous assignment of all proton signals.

2.4.2 ^{1}H NMR Co-conformational Analysis of [2]Rotaxanes

A comparison of the ^{1}H NMR spectra of the rotaxanes to their constituent non-interlocked components in 1:1 $CD_3CN/CDCl_3$ (**Figures 2.29-2.30**) reveals general upfield shifts in the proton resonances arising from both the macrocycle and axle (**Table 2.8**), consistent with the shielding effect that typically accompanies mechanical bond formation.

A detailed examination of the observed chemical shift changes provided interesting insights into the preferred co-conformation of the [2]rotaxanes in the absence of ion binding events. In the axle component of the di(ethylene glycol) (DEG)-based all-XB rotaxane **2.4·XB-XB^{DEG}** (**Figure 2.29a**), the largest changes occurred at the peaks corresponding to xylene protons H_7, which moved upfield by 0.54 ppm in the rotaxane **2.4·XB-XB^{DEG}** relative to the free axle **2.5·XB^{DEG}**. Significant upfield movements were also observed in xylene proton signal H_8 (0.45 ppm) and methylene singlet H_9 (0.35 ppm). In contrast, the di(ethylene glycol) protons H_{10} and H_{11} (0.14 and 0.19 ppm) showed only modest upfield shifts (**Table 2.8**). This suggests that, in the free rotaxane **2.4·XB-XB^{DEG}**, the macrocycle preferentially resides over the xylene spacers rather than the central di(ethylene glycol) station, which is presumably due to favourable π-π interactions between two of the aromatic surfaces of the constituent axle and macrocycle components.

In the analogous HB/XB rotaxane **2.4·XB-HB^{DEG}** (**Figure 2.29b**), the upfield movements of the xylene-derived protons H_7 (0.75 ppm) and H_8 (0.51 ppm) in the rotaxane relative to the axle **2.5·HB^{DEG}** are even larger, as is the case for xylene-proximal methylene singlet H_6 (0.29 ppm). In contrast, the upfield movements in ethylene glycol protons H_{10} and H_{11} are slightly diminished (0.10 and 0.18 ppm) (**Table 2.8**). This suggests that there is an even stronger preference for the macrocycle to reside at the xylene-triazole region of the axle in the mixed HB/XB rotaxane compared to the all-XB rotaxane. This may be due to the propensity

for the axle triazole proton to undergo C-H···O hydrogen bonding with the di(ethylene glycol) oxygen atoms of the macrocycle.[65] This proposed HB interaction between the axle triazole and macrocycle di(ethylene glycol) linker is further supported by the ^{1}H-^{1}H 2D ROESY NMR spectrum of **2.4·XB-HB^{DEG}**, which shows strong cross-peaks between the axle triazole proton H_{trz} and macrocycle ethylene glycol protons $H_{h/i}$.

In the macrocycle, the internal benzene proton H_c exhibits a dramatic upfield shift upon rotaxane formation in both the all-XB rotaxane **2.4·XB-XB^{DEG}** (1.09 ppm) and mixed XB/HB rotaxane **2.4·XB-HB^{DEG}** (1.15 ppm), likely a result of its increased proximity to the shielding ring currents of the aromatic groups in the axle. Interestingly, in the tri(ethylene glycol) (TEG)-based rotaxanes the upfield shifts in H_c, whilst still large, are markedly less pronounced (**2.4·XB-XB^{TEG}**: 0.65 ppm; **2.4·XB-HB^{TEG}**: 0.72 ppm). Presumably, the larger macrocyclic cavity reduces the spectral effects associated with mechanical bond formation.

Further evidence for the greater preference of the macrocycle for the triazole/xylene station of the axle in the mixed XB-HB [2]rotaxanes was obtained by directly comparing the chemical shifts of the axle protons in the analogous pairs of rotaxanes **2.4·XB-XB^{DEG}**/**2.4·XB-HB^{DEG}** and **2.4·XB-XB^{TEG}**/**2.4·XB-HB^{TEG}** (**Table 2.8**). To delineate the contribution of co-conformational effects from the inductive effects from changing the 5-substituent of the triazole moieties, the chemical shift differences of each proton in the corresponding pairs of axle components **2.5·XB^{DEG}**/**2.5·HB^{DEG}** and **2.5·XB^{TEG}**/**2.5·HB^{TEG}** were also determined and found to be < 0.1 ppm for all proton environments.

Notably, the axle xylene proton H_7 was located 0.20 ppm upfield in the mixed XB/HB rotaxane **2.4·XB-HB^{DEG}** relative to the all-XB rotaxane **2.4·XB-XB^{DEG}**. In contrast, a comparison of the non-interlocked axles showed that H_7 is located very slightly downfield (0.006 ppm) in **2.5·HB^{DEG}** relative to **2.5·XB^{DEG}**. This suggests that the greater shielding

experienced by H_7 in **2.4·XB-HB^{DEG}** arises predominantly from co-conformational effects, indicative of the macrocycle showing a greater bias towards the triazole/xylene station in the mixed XB-HB rotaxane. Likewise, the xylene-proximal methylene singlet H_6 occurs 0.17 ppm upfield in **2.4·XB-HB^{DEG}** relative to **2.4·XB-XB^{DEG}**. This is approximately twice the corresponding upfield displacement of H_6 in the non-interlocked axle components **2.5·XB^{DEG}** and **2.5·HB^{DEG}** (0.08 ppm), suggesting that both inductive and co-conformational effects contribute to the greater shielding of H_6 in **2.5·XB-HB^{DEG}**.

Table 2.8. *Comparison of selected ^{1}H NMR chemical shifts of [2]rotaxanes and axles*

Protons	Rotaxane vs. Axle: $\Delta\delta_{2.4/2.5}$ (ppm)[a]				All-XB vs. HB-XB: $\Delta\delta_{HB/XB}$ (ppm)[b]			
	DEG		TEG		DEG		TEG	
	XB-XB	XB-HB	XB-XB	XB-HB	2.4	2.5	2.4	2.5
H_3	0.1598	0.0600	0.0899	0.0522	-0.08	0.0198	-0.0195	0.0182
H_4	0.3234	0.1186	0.1843	0.1089	-0.1647	0.0401	-0.0374	0.038
H_5	0.1142	0.0773	0.1456	0.1219	-0.0798	-0.0429	-0.069	-0.0453
H_6	0.1986	0.2860	0.1789	0.2125	0.1672	0.0798	0.1141	0.0805
H_7	0.5436	0.7512	0.3678	0.4202	0.2016	-0.006	0.0437	-0.0087
H_8	0.4572	0.5098	0.3426	0.4288	0.0302	-0.0224	0.0574	-0.0288
H_9	0.3466	0.3646	0.2533	0.2989	0.0147	-0.0033	0.0412	-0.0044
H_{10}	0.1425	0.0996	0.1215	0.1047	-0.0429	0.0000	-0.0164	0.0004
H_{11}	0.1932	0.1842	0.1661	0.1751	-0.0086	0.0004	0.0098	0.0008
H_{12}	-	-	0.0829	0.0637	-	-	-0.0188	0.0004
H_{trz}	-	0.1365	-	0.1634	-	-	-	-

[a]$\Delta\delta_{2.4/2.5}$ (ppm) = δ(axle) – δ(rotaxane). For example, the [DEG, XB-XB] column shows the Δδ values calculated from: δ(**2.5·XB^{DEG}**) – δ(**2.4·XB-XB^{DEG}**). [b]$\Delta\delta_{HB/XB}$ (ppm) = δ(XB compound) – δ(HB compound). For example, the [DEG, 2.4] column shows the Δδ values calculated from: δ(**2.4·XB-XB^{DEG}**) – δ(**2.4·XB-HB^{DEG}**). All ^{1}H NMR spectra run in 1:1 $CD_3CN/CDCl_3$, 500 MHz, 298 K. Background colours are used to indicate the magnitude of the chemical shift difference. Red: $|\Delta\delta| > 0.3$ ppm; Orange: $0.2 < |\Delta\delta| < 0.3$ ppm; Yellow: $0.1 < |\Delta\delta| < 0.2$ ppm.

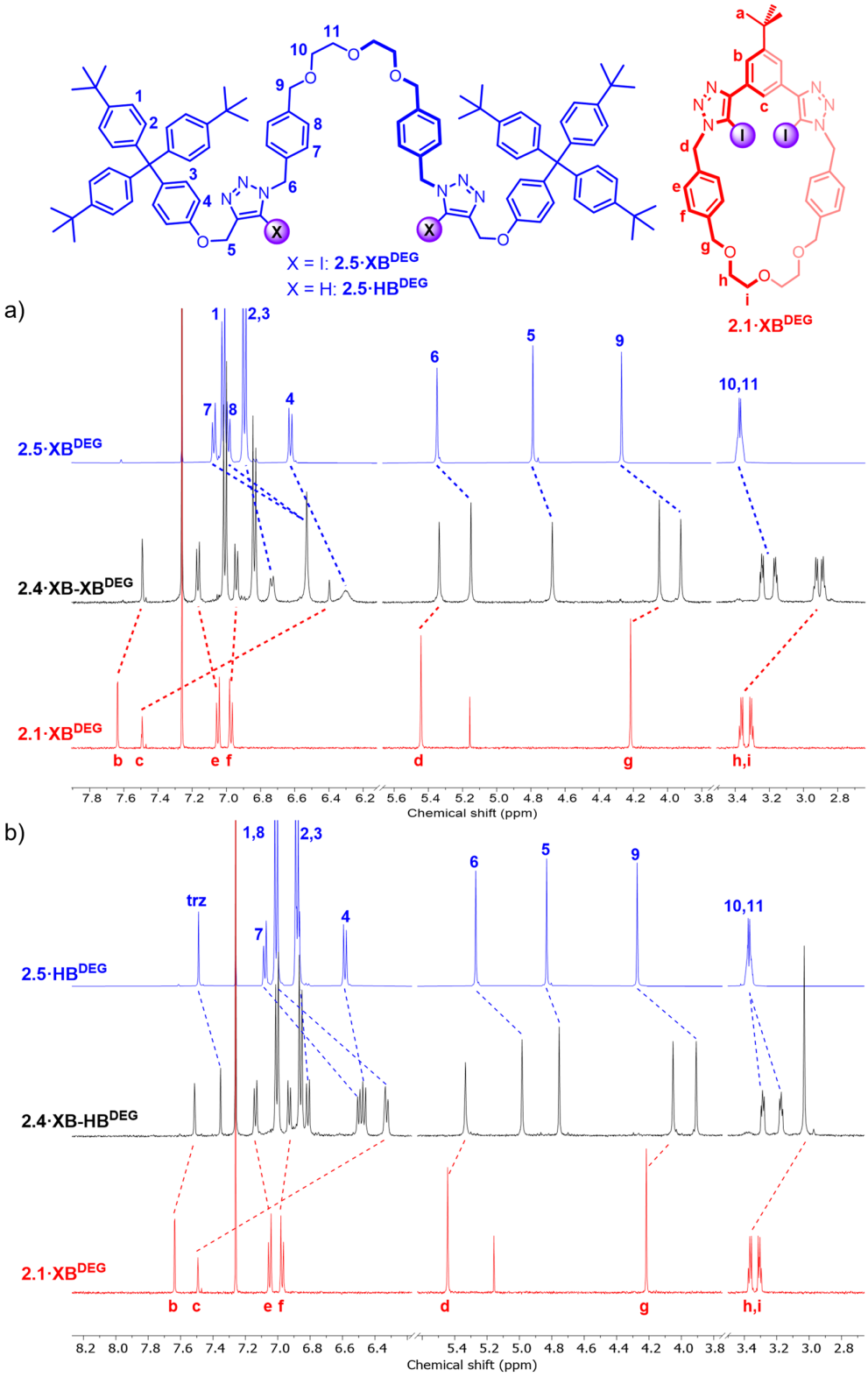


Figure 2.29. *Stacked ^{1}H NMR spectra of the axle (top), [2]rotaxane (middle) and XB macrocycle (bottom) of a)* ***2.4·XB-XB^{DEG}****; b)* ***2.4·XB-HB^{DEG}*** *(500 MHz, $CDCl_3$, 298 K).*

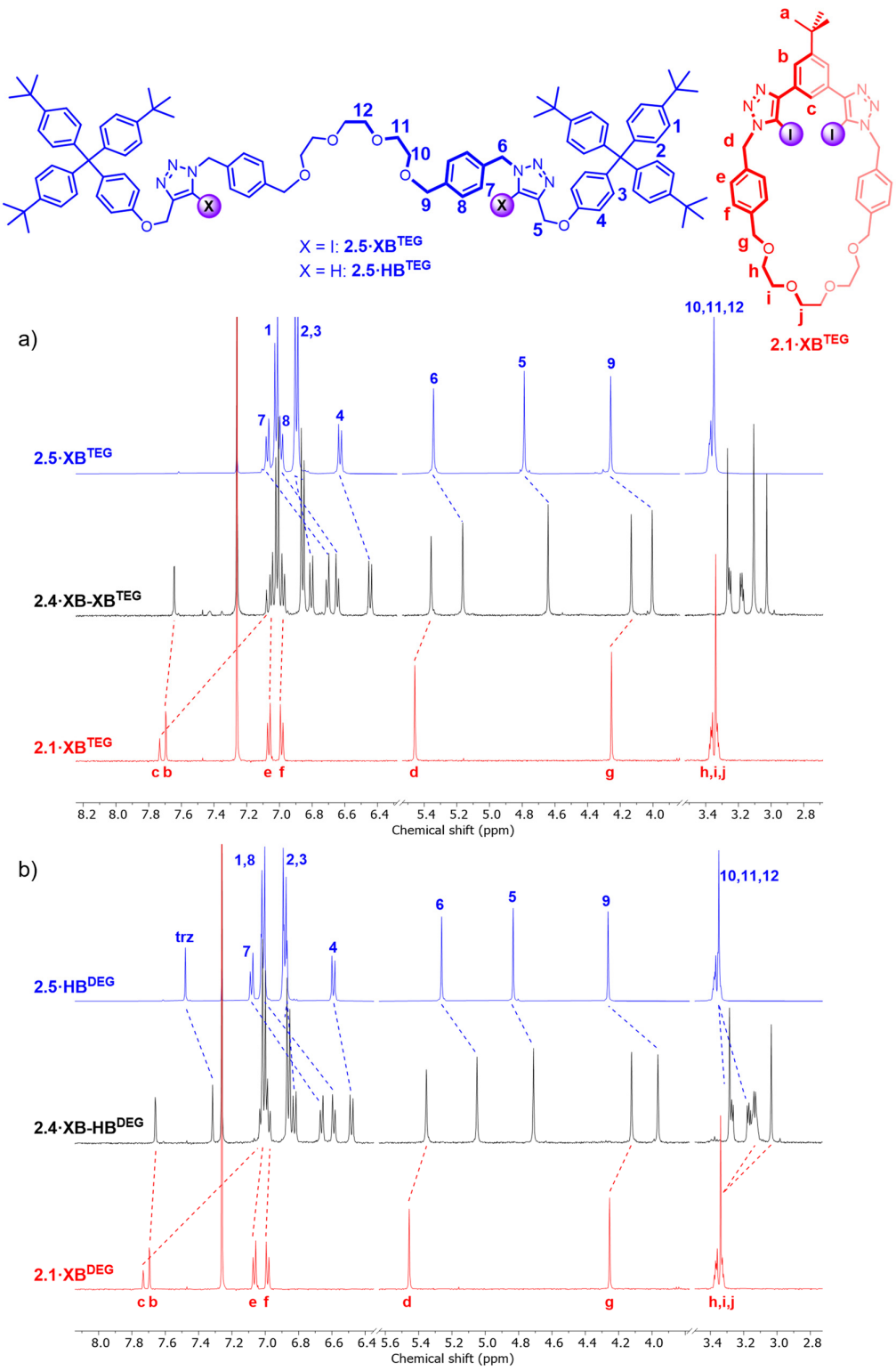


Figure 2.30. *Stacked ^{1}H NMR spectra of the axle (top), [2]rotaxane (middle) and XB macrocycle (bottom) of a)* ***2.4·XB-XB^{TEG}****; b)* ***2.4·XB-HB^{TEG}*** *(500 MHz, $CDCl_3$, 298 K).*

2.4.3 ^{1}H NMR Ion Binding Studies

The cation, anion and ion-pair binding properties of the four rotaxanes were investigated by ^{1}H NMR titrations in 1:1 $CDCl_3/CD_3CN$, under identical conditions to those used previously to investigate the binding properties of the analogous [2]catenanes. A direct comparison of the ion-pair binding properties of the rotaxane and catenane topologies could thus be drawn in this solvent system.

2.4.3.1 Cation Binding Studies

Upon progressive addition of $MBAr^F$ ($M = Na^+$, K^+) to all four rotaxanes, the largest movements were observed in the signals corresponding to protons in the oligo(ethylene glycol) regions (**Figure 2.32b**). In particular, the axle protons H_{10}, H_{11} (as well as H_{12} in the TEG-based rotaxanes **2.4·XB-XB^{TEG}** and **2.4·XB-HB^{TEG}**) shifted upfield, indicative of cation coordination by the oligo(ethylene glycol) oxygen atoms (**Figure 2.32a**). In contrast, the corresponding ethylene glycol protons of the macrocycle H_h and H_i (and H_j) exhibited modest downfield shifts. This is tentatively rationalised by the competing upfield and downfield shifts induced respectively by cation coordination and macrocycle translocation away from the shielding xylene groups of the axle. Significant downfield shifts also occurred in some axle proton signals distal from the proposed cation binding site, most notably xylene protons H_7 and H_8 (in all rotaxanes) and the triazole protons H_{trz} (present only in **2.4·XB-HB^{DEG}** and **2.4·XB-HB^{TEG}**), while H_4, H_5 and H_6 exhibited smaller downfield movements. Taken together, these spectral changes suggest that the macrocycle shuttles to the oligo(ethylene glycol) region of the axle in the presence of a cationic guest, presumably to enable the formation of a 3D cavity in which the polyether regions of the macrocycle and axle are able to convergently bind the cationic guest. Cation binding can therefore serve as a stimulus to induce large amplitude co-conformational changes in dynamic MIM-based receptors.

The binding isotherms obtained by monitoring the chemical shift movements of the ethylene glycol region of the axle (H_{10} and/or H_{12}) were analysed using Bindfit[66] analysis and fitted to a 1:1 host-guest binding model to determine the cation association constants of each rotaxane (**Figure 2.32c-d**, **Table 2.9**). Attempts to fit to various 1:2 host-guest binding models were unsuccessful, concordant with the proposed binding mode in which both oligo(ethylene glycol) regions act convergently to bind one alkali metal cation per rotaxane.

The TEG-based rotaxanes exhibited stronger binding to both Na^+ and K^+ than their respective DEG-based analogues, presumably due to the larger number of polyether oxygen donors available for cation complexation (**Table 2.9**). Similar to the [2]catenane systems, the DEG-based rotaxanes show a preference for the smaller Na^+ cation, while the reverse is true for the TEG-based rotaxanes, in accordance with the anticipated size complementarity between the binding cavity and the preferred cation.

Despite possessing ostensibly identical cation binding sites, the analogous mixed XB/HB rotaxanes display significantly reduced cation affinity compared to the all-XB analogues. This is likely due to the energetic cost of disrupting the intercomponent C-H···O hydrogen bonds between the axle triazole proton and the macrocycle polyether oxygen atoms (**Figure 2.31**) which is consistent with the aforementioned co-conformational bias of the HB rotaxanes. Similar HB interactions were previously observed in the single crystal X-ray structure of a mixed XB/HB catenane.[65]

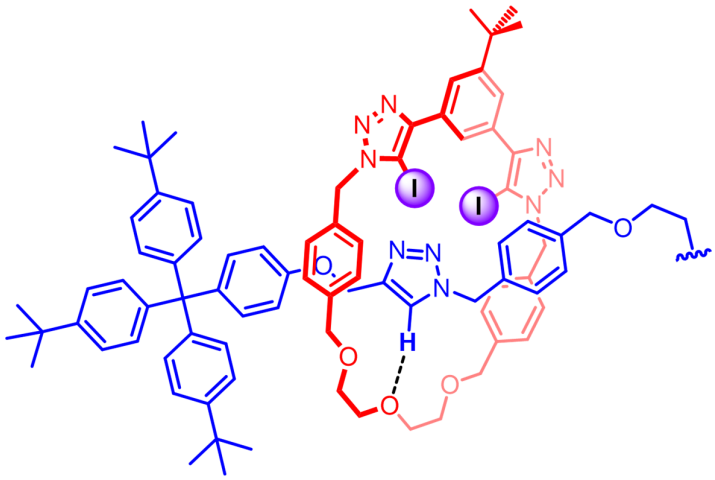


Figure 2.31. *Truncated chemical structure of* ***2.4·XB-HB^{DEG}*** *showing postulated intercomponent hydrogen bonding interactions.*

Compared to the all-XB catenanes, the all-XB rotaxanes **2.4·XB-XB^{DEG}** and **2.4·XB-XB^{TEG}** display significantly weaker cation binding affinities, with the determined K_a values of the [2]rotaxanes being 2-4 fold lower than the corresponding [2]catenanes in all cases **(Table 2.9)**. This suggests a lower degree of pre-organisation in the cation binding sites of the rotaxanes, consistent with the macrocycle having to translocate from the xylene/triazole region of the axle to the central ethylene glycol station in order to participate in cation binding. The greater co-conformational flexibility of the [2]rotaxane topology was therefore concluded to be detrimental for promoting strong binding to cations individually.

Table 2.9. *Cation binding constants (K_a/M^{-1}) of interlocked receptors determined by ^{1}H NMR.*[a]

Guest	**2.4·XB-XB^{DEG}**	**2.4·XB-HB^{DEG}**	**2.4·XB-XB^{TEG}**	**2.4·XB-HB^{TEG}**
Na^+	216(3) **2.2**: 756(11)[b]	110(1) **2.2**: 36(1)[b]	403(5) **2.2**: 753(10)[b]	244(3)
K^+	69(1) **2.2**: 284(2)[b]	N. B.[c]	724(11) **2.2**: 1734(15)[b]	329(4)

[a]K_a values calculated using Bindfit with a 1:1 host-guest binding model. Errors are shown in parentheses and are all <2%. All cations added as BAr^{F-} salts. Solvent = 1:1 $CDCl_3/CD_3CN$. T = 298 K. [Receptor] = 1.0 mM. [b]Where present, the value after "**2.2**:" indicates the previously determined K_a of the analogous [2]catenane for the same metal cation. [c]N.B. = No binding observed.

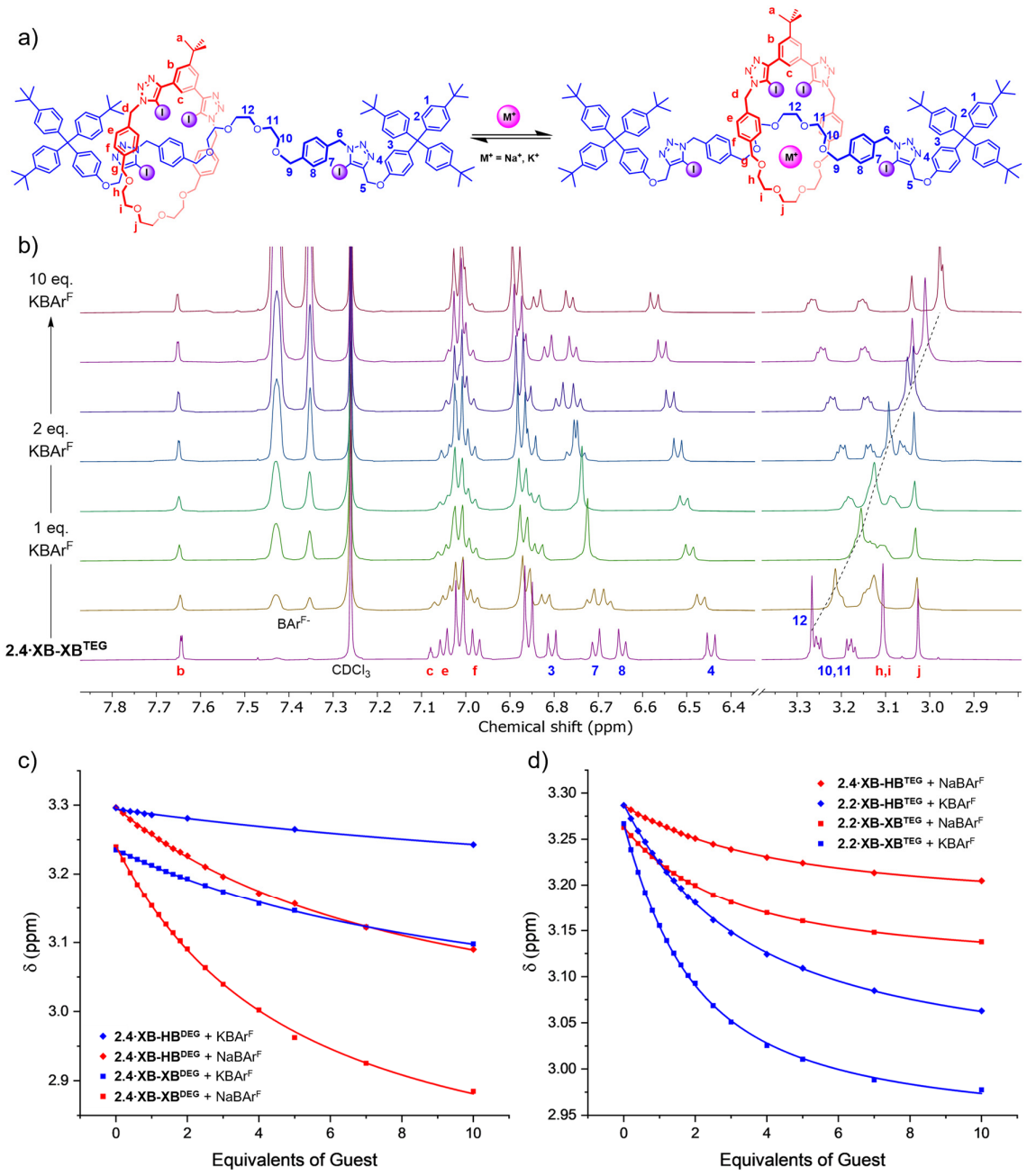


Figure 2.32. *^{1}H NMR alkali metal cation binding studies of [2]rotaxanes. (a) Proposed cation binding mode; (b) Representative stacked ^{1}H NMR titration spectra of* ***2.4·XB-XB^{TEG}*** *upon progressive addition of 10 eq. KBAr^F (500 MHz, 1:1 $CD_3CN/CDCl_3$, 298 K); Binding isotherms of: c)* ***2.4·XB-XB^{DEG}*** *(squares) and* ***2.4·XB-HB^{DEG}*** *(diamonds); d)* ***2.4·XB-XB^{TEG}*** *(squares) and* ***2.4·XB-HB^{TEG}*** *(diamonds) with NaBAr^F (red) and KBAr^F (blue) generated by monitoring the chemical shifts of $H_{h/i}$, fitted to a 1:1 host-guest binding model.*

2.4.3.2 Anion Binding Studies

The anion binding properties of the free rotaxanes were investigated via ^{1}H titration experiments in which halide anions as their tetrabutylammonium (TBA) salts were progressively added to solutions of the rotaxanes in 1:1 $CDCl_3/CD_3CN$.

In the all-XB rotaxanes **2.4·XB-XB^{DEG}** and **2.4·XB-XB^{TEG}**, the macrocycle internal benzene proton H_c, which is typically most the most sensitive proton signal to anion binding to the bis(iodotriazole)benzene XB donor motif, exhibited modest downfield shifts, indicating the participation of the macrocycle XB donor groups in anion binding (**Figure 2.33a-b**). In the mixed HB/XB rotaxanes **2.4·XB-HB^{DEG}** and **2.4·XB-HB^{TEG}**, the signal arising from the internal benzene proton H_c is obscured by the stopper protons and could not be monitored, but it is assumed that anion binding similarly occurs via the macrocycle bidentate XB donor motif. Significant downfield movements of the axle triazole protons H_{trz} were also observed, possibly indicating participation of the triazole proton in halide anion binding via the formation of C-H···X^- HB interactions.

The movements of the selected proton signals were monitored and analysed via Bindfit to determine 1:1 stoichiometric anion association constants for each rotaxane **(Table 2.10)**. The neutral [2]rotaxanes displayed weak halide anion binding in 1:1 $CD_3CN/CDCl_3$, with all K_a values < 200 M^{-1}. In particular, the halide association constants of **2.4·XB-XB^{DEG}** were too low to be determined, while those of **2.4·XB-HB^{DEG}** were significantly lower than the parent macrocycle **2.1·XB^{DEG}**. The weak anion binding affinities of the di(ethylene glycol)-based rotaxanes was attributed to steric crowding from the threaded axle component reducing the accessibility of the macrocyclic binding site. In contrast, the anion association constants of **3·XB-XB^{TEG}** and **3·XB-HB^{TEG}** remain comparable to the parent macrocycles, consistent with the reduced steric crowding in the larger TEG-based macrocycles.

Table 2.10. *Anion binding constants (K_a/M^{-1}) of interlocked receptors determined by ^1H NMR.*[a]

Guest	**2.4·XB-XB^{DEG}**	**2.4·XB-HB^{DEG}**	**2.4·XB-XB^{TEG}**	**2.4·XB-HB^{TEG}**
Cl^-	N.B.[b]	40(1)	73(1)	62(1)
	2.1 (Mac.): 125(2)[c] **2.2** (Cat.): 66(1)[c]		**2.1** (Mac.): 65(1)[c] **2.2** (Cat.): 84(1)[c]	
Br^-	N.B.[b]	77(1)	108(3)	91(2)
	2.1 (Mac.): 154(2)[c] **2.2** (Cat.): 78(1)[c]		**2.1** (Mac.): 97(2)[c] **2.2** (Cat.): 142(1)[c]	
I^-	N.B.[b]	92(2)	150(5)	133(2)
	2.1 (Mac.): 186(3)[c] **2.2** (Cat.): 87(1)[c]		**2.1** (Mac.): 146(3)[c] **2.2** (Cat.): 135(2)[c]	

[a]K_a values calculated using Bindfit with a 1:1 host-guest binding model. Errors are shown in parentheses and are all <2%. All anions added as TBA^+ salts. Solvent = 1:1 $CDCl_3/CD_3CN$. T = 298 K. [Receptor] = 1.0 mM. [b]N.B. = No binding. [c]The values after "Mac." and "Cat." are the previously reported K_a values of the analogous macrocycle and [2]catenane for the same anion. The K_a values of the catenanes have been statistically corrected by a factor of 2 to account for the presence of two bis(iodotriazole)benzene XB donor motifs.

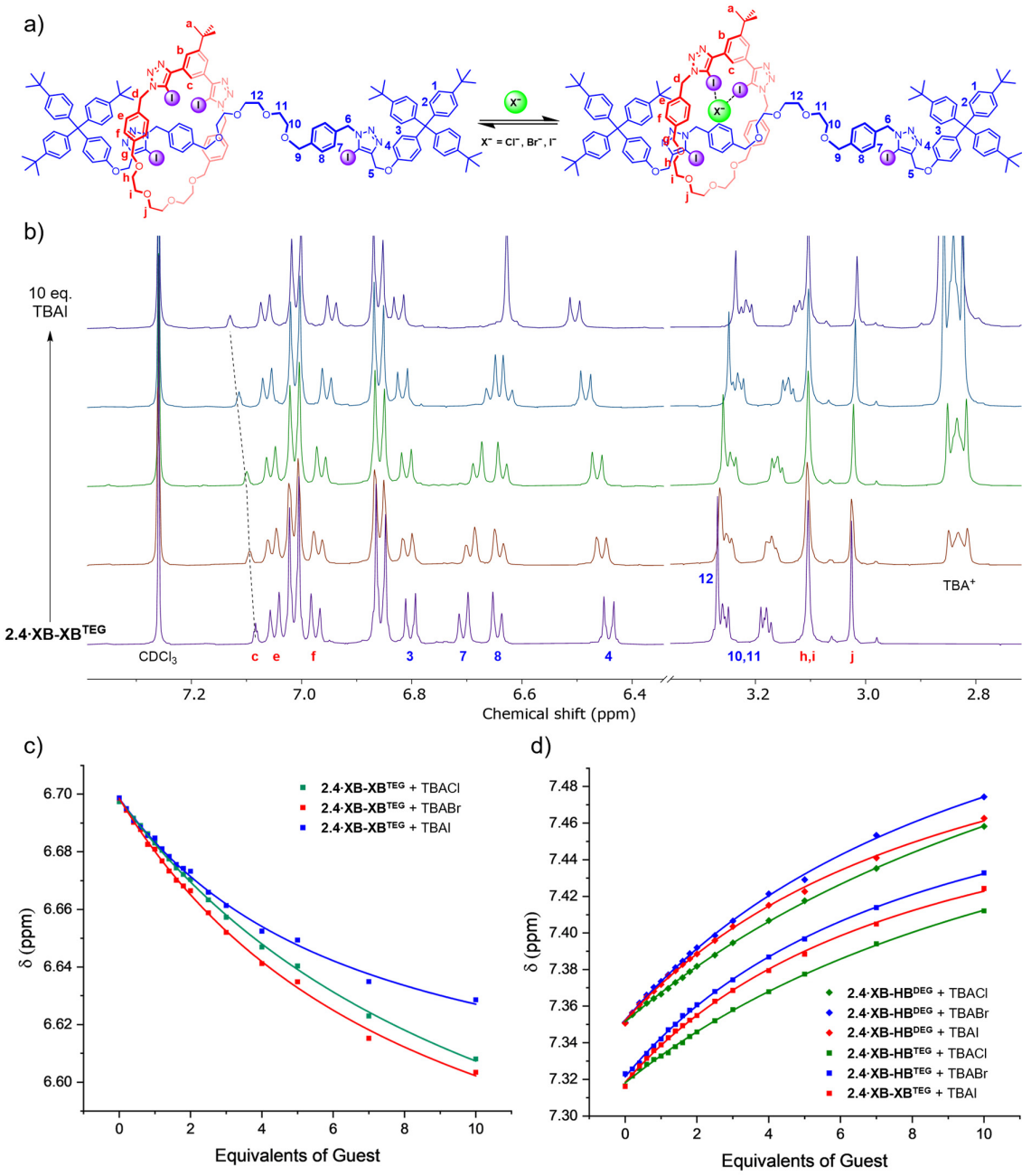


Figure 2.33. *^{1}H NMR halide anion binding studies of [2]rotaxanes. (a) Proposed anion binding mode; (b) Representative stacked ^{1}H NMR titration spectra of* ***2.4·XB-XB^{TEG}*** *upon progressive addition of 10 eq. TBAI (500 MHz, 1:1 $CD_3CN/CDCl_3$, 298 K); Binding isotherms of: c)* ***2.4·XB-XB^{TEG}****, generated by monitoring the chemical shifts of H_7; d)* ***2.4·XB-HB^{DEG}*** *(diamonds) and* ***2.4·XB-HB^{TEG}*** *(squares) with TBACl (green), TBABr (blue) and TBAI (red) generated by monitoring the chemical shifts of H_{trz}, fitted to a 1:1 host-guest binding model.*

2.4.3.3 Ion-Pair Binding

Having studied both the cation and anion binding behaviour of the neutral XB [2]rotaxanes, their ability to bind alkali metal halides as ion pairs was investigated. We initially sought to do so via a similar approach to that used for the [2]catenanes – that is, by comparing the anion binding constants of the free receptor to the *apparent* anion binding constants (K_{app}) of the receptor in the presence of 1 equivalent of the cation. While this approach is a reasonable assumption for cases in which the majority of the receptor exists as the cation-bound complex, it is not valid in the [2]rotaxane systems, which possess modest cation binding constants. As such, a solution containing an equimolar mixture of [2]rotaxane and an alkali metal cation would contain a significant proportion of un-complexed cation and host. Although the mono-cationic receptor complex is expected to bind more strongly to anions on the basis of electrostatic attraction, if the free receptor is present at a significantly higher concentration, it can compete for binding to the anion. The observed peak movements in the ^{1}H NMR spectra, the binding isotherms constructed from monitoring these signals, and the calculated anion binding constants (the 'apparent' anion binding constants) would therefore reflect anion binding to both mono-cationic and neutral species. The lower the initial proportion of the metal-bound complex, the more severely the calculated apparent anion binding constant would underestimate the anion binding affinity of the cation-receptor complex.

An additional complication arises from the formation of a mono-anionic complex upon anion binding to the neutral receptor, which is expected to exhibit enhanced cation affinity relative to the unbound receptor. Therefore, the free metal cations initially present in solution may bind to the mono-anionic complex to form the ternary ion-pair complex (**Figure 2.1**). The simultaneous cation and anion binding processes may both induce shifts in ^{1}H NMR signals, either in parallel or opposite directions. Depending on the binding modes of the guests, some

proton signals may be more sensitive to either cation or anion binding, while others may be influenced by both processes. To reliably determine the apparent anion binding affinities of the rotaxanes, it is therefore imperative to select peaks that shift only in response to the anion and not the cation.

The presence of these parallel equilibria, coupled with the dramatic co-conformational changes in the rotaxanes which also occur upon ion recognition, gave rise to highly complex recognition-induced chemical shift perturbation profile in the ^{1}H NMR titrations which significantly complicates the measurement of K_{app}.

To investigate these effects on determining ion-pair affinity, **2.4·XB-XB^{TEG}** was selected as the subject of the study as it exhibited the largest anion and cation affinities of the [2]rotaxane series. ^{1}H NMR ion-pair titration experiments were performed in the conventional fashion of measuring an enhancement factor, in this case determining the apparent halide association constant of **2.4·XB-XB^{TEG}** in the presence of 1 equivalent K^+ and comparing this value to that in the absence of K^+. In a typical experiment, the chemical shift of the rotaxane's macrocyclic internal benzene proton H_c was monitored with increasing anion concentration which in all cases for the halide titration experiments exhibited a downfield perturbation.

Bindfit[66] analysis of the generated 'binding' isotherms, employing a 1:1 stoichiometric host-guest binding model, determined apparent K_a values of 116(3) M^{-1} (Cl^-), 2655(101) M^{-1} (Br^-) and 1442(84) M^{-1} (I^-). Taking these values at face value would suggest that **2.4·XB-XB^{TEG}** exhibits considerable affinity and selectivity for KBr ion-pairs over the other potassium halide salts investigated. However, a closer and more critical analysis of the ^{1}H NMR spectra in their entirety indicates that these conclusions are not justified.

In the 'KCl' titration, salt recombination was found to be the dominant process, outcompeting ion-pair binding to the receptor, which is consistent with the high lattice enthalpy

of KCl. This is most clearly indicated by monitoring the perturbations in H_4, a signal from the stopper group of the axle, which shifts upfield upon the addition of 1 eq. of TBACl. However, the addition of excess TBACl led instead to a reversal of the direction of movement of H_4, with an incremental downfield shift instead observed up to 10 eq. TBACl. Indeed, a global comparison of the chemical shift values measured in the 'KCl' titration to those of the free rotaxane and those obtained during the anion titration experiments reveal that the addition of 1 eq. TBACl causes K^+ decomplexation through external ion-pairing (**Figure 2.34a**) and once the pre-added equivalent of K^+ becomes saturated with a stoichiometric quantity of chloride, any further perturbations observed are a result of chloride-only binding by **2.4·XB-XB^{TEG}** and not ion-pair 'KCl' binding.

A more ambiguous scenario is observed in the case of the analogous ion-pair 'KBr' titration (**Figure 2.34b**). Superficially, the unidirectional perturbations of the internal benzene proton signal H_c alone would suggest a relatively simple binding situation in which the receptor stabilises a KBr ion-pair. However, monitoring the xylene proton signals $H_{7,8}$ shows an initial downfield shift, up to the addition of 4 eq. of TBABr, after which an upfield shift is observed with bromide equivalents of up to 10 eq. A similar reversal in the direction of peak movements was observed for the ethylene glycol protons $H_{h/i}$ and H_j. In this case, it is clear that during the course of the titration endotopic 'KBr' ion-pair binding occurs up to 4 eq. of Br^-, followed by exotopic ion-pairing, *i.e.* gradual formation of external KBr ion pairs. This suggests that ion-pair binding to **2.4·XB-XB^{TEG}** dominates at low concentrations of bromide, but salt recombination competes significantly with ion-pair binding in the presence of excess bromide. The influence of these competing equilibria on the overall movement of the proton signals will considerably compromise any quantitative information concerning ion-pair binding affinities.

In contrast, analysis of the ^{1}H NMR spectral changes upon TBAI addition suggests that **2.4·XB-XB^{TEG}** is capable of binding KI as an ion-pair (**Figure 2.34c**). As in the previous case, the macrocyclic internal benzene proton H_c exhibits a unidirectional downfield shift with increasing anion concentration, indicative of enhanced anion binding by the metal-rotaxane complex. Crucially, however, in the 'KI' titration, the proton signals arising from the ethylene glycol and axle xylene protons initially undergo chemical shift perturbations consistent with increased cation complexation, but appear to reach saturation in the presence of excess TBAI. This is consistent with a complexation mode in which iodide binding to **2.4·XB-XB^{TEG}** simultaneously enhances the rotaxane's K^+ affinity, such that the rotaxane exists predominantly as the metal-rotaxane complex.

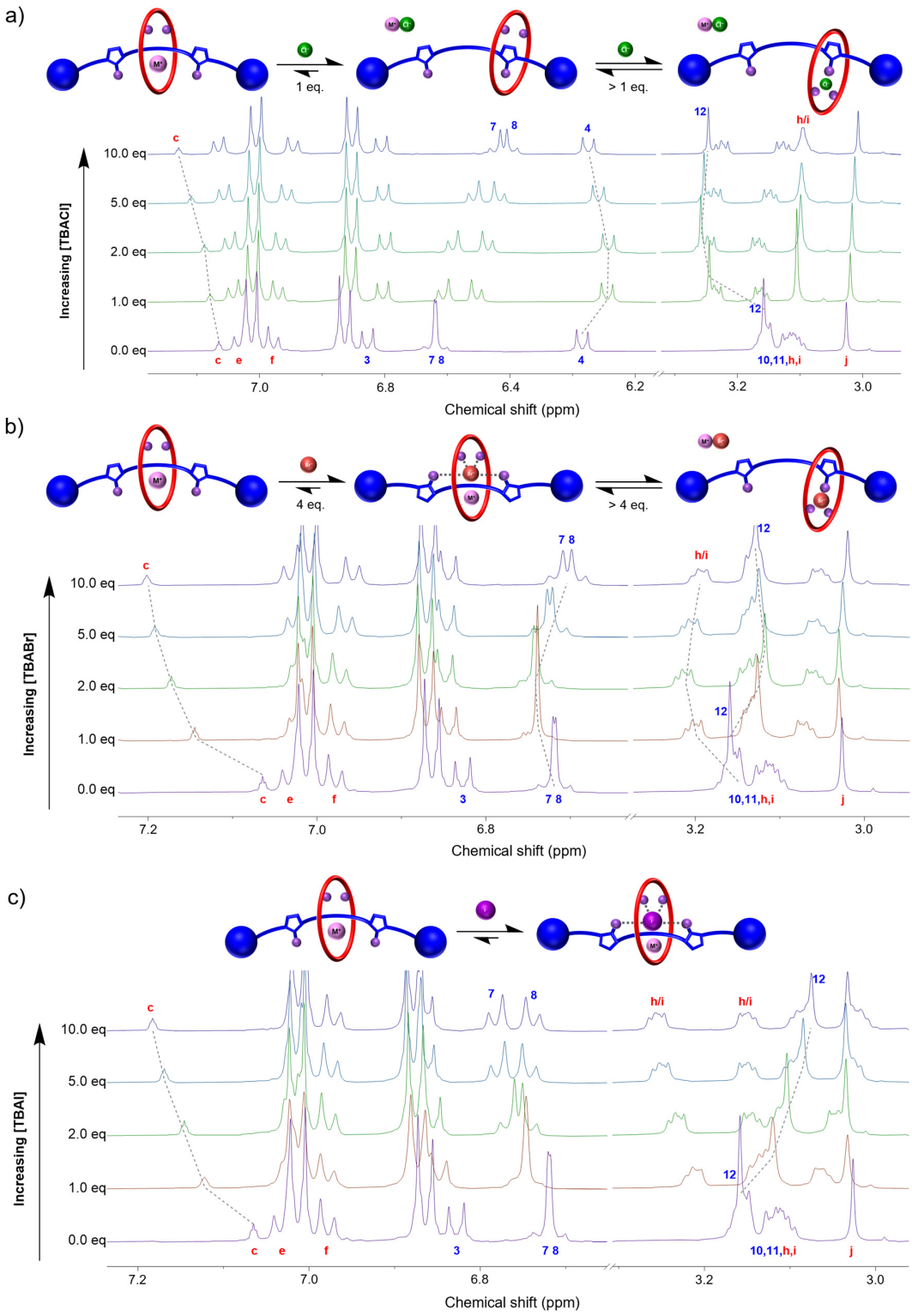


Figure 2.34. *Overlaid ^{1}H NMR ion-pair titration spectra of* ***2.4·XB-XB^{TEG}*** *in the presence of 1 eq. KBAr^{F} upon addition of (a) TBACl, (b) TBABr and (c) TBACl (500 MHz, 298K, 1:1 $CDCl_3/CD_3CN$). The cartoon representations above each set of stacked spectra indicate the dominant equilibria occurring over the course of each titration.*

Given the significant salt recombination occurring in the ion-pair titrations of the rotaxane-cation mixtures with chloride and bromide, only the apparent iodide association constants were selected for further analysis and comparative studies (**Figure 2.35**, **Table 2.11**). Despite being an underestimation of the true anion binding affinity of the metal-rotaxane complexes, the determined apparent iodide binding constants of **2.4·XB-XB^{TEG}** are significantly higher (>8-fold) than the neutral rotaxanes. This positive cooperativity between the cation and anion binding events is consistent with enhanced electrostatic attraction between the oppositely charged co-bound ions, similar to that of the previously reported [2]catenane systems.

Surprisingly, despite the weaker cation binding affinities of the free rotaxanes, the cooperative ion-pairing effect appears to be more pronounced in the all-XB [2]rotaxanes than their catenane counterparts. Rotaxane **2.4·XB-XB^{TEG}** exhibited stronger binding to iodide in the presence of either 1 equiv. Na^+ or K^+ than the analogous catenane (**Table 2.11**), despite the latter possessing higher association constants for both cations *as well as* possessing two bidentate bis(iodotriazole)benzene anion binding motifs. The higher degree of positive cooperativity in the ion-pair binding behaviour of **2.4·XB-XB^{TEG}** relative to the TEG-based [2]catenane is tentatively attributed to the greater co-conformational flexibility of the rotaxane topology, which may allow the iodotriazole donors in both the macrocycle and axle to participate in cooperative anion binding.

To verify this hypothesis, attempts to evaluate the contribution of the axle iodotriazole groups to the ion-pair binding properties of the rotaxanes were undertaken by comparing the apparent anion binding constants of the all-XB and mixed XB-HB rotaxanes. Unfortunately, due to the significantly weaker cation association constants of the mixed XB/HB rotaxanes, the proportion of metal-complexed rotaxane initially present in solution is significantly lower,

affecting the validity of such comparisons. In addition, selecting a suitable signal to monitor ion-pair binding was challenging, as the signal corresponding to H_c in **2.4·XB-HB^{TEG}** is obscured by the stopper proton peaks, while axle triazole proton H_{trz} shifts in response to both cation and anion binding processes (as observed in the cation-only and anion-only titrations). The absence of a tractable proton signal that responds only to anion binding therefore precluded a reliable determination of the K_{app} values of metal-complexed **2.4·XB-HB^{TEG}**. Nonetheless, a global fitting analysis of the isotherms generated by monitoring movements in H_{trz} and H_f allowed us to estimate the upper limits of the anion binding constants, which indeed were found to be lower in the mixed XB/HB rotaxane **2.4·XB-HB^{TEG}** compared to the all-XB analogue **2.4·XB-XB^{TEG}** (**Table 2.11**).

Table 2.11. *Apparent anion binding constants (K_a/M^{-1}) of interlocked receptors determined by ^1H NMR.*[a]

		[2]Rotaxanes		[2]Catenanes	
Receptor	**Cation**	**Proportion bound (%)**[b]	$K_{app}(I^-)$ **(M^{-1})**	**Proportion bound (%)**	$K_{app}(I^-)$ **(M^{-1})**
2.4·XB-XB^{TEG}	Na^+	24	1283(52)	33	818
	K^+	33	1442(84)	47	1050
2.4·XB-HB^{TEG}	Na^+	17	1053(40)	-	-
	K^+	21	844(36)	-	-

[a]K_{app} values calculated using Bindfit with a 1:1 host-guest binding model. Errors (±) are shown in parentheses and are all <10%. All anions added as TBA^+ salts. Solvent = 1:1 $CDCl_3/CD_3CN$. T = 298 K. [Receptor] = [$MBAr^F$] = 1.0 mM. [b]Initial proportion of metal-host complex calculated from cation association constants.

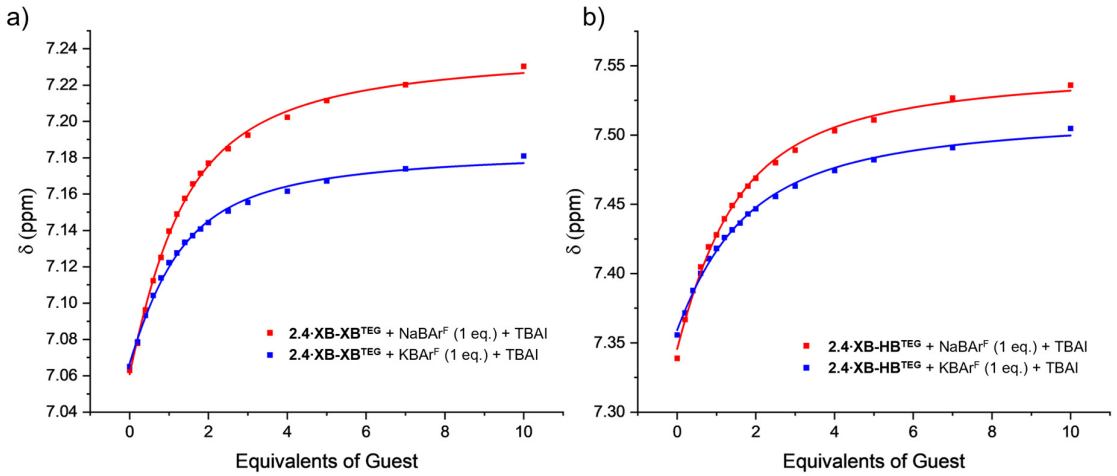


Figure 2.35. *Binding isotherms of: a)* ***2.4·XB-XB^{TEG}*** *(monitoring H_c); b)* ***2.4·XB-HB^{TEG}*** *(monitoring H_{trz}) in the presence of 1 eq. NaBAr^F (red) or KBAr^F (blue) upon progressive addition of TBAI.*

2.5 Conclusions and Future Work

A cation template directed strategy exploiting the orthogonal complexation of sodium or potassium ions by oligo(ethylene glycol) units was developed and used to prepare a family of heteroditopic XB catenanes and rotaxanes for alkali metal halide ion-pair recognition.

^{1}H NMR spectroscopic studies enabled a quantitative determination of the cation, anion and ion-pair binding properties of a series of homo[2]catenanes, indicating a drastic turn-on of cation affinity in the interlocked hosts relative to the parent macrocycles, while solid-state structural analysis provides evidence for cation-induced co-conformational dynamism. Importantly, the weak halide anion affinities of the neutral XB [2]catenanes were significantly augmented by pre-complexation of an alkali metal cation to the receptors, demonstrating cooperative electrostatic effects that make ion-pair receptors highly desirable in supramolecular host-guest recognition. An unexpected switch from a 1:1 to 1:2 host-anion binding stoichiometry in **2.2·XB^{DEG}·Na$^+$** was attributed to the formation of an additional contact ion-pair between the anion and the coordinatively-unsaturated metal centre,

demonstrating an unusual mechanism for modulating the binding mode and stoichiometry of guest binding.

A second-generation hetero[2]catenane containing a modified cation binding site exhibited dramatically enhanced ion-pair binding affinities alongside a notable 3 to 5-fold preference for binding sodium halide over potassium halide ion-pairs. The prodigious binding properties of the hetero[2]catenane were further exploited for selective extraction of sodium halide salts from NaX/KX solid state mixtures into organic solvent media.

A series of hetero[2]rotaxane analogues were also prepared to investigate the effect of interlocked topology on the ion-pair recognition properties of the receptors. Although the [2]rotaxanes exhibited relatively weaker individual cation and anion binding affinities than the analogous [2]catenanes, attributed to a lower degree of pre-organisation, importantly, ion-pair binding studies suggested a higher level of cooperativity between the cation and anion binding events, highlighting the potential utility of mechanical bond co-conformational flexibility in the design of multi-topic interlocked receptors.

2.5.1 Future Work

Future work will involve exploiting the impressive ion-pair binding properties of heteroditopic MIM host molecules to develop selective sensors for alkali metal halide ion-pairs. To this end, photo-active analogues of the [2]catenanes or [2]rotaxanes functionalised with optical reporter groups such as coumarin or anthracene are planned, where the signalling groups are either appended to the periphery of the macrocycle or incorporated into the backbone of the axle (**Figure 2.36**). The sensing properties of these target functionalised heteroditopic receptors will be studied by UV-vis or fluorescence spectroscopy.

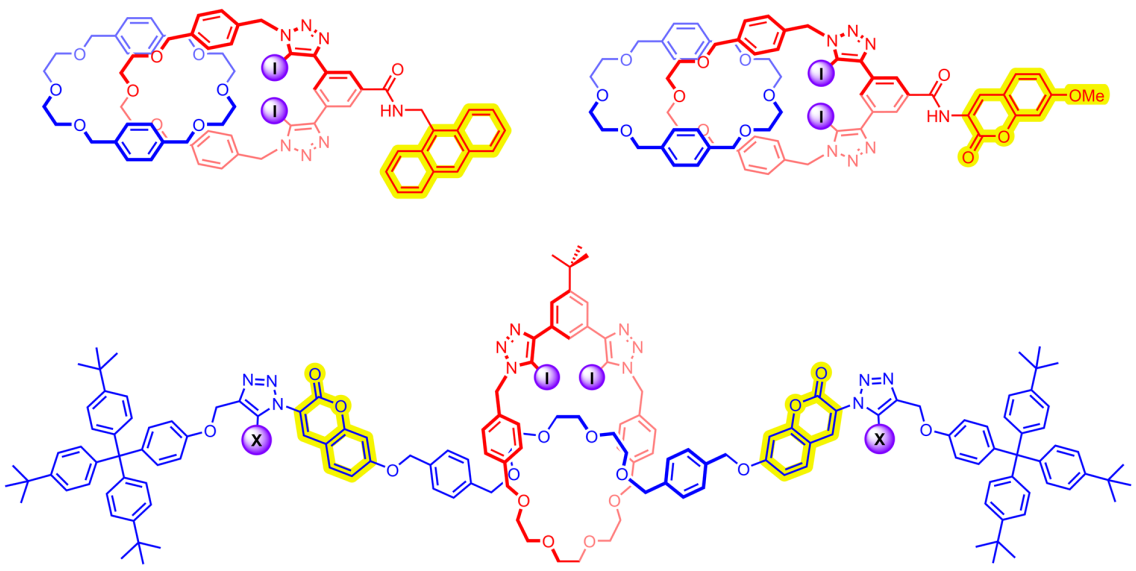


Figure 2.36. *Chemical structures of proposed optical ion-pair sensors with anthracene or coumarin chromophores highlighted in yellow.*

2.6 References for Chapter 2

1. A. J. McConnell, P. D. Beer, *Angew. Chem. Int. Ed.* **2012**, *51*, 5052-5061.
2. J. L. Sessler, S. K. Kim, D. E. Gross, C.-H. Lee, J. S. Kim, V. M. Lynch, *J. Am. Chem. Soc.* **2008**, *130*, 13162-13166.
3. Q. He, G. I. Vargas-Zúñiga, S. H. Kim, S. K. Kim, J. L. Sessler, *Chem. Rev.* **2019**, *119*, 9753-9835.
4. B. Qiao, A. Sengupta, Y. Liu, K. P. McDonald, M. Pink, J. R. Anderson, K. Raghavachari, A. H. Flood, *J. Am. Chem. Soc.* **2015**, *137*, 9746-9757.
5. A. J. McConnell, A. Docker, P. D. Beer, *ChemPlusChem* **2020**, *85*, 1824-1841.
6. P. D. Beer, P. K. Hopkins, J. D. McKinney, *Chem. Commun.* **1999**, 1253-1254.
7. M. Zakrzewski, D. Załubiniak, P. Piątek, *Dalton Trans.* **2018**, *47*, 323-330.
8. Q. He, G. M. Peters, V. M. Lynch, J. L. Sessler, *Angew. Chem. Int. Ed.* **2017**, *56*, 13396-13400.
9. S. G. Galbraith, P. G. Plieger, P. A. Tasker, *Chem. Commun.* **2002**, 2662-2663.
10. T. Bunchuay, A. Docker, U. Eiamprasert, P. Surawatanawong, A. Brown, P. D. Beer, *Angew. Chem. Int. Ed.* **2020**, *59*, 12007-12012.
11. Y. C. Tse, A. Docker, Z. Zhang, P. D. Beer, *Chem. Commun.* **2021**, *57*, 4950-4953.
12. A. Docker, J. G. Stevens, P. D. Beer, *Chem. Eur. J.* **2021**, *27*, 14600-14604.
13. A. Docker, T. Bunchuay, M. Ahrens, A. J. Martinez-Martinez, P. D. Beer, *Chem. Eur. J.* **2021**, *27*, 7837-7841.
14. A. Docker, I. Marques, H. Kuhn, Z. Zhang, V. Félix, P. D. Beer, *J. Am. Chem. Soc.* **2022**, *144*, 14778-14789.
15. Q. He, N. J. Williams, J. H. Oh, V. M. Lynch, S. K. Kim, B. A. Moyer, J. L. Sessler, *Angew. Chem. Int. Ed.* **2018**, *57*, 11924-11928.
16. Q. He, Z. Zhang, J. T. Brewster, V. M. Lynch, S. K. Kim, J. L. Sessler, *J. Am. Chem. Soc.* **2016**, *138*, 9779-9782.
17. A. V. Koulov, J. M. Mahoney, B. D. Smith, *Org. Biomol. Chem.* **2003**, *1*, 27-29.
18. J. M. Mahoney, G. U. Nawaratna, A. M. Beatty, P. J. Duggan, B. D. Smith, *Inorg. Chem.* **2004**, *43*, 5902-5907.

19. A. Galan, D. Andreu, A. M. Echavarren, P. Prados, J. De Mendoza, *J. Am. Chem. Soc.* **1992**, *114*, 1511-1512.
20. W. Walczak, M. Zakrzewski, G. Cichowicz, P. Piątek, *Org. Biomol. Chem.* **2020**, *18*, 694-699.
21. K. M. Bąk, K. Porfyrakis, J. J. Davis, P. D. Beer, *Mater. Chem. Front.* **2020**, *4*, 1052-1073.
22. J. F. Stoddart, *Chem. Soc. Rev.* **2009**, *38*, 1802-1820.
23. E. A. Neal, S. M. Goldup, *Chem. Commun.* **2014**, *50*, 5128-5142.
24. M. Xue, Y. Yang, X. Chi, X. Yan, F. Huang, *Chem. Rev.* **2015**, *115*, 7398-7501.
25. G. Gil-Ramírez, D. A. Leigh, A. J. Stephens, *Angew. Chem. Int. Ed.* **2015**, *54*, 6110-6150.
26. J. E. M. Lewis, M. Galli, S. M. Goldup, *Chem. Commun.* **2017**, *53*, 298-312.
27. W.-X. Gao, H.-J. Feng, B.-B. Guo, Y. Lu, G.-X. Jin, *Chem. Rev.* **2020**, *120*, 6288-6325.
28. H.-N. Zhang, Y.-J. Lin, G.-X. Jin, *J. Am. Chem. Soc.* **2021**, *143*, 1119-1125.
29. G. Baggi, S. J. Loeb, *Chem. Eur. J.* **2017**, *23*, 14163-14166.
30. M. Nandi, S. Bej, T. K. Ghosh, P. Ghosh, *Chem. Commun.* **2019**, *55*, 3085-3088.
31. S.-M. Chan, F.-K. Tang, C.-S. Kwan, C.-Y. Lam, S. C. K. Hau, K. C.-F. Leung, *Mater. Chem. Front.* **2019**, *3*, 2388-2396.
32. T. Shukla, A. K. Dwivedi, R. Arumugaperumal, C.-M. Lin, S.-Y. Chen, H.-C. Lin, *Dyes Pigm.* **2016**, *131*, 49-59.
33. M. Denis, J. Pancholi, K. Jobe, M. Watkinson, S. M. Goldup, *Angew. Chem. Int. Ed.* **2018**, *57*, 5310-5314.
34. A. Caballero, F. Zapata, P. D. Beer, *Coord. Chem. Rev.* **2013**, *257*, 2434-2455.
35. R. J. Goodwin, A. Docker, H. I. MacDermott-Opeskin, H. M. Aitken, M. L. O'Mara, P. D. Beer, N. G. White, *Chem. Eur. J.* **2022**, *28*, e202200389.
36. J. M. Mercurio, F. Tyrrell, J. Cookson, P. D. Beer, *Chem. Commun.* **2013**, *49*, 10793-10795.
37. M. J. Langton, O. A. Blackburn, T. Lang, S. Faulkner, P. D. Beer, *Angew. Chem. Int. Ed.* **2014**, *53*, 11463-11466.
38. N. G. White, P. D. Beer, *Org. Biomol. Chem.* **2013**, *11*, 1326-1333.
39. Y. Cheong Tse, R. Hein, E. J. Mitchell, Z. Zhang, P. D. Beer, *Chem. Eur. J.* **2021**, *27*, 14550-14559.
40. R. C. Knighton, P. D. Beer, *Chem. Commun.* **2014**, *50*, 1540-1542.
41. A. Brown, K. M. Mennie, O. Mason, N. G. White, P. D. Beer, *Dalton Trans.* **2017**, *46*, 13376-13385.
42. M. J. Deetz, R. Shukla, B. D. Smith, *Tetrahedron* **2002**, *58*, 799-805.
43. J. R. Romero, G. Aragay, P. Ballester, *Chem. Sci.* **2017**, *8*, 491-498.
44. M. Denis, L. Qin, P. Turner, K. A. Jolliffe, S. M. Goldup, *Angew. Chem. Int. Ed.* **2018**, *57*, 5315-5319.
45. D.-H. Li, B. D. Smith, *J. Org. Chem.* **2019**, *84*, 2808-2816.
46. C. A. Hunter, H. L. Anderson, *Angew. Chem. Int. Ed.* **2009**, *48*, 7488-7499.
47. A. Arun, A. Docker, H. Min Tay, P. D. Beer, *Chem. Eur. J.* **2023**, *29*, e202301446.
48. E. N. W. Howe, M. Bhadbhade, P. Thordarson, *J. Am. Chem. Soc.* **2014**, *136*, 7505-7516.
49. R. C. Knighton, P. D. Beer, *Org. Chem. Front.* **2021**, *8*, 2468-2472.
50. S.-T. Tung, C.-C. Lai, Y.-H. Liu, S.-M. Peng, S.-H. Chiu, *Angew. Chem. Int. Ed.* **2013**, *52*, 13269-13272.
51. Y.-J. Lee, T.-H. Ho, C.-C. Lai, S.-H. Chiu, *Org. Biomol. Chem.* **2016**, *14*, 1153-1160.
52. A. Inthasot, S.-T. Tung, S.-H. Chiu, *Acc. Chem. Res.* **2018**, *51*, 1324-1337.
53. Y.-W. Wu, P.-N. Chen, C.-F. Chang, C.-C. Lai, S.-H. Chiu, *Org. Lett.* **2015**, *17*, 2158-2161.
54. Y.-W. Wu, S.-T. Tung, C.-C. Lai, Y.-H. Liu, S.-M. Peng, S.-H. Chiu, *Angew. Chem. Int. Ed.* **2015**, *54*, 11745-11749.
55. T.-H. Ho, C.-C. Lai, Y.-H. Liu, S.-M. Peng, S.-H. Chiu, *Chem. Eur. J.* **2014**, *20*, 4563-4567.
56. Y.-J. Lee, K.-S. Liu, C.-C. Lai, Y.-H. Liu, S.-M. Peng, R. P. Cheng, S.-H. Chiu, *Chem. Eur. J.* **2017**, *23*, 9756-9760.
57. D. Brynn Hibbert, P. Thordarson, *Chem. Commun.* **2016**, *52*, 12792-12805.
58. I. Mano, M. Driscoll, *BioEssays* **1999**, *21*, 568-578.
59. P. M. Snyder, *Endocrine Reviews* **2002**, *23*, 258-275.

60. B. Hille, *Biophys. J.* **1978**, *22*, 283-294.
61. T. Dudev, C. Lim, *J. Am. Chem. Soc.* **2010**, *132*, 2321-2332.
62. D. Jagleniec, Ł. Dobrzycki, M. Karbarz, J. Romański, *Chem. Sci.* **2019**, *10*, 9542-9547.
63. D. Jagleniec, S. Siennicka, Ł. Dobrzycki, M. Karbarz, J. Romański, *Inorg. Chem.* **2018**, *57*, 12941-12952.
64. J. Y. C. Lim, T. Bunchuay, P. D. Beer, *Chem. Eur. J.* **2017**, *23*, 4700-4707.
65. H. M. Tay, Y. C. Tse, A. Docker, C. Gateley, A. L. Thompson, H. Kuhn, Z. Zhang, P. D. Beer, *Angew. Chem. Int. Ed.* **2023**, *62*, e202214785.
66. P. Thordarson, *Chem. Soc. Rev.* **2011**, *40*, 1305-1323.

CHAPTER 3

Anion Template-Directed Synthesis of Interlocked Host Structures for Anion Sensing and Transport

Chapter 3: Anion Template-Directed Synthesis of Interlocked Host Structures for Anion Sensing and Transport

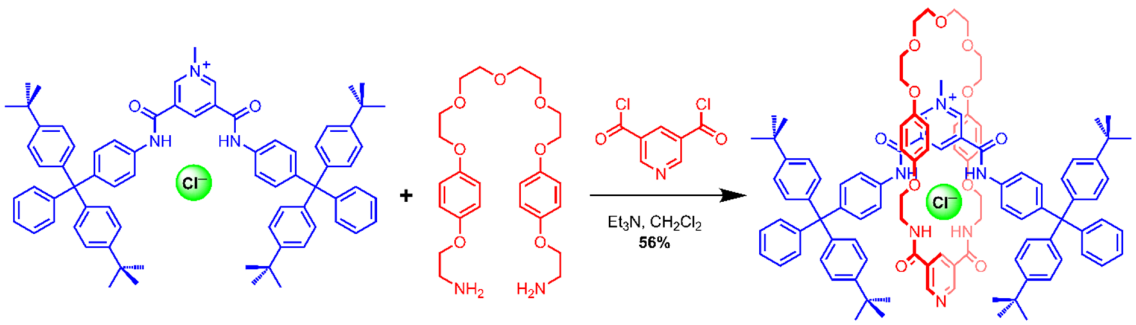
3.1 Introduction

The majority of supramolecular anion receptors capable of functioning in highly competitive aqueous media are cationic in nature, utilising charge-assisted hydrogen bonding and, more recently, halogen bonding interactions. Although favourable electrostatic interactions are a powerful means by which to enhance the anion affinity of a receptor, the non-directional nature of Coulombic interactions makes it difficult to achieve selective anion binding, with highly charged receptors often showing a bias towards highly charged and more charge-dense anions. The presence of counter-anions may also interfere with guest binding by competing with the target anionic guest for the binding cavity of the receptor. From a functional perspective, the reliance on positively charged binding motifs may limit the potential applications of anion receptors; for instance, anion transport across lipid bilayers typically requires lipophilic carrier molecules. Therefore, interest in the design and synthesis of *neutral* anion receptors has been steadily growing in recent years.

3.1.1 Anion template directed synthesis

The last decade or so has seen growing interest in the design of interlocked anion hosts due to their highly pre-organised binding cavities, which have been demonstrated to not only improve the binding affinity of a receptor, but also confer greater selectivity for target anion guest species.[1] The development of discrete anion template-directed methods for mechanical bond formation is therefore highly desirable as a strategy to prepare MIMs that possess 'built-in' anion recognition motifs capable of binding anionic guests after removal of the template.

The first use of discrete anion templates for the preparation of MIMs was pioneered by Beer and co-workers in 2002, who demonstrated that the orthogonal complexation of a chloride anion by a cationic 3,5-bis-amido-*N*-methylpyridinium axle and a bis-vinyl functionalised isophthalamide-containing macrocycle precursor facilitated [2]rotaxane formation via a Grubbs' catalysed ring-closing metathesis (RCM) reaction. The RCM 'clipping' MIM formation approach was successfully used to prepare several cationic rotaxanes and catenanes, but found to be incompatible with pyridyl moieties and other ligating functional groups due to deleterious competing reactions with the ruthenium metal catalyst. To broaden the scope of the anion template-directed methodology, a new macrocyclisation procedure utilising an amide condensation reaction between a bis(amine) and bis(acid chloride) was developed (**Scheme 3.1**).[2] The synthetic versatility of this method provided access to a family of cationic HB and XB MIMs which exhibit impressive anion recognition and sensing capabilities.[3-7]



Scheme 3.1. *Chloride template-directed synthesis of a [2]rotaxane via an amide condensation reaction between a bis(amine) and a bis(acid chloride).*

In contrast, anion template-directed approaches capable of generating *charge-neutral* interlocked host structures are exceedingly rare, with the few reported examples relying primarily on hydrogen bonding interactions with the anion template to direct self-assembly. Jeong and co-workers described an indolocarbazole motif which is capable of forming orthogonal 2:1 host-guest complexes with a chloride template via four convergent NH···Cl⁻

hydrogen bonds (**Figure 3.1a**). A double macrocyclisation reaction using Grubbs' catalysed RCM followed by catalytic hydrogenation afforded the neutral homo[2]catenane in 26% yield. Fluorescence titration experiments in 1% H_2O/acetone (v/v) determined impressive chloride binding by the catenane ($K_a = 1.4 \times 10^5$ M^{-1}), which was a 20-fold enhancement over the non-interlocked macrocycle.[8] The use of the indolocarbazole motif in chloride template-directed [2]catenane synthesis was further explored by Liu and co-workers, who utilised a CuAAC double macrocyclisation procedure to prepare a homo[2]catenane in 15% yield (**Figure 3.1b**). The catenane showed a preference for chloride over other halides and oxoanions in CD_2Cl_2, which the authors attribute to a combination of anion basicity and size complementarity for the interlocked cavity.[9]

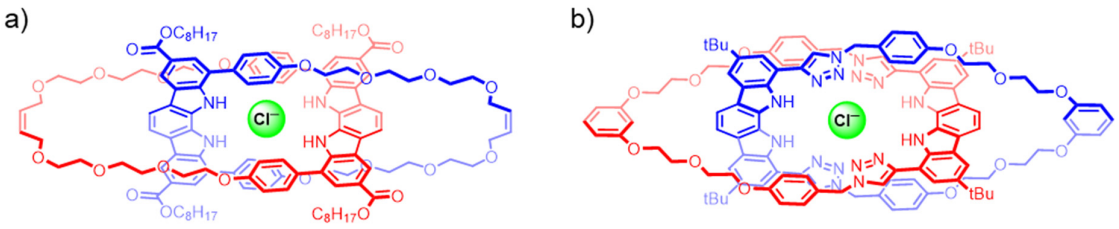


Figure 3.1. *Neutral hydrogen bonding homo[2]catenanes prepared by chloride anion template-directed synthetic methodologies, reported by (a) Jeong and co-workers; (b) Liu and co-workers.*

Very recently, Chmielewski and co-workers reported the use of a sulfate anion to direct the preparation of a neutral homo[2]catenane containing diamidocarbazole anion binding motifs (**Figure 3.2**). The tetrahedral sulfate anion directs orthogonal assembly of the amidocarbazole ligands to form a 2:1 host-guest complex stabilised by four NH···O hydrogen bonds, which underwent a double macrocyclisation reaction via Grubbs' catalysed RCM to afford the neutral [2]catenane. The catenane was capable of preferentially binding sulfate over other oxoanions and halides, with an impressive sulfate association constant of 2.95×10^5 M^{-1} in 9:1 DMSO/H_2O.[10]

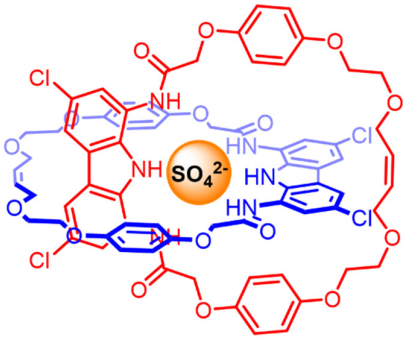


Figure 3.2. *A neutral hydrogen bonding homo[2]catenane prepared by a sulfate anion template-directed synthetic methodology, reported by Chmielewski and co-workers.*

The first example of using XB···anion interactions as the primary templating interaction to prepare a [2]rotaxane was reported recently by Beer and co-workers. A remarkably potent neutral XB motif comprising a bis(iodotriazole) motif functionalised with electron-withdrawing perfluorophenyl (PFP) groups was incorporated into the axle component, which was employed in the chloride template-directed amide condensation methodology developed previously by the group to afford a neutral [2]rotaxane in 17% yield (**Figure 3.3**). The rotaxane demonstrated strong halide binding affinities relative to the non-interlocked components in aqueous-acetone solvent mixtures containing up to 10% water (v/v).[11]

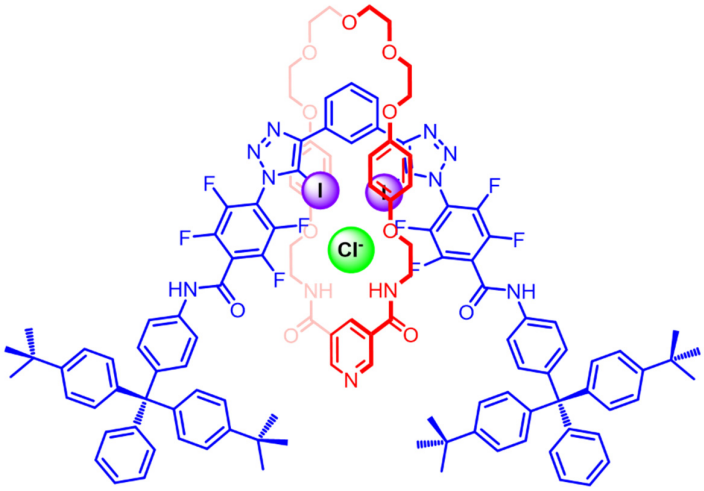


Figure 3.3. *A neutral halogen bonding [2]rotaxane prepared by a chloride anion template-directed synthesis, reported by Beer and co-workers.*

3.1.2 Anion Transport by Mechanically Interlocked Molecules

The regulation of ion concentrations in cells is crucial for maintaining normal physiological function in biological systems. In nature, ion transport is mediated by highly selective protein channels and pumps capable of transporting charged species through otherwise ion-impermeable lipid bilayers. A common feature of ion transport proteins is the presence of sophisticated three dimensionally arranged binding cavities which are electronically and topologically tailored to the target ion. The malfunction of ion transport proteins has been implicated in diseases such as cystic fibrosis and Best's disease, providing a powerful impetus for the use of synthetic ionophores capable of transporting ions, particularly anions, through lipid membranes as potential therapeutics.[12-15]

A persistent challenge in the development of ionophores is achieving levels of affinity and selectivity that are comparable to nature's transport systems. In this context, mechanically interlocked molecules may have an edge over non-interlocked ionophores given the established improvements in guest binding properties elicited by the 3D interlocked binding cavity in MIMs. Surprisingly, however, the use of interlocked structures to mediate ion transport remains rare and have thus far been restricted to [2]rotaxane architectures[16-19] and one catenane-based ion channel system.[20]

The dynamic shuttling behaviour of [2]rotaxanes has been exploited to develop artificial ion channels. Tian and co-workers developed a synthetic [2]rotaxane shuttle containing an axle capable of inserting into and spanning a lipid bilayer, alongside a macrocyclic component tethered to a benzo-18-crown-6 ether cation binding group (**Figure 3.4a**). Ion transport studies in unilamellar lipid vesicles (LUVs) revealed the [2]rotaxane was capable of selectively transporting potassium ions across the membrane, with an EC_{50} value of 1.0 μM with the transporter present at 3.0 mol% relative to the lipid.[17] Building on this strategy,

Qu and co-workers incorporated a photo-switchable azobenzene moiety into the backbone of a [2]rotaxane shuttle for light-gated potassium ion transport (**Figure 3.4b**). Reversible switching between the *trans*- and *cis*-isomers of the azobenzene axle was achieved by alternating 450 nm and 365 nm light stimulus. Importantly, photo-isomerism to the *cis*-isomer was found to switch off potassium ion transport by inhibiting the shuttling motion of the macrocycle along the axle.

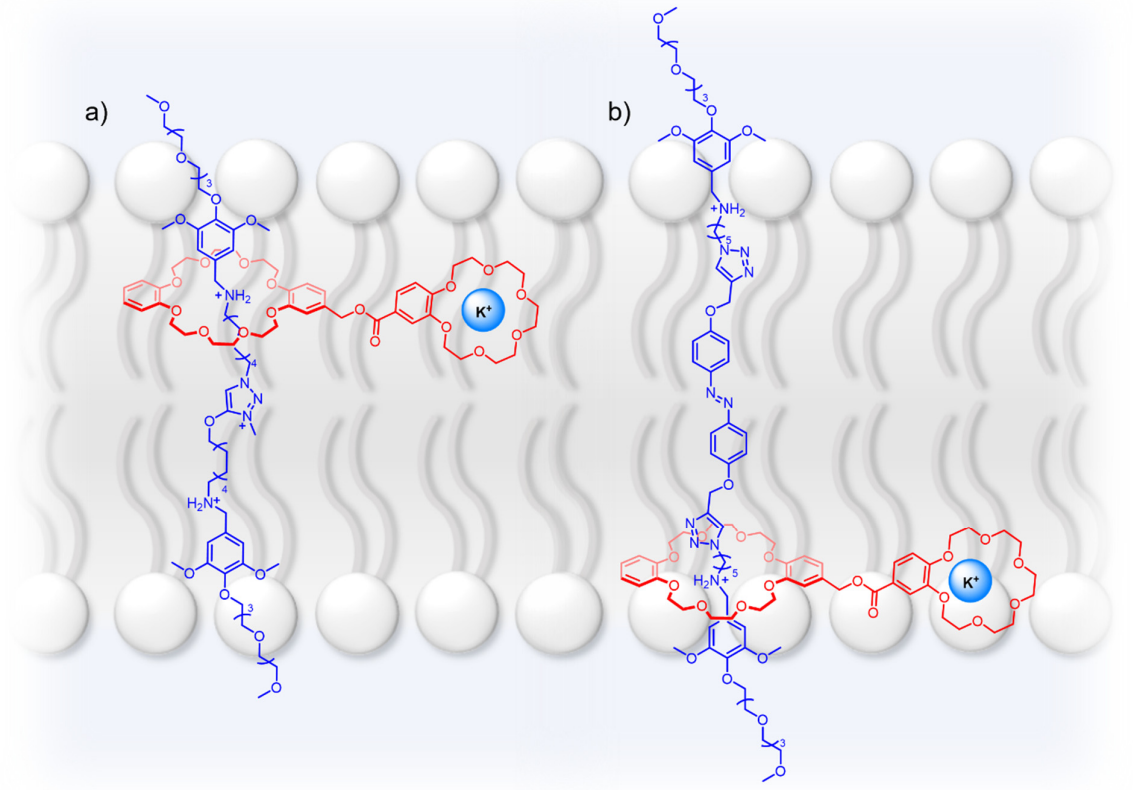


Figure 3.4. *Rotaxane systems for transmembrane cation transport. (a) Potassium-selective [2]rotaxane anionophore developed by Tian and co-workers; (b) Photo-switchable [2]rotaxane for light-gated potassium ion transport.*

Leigh and co-workers synthesised a highly positively charged $(Fe^{II})_6$-coordinated triply-interlocked "Star of David" [2]catenane which was capable of acting as an ion channel for transport of anions across a phospholipid membrane (**Figure 3.5**). Anion transport assays established transport activity increased in the order $F^- < NO_3^- < ClO_4^- < Cl^- < Br^- < I^- \approx$

SCN^-, which the authors attributed to a combination of a Hofmeister binding preference as well as size/shape complementarity for the channel of the catenane. The coordination of multiple Fe(II) ions was found to be crucial for switching "on" ion transport activity, presumably by enhancing the anion binding affinity of the catenane via favourable electrostatic interactions as well as rigidifying the cavity to facilitate the formation of open channels.

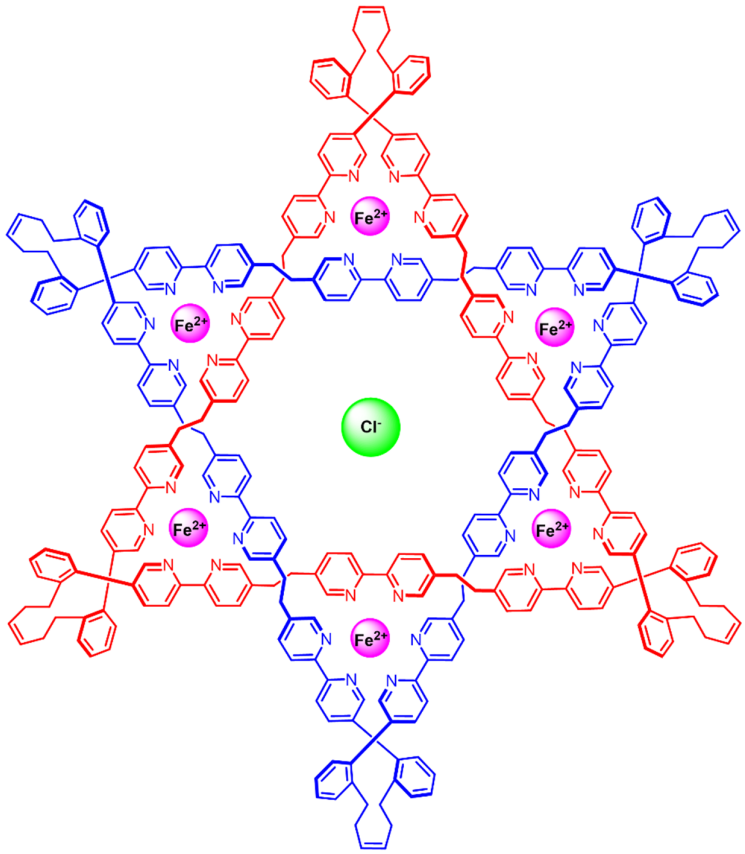


Figure 3.5. *"Star of David" Catenane developed by Leigh and co-workers for transmembrane anion transport via a channel mechanism.*

3.1.3 Anion Sensing by Dynamic Multi-station Rotaxane Shuttles

One of the most fascinating properties of MIMs is the ability of the components to undergo reversible co-conformational changes in response to a stimulus. This dynamic behaviour has been exploited extensively in the design of various molecular machines and

switches.[21, 22] A limited number of studies have utilised anion binding as a stimulus to induce co-conformational changes in MIMs. The majority of these systems are based on multi-station rotaxanes, which produce a photophysical response upon macrocycle translocation from a photoactive station to an anion binding station, thereby enabling optical sensing of the target anion.

An early example of optical anion sensing by a dynamic rotaxane shuttle was reported by Smith and co-workers in 2010. The host design consists of an axle with a central chromophoric squaraine station and peripheral triazole anion binding stations, which is threaded by a tetra-amide macrocycle (**Figure 3.6**). In the absence of a chloride guest the macrocycle preferentially resides at the squaraine station, where it quenches the squaraine fluorescence. Chloride binding in $CDCl_3/CD_3OD$ solvent mixtures induced a translocation of the macrocycle to the triazole station to facilitate convergent chloride binding by the HB donors of the macrocycle and axle, leading to an increase in fluorescence intensity as well as a naked-eye visible colour change from colourless to deep red.

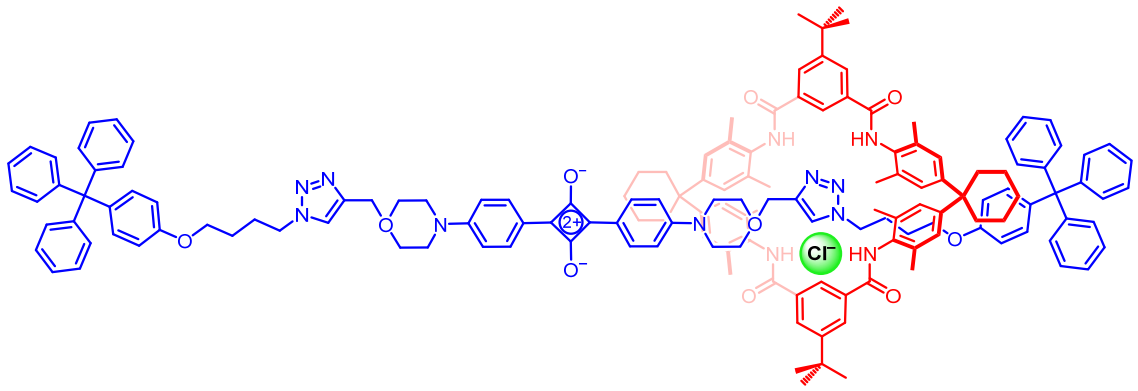


Figure 3.6. *A dynamic multi-station squaraine-based [2]rotaxane for optical sensing of chloride, reported by Smith and co-workers.*

Beer and co-workers designed a two-station [2]rotaxane containing an axle-based naphthalene diimide station and an iodotriazolium XB anion binding station for naked-eye

colourimetric sensing of iodide anions. In the presence of the non-coordinating anion PF_6^-, the macrocycle resides predominantly on the NDI station due to the formation of stable charge transfer interactions between the electron-poor NDI and the electron rich hydroquinone groups of the macrocycle (**Figure 3.7a**). The addition of iodide favours a translocation of the macrocycle to the triazolium or iodotriazolium station, which allows the isophthalimide group of the macrocycle to participate in encapsulation of the halide guest. The loss of the donor-acceptor charge transfer interactions between the NDI units and the macrocycles in the resulting complex is accompanied by a colour change from orange to colourless. Crucially, ^{1}H NMR experiments in 1:1 $CDCl_3/CD_3OD$ indicated that, compared to an analogous prototriazolium-containing HB rotaxane shuttle, the XB rotaxane undergoes a more pronounced macrocycle translocation in the presence of iodide, highlighting the efficacy of highly directional XB interactions in promoting improved binding and sensing capabilities.[23] Using an analogous sensing mechanism, the authors synthesised a four-station [3]rotaxane for selective nitrate sensing by exploiting the complementary trigonal geometry of the nitrate anion and the triangular arrangement of the anion binding motifs in the pincer-like interlocked cavity formed by the axle and the two macrocycles (**Figure 3.7b**).[24]

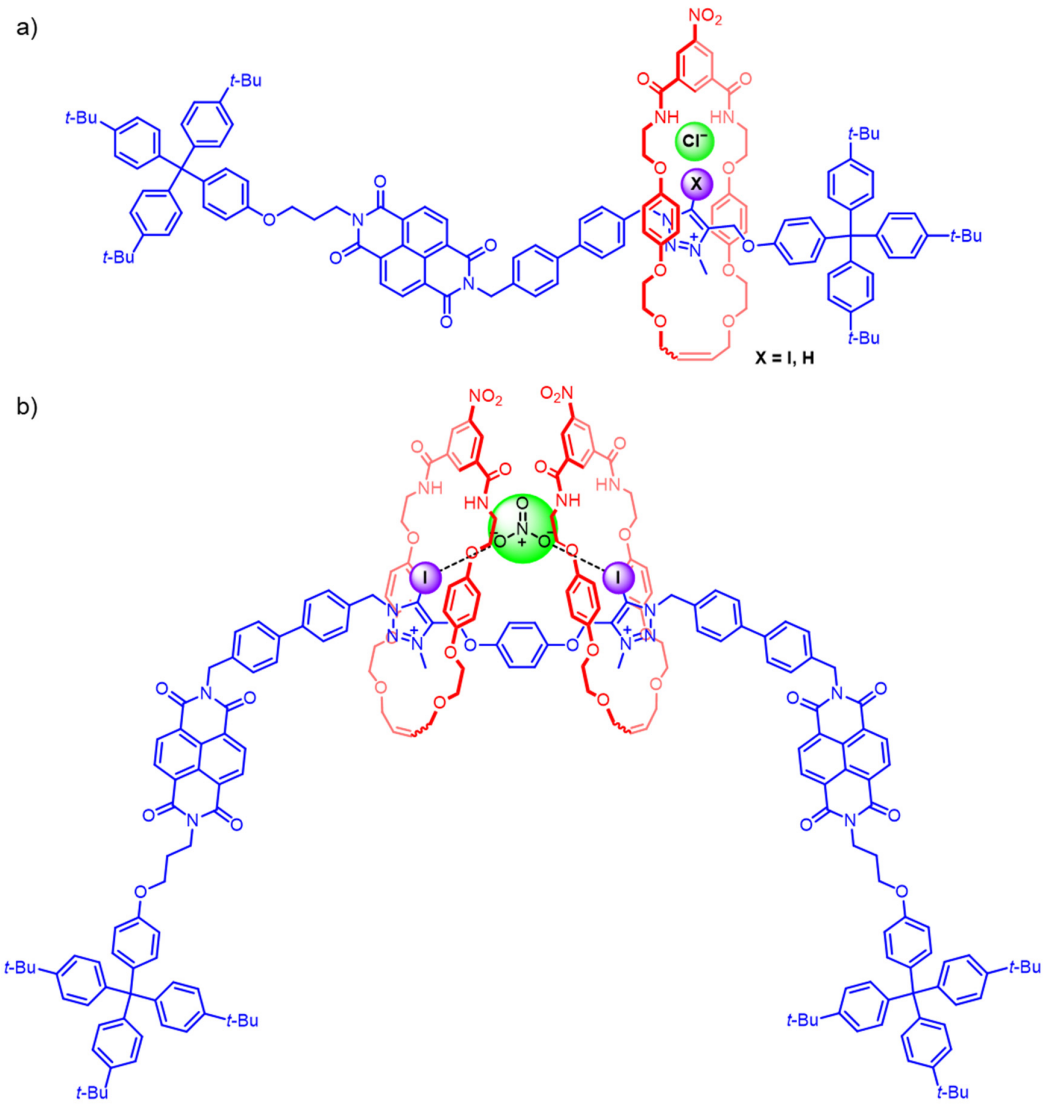


Figure 3.7. *Dynamic halogen bonding interlocked host systems for optical anion sensing via a shuttling mechanism, reported by Beer and co-workers.*

3.1.4 Chapter Aims

The preparation of *neutral* MIMs capable of strong and selective anion recognition remains an ongoing challenge in host-guest supramolecular chemistry, in part due to the scarcity of anion template-directed strategies for MIM synthesis. The development of methodologies for the facile preparation of functional neutral MIMs is therefore highly

desirable in the context of exploiting the unique binding environments of MIMs for applications in anion transport and sensing.

In this chapter, we sought to utilise the exceptionally strong XB···anion interactions between activated XB donor motifs and a discrete chloride anion to develop an anion template-directed strategy to prepare neutral XB interlocked host molecules for anion recognition. To this end, a potent XB motif based on 4,6-dinitro-1,3-bis-iodotriazole was incorporated into macrocycle or axle precursors to facilitate catenane or rotaxane formation respectively in the presence of a chloride template via an amide condensation methodology.

^{1}H NMR binding studies of the interlocked host structures showed a strong binding of halides over oxoanions in aqueous-acetone solvent mixtures. Crucially, the well-defined binding cavities of the interlocked hosts enabled discrimination of chemically-similar halide anions, with the smaller chloride and/or bromide anions able to be encapsulated in the interlocked cavity while the larger iodide anion is sterically excluded.

Encouraged by the promising anion binding behaviour of the neutral MIMs, the potential applications of these interlocked hosts for anion transport and sensing were explored. Anion transport studies conducted on the [2]catenanes established their ability to transport chloride across a lipid bilayer with superior activity and selectivity over the constituent non-interlocked macrocycles, showing for the first time a mechanical bond effect in anion transport (**Figure 3.8a**). A multi-station [2]rotaxane containing chromophoric NDI stations was designed as an optical sensor for halide anions, in which the different halide binding modes was exploited to elicit a selective optical response to chloride over the larger halides (**Figure 3.8b**).

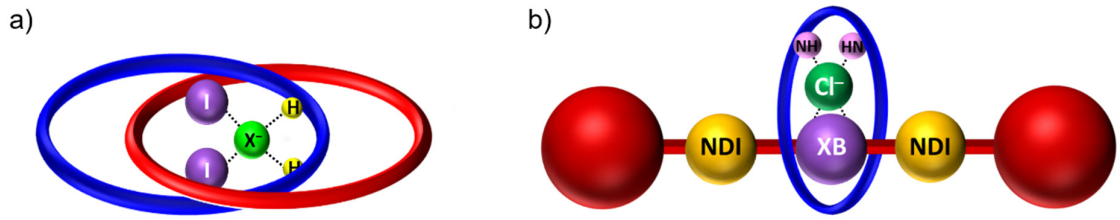


Figure 3.8. *Neutral interlocked XB host architectures based on (a) catenane; (b) rotaxane topologies prepared by a chloride template-directed anion synthesis.*

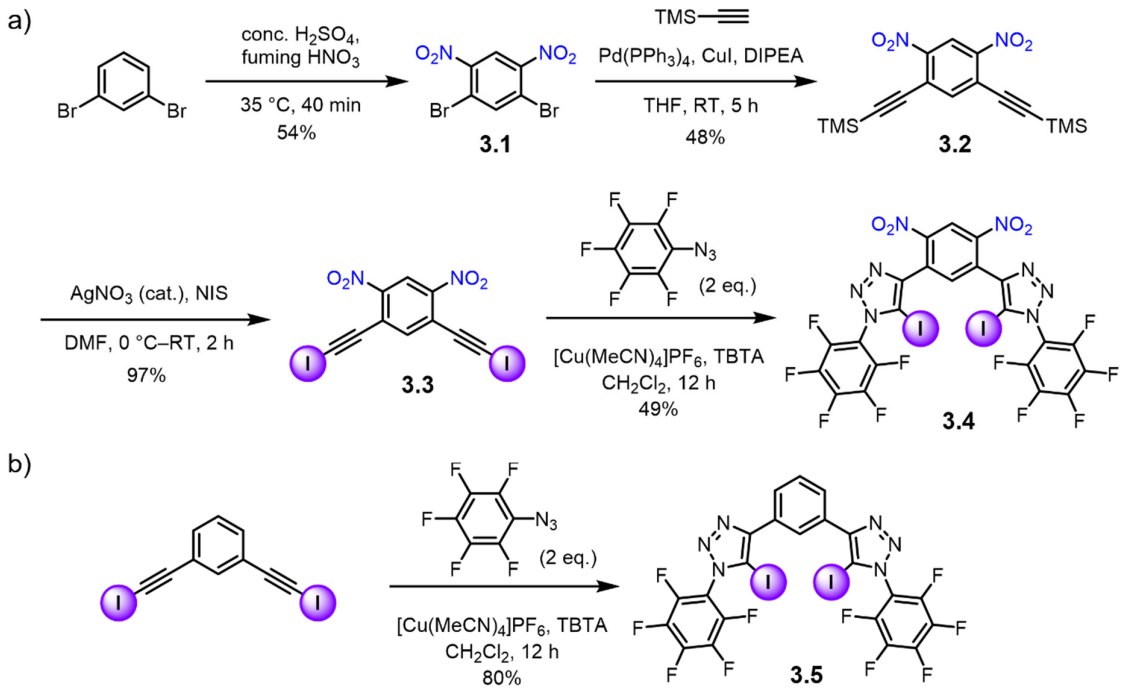
3.2 A Potent Dinitro-Functionalised Halogen Bonding Donor Motif

Inspired by the successful chloride template-directed synthesis of neutral halogen bonding [2]rotaxane systems containing a potent perfluoroaryl-substituted bis-iodotriazole XB donor motif, we sought other electron-withdrawing substituent groups that could be readily incorporated into the central phenyl spacer to further activate the XB donors. To this end, we designed a 4,6-dinitro-1,3-bis-iodotriazole XB binding motif. The nitro group possesses one of the largest positive Hammett substituent constants for a neutral functional group ($\sigma = +0.778$) and is expected to significantly withdraw electron density from the adjacent iodotriazole groups. In addition, the inclusion of substituents *ortho* to the iodotriazole groups may sterically restrict their rotation, thereby pre-organising the XB donors to participate in bidentate anion coordination.

3.2.1 Synthesis of Dinitro-Functionalised Acyclic Receptor

The target intermediate 4,6-dinitro-1,3-bis-iodoalkyne was prepared in three steps from 1,3-dibromobenzene (**Scheme 3.2a**). Nitration of 1,3-dibromobenzene was achieved with fuming HNO_3 and conc. H_2SO_4 to afford 1,3-dibromo-4,6-dinitrobenzene **3.1** in 54% yield, which was subjected to a Sonogashira coupling with TMS-acetylene in the presence of catalytic $Pd(PPh_3)_4$ and CuI under a strictly-controlled reaction time of 5 hours to give the bis-TMS-protected alkyne **3.2** in 48% yield. A one-step deprotection and iodination of **3.2** with N-

iodosuccinimide (NIS) in the presence of catalytic $AgNO_3$ afforded the target bis-iodoalkyne **3.3** in quantitative yield. To investigate the anion binding properties of the 4,6-dinitro-1,3-bis-iodotriazole XB binding motif, an acyclic receptor **3.4** was synthesised in 49% yield via a CuAAC reaction between **3.3** and 2 equivalents of pentafluorophenyl azide. As a control, an analogous receptor **3.5** containing an unsubstituted central phenyl spacer was synthesised in 80% yield via a CuAAC reaction between 2 equivalents of pentafluorophenyl azide and 1,3-bis(iodoethynyl)benzene (**Scheme 3.2b**).



Scheme 3.2. *(a) Synthesis of an acyclic 4,6-dinitrobenzene-1,3-bis-iodotriazole XB receptor **3.4**. (b) Synthesis of an analogous benzene-1,3-bis-iodotriazole XB receptor **3.5**.*

3.2.2 ^{1}H NMR Anion Binding Studies

To study the effect of the nitro substituent groups on the anion binding properties of iodotriazole donors, the chloride binding properties of the acyclic receptor **3.4** were investigated via ^{1}H NMR titrations and compared to that of the phenyl-based receptor **3.5**.

The progressive addition of TBACl to a solution of **3.4** in 2.5% D_2O/acetone induced a downfield movement of the proton signal corresponding to internal benzene proton H_b (**Figure 3.9c**), which is consistent with chloride binding via XB interactions in the bis(iodotriazole) cleft (**Figure 3.9a**). Similar downfield movements of the internal benzene proton signal were observed in the titration of **3.5** under identical conditions (**Figure 3.9d**). Bindfit analysis of the binding isotherms generated by monitoring this proton signal determined 1:1 stoichiometric chloride association constants of the receptors (**Figure 3.9b**, **Table 3.1**). Notably, the dinitro-functionalised receptor showed a dramatic 50-fold enhancement in chloride binding affinity relative to the benzene-based receptor, demonstrating the efficacy of this receptor design in increasing the anion binding potency of the XB donors.

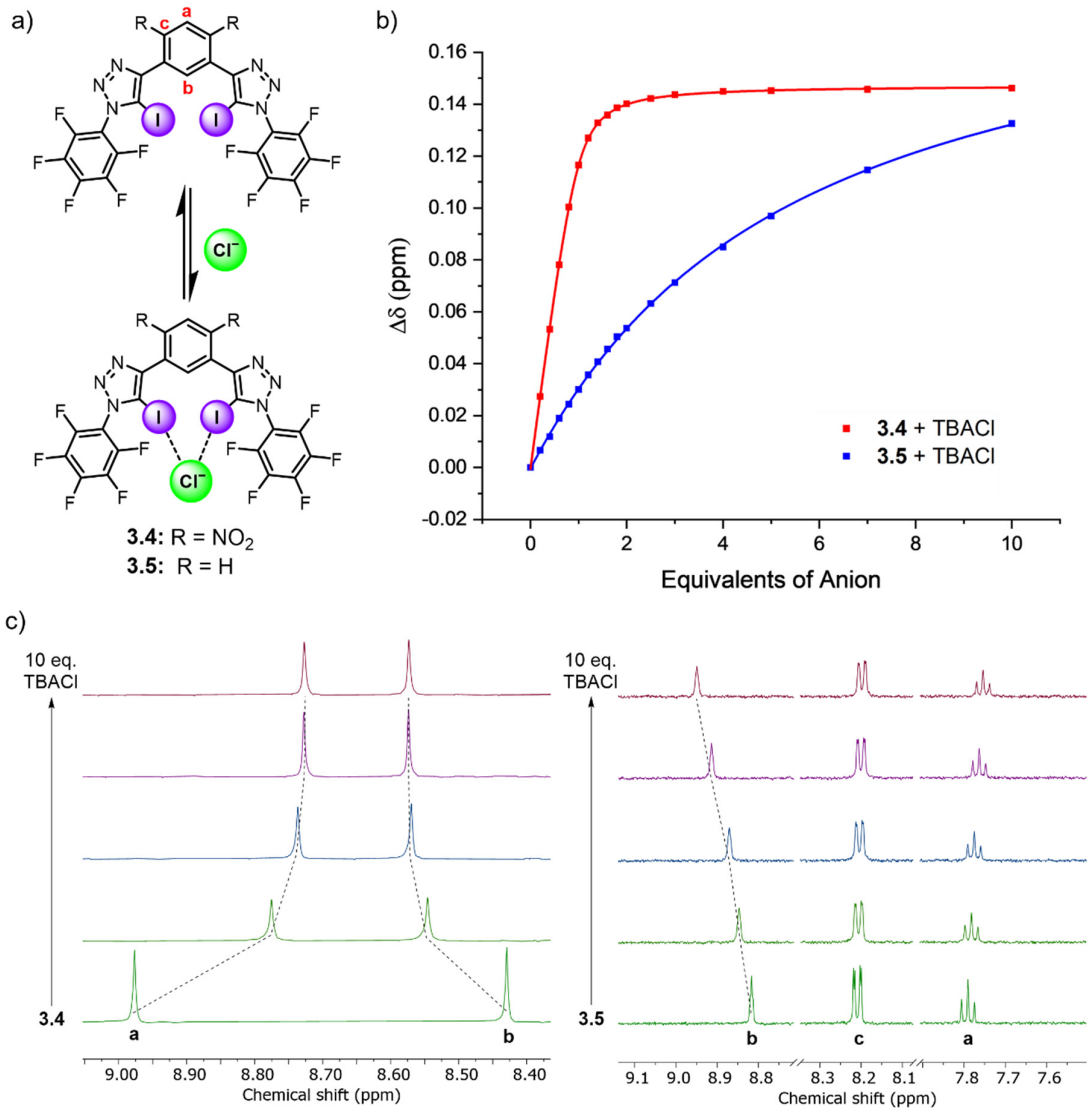


Figure 3.9. *Anion binding studies of acyclic XB receptors* ***3.4*** *and* ***3.5****. (a) Proposed chloride binding mode of the receptors; (b) Normalised binding isotherms generated by monitoring movements of internal benzene proton H_b; (c) Stacked ^{1}H NMR titration spectra of* ***3.4*** *(left) and* ***3.5*** *(right) upon addition of TBACl. In (b)-(c): Solvent = 2.5% D_2O/acetone-d_6 (v/v), T = 298 K, [Receptor] = 1 mM.*

Table 3.1. *Chloride anion association constants (K_a/M^{-1}) for acyclic XB receptors determined by ^{1}H NMR titrations*[a]

Receptor	Chloride association constants (K_a/M^{-1})
3.4	9650(518)
3.5	195(1)

[a]Errors (±) from the fitting process are shown in parentheses and are all < 5%. Chloride added as a TBA^+ salt. Solvent = 97.5/2.5 acetone-d_6/D_2O (v/v). T = 298 K. [Receptor] = 1.0 mM.

3.3 Catenanes for Anion Binding

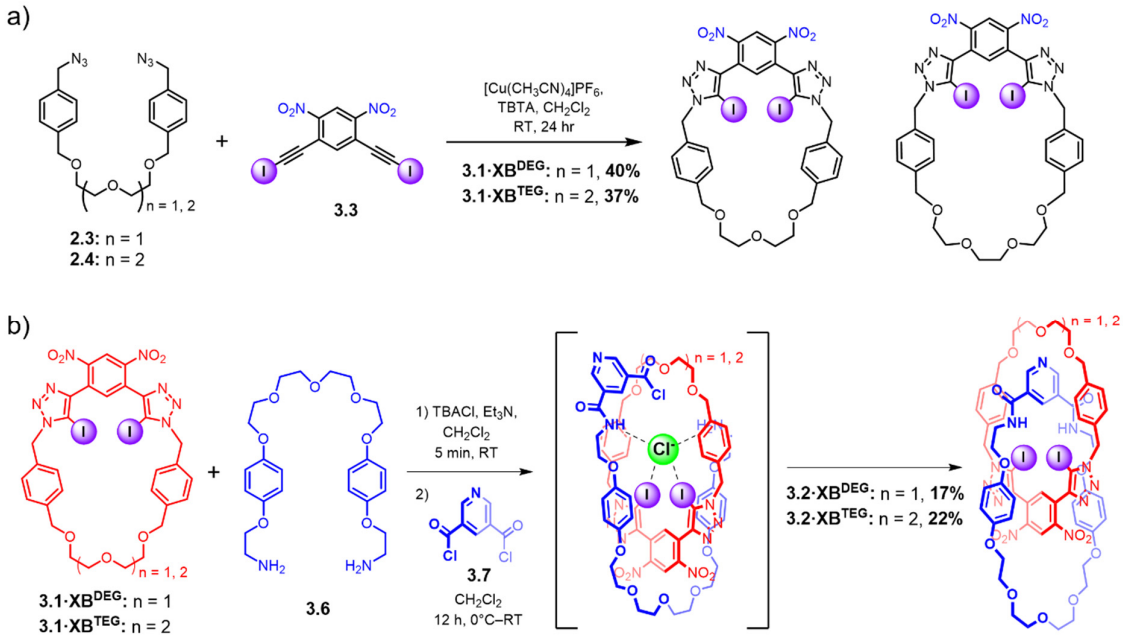
Having established the potent anion binding properties of XB receptors containing the 4,6-dinitro-1,3-bis-iodotriazole motif, attention was directed towards exploiting these strong XB···anion interactions to prepare neutral hetero[2]catenanes. It was envisaged that a macrocycle containing this bidentate XB motif could, in the presence of a chloride anion and bis-amine **3.6**, form a pseudo[2]rotaxane complex stabilised by orthogonal XB···Cl^- and HB···Cl^- interactions. Introduction of a bis(acid chloride) **3.7** to this intermediate would then lead to an amide condensation cyclisation reaction through the aperture of the XB macrocyclic component to form a second interlocked macrocyclic component, thereby generating a hetero[2]catenane.

3.3.1 Anion Template-Directed Synthesis of Neutral Hetero[2]Catenanes

Accordingly, two 4,6-dinitro-1,3-bis-iodotriazole-functionalised XB macrocycles were synthesized *via* a CuAAC reaction between bis(iodoalkyne) **3.3** and oligo(ethylene)-functionalised bis(azides) **2.3** and **2.4** respectively. Aqueous EDTA/NH_4OH work-up and purification by silica gel column chromatography afforded the target macrocycles **3.1·XB^{DEG}** and **3.1·XB^{TEG}** in 40% and 37% yields respectively (**Scheme 3.3a**).

With the XB macrocycles in hand, a chloride template-directed [2]catenane formation reaction was then attempted (**Scheme 3.3b**). To this end, an anhydrous CH_2Cl_2 solution comprising an XB macrocycle, tetrabutylammonium chloride, bis-amine **3.6** and triethylamine was cooled to 0°C, following which a freshly-prepared solution of 3,5-bis-chlorocarbonyl pyridine **3.7** was added dropwise. ESI-MS analysis of the reaction mixtures after 12 hours revealed peaks at m/z 1460 and 1504, corresponding to the target [2]catenanes. Aqueous work up and purification by preparative TLC afforded the [2]catenanes **3.2·XB^{DEG}** and **3.2·XB^{TEG}**

in 22% and 17% yields respectively, which were characterised by ^{1}H, ^{13}C NMR spectroscopy and high-resolution mass spectrometry. This represents, to the best of our knowledge, the first example of the anion templated synthesis of neutral halogen bonding [2]catenanes. Crucially, only a trace amount of the target [2]catenane was formed in the absence of TBACl. In addition, no evidence of interlocked structure formation was observed when a prototriazole-containing HB analogue of macrocycle **3.1·XB^{TEG}** was used, highlighting the key role of XB···chloride interactions in directing the self-assembly of the intermediate pseudo-rotaxane complex.



Scheme 3.3. *Synthesis of neutral XB macrocycles and hetero[2]catenanes via a chloride template-directed synthetic methodology.*

Comparing the ^{1}H NMR spectra of the products to those of the constituent XB macrocycles **3.1·XB^{DEG}** or **3.1·XB^{TEG}** and HB macrocycle **3.8·HB** provided evidence for the formation of an interlocked [2]catenane topology (**Figure 3.10**). The majority of proton signals in the [2]catenanes **3.2·XB^{DEG}** and **3.2·XB^{TEG}** underwent significant upfield shifts relative to the macrocycles, consistent with the increased shielding typically observed upon mechanical bond formation. In particular, large upfield perturbations and splitting were observed in

hydroquinone protons H_6 and H_7, which alongside a concomitant downfield shift of the internal benzene singlet H_b, suggests the formation of donor-acceptor stacking interactions between the electron-rich hydroquinone moieties and the electron-deficient dinitrobenzene motif.

Further insight into the co-conformations of the free [2]catenanes was obtained from 2D ^{1}H-H ROESY NMR spectroscopy (**Figure 3.11**). In both catenanes, through-space cross-peaks were observed between internal pyridyl proton H_2 of the HB macrocycle and internal dinitrobenzene proton H_b of the XB macrocycle, which promisingly suggested that the XB and HB donors of the two interlocked macrocycles are directed towards each other to form a cavity suitable for convergent binding of an anion. Significant cross-peaks were also observed between $H_{6/7}$ and H_b, providing further confirmation of the aforementioned stabilising charge-transfer aromatic stacking interactions between the hydroquinone and dinitrobenzene aromatic moieties.

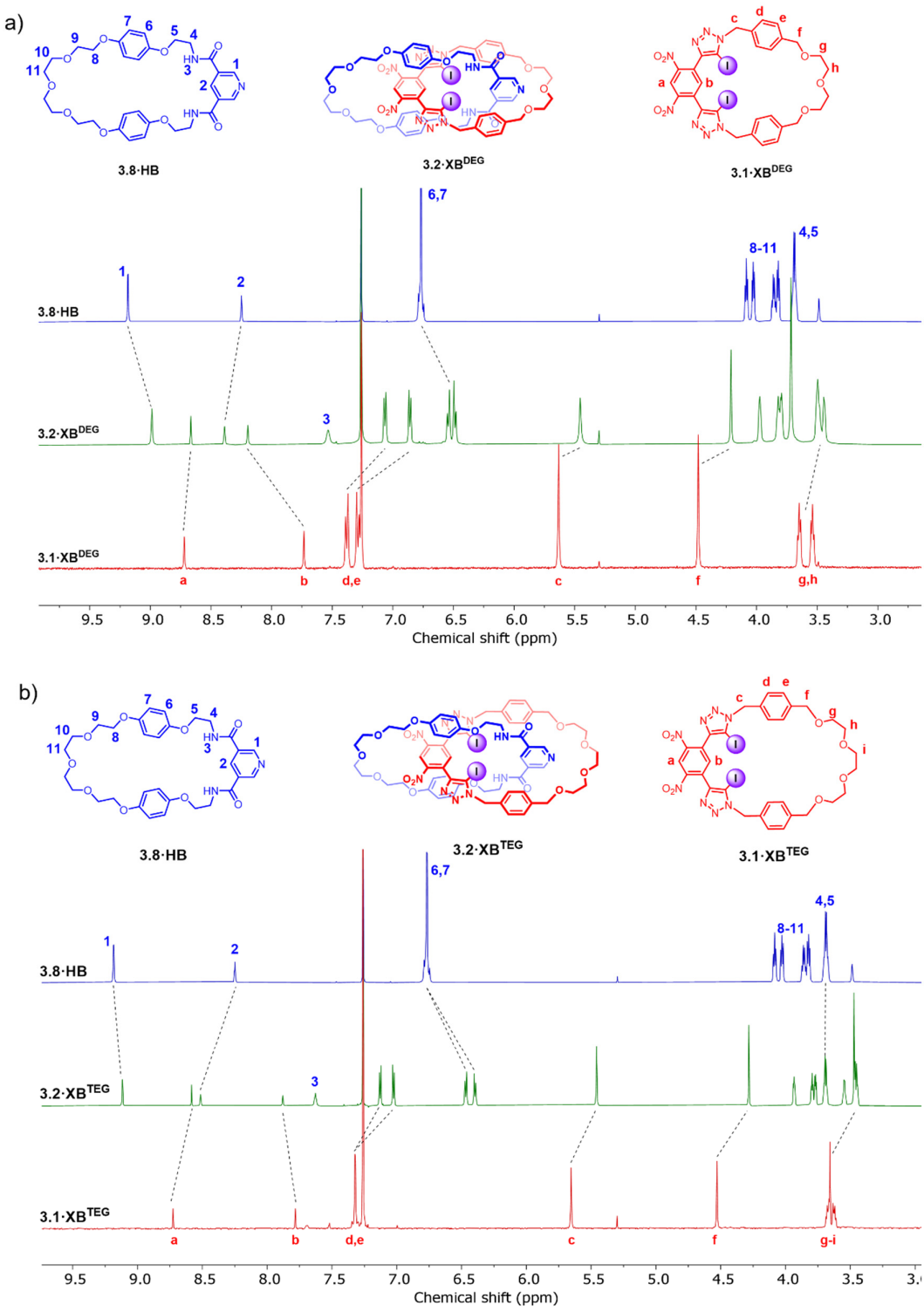


Figure 3.10. *Overlaid ^{1}H NMR spectra of the macrocycle* ***3.8·HB*** *(top), [2]catenane (middle) and corresponding XB macrocycle (bottom) (500 MHz, acetone-d_6, 298 K) for (a)* ***3.2·XB^{DEG}****; (b)* ***3.2·XB^{TEG}****.*

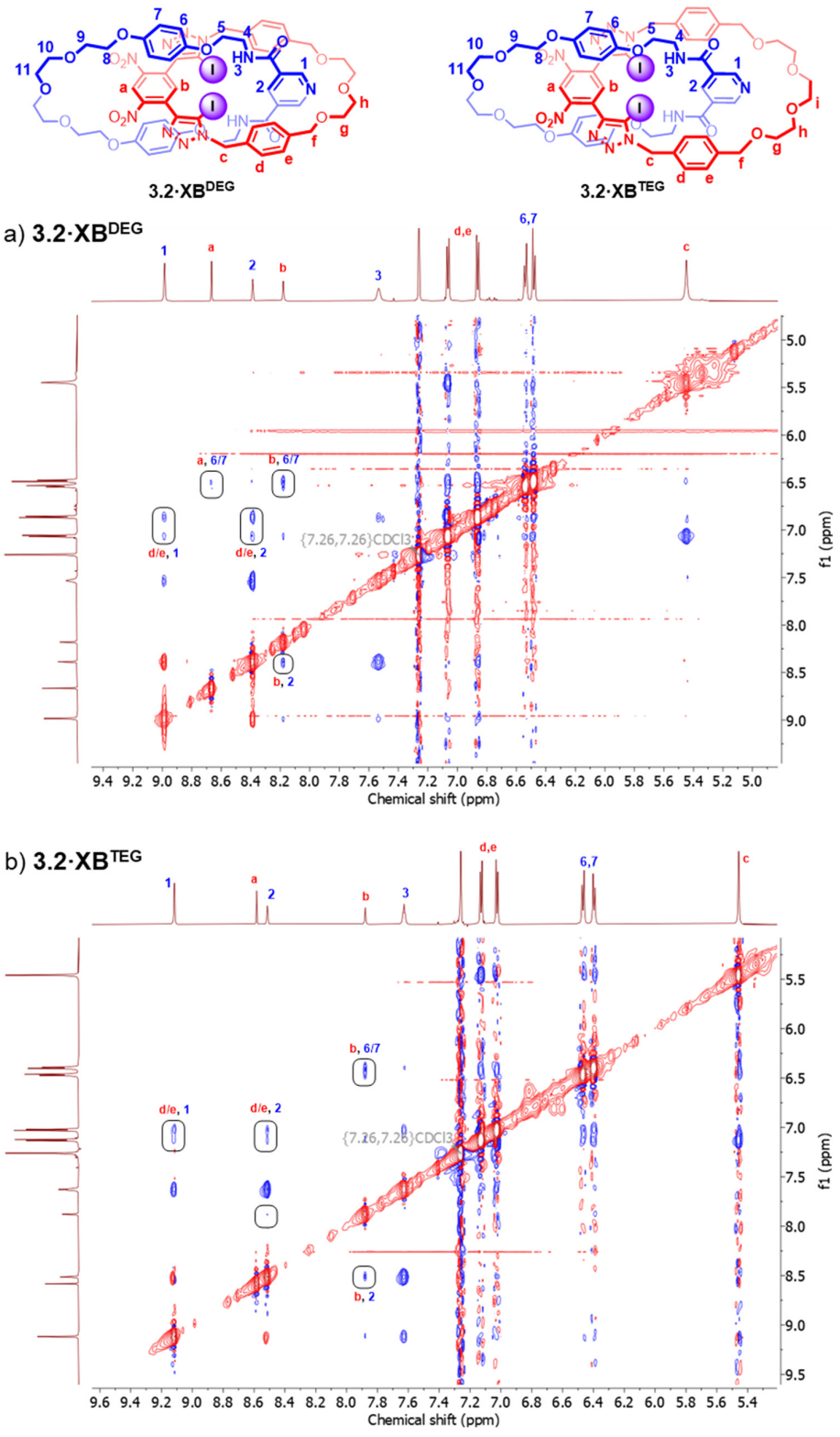


Figure 3.11. *^{1}H-^{1}H 2D ROESY NMR spectra of (a)* ***3.2·XB^{DEG}*** *and (b)* ***3.2·XB^{TEG}*** *(600 MHz, acetone-d_6, 298 K).*

3.3.2 ^{1}H NMR Anion Binding Studies

Encouraged by the promising co-conformational studies of the [2]catenanes which indicated the presence of a pre-organised cavity decorated with convergent XB and HB anion binding motifs, the binding affinities of the neutral interlocked catenane receptors **3.2·XB^{DEG}** and **3.2·XB^{TEG}** for various anions (X = Cl^-, Br^-, I^- and NO_3^-) were studied *via* ^{1}H NMR titration experiments in competitive aqueous-organic solvent mixtures (5:95 D_2O/acetone-*d*$_6$ or 10:90 D_2O/acetone-*d*$_6$ (v/v)). To elucidate the effect of the mechanical bond on the anion binding behaviour of the receptors, analogous titrations were conducted on the corresponding non-interlocked XB macrocycles **3.1·XB^{DEG}** and **3.1·XB^{TEG}**, as well as HB macrocycle **3.8·HB**.

Upon addition of tetrabutylammonium (TBA) halide salts to the macrocycles and catenanes in 5:95 D_2O/acetone-*d*$_6$ (v/v), significant chemical shift perturbations were observed in the protons proximal to the 4,6-dinitro-1,3-bis-iodotriazole motif (H_a, H_b), suggesting that halide binding occurs *via* XB···anion interactions (**Figure 3.12**). In contrast, no significant perturbations of the signals in either the macrocycle or catenane ^{1}H NMR spectra were observed upon addition of excess $TBANO_3$ in 5:95 D_2O/acetone, suggesting that both the macrocyclic and interlocked hosts are incapable of binding nitrate under these solvent conditions. The observed preference of the XB receptors for halides over nitrate is consistent with the known preference of halogen bonding donor groups for softer halide anions over the harder oxoanions[25, 26] and further indicates that the anion binding capabilities of the receptors are driven primarily by the potent XB donor motif.

A more detailed inspection of the halide binding NMR studies revealed marked differences in the perturbation profiles of the catenane proton signals induced by the three halides. Upon progressive addition of Cl^- and Br^- to the catenanes **3.2·XB^{DEG}** and **3.2·XB^{TEG}**, the proton signals corresponding to internal pyridyl proton H_2 and internal dinitrobenzene

proton H_b underwent significant chemical shift perturbations and severe broadening, indicative of the bis(iodotriazole) XB donors and bis(amide) HB donors participating in convergent anion binding (**Figure 3.12b-c**). On the other hand, in the I^- binding study, the magnitude of the downfield shift and degree of broadening in internal pyridyl proton H_2 was greatly attenuated, which may suggest limited participation of the bis(amide) HB donors in binding (**Figure 3.12d**). In addition, some proton signals move in opposite directions upon addition of Cl^-/Br^- *vs.* I^-. For example, the external dinitrobenzene proton H_a shifts significantly downfield in response to Cl^- and Br^- binding, whereas upon addition of I^- the proton instead moves upfield. Similar observations were noted when the titrations were repeated in the more competitive 90:10 acetone-d_6/D_2O (v/v) solvent system. These differing chemical shift perturbation profiles induced by the various halides suggest that the binding mode of iodide to both [2]catenanes differs from that of chloride and bromide.

Conceivably, the larger ionic radius of iodide restricts its access to the interior of the catenane binding cavity, forcing iodide to adopt an 'exotopic' binding mode in which it is bound primarily by the more potent XB on the exterior of the macrocyclic cavity (**Figure 3.12a**). On the other hand, the smaller halides are able to be encapsulated endotopically within the interlocked binding cavity, where they are convergently bound by the XB and HB donors of both macrocycles. Crucially, these differing chemical shift perturbation profiles are not observed for the non-interlocked XB macrocycles **3.1·XB^{DEG}** and **3.1·XB^{TEG}**, which exhibited similar patterns in the movement of their proton signals across all three halides. The role of the catenane host architecture therefore likely plays a pivotal role in eliciting the observed halide size discrimination dependency in the anion binding modes of **3.2·XB^{DEG}** and **3.2·XB^{TEG}**.

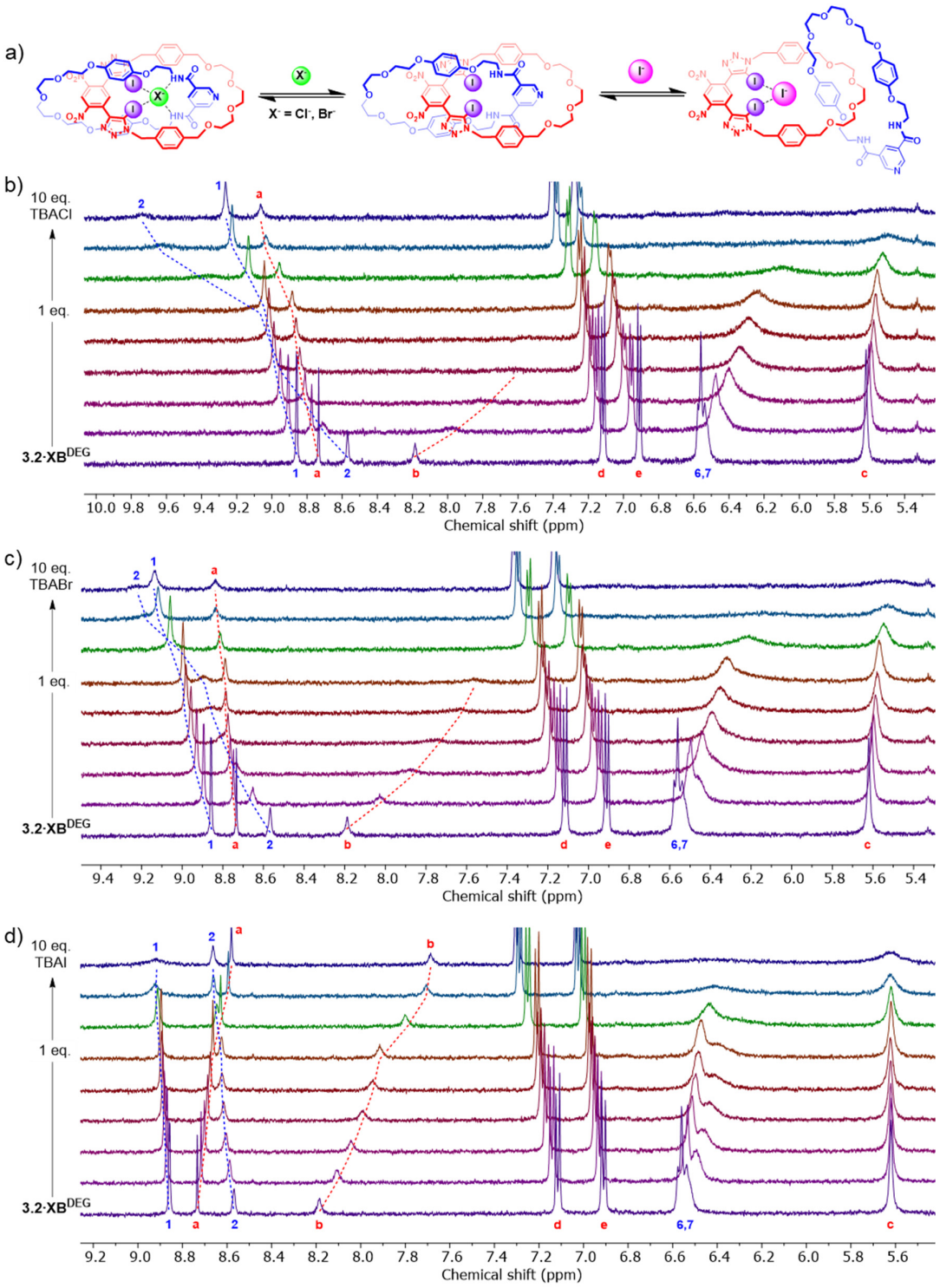


Figure 3.12. *Halide binding studies of [2]catenane* ***3.2·XB^{DEG}****. (a) Proposed endotopic (left) and exotopic (right) binding modes. (b)-(d) Stacked ^{1}H NMR titration spectra of* ***3.2·XB^{DEG}*** *upon addition of: b) TBACl; c) TBABr; d) TBAI. Solvent = 5% D_2O/acetone-d_6 (v/v). T = 298 K. [Receptor] = 1 mM.*

The halide binding constants of the macrocycles **3.1·XB^{DEG}** and **3.1·XB^{TEG}** as well as [2]catenanes **3.2·XB^{DEG}** and **3.2·XB^{TEG}** in 95:5 and 90:10 acetone-d_6/D_2O (v/v) were subsequently determined by Bindfit[27] analysis of the titration data, wherein the binding isotherms generated by monitoring multiple proton resonances proximal to the binding site were fitted to a global 1:1 host-guest stoichiometric binding model (**Figure 3.13**, **Table 3.2**). Notably, the chloride and bromide binding affinities of **3.2·XB^{DEG}** and **3.2·XB^{TEG}** are markedly enhanced relative to their constituent XB and HB macrocycles (**Table 3.2**), which is consistent with the notion that the smaller halide anions bind to the [2]catenanes in an 'endotopic' fashion which benefits from the formation of convergent XB and HB interactions. In contrast, the iodide binding affinities of the [2]catenanes are either of similar strength (**3.2·XB^{TEG}**) or slightly diminished (**3.2·XB^{DEG}**) compared to the respective XB macrocycles, which is again consistent with the proposed exotopic binding mode of iodide wherein anion binding occurs primarily via the XB donor groups.

Table 3.2. *Anion association constants (K_a/M^{-1}) of macrocycles and [2]catenanes determined by ^1H NMR titrations.*

	Anion Association Constant (K_a/M^{-1})						
Solvent	5:95 D_2O/acetone-d_6				10:90 D_2O/acetone-d_6		
	Cl^-	Br^-	I^-	NO_3^-	Cl^-	Br^-	I^-
3.1·XB^{DEG}	220(2)	899(18)	1802(50)	N.B.[b]	22(1)	174(2)	703(12)
3.2·XB^{DEG}	1232(11)	1721(29)	1570(47)	N.B.[b]	170(1)	335(3)	620(5)
3.1·XB^{TEG}	152(2)	690(7)	1556(21)	N.B.[b]	32(1)	160(1)	560(6)
3.2·XB^{TEG}	1260(13)	2345(48)	1749(61)	N.B.[b]	156(1)	347(4)	771(17)
3.8·HB	34(1)	35(1)	21(1)	N.B.[b]	N.M.[c]	N.M.[c]	N.M.[c]

[a] K_a values calculated using Bindfit with a 1:1 host-guest binding model. Errors (±) from the fitting process are shown in parentheses and are all < 5%. All anions added as TBA^+ salts. Solvent = 95:5 or 90:10 acetone-d_6/D_2O. T = 298 K. [Receptor] = 1.0 mM. [b] N.B. = No binding observed. [c] N.M. = Not measured.

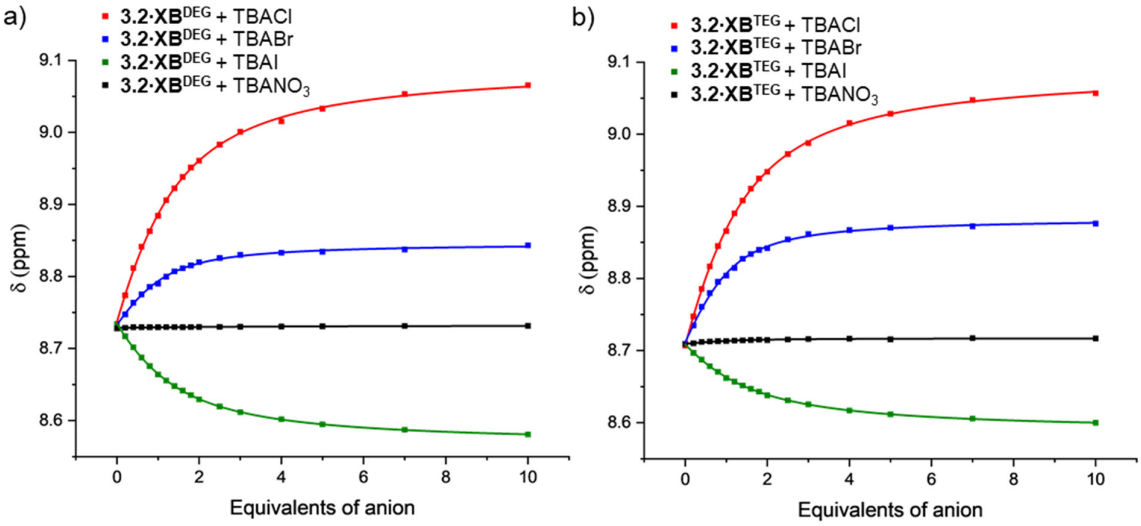


Figure 3.13. *Binding isotherms of: (a)* ***3.2·XB^{DEG}****; (b)* ***3.2·XB^{TEG}****, generated by monitoring the movement of internal pyridyl proton H_2 upon progressive addition of TBAX (X = Cl, Br, I, NO_3) in 5% D_2O/acetone (v/v).*

The halide binding affinities of the XB macrocycles **3.1·XB^{DEG}** and **3.1·XB^{TEG}** follow the trend: $Cl^- < Br^- < I^-$, in line with the 'Hofmeister bias' in which the least extensively hydrated iodide anion is most strongly bound to the receptor in aqueous-containing solvent media (**Figure 3.14a**). On the other hand, the anion association constants of the [2]catenanes **3.2·XB^{DEG}** and **3.2·XB^{TEG}** in 95:5 acetone-d_6/D_2O (v/v) deviate from the trend predicted by the Hofmeister bias and are instead in the order: $Cl^- < I^- < Br^-$ (**Figure 3.14a**). The observed binding preference of the [2]catenanes for Br^- over the other two halides was attributed to the intermediate size of the bromide anion, enabling it to bind within the interlocked cavity while remaining less extensively hydrated compared to chloride. Notably, the larger **3.2·XB^{TEG}** displays a more pronounced preference for bromide over chloride than the smaller catenane **3.2·XB^{DEG}**, presumably due to better size complementarity between bromide and the larger interlocked cavity of the former. Upon moving to the more competitive 90:10 acetone-d_6/D_2O solvent system, the preference of the [2]catenanes for bromide is lost and the trend in binding affinities predicted by the Hofmeister series is restored, indicating that upon raising the water

content of the system, halide binding selectivity becomes increasingly dominated by the degree of anion hydration (**Figure 3.14b**).

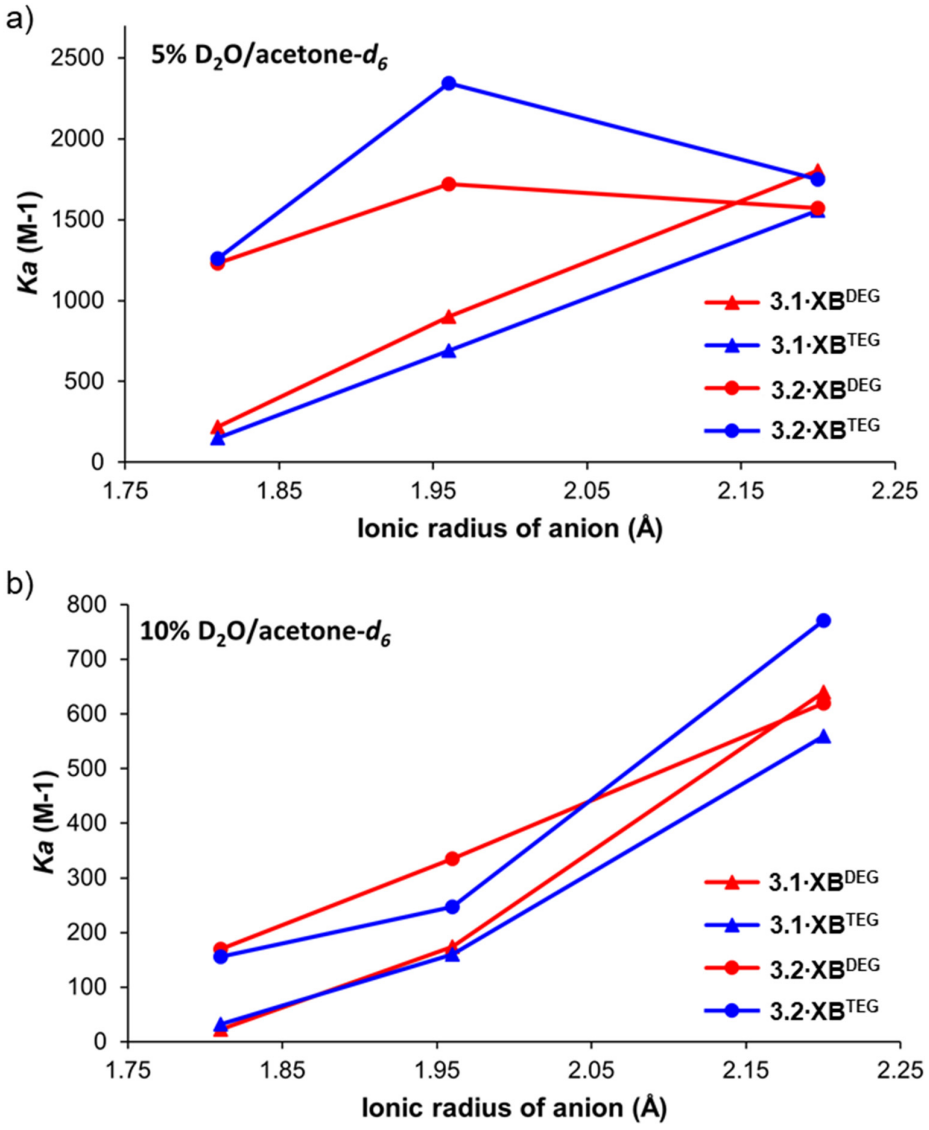


Figure 3.14. *Graphical representation of anion association constants of XB macrocycles and [2]catenanes in a) 5% D_2O/acetone-d_6 (v/v); b) 10% D_2O/acetone-d_6 (v/v).*

The size-driven tendency towards 'anti-Hofmeister' anion binding exhibited by the [2]catenanes can be further illustrated by comparing the anion association constants of the XB macrocycles and the corresponding [2]catenane (**Table 3.3**). This was undertaken by

calculating 'mechanical bond enhancement' (MBE) factors, which are defined for each halide as the ratio: $\ln(K_a^{\mathbf{3.2}})/\ln(K_a^{\mathbf{3.1}})$, where $K_a^{\mathbf{3.2}}$ and $K_a^{\mathbf{3.1}}$ are the anion association constants of the catenane and its constituent XB macrocycle respectively. The MBE values allow us to compare the anion binding energetics of the XB macrocycle and the analogous [2]catenane, and thereby evaluate the effect of the mechanical bond on the anion binding potency of the receptors. We firstly note chloride and bromide exhibit MBE > 1 in all cases, indicative of a mechanical bond induced enhancement in anion binding potency. In contrast, the MBE values of iodide are in some cases <1, indicating attenuated halide affinity upon mechanical bond formation. Importantly, the MBE values universally follow the trend $Cl^- > Br^- > I^-$, showing that the smallest chloride anion consistently experiences the greatest enhancement in binding upon formation of the mechanical bond. This suggests that the trend in halide binding affinity arising from mechanical bonding inherently opposes the trend imposed by the Hofmeister series, presumably due to a halide size-based discrimination effect. Crucially, this pronounced mechanical bond induced enhancement in the binding affinities of the more hydrophilic halides serves as a rare antagonist to the selectivity profiles dictated by the Hofmeister bias. Therefore, it is noteworthy in the wider context of supramolecular anion recognition in aqueous media, the use of XB MIM-based receptors is a promising potential strategy to engineer anti-Hofmeister bias anion selectivity.

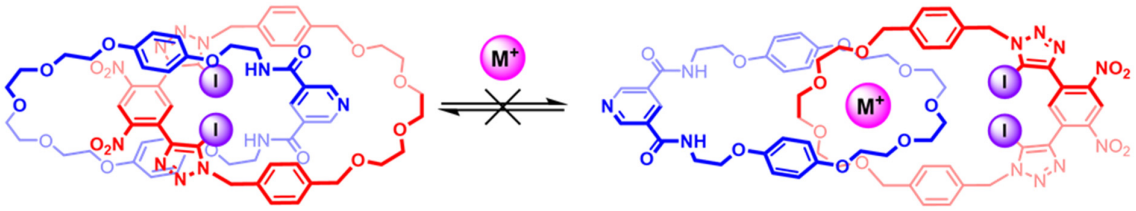
Table 3.3. *Mechanical bond enhancement (MBE) factors of catenane/macrocycle pairs calculated for various halides.*[a]

	MBE (3.2·XB^{DEG}/3.1·XB^{DEG})		**MBE (3.2·XB^{TEG}/3.1·XB^{TEG})**	
Anion	**5% D_2O/acetone-d_6**	**10% D_2O/acetone-d_6**	**5% D_2O/acetone-d_6**	**10% D_2O/acetone-d_6**
Cl^-	1.32	1.66	1.42	1.46
Br^-	1.10	1.13	1.19	1.15
I^-	0.98	0.98	1.02	1.05

[a]MBE = $\ln(K_a^{3.2}/K_a^{3.1})$, calculated using anion association constants (K_a) determined by ^{1}H NMR in 5% D_2O/acetone-d_6 or 10% D_2O/acetone-d_6.

3.3.3 Cation Binding Studies

The presence of polyethylene glycol linkers in both macrocyclic components of the [2]catenanes suggested the possibility of cation coordination via co-conformational circum-rotation of the interlocked rings to generate a binding cavity suitable for binding an alkali metal cation (**Scheme 3.4**). To this end, cation binding studies were conducted on **3.2·XB^{TEG}** by progressive addition of KBAr^{F} in 1:1 $CD_3CN/CDCl_3$. Disappointingly, however, no changes in the ^{1}H NMR spectrum of **3.2·XB^{TEG}** were observed upon addition of up to 10 equivalents of the cation. This weak cation binding could be due to the presence of the hydroquinone linker in the amide-based macrocycle, which may deactivate the corresponding tetraethylene glycol chain towards cation coordination via conjugation of the oxygen lone pair into the aromatic ring. In addition, aromatic stacking between the electron-rich hydroquinone rings and the electron-poor dinitro-bis(iodotriazole)-substituted motif, evidenced by cross-peaks between $H_{6/7}$ and $H_{a/b}$ in the 2D ^{1}H ROESY spectrum of **3.2·XB^{TEG}**, may stabilise the catenane in a co-conformation suitable for anion binding and present an energetic barrier to circum-rotation.

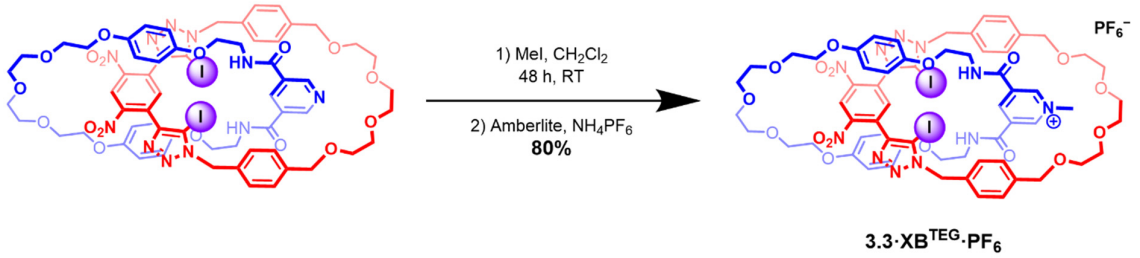


Scheme 3.4. *Proposed cation binding mode of [2]catenane* ***3.2·XB^{TEG}***.

3.3.4 Effects of Methylation on the Anion Binding Properties of the [2]Catenanes

Having determined the anion affinities of the neutral [2]catenanes, we sought to investigate if the halide selectivity profiles could be modulated by post-synthetic methylation of the pyridyl group to generate a monocationic receptor. To this end, the [2]catenane **3.2·XB^{TEG}** was treated with excess methyl iodide in CH_2Cl_2 solution over a period of 48 hrs,

upon which TLC analysis indicated complete consumption of the neutral [2]catenane. The solvent was removed under vacuum to afford the methylated [2]catenane **3.3·XB^{TEG}·I** as the iodide salt. Ion exchange to PF_6^- was achieved by passing an acetone/water solution of the receptor through Amberlite resin pre-loaded with NH_4PF_6 solution to afford **3.3·XB^{TEG}·PF$_6$** in 80% yield (**Scheme 3.5**).



Scheme 3.5. *Synthesis of methylated [2]catenane* ***3.3·XB^{TEG}·PF$_6$.***

Evidence for successful methylation of the pyridyl group and ion exchange was obtained by comparing the ^{1}H NMR spectrum of **3.2·XB^{TEG}** to those of **3.3·XB^{TEG}·I** and **3.3·XB^{TEG}·PF$_6$** in $CDCl_3$ (**Figure 3.15**). Importantly, the appearance of a singlet integrating to 3 protons was observed in the 4-4.5 ppm region of **3.3·XB^{TEG}·I** and **3.3·XB^{TEG}·PF$_6$**, which was assigned to the methyl group protons H_{11}.

The ^{1}H NMR spectrum of **3.3·XB^{TEG}·I** shows evidence of iodide binding via XB interactions with the bis(iodotriazole) motif, as indicated by a dramatic 0.62 ppm downfield shift of internal dinitrobenzene proton H_b relative to the neutral catenane. Broadening of the amide protons H_3 as well as a downfield shift of internal benzene proton H_2 were also observed, suggesting that the iodide counterion also interacts with the pyridinium carboxamide motif of the HB macrocycle, but it is not clear if the XB and HB binding motifs are able to act convergently. The observed proton movements, particularly that of the iodotriazole-adjacent

proton H_b, are reversed upon ion exchange to PF_6^-, consistent wtih the lack of significant XB···anion binding interactions with the non-coordinating PF_6^- anion.

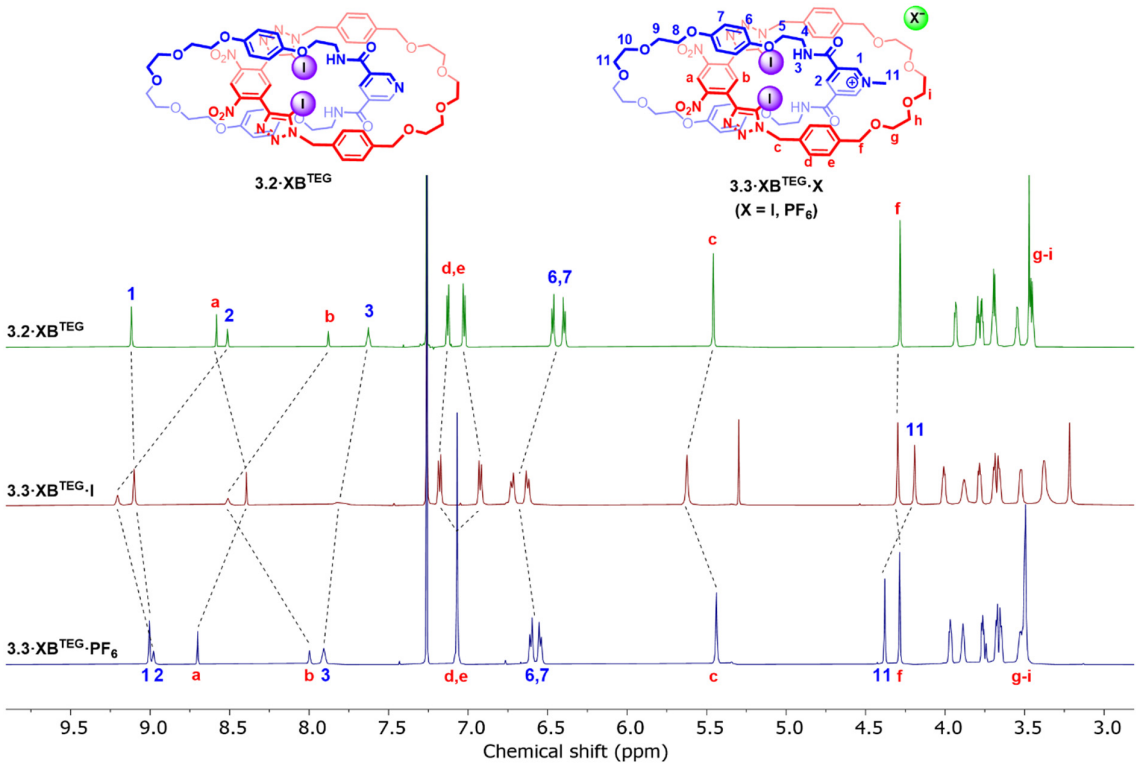


Figure 3.15. *Overlaid ^{1}H NMR spectra of the neutral catenane* ***3.2·XB^{TEG}*** *(top), methylated catenane* ***3.3·XB^{TEG}·I*** *(middle) and ion-exchanged catenane* ***3.3·XB^{TEG}·PF$_6$*** *(bottom) (500 MHz, acetone-d_6, 298 K).*

The ^{1}H-^{1}H 2D ROESY spectrum provides further insights into the co-conformation of the methylated [2]catenane **3.3·XB^{TEG}·PF$_6$** (**Figure 3.16**). Importantly, strong through-space cross-peaks were observed between the methyl singlet H_{11} and the tri(ethylene glycol) protons $H_{g\text{-}i}$, which may suggest at the formation of C-H···O hydrogen bonding interactions between the pyridinium activated methyl group and the oxygen atoms of the opposite macrocycle. Cross-peaks are also seen between dinitrobenzene proton H_b and the hydroquinone protons $H_{6/7}$, which is attributed to the formation of aromatic stacking interactions between the electron-rich hydroquinone moiety and the electron-poor dinitrobenzene. These observations suggest that

methylation of the pyridyl group further stabilises, via the formation of C-H···O hydrogen bonding interactions, the co-conformation of the [2]catenane which is pre-organised for anion binding in the interlocked cavity.

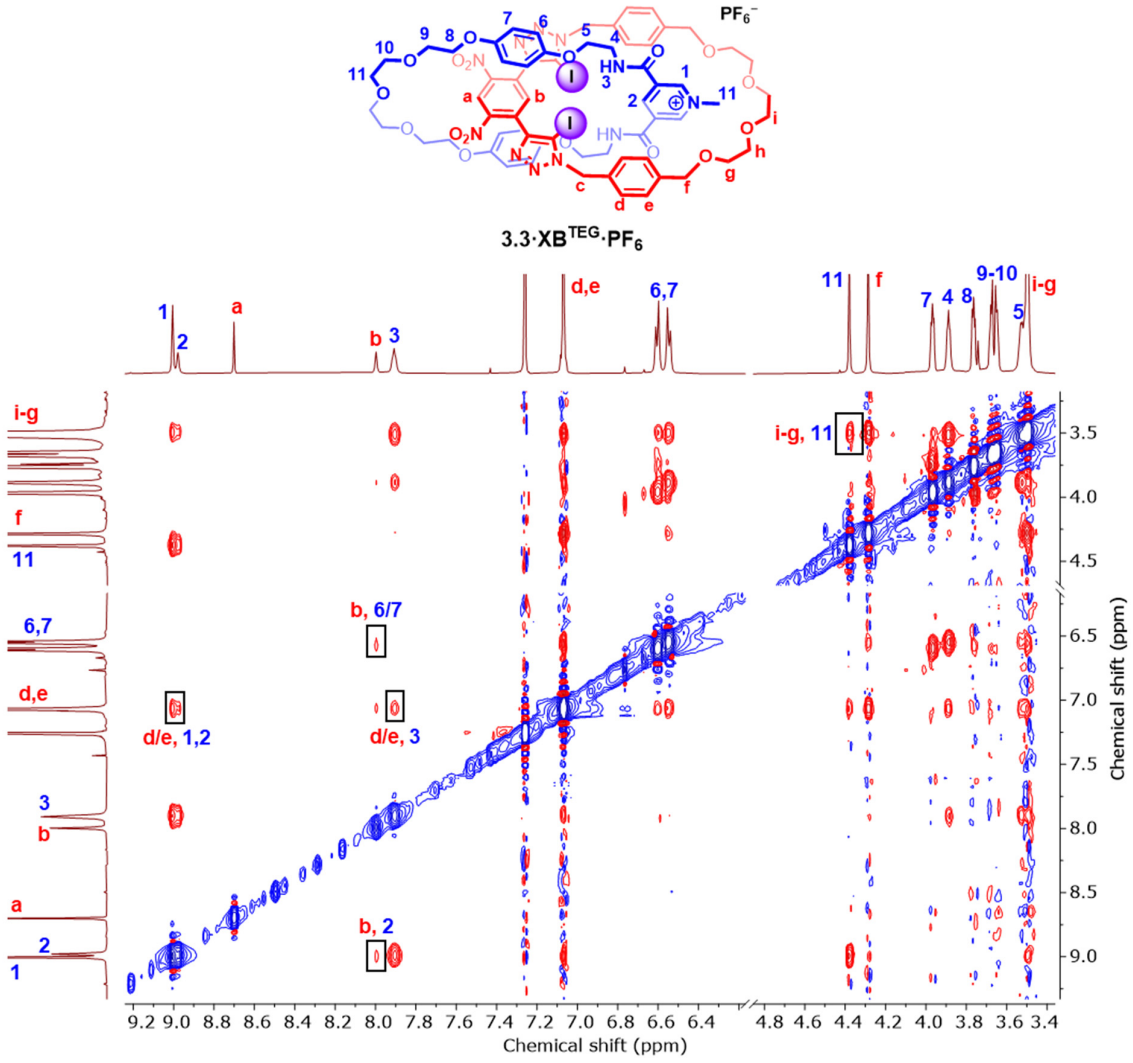


Figure 3.16. *^{1}H-^{1}H 2D ROESY NMR spectra of* ***3.3·XB^{TEG}·PF$_6$*** *(600 MHz, acetone-d$_6$, 298 K).*

The halide binding affinities of **3.3·XB^{TEG}·PF$_6$** were investigated via ^{1}H NMR halide anion titration studies. As anticipated, the introduction of a positive charge significantly enhanced the anion binding affinities of the halides, which were too high to be reliably determined in 5% D$_2$O/acetone-*d$_6$*. In the more competitive solvent 10% D$_2$O/acetone-*d$_6$*

system, the [2]catenane **3.3·XB$^{TEG.}$·PF$_6$** again exhibited chemical shift perturbation profiles consistent with contrasting endotopic and exotopic binding modes in the cases of chloride and iodide respectively (**Figure 3.17a**). This is particularly evident in the movement of dinitrobenzene proton H_b, which upon chloride addition, moves upfield and undergoes severe broadening, indicative of the proton becoming increasingly fixed in the interior of the shielded anion binding cavity (**Figure 3.17b**). In contrast, iodide addition induces a progressive downfield shift of H_b, which is typically observed in acyclic or macrocycle bis(iodotriazole) XB receptors where anion binding occurs via a simple bidentate coordination mode (**Figure 3.17d**). In addition, the internal pyridinium proton H_2 undergoes a downfield shift and broadening upon chloride addition, indicative of the formation of N-H···Cl$^-$ HB interactions, whereas a small upfield shift of H_2 is observed in the presence of iodide. These observations provide compelling evidence for chloride binding endotopically in the interlocked cavity while iodide is bound primarily by the XB bis-iodotriazole donors in an exotopic manner. This suggests that despite charge assistance from the proximal pyridinium group serving to enhance the potency of the isophthalamide HB donor motif, the 2,4-dinitro-1,3-bis-iodotriazole XB motif remains the preferred non-covalent interaction for binding of halides.

An interesting case is observed for bromide addition, which appears at first glance to induce only very small chemical shift perturbations in the proton signals **3.3·XB$^{TEG.}$·PF$_6$**, which superficially suggests a weaker interaction with the bromide anion (**Figure 3.17c**). However, a more detailed inspection of the ^{1}H NMR spectra reveals that the movements of several of the proton signals appear to subtly change direction in the presence of >5 equivalents of bromide. Some examples include: H_2, which initially moves downfield and then upfield; H_a, which moves first downfield and then upfield, as well as $H_{6,7}$, which moves upfield and then slightly downfield. Comparing the movements of these proton signals to the corresponding protons in

the chloride and iodide titrations suggests a scenario in which the bromide-induced chemical shift perturbation profile is a superposition of the chloride and iodide profiles, with 'chloride-like' shifts dominating at low equivalents while 'iodide-like' shifts become more apparent at higher equivalents of bromide.

A physical interpretation of this result could suggest that bromide binding to **3.3·XB^{TEG}·PF$_6$** occurs via a combination of exotopic and endotopic binding modes, with the 1:1 endotopic binding mode favoured at low equivalents of bromide, while at high equivalents an exotopic binding mode is preferred. The observation of dual binding modes for bromide in the methylated [2]catenane **3.3·XB^{TEG}·PF$_6$**, but not the neutral [2]catenane **3.2·XB^{TEG}**, is tentatively attributed to the decreased size of the anion binding cavity due to steric restrictions imposed by the additional methyl group, which reduces its accessibility to the bromide anion.

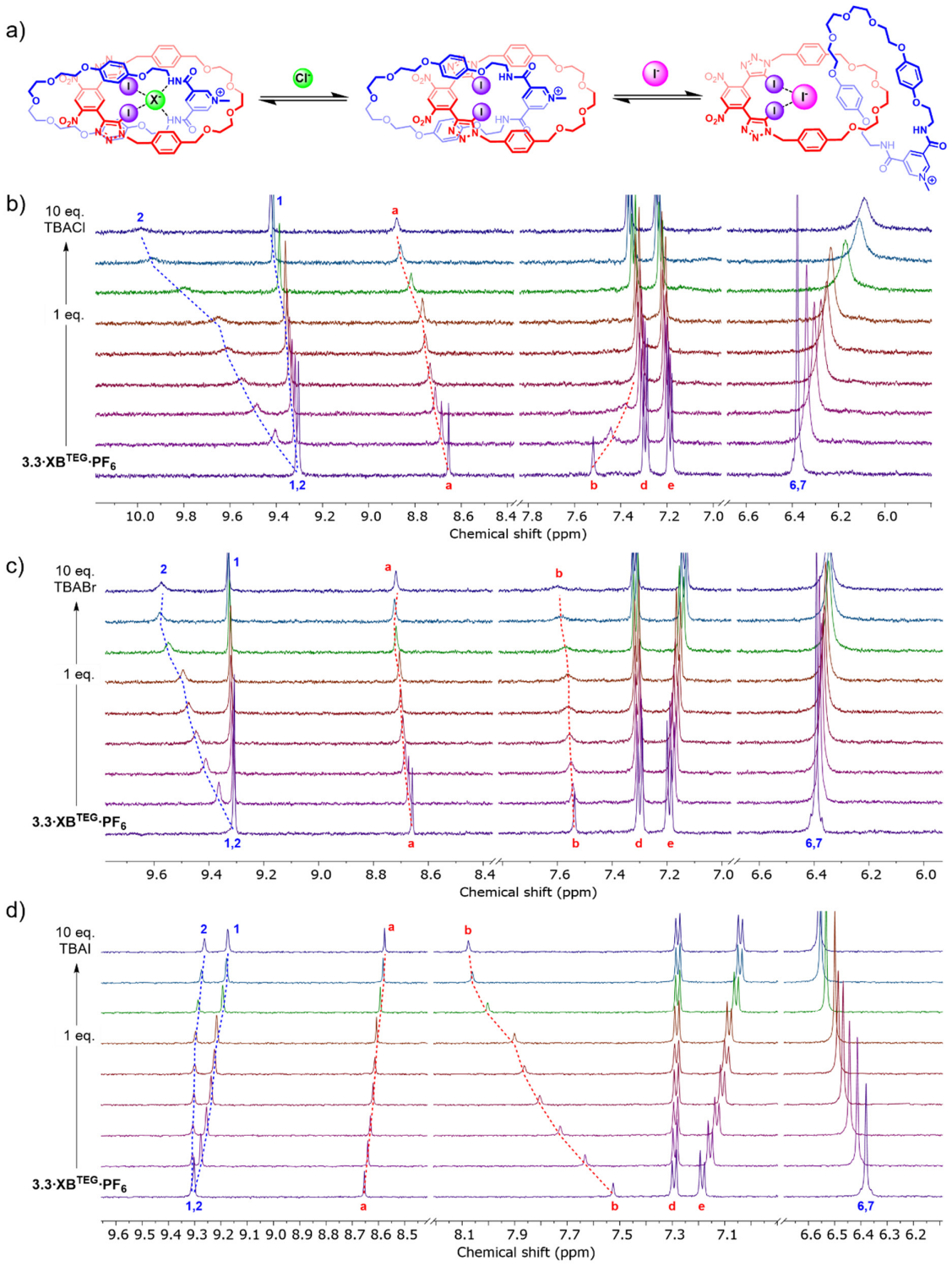


Figure 3.17. *Halide binding studies of [2]catenane* ***3.3·XB^{TEG}·PF$_6$****. (a) Proposed endotopic (left) and exotopic (right) binding modes. (b)-(d) Stacked ^{1}H NMR titration spectra of* ***3.3·XB^{TEG}·PF$_6$*** *upon addition of: b) TBACl; c) TBABr; d) TBAI. Solvent = 10% D_2O/acetone-d_6 (v/v). T = 298 K. [Receptor] = 1 mM.*

The chloride and iodide association constants of **3.3·XB^{TEG}·PF$_6$** were determined by Bindfit analysis of the binding isotherms generated by monitoring the movements of the internal pyridinium proton H_2 and dinitrobenzene proton H_a (**Table 3.4**). The complex binding scenario observed for bromide precluded quantitative analysis of its binding to **3.3·XB^{TEG}·PF$_6$**. A marked enhancement in the anion binding affinities of **3.3·XB^{TEG}·PF$_6$** was observed over the neutral [2]catenane analogue, which is expected given the introduction of a positive charge to the receptor framework.

The iodide association constant remains higher than that of chloride, presumably due to the strong Hofmeister preference for the less solvated iodide anion in the 10% D_2O/acetone-*d*$_6$ solvent system, which contains a high water content. In an analogous manner to the above-described calculation of MBE factors, we calculated a "methylation enhancement" factor for each anion, which is given by $\ln(K_a^{\mathbf{3.3}})/\ln(K_a^{\mathbf{3.2}})$, where $K_a^{\mathbf{3.3}}$ and $K_a^{\mathbf{3.2}}$ respectively refer to the anion association constants of the methylated and neutral catenanes (**Table 3.4**). This analysis indicates that the methylation induces a greater enhancement of chloride anion binding compared to iodide, suggesting that the combined effects of incorporating electrostatic charge and sterically decreasing the size of the interlocked cavity may serve as another potential strategy to further counteract the Hofmeister bias in aqueous-containing solvent systems.

Table 3.4. *Anion association constants and methylation enhancement factors of* ***3.3·XB^{TEG}·PF$_6$,*** *determined by ^{1}H NMR titrations.*[a]

Anion	K_a/M^{-1} (**3.3·XB^{TEG}·PF$_6$**)	Methylation enhancement factor[b]
Cl^-	1647(27)	1.47
I^-	5860(282)	1.31

[a] K_a values calculated using Bindfit with a 1:1 host-guest binding model. Errors (±) from the fitting process are shown in parentheses and are all < 5%. All anions added as TBA^+ salts. Solvent = 90:10 acetone-d_6/D_2O. T = 298 K. [Receptor] = 1.0 mM. [b] Defined as $\ln(K_a^{3.3}/K_a^{3.2})$

3.3.5 Anion Transport Studies

The favourable anion selectivity profiles of the neutral [2]catenanes prompted us to investigate their transmembrane anion transport capabilities. To this end, in collaboration with graduate student Toby Johnson of Matthew Langton's group, anion transport assays were conducted in 1-palmitoyl-2-oleoyl-*sn*-glycero-3-phosphocholine large unilamellar vesicles (POPC LUVs, lipid concentration 31 μM) loaded with the pH responsive dye 8-hydroxypyrene-1,3,6-trisulfonate (HPTS) and buffered to pH 7.0 with HEPES in NaCl solution. In a typical experiment, a pH gradient was applied by addition of a NaOH base pulse (5 mM), followed by addition of the macrocycle or catenane carrier in DMSO (<0.5% v/v). The ability of the transporter to dissipate the pH gradient by Cl^-/OH^- antiport (or the functionally equivalent H^+/Cl^- symport) was determined by recording the change in the HPTS emission I_{rel} (λ_{em} = 510 nm) over time following excitation at λ_{ex} = 405/460 nm. At the end of the experiment, the detergent (Triton X-100) was added to lyse the vesicles for calibration. To study the relative rates of Cl^- *vs.* H^+/OH^- transport, the assay was repeated in the presence of carbonyl cyanide-*p*-trifluoromethoxyphenylhydrazone (FCCP), a weak acid protonophore which facilitates fast electrogenic H^+ transport to ensure that Cl^- transport is the rate limiting step. This decoupling of the anionophore-mediated OH^-/Cl^- antiport (or H^+/Cl^- symport) processes allows us to directly measure the rate of carrier-mediated electrogenic Cl^- transport in the presence of FCCP, and the rate of H^+/OH^- transport in its absence (**Figure 3.18**). A Cl^- > H^+/OH^- selective transporter would therefore be expected to show low transport activity in the absence of FCCP, and enhanced activity in its presence. In contrast, if the rate of transport remains the same in the presence and absence of FCCP, this suggests that Cl^- transport is inherently rate-limiting and that the transporter shows no Cl^- > H^+/OH^- selectivity. In the case of halogen bonding anionophores, it has been established that the selectivities determined using

this method reflects $Cl^- > OH^-$ rather than $Cl^- > H^+$ selectivity due to the low basicity of the triazole binding site.[28, 29]

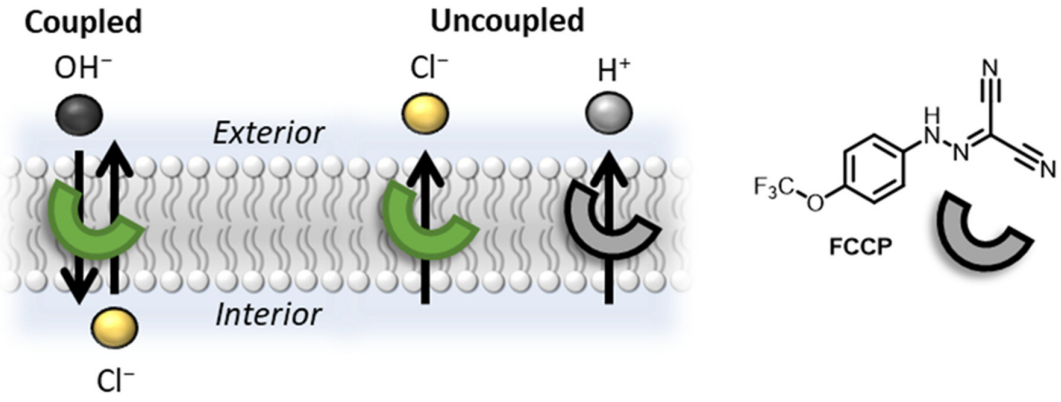


Figure 3.18. *Investigating $Cl^- > H^+/OH^-$ anion transport selectivity of mobile carriers with FCCP. Schematic of the coupled Cl^-/OH^- antiport mechanism (without FCCP) and uncoupled Cl^- transport (with FCCP).*

The activities of the macrocyclic and catenane receptors in the presence and absence of FCCP were quantified through the determination of EC_{50} values, which is the concentration required to reach half-maximal activity, by fitting the dose-response curves to the Hill equation (**Table 3.5**, **Figure 3.19c-d**). The XB macrocycles **3.1·XB^{DEG}** and **3.1·XB^{TEG}** exhibited significant transport activity in the presence of FCCP, with EC_{50} values of 2.2 and 2.1 mol% respectively, but negligible activity in its absence, indicating a highly selective $Cl^- > OH^-$ transport process. In contrast, the HB macrocycle **3.8·HB** was inactive, both in the presence and absence of FCCP, consistent with the low anion binding affinity observed in solution (**Figure 3.19a**). The [2]catenane transporters **3.2·XB^{DEG}** and **3.2·XB^{TEG}** also exhibit high chloride transport activity in the presence of FCCP with EC_{50} values of 0.6 mol% and 1.4 mol% respectively (**Table 3.5**), but were inactive in its absence (**Figure 3.19b**), again suggesting a highly selective [2]catenane-mediated $Cl^- > OH^-$ transport process. To the best of our knowledge, these represent the first interlocked catenane mobile carriers reported to date.

Crucially, the catenanes exhibit improved activity compared to their macrocyclic analogues **3.1·XB^{DEG}** and **3.1·XB^{TEG}** despite the increased size of the catenanes compared to the analogous macrocycles, which is particularly noteworthy given that an increase in the size of a mobile carrier is often detrimental to its transport activity. Conceivably, the enhanced transport kinetics observed for the catenanes arises due to a combination of their enhanced anion binding strength with respect to the macrocycles, as well as a greater degree of anion encapsulation within the globular, compact catenane structure.

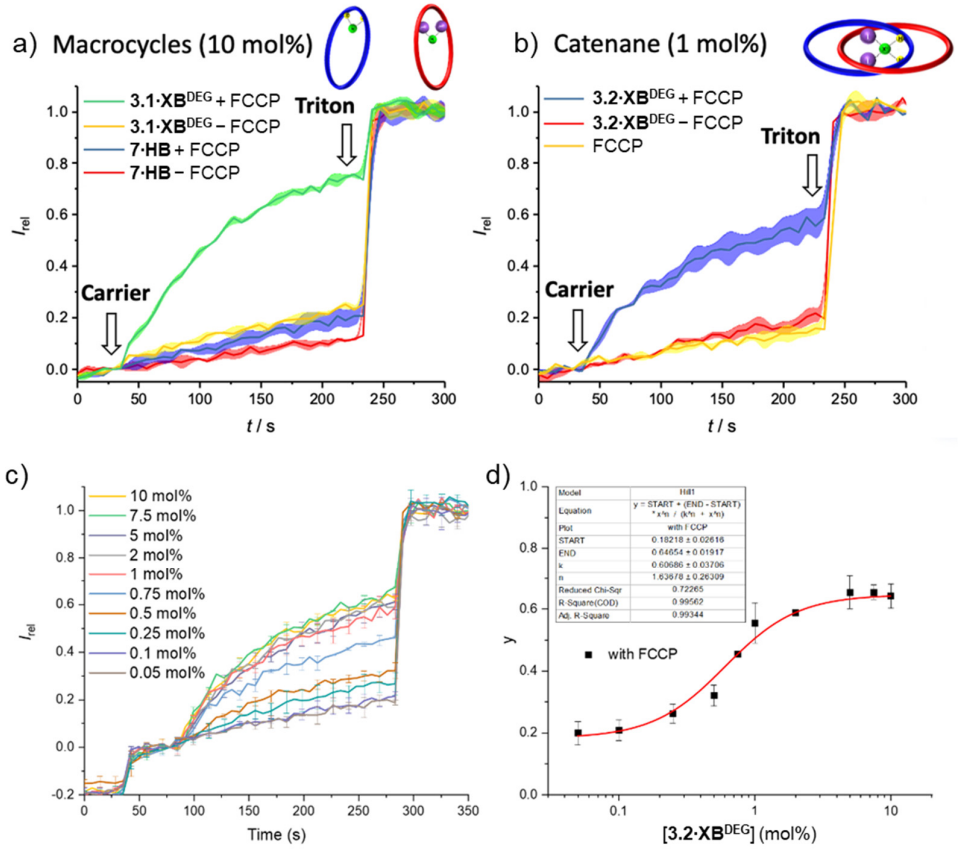


Figure 3.19. *Anion transport in the HPTS assay with and without FCCP. (a) Change in ratiometric emission, I_{rel} (λ_{em} = 510 nm; λ_{ex1} = 405 nm, λ_{ex2} = 460 nm), upon addition of macrocycle carrier in DMSO (10 mol% with respect to lipid) to POPC LUVs (31 μM) containing 1 mM HPTS, 100 mM internal and external NaCl, buffered with 10 mM HEPES at pH 7.0. Protonophore FCCP added prior to the start of each run in DMSO (0.8 mol%), before the NaOH base pulse (5 mM). (b) Transport activity for [2]catenane **3.2·XB^{DEG}** (1 mol%) for Cl^- (with FCCP) and for OH^- (without FCCP). (c) Change in I_{rel} over time upon addition of varying concentrations (mol%) of **3.2·XB^{DEG}**. (b) Dose-response curve of **3.2·XB^{DEG}** fitted to the Hill equation for determination of EC_{50}.*

The $Cl^- > OH^-$ selectivity of the carriers can be quantified via determination of a selectivity factor *F*, defined $F = EC_{50}(Cl^-)/EC_{50}(Cl^-)^{FCCP}$, such that a higher value of *F* indicates greater $Cl^- > OH^-$ selectivity. Due to the inactivity of the catenanes in the absence of FCCP, precise values of $EC_{50}(Cl^-)$ could not be determined, precluding an exact determination of *F*. Nonetheless, the lower bounds for selectivity were estimated to be $F > 49$ for the smaller catenane **3.2·XB^{DEG}** and $F > 21$ for the larger catenane **3.2·XB^{TEG}** (**Table 3.5**). This $Cl^- > OH^-$ selectivity is notably higher than the corresponding macrocycles **3.1·XB^{DEG}** ($F > 13$) and **3.1·XB^{TEG}** ($F > 14$), demonstrating the crucial role of the mechanical bond in the catenane in eliciting both improved selectivity and activity in anion transport. Indeed, [2]catenane **3.2·XB^{DEG}** is one of the most $Cl^- > OH^-$ selective anionophores reported,[30-32] outperforming previously reported isostructural acyclic iodotriazole based anionophores ($F = 2$-14).[28, 29, 33]

Table 3.5. *Transport activities of macrocycle and [2]catenane mobile carriers.*

Mobile Carrier	$EC_{50}(Cl^-)^{FCCP}$ / mol% [a]	$EC_{50}(Br^-)^{FCCP}$ / mol% [a]	$F(Cl^-/OH^-)$ [b]	$F(Cl^-/Br^-)$ [c]	$F(Cl^-/NO_3^-)$ [d]
1·XB^{DEG}	2.2 (0.1)	-	>13	-	-
2·XB^{DEG}	0.61 (0.04)	0.29 (0.02)	>49	0.48	>49
1·XB^{TEG}	2.1 (0.2)	-	>14	-	-
2·XB^{TEG}	1.4 (0.2)	0.34 (0.02)	>21	0.24	>21

[a] EC_{50} is defined as the effective concentration required to achieve 50% activity in the HPTS assay in the presence of FCCP (0.8 mol% with respect to lipid) with the anion specified present in both the intra and extravesicular solution of POPC LUVs (31 μM). [b] Factor of enhancement in the transport rate between Cl^- and OH^- ($F(Cl^-/OH^-) = EC_{50}(Cl^-)/EC_{50}(Cl^-)^{FCCP}$. [c] Factor of enhancement in the transport rate between Cl^- and Br^- ($F(Cl^-/Br^-) = EC_{50}(Br^-)^{FCCP}/EC_{50}(Cl^-)^{FCCP}$. [d] Factor of enhancement in the transport rate between Cl^- and NO_3^- ($F(Cl^-/NO_3^-) = EC_{50}(NO_3^-)^{FCCP}/EC_{50}(Cl^-)^{FCCP}$. $EC_{50}(Cl^-)$ and $EC_{50}(NO_3^-)^{FCCP}$ were too inactive to determine (>30 mol% with respect to lipid), considering the EC_{50} value as 30 in selectivity factor calculations.

To investigate the mechanism of anion transport mediated by the macrocyclic and catenane XB transporters, their activities were examined within the gel phase of dipalmitoylphosphatidylcholine (DPPC) LUVs at 25 °C. The absence of observable ion transport under these conditions, alongside restoration of activity at 45 °C, above the gel–liquid

phase transition temperature (T_m = 41 °C), is consistent with a mobile carrier mechanism. The initial anion transport rate, k_{ini}, exhibited a linear dependence on the concentration of **3.2·XB^{DEG}**, implying that a single transporter molecule is involved in the rate-limiting step of the transport process. This suggests that the interlocked transporter **3.2·XB^{DEG}** facilitates anion transport *via* a unimolecular mobile carrier mechanism, rather than through self-assembly of a membrane spanning ion channel. Exchanging the chloride anion in the buffer for the large hydrophilic gluconate anion entirely arrests transport, indicative of a solely anion selective mobile carrier process and ruling out Na^+/H^+ antiport involvement in dissipating the pH gradient.

Finally, we explored whether the unique solution phase anion binding selectivities imparted by the interlocked nature of the catenane systems was translated to observed transport selectivities across lipid bilayer membranes. To this end, we repeated the transport assays with catenanes **3.2·XB^{DEG}** and **3.2·XB^{TEG}** but with different anions present in the internal and external buffer (**Figure 3.20a**). These studies revealed that, as with solution phase binding, the catenanes preferentially transported bromide over chloride, while no activity was observed for nitrate transport.[34] Overall, this translates to a transport selectivity profile of $Br^- > Cl^- \gg OH^- \sim NO_3^-$. Comparative studies on a simple mono-aryl thiourea derivative reveals a contrasting transport selectivity trend of $NO_3^- > Br^- > Cl^-$ under analogous conditions (**Figure 3.20b**). In general, selectivity for halides over nitrate in carrier mediated ion transport is unusual, as the latter anion is often readily transported due to its comparably higher lipophilicity, even in acyclic HB receptor systems which exhibit preferential chloride over nitrate binding selectivities in solution-phase binding studies.[35] The selectivity of the smaller catenane **3.2·XB^{DEG}** for $Cl^- > NO_3^-$ is particularly notable ($F > 49$), and to the best of our knowledge is the most $Cl^- > NO_3^-$ selective synthetic anionophore reported to date, outperforming previously

reported chloride selective tripodal systems by a factor of 5.[35] This suggests that the stringent geometric constraints imparted by the [2]catenane interlocked anion binding cavity may facilitate direct translation of anion binding preference into transport activity, enabling highly selective halide over oxoanion (NO_3^- and OH^-) transport behaviour to be achieved.

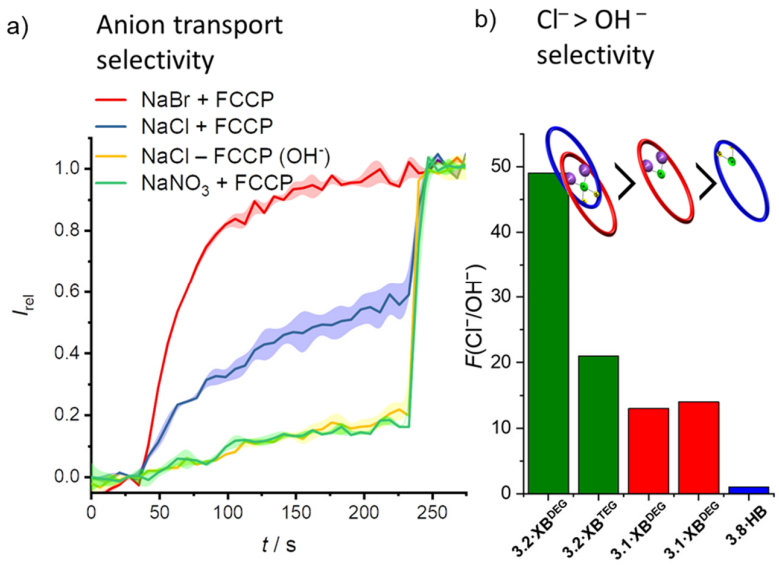


Figure 3.20. *(a) Transport activity of* ***3.2·XB^{DEG}*** *(1 mol%) for different anions in the HPTS assay. Change in ratiometric emission, I_{rel} (λ_{em} = 510 nm; λ_{ex1} = 405 nm, λ_{ex2} = 460 nm), upon addition of* ***3.2·XB^{DEG}*** *in DMSO (1 mol% with respect to lipid) to POPC LUVs (31 μM) containing 1 mM HPTS, 100 mM internal and external NaX, where X = Cl^-, Br^-, NO_3^-, buffered with 10 mM HEPES at pH 7.0. Protonophore FCCP added prior to the start of each run in DMSO (0.8 mol%), before the NaOH base pulse (5 mM). (b) Cl^- > OH^- selectivity factors F, (where $F = EC_{50}(Cl^-)/EC_{50}(Cl^-)^{FCCP}$*

3.4 A Multi-station Rotaxane Shuttle for Selective Chloride Sensing

The pivotal role played by chloride[36] and iodide[37] in various aspects of human health provides an impetus for the development of chemo-sensors capable of distinguishing these chemically-similar halide anions. However, as discussed above, achieving selective chloride over iodide recognition and sensing in aqueous-containing media remains a persistent challenge[8, 38, 39] due to the extensive solvation of chloride by water molecules, which typically confers a Hofmeister bias in halide binding affinities, *i.e.* $Cl^- < Br^- < I^-$.

Intrigued by the observed anti-Hofmeister binding preferences of the [2]catenanes, which we attributed to the ability of the catenanes to encapsulate the smaller halides in a solvent-shielded interlocked cavity, we sought to exploit this size-driven endotopic binding mode to develop a multi-station [2]rotaxane capable of selective optical sensing of chloride/bromide over iodide.

The host design involves an isophthalamide-based macrocycle threaded onto a 3-station axle containing naphthalene diimide (NDI) stations as optical reporter groups, as well as a central bis(iodotriazole) based halogen bonding (XB) station for anion binding (**Figure 3.21**). In the absence of guest ions, the macrocycle would conceivably reside preferentially over the NDI stations, a co-conformation stabilised by the formation of aromatic donor-acceptor charge transfer interactions between the electron-poor NDI and the electron-rich hydroquinone groups of the macrocycle. The addition of chloride is expected to induce macrocycle translocation to the halogen bonding station of the axle to facilitate the formation of XB···Cl^- and HB···Cl^- interactions with the axle and macrocycle respectively. The resulting spatial separation of the NDI and hydroquinone groups would lead to a reduction in the intensity of the charge transfer absorption band, thereby enabling optical sensing of chloride. In contrast, no optical response

is expected in the case of iodide binding due to the steric inaccessibility of the interlocked cavity to the larger iodide guest.

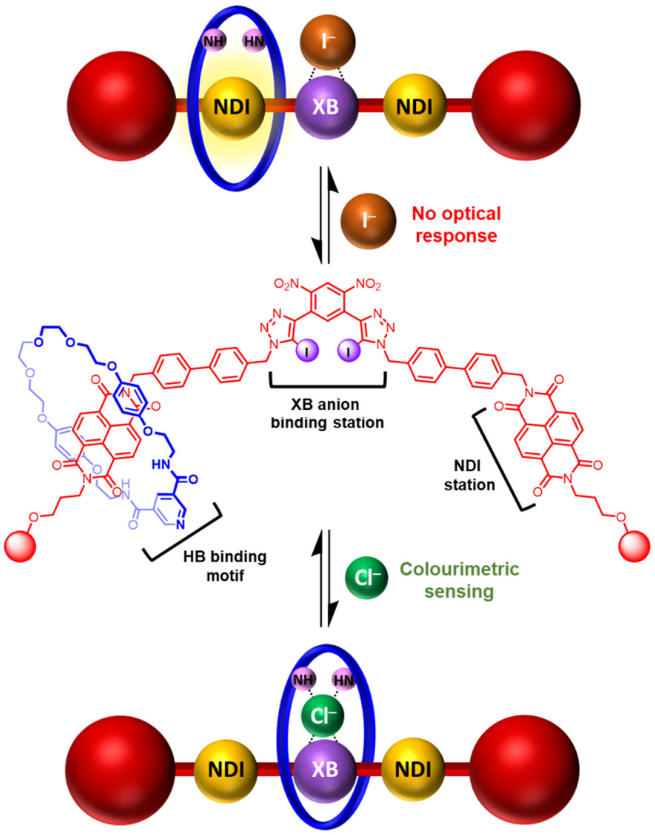
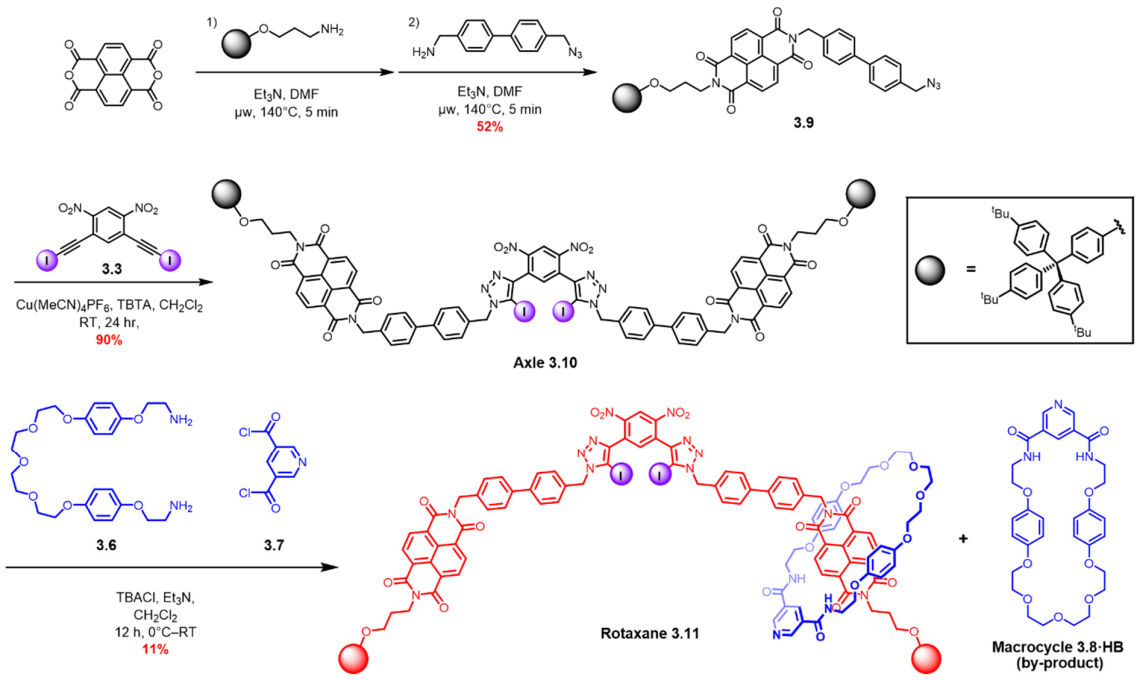


Figure 3.21. *Schematic representation of 3-station-[2]rotaxane acting as a selective optical sensor for chloride over iodide anions.*

3.4.1 Synthesis and Characterisation

Encouraged by the efficacy of the chloride template-directed method in the synthesis of neutral hetero[2]catenanes, we sought to employ a similar strategy to prepare a multi-station [2]rotaxane. To this end, NDI-functionalised stopper azide **3.9** was prepared via a literature procedure.[23] A CuAAC reaction between 4,6-dinitro-1,3-bis-iodoalkyne **3.3** and two equivalents of **3.9** afforded the desired 3-station axle **3.10** in 90% yield (**Scheme 3.6**).

With NDI-functionalised axle **3.10** in hand, the target [2]rotaxane **3.11** was prepared via a chloride anion-directed amide condensation cyclisation reaction between bis(amine) **3.6** and 3,5-bis(chlorocarbonyl) pyridine **3.7** to form the interlocked product (**Scheme 3.6**). In a typical reaction, a solution of freshly-prepared **3.7** was added dropwise to a cooled solution of axle **3.10**, tetrabutylammonium chloride (TBACl), bis(amine) **3.6** and triethylamine in anhydrous CH_2Cl_2. The reaction mixture was allowed to stir overnight at room temperature, then subjected to a basic work-up and purification by iterative preparative TLC to afford the target [2]rotaxane **3.11** as a bright orange solid in an isolated yield of 11%, which was characterised by ^{1}H NMR, ^{13}C NMR and high-resolution mass spectrometry.



Scheme 3.6. *Synthesis of 3-station axle **3.10** and rotaxane **3.11** via a chloride template-directed synthetic strategy.*

A comparison of the ^{1}H NMR spectrum of **3.11** to the corresponding spectra of the axle **3.10** and macrocycle **3.8·HB** components indicates successful mechanical bond formation (**Figure 3.22**). The hydroquinone protons of the macrocycle $H_{6,7}$ undergo a significant upfield

shift ($\Delta\delta$ = 1.06 ppm), which is diagnostic of the formation of aromatic stacking interactions with the aryl components of the axle. Pronounced upfield shifts were also observed in the protons of the tetra(ethylene glycol) linker $H_{8\text{-}11}$, presumably due to their increased proximity to the shielding ring currents of the axle aryl groups, while the internal pyridyl proton H_2 shifts downfield in a manner similar to that observed in the [2]catenanes, which is also consistent with reports of interlocked structures featuring an isophthalamide-based macrocycle.[23, 24, 40] The changes in the chemical shift values of the axle protons are considerably more modest, with the most notable changes being a downfield shift of the NDI protons $H_{i,j}$ ($\Delta\delta$ = 0.07 ppm). This is in contrast to previously reported structurally-comparable [2]rotaxane shuttles,[23, 24] in which the NDI proton signals were shifted upfield by a considerable margin when sandwiched between two hydroquinone groups. The modest chemical shift changes in the proton signals arising from the axle possibly indicate the presence of other competing factors that influence the observed chemical shift values of rotaxane **3.11**, particularly given the conformational flexibility of the axle which may promote the formation of secondary intercomponent contacts.

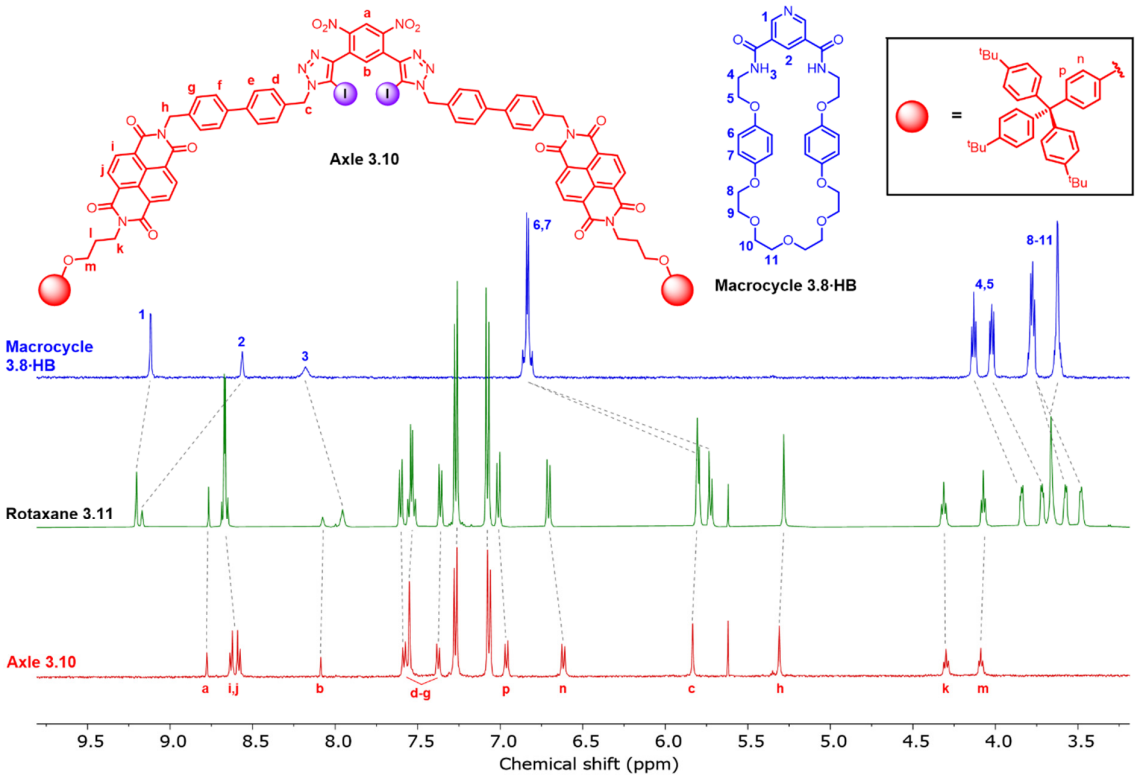


Figure 3.22. *Overlaid ^{1}H NMR spectra of HB macrocycle* ***3.8·HB*** *(top), [2]rotaxane* ***3.11*** *(middle) and axle* ***3.10*** *(bottom) (500 MHz, acetone-d_6, 298 K).*

Further insights into the co-conformation of **3.11** were obtained from the 2D ^{1}H-^{1}H ROESY spectrum (**Figure 3.22**). Strong through-space cross-peaks were observed between the NDI protons $H_{i,j}$ and several macrocycle-derived proton signals in the spectrum, most notably the hydroquinone protons $H_{6,7}$, providing further evidence for the formation of π-stacking interactions between the NDI and hydroquinone moieties. Significant intercomponent cross-peaks were also observed between $H_{6,7}$ and the NDI-adjacent biphenyl protons $H_{g,f}$, while no cross peaks were observed between the dinitrobenzene protons H_a and H_b and the macrocycle. This is concordant with the macrocycle displaying a co-conformational bias towards residing at the peripheral regions of the axle rather than the central halogen bonding station. This co-conformation is expected to be favoured by the formation of stabilising aromatic charge-transfer interactions between the electron-deficient NDI and the electron-rich hydroquinone

moieties, as indicated by the appearance of a characteristic charge-transfer absorption at λ = 450 nm (**Figure 3.26**).

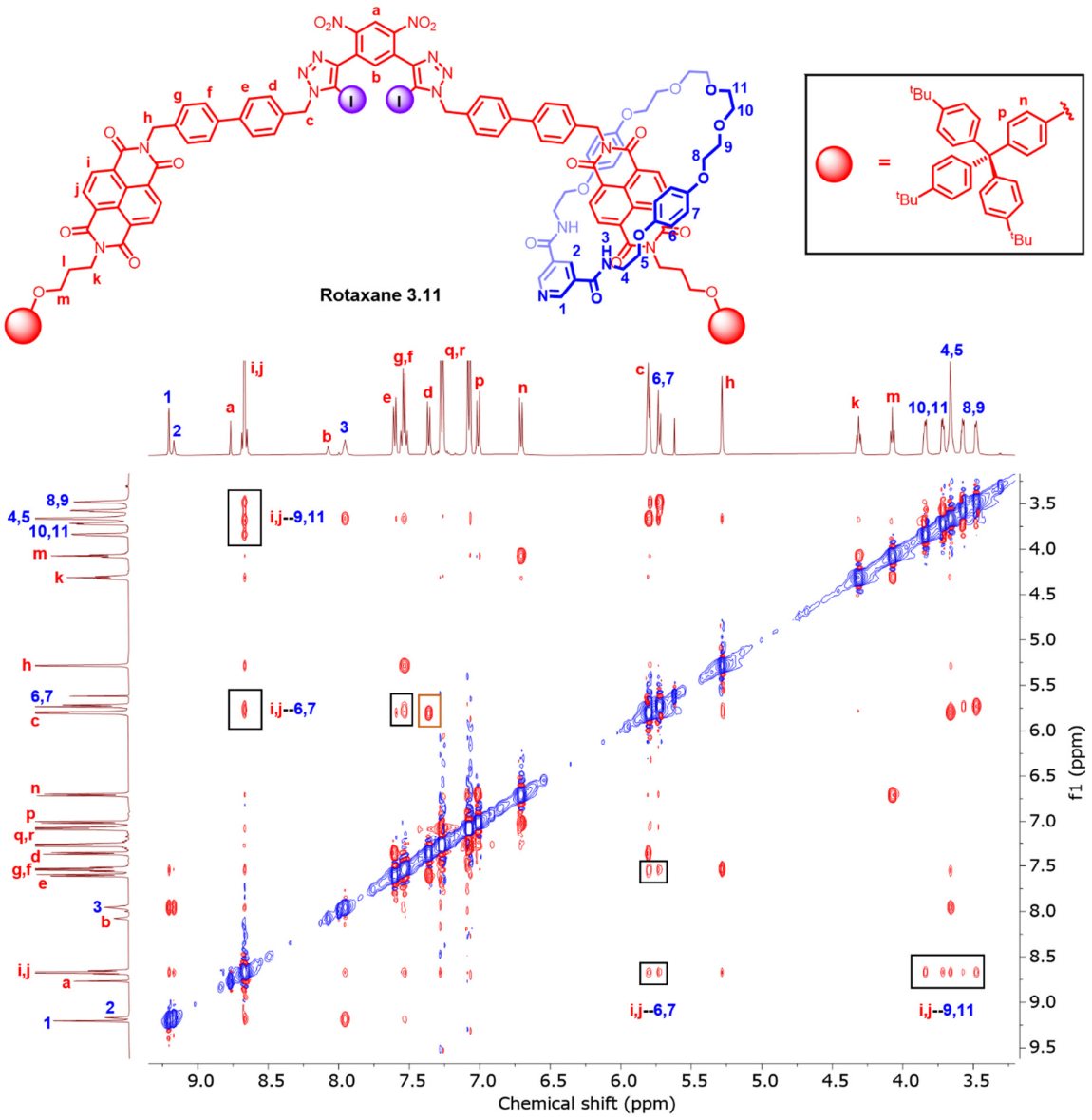


Figure 3.23. *^{1}H-^{1}H 2D ROESY NMR spectrum of 3-station-[2]rotaxane* ***3.12*** *(600 MHz, acetone-d_6, 298 K).*

3.4.2 ^{1}H NMR Anion Binding Studies

The halide anion binding properties, and in particular the effect of halide binding on the co-conformation of rotaxane **3.11**, were initially studied by ^{1}H NMR spectroscopic binding

studies. To this end, aliquots of TBAX salts (X = Cl, Br, I) were added progressively to a 0.5 mM solution of the host in the moderately competitive 2.5% D_2O/acetone (v/v) solvent mixture.

Significant chemical shift perturbations in the rotaxane NMR spectrum were observed in response to increasing halide concentration, particularly in the 2,4-dinitrobenzene protons H_a and H_b, indicative of anion binding at the central XB motif of the axle component (**Figure 3.24**). Pleasingly, the magnitude and direction of the changes, particularly of the proton signals proximal to the macrocycle HB binding site, differed depending on the identity of the halide guest, suggesting that, similar to the situation observed with the [2]catenanes, the halides adopt different binding modes to rotaxane **3.11**.

Addition of chloride anions induces pronounced downfield shifts of the rotaxane's internal pyridyl proton H_2 and amide protons H_3, indicating that the macrocycle component HB binding motif is involved in anion binding (**Figure 3.24b**). The proton signals near the axle XB binding station also undergo significant changes, including a downfield movement of the external nitrobenzene proton H_a and significant broadening of internal nitrobenzene proton H_b. Taken together, these changes suggest that the small chloride anion is convergently bound by the bis-iodotriazole XB motif of the axle and isophthalamide HB donor of the macrocycle. This chloride-induced chemical shift perturbation profile is similar to that of the [2]catenanes **3.2·XB^{DEG}** and **3.2·XB^{TEG}**, indicating that the rotaxane interlocked cavity is similarly capable of encapsulating the small chloride guest. In rotaxane **3.11**, the adoption of this endotopic binding mode necessitates a translocation of the macrocycle to the central XB bis(iodotriazole station), as suggested by a large upfield shift of the iodotriazole-adjacent methylene singlet H_c, which likely experiences greater shielding as a result of its increased proximity to the ring currents of the macrocycle hydroquinone groups. Significant chemical shift changes were also

observed in the macrocycle protons $H_{4,5}$ and $H_{8\text{-}11}$, which are distal from the anion binding site, thereby suggesting that chloride binding induces a co-conformational change in the host.

In contrast, little to no changes to the macrocycle proton signals were observed upon addition of iodide (**Figure 3.24d**). The axle protons H_a and H_b move upfield and downfield respectively with increasing concentrations of iodide, displaying a similar response to that of acyclic receptor **3.4**, while the protons of the macrocycle isophthalamide group (H_1, H_2, H_3) experience no significant perturbations. This suggests that iodide is bound primarily by XB···anion interactions with the iodotriazole XB donors of the axle, with minimal participation of the isophthalamide group of the macrocycle. This is consistent with the larger ionic radius of the iodide anion precluding access to the interlocked binding cavity of the rotaxane and forcing it to adopt an exotopic binding mode. Importantly, no significant movements were observed in proton signals distal from the XB binding site, suggesting that the co-conformation of rotaxane **3.11** does not change significantly in response to iodide binding.

Addition of bromide produces a chemical shift perturbation profile which appears to be intermediate between the extreme cases of chloride and iodide (**Figure 3.24c**). With increasing bromide concentration, the macrocycle protons H_2 and H_3 move progressively downfield (similar to the chloride binding experiments), while axle proton H_a moves upfield (similar to the iodide binding experiments), albeit with greatly attenuated magnitudes relative to the corresponding chloride/iodide-induced changes. Given that the ionic radius of the bromide anion falls in between that of the other two halides, it is conceivable that the **3.11**·$\mathbf{Br^-}$ complex in solution exists as a mixture of the competing endotopic and exotopic binding modes in fast exchange, a similar scenario to that observed for the methylated [2]catenane **3.3**·$\mathbf{XB^{TEG}}$·$\mathbf{PF_6}$.

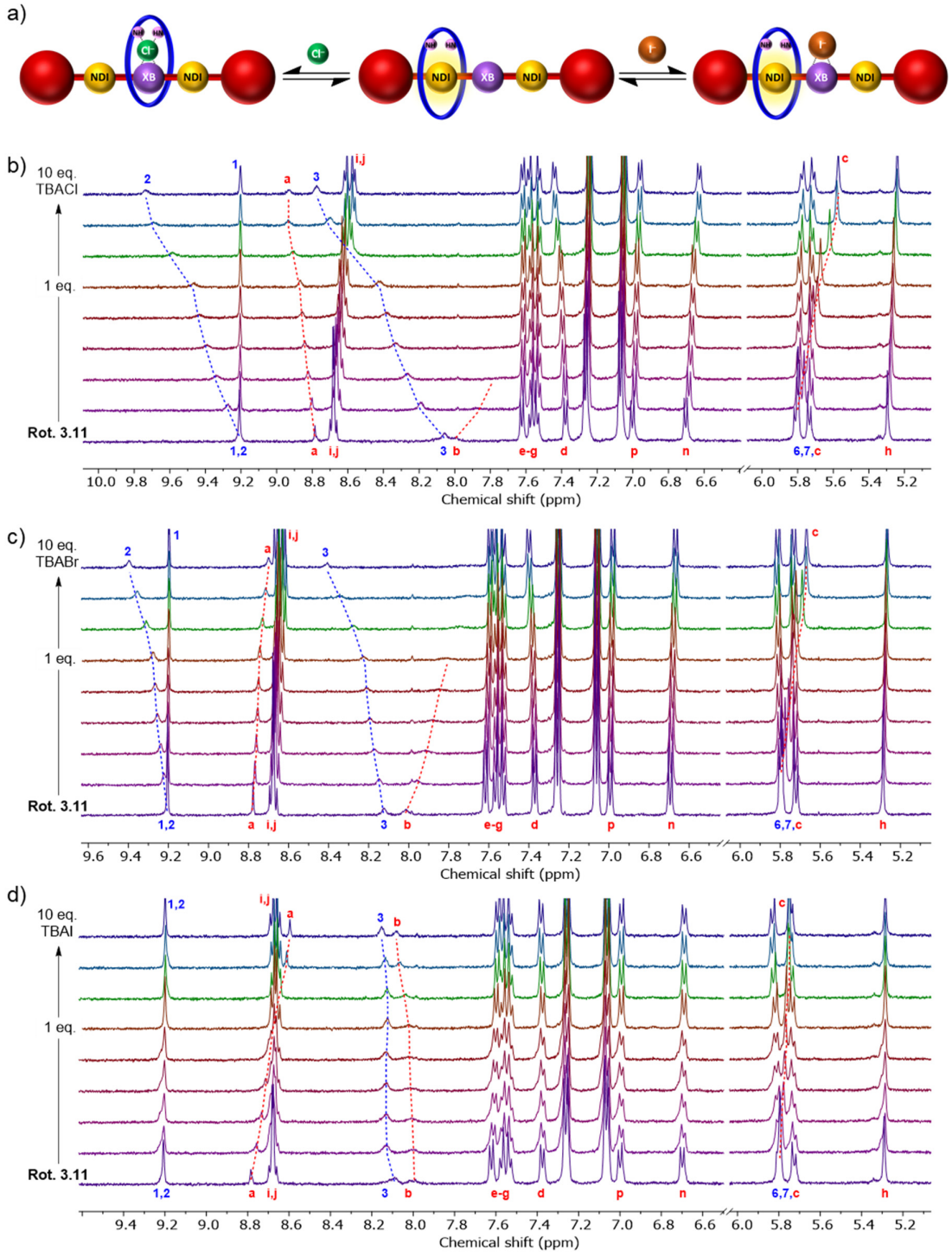
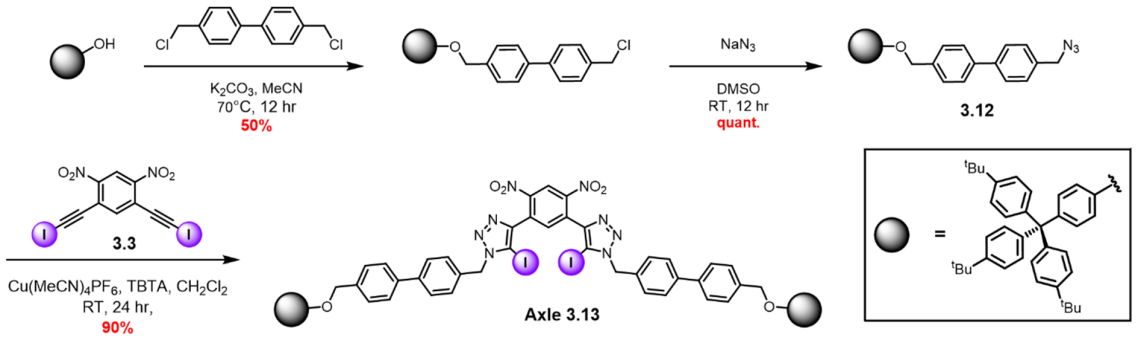


Figure 3.24. *Halide binding studies of [2]rotaxane* ***3.11****. (a) Proposed endotopic (left) and exotopic (right) binding modes. (b)-(d) Stacked* ^{1}*H NMR titration spectra of* ***3.11*** *upon addition of: b) TBACl; c) TBABr; d) TBAI. Solvent = 2.5%* D_2O*/acetone-*d_6 *(v/v). T = 298 K. [Receptor] = 0.5 mM.*

Analogous titration studies were attempted on the non-interlocked NDI-functionalised XB axle **3.10**. Unfortunately, the low solubility of **3.10** in 2.5% D_2O/acetone-d_6 precluded a direct comparison of the axle and rotaxane binding properties. To determine the anion affinities of the XB donor-containing axle motif, a more soluble "model axle" **3.13** was prepared (**Scheme 3.7**). Axle **3.13** is structurally similar to **3.10** but does not feature the NDI units, which are not anticipated to influence the anion binding properties of the XB donor unit.



Scheme 3.7. *Synthesis of XB axle* ***3.13*** *for comparative halide binding studies.*

Importantly, unlike rotaxane **3.11,** axle **3.13** displayed similar chemical shift perturbation profiles in response to all three halides. In particular, a progressive upfield movement of H_a and downfield movement of H_b were observed with increasing halide concentration, providing strong evidence that the variation in anion binding modes seen in rotaxane **3.11** arises from a mechanical bond effect.

The anion association constants of rotaxane **3.11** and axle **3.13** in 2.5% D_2O/acetone-d_6 were subsequently determined by a global Bindfit[41] analysis of the titration data (**Figure 3.25**), which determined 1:1 host-guest stoichiometric association constants for chloride and iodide binding, summarised in **Table 3.6**. The complex scenario indicated by the bromide-induced chemical shifts of rotaxane **3.11**, with qualitative ^1H NMR analysis suggesting both endotopic and exotopic binding of bromide, is challenging to model from the titration data and

prohibits a reliable determination of bromide association constants. Such a situation highlights the need for judicious consideration of all possible equilibria as well as the underlying chemical structures when attempting to extract quantitative information from a host-guest binding experiment, which is expected to become more important with the development of increasingly large and complex supramolecular systems.[42]

Table 3.6. *Halide anion association constants (K_a/M^{-1}) for rotaxane **3.11** and axle **3.13** determined by ^1H NMR titrations.*[a]

	Anion Association Constant K_a (M^{-1})	
Anion	**Rotaxane 3.11**	**Axle 3.13**
Cl^-	3250(102)	770(12)
Br^-	N.D.[b]	2370(52)
I^-	2720(201)	2584(86)

[a]K_a values calculated using Bindfit with a 1:1 host-guest binding model. Errors (±) are all < 5%. All anions added as TBA^+ salts. Solvent = 2.5% D_2O/acetone-d_6. T = 298 K. [Receptor] = 0.5 mM. [b]Not determined (see text for discussion).

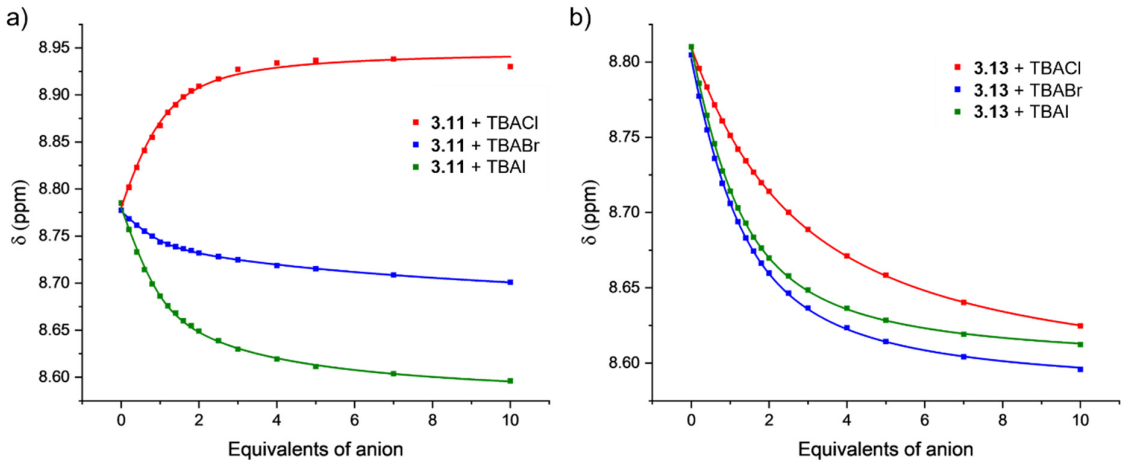


Figure 3.25. *Binding isotherms of: (a) rotaxane **3.11**, showing changes in the chemical shift of internal pyridyl proton H_2, (b) axle **3.13**, showing changes in the external nitrobenzene proton H_a, with increasing equivalents of TBAX salts (X = Cl, Br, I, NO_3). [Receptor] = 0.5 mM. Solvent = 95:5 acetone-d_6/D_2O (v/v). T = 298 K.*

Inspection of the anion association constants summarised in **Table 3.6** reveal trends consistent with the proposed binding modes for the various halides. The simple 1-station XB axle **3.13** shows an increase in anion binding affinities in the order Cl^- << Br^- < I^-. This is

consistent with the binding preference conferred by the Hofmeister series, wherein the most extensively hydrated chloride anion is least strongly bound to the receptor in aqueous containing solvent mixtures.

Notably, this is not the case for rotaxane **3.11**, which exhibits stronger binding to chloride than iodide, displaying an 'anti-Hofmeister' binding preference. Indeed, rotaxane **3.11** displays a significant 4.3-fold enhancement in chloride binding affinity relative to axle **3.13**. This is consistent with the proposed endotopic chloride binding mode, in which binding affinity is enhanced by encapsulation of chloride in the rotaxane's solvent-shielded cavity alongside the formation of convergent interactions involving both the XB and HB binding motifs in **3.11**. In contrast, the iodide association constants of rotaxane **3.11** and axle **3.13** are similar within experimental error, providing strong evidence that the iodide ion interacts almost exclusively with the XB donor motif of the axle and does not benefit from an enhancement in binding affinity originating from its encapsulation in the interlocked cavity. Crucially, the enhancement in chloride but attenuation of iodide binding affinity of the rotaxane relative to the non-interlocked axle demonstrates the efficacy of using mechanically bonded hosts to achieve highly selective enhancements in guest binding affinities.

3.4.3 UV-Vis Studies

The UV-visible spectrum of the free rotaxane **3.11** in 2.5% H_2O/acetone contained a broad absorption at λ = 450 nm, diagnostic of donor-acceptor charge-transfer interactions formed between the NDI stations of the axle and the hydroquinone groups of the macrocycle (**Figure 3.26a**). In contrast, no significant absorption intensity was observed in the non-interlocked NDI-containing axle **3.10** (**Figure 3.26b**), confirming that the observed absorption originates from intercomponent charge-transfer interactions.

Encouraged by the ^{1}H NMR anion binding studies which indicate a chloride-induced translocation of the macrocycle to the XB binding site, attention was directed towards investigating the optical response of rotaxane **3.11** towards anion binding. To this end, preliminary UV-vis spectroscopic sensing studies were conducted on a 0.25 mM solution of **3.11** in 2.5% H_2O/acetone, wherein the UV-vis absorption spectrum of the host solution was recorded before and after the addition of 20 equivalents TBAX (X = Cl, Br, I) (**Figure 3.26**).

Pleasingly, upon addition of chloride anions to rotaxane **3.11**, a significant (42%) reduction of the absorption intensity at 450 nm was observed, which was accompanied by a subtle discolouration of the bright orange solution, consistent with a reduction in the NDI-hydroquinone charge-transfer interaction resulting from translocation of the macrocycle to the central XB anion binding station. Notably, the bromide-induced reduction in absorption intensity at 450 nm was considerably smaller (10%), while iodide addition results in essentially no change in the charge-transfer band. This serves as an effective demonstration of exploiting the binding cavity of an interlocked molecule to simultaneously achieve an enhancement in binding affinity as well as a selective optical sensing response for a target guest ion.

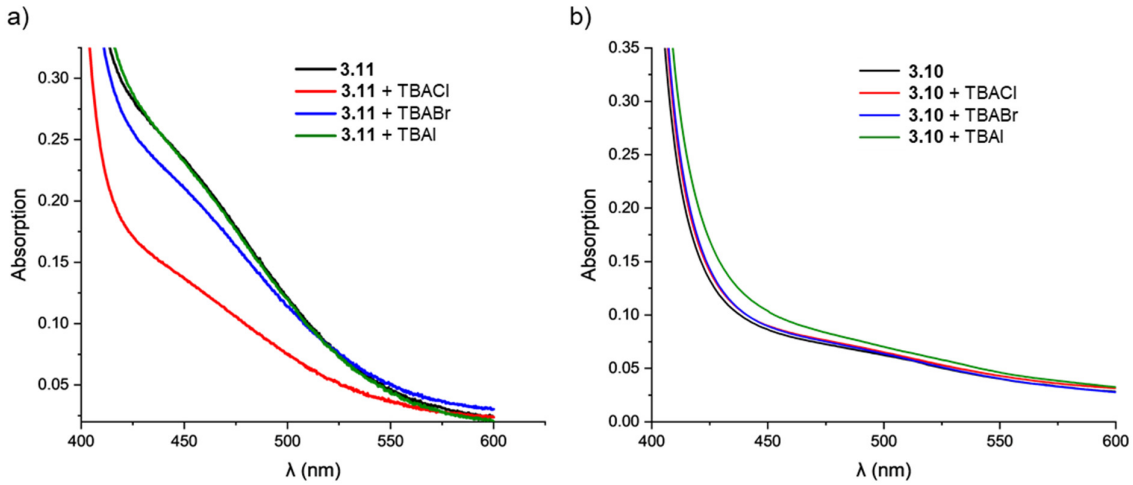


Figure 3.26. *UV-Vis spectra showing the effects of adding 20 equivalents of TBAX (X = Cl, Br, I) into a solution of (a) rotaxane **3.11**; (b) axle **3.10** in 2.5% H_2O/acetone. [Host] = 0.25 mM. T = 298 K.*

3.5 Conclusions and Future Work

To summarise, the impressive chloride binding properties of a 4,6-dinitro-1,3-bis-iodotriazole motif were exploited to develop a chloride template-directed synthetic methodology to prepare neutral interlocked host molecules. A common feature of the resulting host molecules is the presence of an interlocked binding cavity decorated with XB and HB binding sites, which prompted us to investigate their halide binding properties. The interlocked hosts displayed contrasting halide binding modes in aqueous-acetone solvent systems, with the smaller halides (Cl^- and/or Br^-) binding in an endotopic manner within the cavity, while the larger I^- is bound exotopically via XB···I^- interactions with the potent dinitro-bis-iodotriazole XB motif. These differences in halide binding mode gave rise to a tendency towards "anti-Hofmeister" binding behaviour in the interlocked hosts, in which the observed enhancement in the anion association constants upon mechanical bond formation increases in the order $I^- < Br^- < Cl^-$. These unusual binding properties, which arise from the spatial restrictions imposed by the mechanical bond, were exploited to develop supramolecular systems for anion transport and sensing.

The compact nature of the neutral [2]catenanes prompted an investigation into their potential applications in transmembrane halide transport. Transmembrane anion transport studies conducted in POPC LUVs revealed that the neutral catenanes were effective anion transporters, out-performing their macrocyclic components, representing, to the best of our knowledge, the first catenane-based anionophore. Furthermore, the intrinsic binding preferences of the [2]catenanes for halides over oxoanions were directly translated into observed anion transport selectivity trends, resulting in catenane anionophores with high halide over hydroxide and nitrate selectivity, which is particularly critical for potential therapeutic applications. The remarkable transport selectivity demonstrated by the [2]catenane hosts may

open up new avenues for exploiting mechanically interlocked anion transporters for the development of novel and highly selective transport systems for therapeutic applications.

The co-conformational dynamism of multi-station rotaxane shuttles was exploited to develop a 3-station XB [2]rotaxane which shows potential for selective chloride over iodide optical sensing. Chloride binding to the rotaxane induced a translocation of the macrocycle from the NDI station to the bis-iodotriazole station to facilitate the formation of convergent XB···Cl^- and HB···Cl^- interactions, leading to an optical chemo-sensing response corresponding to a significant reduction in the intensity of the NDI-hydroquinone charge transfer absorption band. In contrast, no optical response was observed for the larger iodide ion, which is incapable of binding within the interlocked cavity. This work illustrates the potential efficacy of using mechanically interlocked host molecules as a strategy to not only enhance the binding affinity and selectivity of anion receptors using the mechanical bond effect, but also through their inherent dynamism achieve selective optical sensing of a target ion over other chemically similar guest species.

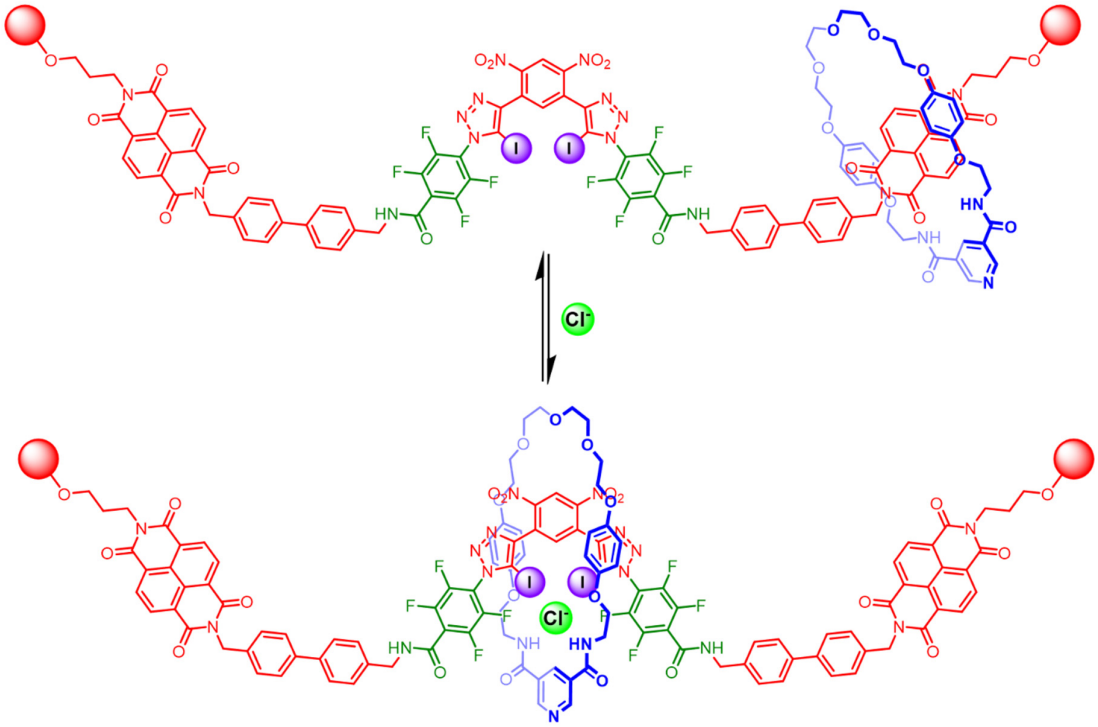
3.5.1 Future Work

There is substantial scope for future extensions of this work given the broad applicability of the methodologies and principles developed in this chapter to the design of future interlocked anion receptors.

The 4,6-dinitro-1,3-bis-iodotriazole group is a potent and synthetically accessible bidentate XB motif which can be incorporated into a range of acyclic, macrocyclic and interlocked anion receptors to enhance their anion binding affinities. Its demonstrated capability in facilitating chloride template-directed mechanical bond formation could conceivably be extended to the synthesis of higher-order interlocked structures. For example, sequential anion template-directed macrocycle clipping reactions around a long axle could

serve as a potential strategy to prepare oligo-rotaxanes. The chloride template-directed strategy could also be combined with other template-directed strategies to prepare higher-order catenanes, as described in **Chapter 4**.

The multi-station [2]rotaxane described in Section 3.4, which utilises the co-conformational dynamism of interlocked systems alongside the size complementarity of the binding cavity for chloride to achieve a selective optical chemo-sensing response, is a particularly promising system with scope for further improvement in performance. For instance, appending electron-withdrawing perfluoroaryl groups to the bis-iodotriazole motif may further augment its anion binding affinity (**Scheme 3.8**), which would conceivably facilitate a greater degree of macrocycle translocation to the XB station upon chloride binding, translating to a more pronounced sensing response to enable naked-eye detection of chloride.



Scheme 3.8. *Proposed enhanced chloride binding and optical sensing by a potent XB multi-station [2]rotaxane.*

3.6 References for Chapter 3

1. K. M. Bąk, K. Porfyrakis, J. J. Davis and P. D. Beer, *Mater. Chem. Front.*, 2020, **4**, 1052-1073.
2. L. M. Hancock, L. C. Gilday, S. Carvalho, P. J. Costa, V. Félix, C. J. Serpell, N. L. Kilah and P. D. Beer, *Chem. Eur. J.*, 2010, **16**, 13082-13094.
3. T. Bunchuay, A. Docker, A. J. Martinez-Martinez and P. D. Beer, *Angew. Chem. Int. Ed.*, 2019, **58**, 13823-13827.
4. L. M. Hancock, E. Marchi, P. Ceroni and P. D. Beer, *Chem. Eur. J.*, 2012, **18**, 11277-11283.
5. N. H. Evans, C. J. Serpell and P. D. Beer, *Chem. Commun.*, 2011, **47**, 8775-8777.
6. L. M. Hancock, L. C. Gilday, N. L. Kilah, C. J. Serpell and P. D. Beer, *Chem. Commun.*, 2011, **47**, 1725-1727.
7. N. H. Evans, C. J. Serpell and P. D. Beer, *New J. Chem.*, 2011, **35**, 2047-2053.
8. M. K. Chae, J.-m. Suk and K.-S. Jeong, *Tetrahedron Lett.*, 2010, **51**, 4240-4242.
9. Y. Zhao, Y. Li, Y. Li, H. Zheng, X. Yin and H. Liu, *Chem. Commun.*, 2010, **46**, 5698-5700.
10. K. M. Bąk, B. Trzaskowski and M. J. Chmielewski, *Chem. Sci.*, 2024, **15**, 1796-1809.
11. A. Docker, Y. C. Tse, H. M. Tay, A. J. Taylor, Z. Zhang and P. D. Beer, *Angew. Chem. Int. Ed.*, 2022, **61**, e202214523.
12. J. T. Davis, P. A. Gale and R. Quesada, *Chem. Soc. Rev.*, 2020, **49**, 6056-6086.
13. X. Wu, E. N. W. Howe and P. A. Gale, *Acc. Chem. Res.*, 2018, **51**, 1870-1879.
14. L. E. Bickerton, T. G. Johnson, A. Kerckhoffs and M. J. Langton, *Chem. Sci.*, 2021, **12**, 11252-11274.
15. A. Barba-Bon, M. Nilam and A. Hennig, *ChemBioChem*, 2020, **21**, 886-910.
16. D. B. Smithrud, L. Powers, J. Lunn, S. Abernathy, M. Peschka, S.-m. Ho and P. Tarapore, *ACS Medicinal Chemistry Letters*, 2017, **8**, 163-167.
17. S. Chen, Y. Wang, T. Nie, C. Bao, C. Wang, T. Xu, Q. Lin, D.-H. Qu, X. Gong, Y. Yang, L. Zhu and H. Tian, *J. Am. Chem. Soc.*, 2018, **140**, 17992-17998.
18. C. Wang, S. Wang, H. Yang, Y. Xiang, X. Wang, C. Bao, L. Zhu, H. Tian and D.-H. Qu, *Angew. Chem. Int. Ed.*, 2021, **60**, 14836-14840.
19. S. Pang, X. Sun, Z. Yan, C. Wang, K. Ye, S. Ma, L. Zhu and C. Bao, *Chem. Commun.*, 2023, **59**, 3866-3869.
20. D. P. August, S. Borsley, S. L. Cockroft, F. della Sala, D. A. Leigh and S. J. Webb, *J. Am. Chem. Soc.*, 2020, **142**, 18859-18865.
21. J. F. Stoddart, *Angew. Chem. Int. Ed.*, 2017, **56**, 11094-11125.
22. A. W. Heard and S. M. Goldup, *ACS Cent. Sci.*, 2020, **6**, 117-128.
23. T. A. Barendt, S. W. Robinson and P. D. Beer, *Chem. Sci.*, 2016, **7**, 5171-5180.
24. T. A. Barendt, A. Docker, I. Marques, V. Félix and P. D. Beer, *Angew. Chem. Int. Ed.*, 2016, **55**, 11069-11076.
25. B. R. Mullaney, A. L. Thompson and P. D. Beer, *Angew. Chem. Int. Ed.*, 2014, **53**, 11458-11462.
26. A. E. Hess and P. D. Beer, *Org. Biomol. Chem.*, 2016, **14**, 10193-10200.
27. D. Brynn Hibbert and P. Thordarson, *Chem. Commun.*, 2016, **52**, 12792-12805.
28. T. G. Johnson, A. Docker, A. Sadeghi-Kelishadi and M. J. Langton, *Chem. Sci.*, 2023, **14**, 5006-5013.
29. L. E. Bickerton, A. J. Sterling, P. D. Beer, F. Duarte and M. J. Langton, *Chem. Sci.*, 2020, **11**, 4722-4729.
30. X. Wu, L. W. Judd, E. N. W. Howe, A. M. Withecombe, V. Soto-Cerrato, H. Li, N. Busschaert, H. Valkenier, R. Pérez-Tomás, D. N. Sheppard, Y.-B. Jiang, A. P. Davis and P. A. Gale, *Chem*, 2016, **1**, 127-146.
31. S. J. Wezenberg, L.-J. Chen, J. E. Bos, B. L. Feringa, E. N. W. Howe, X. Wu, M. A. Siegler and P. A. Gale, *J. Am. Chem. Soc.*, 2022, **144**, 331-338.

32. A. Singh, A. Torres-Huerta, T. Vanderlinden, N. Renier, L. Martínez-Crespo, N. Tumanov, J. Wouters, K. Bartik, I. Jabin and H. Valkenier, *Chem. Commun.*, 2022, **58**, 6255-6258.
33. L. E. Bickerton, A. Docker, A. J. Sterling, H. Kuhn, F. Duarte, P. D. Beer and M. J. Langton, *Chem. Eur. J.*, 2021, **27**, 11738-11745.
34. *Accurate quantification of iodide transport rates could not be achieved due to high background activity in these assays.*
35. Y. Yang, X. Wu, N. Busschaert, H. Furuta and P. A. Gale, *Chem. Commun.*, 2017, **53**, 9230-9233.
36. M. P. Anderson, R. J. Gregory, S. Thompson, D. W. Souza, S. Paul, R. C. Mulligan, A. E. Smith and M. J. Welsh, *Science*, 1991, **253**, 202-205.
37. F. Delange, *Thyroid*, 1994, **4**, 107-128.
38. K. Dabrowa, F. Ulatowski, D. Lichosyt and J. Jurczak, *Org. Biomol. Chem.*, 2017, **15**, 5927-5943.
39. X. Wu, P. Wang, P. Turner, W. Lewis, O. Catal, D. S. Thomas and P. A. Gale, *Chem*, 2019, **5**, 1210-1222.
40. A. Brown, T. Lang, K. M. Mullen and P. D. Beer, *Org. Biomol. Chem.*, 2017, **15**, 4587-4594.
41. P. Thordarson, *Chem. Soc. Rev.*, 2011, **40**, 1305-1323.
42. H.-J. Schneider, *Angew. Chem. Int. Ed.*, 2009, **48**, 3924-3977.

CHAPTER 4

Preparation of Higher Order Catenanes via Orthogonal Template-Directed Strategies

Chapter 4: Preparation of Higher-Order Catenanes via Orthogonal Template-Directed Strategies

4.1 Introduction

Since the first report of a statistical catenane synthesis by Wassermann more than 60 years ago, the topological complexity of this class of molecules has been a source of both fascination and frustration to supramolecular chemists. Despite the growing arsenal of template-directed methods to facilitate mechanical bond formation, thus far only the simplest 'Hopf' link, a [2]catenane with two molecular crossing points, can be accessed in a relatively straightforward manner.[1]

In contrast, there is a dearth of strategies for the preparation of higher order [n]catenanes ($n \geq 3$), of which those capable of generating functional catenanes in appreciable yields are even rarer. The synthesis of higher order catenanes is complicated by additional considerations such as an increase in the number of bond-forming reactions needed, competing equilibria leading to the formation of side products, and consequentially greater challenges associated with purification of the target [n]catenane. Another important consideration is the heightened possibility of topological isomerism as the number of macrocyclic components increases. A myriad of possible different interlocking patterns exists for [n]catenanes with $n > 3$, of which the radial isomer, consisting of $n-1$ macrocycles threaded around a large central macrocycle, is the most common.

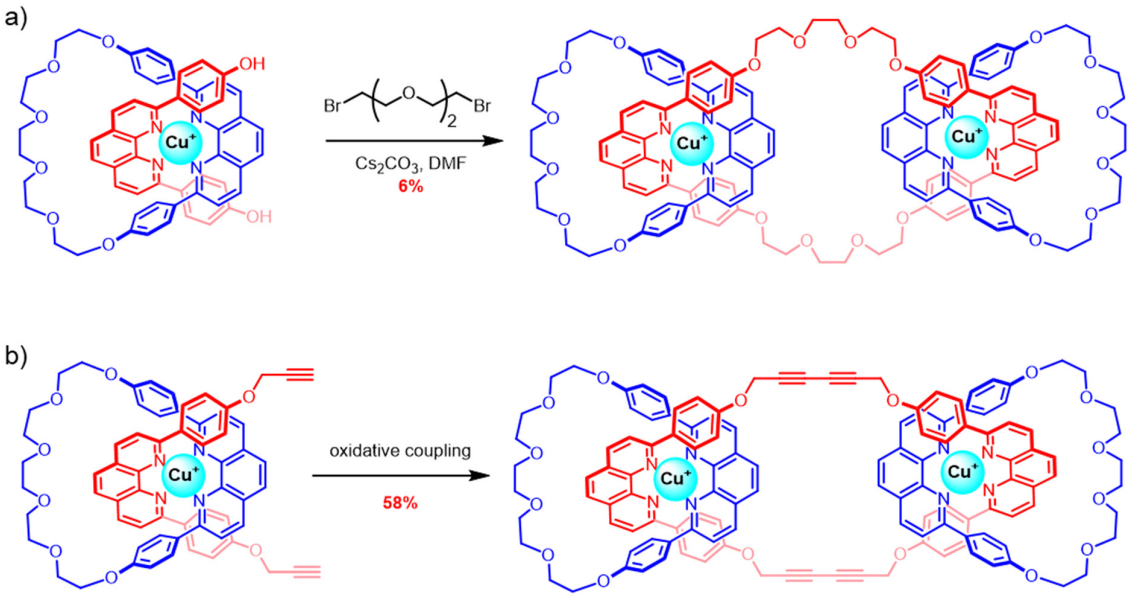
The difficulty associated with preparing higher order catenanes has thus far limited their applications as sensors, switches and molecular machines. Nonetheless, there are hints of their potential superiority over simpler interlocked systems, such as in a report by Leigh and co-

workers, who demonstrated unidirectional motion in a [3]catenane-based molecular motor but not the [2]catenane analogue.[2] Additionally, in the context of supramolecular host-guest chemistry, particularly ion-pair recognition, the use of higher order catenane receptors containing interlocked binding sites for *both* guest ions is an intriguing strategy to enhance the affinity and selectivity of ion-pair binding via the mechanical bond effect (MBE). The development of synthetic strategies to access these exotic molecules is therefore highly desirable and a promising avenue through which to extend the suite of applications in which mechanically bonded architectures can be exploited.

4.1.1 Strategies for the Preparation of Higher Order [n]Catenanes (n > 2)

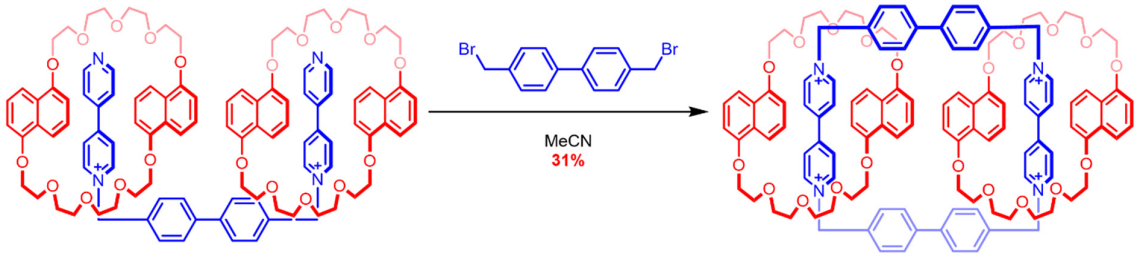
4.1.1.1 Linear [3]Catenanes

One of the earliest [3]catenanes was reported in 1985 by Sauvage and co-workers, who dimerised two pseudo[2]rotaxane complexes formed by the Cu(I)-directed self-assembly of a 1,10-phenanthroline-containing macrocycle and acyclic thread. The original system employed a Williamson ether synthesis to link two such pseudo[2]rotaxanes complexes, affording a [3]catenane in a modest yield of 6% (**Scheme 4.1a**).[3] The subsequent use of an oxidative coupling reaction between terminal acetylene units dramatically improved the yield of the [3]catenane formation step to 58% (**Scheme 4.1b**).[4] Besides the target [3]catenane, this approach was also found to produce a complex mixture of higher order radial [n]catenanes, which were presumably formed via intermolecular oligomersation of the pseudo[2]rotaxane precursors. Analysis of the mixture by electrospray mass spectrometry provided evidence for the formation of catenanes containing up to seven rings; however, only catenanes with $n \leq 5$ could be isolated.[5] These studies revealed the possibility of generating higher order radial [n]catenanes by oligomerisation of pseudo[2]rotaxanes, while highlighting the need to control the degree of oligomerisation so as to avoid a broad distribution of products.



Scheme 4.1. *Sauvage's Cu(I)-templated preparation of [3]catenanes using: a) Williamson ether synthesis; b) Oxidative coupling.*

A strategy for the controlled preparation of a [3]catenane was reported by Stoddart and co-workers, who employed a large central macrocycle containing two recognition sites. This templating approach builds on their initial synthesis of a [2]catenane by exploiting the donor-acceptor charge-transfer interactions between an electron rich macrocycle and an electron-deficient cyclobis(paraquat-*p*-phenylene) macrocycle. Increasing the size of the central electron-deficient macrocycle through the use of biphenylene linkers allowed two electron-rich macrocycles to simultaneously thread through its cavity, generating a [3]catenane in up to 31% yield (**Scheme 4.2**).[6]



Scheme 4.2. *Stoddart's synthesis of a [3]catenane using donor-acceptor charge transfer interactions.*

While increasing the size of the central macrocycle is often necessary to alleviate the steric repulsions associated with having multiple species threaded through the central cavity, the cyclisation of large rings is often challenging and proceeds in lower yields. Recognising this issue, Loeb and co-workers proposed the use of an external template to aid in ring-closure (**Figure 4.1**). The authors developed a one-step self-assembly procedure to prepare a [3]catenane by exploiting the threading of a dipyridinium species through a crown ether macrocycle, in which crucially the crown ether plays the dual roles of serving as an interlocked component and a template for the formation of the large central macrocycle. A variety of crown ethers were investigated, of which dibenzo-24-crown-8 ether (DB24C8) was found to give the highest yield of cyclic products. Evidence for its role as a template was provided by single crystal X-ray diffraction studies, which showed the formation of a [3]catenane-DB24C8 host-guest adduct, in which the DB24C8 guest is bound within the central cavity of the large macrocycle where it is stabilised by a variety of π-stacking and C-H···π interactions.[7]

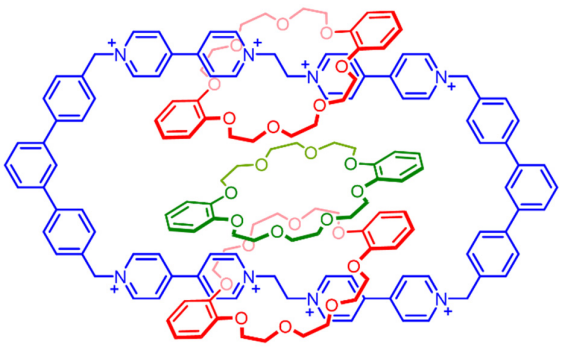


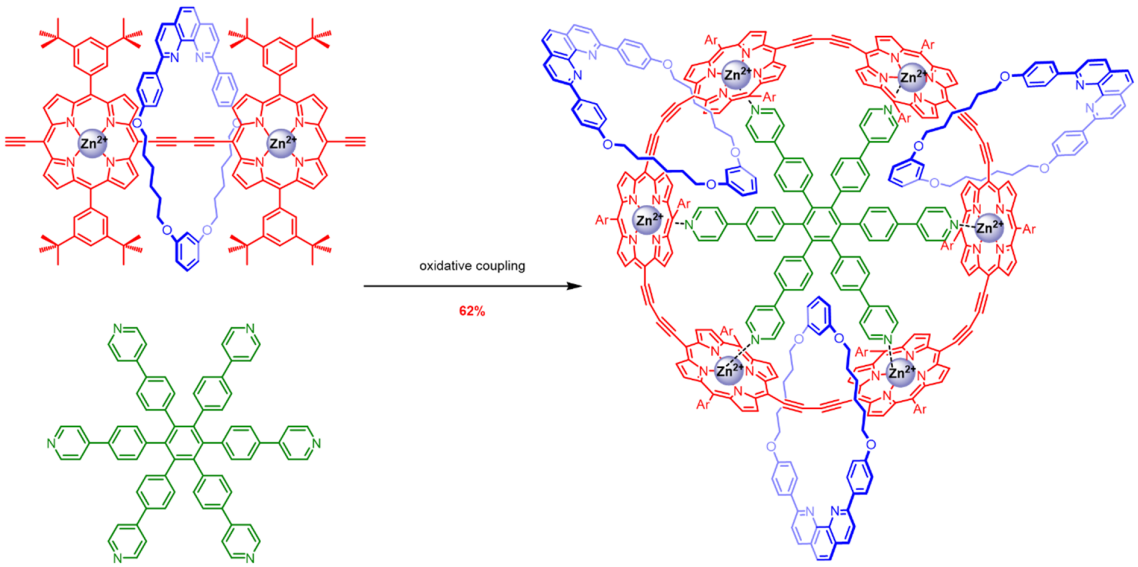
Figure 4.1. *Loeb's preparation of a [3]catenane using a DB24C8 template.*

Other approaches for the preparation of [3]catenanes have also been reported by Fujita, who observed [3]catenane assembly during thermodynamic re-organisation of Pd(II)-based macrocycles,[8] and by Sanders, who used dynamic combinatorial chemistry to prepare a [3]catenane by disulfide bond formation between cysteine-functionalised linear building blocks.[9]

4.1.1.2 Higher Order [n]Catenanes (n > 3)

Higher order catenanes with n > 3 can exist as radial, linear or branched topological isomers. Of these, reports of radial [n]catenanes are the most common because they can be prepared by oligomerisation of pseudo[2]rotaxane (or rotaxane) units.

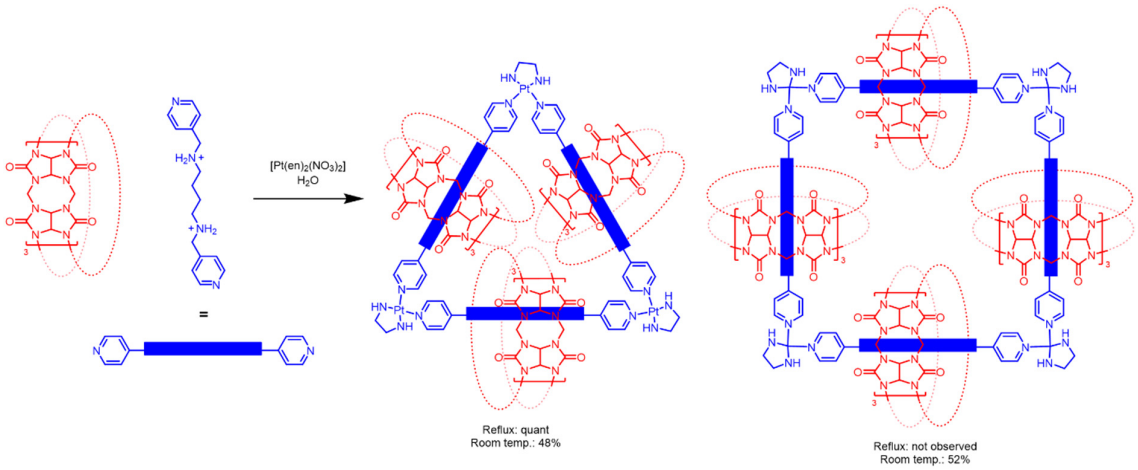
This strategy was employed was Anderson and co-workers to prepare a radial[4]catenane containing three phenanthroline-containing macrocycles threaded onto a six-porphyrin central nanoring (**Scheme 4.3**). The authors prepared the [4]catenane from a porphyrin-stoppered [2]rotaxane precursor functionalised with terminal, which underwent cyclotrimerization via an oxidative homocoupling reaction to afford the target radial [4]catenane in 62% yield.[10] In this case, excellent control over the degree of oligomerisation was achieved via the use of a hexapyridyl template, which coordinates to six Zn(II) centres from three [2]rotaxanes to direct trimerization.



Scheme 4.3. *Anderson's preparation of a radial [4]catenane using a hexapyridyl template.*

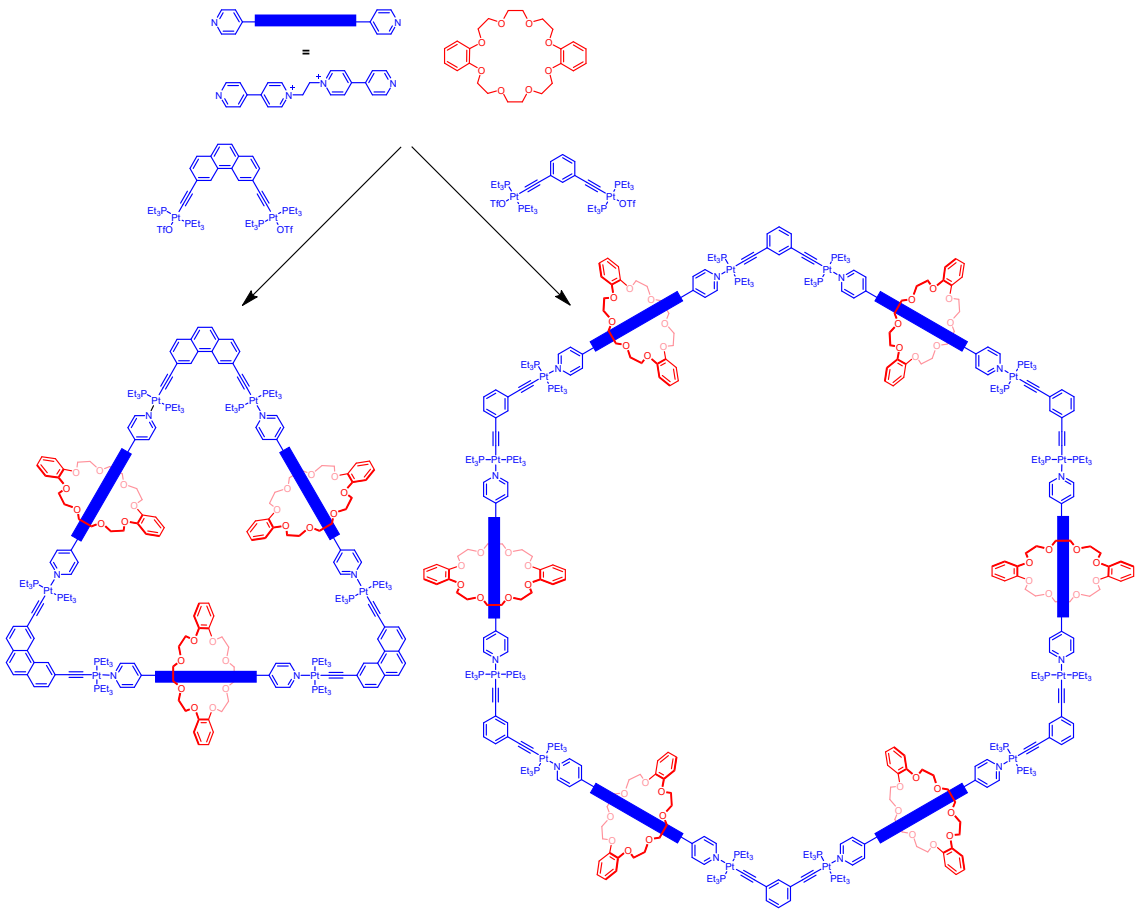
Another example of radial catenane synthesis via oligomerisation of pseudorotaxane subunits was reported by Kim and co-workers, who exploited the ability of cucurbit[6]uril

(CB[6]) to form highly stable inclusion complexes with linear diammonium salts to direct pseudo[2]rotaxane formation between bis-pyridyl functionalised 1,4-butyldiammonium and CB[6] (**Scheme 4.4**). Refluxing the pseudo[2]rotaxane precursor with Pt(II) led to trimerization, affording a [4]catenane in almost quantitative yield. Interestingly, conducting the reaction at room temperature led instead to a mixture of [4]- and [5]catenanes, with the [5]catenane slightly favoured (52%). The authors attribute this behaviour to the greater difficulty of overcoming the steric repulsion between the CB[6] subunits at room temperature, leading to the [5]catenane being the favoured kinetic product.



Scheme 4.4. *Kim's synthesis of radial [4]- and [5]catenanes under kinetic vs. thermodynamic control.*

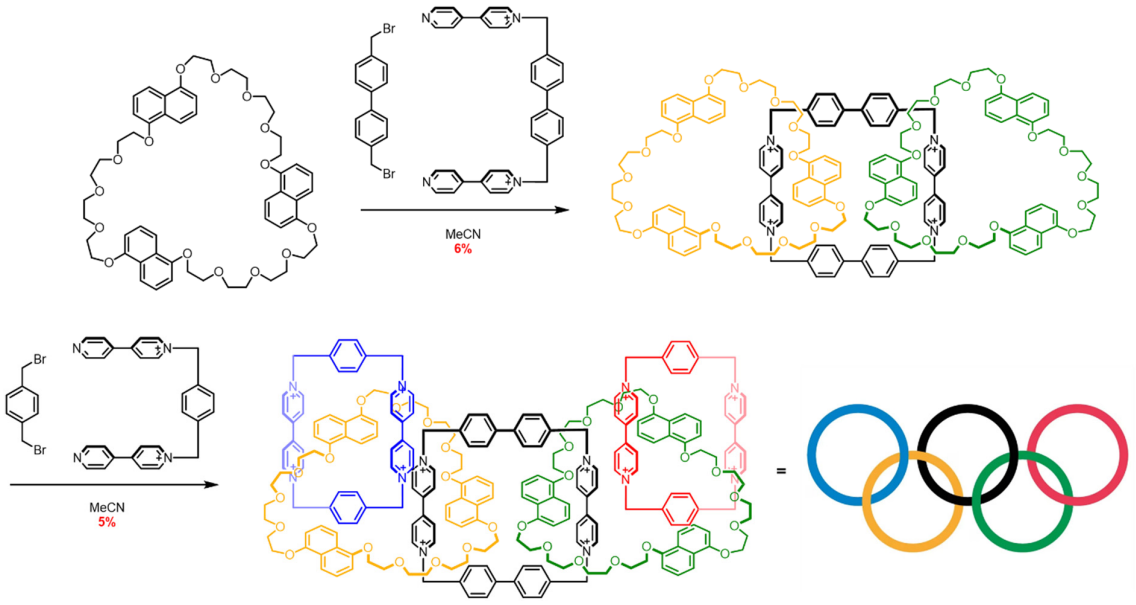
Controlling the degree of cyclic oligomerisation in radial catenane synthesis can also be accomplished by using building blocks with well-defined geometries. This was demonstrated by Stang and co-workers, who achieved exclusive formation of either a [4]- or [7]catenane by varying the geometry of the bis(alkyne) building blocks (**Scheme 4.5**). In the former case, a 3,6-phenanthrene spacer is used to ensure an angle of 120° between the bis(alkynes), facilitating the preparation of a [4]catenane featuring a triangular central macrocycle. In contrast, the use of a 1,3-benzyl spacer with a 60° angle between the bis(alkynes) directs the formation of a [7]catenane containing a hexagonal central macrocycle.[11]



Scheme 4.5. *Stang's synthesis of radial [4]- and [7]catenanes using linkers of different geometries.*

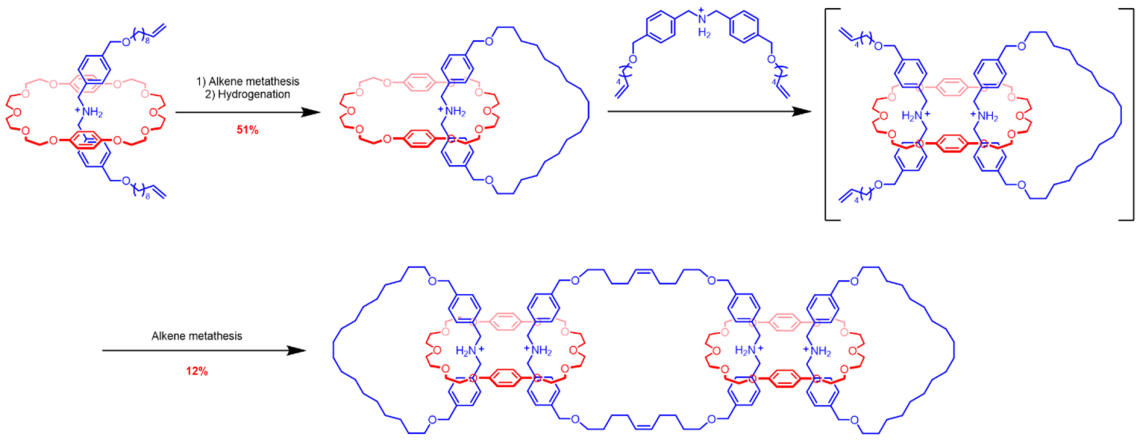
In contrast to radial [n]catenanes, very few examples of linear [n]catenanes (n > 3) have been reported to date. Perhaps the most well-known example of a linear [5]catenane is the molecule dubbed 'Olympiadane' by Stoddart and co-workers, who asserted that the linear connectivity of its five interlocked macrocycles resembles the logo of the Olympic games. The preparation of Olympiadane required two mechanical bond forming steps, both of which exploit donor-acceptor charge transfer interactions between macrocycles containing electron-deficient paraquat and electron-rich 1,5-dioxynaphthalene units (**Scheme 4.6**). In the first step, the cyclisation of an electron-deficient bis-paraquat macrocycle around two tris-1,5-dioxynaphthalene-functionalised macrocycles gave a [3]catenane in 6% yield. Each peripheral electron-rich macrocycle then served as a templating site for the threading and cyclisation of a

new interlocked paraquat-containing macrocycle to generate the target[5]catenane in 5% yield. Evidence for the linear topology of the product was provided by tandem mass spectrometry and variable temperature ^{1}H NMR.[12]



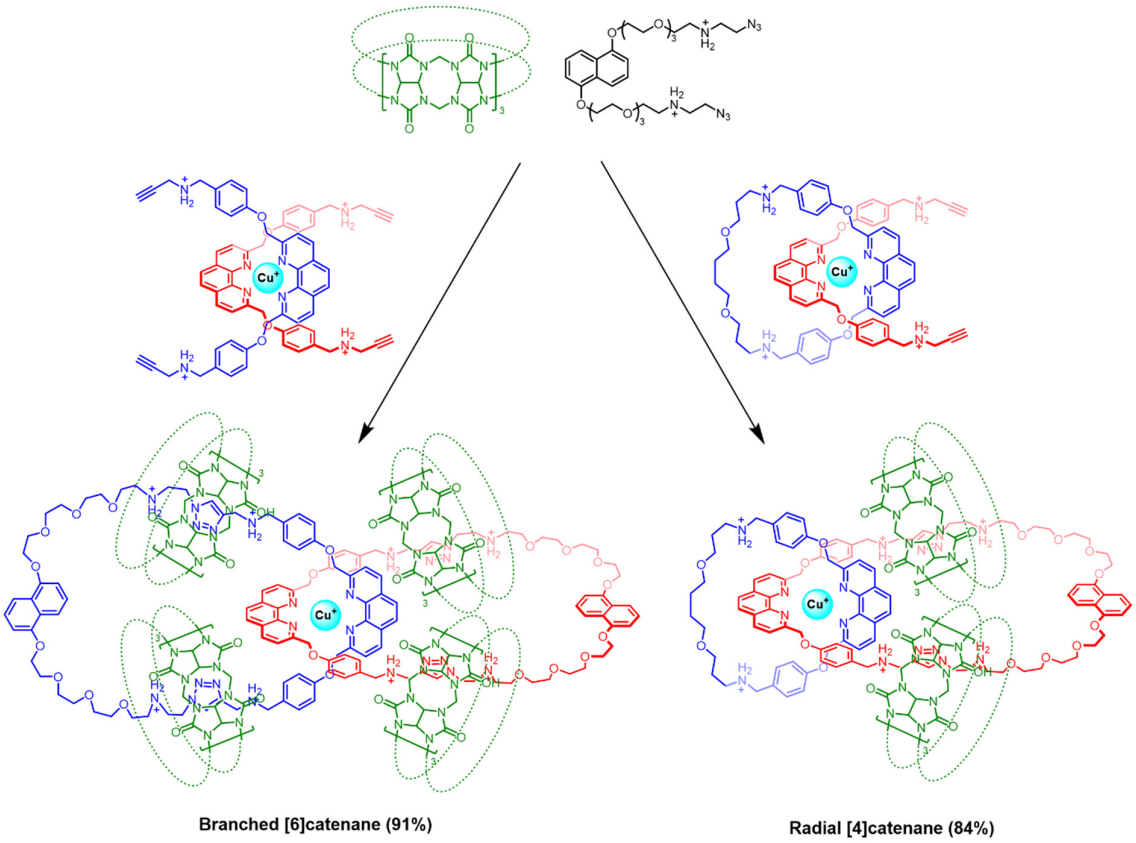
Scheme 4.6. *Stoddart's synthesis of Olympiadane using donor-acceptor charge transfer interactions.*

Hajime and co-workers subsequently reported the stepwise synthesis of another linear [5]catenane by exploiting the threading of ammonium species through the cavity of crown ether-like macrocycles (**Scheme 4.7**). Unlike Stoddart's Olympiadane synthesis, the authors first assembled a [2]catenane by *intra*molecular alkene metathesis of a dialkylammonium precursor threaded through a bis(*p*-phenylene)-34-crown-10 ether macrocycle (BPP34C10). A shorter dialkylammonium unit was subsequently threaded through the BPP34C10 cavity of the [2]catenane, which was dimerised via *inter*molecular alkene metathesis to form the [5]catenane in 12% yield. The length of the dialkylammonium precursors was found to be crucial, with a longer linker favouring intramolecular cyclisation while a shorter linker favours intermolecular dimerization.[13]



Scheme 4.7. *Hajime's synthesis of a linear [5]catenane using alkylammonium-crown ether interactions.*

The above examples all utilise a single type of non-covalent interaction to direct the formation of higher order catenanes, giving rise to catenane products in which at least two of the macrocycles are identical. In principle, the use of orthogonal interactions could serve a powerful potential strategy to access hetero[n]catenanes containing a variety of different macrocycles. To the best of our knowledge, the only example of using orthogonal interactions to assemble higher order catenanes was reported by Au-Yeung and co-workers, who combined the well-established Cu(I)-phenanthroline coordination and CB[6]-diammonium interactions to direct the formation of a rare branched [6]catenane in 91% yields (**Scheme 4.8**). Replacing one of the acyclic phenanthroline precursors with a macrocycle containing the same recognition motif gave rise to a radial [4]catenane in which one of the three macrocycles threaded around the central ring is unique, thereby demonstrating the potential of using orthogonal supramolecular interactions to de-symmetrise catenanes or access unusual topologies.[14]



Scheme 4.8. *Au-Yeung's synthesis of a branched [6]catenane and radial [4]catenane using orthogonal templating interactions.*

4.1.2 Applications of Higher Order Catenanes

Due to the inherent difficulties associated with the preparation of higher order catenanes, the vast majority of reports are focused on characterising the topology of the interlocked products rather than exploring their properties and potential applications. Indeed, current methods for the synthesis of higher order catenanes often place major restrictions on the size and type of macrocycles present in the catenanes which makes it difficult to incorporate functionally useful motifs into these molecules.

Leigh and co-workers reported a [3]catenane capable of functioning as an artificial unidirectional molecular rotor (**Figure 4.2a**). The authors exploited hydrogen bonding interactions between the components to template the formation of a [2]catenane and a

[3]catenane, wherein the large macrocycle contains three non-identical hydrogen bonding stations exhibiting different binding affinities for the smaller macrocycle(s). Two of the stations are able to undergo photoisomerization, which lowers their binding affinity to the smaller macrocycle(s), inducing translocation of the macrocycle to the next strongest binding station. The authors found that the [2]catenane moves with high positional integrity between the stations upon photo-switching but with no directional bias. In contrast, in the [3]catenane, each ring is able to block the passage of the other in a particular direction, giving rise to unidirectional macrocycle translocation upon photo-switching, evidence for which was obtained via a series of kinetic studies. This novel study elegantly demonstrates the unique advantages that higher order catenanes may offer in the design of sophisticated molecular machines.[2]

A rare example of a dynamic hetero[3]catenane system capable of optical anion sensing was reported by Beer and co-workers. The large central macrocycle of the hetero[3]catenane comprises a tetrachloro-functionalised perylene diimide (PDI) unit as well as two triazolium anion-binding stations (**Figure 4.2b**). In polar protic solvents, the smaller peripheral isophthalamide-functionalised macrocycles reside over the PDI station, stabilised by aromatic donor-acceptor charge transfer interactions that give rise to a characteristic UV-vis absorption. Addition of chloride induced a translocation of the isophthalamide macrocycles to the triazolium binding sites, leading to a reduction in the charge-transfer absorption band and a concomitant naked eye colour change from red to orange. A significant enhancement of the PDI fluorescence was also observed upon chloride binding in a solvent mixture of 45:45:10 $CHCl_3/CH_3OH/H_2O$, highlighting the catenane's potential to be used as a fluorescent anion sensor in competitive media.[15]

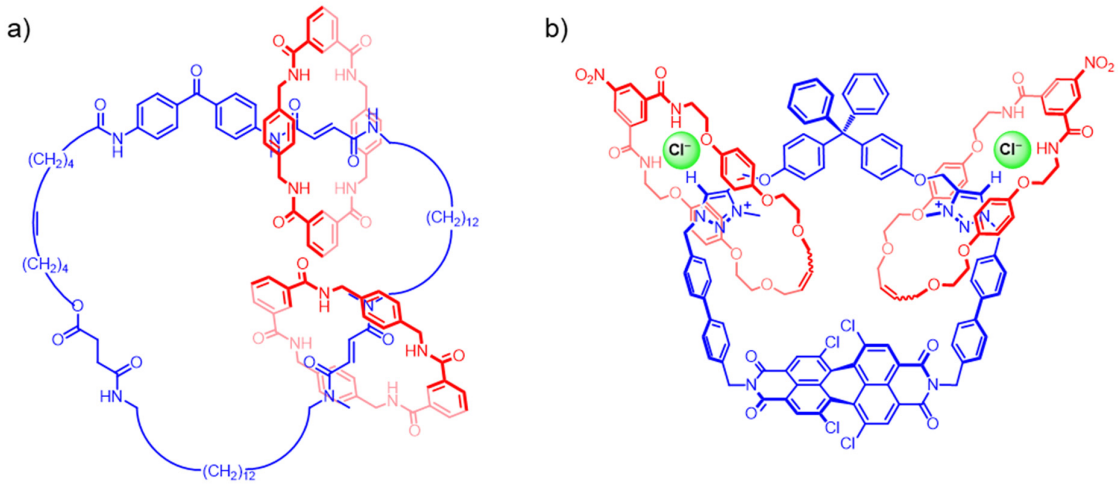


Figure 4.2. *a) Leigh's [3]catenane-based unidirectional molecular motor; b) Beer's [3]catenane for optical anion sensing.*

4.1.3 Chapter Aims

The scarcity of synthetic methods for the preparation of functional higher order catenanes has severely hindered efforts to explore the properties and potential applications of this fascinating class of molecules. The preparation of a heteroditopic [3]catenane containing interlocked binding cavities for both a cationic and anionic guest is a particularly desirable target given the demonstrated improvements in individual ion binding affinities and selectivities achieved by encapsulating these guest ions in MIM-based hosts.

To this end, ambitiously we sought to combine the orthogonal alkali metal cation and chloride anion template-directed methodologies discussed in Chapters 2 and 3 respectively, for the stepwise preparation of a hetero[3]catenane (**Figure 4.3**). Conceivably, the presence of pre-organised cation and anion binding cavities in the [3]catenane would markedly enhance its alkali metal halide ion-pair recognition properties relative to the [2]catenanes and [2]rotaxanes discussed in the previous chapters. This chapter outlines various [3]catenane designs and the synthetic challenges associated with each route. Preliminary solid-state evidence indicating the potent ion-pair recognition capability of the [3]catenane will also be presented.

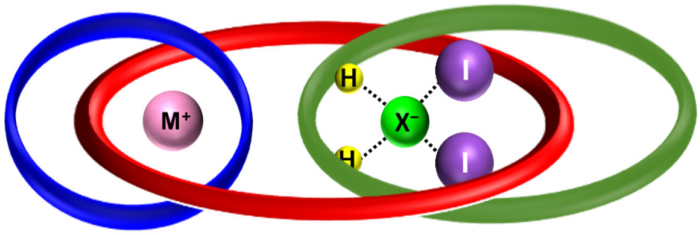
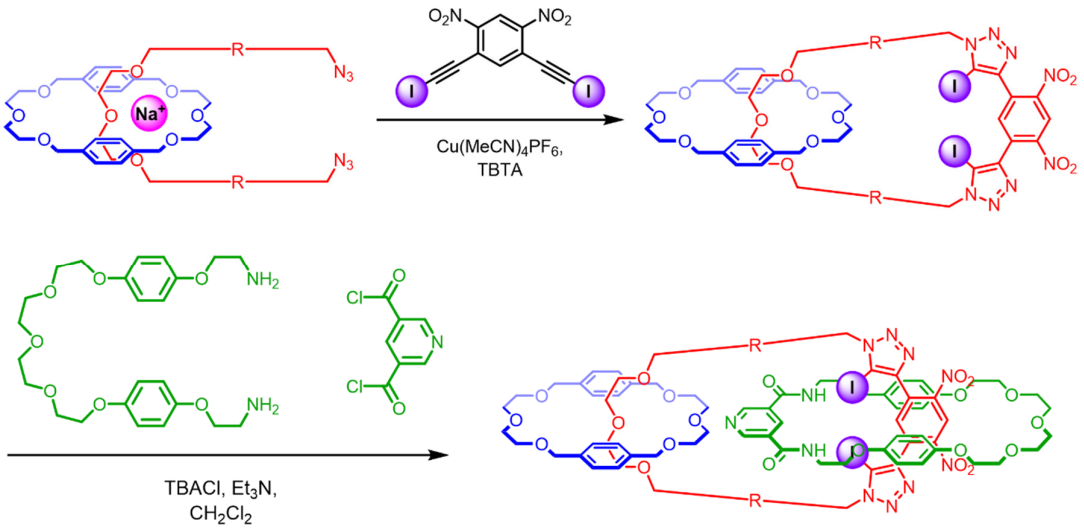


Figure 4.3. *Cartoon representation of a target heteroditopic [3]catenane containing interlocked binding cavities for both the cation and anion guests.*

4.2 A Heteroditopic [3]Catenane for Ion-Pair Recognition

4.2.1 Synthesis

Motivated by the efficacy of our alkali metal cation and chloride anion template-directed strategies for the preparation of interlocked host molecules for ion recognition, we envisaged combining these methods to generate a hetero[3]catenane containing a oligo(ethylene glycol)-based interlocked cavity for cation binding alongside a XB- and HB-decorated cavity for halide binding. The proposed general synthetic approach involves two mechanical bond forming steps. Firstly, an alkali metal cation directs the formation of a [2]catenane, wherein, crucially, the CuAAC-mediated macrocycle clipping reaction generates a 4,6-dinitro-1,3-bis-iodotriazole group. This potent XB motif is then well-placed to facilitate a chloride template-directed amide condensation reaction between a bis-amine and a bis-acid chloride to form the third interlocked macrocycle (**Scheme 4.9**).



Scheme 4.9. *General synthetic approach for the preparation of a heteroditopic [3]catenane.*

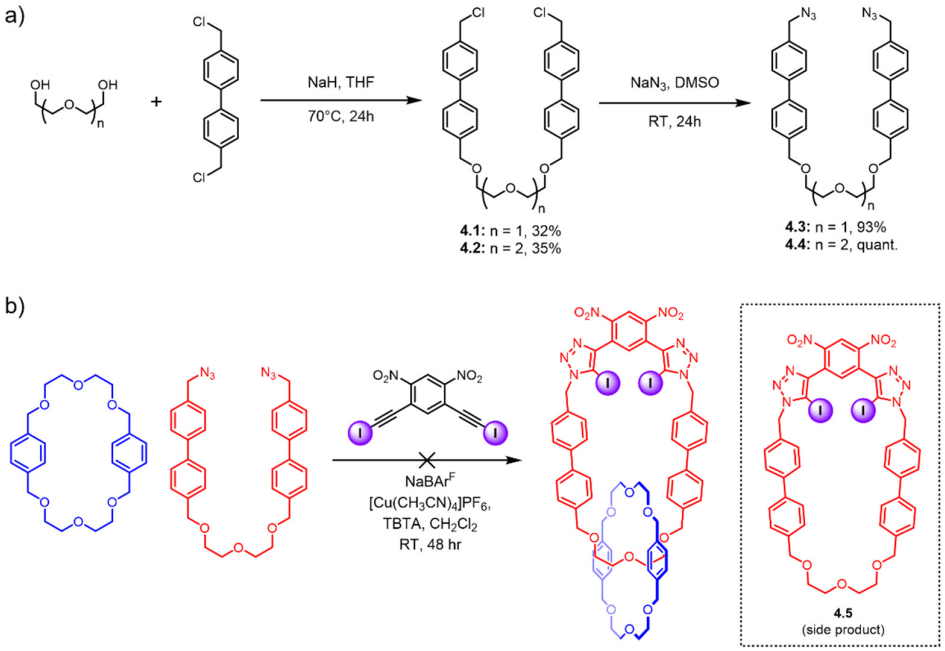
4.2.1.1 Sodium Cation Template-Directed Formation of a [2]Catenane

Initial host designs sought to employ chemically similar synthons to those developed in Chapters 2 and 3. However, the need for an expanded central macrocycle with a sufficiently large cavity to accommodate two threaded species necessitated the preparation of longer bis-azide precursors. We first decided to prepare bis-azides in which biphenyl linkers separate the oligo(ethylene glycol) cation binding site from the terminal azide groups.

The target bis-azides were prepared using similar synthetic procedures to those employed in the preparation of **2.3** and **2.4**. Alkylation of di- or tri(ethylene glycol) with excess 4,4'-bis(chloromethyl)-1,1'-biphenyl in the presence of NaH produced the dichlorides **4.1** and **4.2** in 32% and 35% yields respectively. Treatment of the dichlorides with NaN_3 in DMSO solution afforded the target bis-azides **4.3** and **4.4** in near-quantitative yields (**Scheme 4.10a**).

With the bis-azides in hand, the formation of a hetero[2]catenane via an alkali metal template-directed methodology was attempted (**Scheme 4.10b**). To this end, a mixture containing bis-azide **4.3**, $NaBAr^F$ and bis-di(ethylene glycol)-functionalised macrocycle **2.7** were pre-complexed in dry CH_2Cl_2, followed by dropwise addition of CH_2Cl_2 solutions

containing 4,6-dinitro-1,3-bis-iodoalkyne **3.3** and $[Cu(MeCN)_4]PF_6$/TBTA. The reaction was allowed to stir for 3 days, after which TLC analysis indicated complete consumption of the bis-azide and the formation of a complex mixture of compounds, including the non-interlocked XB macrocycle as well as several more polar species. ESI-MS analysis of the crude mixture suggested that a trace amount of the desired [2]catenane had been formed, as indicated by the appearance of a small peak with m/z = 1433. The reaction was subjected to a basic work-up with aqueous EDTA solution and purification by preparative TLC. Unfortunately, however, the low yields and sheer number of side-products resulted in the desired [2]catenane not being isolated. The major side-product of the reaction appeared to be the non-interlocked XB macrocycle **4.5**, which was isolated in 25% yield. Mass spectrometric analysis of the polar components of the mixture, which were formed in minute quantities, suggested the presence of a [2+2] macrocycle, as well as several oligomeric species.



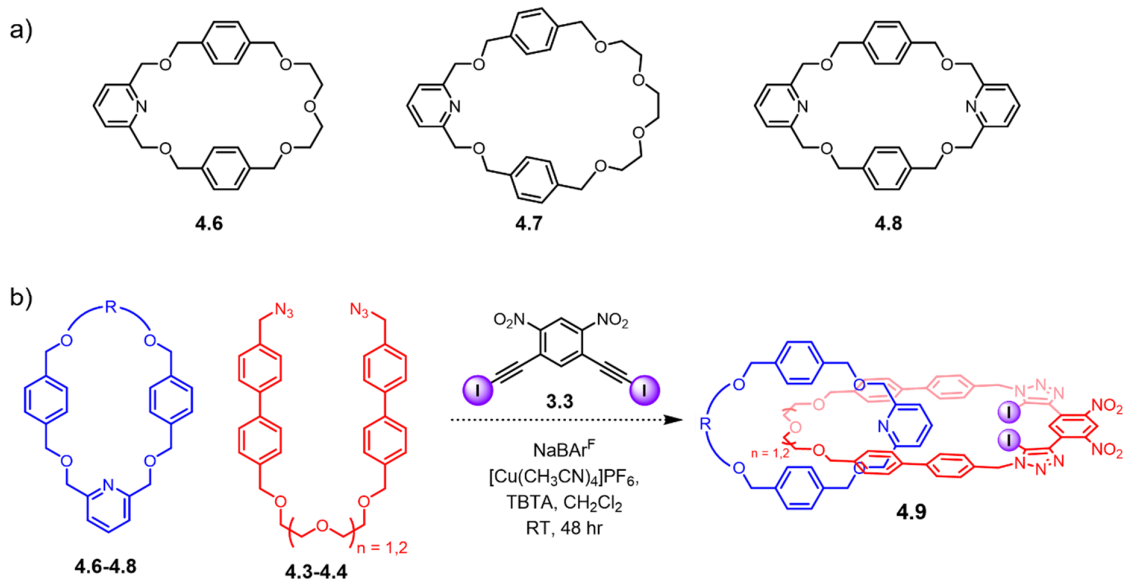
Scheme 4.10. *a) Preparation of extended bis-azides* ***4.3*** *and* ***4.4****; b) Attempted synthesis of a [2]catenane via a sodium cation template-directed strategy.*

Repeating the reaction with the shorter xylene-based bis-azide **2.3**, which had been previously employed in the sodium cation template-directed formation of heteroditopic homo- and hetero[2]catenanes (described in **Chapter 2**), similarly yielded a complex mixture from which the desired hetero[2]catenane could not be isolated. The failure to obtain the desired [2]catenane was attributed to the susceptibility of the 4,6-dinitro-1,3-bis-iodoalkyne towards de-iodination via nucleophilic attack, which when combined with the inherently low yield of hetero[2]catenane formation using macrocycle **2.7** (described in **Section 2.3.1**), likely generates only trace amounts of the desired catenane product.

These observations were concordant with a recent study by Chiu and co-workers, who noted that attempts to prepare hetero[2]catenanes via Na^+ template-directed threading of acyclic di(ethylene glycol) precursors through the cavity of bis-di(ethylene glycol)-incorporated macrocycles like **2.7** typically resulted in low reaction yields. This was attributed to the poorly directional metal cation binding of macrocycle-incorporated di(ethylene glycol) chains, leading to both desired internal threading and undesired external binding. The authors showed that hetero[2]catenanes yields could be improved through the use of 2,6-dimethanolpyridine-containing macrocycles, where sodium cation binding within the macrocycle cavity favoured the formation of a threaded pseudo[2]rotaxane species.[16]

These findings prompted an investigation into sodium ion template-directed hetero[2]catenane formation using 2,6-dimethanolpyridine-containing macrocycles. Accordingly, three macrocycles **4.6-4.8** containing this recognition motif were prepared using modified literature procedures (**Scheme 4.11a**).[17] A series of hetero[2]catenane formation reactions were undertaken utilising different combinations of the two bis-azides (**4.3** and **4.4**) and the three macrocycles (**Scheme 4.11b**), the results of which are summarised in **Table 4.1**. Pleasingly, the use of a 2,6-dimethanolpyridine-containing macrocycle in conjunction with

di(ethylene glycol)-based bis-azide **4.3** as complementary binding units for the sodium cation template markedly improved the yields of the target hetero[2]catenanes. However, purification of the mixtures remained a challenge, with ^{1}H NMR analysis revealing the presence of persistent impurities despite iterative chromatographic purification. In general, the use of precursors containing longer oligo(ethylene glycol) units typically resulted in more challenging purifications due to the increased polarity of the products.



Scheme 4.11. *a) Macrocycles containing the 2,6-dimethanolpyridine motif; b) General sodium cation template-directed synthesis of a [2]catenane using different combinations of macrocycle and bis-azide precursors.*

Table 4.1. *Alkali metal cation template-directed synthesis of hetero[2]catenanes using various bis-azide and macrocyclic precursors.*

	Bis-azide **4.3**		Bis-azide **4.4**	
Macrocycle	[2]catenane	Yield (%)	[2]catenane	Yield (%)
4.6	**4.9**$^{\text{DEG-4.6}}$	**14**	**4.9**$^{\text{TEG-4.6}}$	< 5[a]
4.7	**4.9**$^{\text{DEG-4.7}}$	6[a]	**4.9**$^{\text{TEG-4.7}}$	< 5[a]
4.8	**4.9**$^{\text{DEG-4.8}}$	< 10[a]	**4.9**$^{\text{TEG-4.8}}$	N.D.[b]

[a] Impurities observed in ^{1}H NMR spectra of product despite multiple rounds of purification by preparative TLC.
[b] N.D. = Not done.

Hetero[2]catenane **4.9**$^{\mathbf{DEG\text{-}4.6}}$, formed via the sodium cation directed threading of bis-azide **4.3** through the cavity of macrocycle **4.6**, was isolated in the highest yield and purity. Evidence for the interlocked nature of **4.9**$^{\mathbf{DEG\text{-}4.6}}$ was obtained by comparing its ^{1}H NMR spectrum to that of the constituent macrocycles **4.5** and **4.6** (**Figure 4.4**). Significant upfield perturbations were observed in the proton signals arising from macrocycle **4.6**, presumably due to their enforced proximity to the shielding ring currents generated by the biphenyl spacers of macrocycle **4.5**. In macrocycle **4.5**, the most prominent changes were observed in the proton signals proximal to the ethylene glycol region, particularly $H_{i,j}$ and H_h which moved upfield, suggesting that this region of the macrocycle participates in intercomponent interactions with **4.6**. In contrast, only small perturbations occurred in the dinitrobenzene proton signals H_a and H_b, which promisingly suggests that the XB motif of **4.5** remains sterically accessible for chloride binding.

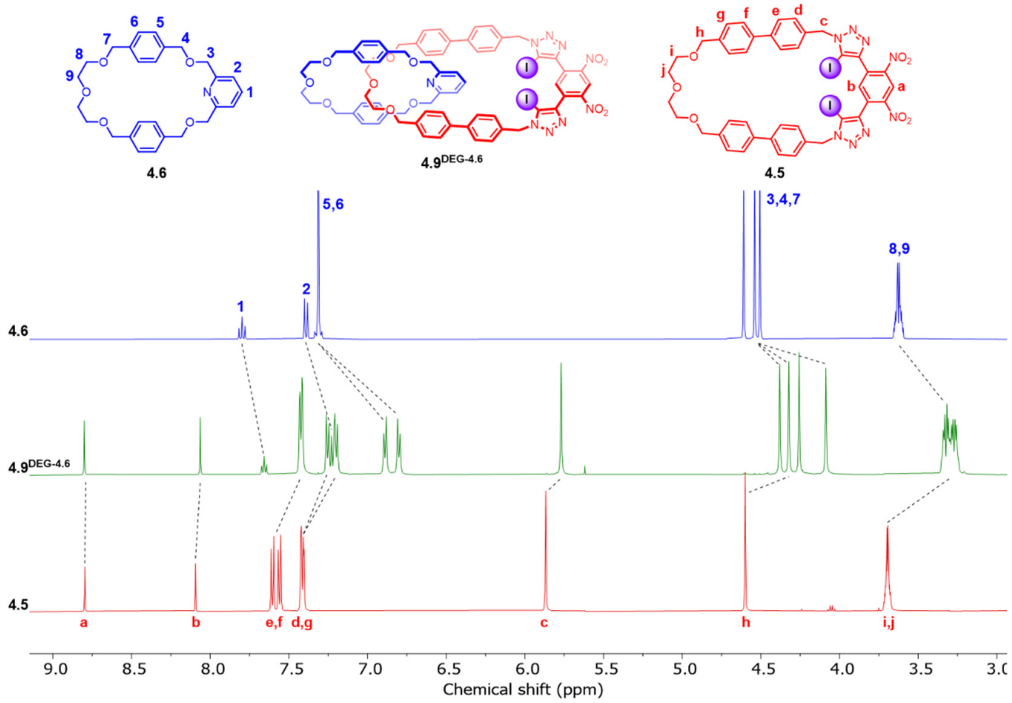
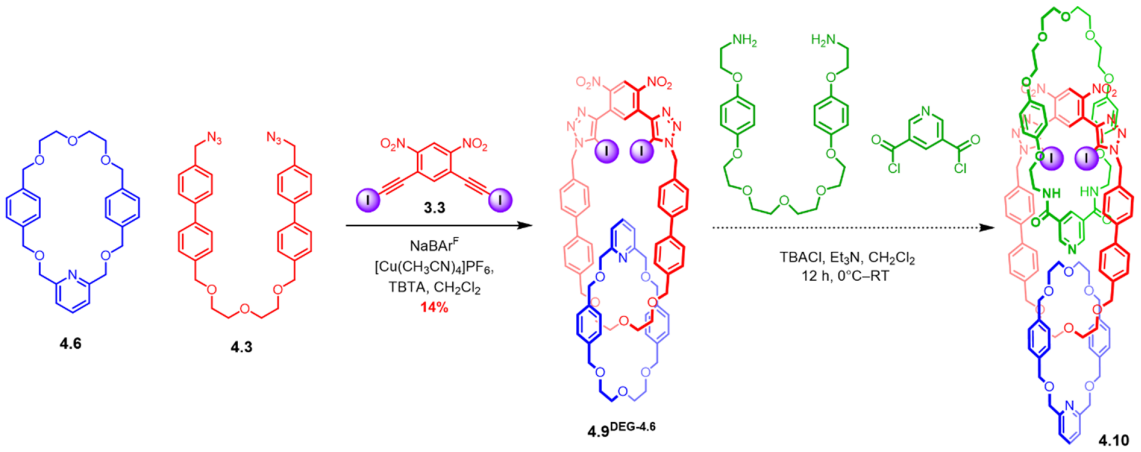


Figure 4.4. *Stacked ^{1}H NMR spectra of macrocycle* ***4.6*** *(top), [2]catenane* ***4.9***$^{\mathbf{DEG\text{-}4.6}}$ *(middle) and XB macrocycle* ***4.5*** *(bottom) (500 MHz, acetone-d_6, 298 K).*

4.2.1.2 Chloride Anion Template-Directed Formation of a [3]Catenane

With the XB [2]catenane **4.9**$^{DEG\text{-}4.6}$ in hand, the chloride template-directed preparation of a [3]catenane was undertaken (**Scheme 4.12**). A solution of [2]catenane **4.9**$^{DEG\text{-}4.6}$, bis-amine **3.6**, TBACl and Et_3N in anhydrous CH_2Cl_2 was cooled to 0°C, followed by dropwise addition of solution of a freshly prepared bis-acid chloride **3.7** in CH_2Cl_2. The reaction mixture was allowed to warm to room temperature and stirred overnight. Pleasingly, ESI-MS analysis of the crude suggested the formation of the target [3]catenane, as evidenced by the appearance of an ion peak with m/z = 2062. Following aqueous work-up with K_2CO_3 solution and preparative TLC purification of the reaction mixture, a small quantity of the putative [3]catenane **4.10** was isolated as an orange solid in approximately 5% yield.



Scheme 4.12. *Synthesis of [3]catenane* ***4.10*** *via orthogonal cation and anion template-directed methods.*

4.2.2 Characterisation

4.2.2.1 ^{1}H NMR and Mass Spectrometric Studies

Attention was then directed to determining the identity and topology of the reaction product **4.10**, which proved to be a non-trivial endeavour as the low reaction yields, complex product mixtures, and loss of product following multiple rounds of chromatographic purification posed significant barriers to scale-up efforts.

Notably, the high resolution ESI+ve mass spectrum of **4.10** revealed the presence of a major peak with m/z = 2062.5374, which exhibited an isotope distribution that is in excellent agreement with the predicted chemical composition of the [3]catenane (**Figure 4.5**).

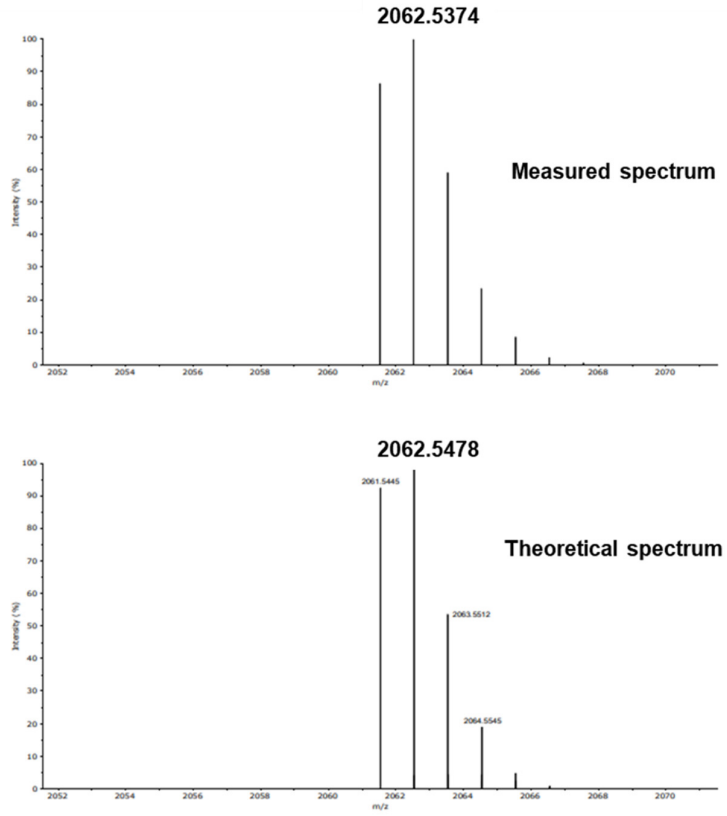


Figure 4.5. *High resolution mass spectrum (ESI +ve) of* ***4.10*** *(top: measured; bottom: simulated).*

^{1}H NMR analysis of the compound in $CDCl_3$ revealed a series of broad peaks, with the majority of proton signals falling in the 3.0 – 4.5 ppm and 6.5 – 7.75 ppm regions. A series of lower intensity signals were also observed further downfield (δ > 8.5 ppm), which are typical of dinitrobenzene and pyridyl proton signals (**Figure 4.6**). The general distribution of the proton signals appears to be consistent with the functional groups present in the [3]catenane. However, the broad and overlapping nature of the proton signals precluded definitive spectral assignment.

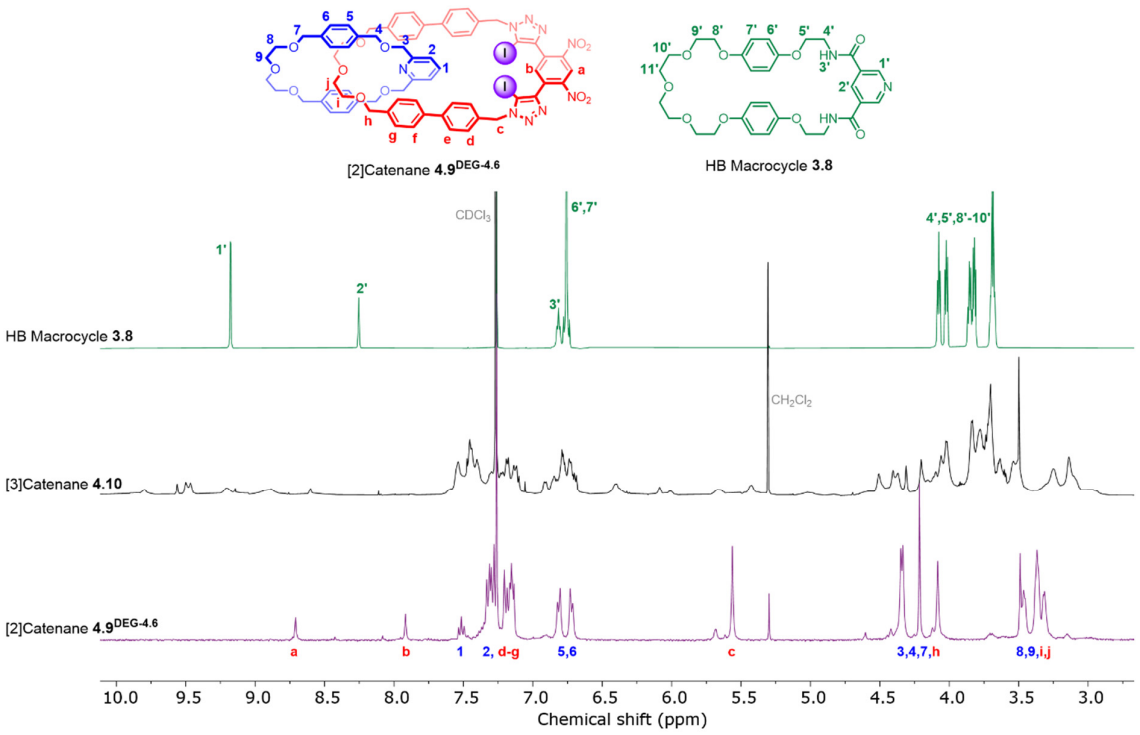


Figure 4.6. *Stacked ^{1}H NMR spectra of HB macrocycle* ***3.8*** *(top), [3]catenane* ***4.10*** *(middle) and [2]catenane* ***4.9$^{DEG-4.6}$*** *(bottom) ($CDCl_3$, 500 MHz, 298 K).*

Variable temperature NMR (VT-NMR) studies in $CDCl_3$ and acetone-d_6 were conducted in an attempt to improve the spectral resolution of the ^{1}H NMR spectrum. Pleasingly, heating a solution of **4.10** in acetone-d_6 to 318 K markedly reduced the linewidths of the proton signals (**Figure 4.7**). In contrast, cooling the solution to 193 K resulted in further broadening and splitting of the proton resonances, which in some cases could not be distinguished from the baseline due to low concentration of the compound in solution. This behaviour is consistent with previous reports of dynamic higher-order [n]catenanes, which exhibit split and broadened spectra at low temperatures due to the hindered co-conformational circum-rotation of the constituent macrocycles, whereas at higher temperature, sharper proton signals are observed due to the rapid re-orientations of the macrocycles relative to the NMR timescale.[12]

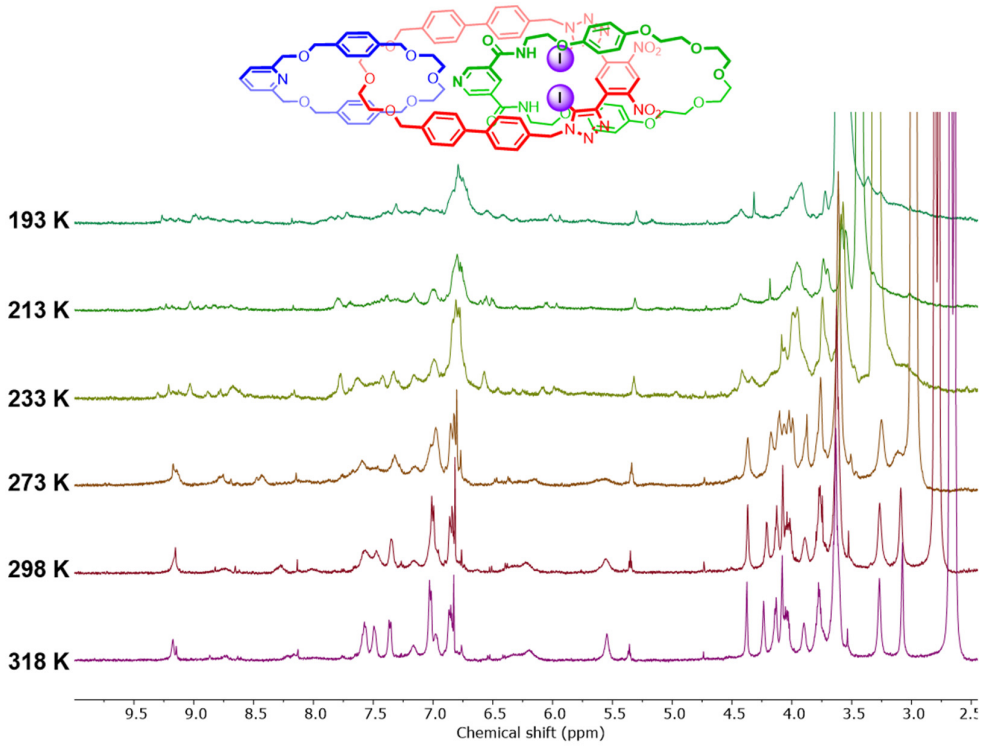


Figure 4.7. *Variable temperature ^{1}H NMR spectra of* ***4.10*** *(acetone-d_6, 500 MHz).*

It was envisaged that sodium cation binding in the interlocked cavity of the [3]catenane may "lock" the orientation of macrocycle **4.6** relative to the large central macrocycle **4.5** as an alternative means to tune the linewidths in the ^{1}H NMR spectrum of **4.10**. To this end, aliquots of $NaBAr^{F}$ were progressively added to a 1 mM solution of **4.10** in 1:1 $CDCl_3/CD_3CN$ (v/v). With increasing concentration of the sodium cation guest, notable chemical shift perturbations were observed in the ^{1}H NMR spectrum of the receptor, with a number of broad proton signals undergoing gradual splitting and sharpening (**Figure 4.8**). Qualitative analysis of these changes suggests that sodium cation binding to the receptor gives rise to a co-conformationally "locked" complex with sharp proton signals, which exists in fast exchange with the free receptor and increasingly becomes the dominant species upon addition of excess sodium ions. However, the complexity of the spectral changes precluded a quantitative determination of the sodium cation association constant of **4.10**.

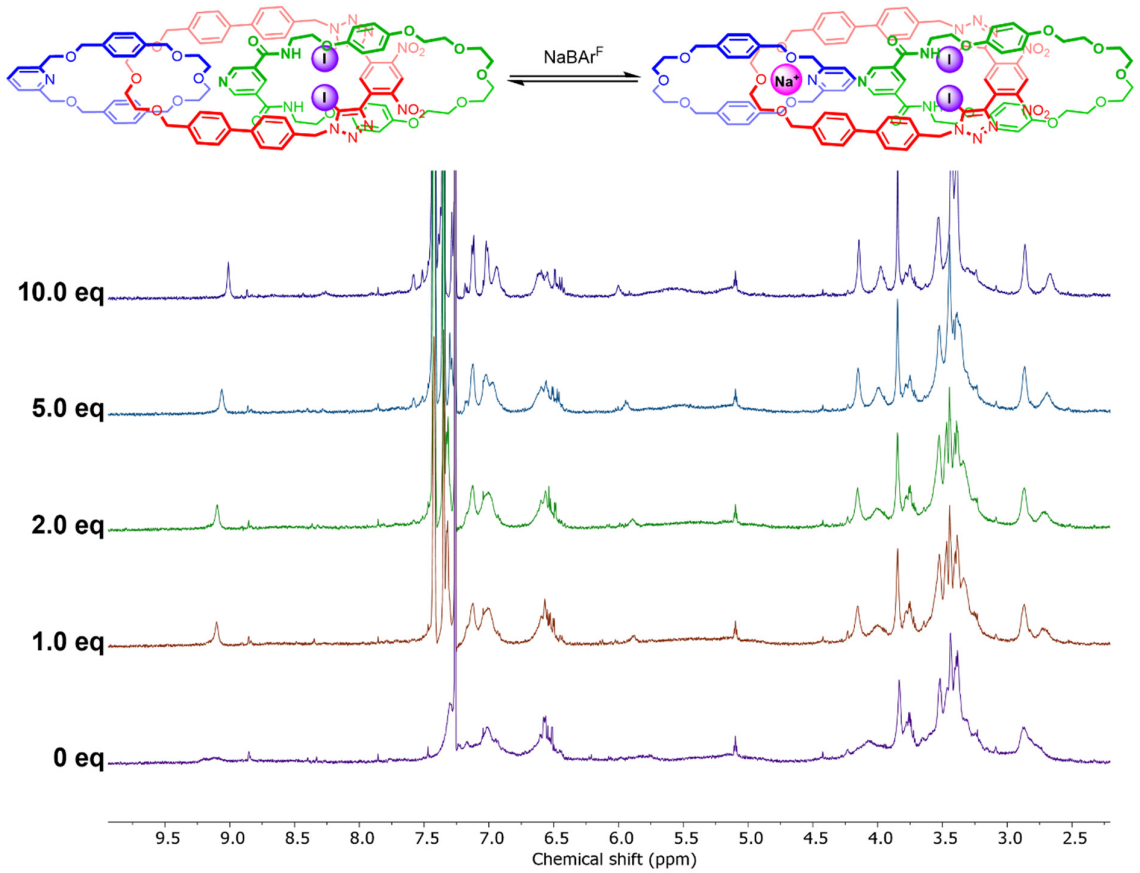


Figure 4.8. *Overlaid ^{1}H NMR titration spectra of* ***4.10*** *upon progressive addition of 10 eq. NaBAr^F (500 MHz, 1:1 $CD_3CN/CDCl_3$, 298 K).*

4.2.2.2 Single Crystal X-ray Diffraction Studies

Unequivocal evidence for the formation of a [3]catenane topology was obtained by solid-state crystallographic studies. Slow evaporation of the titration solution of **4.10** containing 10 equivalents of NaBAr^F in 1:1 $CDCl_3/CD_3CN$ led to the formation a small needle-like orange crystals suitable for analysis by SCXRD. The crystals were solved in the triclinic space group *P*-1, revealing, to our delight, the desired hetero[3]catenane bound to a sodium chloride ion pair (**Figure 4.9**). The chloride ions likely arise from the decomposition of the chloroform solvent. Importantly, the solid-state structure confirms the proposed binding mode of the charged guests, with both ions residing in their respective interlocked binding cavities; the Na^+ guest is orthogonally complexed by the di(ethylene glycol) and 2,6-dimethanolpyridine

motifs of macrocycles **4.4** and **4.5** respectively, while the Cl^- guest participates in XB and HB interactions with the bis-iodotriazole motif of **4.5** and the isophthalamide group of **3.8** respectively.

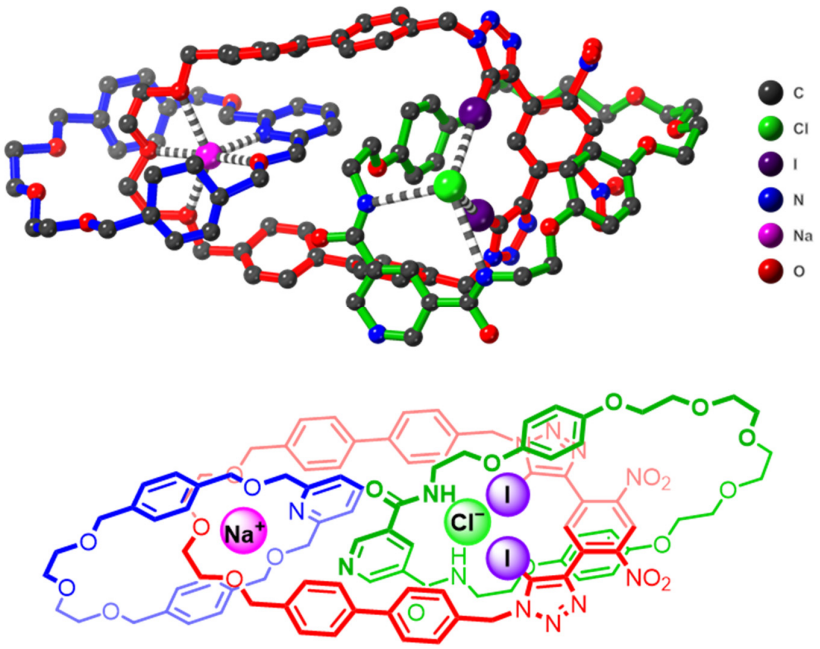


Figure 4.9. *Solid-state XRD structure of* ***4.10*** *bound to an NaCl ion-pair in a host-separated binding mode. Hydrogen atoms have been omitted for clarity. Atom colours are as follows: black (carbon), blue (nitrogen), red (oxygen), purple (iodine), pink (sodium), green (chlorine). The chemical structure of the catenane is shown below for reference.*

The demonstrated binding of a sodium chloride ion-pair by the receptor is particularly noteworthy due to the high lattice enthalpy of NaCl, which strongly favours salt recombination and precipitation over ion-pair binding. Only a few examples exist of heteroditopic receptors capable of stabilising NaCl ion pairs, and to the best of our knowledge, NaCl ion-pair binding by receptors using XB interactions as the primary anion binding interaction is unprecedented. Indeed, NaCl salt recombination in 1:1 $CDCl_3/CD_3CN$ was observed with all of the heteroditopic receptor systems described in Chapter 2, even the potent and NaX-selective hetero[2]catenane **2.3·XB^{DEG}**. The observed binding of NaCl by [3]catenane **4.10** therefore

provides promising preliminary evidence for the efficacy of using multiple interlocked binding cavities to enhance the ion-pair recognition properties of heteroditopic receptors.

4.3 Modifications to [3]Catenane Design

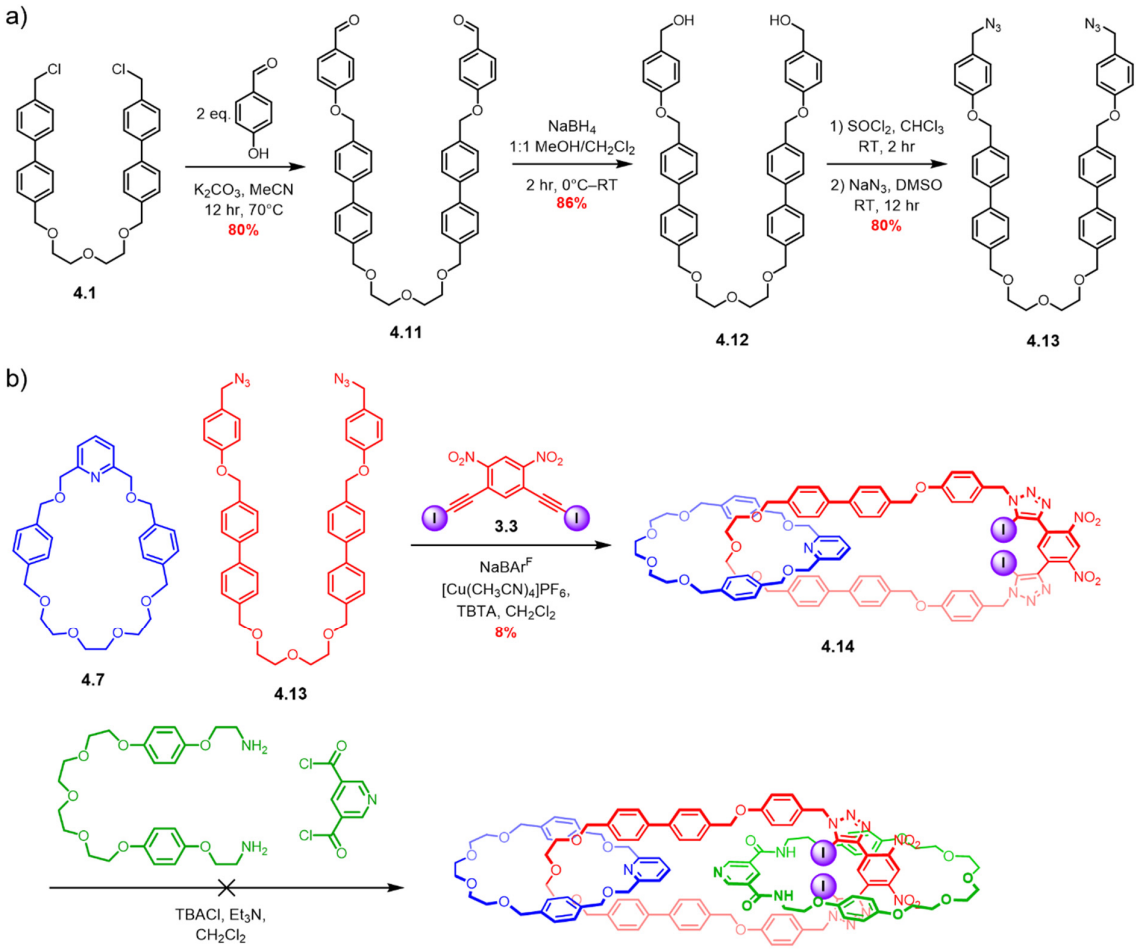
The solid-state structure determination of the NaCl ion-pair complex of [3]catenane **4.10**, which not only ascertained the formation of a [3]catenane topology, but also hinted at its superior ion-pair binding properties over analogous [2]catenanes, prompted the exploration of alternative synthetic routes to access heteroditopic [3]catenanes in improved yield and purity, with the goal of obtaining an analytically pure sample in sufficient quantities to conduct ^{1}H NMR ion-pair binding studies. Primarily this was undertaken by altering the size and chemical properties of the central macrocycle in the [3]catenane structure. Various central macrocycle designs were explored and are discussed in the following sections.

4.3.1 Expanded Central Macrocycles

As demonstrated in Stoddart's preparation of [3]- and [5]catenanes, a simple yet effective approach to improve the yield of higher order interlocked products is to increase the cavity size of the central macrocycle. With this in mind, an extended bis-azide precursor was designed containing an additional phenyl spacer between the biphenyl linkers and the terminal azide groups. To this end, the di(ethylene glycol)-based dichloride **4.1** was coupled with 2 equivalents of 4-hydroxybenzaldehyde via a Williamson ether synthesis to afford the dialdehyde **4.11** in 90% yield, which was quantitatively reduced to the diol by reaction with $NaBH_4$. Chlorination of the diol was achieved by treatment with excess $SOCl_2$ in $CHCl_3$ solution, which upon removal of the solvent in *vacuo* afforded the extended dichloride, which was immediately reacted with excess NaN_3 in DMSO solution to yield the target extended bis-azide **4.13** in quantitative yield (**Scheme 4.13a**).

With bis-azide **4.13** in hand, [2]catenane formation was undertaken via the previously described cation template-directed method, wherein a sodium cation facilitates pseudo[2]rotaxane assembly between bis-azide **4.13** and 2,6-dimethanolpyridine-containing macrocycle **4.6**, followed by a CuAAC cyclisation reaction with 4,6-dinitro-1,3-bis-iodoalkyne **3.3** (**Scheme 4.13b**). The target hetero[2]catenane **4.14** was formed in a low estimated yield of 8%, which was attributed to the increased length and flexibility of the bis-azide linker favouring oligomerisation over macrocyclization. Additionally, purification of the [2]catenane product proved to be challenging, with ^{1}H NMR analysis indicating the presence of impurities despite multiple rounds of chromatographic purification.

Nonetheless, the preparation of a [3]catenane was attempted using an impure sample of [2]catenane **4.14** via the chloride template-directed amide condensation strategy described previously (**Scheme 4.13b**). Mass spectrometric analysis of the reaction mixture revealed a small peak with an m/z value corresponding to the desired [3]catenane. However, attempts to isolate the product afforded only trace amounts of a sample that exhibited broad ^{1}H NMR proton resonances. Given that this route is synthetically more demanding than the initial synthesis, yet appears to offer no discernible advantages in reaction yield or ^{1}H NMR signal resolution, this central macrocycle design was not pursued.

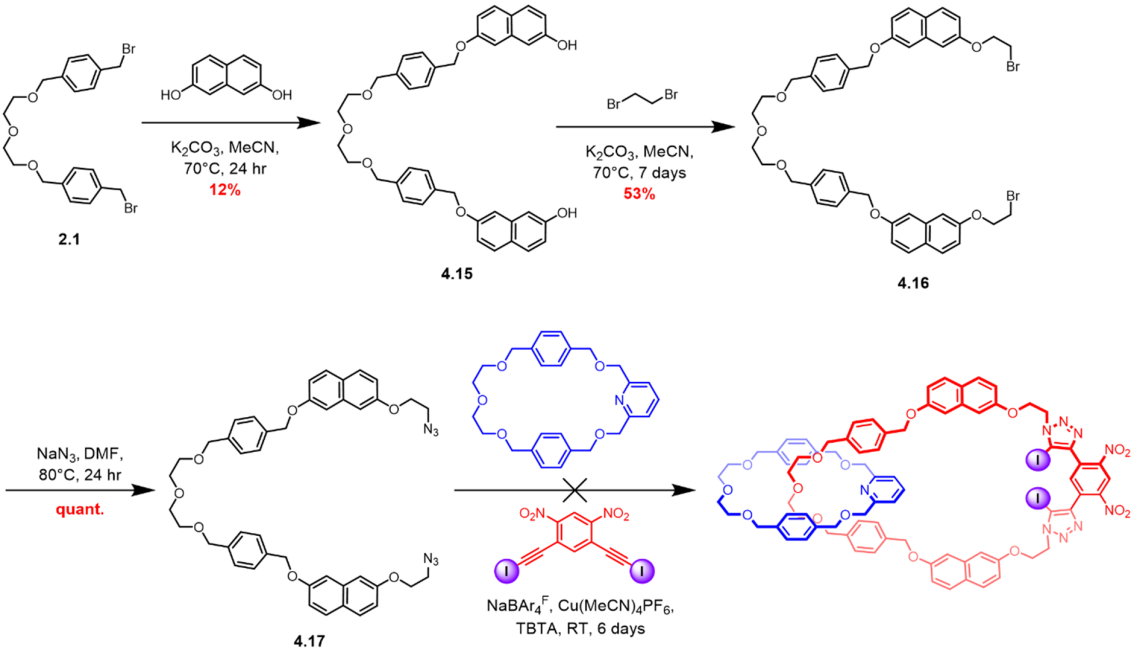


Scheme 4.13. *a) Preparation of extended bis-azide* ***4.13****; b) Attempted synthesis of a [3]catenane containing an expanded central macrocycle based on* ***4.13****.*

A related [3]catenane design features an expanded central macrocycle containing 2,7-dihydroxynaphthalene spacer units. Naphthalene units have previously been used in the synthesis of [2]catenanes for fluorescent anion sensing, wherein the naphthalene group plays the dual roles of a spacer and a chromophore.[18, 19]

The target naphthalene-functionalised bis(azide) was prepared in three steps from di(ethylene glycol)-based dibromide **2.1** (**Scheme 4.14**). A statistical Williamson ether synthesis between **2.1** and excess 2,7-dihydroxynaphthalene afforded the diol **4.15** in 12% yield, which was subsequently alkylated by reaction with excess 1,2-dibromoethane. Quantitative

azidation of the resulting dibromide **4.16** was achieved with NaN_3 in DMF solvent to obtain the bis-azide **4.17** in quantitative yield. The low yields of the intermediates **4.15** and **4.16** were attributed to the statistical nature of the alkylation reactions as well as partial oxidation of the naphthalene group. The sodium template-directed preparation of a [2]catenane was then attempted under standard CuAAC reaction conditions but proved to be unsuccessful, with only a mixture of oligomeric products obtained. These studies reiterated the challenges associated with tuning the macrocycle size in higher order catenanes, with ring-closing becoming increasingly unfavourable as the size and flexibility of the macrocycles increases.



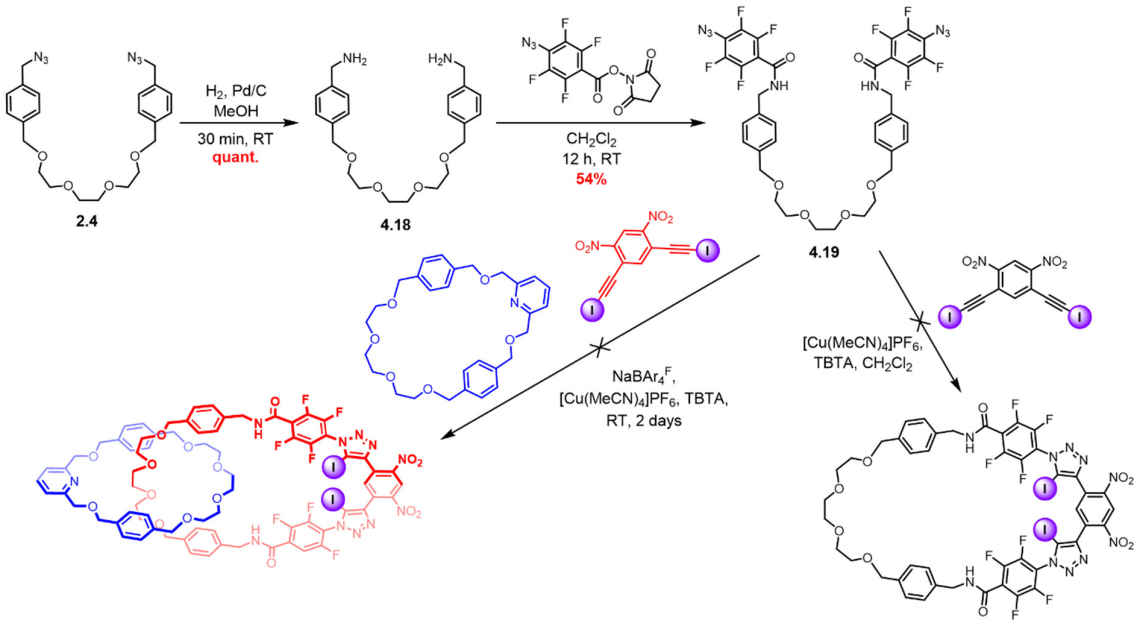
Scheme 4.14. *Attempted sodium cation template-directed synthesis of a [2]catenane using a naphthalene-functionalised bis-azide.*

4.3.2 Perfluorophenyl (PFP)-functionalised Central Macrocycles

An alternative approach to increase the yield of the anion template-directed [3]catenane formation reaction is to enhance the anion binding potency of the bis-iodotriazole motif through the covalent attachment of additional electron-withdrawing groups. To this end, a perfluorophenyl-functionalised bis-azide was sought which could conceivably undergo a

CuAAC reaction with the 4,6-dinitro-1,3-bis-iodoalkyne to give a highly activated XB donor motif.

The target PFP-functionalised bis-azide was prepared by Pd/C catalysed hydrogenation of bis-azide **2.4** under a strictly controlled reaction time of 30 minutes to afford bis-amine **4.18**. An amide coupling reaction between **4.18** and an activated *N*-hydroxysuccinimide ester derivative of 4-azido-2,3,5,6-tetrafluorobenzoic acid afforded the target bis-azide **4.19** in 54% yield. Unfortunately, however, attempts to form a hetero[2]catenane via a sodium template-directed route were unsuccessful, with degradation of the amide-linked PFP-functionalised compounds observed during preparative TLC purification (**Scheme 4.15**).

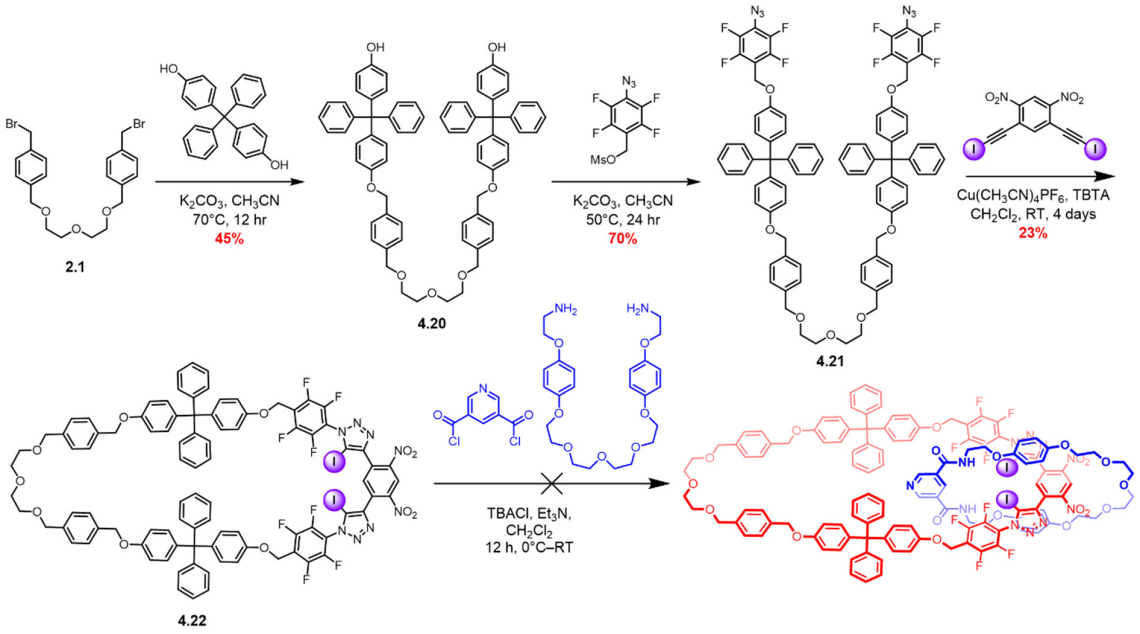


Scheme 4.15. *Attempted sodium cation template-directed [2]catenane synthesis using a PFP-functionalised bis-azide.*

An alternative PFP-functionalised central macrocycle containing a terphenyl spacer was explored. The inclusion of rigid tetrahedral terphenyl spacers has previously been shown to promote ring-closing of large macrocycles.[15] The steric bulk of this group may also serve to spatially separate the two peripheral macrocycles in the [3]catenane, thereby limiting the

potential interference from the first threaded macrocycle during the second anion template-directed mechanical bond formation reaction. However, a drawback of this design is that the bulky terphenyl linkers prevent sodium-directed threading of the bis-azide through the cavity of the 2,6-dimethanolpyridine functionalised macrocycles. Therefore, a less elegant synthetic approach was adopted, requiring first the preparation of a non-interlocked central macrocycle via a CuAAC clipping reaction with a bis-iodoalkyne, before sequentially attempting anion- and cation template-directed catenane formation.

The desired bis-azide **4.21** was prepared via a two-step route involving statistical Williamson ether synthesis followed by alkylation of the pendant diols. Pleasingly, the ether linked PFP moieties appeared to be more stable to chromatographic purification than the previously-employed amide linkage, giving the desired large central macrocycle **4.22** in 23% yield. However, attempts to form a [2]catenane via chloride template-directed synthesis yielded no interlocked product, with the only new species isolated being the non-interlocked isophthalamide-functionalised HB macrocycle **3.8**. This could be due to the terphenyl groups obstructing access to the bis-iodotriazole anion binding motif, as suggested by preliminary modelling studies (**Scheme 4.16**).

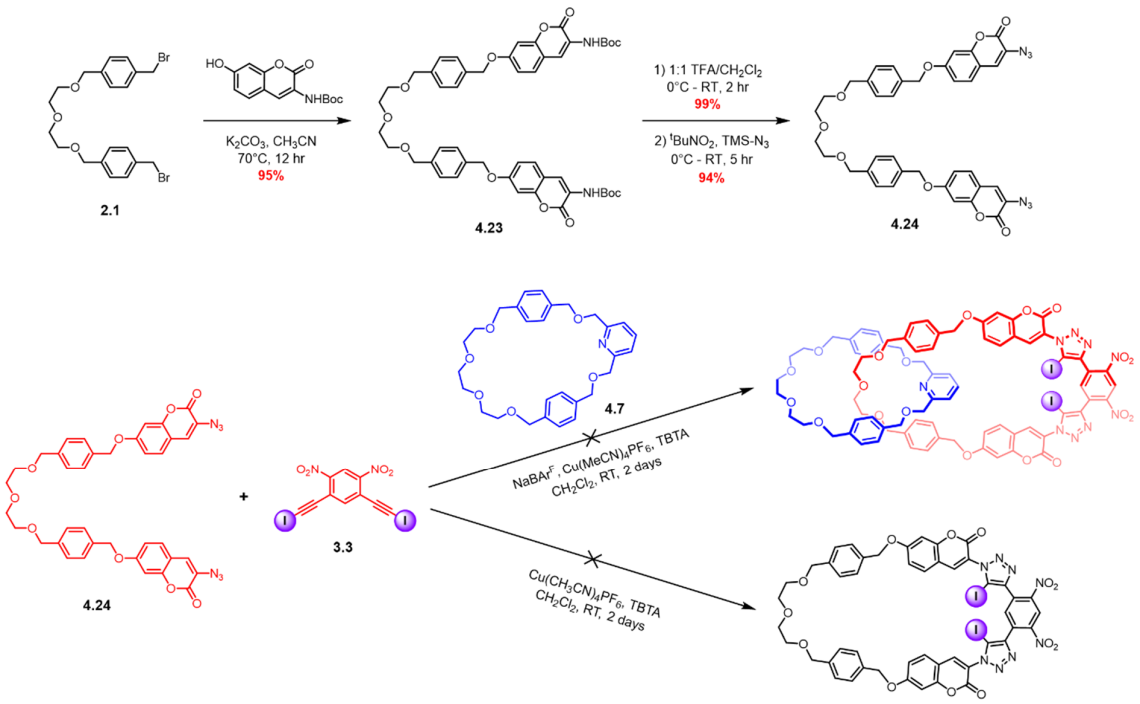


***Scheme 4.16**. Attempted chloride anion template-directed [2]catenane synthesis using terphenyl-containing macrocycle.*

4.3.3 A Coumarin-containing Central Macrocycle

The incorporation of coumarin fluorophores as spacer units in the central macrocycle was explored as a strategy to simultaneously increase the size and the anion binding potency of the central macrocycle. Given the electron-deficient nature of coumarin, it was anticipated that the direct covalent attachment of these groups to the iodotriazole binding groups would enhance the potency of the XB donor motif in a manner analogous to the above-described dinitrobenzene and PFP moieties. The rigidity of the coumarin spacer also serves as a way to increase the size of the macrocycle without a concomitant increase in the number of rotatable bonds present. Additionally, the incorporation of a bright fluorophore like coumarin, which has previously been used in the development of optical anion sensors,[20] opens up the possibilities of studying the binding properties of the hosts by fluorescence titrations, which can be performed at much lower concentrations than ^{1}H NMR titration experiments.

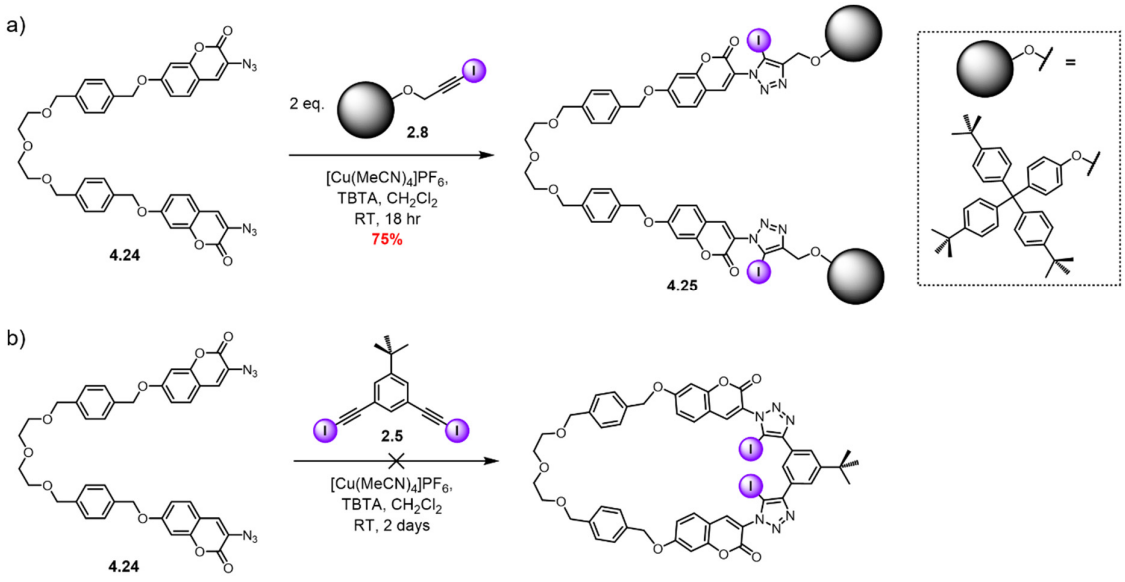
The coumarin bis-azide was synthesised in excellent yields over three steps. The reaction of dibromide **2.1** with a Boc-protected coumarin derivative in the presence of K_2CO_3 afforded bis-coumarin **4.23** in 95% yield. The Boc group was deprotected using TFA to give the bis-amine, which was immediately treated with $^tBu\text{-}NO_2$ and $TMS\text{-}N_3$ to afford the target bis-azide **4.24**. However, attempts to either prepare the non-interlocked macrocycle or perform sodium template-directed [2]catenane formation via a CuAAC reaction with 4,6-dinitro-1,3-bis-iodoalkyne were both unsuccessful, despite stirring the reaction mixtures for an extended period of time and increasing the loading of the Cu(I) catalyst. In both cases, a significant amount of the bis-iodoalkyne was recovered, while the azide appeared to have degraded into a mixture of highly polar and poorly-separated species (**Scheme 4.17**).



Scheme 4.17. *Attempted macrocycle and sodium cation template-directed [2]catenane synthesis using a coumarin-functionalised bis-azide.*

A series of control experiments were conducted to determine the reasons for the failure to obtain any macrocyclic or interlocked products. To firstly establish that the bis(coumarin

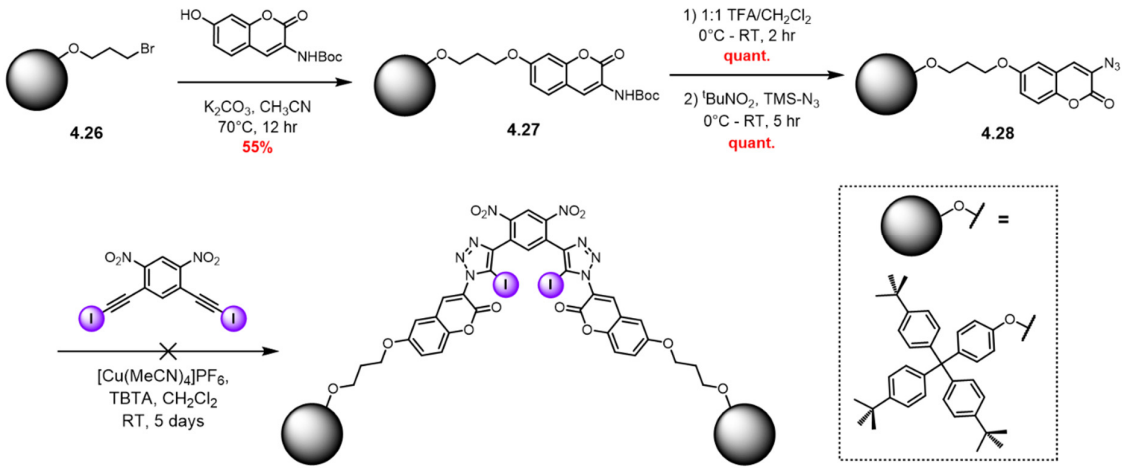
azide) **4.24** is capable of undergoing CuAAC reactions with iodoalkynes, **4.24** was reacted with two equivalents of iodoalkyne stopper in the presence of catalytic $[Cu(MeCN)_4]PF_6$ and TBTA ligand, which afforded the bis-iodotriazole **4.25** in 75% yield (**Scheme 4.18a**). In contrast, attempts to form an XB macrocycle via a CuAAC reaction between **4.24** and *tert*-butyl-functionalised bis-iodoalkyne **2.5** under high dilution conditions led to the formation of a highly polar mixture of oligomers, suggesting that macrocycle formation may be prohibited by severe ring strain in the target macrocycle (**Scheme 4.18b**).



Scheme 4.18. *Investigating the reactivity of the bis(coumarin-azide)* ***4.24****. a) CuAAC-mediated reaction of* ***4.24*** *with 2 equivalents of iodoalkyne stopper* ***2.8****; b) Attempted CuAAC-mediated macrocycle formation between* ***4.24*** *and bis-iodoalkyne* ***2.5****.*

Given the conformational restrictions associated with macrocycle formation, we turned our attention to exploiting coumarin motifs in the development of neutral anion sensing rotaxanes. To this end, a mono-coumarin azide stopper **4.28** was prepared via an analogous synthetic route and subjected to a click reaction with 4,6-dinitro-1,3-bis-iodoalkyne in an attempt to prepare a bis-coumarin-functionalised XB axle (**Scheme 4.19**). However, the desired product was not detected by mass spectrometric analysis of the reaction mixture, with TLC

analysis indicating degradation of the coumarin azide stopper. These results suggest that the electron-deficient azide and alkyne coupling partners are incompatible under CuAAC reaction conditions, although further investigation is required to understand the processes leading to degradation of the coumarin azide.



Scheme 4.19. *Attempted preparation of a coumarin-functionalised axle for anion template-directed [2]rotaxane synthesis.*

4.4 Conclusions and Future Work

In this chapter, the use of orthogonal cation and anion template directed methodologies was investigated as a novel approach to prepare heteroditopic [3]catenanes for potent ion-pair recognition. Cation template-directed [2]catenane formation was achieved by exploiting the sodium cation-directed assembly of a pseudo[2]rotaxane complex between a 2,6-dimethanolpyridine-containing macrocycle **4.6** and an extended bis-azide **4.4**, which underwent a CuAAC ring closing reaction with bis-iodoalkyne **3.3** to form the first mechanical bond and a potent dinitro-functionalised bis-iodotriazole XB motif in the same step. The strong chloride binding affinity of this XB motif was utilised in a second mechanical bond forming step to generate the target [3]catenane **4.10.** Although the low yield, challenging purification and poor spectra resolution of the product precluded quantitative ^{1}H NMR ion-pair binding

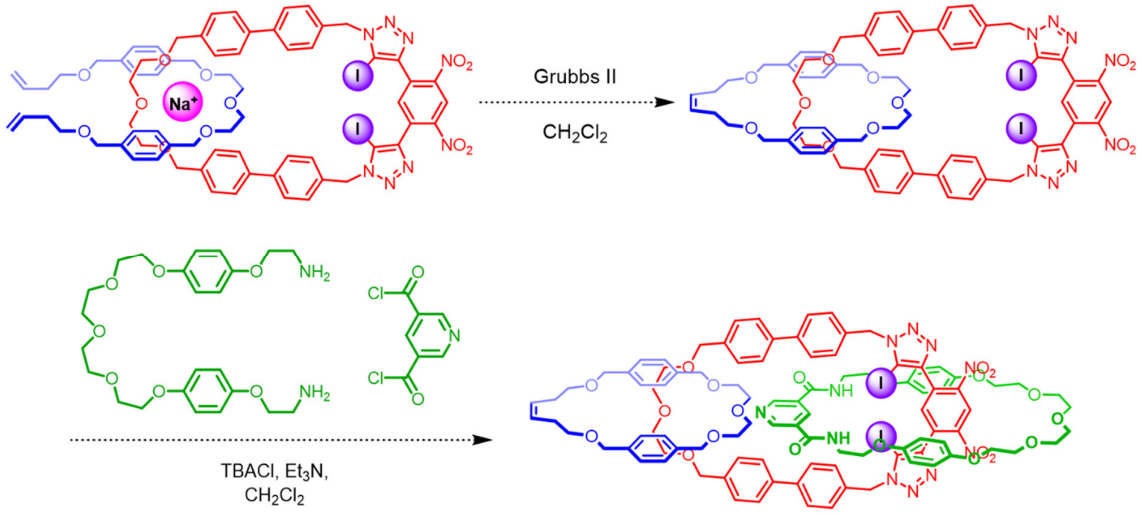
studies, a promising solid-state crystallographic investigation suggested the heteroditopic [3]catenane was capable of stabilising NaCl ion-pairs, a notoriously difficult feat given the high lattice enthalpy of this salt.

Attempts to prepare heteroditopic [3]catenane derivatives in improved yields and purity resulted in an extensive synthetic investigation into the effects of altering the size and chemical properties of the catenane's central macrocycle component. Efforts to increase the cavity size of the macrocycle as well as the anion binding potency of the bis-iodotriazole motif were undertaken via the incorporation of various spacer groups. However, these efforts were thwarted by the low yields of the intermediate [2]catenane, which highlights the need to develop ring-closing procedures that allow more efficient translation of the cation and anion template-directed pseudorotaxane complexes into mechanically bonded products.

4.4.1 Future Work

Future work on this project would focus on developing synthetic strategies capable of generating a heteroditopic [3]catenane in sufficient yields to enable quantitative determination of its ion-pair binding properties by ^{1}H NMR titration studies. One possible approach involves the use of Grubbs' catalysed olefin ring closing metathesis (RCM) to facilitate cyclisation, which has the advantage of being an intramolecular process. One proposed synthetic route involves first the formation of the central XB macrocycle **4.5**, which has been achieved in 40% yield via a CuAAC reaction between bis-azide **4.3** and iodoalkyne **3.3**. This will be followed by sodium cation directed threading of an acyclic di(ethylene glycol)-containing bis-alkene through the macrocycle cavity, which could undergo Grubbs' catalysed RCM to form the [2]catenane intermediate compound. Finally, a subsequent chloride template-directed amide condensation step would conceivably generate the target heteroditopic [3]catenane. Although this approach requires an additional reaction step, the [2]catenane formation step no longer

relies on the challenging CuAAC-mediated intermolecular clipping reaction between a bis-iodoalkyne and an extended flexible bis-azide precursor, which may lead to an overall improvement in the yield of the desired catenane (**Scheme 4.20**).



Scheme 4.20. *Proposed sequential cation and anion template-directed synthesis of a heteroditopic [3]catenane using an olefin metathesis reaction in the first mechanical bond forming step.*

4.5 References for Chapter 4

1. H. Y. Au-Yeung, C.-C. Yee, A. W. Hung Ng and K. Hu, *Inorg. Chem.*, 2018, **57**, 3475-3485.
2. D. A. Leigh, J. K. Y. Wong, F. Dehez and F. Zerbetto, *Nature*, 2003, **424**, 174-179.
3. J. P. Sauvage and J. Weiss, *J. Am. Chem. Soc.*, 1985, **107**, 6108-6110.
4. C. O. Dietrich-Buchecker, C. Hemmert, A. K. Khemiss and J. P. Sauvage, *J. Am. Chem. Soc.*, 1990, **112**, 8002-8008.
5. F. Bitsch, C. O. Dietrich-Buchecker, A. K. Khemiss, J. P. Sauvage and A. Van Dorsselaer, *J. Am. Chem. Soc.*, 1991, **113**, 4023-4025.
6. P. R. Ashton, C. L. Brown, E. J. T. Chrystal, T. T. Goodnow, A. E. Kaifer, K. P. Parry, A. M. Z. Slawin, N. Spencer, J. F. Stoddart and D. J. Williams, *Angew. Chem. Int. Ed. Engl.*, 1991, **30**, 1039-1042.
7. A. L. Hubbard, G. J. E. Davidson, R. H. Patel, J. A. Wisner and S. J. Loeb, *Chem. Commun.*, 2004, 138-139.
8. A. Hori, K. Kumazawa, T. Kusukawa, D. K. Chand, M. Fujita, S. Sakamoto and K. Yamaguchi, *Chem. Eur. J.*, 2001, **7**, 4142-4149.
9. F. B. L. Cougnon, N. A. Jenkins, G. D. Pantoş and J. K. M. Sanders, *Angew. Chem. Int. Ed.*, 2012, **51**, 1443-1447.
10. M. J. Langton, J. D. Matichak, A. L. Thompson and H. L. Anderson, *Chem. Sci.*, 2011, **2**, 1897-1901.
11. S. Li, J. Huang, F. Zhou, T. R. Cook, X. Yan, Y. Ye, B. Zhu, B. Zheng and P. J. Stang, *J. Am. Chem. Soc.*, 2014, **136**, 5908-5911.
12. D. B. Amabilino, P. R. Ashton, A. S. Reder, N. Spencer and J. F. Stoddart, *Angew. Chem. Int. Ed. Engl.*, 1994, **33**, 1286-1290.

13. H. Iwamoto, S. Tafuku, Y. Sato, W. Takizawa, W. Katagiri, E. Tayama, E. Hasegawa, Y. Fukazawa and T. Haino, *Chem. Commun.*, 2016, **52**, 319-322.
14. K. Wang, C.-C. Yee and H. Y. Au-Yeung, *Chem. Sci.*, 2016, **7**, 2787-2792.
15. T. A. Barendt, L. Ferreira, I. Marques, V. Félix and P. D. Beer, *J. Am. Chem. Soc.*, 2017, **139**, 9026-9037.
16. C.-Y. Chen, H.-C. Xu, T.-H. Ho, C.-J. Hsu, C.-C. Lai, Y.-H. Liu, S.-M. Peng and S.-H. Chiu, *J. Org. Chem.*, 2021, **86**, 13491-13502.
17. Y.-H. Lin, C.-C. Lai and S.-H. Chiu, *Org. Biomol. Chem.*, 2014, **12**, 2907-2917.
18. A. Caballero, F. Zapata, N. G. White, P. J. Costa, V. Félix and P. D. Beer, *Angew. Chem. Int. Ed.*, 2012, **51**, 1876-1880.
19. J. M. Mercurio, A. Caballero, J. Cookson and P. D. Beer, *RSC Adv.*, 2015, **20**, 9298-9306.
20. E. J. Mitchell, A. J. Beecroft, J. Martin, S. Thompson, I. Marques, V. Félix and P. D. Beer, *Angew. Chem. Int. Ed.*, 2021, **60**, 24048-24053.

CHAPTER 5

Conclusions

Chapter 5: Conclusions

The work presented in this thesis seeks to develop novel template-directed methodologies to prepare functional mechanically interlocked host molecules capable of strong and selective ion recognition. In particular, the integration of halogen bonding (XB) donor motifs into the host architectures was targeted as a means to tune their anion binding affinity and selectivity profiles.

In Chapter 2, the ion-pair binding properties of a family of heteroditopic XB catenanes and rotaxanes, prepared via an alkali metal cation template-directed approach, are discussed (**Figure 5.1**). Extensive quantitative ^{1}H NMR titration studies with alkali metal cations, halide anions and their respective ion-pairs enabled elucidation of the effects of cavity size, binding motifs and host topology on the ion recognition properties of the receptors, in particular the degree of positive cooperativity associated with ion-pair binding.

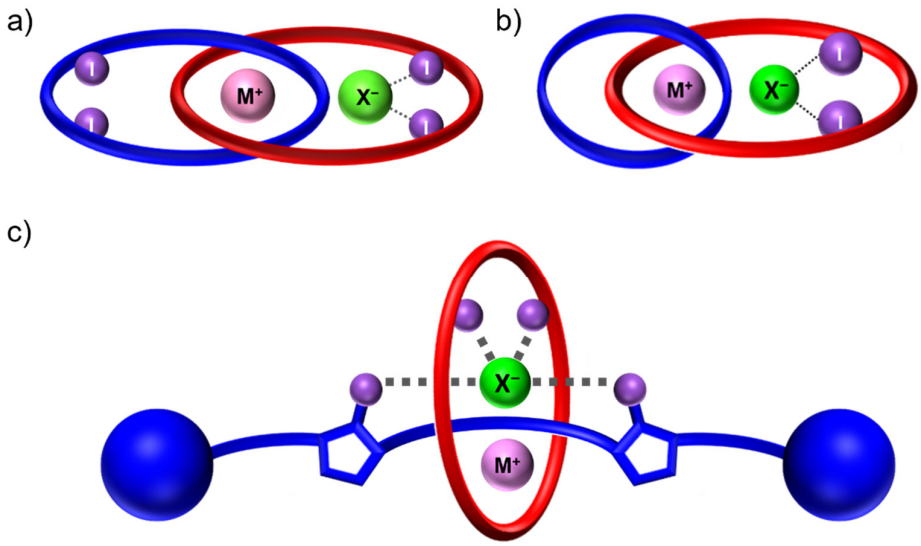


Figure 5.1. *Cartoon representations of the neutral heteroditopic (a) homo[2]catenane; (b) hetero[2]catenane; (c) [2]rotaxane host molecules for ion-pair recognition, discussed in Chapter 2.*

An alkali metal cation template-directed approach was initially employed to prepare a series of unprecedented neutral XB heteroditopic homo[2]catenanes, comprising oligo(ethylene glycol) motifs for alkali metal cation binding and XB donor motifs for anion recognition (**Figure 5.1a**). ^{1}H NMR binding studies revealed the relatively weak halide anion affinities of the catenanes were significantly enhanced by pre-complexation of an alkali metal cation, highlighting evidence for the favourable proximal cooperative electrostatic effects that operate during ion-pair recognition. An unexpected switch from a 1:1 to a 1:2 host-anion binding stoichiometry was observed in the sodium complex of the smaller homo[2]catenane, which was attributed to the formation of an additional contact ion-pair between the anion and the coordinatively-unsaturated metal centre. This constitutes an unusual example of an ion-pair receptor in which the binding stoichiometry of the anion can be indirectly modulated by changing the size of the cation binding site, which may be valuable in informing the considered design of future multicomponent interlocked receptors for ion-pairs.

Building on these initial studies, a hetero[2]catenane ion-pair host system was developed containing a more potent bis-di(ethylene glycol) cation binding site (**Figure 5.1b**). ^{1}H NMR cation binding studies revealed a dramatic enhancement in sodium and potassium alkali metal cation affinity relative to the homo[2]catenane systems, as well as considerable sodium over potassium selectivity. Ion-pair titrations showed strong binding of alkali metal halide salts with significant cooperativity between the cation and anion binding events, reflected in a significant ‘switch-on’ of the catenane’s anion affinity upon pre-complexation with a metal cation. Importantly, the catenane was found to bind sodium halide salts 3-5 times more strongly than the corresponding potassium halide salts. Solid-liquid extraction studies highlighted the capability of the catenane to function as an alkali metal halide salt extractant, in which the observed selectivity preference for NaX over KX ion-pair binding in solution-

state NMR studies impressively translated to superior extraction of sodium halide salts from a competitive solid mixture of NaX/KX salts.

Motivated by the promising ion-pair binding properties of the catenanes, their XB heteroditopic [2]rotaxane analogues were investigated by performing a stoppering-type reaction of the intermediate pseudo[2]rotaxane assembly with sterically encumbering terphenyl groups (**Figure 5.1c**). The co-conformations of the rotaxanes in the absence and presence of charged guests were investigated by ^{1}H NMR studies, revealing translocation of the macrocycle towards the central ethylene glycol stations upon alkali metal cation complexation. Comparing the apparent alkali metal cation iodide ion-pair binding K_{app} values of the [2]rotaxanes and the [2]catenane analogues revealed a notably higher degree of positive cooperativity between cation and anion binding events in the rotaxane topology, highlighting the advantages of greater mechanical bond co-conformational flexibility in the design of future multi-topic interlocked receptors.

In Chapter 3, the exceptionally strong XB···anion interactions between activated XB donor motifs and a discrete chloride anion were utilised to prepare neutral interlocked host molecules for anion recognition, transport and sensing (**Figure 5.2**).

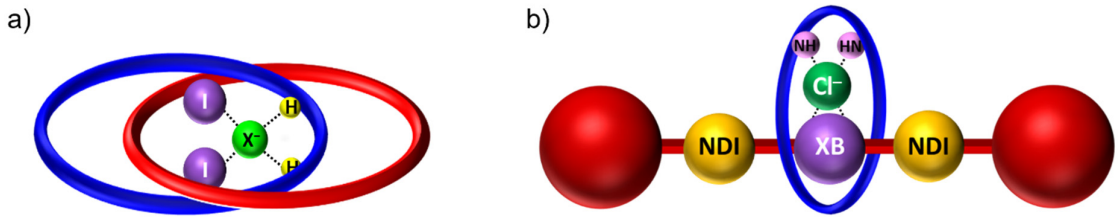


Figure 5.2. *Cartoon representations of the neutral XB (a) [2]catenane; (b) [2]rotaxane host molecules for anion recognition, discussed in Chapter 3.*

A novel 4,6-dinitro-1,3-bis-iodotriazole XB donor motif was exploited to facilitate an anion template-directed catenane formation reaction, in which a chloride ion simultaneously

coordinates the XB macrocycle and a bis(amine) to form a complex containing orthogonal HB···Cl^- and XB···Cl^- interactions. Introduction of a reactive bis-acid chloride such as 3,5-bis-chlorocarbonyl pyridine facilitated an amide condensation cyclisation reaction to afford the target hetero[2]catenanes (**Figure 5.2a**). ^{1}H NMR anion binding studies revealed a marked enhancement in chloride and bromide affinities relative to the constituent XB macrocycle, attributed to the formation of convergent XB···anion and HB···anion interactions within the interlocked cavity. Importantly, the catenane exhibited a preference for binding bromide over iodide in 95:5 acetone-d_6/D_2O, and no binding of nitrate, highlighting the potential of exploiting the interlocked cavity to achieve anti-Hofmeister anion binding behaviour. Transmembrane anion transport studies conducted in POPC LUVs revealed that the neutral catenanes were effective anion transporters, out-performing their macrocyclic components, representing, to the best of our knowledge, the first catenane-based anionophore. Importantly, the intrinsic anion binding selectivity of the interlocked host cavity was directly translated into the observed anion transport selectivity trend, resulting in catenane anionophores with high halide over hydroxide and nitrate selectivity, which is particularly critical for potential therapeutic applications.

The halide size-dependence of the binding modes exhibited by interlocked hosts synthesised using this anion template-directed method was further exploited to design a 3-station [2]rotaxane for chloride-selective optical sensing in aqueous-acetone solvent mixtures (**Figure 5.2b**). 1D and 2D ^{1}H NMR analysis of the rotaxane suggested a co-conformation in which the macrocycle resides preferentially at the axle NDI stations, which is driven by the formation of intercomponent NDI-hydroquinone aromatic donor-acceptor charge transfer interactions. ^{1}H NMR anion binding studies with various halides reveals that chloride binding to the [2]rotaxane occurs via an endotopic binding mode, which is accompanied by macrocycle

translocation to the central XB station. This co-conformational change induced by chloride binding led to an optical chemo-sensing response corresponding to a significant reduction in the intensity of the charge transfer absorption band. Crucially, no significant changes in the UV-vis spectrum were observed upon addition of bromide or iodide, which are too large to fit in the binding cavity. This work serves as a proof-of-concept of using the inherent dynamism of mechanically bonded systems to achieve selective optical sensing of a target ion over other chemically similar guest species.

In Chapter 4, attention turned to the ambitious goal of integrating the cation and anion template-directed methodologies to prepare a heteroditopic [3]catenane (**Figure 5.3**). The target [3]catenane would possess interlocked binding cavities for both cationic and anionic guests, and is expected to display highly potent and selective ion-pair recognition. Various [3]catenane host designs were explored, amongst which the use of an expanded biphenyl-containing macrocycle was found to successfully generate a [3]catenane product. Solid state crystallographic studies of the [3]catenane promisingly indicated its ability to bind an NaCl ion-pair in a host-separated binding mode wherein each guest ion is encapsulated in an interlocked binding cavity. Future work on this project involves optimising the synthesis and purification of the product to facilitate solution state ^{1}H NMR ion-pair binding studies.

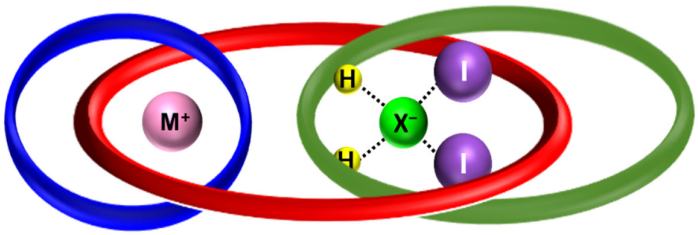


Figure 5.3. *Cartoon representation of the heteroditopic [3]catenane discussed in Chapter 4.*

In summary, the results of this thesis demonstrate the efficacy of combining mechanically bonded architectures with halogen bonding donor motifs to achieve strong and selective recognition of target guest ions. Exploiting size complementarity between the interlocked binding cavity and the target cation or anion guest proved to be a powerful strategy to modulate both the affinity and selectivity profiles of the MIM hosts, allowing discrimination between chemically-similar alkali metal cations or halide anions. The inherent dynamic nature of interlocked molecules also facilitates large-amplitude co-conformational changes in response to guest binding, which holds considerable promise as a means to introduce additional sensing and switching functionality into the host molecules. These findings demonstrate the considerable potential of exploiting the unique topology and dynamic nature of mechanically interlocked architectures to develop novel host molecules capable of ion recognition, sensing, transport and extraction. Future progress in this field would involve the development of synthetic strategies to prepare complex interlocked host assemblies capable of displaying increasingly sophisticated responses to ion binding.

CHAPTER 6

Experimental

Chapter 6: Experimental

6.1 General Considerations

6.1.1 Chemicals and Solvents

All solvents and reagents used in this thesis were purchased from commercial suppliers and used as received unless otherwise stated. Dry organic solvents were degassed by purging with nitrogen and dehydrated by passing through an MBraun MPSP-800 column. Water was deionised and micro-filtered using a Milli-Q® Millipore machine. TBA salts and $[Cu(MeCN)_4]PF_6$ were stored in vacuum desiccators containing anhydrous P_2O_5 powder in between usage. TBTA was synthesised according to a reported procedure[1] and stored at room temperature. Et_3N was distilled from KOH and stored over the same base prior to use. Ratios of solvent mixtures are reported by volume. Brine refers to a saturated aqueous solution of NaCl, and basic EDTA (aq.) refers to an aqueous solution of 0.02 M EDTA with 1% NH_3 (28–30%) solution. Thin layer chromatography (TLC) analysis was performed using Merck silica Kieselgel 60 F254 0.25 mm plates, with spots visualised under UV light (254 nm) and/or staining with basic $KMnO_4$ solution/iodine vapour. Column chromatography was carried out on Merck silica gel 60 under a positive pressure of nitrogen, and preparative TLC was performed on 20 × 20 cm plates with a silica layer of thickness 1 mm. Microwave-assisted reactions were performed in a Biotage Initiator 2.0 reactor using sealed standard Biotage pyrex-glass microwave vials.

6.1.2 Instrumentation

NMR spectra for the nuclei ^{1}H and ^{13}C were recorded on Bruker Avance III 400 HD nanobay NMR machines (Hg400 and Venus400) each equipped with a 9.4 T magnet, or Bruker Avance III 500 HD NMR machine (AVD500) equipped with a 11.75 T magnet, or Bruker Avance

NMR machine (AVC500) equipped with a 11.75 T magnet and a ^{13}C detect cryoprobe, or Bruker NEO 600 with broadband helium cryoprobe. All chemical shifts are reported in part per million (ppm) with signals splitting denoted as singlet (s), broad singlet (brs), doublet (d), triplet (t), quartet (q), quintet (quint.), septet (sept.) and multiplet (m). ^{1}H and ^{13}C NMR spectra are calibrated to the residual solvent peak, or to the solvent with the higher number of deuterium atoms for mixed solvent systems, and are assigned with aid from 2D NMR spectroscopies including COSY and ROESY. Low resolution ESI mass spectra were recorded on a Waters LCT Premier XE bench-top orthogonal acceleration time-of-flight LC-MS system. High resolution ESI spectra were recorded on a Bruker micrOTOF spectrometer. Tandem ESI mass spectra were recorded on a Xevo G2-S mass spectrometer with a collision energy of 40 V. UV–visible absorption spectra were recorded on a V-770 UV-Visible/NIR Spectrophotometer equipped with a Peltier temperature controller, using quartz cuvettes of 1 cm path length.

6.1.3 ^{1}H NMR Titration Protocol

^{1}H NMR titration experiments were performed on a Bruker Avance III NMR 500 MHz spectrometer (AVD500) at 298 K. In a typical experiment, aliquots of a 50 mM stock solution containing the guest ion were added to 0.5 mL of a 1.0 mM host solution, where 1.0 equivalent of guest ion added corresponds to 10.0 μL of the stock solution. The samples were thoroughly mixed before recording the ^{1}H NMR spectra. 17 data points corresponding to 0.0, 0.2, 0.4, 0.6, 0.8, 1.0, 1.2, 1.4, 1.6, 1.8, 2.0, 2.5, 3.0, 4.0, 5.0, 7.0 and 10.0 equivalents of added charged guest were obtained. The binding of charged guest with all hosts were found to be fast on the NMR timescale. Stability constants were determined using Bindfit[2] software, employing a 1:1 host-guest stoichiometric binding model unless otherwise specified.

6.1.4 Solid-liquid Extraction Protocol

In a typical SLE experiment, an excess of a solid alkali metal salt (MX, where M = Na, K; X = Cl, Br, I) was added to 1.0 mM a solution of the receptor in $CDCl_3$ (700 μL) and the mixture was vigorously sonicated for 20 min. The excess salt was subsequently removed by filtration through a syringe filter. A post-extraction ^1H NMR spectrum of the filtrate was collected using a Bruker AVIII 500 MHz spectrometer at 298 K and compared to the pre-extraction ^1H NMR spectrum.

6.1.5 Optical Studies

The UV-visible spectroscopic studies reported in Chapter 3 were recorded using a V-770 UV-Visible/NIR Spectrophotometer equipped with a Peltier temperature controller, using quartz cuvettes of 1 cm path length. Experiments were conducted at 25 °C unless otherwise stated. The receptor was dissolved in 2.5% H_2O/acetone at a concentration of 0.25 mM. The TBA salt of the anionic guest was dissolved in the stock solution at a concentration of 25 mM. The UV-vis spectrum of the host solution (0.5 mL) was recorded between 400-650 nm. Subsequently, a single aliquot of the guest solution (0.2 mL, 20 equivalents of guest) was added to the host solution. The sample was mixed and the UV-visible spectra recorded. The process was repeated for each guest anion.

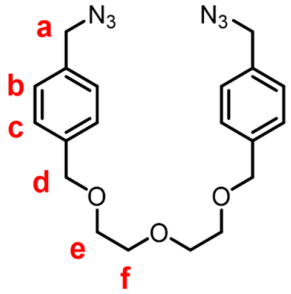
6.2 Synthesis and Characterisation of Novel Compounds

6.2.1 Compounds from Chapter 2

The dibromides **2.1** and **2.2**,[3] bis-alkynes **2.5** and **2.6**,[4] alkali metal salts $NaBAr^F$ and $KBAr^F$,[5] macrocycle **2.7**,[6] and stopper alkynes **2.8**[7] and **2.9**[8] were prepared according to previous literature reports.

General Procedure 2A: Conversion of Dibromides to Bis-azides

Diethylene glycol-based bis-azide (2.3)



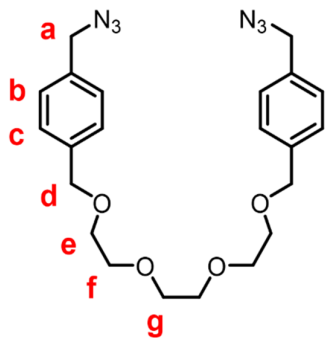
Dibromide **2.1** (1.38 g, 2.92 mmol) was dissolved in DMSO (18 mL). Sodium azide (0.76 g, 11.69 mmol) was added and the reaction mixture was stirred at room temperature overnight. The crude reaction mixture was diluted with H_2O (50 mL) and extracted with diethyl ether (30 mL × 3). The combined organic layer was washed with brine (30 mL × 3), dried over anhydrous $MgSO_4$, filtered and concentrated in vacuo to afford **2.3** as a yellow oil (1.16 g, quant.).

^{1}H NMR (500 MHz, $CDCl_3$) δ 7.40 – 7.34 (m, 4H, H_b), 7.30 – 7.27 (m, 4H, H_c), 4.58 (s, 4H, H_a), 4.32 (s, 4H, H_d), 3.75 – 3.60 (m, 8H, $H_{e,f}$).

^{13}C NMR (126 MHz, $CDCl_3$) δ 138.70, 134.78, 128.43, 128.27, 72.98, 70.86, 69.76, 54.69.

HRMS (ESI +ve) m/z: 419.1793 ($[M+Na]^+$, $C_{20}H_{24}O_3N_6Na$ requires 419.1802).

Triethylene glycol-based bis-azide (2.4)



Following general procedure 2A, the reaction of dibromide **2.2** (2.59 g, 5.01 mmol) and sodium azide (1.30 g, 20.1 mmol) yielded the desired product as a yellow oil (2.19 g, quant).

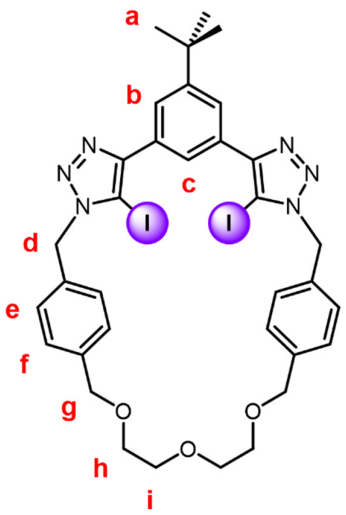
^{1}H NMR (500 MHz, acetone-d_6) δ 7.38 (m, J = 8.3 Hz, 8H, $H_{b,c}$), 4.56 (s, 4H, H_a), 4.42 (s, 4H, H_d), 3.69 – 3.57 (m, 12H, $H_{e,f,g}$).

^{13}C NMR (126 MHz, acetone-d_6) δ 140.08, 135.75, 129.21, 128.66, 73.05, 71.35, 71.29, 70.58, 54.84.

HRMS (ESI +ve) m/z: 463.2057 ($[M+Na]^+$, $C_{22}H_{28}O_3N_6Na$ requires 463.2064).

General Procedure 2B: CuAAC-mediated Macrocyclisation Reaction

Diethylene glycol-based halogen bonding macrocycle (2.1·XB^{DEG}).



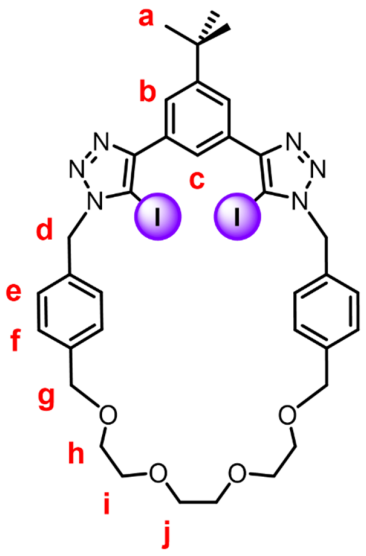
$[Cu(CH_3CN)_4]PF_6$ (172 mg, 0.46 mmol) and TBTA (122 mg, 0.23 mmol) were dissolved in dry, degassed CH_2Cl_2 (180 mL) and the mixture was stirred at room temperature under N_2 for 15 minutes. A solution of diethylene glycol-based bis-azide **2.3** (365 mg, 0.92 mmol) in dry, degassed CH_2Cl_2 (2 mL) was added, followed by the dropwise addition of a solution of bis(iodoalkyne) **2.5** (400 mg, 0.92 mmol) in dry, degassed CH_2Cl_2 (2 mL). The reaction mixture was stirred overnight at room temperature under N_2 in the dark. The crude reaction mixture was diluted with CH_2Cl_2 and washed with aqueous EDTA/NH_4OH solution (50 mL x 2) and brine (50 mL). The organic layer was dried over anhydrous $MgSO_4$, filtered and concentrated on the rotary evaporator. The residue was purified by silica gel chromatography (eluent: 15% EtOAc/DCM) to give **2.1·XB^{DEG}** as a white solid (265 mg, 35%).

^{1}H NMR (500 MHz, acetone-d_6) δ 7.94 (d, J = 1.6 Hz, 2H, H_b), 7.88 (d, J = 1.6 Hz, 1H, H_c), 7.31 (d, J = 8.1 Hz, 4H, H_e), 7.21 (d, J = 8.1 Hz, 4H, H_f), 5.78 (s, 4H, H_d), 4.46 (s, 4H, H_g), 3.61 – 3.48 (m, 8H, $H_{h,i}$), 1.45 (s, 9H, H_a).

^{13}C NMR (126 MHz, acetone-d_6) δ 153.14, 152.29, 139.68, 135.66, 131.92, 129.20, 128.63, 125.99, 125.44, 79.01, 73.33, 71.26, 70.60, 35.72, 31.75.

HRMS (ESI +ve) m/z: 831.1000 ($[M+H]^+$, $C_{34}H_{37}O_3N_6I_2$ requires 831.1011).

Triethylene glycol-based halogen bonding macrocycle (2.1·XB^{TEG})



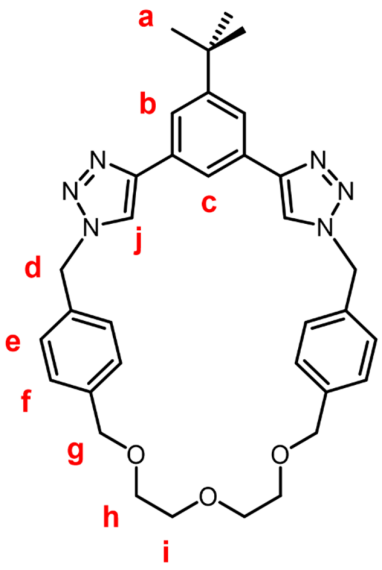
Using General Procedure 2B, the CuAAC click reaction between triethylene glycol-based bis-azide **2.4** (391 mg, 0.89 mmol) and bis(iodoalkyne) **2.5** (385 mg, 0.89 mmol), followed by purification by silica gel chromatography (eluent: 30% EtOAc/DCM) yielded **2.1·XB^{TEG}** as a white solid (348 mg, 45%).

^{1}H NMR (500 MHz, acetone-d_6) δ 8.12 (t, J = 1.6 Hz, 1H, H_c), 8.00 (d, J = 1.6 Hz, 2H, H_b), 7.34 (d, J = 8.1 Hz, 4H, H_e), 7.24 (d, J = 8.1 Hz, 4H, H_f), 5.79 (s, 4H, H_d), 4.50 (s, 4H, H_g), 3.61 – 3.50 (m, 12H, $H_{h,i,j}$), 1.45 (s, 9H, H_a).

^{13}C NMR (126 MHz, acetone-d_6) δ 152.92, 151.69, 140.05, 135.57, 131.96, 128.84, 128.44, 125.84, 124.84, 79.32, 79.28, 73.16, 71.51, 71.40, 70.86, 35.78, 31.76.

HRMS (ESI +ve) m/z: 875.1256 ($[M+H]^+$, $C_{36}H_{41}O_4N_6I_2$ requires 875.1273).

Diethylene glycol-based hydrogen bonding macrocycle (2.1·HB^{DEG})



Using General Procedure 2B, the CuAAC click reaction between diethylene glycol-based bis-azide **2.3** (159 mg, 0.87 mmol) and bis(alkyne) **2.6** (346 mg, 0.87 mmol), followed by purification by silica gel chromatography (eluent: 30% EtOAc/DCM) yielded **2.1·HB^{DEG}** as a white solid (165 mg, 33%).

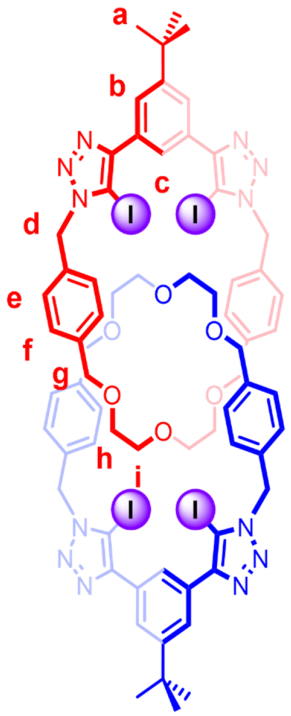
^{1}H NMR (500 MHz, acetone-d_6) δ 8.17 (d, J = 1.5 Hz, 2H, H_b), 8.01 (s, 2H, H_j), 7.84 (t, J = 1.5 Hz, 1H, H_c), 7.38 (d, J = 8.2 Hz, 4H, $H_{e,f}$), 7.31 (d, J = 8.2 Hz, 4H, $H_{e,f}$), 5.65 (s, 4H, H_d), 4.52 (s, 4H, H_g), 3.68-3.63 (m, 8H, $H_{h,i}$), 1.45 (s, 9H, H_a).

^{13}C NMR (126 MHz, acetone-d_6) δ 152.10, 147.82, 139.10, 134.91, 131.49, 128.41, 128.18, 121.35, 120.61, 120.18, 72.32, 70.34, 69.90, 53.30, 34.64, 30.77.

HRMS (ESI +ve) m/z: 579.3070 ($[M+H]^+$, $C_{34}H_{39}O_3N_6$ requires 579.3084).

General Procedure 2C: Alkali Metal-templated Synthesis of [2]Catenanes

Diethylene glycol-based halogen bonding [2]catenane (2.2·XB^{DEG})



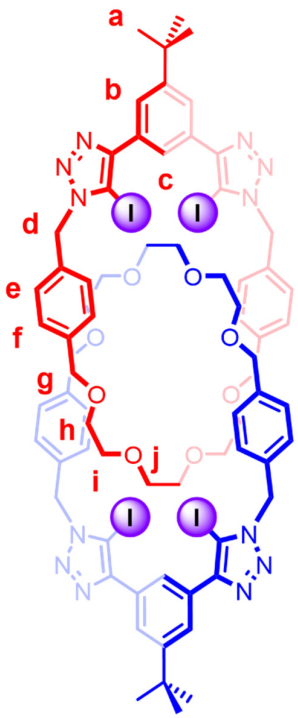
Macrocycle **2.1·XB^{DEG}** (50.0 mg, 0.060 mmol) and NaBAr^{F} (53.4 mg, 0.060 mmol) were dissolved in dry, degassed CH_2Cl_2 (4 mL) and stirred for 30 minutes at room temperature. A solution of bis-azide **2.3** (23.9 mg, 0.060 mmol) in CH_2Cl_2 (2 mL) was added and the mixture stirred for a further 30 minutes. A solution of bis(iodoalkyne) **2.5** (26.1 mg, 0.060 mmol) in CH_2Cl_2 (2 mL) was added, followed by a dropwise addition of a premixed solution of $[Cu(CH_3CN)_4]PF_6$ (11.2 mg, 0.030 mmol) and TBTA (16.0 mg, 0.030 mmol) in CH_2Cl_2 (4 mL). The reaction mixture was stirred at room temperature in the dark for 48 hours, then was diluted with CH_2Cl_2 (40 mL). The organic layer was washed with EDTA/NH_4OH (2 × 25 mL) and H_2O (2 × 25 mL), dried over $MgSO_4$, filtered and concentrated under vacuum. The crude was purified by preparative TLC (eluent: 50:50:1 CH_2Cl_2/EtOAc/MeOH) to afford **2.2·XB^{DEG}** as a white solid (20 mg, 20%).

^{1}H NMR (500 MHz, acetone-d_6) δ 7.83 (d, J = 1.6 Hz, 4H, H_b), 7.44 (t, J = 1.6 Hz, 2H, H_c), 7.17 – 7.10 (m, 8H, H_e), 6.89 – 6.81 (m, 8H, H_f), 5.62 (s, 8H, H_d), 3.98 (s, 8H, H_g), 2.99 (m, 16H, $H_{h,i}$), 1.44 (s, 18H, H_a) ppm.

^{13}C NMR (126 MHz, acetone-d_6) δ 152.66, 152.49, 139.96, 135.21, 132.08, 129.40, 129.01, 126.66, 126.01, 80.17, 73.02, 70.79, 70.02, 35.74, 32.80, 31.82 ppm.

HRMS (ESI +ve) m/z: 1661.1899 ($[M+H]^+$, $C_{68}H_{73}O_6N_{12}I_4$ requires 1661.1949).

Triethylene glycol-based halogen bonding [2]catenane (2.2·XB^{TEG})



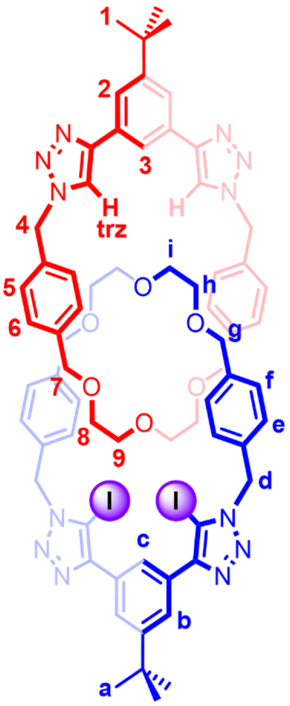
Following general procedure 2C, the reaction between macrocycle **2.1·XB^{TEG}** (50.0 mg, 0.057 mmol), NaBAr^{F} (50.6 mg, 0.057 mmol), bis-azide **2.4** (25.2 mg, 0.057 mmol), bis-iodoalkyne **5** (24.8 mg, 0.057 mmol), [Cu(CH$_3$CN)$_4$]PF$_6$ (10.7 mg, 0.026 mmol) and TBTA (15.2 mg, 0.026 mmol), followed by iterative preparative TLC purification (eluent: 50:50:2 CH$_2$Cl$_2$/EtOAc/MeOH) afforded **2.2·XB^{TEG}** as a white solid (18 mg, 18%).

^{1}H NMR (500 MHz, acetone-*d*$_6$) δ 7.95 (d, *J* = 1.6 Hz, 4H, H$_b$), 7.84 (t, *J* = 1.6 Hz, 2H, H$_c$), 7.09 (d, *J* = 8.0 Hz, 8H, H$_e$), 7.00 (d, *J* = 8.0 Hz, 8H, H$_f$), 5.62 (s, 8H, H$_d$), 4.17 (s, 8H, H$_g$), 3.28 – 3.17 (m, 24H, H$_{h,i,j}$), 1.45 (s, 18H, H$_a$).

^{13}C NMR (126 MHz, acetone-*d*$_6$) δ 152.67, 151.66, 140.02, 135.21, 131.97, 128.80, 128.77, 125.75, 125.26, 79.93, 73.09, 71.34, 71.16, 70.75, 35.81, 31.84, 23.49.

HRMS (ESI +ve) m/z: 1749.2437 ([M+H]$^+$, C$_{72}$H$_{81}$O$_8$N$_{12}$I$_4$ requires 1749.2474).

Diethylene glycol-based halogen- and hydrogen bonding [2]catenane (2.2·HBXB^{DEG})



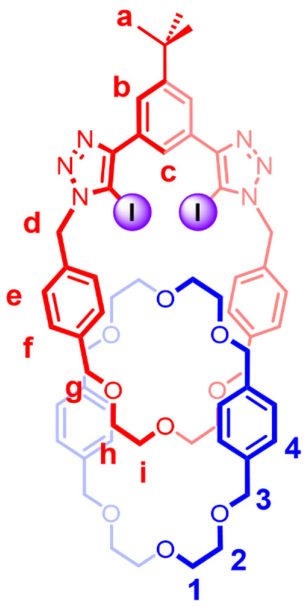
Following General Procedure 2C, the reaction between macrocycle **2.1·HB^{DEG}** (50.0 mg, 0.086 mmol), NaBAr^{F} (76.6 mg, 0.086 mmol), bis-azide **2.4** (34.3 mg, 0.086 mmol), bis-iodoalkyne **2.5** (37.5 mg, 0.086 mmol), [Cu(CH$_3$CN)$_4$]PF$_6$ (16.1 mg, 0.043 mmol) and TBTA (22.3 mg, 0.043 mmol), followed by iterative preparative TLC purification (50:50:2 CH$_2$Cl$_2$/EtOAc/MeOH) afforded **2.2·HBXB^{DEG}** as a white solid (4.8 mg, 4%).

^{1}H NMR (500 MHz, acetone-*d*$_6$) δ 8.17 (d, *J* = 1.5 Hz, 2H, H$_2$), 8.01 (s, 2H, H$_{trz}$), 7.81 (s, 1H, H$_3$), 7.78 (d, *J* = 1.5 Hz, 2H, H$_b$), 7.37 (d, *J* = 8.3 Hz, 4H, H$_e$), 7.19 (s, 1H, H$_c$), 6.98 (d, *J* = 8.3 Hz, 4H, H$_f$), 6.79 (d, *J* = 8.1 Hz, 4H, H$_5$), 6.62 (d, *J* = 8.1 Hz, 4H, H$_6$), 5.71 (s, 4H, H$_d$), 5.13 (s, 4H, H$_4$), 4.20 (s, 4H, H$_7$), 4.01 (s, 4H, H$_g$), 3.61 – 3.57 (m, 4H, H$_{8/9}$), 3.49 – 3.44 (m, 4H, H$_{8/9}$), 2.89 – 2.85 (m, 4H, H$_{h/i}$), 2.83 – 2.81 (m, 4H, H$_{h/i}$), 1.45 (s, 9H, H$_a$), 1.42 (s, 9H$_1$).

^{13}C NMR (126 MHz, acetone-d_6) δ 152.76, 152.44, 152.28, 148.44, 139.52, 139.40, 135.86, 134.81, 132.62, 131.75, 130.00, 129.41, 128.81, 126.86, 125.69, 121.94, 121.89, 73.31, 72.92, 71.19, 70.98, 70.55, 69.75, 54.55, 54.16, 35.57, 35.55, 31.79, 31.66, 24.42, 23.33, 14.36, 13.84.

HRMS (ESI +ve) m/z: 1409.4000 ($[M+H]^+$, $C_{68}H_{77}O_6N_{12}$ requires 1409.4016).

Bis-di(ethylene glycol)-based halogen bonding hetero[2]catenane (2.3·XB^{DEG})



Following General Procedure 2C, the reaction between macrocycle **2.7** (30.0 mg, 0.076 mmol), $NaBAr^F$ (63.8 mg, 0.072 mmol), bis-azide **2.3** (28.6 mg, 0.072 mmol), bis-iodoalkyne **2.5** (31.3 mg, 0.072 mmol), $[Cu(CH_3CN)_4]PF_6$ (13.4 mg, 0.036 mmol) and TBTA (19.1 mg, 0.036 mmol), followed by iterative preparative TLC purification in 7:3 EtOAc/CH_2Cl_2, then in 4:96 MeOH/DCM afforded **2.3·XB^{DEG}** as a white solid (10 mg, 11%).

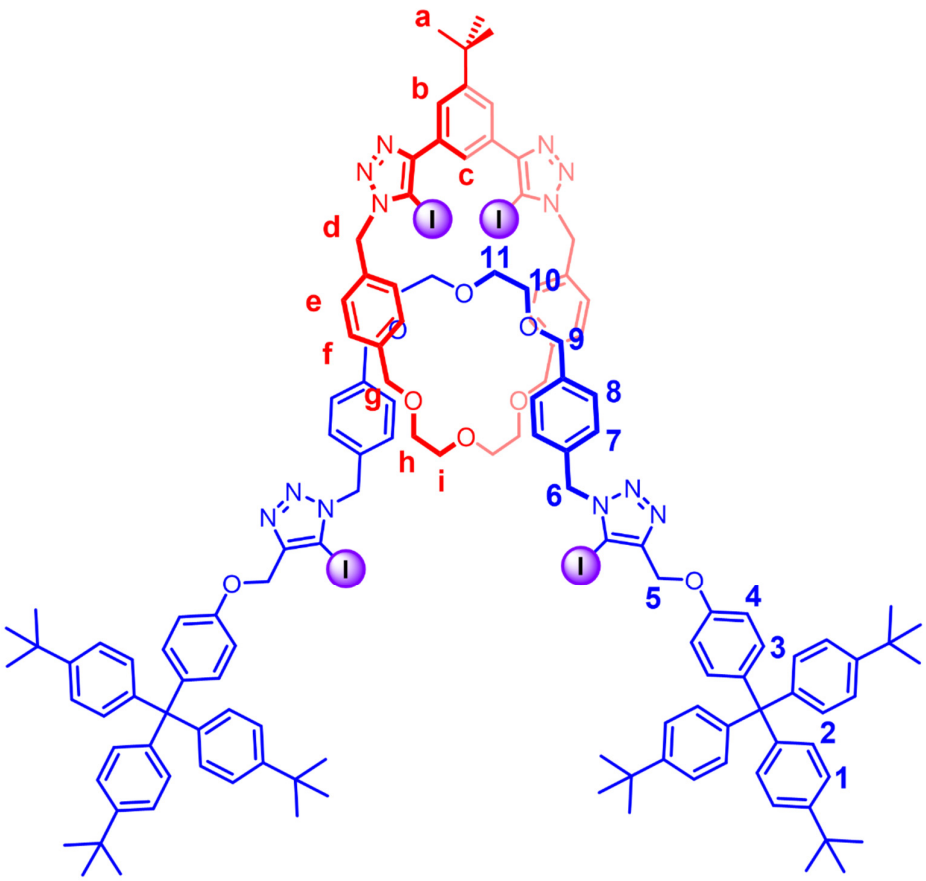
^{1}H NMR (600 MHz, $CDCl_3$) δ 7.78 (d, J = 1.6 Hz, 2H, H_b), 7.33 (d, J = 7.9 Hz, 4H, H_e), 7.17 (d, J = 7.9 Hz, 4H, H_f), 7.12 (d, J = 1.6 Hz, 1H, H_c), 6.71 (s, 8H, H_4), 5.66 (s, 4H, H_d), 4.10 (s, 8H, H_3), 4.08 (s, 4H, H_g), 3.34 (t, J = 5.7 Hz, 8H, $H_{1/2}$), 3.26 (t, J = 5.7 Hz, 8H, $H_{1/2}$), 2.89 (s, 8H, H_h, H_i), 1.40 (s, 9H, H_a).

^{13}C NMR (151 MHz, $CDCl_3$) δ 152.22, 152.07, 139.80, 137.14, 133.48, 130.21, 129.56, 128.98, 128.73, 128.07, 125.98, 125.31, 73.19, 72.15, 70.40, 69.52, 68.94, 68.43, 54.47, 35.20, 31.48, 29.85.

HRMS (ESI +ve) m/z: 1247.3160 ($[M+H]^+$, $C_{58}H_{69}O_9N_6I_2$ requires 1247.3210).

General Procedure 2D: Cation Template-Directed Synthesis of All-XB [2]Rotaxanes

Diethylene glycol-based halogen bonding rotaxane (2.4·XB-XB^{DEG})



Macrocycle **2.1·XB^{DEG}** (20.0 mg, 0.024 mmol) and NaBAr^{F} (21.4 mg, 0.024 mmol) were dissolved in dry, degassed CH_2Cl_2 (1.0 mL) and stirred for 30 minutes at room temperature. A solution of bis-azide **2.3** (9.6 mg, 0.024 mmol) in CH_2Cl_2 (1 mL) was added and the mixture stirred for a further 30 minutes. A solution of iodoalkyne stopper **2.8** (40.3 mg, 0.060 mmol) in CH_2Cl_2 (1.0 mL) was added, followed by a dropwise addition of a premixed solution of $[Cu(CH_3CN)_4]PF_6$ (4.5 mg, 0.012 mmol) and TBTA (6.4 mg, 0.012 mmol) in CH_2Cl_2 (1.0 mL). The reaction mixture was stirred at room temperature in the dark for 48 hours, then was diluted with CH_2Cl_2 (25 mL). The organic layer was washed with EDTA/NH_4OH (2 × 20 mL) and H_2O (2 × 20 mL), dried over $MgSO_4$, filtered and concentrated under vacuum. The crude was

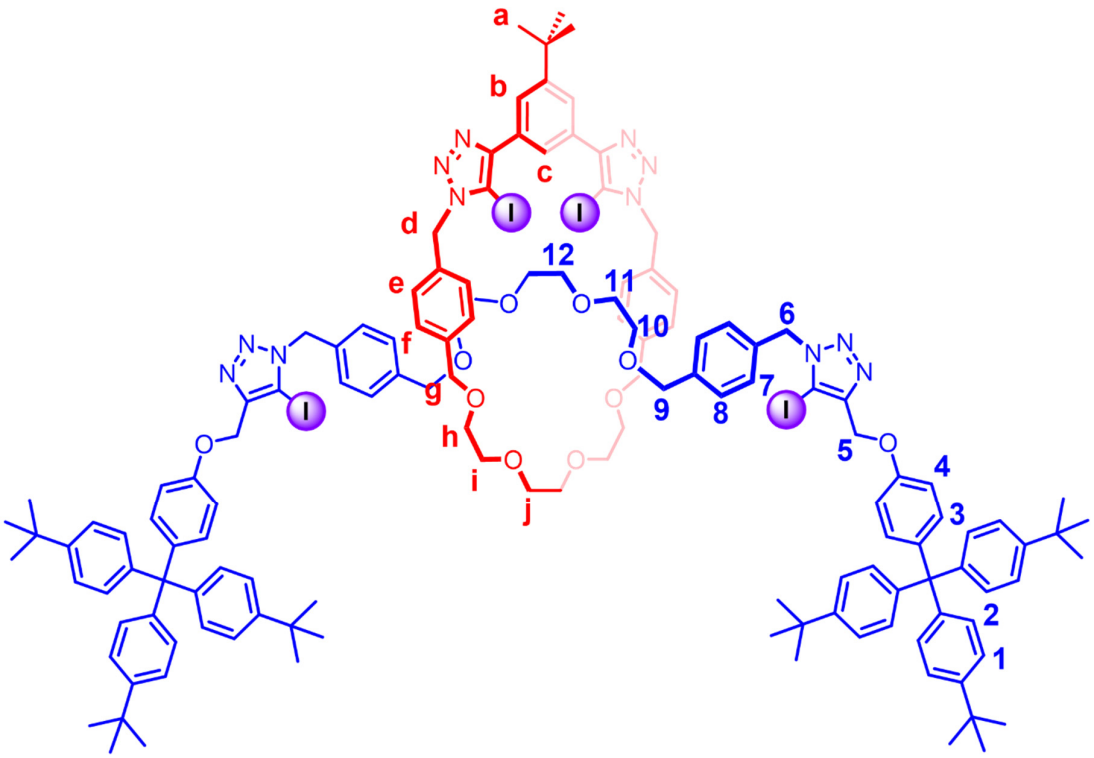
purified by preparative TLC in 75:25 CH_2Cl_2/EtOAc to afford the target rotaxane **2.4·XB-XB^{DEG}** as a white solid (13.0 mg, 21%).

^{1}H NMR (600 MHz, $CDCl_3$) δ 7.73 (s, 2H, H_b), 7.48 (d, *J* = 7.7 Hz, 4H, H_e), 7.26 – 7.25 (m, H_f + $CDCl_3$), 7.22 (d, *J* = 8.6 Hz, 12H, H_1), 7.07-7.04 (m, 16H, H_2, H_3), 6.76 (d, *J* = 8.7 Hz, 4H, H_4), 6.58-6.57 (m, 8H, H_7, H_8), 6.47 (s, 1H_c), 5.57 (s, 4H, H_d), 5.31 (s, 4H, H_6), 4.98 (s, 4H, H_5), 4.35 (s, 4H, H_g), 4.09 (s, 4H, H_9), 3.52 (br s, 4H, $H_{10/11}$), 3.42 (br s, 4H, $H_{10/11}$), 3.27-3.24 (m, 8H, H_h, H_i), 1.57 (s, 9H, H_a), 1.30 (s, 54H, stopper-*tert*-butyl).

^{13}C NMR (151 MHz, $CDCl_3$) δ 156.34, 151.76, 148.46, 147.77, 144.22, 140.35, 139.75, 139.13, 138.44, 134.96, 134.14, 133.08, 132.39, 130.88, 130.22, 129.45, 129.38, 127.87, 127.73, 125.80, 125.23, 124.20, 113.61, 81.53, 73.15, 72.49, 70.75, 70.31, 69.72, 69.27, 63.21, 61.80, 54.40, 54.01, 35.18, 34.44, 31.59, 29.85.

HRMS (ESI +ve) m/z: 2564.7883 ($[M+H]^+$, $C_{134}H_{151}O_8N_{12}I_4$ requires 2564.7985).

Triethylene glycol-based halogen bonding rotaxane (2.4·XB-XB^{TEG})



Following General Procedure 2D, the reaction between macrocycle **2.1·XB^{TEG}** (20.0 mg, 0.023 mmol), KBAr^{F} (20.6 mg, 0.023 mmol), bis-azide **2.4** (9.9 mg, 0.023 mmol), iodoalkyne stopper **2.8** (38.2 mg, 0.057 mmol), [Cu(CH$_3$CN)$_4$]PF$_6$ (4.3 mg, 0.011 mmol) and TBTA (6.1 mg, 0.011 mmol), followed by iterative preparative TLC purification in 70:30:1 CH$_2$Cl$_2$/EtOAc/MeOH, then in 4:96 MeOH/DCM afforded **2.4·XB-XB^{TEG}** as a white solid (12.5 mg, 20%).

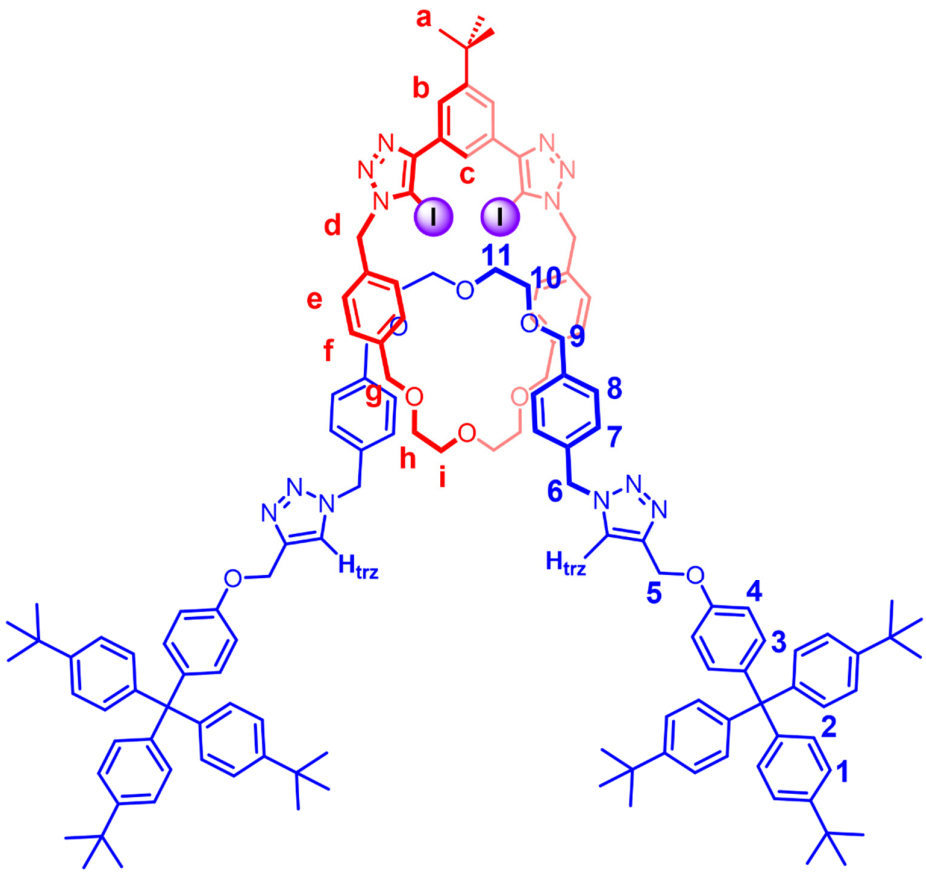
^{1}H NMR (600 MHz, CDCl$_3$) δ 7.91 (s, 2H, H$_b$), 7.33 (d, *J* = 8.2 Hz, 4H, H$_e$), 7.26 – 7.24 (m, H$_f$, H$_c$ + CDCl$_3$) 7.22 (d, *J* = 8.7 Hz, 12H$_1$), 7.06 (d, *J* = 8.6 Hz, 16H, H$_2$, H$_3$), 6.85 (d, *J* = 8.2 Hz, 4H, H$_7$), 6.81 (m, 4H, H$_8$), 6.77 (d, *J* = 8.9 Hz, 4H, H$_4$), 5.58 (s, 4H$_d$), 5.34 (s, 4H$_6$), 4.93 (s, 4H, H$_5$), 4.41 (s, 4H, H$_g$), 4.20 (s, 4H, H$_9$), 3.62 – 3.49 (m, 8H, H$_i$, H$_{11}$), 3.45 – 3.40 (m, 12H, H$_h$, H$_{10}$, H$_{12/j}$), 3.34 (s, 4H, H$_{12/j}$), 1.40 (s, 9H, H$_a$), 1.30 (s, 54H, stopper-*tert*-butyl).

^{13}C NMR (151 MHz, $CDCl_3$) δ 156.22, 150.88, 148.35, 147.65, 144.08, 140.19, 138.98, 138.48, 133.81, 133.13, 132.27, 130.74, 130.03, 128.52, 128.46, 127.89, 127.86, 125.58, 124.07, 113.47, 81.13, 72.85, 72.49, 70.54, 70.46, 69.81, 69.58, 63.07, 61.59, 54.17, 53.92, 35.11, 34.31, 29.71.

HRMS (ESI +ve) m/z: 2651.8406 ($[M+H]^+$, $C_{138}H_{159}O_{10}N_{12}I_4$ requires 2651.8481).

General Procedure 2E: CuAAC-mediated Active Metal Template Synthesis of XB-HB [2]Rotaxanes

Diethylene glycol-based mixed halogen/hydrogen bonding rotaxane (2.4·XB-HB^{DEG})



Macrocycle **2.1·XB^{DEG}** (25.0 mg, 0.030 mmol) and $[Cu(CH_3CN)_4]PF_6$ (10.8 mg, 0.029 mmol) were suspended in dry, degassed 1,2-dichloroethane (2.0 mL) and stirred for 30 minutes at room temperature. A solution of bis-azide **2.3** (48 mg, 0.12 mmol) in 1,2-dichloroethane (1.0 mL) was added, followed by a solution of stopper alkyne **2.9** (131 mg, 0.24 mmol) in 1,2-dichloroethane (2.0 mL). The reaction mixture was heated to 80°C for 3 days, then cooled to room temperature and diluted with CH_2Cl_2 (25 mL). The organic layer was washed with EDTA/NH_4OH (2 × 20 mL) and H_2O (2 × 20 mL), dried over $MgSO_4$, filtered and concentrated

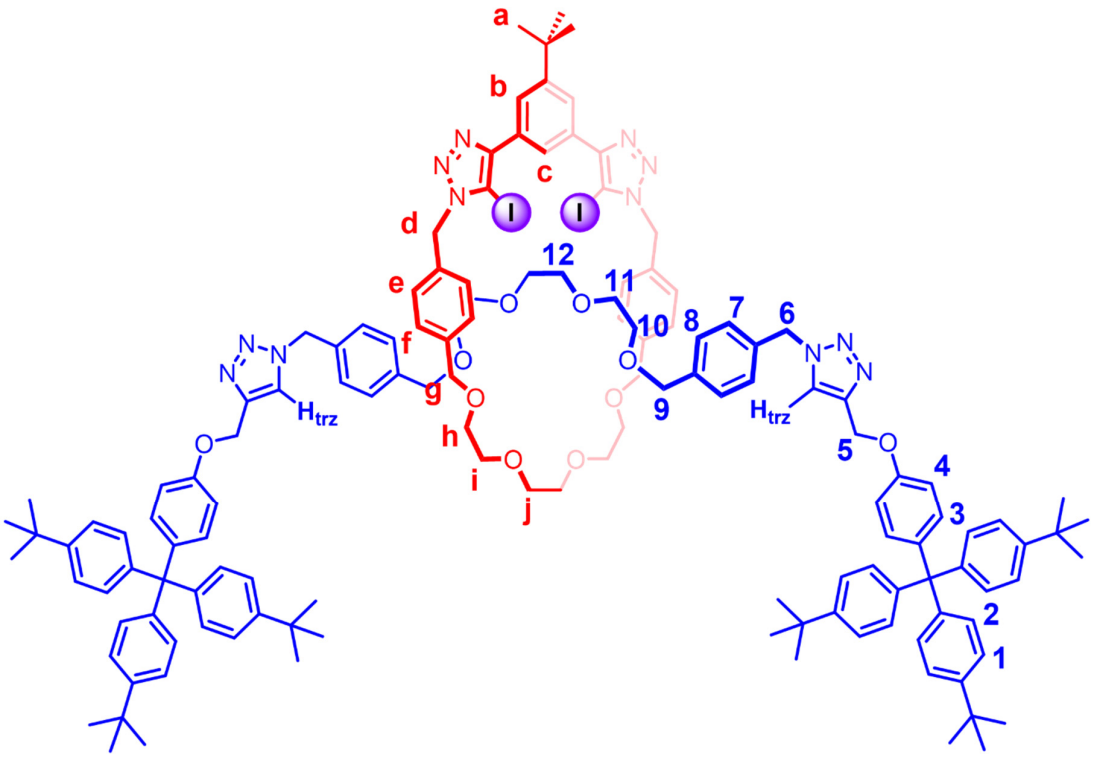
under vacuum. The crude was purified by preparative TLC in 75:25 CH_2Cl_2/EtOAc to afford the target rotaxane **2.4·XB-HB^{DEG}** as a white solid (14.6 mg, 21%).

^{1}H NMR (700 MHz, $CDCl_3$) δ 7.79 (d, *J* = 1.6 Hz, 2H, H_b), 7.51 (s, 2H_{trz}), 7.46 (d, *J* = 8.1 Hz, 4H, H_e), 7.29 – 7.24 (m, H_f + $CDCl_3$), 7.23 – 7.20 (m, 12H, H_1), 7.09 – 7.04 (m, 16H, H_2, H_3), 6.84 – 6.80 (m, 4H, H_4), 6.62 (d, *J* = 7.7 Hz, 4H, H_7), 6.39 (br s, 4H, H_8), 6.33 (t, *J* = 1.6 Hz, 1H, H_c), 5.57 (s, 4H, H_d), 5.17 (s, 4H, H_6), 5.10 (s, 4H, H_5), 4.34 (s, 4H, H_g), 4.08 (s, 4H, H_9), 3.56 (t, *J* = 4.8 Hz, 4H, H_{11}), 3.41 (br s, 4H, H_{10}), 3.37 (m, 8H, H_h, H_i), 1.39 (s, 9H, H_a), 1.29 (s, 54H, stopper-*tert*-butyl).

^{13}C NMR (176 MHz, $CDCl_3$) δ 156.29, 152.19, 151.61, 148.51, 144.19, 144.07, 140.34, 138.85, 138.60, 134.30, 133.78, 132.50, 130.88, 129.97, 129.59, 129.35, 128.01, 127.83, 125.54, 124.71, 124.20, 123.82, 113.40, 78.03, 73.42, 72.47, 70.74, 70.65, 69.93, 69.71, 63.21, 62.05, 54.40, 53.67, 35.19, 34.45, 31.55, 31.53.

HRMS (ESI +ve) m/z: 2311.9924 ($[M+H]^+$, $C_{134}H_{153}N_{12}O_8I_2$ requires 2312.0023).

Triethylene glycol-based mixed halogen/hydrogen bonding rotaxane (2.4·XB-HB^{TEG})



Following General Procedure 2E, the reaction between macrocycle **2.1·XB^{TEG}** (25.0 mg, 0.029 mmol), bis-azide **2.4** (38 mg, 0.11 mmol), protoalkyne stopper **2.9** (124 mg, 0.23 mmol) and $[Cu(CH_3CN)_4]PF_6$ (10.4 mg, 0.029 mmol) in CH_2Cl_2 (5.0 mL) at room temperature for 7 days, followed by iterative preparative TLC purification in 97:3 CH_2Cl_2/MeOH, afforded **2.4·XB-HB^{TEG}** as a white solid (12.0 mg, 17%).

^{1}H NMR (600 MHz, acetone-d_6) δ 7.96 (d, J = 1.6 Hz, 2H, H$_b$), 7.82 (s, 2H, H$_{trz}$), 7.57 (t, J = 1.6 Hz, 1H, H$_c$), 7.29 (m, 16H, H$_1$, H$_e$), 7.23 (d, J = 8.4 Hz, 4H, H$_f$), 7.09 (d, J = 8.8 Hz, 12H, H$_2$), 7.03 (d, J = 9.1 Hz, 4H, H$_3$), 6.98 (d, J = 8.3 Hz, 4H, H$_8$), 6.94 (d, J = 8.3 Hz, 4H, H$_7$), 6.79 (d, J = 9.0 Hz, 4H, H$_4$), 5.68 (s, 4H, H$_d$), 5.38 (s, 4H, H$_6$), 5.00 (s, 4H, H$_5$), 4.37 (s, 4H, H$_g$), 4.25 (s, 4H, H$_9$), 3.51 (m, 8H, H$_{10}$, H$_{12}$), 3.43 – 3.41 (m, 4H, H$_{11}$), 3.40 – 3.35 (m, 8H, H$_h$, H$_i$), 3.27 (s, 4H, H$_j$), 1.41 (s, 9H$_a$), 1.29 (s, 54H, stopper-*tert*-butyl).

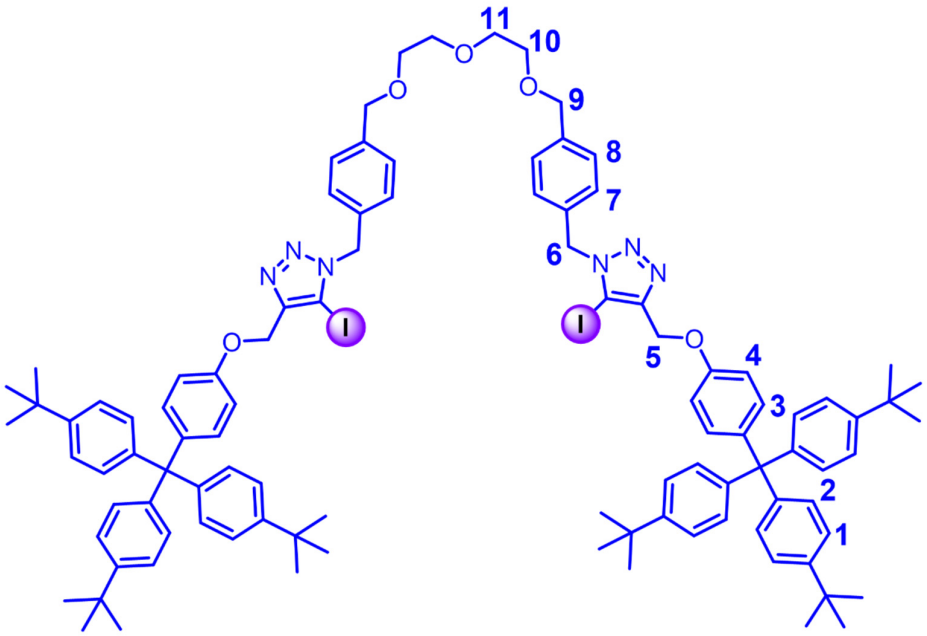
^{13}C NMR (151 MHz, acetone-d_6) δ 157.43, 152.50, 151.44, 149.14, 145.25, 144.51, 140.43, 139.92, 139.86, 135.53, 135.37, 132.79, 131.60, 131.45, 129.03, 128.90, 128.80, 128.52, 125.67, 125.08, 124.81, 124.30, 114.32, 79.29, 73.12, 72.84, 71.29, 71.24, 71.18, 71.10, 70.66, 70.47, 63.90, 62.27, 54.67, 53.99, 35.61, 34.88, 31.71, 30.34.

HRMS (ESI +ve) m/z: 2400.0461 ($[M+H]^+$, $C_{138}H_{161}N_{12}O_{10}I_2$ requires 2400.0548).

Characterisation of Axle By-Products

The non-interlocked axle components (**2.5·XB^{DEG}**, **2.5·XB^{TEG}**, **2.5·HB^{DEG}**, **2.5·HB^{TEG}**) were formed as by-products of the corresponding rotaxane-formation reactions. An analytical sample of each axle was isolated from the preparative TLC plate and characterised by ^{1}H NMR, ^{13}C NMR and HR-MS.

Diethylene glycol-based halogen bonding axle (2.5·XB^{DEG})



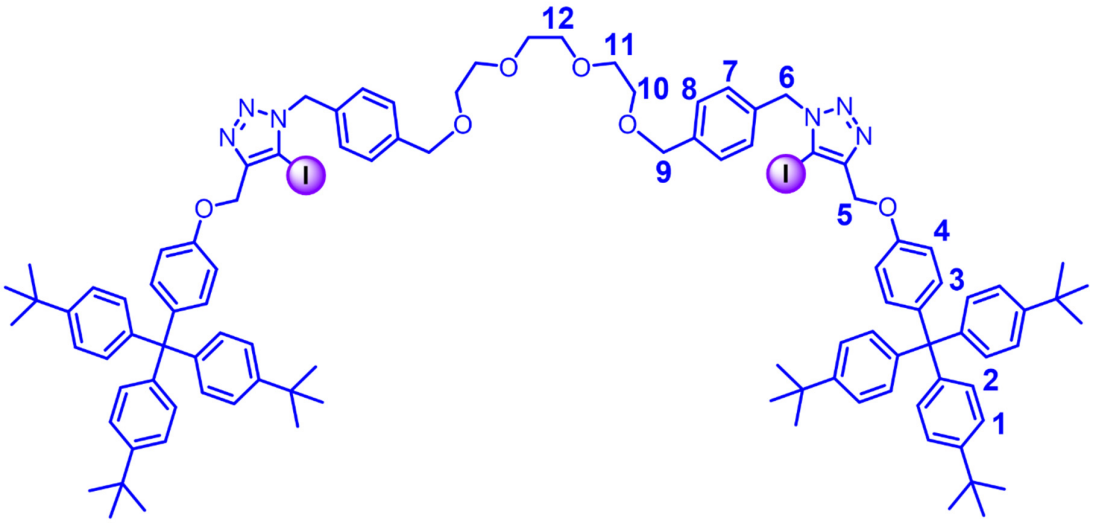
Isolated as a by-product of **2.4·XB-XB^{DEG}** formation as a white powder (12 mg, 29%).

^{1}H NMR (500 MHz, 1:1 $CDCl_3$/CD_3CN) δ 7.07 (d, *J* = 8.2 Hz, 4H, $H_{7/8}$), 7.03 – 6.98 (m, 16H, H_1, $H_{7/8}$), 6.89 (d, *J* = 8.9 Hz, 16H, H_2, H_3), 6.63 (d, *J* = 9.0 Hz, 4H, H_4), 5.35 (s, 4H, H_6), 4.79 (s, 4H, H_5), 4.27 (s, 4H, H_9), 1.05 (s, 54H, stopper-*tert*-butyl).

^{13}C NMR (126 MHz, 1:1 $CDCl_3$/CD_3CN) δ 155.52, 147.63, 146.99, 143.66, 139.63, 138.36, 133.16, 131.23, 129.73, 127.36, 127.14, 123.64, 113.10, 81.22, 71.66, 69.74, 68.99, 62.37, 61.12, 53.20, 33.45, 30.36.

HRMS (ESI +ve) m/z: 1733.7031 ($[M+H]^+$, $C_{100}H_{115}N_6O_5I_2$ requires 1733.7018).

Triethylene glycol-based halogen bonding axle (2.5·XB^{TEG})



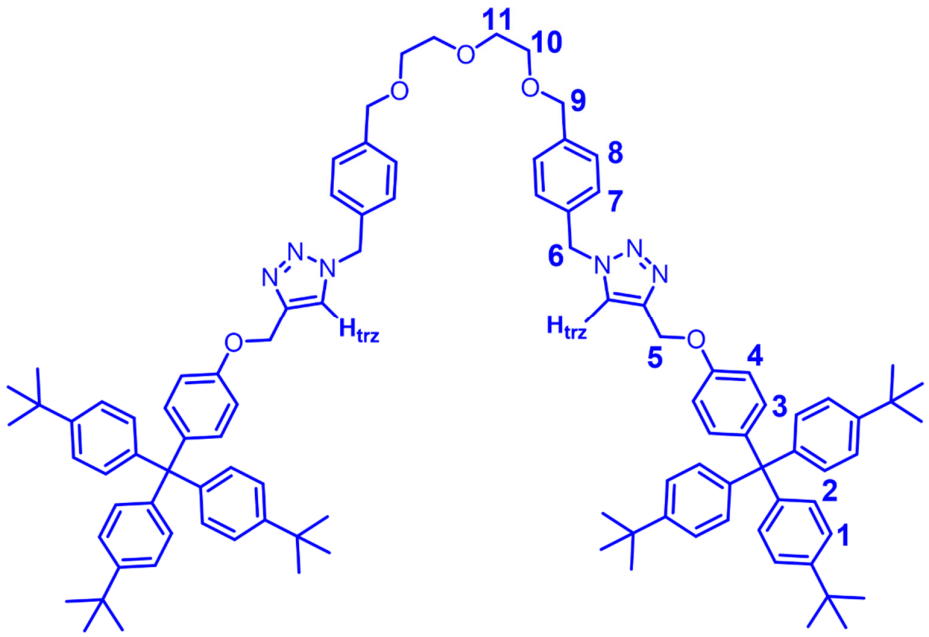
Isolated as a by-product of **2.4·XB-XB^{TEG}** formation as a white powder (8.2 mg, 20%).

^{1}H NMR (500 MHz, 1:1 $CDCl_3/CD_3CN$) δ 7.07 (d, *J* = 8.0 Hz, 4H, $H_{7/8}$), 7.02 – 6.98 (m, 16H, $H_{7/8}$, H_1), 6.89 (d, *J* = 8.6 Hz, 16H, H_2, H_3), 6.63 (d, *J* = 8.9 Hz, 4H, H_4), 5.34 (s, 4H, H_6), 4.79 (s, 4H, H_5), 4.26 (s, 4H, H_9), 3.41 – 3.32 (m, 12H, H_{10}, H_{11}, H_{12}), 1.05 (s, 54H, stopper-*tert*-butyl).

^{13}C NMR (126 MHz, 1:1 $CDCl_3/CD_3CN$) δ 155.53, 147.63, 146.99, 143.66, 139.63, 138.35, 133.15, 131.23, 129.73, 127.38, 127.13, 123.64, 113.09, 81.18, 71.64, 69.74, 69.70, 68.98, 62.37, 61.11, 53.19, 33.45, 30.36.

HRMS (ESI +ve) m/z: 1777.7202 ($[M+H]^+$, $C_{102}H_{119}N_6O_6I_2$ requires 1777.7281).

Diethylene glycol-based hydrogen bonding axle (2.5·HB^{DEG})



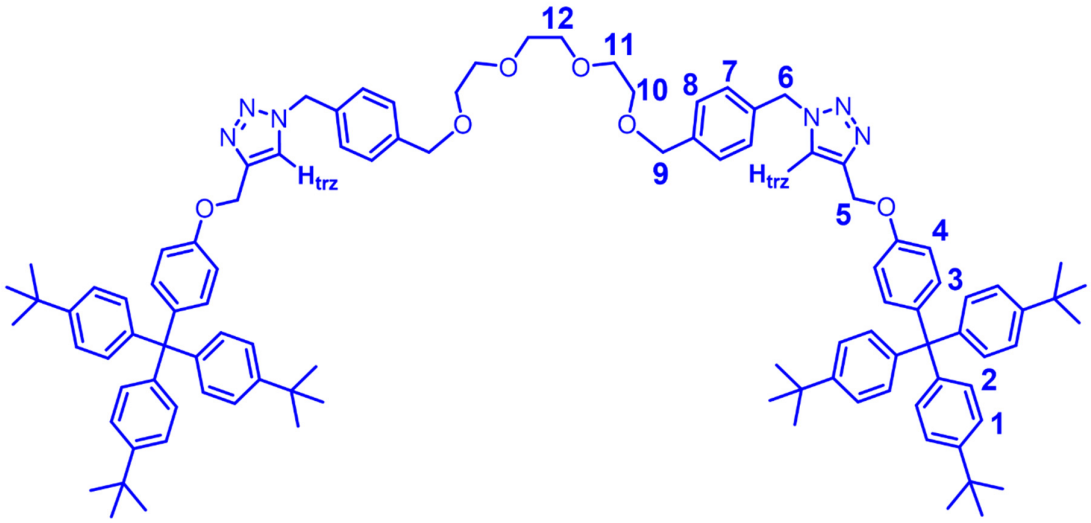
Isolated as a by-product of **2.4·XB-HB^{DEG}** formation as a white powder (73.0 mg, 41%).

^{1}H NMR (500 MHz, 1:1 $CDCl_3/CD_3CN$) δ 7.49 (s, 2H, H_{trz}), 7.08 (d, *J* = 8.2 Hz, 4H, $H_{7/8}$), 7.01 (d, *J* = 8.7 Hz, 16H, $H_{7/8}$, H_1), 6.89 – 6.86 (m, 16H, H_2, H_3), 6.58 (d, *J* = 9.0 Hz, 4H, H_4), 5.27 (s, 4H, H_6), 4.83 (s, 4H, H_5), 4.27 (s, 4H, H_9), 3.37 (m, 8H, H_{10}, H_{11}), 1.05 (s, 54H, stopper-*tert*-butyl).

^{13}C NMR (126 MHz, 1:1 $CDCl_3/CD_3CN$) δ 155.53, 147.62, 143.66, 143.24, 139.35, 138.44, 133.81, 131.21, 129.72, 127.43, 123.62, 122.86, 112.79, 71.64, 69.74, 68.97, 62.34, 60.90, 52.85, 33.45, 30.35.

HRMS (ESI +ve) m/z: 1481.9003 ($[M+H]^+$, $C_{100}H_{117}N_6O_5$ requires 1481.9085).

Triethylene glycol-based hydrogen bonding axle (2.5·HB^{TEG})



Isolated as a by-product of **2.4·XB-HB^{TEG}** formation as a white powder (40.9 mg, 25%).

^{1}H NMR (500 MHz, 1:1 $CDCl_3/CD_3CN$) δ 7.48 (s, 2H, H_{trz}), 7.08 (d, *J* = 8.2 Hz, 4H, $H_{7/8}$), 7.03 – 7.00 (m, 16H, $H_{7/8}$, H_1), 6.89 – 6.87 (m, 16H, H_2, H_3), 6.59 (d, *J* = 9.0 Hz, 4H, H_4), 5.26 (s, 4H, H_6), 4.83 (s, 4H, H_5), 4.26 (s, 4H, H_9), 3.41 – 3.32 (m, 12H, H_{10}, H_{11}, H_{12}), 1.05 (s, 54H, stopper-*tert*-butyl).

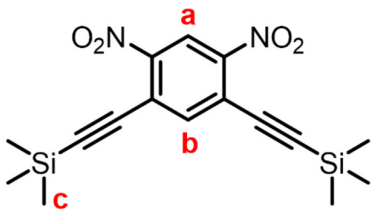
^{13}C NMR (126 MHz, 1:1 $CDCl_3/CD_3CN$) δ 155.54, 147.63, 143.67, 143.25, 139.35, 138.43, 133.80, 131.21, 129.72, 127.45, 127.42, 123.63, 122.84, 112.79, 71.63, 69.74, 69.70, 68.96, 62.34, 60.90, 52.85, 33.45, 30.35.

HRMS (ESI +ve) m/z: 1525.9269 ($[M+H]^+$, $C_{102}H_{121}N_6O_6$ requires 1525.9348).

6.2.2 Compounds from Chapter 3

The dinitro-functionalised dibromide **3.1**,[9] bis-amine **3.6**,[10] macrocycle **3.8·HB**,[10] NDI-functionalised stopper azide **3.9**[11] and biphenyl-functionalised stopper azide **3.12**[11] were prepared according to literature reports.

4,6-Dinitro-1,3-bis-(TMS-alkyne) (3.2)



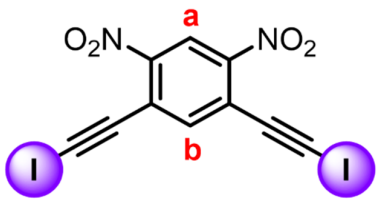
4,6-Dinitro-1,3-dibromobenzene **3.1** (1.00 g, 3.08 mmol), $Pd(PPh_3)_4$ (177 mg, 1.53 mmol) and CuI (58 mg, 0.305 mmol) were suspended in dry degassed THF (20 ml), to which was added DIPEA (5.34 ml, 30.7 mmol) and TMS acetylene (4.34 ml, 30.6 mmol) and left to stir for 5 hours at room temperature, after which the mixture was filtered through celite, the filtrate concentrated *in vacuo* and the crude residue dissolved in CH_2Cl_2 (25 mL). The organic layer was washed with EDTA/NH_4OH (2 × 20 mL) and brine (2 × 20 mL). The organic layer was dried over $MgSO_4$ and concentrated to dryness, after which the crude was subjected to silica gel flash column chromatography (eluent: 3:7 CH_2Cl/hexane) to afford **3.2** as a yellow solid (533 mg, 48%).

^{1}H NMR (500 MHz, $CDCl_3$) δ 8.75 (s, 1H, H_a), 7.91 (s, 1H, H_b), 0.30 (s, 18H, H_c).

^{13}C NMR (126 MHz, $CDCl_3$) δ 77.95, 71.84, 53.07, 51.83, 41.25, 27.36, -70.38.

HRMS (ESI+ve) m/z: 361.1033 ($[M+H]^+$, $C_{16}H_{21}O_4N_2Si_2$ requires 361.1034)

4,6-Dinitro-1,2-bis-iodoalkyne (3.3)



3.2 (520 mg, 1.44 mmol) was dissolved in anhydrous DMF (20 ml), to which was added $AgNO_3$ (48 mg, 0.213 mmol). The suspension was cooled to 0 °C, at which point NIS (735 mg, 4.33 mmol) was added portion-wise and left to stir at 0 °C for 10 minutes, after which the reaction was allowed to stir at room temperature for 2 hours in the dark. The reaction mixture was diluted with H_2O (250 mL) and extracted with Et_2O (3 × 100 mL). The combined organic phases were washed with H_2O (2 × 200 mL), dried over $MgSO_4$ and concentrated in vacuo to afford **3.3** as a yellow solid (655 mg, quant.).

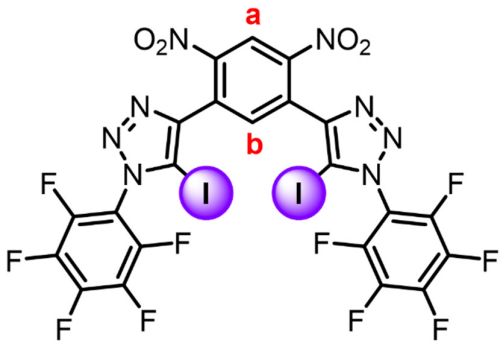
^{1}H NMR (500 MHz, $CDCl_3$) δ 8.81 (s, 1H, H_a), 7.92 (s, 1H, H_b).

^{13}C NMR (126 MHz, $CDCl_3$) δ 148.28, 143.60, 123.19, 122.01, 87.53, 26.15.

HRMS (MSS-ve) m/z: 467.8091 ($[M]^-$, $C_{10}H_2O_4N_2I_2$ requires 467.8109).

General Procedure 3A: CuAAC-mediated Synthesis of Acyclic XB Receptors

Dinitrobenzene-based acyclic XB receptor (3.4)



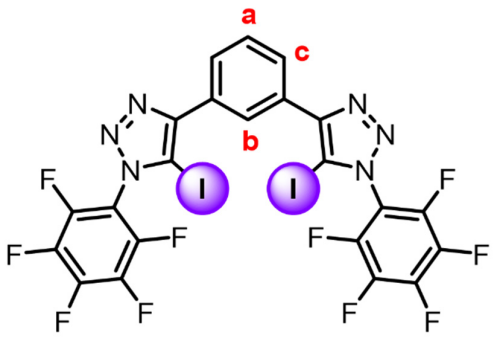
$[Cu(MeCN)_4]PF_6$ (20 mg, 0.053 mmol) and TBTA (14 mg, 0.026 mmol) were dissolved in dry, degassed CH_2Cl_2 (3 mL) and stirred for 20 minutes. Bis-iodoalkyne **3.3** (50 mg, 0.11 mmol) was added in dry, degassed CH_2Cl_2 (2 mL) before the addition of perfluorophenyl azide (44 mg, 0.22 mmol). The resulting mixture was stirred at room temperature overnight under an atmosphere of N_2. The crude was diluted with CH_2Cl_2 (10 mL) and washed with an EDTA/NH_4OH solution (2 × 15 mL) followed by brine (2 × 15 mL). The organic layer was dried over $MgSO_4$ and concentrated under reduced pressure. The residue was purified by silica gel flash column chromatography (eluent: 1:1 CH_2Cl_2/hexane) to afford **3.4** as an orange solid (46 mg, 49%).

^{1}H NMR (500 MHz, $CDCl_3$) δ 8.91 (d, J = 4.5 Hz, 1H, H_a), 8.18 (d, J = 4.5 Hz, 1H, H_b).

^{13}C NMR (126 MHz, $CDCl_3$) δ 148.28, 147.06, 143.95 (dm, J = 263 Hz), 143.95 (dm, J = 263 Hz), 143.68 (dm, J = 258 Hz), 138.22 (dm, J = 257 Hz) 137.44, 128.92, 122.68, 111.85 (t, J = 13.9 Hz), 84.84.

HRMS (ESI+ve) m/z: 886.8192 ($[M+H]^+$, $C_{22}H_3O_4N_8F_{10}I_2$ requires 886.8201).

Phenyl-based acyclic XB receptor (3.5)



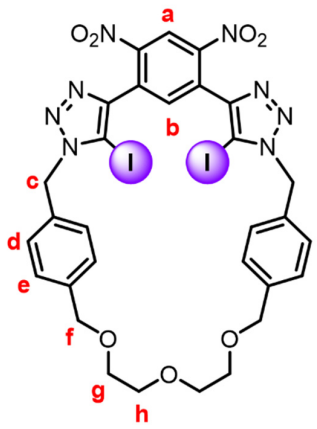
Following General Procedure 3A, the reaction between 1,3-bis(iodoethynyl)benzene (40 mg, 0.11 mmol), perfluorophenyl azide (44 mg, 0.22 mmol), $[Cu(MeCN)_4]PF_6$ (20 mg, 0.053 mmol) and TBTA (14 mg, 0.026 mmol), followed by silica gel flash column chromatography (eluent: 2:8 CH_2Cl_2/hexane) afforded **3.5** as a white solid (59 mg, 70%).

^{1}H NMR (500 MHz, DMSO-d_6) δ 8.75 (t, J = 1.7 Hz, 1H, H_b), 8.16 (dd, J = 7.8, 1.8 Hz, 2H, H_c), 7.69 (t, J = 7.8 Hz, 1H, H_a).

^{13}C NMR (126 MHz, DMSO-d_6) δ 146.67, 143.34 –140.97 (Coincident ^{13}C signals), 137.68 (d, J = 251.9 Hz), 130.19, 130.05, 125.83, 124.72, 122.55, 112.47 (d, J = 13.6 Hz).

HRMS (ESI+ve) m/z: 545.0578 ($[M+H]^+$, $C_{22}H_7F_{10}N_6$ requires 545.0573).

Diethylene glycol-based halogen bonding macrocycle (3.1·XB^{DEG})



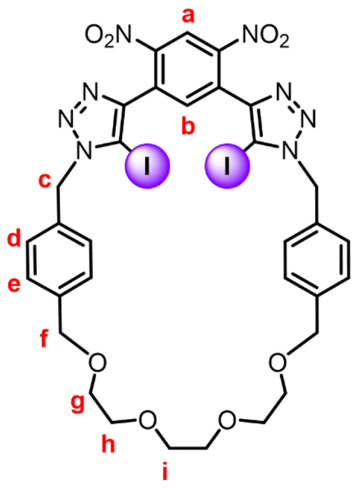
Using General Procedure 2B, the CuAAC click reaction between diethylene glycol-based bis-azide **2.3** (85 mg, 0.21 mmol) and bis(iodoalkyne) **3.3** (100 mg, 0.21 mmol), $[Cu(MeCN)_4]PF_6$ (40 mg, 0.11 mmol) and TBTA (28 mg, 0.053 mmol), followed by purification by silica gel chromatography (eluent: 10% EtOAc/CH_2Cl_2) afforded **3.1·XB^{DEG}** as a yellow solid (78 mg, 42%).

^{1}H NMR (500 MHz, $CDCl_3$) δ 8.72 (s, 1H, H_a), 7.73 (s, 1H, H_b), 7.38 (d, J = 8.2 Hz, 4H, H_d), 7.29 (d, J = 8.1 Hz, 4H, H_e), 5.63 (s, 4H, H_c), 4.48 (s, 4H, H_f), 3.65 (t, J = 5.0 Hz, 4H, $H_{g/h}$), 3.54 (t, J = 5.0 Hz, 4H, $H_{g/h}$).

^{13}C NMR (126 MHz, $CDCl_3$) δ 148.34, 146.57, 139.03, 137.10, 133.12, 129.67, 128.84, 128.79, 122.01, 79.70, 73.02, 70.78, 69.77, 54.69.

HRMS (ESI +ve) m/z: 865.0065 ($[M+H]^+$, $C_{30}H_{27}O_7N_8I_2$ requires 865.0087).

Triethylene glycol-based halogen bonding macrocycle (3.1·XB^{TEG})



Using General Procedure 2B, the CuAAC click reaction between triethylene glycol-based bis-azide **2.4** (100 mg, 0.23 mmol) and bis(iodoalkyne) **3.3** (108 mg, 0.23 mmol), $[Cu(CH_3CN)_4]PF_6$ (43 mg, 0.12 mmol) and TBTA (31 mg, 0.058 mmol), followed by purification by silica gel chromatography (eluent: 30% EtOAc/CH_2Cl_2) afforded **3.1·XB^{TEG}** as an orange solid (76 mg, 37%).

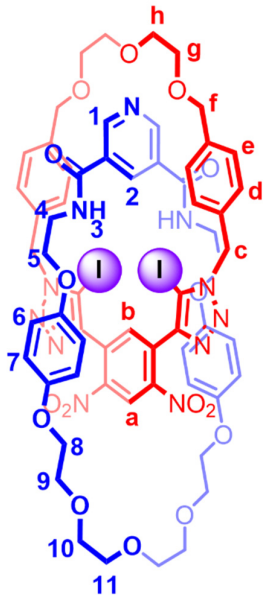
^{1}H NMR (500 MHz, $CDCl_3$) δ 8.72 (s, 1H, H_a), 7.79 (s, 1H, H_b), 7.32 (d, J = 2.6 Hz, 8H, H_d, H_e), 5.65 (s, 4H, H_c), 4.53 (s, 4H, H_f), 3.69 – 3.65 (m, 8H, $H_{g/h}$, H_i), 3.62 (dd, J = 5.7, 3.0 Hz, 4H, $H_{g/h}$).

^{13}C NMR (126 MHz, $CDCl_3$) δ 148.30, 146.50, 139.38, 137.00, 132.97, 129.65, 128.44, 128.21, 122.06, 79.92, 72.84, 71.18, 70.98, 70.36, 54.70.

HRMS (ESI +ve) m/z: 909.0331 ($[M+H]^+$, $C_{32}H_{31}O_8N_8I_2$ requires 909.0349).

General Procedure 3B: Chloride Template-Directed [2]Catenane Synthesis

Diethylene glycol-based halogen bonding [2]catenane (3.2·XB^{DEG})



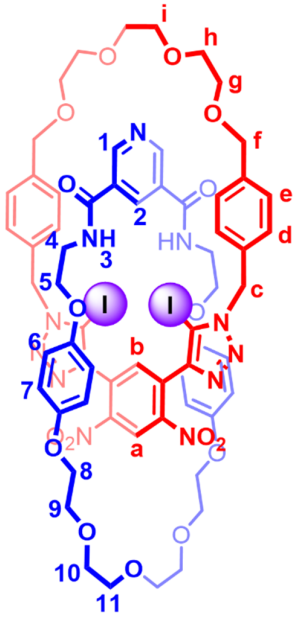
3,5-Pyridinedicarboxylic acid (58 mg, 0.34 mmol) was suspended in neat oxalyl chloride (2 ml), to which was added one drop of DMF. After stirring for 2 hours, the mixture became homogenous, at which point the volatiles were removed in vacuo to afford the corresponding bis-acid chloride **3.7**. In a separate flask, **3.1·XB^{DEG}** (30 mg, 0.034 mmol), bis-amine **3.6** (161 mg, 0.34 mmol), TBACl (9.6 mg, 0.034 mmol) and NEt_3 (0.1 mL) were dissolved in anhydrous CH_2Cl_2 (12 mL) and cooled to 0 °C. Bis-acid chloride **3.7** was dissolved in anhydrous CH_2Cl_2 (3 mL) and added dropwise to reaction mixture, after which the mixture was allowed to warm to room temperature and stirred overnight. The reaction mixture was diluted with CH_2Cl_2 (50 mL) and washed with sat. K_2CO_3 (aq) (2 × 30 mL) and H_2O (2 × 30 mL), the collected organic phase was dried over $MgSO_4$, concentrated to dryness *in vacuo* and purified by preparative thin layer chromatography (25:1 CH_2Cl_2/MeOH) to yield **3.2·XB^{DEG}** as a yellow solid (8.5 mg, 17%).

^{1}H NMR (600 MHz, $CDCl_3$) δ 8.98 (s, 2H, H_1), 8.67 (s, 1H, H_a), 8.39 (s, 1H, H_2), 8.18 (s, 1H, H_b), 7.53 (br s, 2H, H_3), 7.06 (d, *J* = 8.1 Hz, 4H, H_d), 6.86 (d, *J* = 8.1 Hz, 4H_e), 6.54 (d, *J* = 9.2 Hz, 4H, H_7), 6.48 (d, *J* = 9.1 Hz, 4H, H_6), 5.45 (s, 4H, H_c), 4.21 (s, 4H, H_f), 3.99 – 3.95 (m, 4H, H_8), 3.84 – 3.77 (m, 8H, H_5, H_9), 3.71 (s, 8H, H_{10}, H_{11}), 3.52 – 3.41 (m, 12H, H_g, H_h, H_4).

^{13}C NMR (151 MHz, acetone-d_6) δ 165.13, 153.09, 152.40, 152.09, 148.29, 146.76, 137.88, 137.72, 133.52, 132.84, 129.59, 128.44, 128.40, 128.22, 121.67, 115.56, 114.95, 80.66, 73.17, 70.90, 70.80, 70.71, 69.95, 69.84, 68.10, 66.51, 54.24, 40.01, 29.85.

HRMS (ESI +ve) m/z: 1460.2571 ($[M+H]^+$, $C_{61}H_{64}O_{16}N_{11}I_2$ requires 1460.2617).

Triethylene glycol-based halogen bonding [2]catenane (3.2·XB^{TEG})



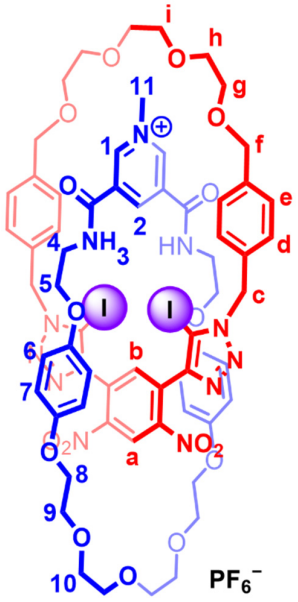
Following General Procedure 3B, the reaction between 3,5-pyridinedicarboxylic acid (55 mg, 0.33 mmol), **3.1·XB^{TEG}** (30 mg, 0.033 mmol), bis-amine **3.6** (153 mg, 0.33 mmol), TBACl (9 mg, 0.033 mmol) and NEt_3 (0.1 ml), followed by purification by preparative thin layer chromatography (25:1 CH_2Cl_2/MeOH), afforded **3.2·XB^{TEG}** as a yellow solid (11 mg, 22%).

^{1}H NMR (600 MHz, $CDCl_3$) δ 9.12 (d, *J* = 2.1 Hz, 2H, H_1), 8.58 (s, 1H, H_a), 8.51 (s, 1H, H_2), 7.88 (s, 1H, H_b), 7.63 (t, *J* = 5.4 Hz, 2H, H_3), 7.13 (d, *J* = 8.2 Hz, 4H, H_d), 7.03 (d, *J* = 8.2 Hz, 4H, H_e), 6.47 (d, *J* = 9.1 Hz, 4H, H_7), 6.40 (d, *J* = 9.1 Hz, 4H, H_6), 5.46 (s, 4H, H_c), 4.28 (s, 4H, H_f), 3.96 – 3.91 (m, 4H, H_8), 3.79 (t, *J* = 5.0 Hz, 4H, H_5), 3.78-3.76 (m, 4H, H_9), 3.69 (m, 8H, H_{10}, H_{11}), 3.55 (m, 4H, H_4), 3.49 – 3.43 (m, 12H, H_g, H_h, H_i).

^{13}C NMR (151 MHz, $CDCl_3$) δ 165.43, 153.05, 152.37, 152.18, 148.18, 146.16, 138.54, 136.48, 133.31, 132.61, 129.08, 128.90, 128.30, 128.12, 121.67, 115.50, 115.03, 81.15, 72.82, 70.86, 70.83, 70.77, 70.70, 70.04, 69.94, 68.09, 66.65, 54.34, 40.08, 29.85.

HRMS (ESI +ve) m/z: 1504.2837 ($[M+H]^+$, $C_{63}H_{68}O_{17}N_{11}I_2$ requires 1504.2879).

Methylated triethylene glycol-based halogen bonding [2]catenane ($3.3{\cdot}XB^{TEG}{\cdot}PF_6$)



Tri-ethylene glycol-based XB [2]catenane **$3.2{\cdot}XB^{TEG}$** (4.1 mg, 0.0027 mmol) was dissolved in anhydrous CH_2Cl_2 (0.5 mL), to which was added MeI (50 µL). The reaction was allowed to stir overnight at room temperature, after which a further aliquot of MeI (20 µL) was added. The reaction was allowed to stir for a further 6 hours, after which the solvent was removed *in vacuo* to afford **$3.3{\cdot}XB^{TEG}{\cdot}I$** as a yellow solid. Subsequent anion exchange was performed by dissolving the crude in a solvent mixture of 1% H_2O/acetone (v/v) (10 mL) and passing the solution three times through a column of Amberlite® resin loaded with hexafluorophosphate to yield **$3.3{\cdot}XB^{TEG}{\cdot}PF_6$** as an orange solid (3.3 mg, 80%).

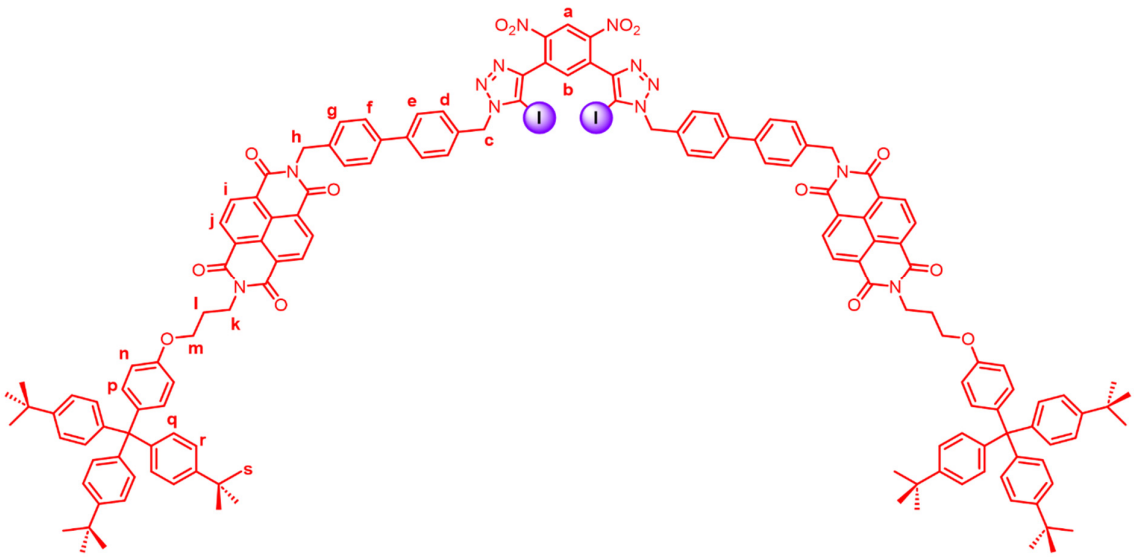
^{1}H NMR (600 MHz, $CDCl_3$) δ 9.00 (s, 2H, H_1), 8.98 (s, 1H, H_2), 8.70 (s, 1H, H_a), 8.00 (s, 1H, H_b), 7.91 (t, J = 5.4 Hz, 2H, H_3), 7.07 (s, 8H, $H_{d,e}$), 6.60 (d, J = 8.6 Hz, 4H, $H_{6/7}$), 6.55 (d, J = 8.6 Hz, 4H, $H_{6/7}$), 5.44 (s, 4H, H_c), 4.38 (s, 3H, H_{11}), 4.29 (s, 4H, H_f), 3.97 (dd, J = 5.8, 3.3 Hz, 4H, H_7), 3.89 (t, J = 4.8 Hz, 4H, H_4), 3.79 – 3.73 (m, 4H, H_8), 3.70 – 3.62 (m, 8H, $H_{9,10}$), 3.55 – 3.47 (m, 16H, H_5, $H_{i\text{-}g}$).

^{13}C NMR (151 MHz, $CDCl_3$) δ 160.74, 153.05, 152.27, 147.91, 146.41, 146.22, 141.31, 138.32, 137.54, 133.92, 133.68, 129.46, 128.27, 127.93, 121.67, 115.57, 114.86, 81.84, 72.59, 70.65, 70.59, 70.31, 70.25, 70.01, 69.81, 69.53, 67.88, 66.16, 53.97, 53.81, 49.09, 40.52, 31.74, 29.71, 29.28.

HRMS (ESI +ve) m/z: 1518.3109 ($[M\text{-}PF_6]^+$, $C_{64}H_{70}O_{17}N_{11}I_2$ requires 1518.3041).

General Procedure 3C: CuAAC-mediated Synthesis of XB Axles

3-station-bis(iodotriazole)-bis(naphthalene diimide) functionalised axle (3.10)



$[Cu(MeCN)_4]PF_6$ (12 mg, 0.032 mmol) and TBTA (8.5 mg, 0.016 mmol) were dissolved in dry, degassed CH_2Cl_2 (2 mL) and the mixture was stirred at room temperature under N_2 for 15 minutes. A solution of naphthalene diimide funcionalised stopper azide **3.9** (146 mg, 0.14 mmol) in dry, degassed CH_2Cl_2 (1.5 mL) was added, followed by 2,4-dinitro-bis(iodoalkyne) **3.3** (30 mg, 0.064 mmol) in dry, degassed CH_2Cl_2 (1.5 mL). The reaction mixture was stirred overnight at room temperature under N_2 in the dark. The crude reaction mixture was diluted with CH_2Cl_2 and washed with aqueous EDTA/NH_4OH solution (50 mL × 2), water (50 mL × 2) and brine (50 mL). The organic layer was dried over anhydrous $MgSO_4$, filtered and concentrated on the rotary evaporator. The residue was purified by silica gel chromatography (eluent: 0.5% MeOH/DCM) to give **3.10** as an orange solid (146 mg, 91%).

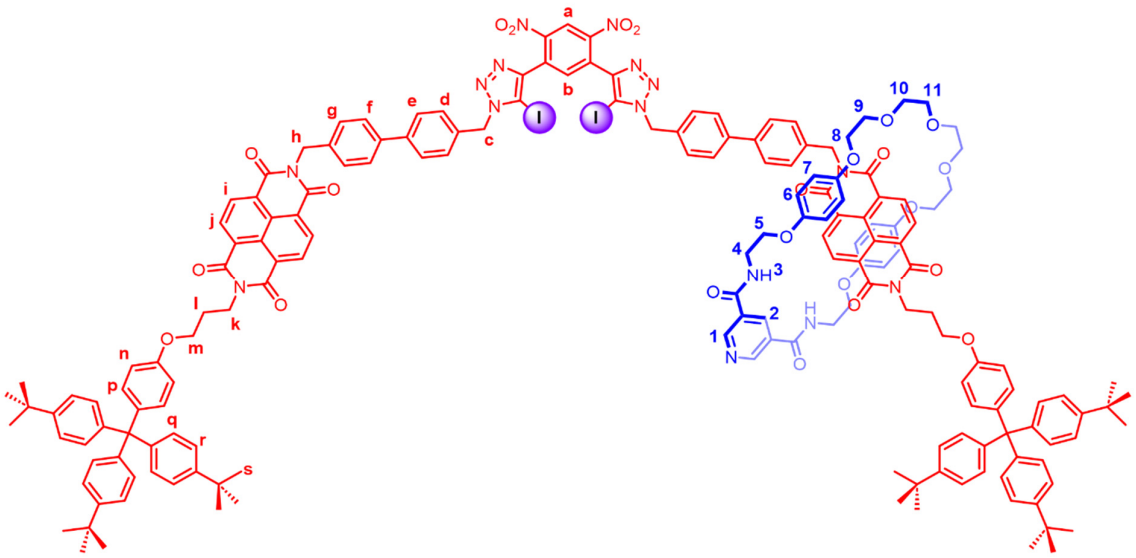
^{1}H NMR (500 MHz, $CDCl_3$) δ 8.79 – 8.68 (m, 9H, $H_{a,i,j}$), 7.95 (s, 1H, H_b), 7.62 (d, J = 8.4 Hz, 4H, H_e), 7.53 (m, 8H, $H_{g,f}$), 7.32 (d, J = 8.5 Hz, 4H, H_d), 7.22 (d, J = 8.7 Hz, 12H, $H_{q/r}$), 7.05 (d, J = 8.7 Hz, 12H, $H_{q/r}$), 7.01 (d, J = 9.0 Hz, 4H, H_p), 6.63 (d, J = 9.0 Hz, 4H, H_n), 5.69 (s,

5H, H_c), 5.42 (s, 4H, H_h), 4.41 (t, J = 7.0 Hz, 4H, H_k), 4.09 (t, J = 6.1 Hz, 4H, H_m), 2.24 (m, 4H, H_l), 1.29 (s, 54H, H_s).

^{13}C NMR (126 MHz, $CDCl_3$) δ 163.05, 162.96, 156.66, 148.46, 147.89, 146.69, 144.27, 141.41, 139.92, 139.82, 137.38, 136.19, 132.76, 132.32, 131.36, 131.17, 130.85, 129.86, 129.79, 128.31, 127.87, 127.45, 126.90, 126.86, 126.71, 124.18, 122.23, 113.07, 80.55, 66.11, 63.18, 54.63, 43.87, 38.81, 34.44, 31.53, 28.11.

HRMS (ESI +ve) m/z: 2531.8137 ($[M+H]^+$, $C_{146}H_{133}N_{12}O_{14}I_2$ requires 2531.8154).

XB 3-station-[2]rotaxane (3.11).



3,5-Pyridinedicarboxylic acid (34 mg, 0.20 mmol) was suspended in neat oxalyl chloride (2 ml), to which was added one drop of DMF. After stirring for 2 hours, the mixture became homogenous, at which point the volatiles were removed in vacuo to afford the corresponding bis-acid chloride. In a separate flask, axle **3.10** (50 mg, 0.020 mmol), bis-amine **3.6** (92 mg, 0.20 mmol), TBACl (5.6 mg, 0.020 mmol) and NEt_3 (0.1 mL) were dissolved in anhydrous CH_2Cl_2 (10 ml) and cooled to 0 °C. A freshly-prepared solution of bis-acid chloride **3.7** was dissolved in anhydrous CH_2Cl_2 (3 mL) and added dropwise to reaction mixture, after which the mixture was allowed to warm to room temperature and stirred overnight. The reaction mixture was diluted with CH_2Cl_2 (50 mL) and washed with sat. K_2CO_3 (aq) (2 × 30 mL) and H_2O (2 × 30 mL), the collected organic phase was dried over $MgSO_4$, concentrated to dryness *in vacuo* and purified by iterative preparative thin layer chromatography (4% MeOH/CH_2Cl_2 followed by 40% acetone/toluene) to yield rotaxane **3.11** as an orange solid (7.0 mg, 11%).

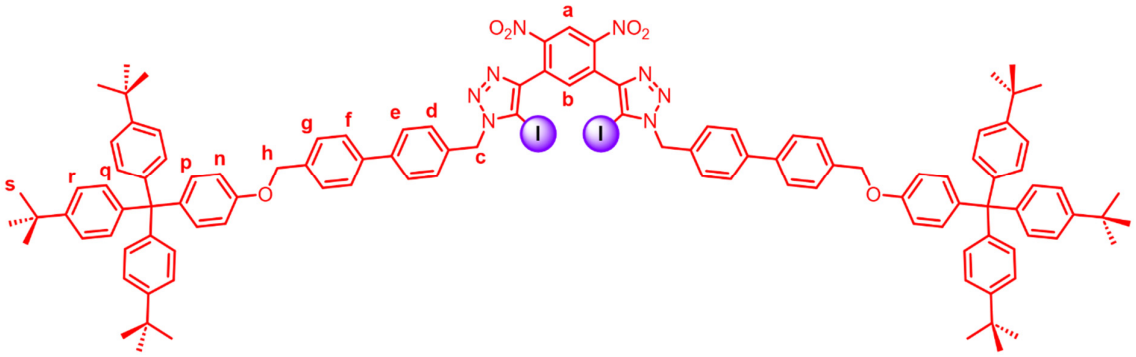
^{1}H NMR (500 MHz, acetone-d_6) δ 9.21 (d, J = 2.2 Hz, 2H, H_2), 9.17 (d, J = 2.2 Hz, 1H, H_1), 8.77 (s, 1H, H_a), 8.70 – 8.63 (m, 8H, $H_{i,j}$), 8.08 (s, 1H, H_b), 7.96 (br, 2H, H_3), 7.60 (d, J = 8.2

Hz, 4H, H_e), 7.57 – 7.50 (m, 8H, $H_{f,g}$), 7.36 (d, *J* = 8.2 Hz, 4H, H_d), 7.29 – 7.24 (m, 12H, H_q), 7.10 – 7.05 (m, 12H, H_r), 7.04 – 6.99 (d, *J* = 8.9 Hz, 4H, H_p), 6.74 – 6.67 (d, *J* = 8.9 Hz, 4H, H_n), 5.80 (m, 8H, $H_{c,6}$), 5.75 – 5.70 (m, 4H, H_7), 5.28 (s, 4H, H_h), 4.31 (t, *J* = 7.0 Hz, 4H, H_k), 4.07 (t, *J* = 6.1 Hz, 4H, H_m), 3.91 – 3.82 (m, 4H, $H_{8\text{-}11}$), 3.75 – 3.71 (m, 4H, $H_{8\text{-}11}$), 3.66 (s, 8H, $H_{4,5}$), 3.60 – 3.55 (m, 4H, $H_{8\text{-}11}$), 3.48 (m, 4H, $H_{8\text{-}11}$), 2.20 (m, 4H, H_l), 1.27 (s, 54H, H_s).

^{13}C NMR (151 MHz, $CDCl_3$) δ 165.56, 163.38, 163.11, 156.72, 153.15, 152.46, 151.60, 148.48, 147.87, 146.64, 144.25, 141.20, 140.08, 139.99, 137.28, 136.05, 132.90, 132.38, 131.34, 131.26, 131.00, 130.85, 130.08, 129.75, 128.84, 128.39, 127.85, 127.39, 126.62, 126.53, 126.50, 126.28, 124.19, 122.20, 114.49, 113.94, 113.21, 80.66, 70.97, 69.65, 67.45, 67.21, 66.10, 63.19, 54.61, 44.00, 40.51, 38.73, 34.44, 31.53, 29.85, 28.24.

HRMS (ESI +ve) m/z: 3127.0562 ($[M+H]^+$, $C_{177}H_{170}N_{15}O_{23}I_2$ requires 3127.0678).

1-station-bis(iodotriazole) functionalised axle (3.13)



Following General Procedure 3C, the reaction between a biphenyl-functionalised stopper azide **3.12** (34 mg, 0.047 mmol), 2,4-dinitro-1,3-bis(iodoalkyne) **3.3** (10 mg, 0.021 mmol), $[Cu(MeCN)_4]PF_6$ (4.0 mg, 0.011 mmol) and TBTA (2.8 mg, 0.005 mmol), followed by purification via silica gel chromatography (eluent: 1% EtOAc/DCM), afforded **3.13** as a yellow solid (35 mg, 87%).

^{1}H NMR (500 MHz, acetone-d_6) δ 8.80 (s, 1H, H_a), 7.99 (s, 1H, H_b), 7.60 (m, 8H, $H_{e,f}$), 7.50 (d, J = 8.4 Hz, 4H, H_g), 7.36 (d, J = 8.4 Hz, 4H, H_d), 7.23 (d, J = 8.7 Hz, 12H, H_r), 7.14 – 7.05 (m, 16H, $H_{p,q}$), 6.85 (d, J = 9.0 Hz, 4H, H_n), 5.73 (s, 4H, H_c), 5.06 (s, 4H, H_h), 1.30 (s, 54H, H_s).

^{13}C NMR (151 MHz, $CDCl_3$) δ 156.78, 148.48, 147.92, 146.73, 144.26, 141.54, 140.12, 140.00, 137.41, 136.87, 132.76, 132.47, 130.89, 129.83, 128.35, 128.25, 127.92, 127.45, 124.20, 122.25, 113.45, 80.56, 69.78, 63.23, 54.69, 34.45, 31.54.

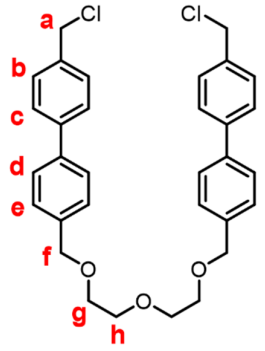
HRMS (ESI +ve) m/z: 1919.6820 ($[M+H]^+$, $C_{112}H_{113}N_8O_6I_2$ requires 1919.6867).

6.2.3 Compounds from Chapter 4

The 2,6-dimethanolpyridine-functionalised macrocycles **4.6-4.8**,[3, 12] bis-amine **4.18**[12] and stopper bromide **4.26**[13] were prepared according to literature reports.

General Procedure 4A: Synthesis of Oligo(Ethylene Glycol)-Based Dichlorides

Diethylene glycol-based dichloride (4.1)



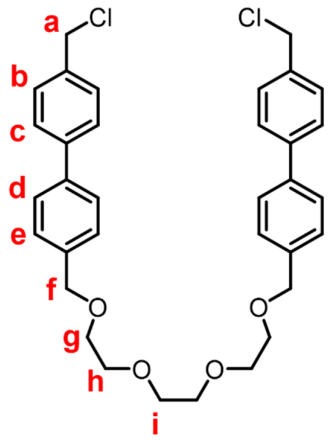
To a solution of diethylene glycol (1.0 mL, 11.1 mmol) in THF (100 mL), NaH (0.80 g, 33.3 mmol) was added portion-wise and the suspension was allowed to stir at room temperature for 20 minutes. 4,4'-bis(chloromethyl)-biphenyl (11.2 g, 44.5 mmol) was added and the reaction mixture was stirred at reflux for 24 hours, after which the precipitate was removed by filtration, and the filtrate concentrated *in vacuo*. The residue was redissolved in CH_2Cl_2 (100 mL), the organic layer washed with H_2O (2 × 100 mL) and brine (2 × 100 mL), dried over $MgSO_4$ and the solvent removed under vacuum. Purification by silica gel column chromatography (eluent: 2% EtOAC/CH_2Cl_2) afforded the dichloride **2.1** as a white solid (1.90 g, 32%).

^{1}H NMR (400 MHz, $CDCl_3$) δ 7.55 (m, 8H, $H_{c,d}$), 7.43 (m, 8H, $H_{b,e}$), 4.63 (s, 4H, $H_{a/f}$), 4.62 (s, 4H, $H_{a/f}$), 3.77 – 3.66 (m, 8H, $H_{g,h}$).

^{13}C NMR (126 MHz, $CDCl_3$) δ 141.23, 139.93, 137.85, 136.59, 129.21, 128.38, 127.55, 127.25, 73.09, 70.93, 69.75, 46.19.

HRMS (ESI +ve) m/z: 535.1809 ($[M+H]^+$, $C_{32}H_{33}Cl_2O_3$ requires 535.1801).

Triethylene glycol-based dichloride (4.2)



Following General Procedure 4A, the reaction between tri(ethylene glycol) (1.0 mL, 7.32 mmol), NaH (0.70 g, 29.3 mmol) and 4,4'-bis(chloromethyl)-biphenyl (7.36 g, 29.3 mmol), followed by purification via silica gel column chromatography (eluent: 5% EtOAc/CH_2Cl_2), afforded the dichloride **4.2** as a white solid (1.48 g, 35%).

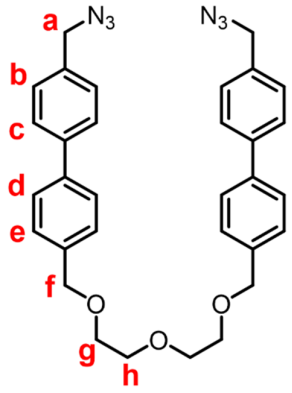
^{1}H NMR (400 MHz, $CDCl_3$) δ 7.58 – 7.53 (m, 8H, $H_{c,d}$), 7.44 (d, J = 8.3 Hz, 4H, $H_{b/e}$), 7.41 (m, J = 8.3 Hz, 4H, $H_{b/e}$), 4.63 (s, 4H, $H_{a/f}$), 4.61 (s, 4H, $H_{a/f}$), 3.77 – 3.63 (m, 12H, $H_{g,h,i}$).

^{13}C NMR (126 MHz, $CDCl_3$) δ 141.21, 139.92, 137.83, 136.58, 129.19, 128.36, 127.54, 127.23, 73.06, 70.85, 69.71, 46.17. *Undetected aliphatic signal believed to be coincident.*

HRMS (ESI +ve) m/z: 579.2070 ($[M+H]^+$, $C_{34}H_{37}Cl_2O_4$ requires 579.2063).

General Procedure 4B: Conversion of Dichlorides to Bis-azides

Diethylene glycol-based bis-azide (4.3)



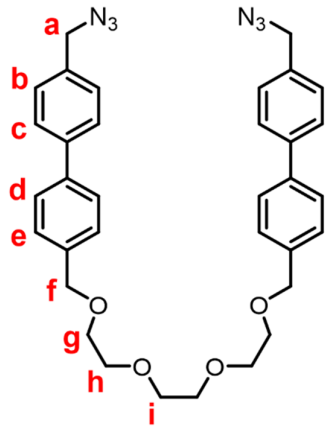
Dichloride **4.1** (1.0 g, 1.87 mmol) was dissolved in DMSO (9 mL). Sodium azide (0.49 g, 7.48 mmol) was added and the reaction mixture was stirred at room temperature overnight. The crude reaction mixture was diluted with H_2O (50 mL) and extracted with diethyl ether (30 mL × 3). The combined organic layer was washed with brine (30 mL × 3), dried over anhydrous $MgSO_4$, filtered and concentrated in vacuo to afford **2.4** as a white solid (0.95 g, 93%).

^{1}H NMR (400 MHz, $CDCl_3$) δ 7.58 (d, J = 7.9 Hz, 4H, H_d), 7.55 (d, J = 7.9 Hz, 4H, H_c), 7.42 (d, J = 7.9 Hz, 4H, H_e), 7.37 (d, J = 7.9 Hz, 4H, H_b), 4.63 (s, 4H, H_f), 4.38 (s, 4H, H_a), 3.77 – 3.66 (m, 8H, $H_{g,h}$).

^{13}C NMR (126 MHz, $CDCl_3$) δ 141.08, 139.93, 137.80, 134.48, 128.78, 128.37, 127.60, 127.21, 73.07, 70.90, 69.72, 54.66.

HRMS (ESI +ve) m/z: 549.2615 ($[M+H]^+$, $C_{32}H_{33}N_6O_3$ requires 549.2609).

Diethylene glycol-based bis-azide (4.4)



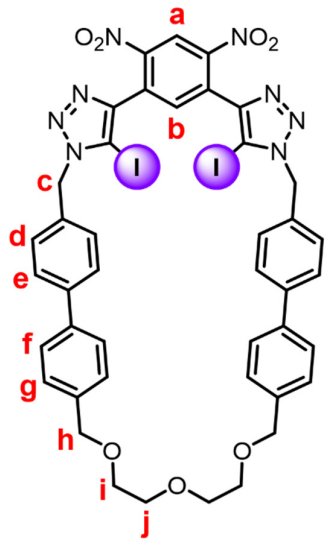
Following general procedure 4B, the reaction of dichloride **4.2** (1.46 g, 2.53 mmol) and sodium azide (0.66 g, 10.1 mmol) yielded the desired product as a white solid (1.48 g, quant).

^{1}H NMR (400 MHz, $CDCl_3$) δ 7.59 (d, *J* = 6.3 Hz, 4H, H_d), 7.56 (d, *J* = 6.2 Hz, 4H, H_c), 7.44 – 7.41 (d, *J* = 6.3 Hz, 4H, H_e), 7.37 (d, *J* = 6.3 Hz, 4H, H_b), 4.61 (s, 4H, H_f), 4.38 (s, 4H, H_a), 3.74 – 3.65 (m, 12H, $H_{g,h,i}$).

^{13}C NMR (126 MHz, $CDCl_3$) δ 141.08, 139.93, 137.79, 134.48, 128.78, 128.36, 127.61, 127.21, 73.05, 70.85, 69.70, 54.66. *Undetected aliphatic signal believed to be coincident.*

HRMS (ESI +ve) m/z: 593.2865 ($[M+H]^+$, $C_{34}H_{37}N_6O_4$ requires 593.2871).

Biphenyl-based XB Macrocycle (4.5)



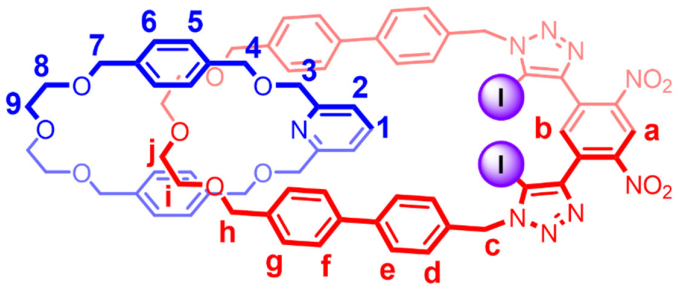
Using General Procedure 2B, the CuAAC click reaction between bis-azide **4.3** (114 mg, 0.21 mmol) and bis(iodoalkyne) **3.3** (100 mg, 0.21 mmol), $[Cu(MeCN)_4]PF_6$ (40 mg, 0.11 mmol) and TBTA (28 mg, 0.053 mmol), followed by purification by silica gel chromatography (eluent: 8% EtOAc/CH_2Cl_2) afforded macrocycle **4.5** as a yellow solid (86 mg, 40%).

^{1}H NMR (400 MHz, $CDCl_3$) δ 8.74 (s, 1H, H_a), 7.77 (s, 1H, H_b), 7.53 (d, J = 8.2 Hz, 4H, H_f), 7.47 (d, J = 8.2 Hz, 4H, H_e), 7.41 (d, J = 8.3 Hz, 4H, H_g), 7.38 (d, J = 8.2 Hz, 4H, H_d), 5.70 (s, 4H, H_c), 4.61 (s, 4H, H_h), 3.86 – 3.62 (m, 8H, $H_{i,j}$).

^{13}C NMR (126 MHz, $CDCl_3$) δ 148.32, 146.57, 141.72, 139.54, 137.98, 137.08, 132.65, 129.64, 128.86, 128.38, 127.79, 127.19, 122.10, 79.89, 73.06, 71.04, 69.94, 54.62.

HRMS (ESI +ve) m/z: 1017.5981 ($[M+H]^+$, $C_{42}H_{35}N_8O_7I_2$ requires 1017.5994).

XB hetero[2]catenane ($4.9^{DEG\text{-}4.6}$)



Following General Procedure 2C, the reaction between macrocycle **4.6** (40.0 mg, 0.088 mmol), $NaBAr^F$ (78.8 mg, 0.088 mmol), bis-azide **4.3** (47.6 mg, 0.088 mmol), bis-iodoalkyne **3.3** (41.6 mg, 0.088 mmol), $[Cu(CH_3CN)_4]PF_6$ (16.4 mg, 0.044 mmol) and TBTA (23.6 mg, 0.044 mmol), followed by iterative preparative TLC purification (eluent: 60:40:1 CH_2Cl_2/EtOAc/MeOH, then 2.5% MeOH/CH_2Cl_2), afforded [2]catenane **4.9** as an orange solid (18 mg, 14%).

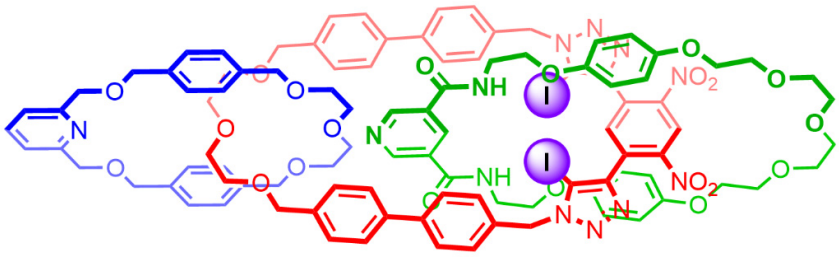
^{1}H NMR (500 MHz, acetone-d_6) δ 8.80 (s, 1H, H_a), 8.06 (s, 1H, H_b), 7.66 (t, J = 7.8 Hz, 1H, H_1), 7.42 (m, 8H, $H_{e,f}$), 7.28 – 7.17 (m, 8H, $H_{d,g,2}$), 6.89 (d, J = 7.6 Hz, 4H, H_5), 6.80 (d, J = 7.6 Hz, 4H, H_6), 5.77 (s, 4H, H_c), 4.38 (s, 4H, H_4), 4.32 (s, 4H, H_h), 4.26 (s, 4H, H_3), 4.09 (s, 4H, H_7), 3.36 – 3.25 (m, 16H, $H_{i,j,8,9}$).

^{13}C NMR (151 MHz, acetone-d_6) δ 158.78, 149.48, 146.99, 141.33, 139.80, 139.00, 138.25, 137.82, 137.46, 136.81, 134.22, 130.04, 129.20, 128.95, 128.90, 128.86, 128.28, 127.65, 122.84, 120.23, 82.57, 73.46, 72.96, 72.83, 72.28, 71.00, 70.91, 69.97, 69.66, 54.73.

HRMS (ESI +ve) m/z: 1466.2897 ($[M+H]^+$, $C_{69}H_{66}N_9O_{12}I_2$ requires 1466.2915).

Note: Only the spectral data for the highest-yielding [2]catenane ***4.9$^{DEG\text{-}4.6}$*** *has been included due to the challenging purification and low yields of the other analogues.*

Hetero[3]catenane (4.10)

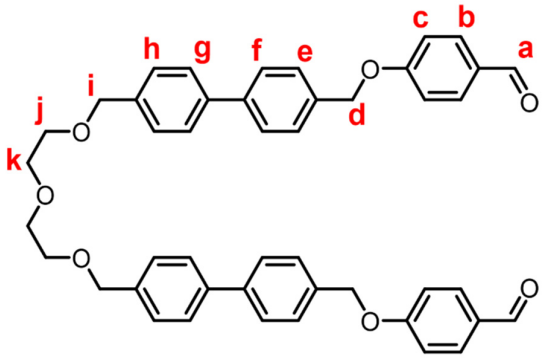


Following General Procedure 3B, the reaction between 3,5-pyridinedicarboxylic acid (17 mg, 0.10 mmol), **4.9**$^{\mathbf{DEG\text{-}4.6}}$ (15 mg, 0.010 mmol), bis-amine **3.6** (48 mg, 0.10 mmol), TBACl (2.9 mg, 0.010 mmol) and NEt_3 (0.5 ml), followed by purification by iterative preparative thin layer chromatography (50:50:4 CH_2Cl_2/EtOAc/MeOH), afforded **4.10** as a yellow solid (2.5 mg, 12%).

^{1}H NMR and **^{13}C NMR** spectral data could not be obtained due to the low yield of **4.10** as well as broadening of NMR resonances (see **Section 4.22** for details).

HRMS (ESI +ve) m/z: 2062.5374 ($[M+H]^+$, $C_{100}H_{103}N_{12}O_{21}I_2$ requires 2062.5478).

Extended biphenyl-containing dialdehyde (4.11)



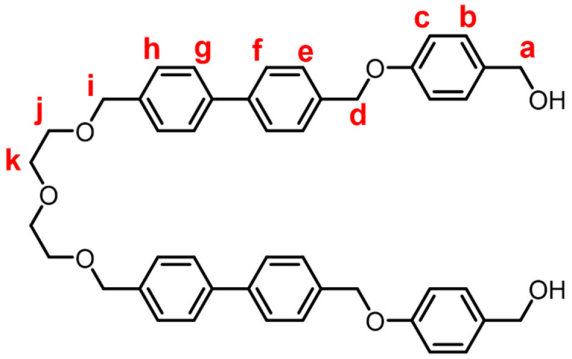
4-Hydroxybenzaldehyde (0.34 g, 2.8 mmol) and K_2CO_3 (0.62 g, 4.5 mmol) were suspended in anhydrous MeCN (20 mL) and stirred at room temperature for 15 minutes. Dichloride **4.1** (0.60 g, 1.1 mmol) was added and the reaction mixture allowed to stir at reflux for 12 hours, after which it was diluted with CH_2Cl_2 (60 mL), washed with H_2O (2 × 50 mL) and brine (2 × 50 mL), dried over $MgSO_4$ and concentrated under vacuum. The residue was purified by silica gel column chromatography (eluent: 3% EtOAc/CH_2Cl_2) to afford dialdehyde **4.11** as a white solid (0.63 g, 80%).

^{1}H NMR (400 MHz, $CDCl_3$) δ 9.81 (s, 2H, H_a), 7.79 – 7.76 (m, 4H, H_b), 7.55 – 7.51 (m, 4H, H, H_g), 7.51 – 7.47 (m, 4H, H_f), 7.41 (d, J = 8.1 Hz, 4H, H_h), 7.35 (d, J = 8.2 Hz, 4H, H_e), 7.03 – 7.00 (m, 4H, H_c), 5.10 (s, 4H, H_d), 4.55 (s, 4H, H_i), 3.69 – 3.58 (m, 8H, $H_{j,k}$).

^{13}C NMR (101 MHz, $CDCl_3$) δ 190.91, 163.84, 141.18, 140.01, 137.80, 135.01, 132.16, 130.31, 128.39, 128.14, 127.54, 127.24, 115.29, 77.48, 77.16, 76.84, 73.09, 70.91, 70.18, 69.74.

HRMS (ESI +ve) m/z: 707.3012 ($[M+H]^+$, $C_{46}H_{43}O_7$ requires 707.3003).

Extended biphenyl-containing diol (4.12)



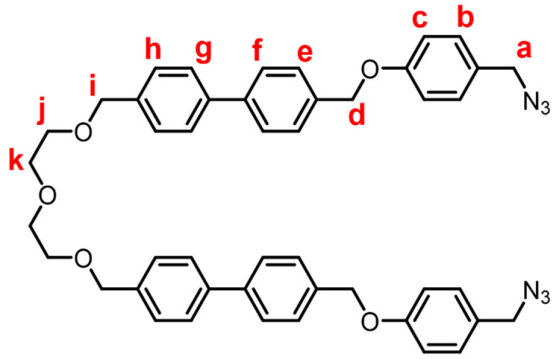
Dialdehyde **4.11** (0.75 g, 1.1 mmol) was suspended in MeOH/CH_2Cl_2 (12 mL, 1:1 v/v) and cooled to 0°C. Sodium borohydride (96 mg, 2.6 mmol) was added portion-wise and the reaction mixture was allowed to stir at room temperature for 2 hours. The reaction was quenched with aqueous sat. NH_4Cl (20 mL) and diluted with CH_2Cl_2 (30 mL). The organic layer was washed with H_2O (2 × 25 mL) and brine (2 × 25 mL), dried over $MgSO_4$ and concentrated under vacuum to afford diol **4.12** as a white solid (0.65 g, 86%).

^{1}H NMR (400 MHz, $CDCl_3$) δ 7.61 – 7.52 (m, 8H, $H_{f,g}$), 7.48 (d, J = 8.1 Hz, 4H, H_h), 7.42 (d, J = 7.9 Hz, 4H, H_e), 7.29 (d, J = 8.4 Hz, 4H, H_b), 6.98 (d, J = 8.6 Hz, 4H, H_c), 5.09 (s, 4H, H_d), 4.62 (s, 8$H_{a,i}$), 3.75 – 3.67 (m, 8H, $H_{j,k}$).

^{13}C NMR (126 MHz, $CDCl_3$) δ 158.57, 140.82, 140.21, 137.68, 136.07, 133.60, 128.83, 128.38, 128.09, 127.43, 127.24, 115.10, 73.12, 70.93, 69.96, 69.73, 65.21.

HRMS (ESI +ve) m/z: 717.3320 ($[M+H]^+$, $C_{46}H_{47}O_7$ requires 711.3316).

Extended biphenyl-containing bis-azide (4.13)



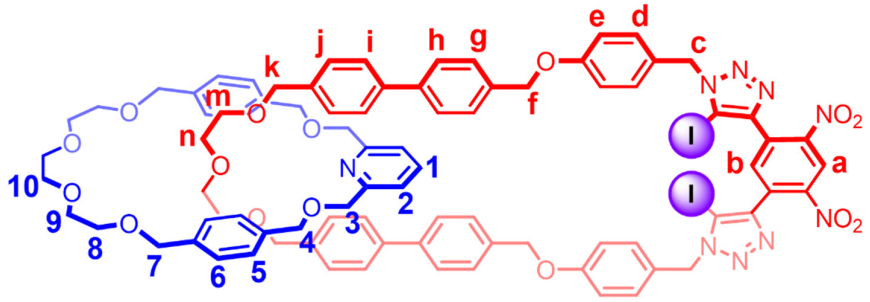
Diol **4.12** (100 mg, 0.14 mmol) was suspended in anhydrous $CHCl_3$ (10 mL), to which was added $SOCl_2$ (61 µL, 0.84 mmol) dropwise and a catalytic amount of DMF. The reaction mixture was stirred under N_2 atmosphere for 2 hours, then diluted with CH_2Cl_2 (10 mL), washed with H_2O (2 × 25 mL) and brine (2 × 25 mL), dried over $MgSO_4$ and concentrated under vacuum to afford the dichloride as a white solid (100 mg, 96%), which was used immediately without further purification. Following general procedure 4B, the reaction of the dichloride (100 mg, 0.13 mmol) and sodium azide (35 mg, 0.54 mmol) yielded the desired bis-azide **4.13** as a white solid (85 mg, 83%).

^{1}H NMR (400 MHz, $CDCl_3$) δ 7.62 – 7.54 (m, 8H, $H_{f,g}$), 7.51 – 7.46 (m, 4H, H_h), 7.45 – 7.40 (m, 4H, H_e), 7.27 – 7.23 (m, 4H, H_b), 7.03 – 6.98 (m, 4H, H_c), 5.10 (s, 4H, H_d), 4.63 (s, 4H, H_i), 4.28 (s, 4H, H_a), 3.76 – 3.67 (m, 8H, $H_{j,k}$).

^{13}C NMR (126 MHz, $CDCl_3$) δ 158.97, 140.89, 140.19, 137.69, 135.89, 129.91, 128.38, 128.12, 127.91, 127.46, 127.24, 115.29, 73.12, 70.92, 69.97, 69.73, 54.54.

HRMS (ESI +ve) m/z: 761.3440 ($[M+H]^+$, $C_{46}H_{45}N_6O_5$ requires 761.3446).

Extended XB hetero[2]catenane (4.14)

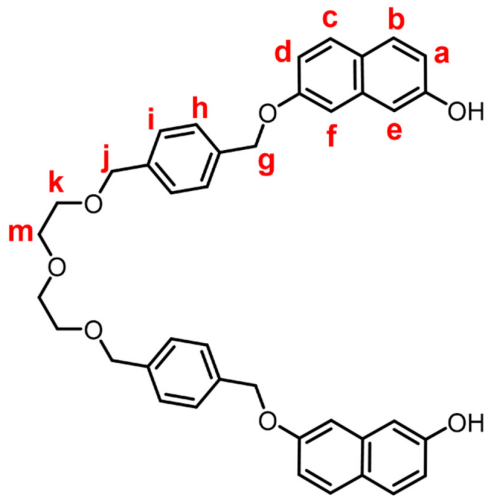


Following General Procedure 2C, the reaction between macrocycle **4.7** (15.0 mg, 0.030 mmol), $NaBAr^F$ (26.9 mg, 0.030 mmol), bis-azide **4.13** (23.0 mg, 0.030 mmol), bis-iodoalkyne **3.3** (14.2 mg, 0.030 mmol), $[Cu(CH_3CN)_4]PF_6$ (5.7 mg, 0.015 mmol) and TBTA (8.1 mg, 0.015 mmol), followed by iterative preparative TLC purification (eluent: 90:10:1 CH_2Cl_2/acetone/MeOH, then 100:1:1 CH_2Cl_2/EtOAc/MeOH) afforded [2]catenane **4.14** as an orange solid (4.2 mg, 8%).

^{1}H NMR (400 MHz, acetone-d_6) δ 8.80 (s, 1H, H_a), 7.87 (s, 1H, H_b), 7.52 (d, J = 7.9 Hz, 9H, $H_{i,j,1}$), 7.40 (d, J = 7.9 Hz, 4H, $H_{g/j}$), 7.33 (d, J = 8.0 Hz, 4H, $H_{g/j}$), 7.25 (d, J = 7.8 Hz, 2H, H_2), 7.14 (d, J = 8.1 Hz, 4H, H_d), 7.03 (d, J = 7.7 Hz, 4H, $H_{5/6}$), 6.97 (d, J = 7.7 Hz, 4H, $H_{5/6}$), 6.70 (d, J = 8.1 Hz, 4H, H_e), 5.66 (s, 4H, H_f), 4.73 (s, 4H, $H_{3/4/7/k/f}$), 4.63 (s, 4H, $H_{3/4/7/k/f}$), 4.43 (s, 4H, $H_{3/4/7/k/f}$), 4.27 (s, 4H, $H_{3/4/7/k/f}$), 4.20 (s, 4H, $H_{3/4/7/k/f}$), 3.71 (s, 8H, $H_{m,n}$), 3.34 – 3.23 (m, 12H, $H_{8,9,10}$).

HRMS (ESI +ve) m/z: 1722.3983 ($[M+H]^+$, $C_{85}H_{82}I_2N_9O_{15}$ requires 1722.4015).

Naphthalene-functionalised diol (4.15)

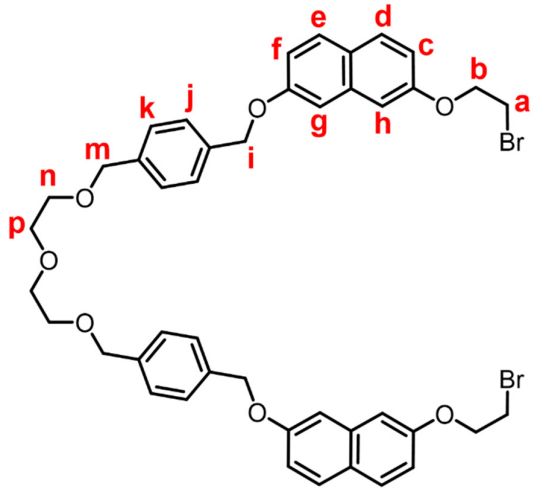


2,7-Dihydroxynaphthalene (0.68 g, 4.2 mmol) and K_2CO_3 (0.29 g, 2.1 mmol) were suspended in anhydrous MeCN (16 mL) and allowed to stir at room temperature for 15 minutes, following which dibromide **2.1** (0.40 g, 0.85 mmol) was added. The reaction mixture was stirred at reflux for 24 hours, then diluted with CH_2Cl_2 (50 mL), washed with H_2O (2 × 50 mL) and brine (2 × 50 mL), dried over $MgSO_4$ and concentrated under vacuum. The residue was purified by silica gel column chromatography (eluent: 1:1 EtOAc/*n*-hexane) to afford diol **4.15** as a white solid (64 mg, 12%).

^{1}H NMR (400 MHz, $CDCl_3$) δ 7.67 (d, J = 8.8 Hz, 4H, $H_{b,c}$), 7.44 (d, J = 7.9 Hz, 4H, $H_{h/i}$), 7.39 (d, J = 7.9 Hz, 4H, $H_{h/i}$), 7.07 (dd, J = 8.9, 2.5 Hz, 2H, $H_{a/d}$), 7.00 (dd, J = 8.5, 2.5 Hz, 4H, $H_{e,f}$), 6.96 (dd, J = 8.7, 2.5 Hz, 2H, $H_{a/d}$), 5.13 (s, 4H, H_g), 4.61 (s, 4H, H_j), 3.74 – 3.65 (m, 8H, $H_{k,m}$).

HRMS (ESI +ve) m/z: 631.2694 ($[M+H]^+$, $C_{40}H_{39}O_7$ requires 631.2690).

Naphthalene-functionalised dibromide (4.16)

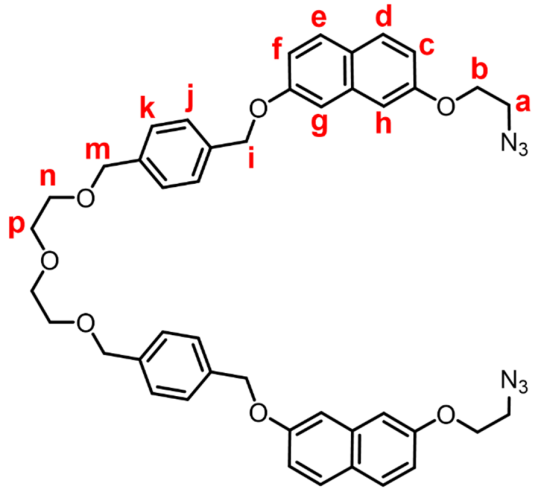


Diol **4.15** (64 mg, 0.10 mmol) and K_2CO_3 (35 mg, 0.25 mmol) were suspended in anhydrous MeCN (3 mL) and allowed to stir at room temperature for 15 minutes, following which 1,2-dibromoethane (175 μL, 2.0 mmol) was added. The reaction mixture was allowed to stir at reflux for 7 days, then diluted with CH_2Cl_2 (20 mL), washed with H_2O (2 × 20 mL) and brine (2 × 20 mL), dried over $MgSO_4$ and concentrated under vacuum. The residue was purified by silica gel column chromatography (eluent: 1:4 EtOAc/*n*-hexane) to afford dibromide **4.16** as a white solid (45 mg, 53%).

^{1}H NMR (400 MHz, $CDCl_3$) δ 7.66 (m, 4H, $H_{d,e}$), 7.44 (d, J = 8.1 Hz, 4H, $H_{j/k}$), 7.38 (d, J = 8.1 Hz, 4H, $H_{j/k}$), 7.11 – 7.05 (m, 4H, $H_{c/f,g/h}$), 7.04 – 6.99 (m, 4H, $H_{c/f,g/h}$), 5.14 (s, 4H, H_i), 4.59 (s, 4H, H_m), 4.37 (t, J = 6.3 Hz, 4H, H_a), 3.74 – 3.63 (m, 12H, $H_{b,n,p}$).

HRMS (ESI +ve) m/z: 843.1540 ($[M+H]^+$, $C_{44}H_{45}O_7Br_2$ requires 843.1527).

Naphthalene-functionalised bis-azide (4.17)



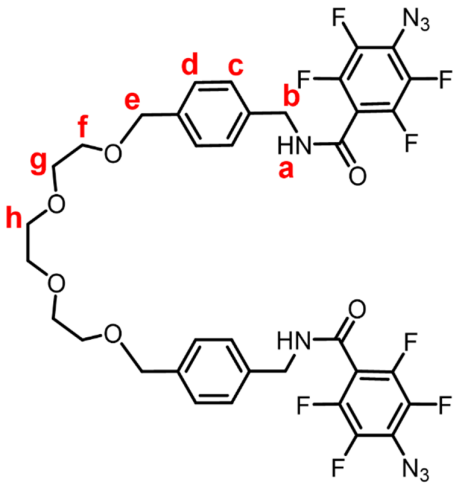
Dibromide **4.16** (45 mg, 0.053 mmol) and sodium azide (21 mg, 0.32 mmol) were suspended in DMF (3 mL) and the reaction mixture was allowed to stir at 80°C for 24 hours. The reaction mixture was diluted with EtOAc (30 mL), washed with H_2O (2 × 20 mL) and brine (2 × 20 mL), dried over $MgSO_4$ and concentrated under vacuum to afford bis-azide **4.17** as a pale pink solid (42 mg, quant.).

^{1}H NMR (400 MHz, $CDCl_3$) δ 7.74 – 7.63 (m, 4H, $H_{d,e}$), 7.44 (d, J = 8.0 Hz, 4H, $H_{j/k}$), 7.38 (d, J = 8.0 Hz, 4H, $H_{j/k}$), 7.12 – 7.05 (m, 4H, $H_{c/f,g/h}$), 7.05 – 7.00 (m, 4H, $H_{c/f,g/h}$), 5.14 (s, 4H, H_i), 4.59 (s, 4H, H_m), 4.37 (t, J = 6.3 Hz, 4H, H_a), 3.74 – 3.63 (m, 12H, $H_{b,n,p}$).

^{13}C NMR (126 MHz, $CDCl_3$) δ 157.55, 156.93, 138.32, 136.39, 135.81, 129.49, 129.37, 128.12, 127.70, 124.82, 116.87, 116.30, 106.81, 106.54, 73.10, 70.87, 69.94, 69.70, 67.01, 50.30.

HRMS (ESI +ve) m/z: 769.3351 ($[M+H]^+$, $C_{44}H_{45}N_6O_7$ requires 769.3344).

Perfluorophenyl-functionalised bis-azide (4.19)

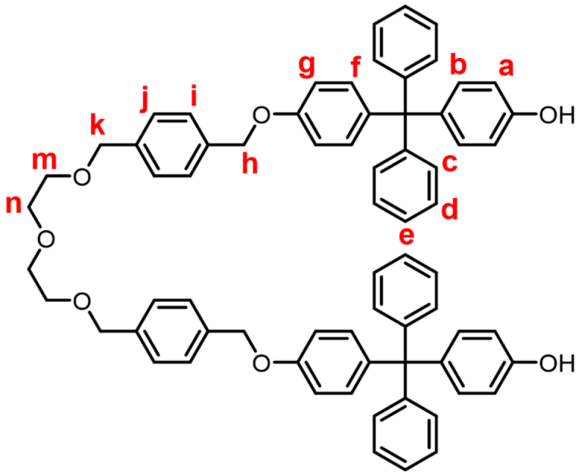


A solution of bis-amine **4.18** (154 mg, 0.40 mmol) and *N*-hydroxysuccinimide-4-azido-2,3,5,6-tetrafluorobenzoate (330 mg, 0.99 mmol) in anhydrous CH_2Cl_2 (5 mL) was allowed to stir at room temperature for 12 hours. The reaction mixture was diluted with CH_2Cl_2 (20 mL), washed with H_2O (2 × 20 mL) and brine (2 × 20 mL), dried over $MgSO_4$ and concentrated in vacuum. The residue was purified by alumina flash column chromatography (eluent: 7:3 EtOAc/*n*-hexane) to afford the bis-azide **4.19** as an off-white solid (176 mg, 54%).

^{1}H NMR (400 MHz, $CDCl_3$) δ 7.31 (d, J = 7.9 Hz, 4H, $H_{c/d}$), 7.26 (d, J = 8.1 Hz, 4H, $H_{c/d}$), 6.58 (br t, 2H, H_a), 4.55 (d, J = 5.7 Hz, 4H, H_b), 4.53 (s, 4H, H_e), 3.72 – 3.59 (m, 12H, $H_{f,g,h}$).

HRMS (ESI +ve) m/z: 823.2228 ($[M+H]^+$, $C_{36}H_{31}N_8O_6F_8$ requires 823.2233).

Terphenyl-functionalised diol (4.20)

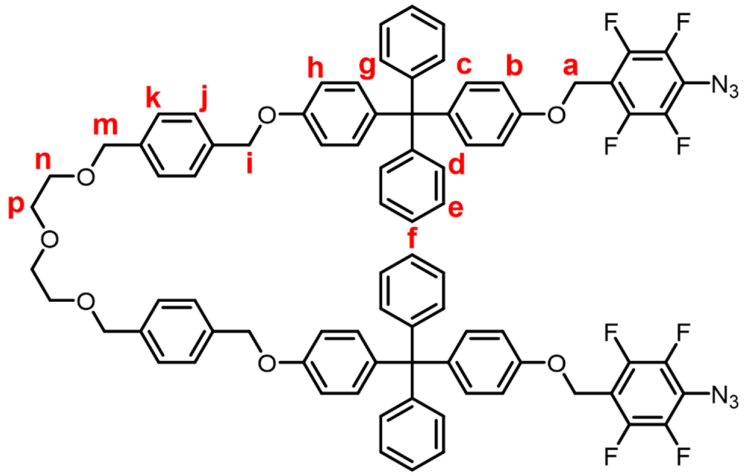


(Diphenylmethylene)diphenol (0.60 g, 1.7 mmol) and K_2CO_3 (0.12 g, 0.85 mmol) were suspended in anhydrous MeCN (8 mL) and allowed to stir at room temperature for 15 minutes, following which dibromide **2.1** (0.20 g, 0.42 mmol) was added. The reaction mixture was stirred at reflux for 12 hours, then diluted with CH_2Cl_2 (50 mL), washed with H_2O (2 × 50 mL) and brine (2 × 50 mL), dried over $MgSO_4$ and concentrated under vacuum. The residue was purified by silica gel column chromatography (eluent: 1:1 EtOAc/*n*-hexane) to afford diol **4.20** as a white solid (0.19 g, 45%).

^{1}H NMR (400 MHz, $CDCl_3$) δ 7.41 – 7.31 (m, 8H, $H_{i,j}$), 7.27 – 7.13 (m, 20H, $H_{c,d,e}$), 7.11 – 6.99 (m, 8H, $H_{b,f}$), 6.82 (d, J = 8.9 Hz, 4H, H_g), 6.73 – 6.66 (m, 4H, H_a), 5.00 (s, 4H, H_h), 4.78 (s, 2H, O**H**), 4.57 (s, 4H, H_k), 3.73 – 3.61 (m, 8H, $H_{k,m,n}$).

HRMS (ESI +ve) m/z: 1015.4581 ($[M+H]^+$, $C_{70}H_{63}O_7$ requires 1015.4568)

Terphenyl- and perfluorophenyl-functionalised bis-azide (4.21)



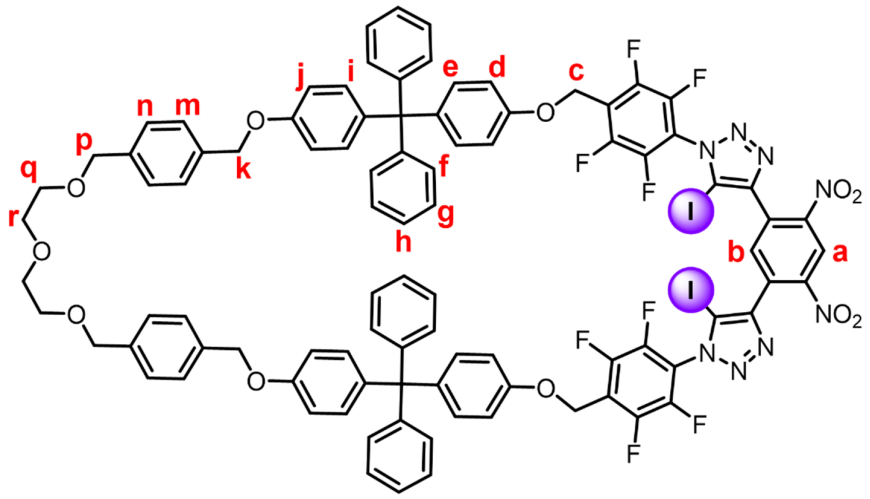
Diol **4.20** (190 mg, 0.19 mmol) and K_2CO_3 (78 mg, 0.56 mmol) were suspended in anhydrous MeCN (8 mL) and allowed to stir at room temperature for 15 minutes, following which 4-azido-2,3,5,6-tetrafluorobenzyl methanesulfonate (123 mg, 0.42 mmol) was added. The reaction mixture was stirred at 50°C for 24 hours, then diluted with CH_2Cl_2 (20 mL), washed with H_2O (2 × 20 mL) and brine (2 × 20 mL), dried over $MgSO_4$ and concentrated under vacuum. The residue was purified by silica gel column chromatography (eluent: 2% MeOH/CH_2Cl_2) to afford bis-azide **4.21** as a white solid (186 mg, 70%).

^{1}H NMR (400 MHz, $CDCl_3$) δ 7.42 – 7.32 (m, 8H, $H_{j,k}$), 7.25 – 7.21 (m, 8H, H_e), 7.21 – 7.15 (m, 12H, $H_{d,f}$), 7.15 – 7.06 (m, 8H, $H_{c,g}$), 6.88 – 6.79 (m, 8H, $H_{b,h}$), 5.07 (s, 4H, H_a), 5.01 (s, 4H, H_i), 4.58 (s, 4H, H_m), 3.74 – 3.61 (m, 8H, $H_{m,n,p}$).

^{13}C NMR (126 MHz, $CDCl_3$) δ 156.94, 156.09, 147.24, 140.57, 139.47, 138.26, 136.55, 132.43, 132.27, 131.17, 128.09, 127.76, 127.58, 126.02, 113.73, 113.68, 73.12, 70.87, 69.90, 69.68, 63.81.

HRMS (ESI +ve) m/z: 1421.4804 ($[M+H]^+$, $C_{84}H_{65}N_6O_7F_8$ requires 1421.4782)

Terphenyl- and perfluorophenyl-functionalised XB macrocycle (4.22)

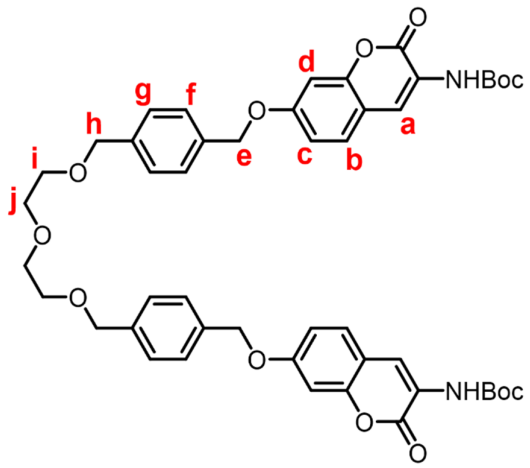


Using General Procedure 2B, the CuAAC click reaction between bis-azide **4.21** (40 mg, 0.028 mmol) and bis(iodoalkyne) **3.3** (13.2 mg, 0.028 mmol), $[Cu(MeCN)_4]PF_6$ (5.2 mg, 0.014 mmol) and TBTA (3.7 mg, 0.007 mmol), followed by purification by silica gel chromatography (eluent: 25:1 CH_2Cl_2/EtOAc) afforded macrocycle **4.22** as a yellow solid (12 mg, 23%).

^{1}H NMR (400 MHz, $CDCl_3$) δ 8.86 (s, 1H, H_a), 8.12 (s, 1H, H_b), 7.36 (m, 8H, $H_{m,n}$), 7.26 – 7.17 (m, 20H, $H_{f,g,h}$), 7.14 (d, J = 8.8 Hz, 4H, $H_{e/i}$), 7.07 (d, J = 8.8 Hz, 4H, $H_{e/i}$), 6.87 (d, J = 8.8 Hz, 4H, $H_{d/j}$), 6.83 (d, J = 8.8 Hz, 4$H_{d/j}$), 5.30 (s, 4H, H_c), 5.02 (s, 4H_k), 4.56 (s, 4H_p), 3.72 – 3.61 (m, 8H, $H_{q,r}$).

HRMS (ESI +ve) m/z: 1889.2906 ($[M+H]^+$, $C_{94}H_{67}N_8O_{11}F_8I_2$ requires 1889.2885)

Boc-protected bis-coumarin (4.23)



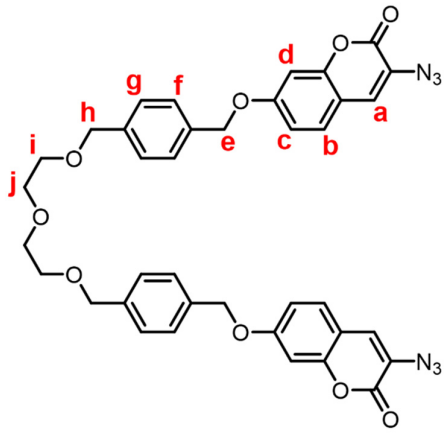
3-Azido-7-hydroxy-coumarin (0.39 g, 1.40 mmol) and K_2CO_3 (0.35 g, 2.54 mmol) were suspended in anhydrous MeCN (10 mL) and allowed to stir at room temperature for 15 minutes, following which dibromide **2.1** (0.30 g, 0.64 mmol) was added. The reaction mixture was stirred at reflux for 12 hours, then diluted with CH_2Cl_2 (40 mL), washed with H_2O (2 × 40 mL) and brine (2 × 40 mL), dried over $MgSO_4$ and concentrated under vacuum. The residue was purified by silica gel column chromatography (eluent: 10:1 CH_2Cl_2/EtOAc) to afford bis-coumarin **4.23** as a white solid (0.52 g, 95%).

^{1}H NMR (400 MHz, $CDCl_3$) δ 8.22 (s, 2H, N**H**Boc), 7.42 – 7.32 (m, 10H, $H_{b,g,f,}$), 7.28 (s, 2H, H_a), 6.92 (dd, *J* = 8.6, 2.5 Hz, 2H, H_c), 6.86 (d, *J* = 2.5 Hz, 2H, H_d), 5.08 (s, 4H, H_e), 4.58 (s, 4H, H_h), 3.72 – 3.63 (m, 8H, $H_{i,j}$), 1.52 (s, 18H, Boc-C**H**$_3$).

HRMS (ESI +ve) m/z: 865.3541 ($[M+H]^+$, $C_{48}H_{53}N_2O_{13}$ requires 865.3542)

General Procedure 4C: Azidation of Coumarin Moieties

Coumarin-functionalised bis-azide (4.24)



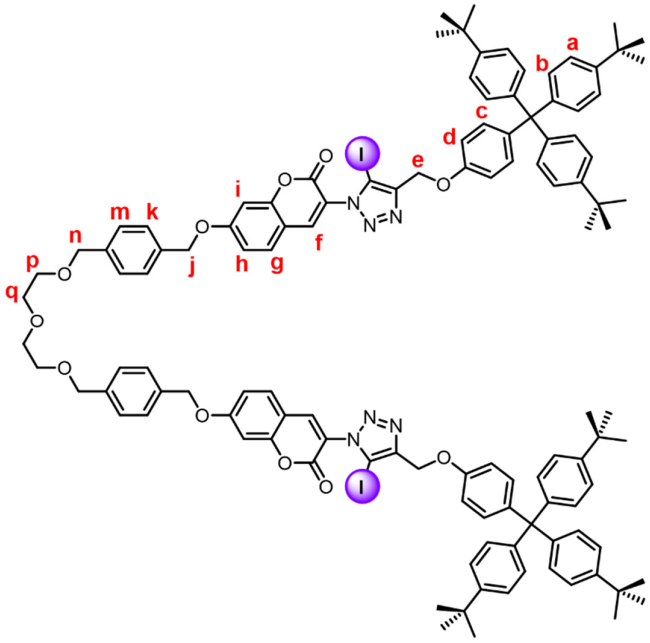
Bis-coumarin **4.23** (0.52 g, 0.601 mmol) was dissolved in CH_2Cl_2 (2 mL) and cooled to 0°C, following which trifluoroacetic acid (2 mL) was added slowly. The reaction was allowed to gradually warm to room temperature and stirred for 2 hours, then diluted with CH_2Cl_2 (20 mL), washed with aqueous sat. $NaHCO_3$ (3 × 20 mL), H_2O (2 × 20 mL) and brine (2 × 20 mL), dried over $MgSO_4$ and concentrated under vacuum to afford the bis-amine (0.39 g, 99%) which was immediately used without further purification. The bis-amine was suspended in THF (10 mL) and cooled to 0°C, to which was sequentially added *tert*-butyl nitrite (226 µL, 1.90 mmol), and trimethylsilyl azide (284 µL, 2.14 mmol). The reaction mixture was allowed to slowly warm to room temperature and stirred for 5 hours, then concentrated under vacuum to afford the bis-azide **4.24** as a yellow solid (0.40 g, 94%).

^{1}H NMR (400 MHz, $CDCl_3$) δ 7.38 (s, 8H, $H_{f,g}$), 7.30 (d, J = 8.6 Hz, 2H, H_b), 7.15 (s, 2H, H_a), 6.92 (dd, J = 8.6, 2.4 Hz, 2H, H_c), 6.87 (d, J = 2.4 Hz, 2H, H_d), 5.09 (s, 4H, H_e), 4.58 (s, 4H, H_h), 3.77 – 3.62 (m, 8H, $H_{i,j}$).

^{13}C NMR (126 MHz, $CDCl_3$) δ 160.92, 157.81, 153.04, 138.83, 135.17, 128.28, 128.20, 127.73, 126.43, 123.60, 114.08, 112.98, 101.90, 73.01, 70.88, 70.52, 69.78.

HRMS (ESI +ve) m/z: 717.2307 ([M+H]$^+$, $C_{38}H_{33}N_6O_9$ requires 717.2304).

Coumarin-functionalised bis-triazole (4.25)



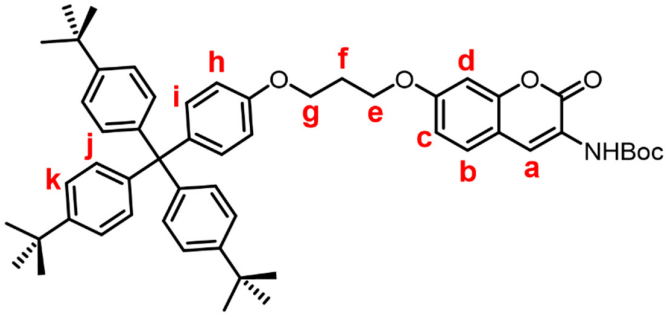
$[Cu(MeCN)_4]PF_6$ (2.6 mg, 0.007 mmol) and TBTA (1.9 mg, 0.003 mmol) were dissolved in dry, degassed CH_2Cl_2 (1 mL) and stirred for 20 minutes. Solutions of bis-azide **4.24** (10 mg, 0.014 mmol) in CH_2Cl_2 (1 mL) and stopper iodoalkyne **2.8** (20.5 mg, 0.031 mmol) in CH_2Cl_2 (1 mL) were added sequentially. The resulting mixture was stirred at room temperature overnight under an atmosphere of N_2, then diluted with CH_2Cl_2 (10 mL) and washed with an EDTA/NH_4OH solution (2 × 15 mL), H_2O (2 × 15 mL) and brine (2 × 15 mL), dried over $MgSO_4$ and concentrated under reduced pressure. The residue was purified by silica gel column chromatography (eluent: 100:7 CH_2Cl_2/EtOAc) to afford **4.25** a white solid (20 mg, 70%).

^{1}H NMR (400 MHz, $CDCl_3$) δ 7.97 (s, 2H, H_f), 7.52 (d, J = 8.7 Hz, 2H, H_g), 7.41 (s, 8H, $H_{k,m}$), 7.25 – 7.21 (m, 12H, H_a), 7.15 – 7.07 (m, 16H, $H_{b,c}$), 7.03 (dd, J = 8.7, 2.4 Hz, 2H, H_h), 6.98 (d, J = 2.4 Hz, 2H, H_i), 6.95 – 6.91 (m, 4H, H_d), 5.18 (s, 4H, $H_{e/j}$), 5.16 (s, 4H, $H_{e/j}$), 4.60 (s, 4H, H_n), 3.75 – 3.63 (m, 8H, $H_{p,q}$), 1.30 (s, 54H, stopper-^{t}Bu-C**H**$_3$).

^{13}C NMR (126 MHz, $CDCl_3$) δ 163.85, 156.39, 156.29, 148.49, 148.24, 144.22, 142.58, 140.52, 139.06, 134.70, 132.47, 130.89, 130.53, 128.28, 127.78, 124.21, 120.73, 114.80, 113.65, 111.39, 102.26, 83.83, 72.99, 70.88, 70.82, 69.82, 63.24, 61.78, 34.44, 31.53.

HRMS (ESI +ve) m/z: 2053.7315 ($[M+H]^+$, $C_{118}H_{123}N_6O_{11}I_2$ requires 2053.7334).

Boc-protected Coumarin Stopper (4.27)



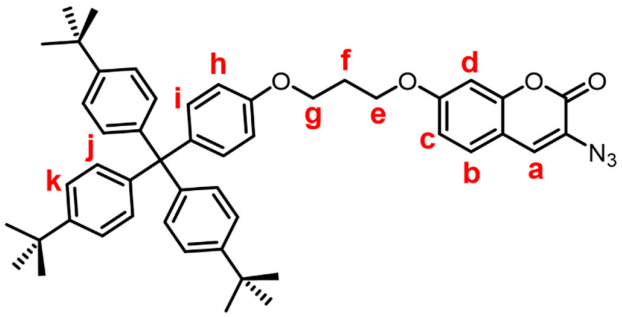
3-Boc-7-hydroxy-coumarin (0.12 g, 0.44 mmol) and K_2CO_3 (0.11 g, 0.80 mmol) were suspended in anhydrous MeCN (10 mL) and allowed to stir at room temperature for 15 minutes, following which stopper bromide **4.26** (0.25 g, 0.40 mmol) was added. The reaction mixture was stirred at reflux for 12 hours, then diluted with CH_2Cl_2 (40 mL), washed with H_2O (2 × 40 mL) and brine (2 × 40 mL), dried over $MgSO_4$ and concentrated under vacuum. The residue was purified by silica gel column chromatography (eluent: CH_2Cl_2) to afford coumarin stopper **4.27** as a yellow solid (0.18 g, 55%).

^{1}H NMR (400 MHz, $CDCl_3$) δ 8.23 (s, 1H, N**H**Boc), 7.34 (d, J = 8.6 Hz, 1H, H_b), 7.29 (s, 1H, H_a), 7.25 – 7.20 (m, 6H, H_j), 7.10 – 7.05 (m 8H, $H_{k,i}$), 6.86 (dd, J = 8.6, 2.4 Hz, 1H, H_c), 6.83 (d, J = 2.4 Hz, 1H, H_d), 6.80 – 6.75 (m, 2H, H_h), 4.20 (m, 2H, H_e), 4.14 (m, 2H, H_g), 2.27 (m, 2H, H_f), 1.53 (s, 9H, Boc-CH_3), 1.30 (s, 27H, stopper-^{t}Bu-CH_3).

^{13}C NMR (126 MHz, $CDCl_3$) δ 160.03, 156.52, 152.62, 150.93, 148.31, 144.11, 139.81, 132.29, 130.71, 128.09, 124.04, 122.14, 121.26, 113.34, 112.94, 101.33, 65.04, 63.88, 63.05, 53.43, 34.30, 31.39, 29.17, 28.24.

HRMS (ESI +ve) m/z: 822.4731 ($[M+H]^+$, $C_{54}H_{64}O_6N$ requires 822.4734).

Coumarin-Functionalised Azide Stopper (4.28)



Following General Procedure 4C, the reaction between Boc-protected coumarin stopper **4.27** (0.18 g, 0.21 mmol) and trifluoroacetic acid (2 mL) in CH_2Cl_2 (2 mL) afforded the amine stopper in quantitative yield, which was subsequently reacted with *tert*-butyl nitrite (40 µL, 0.33 mmol), and trimethylsilyl azide (50 µL, 0.37 mmol) to afford the azide stopper as a yellow powder (0.16 g, quant).

^{1}H NMR (500 MHz, $CDCl_3$) δ 7.32 – 7.27 (m, 1H, H_b), 7.26 – 7.19 (m, 6H, H_j), 7.16 (s, 1H, H_a), 7.13 – 7.04 (m, 8H, $H_{k,i}$), 6.87 – 6.84 (m, 2H, $H_{c,d}$), 6.80 – 6.75 (m, 2H, H_h), 4.21 (t, J = 6.1 Hz, 2H, H_e), 4.13 (t, J = 5.9 Hz, 2H, H_g), 3.78 – 3.71 (m, 2H, H_f), 1.30 (s, 27H, stopper-^{t}Bu-CH_3).

^{13}C NMR (126 MHz, $CDCl_3$) δ 161.23, 157.87, 156.63, 153.14, 148.48, 144.24, 140.01, 132.44, 130.85, 128.23, 126.52, 124.19, 123.46, 113.68, 113.08, 112.79, 101.53, 68.12, 65.34, 63.94, 63.20, 34.44, 31.53, 29.26, 25.77.

HRMS (ESI +ve) m/z: 770.3933 ($[M+Na]^+$, $C_{49}H_{53}O_4N_3Na$ requires 770.3934)

6.3 References for Chapter 6

1. T. R. Chan, R. Hilgraf, K. B. Sharpless and V. V. Fokin, *Org. Lett.*, 2004, **6**, 2853-2855.
2. P. Thordarson, *Chem. Soc. Rev.*, 2011, **40**, 1305-1323.
3. Y.-H. Lin, C.-C. Lai and S.-H. Chiu, *Org. Biomol. Chem.*, 2014, **12**, 2907-2917.
4. Y. C. Tse, A. Docker, Z. Zhang and P. D. Beer, *Chem. Commun.*, 2021, **57**, 4950-4953.
5. A. J. Martínez-Martínez and A. S. Weller, *Dalton Trans.*, 2019, **48**, 3551-3554.
6. P.-N. Cheng, C.-F. Lin, Y.-H. Liu, C.-C. Lai, S.-M. Peng and S.-H. Chiu, *Org. Lett.*, 2006, **8**, 435-438.
7. N. L. Kilah, M. D. Wise, C. J. Serpell, A. L. Thompson, N. G. White, K. E. Christensen and P. D. Beer, *J. Am. Chem. Soc.*, 2010, **132**, 11893-11895.
8. V. Aucagne, K. D. Hänni, D. A. Leigh, P. J. Lusby and D. B. Walker, *J. Am. Chem. Soc.*, 2006, **128**, 2186-2187.
9. A. V. Lunchev, V. C. Hendrata, A. Jaggi, S. A. Morris, R. Ganguly, X. Chen, H. Sun and A. C. Grimsdale, *J. Mater. Chem. C*, 2018, **6**, 3715-3721.
10. K.-Y. Ng, V. Felix, S. M. Santos, N. H. Rees and P. D. Beer, *Chem. Commun.*, 2008, 1281-1283.
11. T. A. Barendt, S. W. Robinson and P. D. Beer, *Chem. Sci.*, 2016, **7**, 5171-5180.
12. C.-Y. Chen, H.-C. Xu, T.-H. Ho, C.-J. Hsu, C.-C. Lai, Y.-H. Liu, S.-M. Peng and S.-H. Chiu, *J. Org. Chem.*, 2021, **86**, 13491-13502.
13. H. Zheng, W. Zhou, J. Lv, X. Yin, Y. Li, H. Liu and Y. Li, *Chem. Eur. J.*, 2009, **15**, 13253-13262.

APPENDIX

Appendix

Single Crystal X-ray Diffraction Studies

Single crystals of **2.2·XB^{TEG}**, **2.2·XB^{DEG}·TBACl**, **2.2·XB^{DEG}·NaI·H$_2$O**, **2.2·XB^{TEG}·NaI**, **2.2·HBXB^{DEG}**, **2.3·XB^{DEG}·NaI** and **4.10·NaCl** suitable for X-ray analysis were each coated with perfluoropolyether oil, mounted on a 200 μm MiTeGen loop and placed in a cold nitrogen stream (150 K)[1] on an Oxford Diffraction Supernova X-ray diffractometer. Diffraction intensities were measured using monochromated Cu K$_\alpha$ diffraction. Data collection, indexing, initial cell refinements, frame integration, final cell refinements and absorption corrections were performed using CrysAlisPro. Crystal structures were solved by SuperFlip[2] or ShelXS[3] and refined using full matrix least-squares on F^2 with Crystals.[4] Hydrogen atoms were included into the model at geometrically calculated positions and refined using a riding model.[5]

Details of the data quality and a summary of the residual values for the refinements are included in Tables A1-4. The data is provided free of charge by the joint Cambridge Crystallographic Data Centre and Fachinformationszentrum Karlsruhe Access Structures service www.ccdc.cam.ac.uk/structures with deposition numbers 2211706 (**2.2·XB^{TEG}**), 2211716 (**2.2·XB^{DEG}·TBACl**), 2211724 (**2.2·XB^{DEG}·NaI·H$_2$O**), 2211718 (**2.2·XB^{TEG}·NaI**), 2211717 (**2.2·HBXB^{DEG}**), 2348225 (**2.3·XB^{DEG}·NaI**). The data for **4.10·NaCl** is provided with this thesis as an accompanying CIF.

Table A1. *Selected crystallographic data for* ***2.2·XB^{TEG}*** *and* ***2.2·XB^{DEG}·TBACl***

Compound	**2.2·XB^{TEG}**	**2.2·XB^{DEG}·TBACl**
Formula	$C_{36}H_{40}I_2N_6O_4$	$C_{84}H_{108}Cl\ I_4N_{13}O_6$
Formula Weight	874.56	1938.93
Temp (K)	150(2)	150(2)
Crystal system	monoclinic	tetragonal
Space Group	Pc	P4/n
***a* (Å)**	14.3321(2)	36.7661(10)
***b* (Å)**	34.2258(6)	36.7661(10)
***c* (Å)**	14.8140(2)	13.8468(8)
α (°)	90	90
β (°)	98.7161(14)	90
γ (°)	90	90
Cell Volume (Å^3)	7182.76(19)	18717.4(15)
Z	8	8
Reflections collected (all)	87363	99032
Reflections (unique)	17373	18458
R_{int}	0.096	0.122
R_1 ($I > 2\sigma(I)$)	0.0743	0.1177
wR_2 (all data)	0.1802	0.2679

Table A2. *Selected crystallographic data for* ***2.2·XB^{DEG}·NaI·H$_2$O*** *and* ***2.2·XB^{TEG}·NaI***

Compound	**2.2·XB^{DEG}·NaI·H$_2$O**	**2.2·XB^{TEG}·NaI**
Formula	$C_{68}H_{74}I_5N_{12}NaO_7$	$C_{72}H_{80}I_5N_{12}NaO_8$
Formula Weight	1828.92	1899.01
Temp (K)	150(2)	150(2)
Crystal system	monoclinic	monoclinic
Space Group	$P2_1/n$	$P2_1/c$
***a* (Å)**	18.8455(5)	12.8306(2)
***b* (Å)**	18.1755(5)	26.6737(4)
***c* (Å)**	24.7474(9)	26.0769(4)
α (°)	90	90
β (°)	95.831(3)	96.7556(15)
γ (°)	90	90
Cell Volume (Å^3)	8432.8(4)	8862.6(2)
Z	4	4
Reflections collected (all)	60082	85459
Reflections (unique)	16973	18071
***R*$_{int}$**	0.101	0.094
***R*$_1$ (*I* > 2σ(*I*))**	0.1474	0.0917
w*R*$_2$ (all data)	0.3874	0.2520

Table A3. *Selected crystallographic data for* ***2.2·HBXB^{DEG}*** *and* ***2.3·XB^{DEG}·NaI***

Compound	**2.2·HBXB^{DEG}**	**2.3·XB^{DEG}·NaI**
Formula	$C_{71}H_{80}I_2N_{12}O_7$	$C_{59}H_{68}I_3N_6NaO_9$
Formula Weight	1467.27	1396.87
Temp (K)	150(2)	150.15(2)
Crystal system	triclinic	monoclinic
Space Group	P-1	$P2_1/n$
***a* (Å)**	13.7114(3)	21.3809(4)
***b* (Å)**	16.6936(6)	11.8823(2)
***c* (Å)**	17.3863(4)	26.6796(5)
α (°)	68.872(3)	90
β (°)	84.057(2)	100.995(2)
γ (°)	68.699(3)	90
Cell Volume (Å^3)	3456.77(19)	6653.6(2)
Z	2	4
Reflections collected (all)	64271	83698
Reflections (unique)	14222	13822
R_{int}	0.086	0.0755
R_1 ($I > 2\sigma(I)$)	0.0527	0.0454
wR_2 (all data)	0.1447	0.1385

Table A4. *Selected crystallographic data for* ***4.10·NaCl***

Compound	
Formula	$C_{100}N_{12}O_{21}I_2Cl_1Na_1$
Formula Weight	1996.35
Temp (K)	150.01(18)
Crystal system	triclinic
Space Group	P-1
***a* (Å)**	15.4754(4)
***b* (Å)**	15.8405(4)
***c* (Å)**	44.5771(9)
α (°)	83.865(2)
β (°)	85.070(2)
γ (°)	73.881(2)
Cell Volume (Å^3)	10419.7(4)
Z	4
Reflections collected (all)	115516
Reflections (unique)	14880
R_{int}	0.2936
R_1 ($I > 2\sigma(I)$)	0.2031
wR_2 (all data)	0.5204

The data for **4.10·NaCl** was weak, with visibly poor crystal quality and diffraction, thought to be caused in part by solvent loss. Despite several attempts to obtain better data or to improve the integration of these data, the results were still poor. In addition, on inspection of the raw frame data, the crystal was found to be twinned and the data was processed taking this into account. The best refinement came from including data from only one component and omitting the poorly fitting low angle reflections. The structure solved in the triclinic space group *P*-1, but on refinement many of the displacement ellipsoids were poorly shaped. The poor quality and weakness of the data precluded a full anisotropic refinement of the structure.

Nevertheless, there is no doubt about the connectivity, the interlocked nature of the structure, and the location of the sodium and chloride ions situated in the interlocked binding cavities.

Binding Model Analysis of Ion-Pair Titrations of 2.2·XB^{DEG} and 2.2·XB^{TEG}

Since metal complexation to the [2]catenane produces a monocationic species, there is a possibility of 1:2 host-guest binding that utilises multiple anion binding sites in the [2]catenanes. As such, all binding isotherms were fitted to both the 1:1 host-guest binding model, as well as four variants of the 1:2 host-guest binding model.

To determine which model best applies to the data, the covariance values of the various fits were compared. Following an approach used by Thordarson and co-workers,[6] a parameter known as the cov_{fit} factor was introduced, which defined as the ratio of cov_{fit} for the simple 1:1 model to cov_{fit} for each of the 1:2 models. In general, the better a model fits the data, the lower the value of cov_{fit} and hence the higher the value of the cov_{fit} factor. However, the number of fitted parameters should also be considered, as complex binding models with a larger number of fitted parameters, such as the 1:2 (Full) model, may appear to fit better to the data and yield an apparently lower cov_{fit}. Therefore, the more complex 1:2 binding models were only considered applicable if they possess a significantly lower cov_{fit} than the simple 1:1 model – that is, cov_{fit} factor > 10. The binding models and corresponding K_1 and K_2 values obtained from this analysis are shown in **Table A5**.

Table A5. *Apparent anion association constants (K_a/M^{-1}) for [2]catenanes* ***2.2·XB^{DEG}*** *and* ***2.2·XB^{TEG}*** *in the presence of 1 equiv. M^IBAr^F (M^I = Na, K) determined by ^{1}H NMR titrations.*[a]

Host	Cation	% cat·M^I	Anion	Binding model	K_1	K_2	Cov_{fit} ($\times10^{-4}$)	cov_{fit} factor
2·XB^{DEG}	Na^+	33	Br^-	1:1	724	-	5.1	1.000
				1:2 (Full)[b]	**1900**	**435**	**0.43**	**11.988**
				1:2 (Non-cooperative)	1670	418	0.44	11.801
				1:2 (Additive)	543	< 0	1.3	3.947
				1:2 Statistical)	5.81	1.45	2030	< 0.01
			I^-	1:1	919	-	18	1.000
				1:2 (Full)[b]	**3080**	**787**	**1.1**	**15.869**
				1:2 (Non-cooperative)	616	154	3.8	4.750
				1:2 (Additive)	573	< 0	5.0	3.604
				1:2 Statistical)	4.86	1.22	2450	0.007
	K^+	17	Br^-	**1:1**[b]	**432**	**-**	**5.3**	**1.000**
				1:2 (Full)	10600	245	1.8	3.047
				1:2 (Non-cooperative)	692	173	9.3	0.574
				1:2 (Additive)	592	0.462	2.7	1.953
				1:2 Statistical)	3.09	0.772	1280	0.004
			I^-	**1:1**[b]	**487**	**-**	**3.4**	**1.000**
				1:2 (Full)	5190	350	1.6	2.197
				1:2 (Non-cooperative)	984	246	2.5	1.384
				1:2 (Additive)	435	< 0	3.0	1.133
				1:2 Statistical)	3.02	0.754	1470	0.002
2·XB^{TEG}	Na^+	37	Br^-	**1:1**[b]	**745**	**-**	**1.9**	**1.000**
				1:2 (Full)	936	47.0	1.6	1.198
				1:2 (Non-cooperative)	1040	261	7.1	0.266
				1:2 (Additive)	808	0.186	1.6	1.180
				1:2 Statistical)	4.99	1.25	2000	0.001
			I^-	**1:1**[b]	**817**	**-**	**5.3**	**1.000**
				1:2 (Full)	1280	82.5	4.1	1.307
				1:2 (Non-cooperative)	1120	279	13	0.395
				1:2 (Additive)	953	0.284	4.2	1.261
				1:2 Statistical)	4.12	1.03	2130	0.002
	K^+	48	Br^-	**1:1**[b]	**983**	**-**	**5.2**	**1.000**
				1:2 (Full)	2010	132	2.4	2.191
				1:2 (Non-cooperative)	1337	334	17	0.306
				1:2 (Additive)	1223	0.374	2.7	1.936
				1:2 Statistical)	4.01	1.00	2390	0.002
			I^-	**1:1**[b]	**1050**	**-**	**3.0**	**1.000**
				1:2 (Full)	1680	87.4	0.80	3.769
				1:2 (Non-cooperative)	1450	362	14	0.212
				1:2 (Additive)	1270	0.271	0.88	3.415
				1:2 Statistical)	3.23	0.808	2490	0.001

[a]*Ka* values calculated using Bindfit. Errors (±) are all < 5% unless otherwise stated. All anions added as TBA^+ salts. Solvent = 1:1 $CDCl_3/CD_3CN$. *T* = 298 K. [Receptor] = 1.0 mM. [b]Most appropriate binding model determined from cov_{fit} analysis.

References for Appendix

1. J. Cosier and A. M. Glazer, *J. Appl. Crystallogr.*, 1986, **19**, 105-107.
2. L. Palatinus and G. Chapuis, *J. Appl. Crystallogr.*, 2007, **40**, 786-790.
3. G. Sheldrick, *Acta Cryst. A*, 2015, **71**, 3-8.
4. R. Cooper, P. Betteridge, D. Watkin, K. Prout and J. Carruthers, *J. Appl. Crystallogr.*, 2003, **36**, 1487.
5. R. Cooper, A. Thompson and D. Watkin, *J. Appl. Crystallogr.*, 2010, **43**, 1100-1107.
6. E. N. W. Howe, M. Bhadbhade and P. Thordarson, *J. Am. Chem. Soc.*, 2014, **136**, 7505-7516.

"[n]Ring[s] to rule them all,
[n]Rings[s] to find them.
[n]Ring[s] to bring them all,
And in the darkness bind them."

J. R. R. Tolkien
The Fellowship of the Ring